The identification of natural organic components in the construction materials of ancient earthen sites in China



Yushen He 1059204

School of Archaeology, University of Oxford

Supervisors: Prof. Mark Pollard &Dr. Thibaut Deviese

Abstract: This research begins with a review of the previous research on the application and identification of natural organic materials, such as starch and sugar, in ancient architectures in China. The review reveals that most (92.7%) of the existing methods relied upon “spot test”: a basic form of chemical reaction-based analysis. These tests are generally insufficient in sensitivity and specificity for the dependable identification of organic materials. Moreover, a significant gap is identified in the lack of blank tests for detecting organic residues in foundational materials like earth, which is crucial for establishing a baseline in such studies.

Through the analysis of modern and archaeological samples, the research develops and applies a novel analytical strategy for identifying starch and disaccharides. The new protocol includes pretreatment, sample screening, extraction of organics and identification at the molecular level, moving beyond the limitations of most existing analytical methods. The research explores the application of 8 analytical methods to develop this new protocol. Amongst them, FTIR and LOI are found suitable for the screening step. MALDI-TOF-MS and LC-MS/MS are effective in detecting starch and sucrose in earth samples at low detection limits. Significant findings from this new protocol include the identification of starch and sucrose in several archaeological samples, evidencing the artificial addition of these organics in earthen constructions. The outcomes not only enhance the methodology in archaeological science but also have important implications for the analysis and conservation of ancient sites.

Keywords: ancient Chinese architecture earthen construction natural organic materials novel analytical strategy

Acknowledgements

I would like to express my sincere thanks to my supervisors, Prof. Mark Pollard and Dr. Thibaut Deviese, for their guidance and advice throughout my DPhil studies. Their support has been essential to my research. I am particularly grateful to Prof. Pollard for his support during the toughest times when I was attacked in Oxford, helping me to overcome those difficult days.

I would like to thank all the faculty, staff, and fellow students at the School of Archaeology for their invaluable assistance and support, especially the assistance provided by Prof. Amy Bogaard, Prof. Greger Larson, Dr. Chris Doherty and Dr. Peter Ditchfield during my transfer and confirmation. Additionally, I extend my gratitude to Prof. Yanyi Huang and Guanbo Wang from the Biomedical Pioneering Innovation Center (BIOPIC) at Peking University for their support and guidance. My acknowledgements also go to Fei Zhang at the Analytical Instrumentation Centre, College of Chemistry and Molecular Engineering, Peking University, and to Xiaopeng Yao, Hulingxiao Chai, and Xiang Xu at the Institute of Cell Analysis, Shenzhen Bay Laboratory for their help with experiments. Further, I appreciate Prof. Shuanglin Zhou at the School of Archaeology and Museology, Peking University, and Biao Cui at Zhejiang Provincial Institute of Cultural Relics and Archaeology for their assistance in providing samples.

I owe a deep sense of gratitude to my parents for their unwavering support and

encouragement throughout my DPhil journey. A special acknowledgment goes to my wife, who has been a constant companion by my side throughout these years. Her presence was particularly comforting during the times when I was overwhelmed by the panic and negative feelings caused by the attack I experienced and the challenges of the pandemic. Her unwavering support and understanding allowed me to get through these tough periods and continue focusing on my research. Her love and patience are more than I could ever ask for.

Abbreviations and Acronyms 11

1. Introduction 12

2. Background 16

2.1. Traditional building materials in China 16

2.2. Construction of earthen sites in China 19

2.2.1. The history of ancient earthen sites in China 19

2.2.2. The construction of ancient earthen sites in China 25

2.2.2.1. The excavation method 26

2.2.2.2. The rammed earth method 29

2.2.2.3. The cob method 33

2.2.2.4. The wooden wattle and mud daub method 35

2.2.2.5. The adobe building method 36

2.3. The organic materials used in ancient sites in China 38

2.3.1. Starch (sticky rice and flour) 42

2.3.2. Sugar 46

2.3.3. Protein 48

2.3.4. Blood (pig blood) 52

2.3.5. Lipid 55

2.3.6. Other natural organic materials 57

2.4. Organics in natural loess 60

2.4.1. The genesis and distribution of loess 60

2.4.2. Sources of organic matter in loess 62

2.4.3. The organic matter content in loess in China.....63

2.4.4. The composition of organic matter in loess in China 65

3. Materials 68

3.1. Modern samples.....68

3.2. Archaeological samples 75

3.3. Artificially aged samples 82

4. The iodine-starch test.....88

4.1. Samples.....88

4.2. Methods.....88

4.3. Results.....89

4.4. Discussion.....92

4.5. Conclusions.....95

5. Fourier transform infrared spectroscopy (FTIR) 96

5.1. Samples.....96

5.2. Methods.....97

5.3. Results.....97

5.4. Discussion.....98

5.4.1. The characteristic peaks of the sticky rice in FTIR 98

5.4.2. The detection limit of FTIR 106

5.4.3. Shortcomings of FTIR 108

5.5. Conclusions.....110

6. Sequential loss on ignition (LOI) and thermogravimetric analysis -differential

scanning calorimetry-differential thermal analysis (TGA-DSC-DTA) 112

6.1. Samples 112

6.2. Methods 113

6.3. Results 115

6.4. Discussion 118

6.4.1. TGA-DTA-DSC and LOI 118

6.4.2. The detection limit of LOI 123

6.4.3. Shortcomings of LOI 124

6.5. Conclusions 126

7. Thermogravimetric analysis-Fourier transform infrared spectroscopy (TGA-FTIR) and Thermogravimetric analysis- mass spectrometry (TGA-MS) 127

7.1. Samples 127

7.2. Methods 128

7.3. Results and discussion 128

7.3.1. The potential of TGA-FTIR in the identification step 128

7.3.2. The potential of TGA-MS in the identification step 138

7.5. Conclusions 146

8. Matrix assisted laser desorption ionization-time of flight-mass spectrometry (MALDI-TOF-MS) 148

8.1. Samples 148

8.2. Methods 148

8.3. Results and discussion 151

8.3.1. The identification of starch in MALDI-TOF-MS 151

8.3.2. The detection limit of MALDI-TOF-MS 168

8.3.3. Optimisation of the extraction process 177

8.3.4. The influence of cellulose in the earth samples 182

8.3.5. Degradation of starch in earth samples 190

8.5. Conclusions 198

9. Liquid chromatography-tandem mass spectrometry (LC-MS/MS) 200

9.1. Samples 200

9.2. Methods 202

9.2.1. Sample preparation 202

9.2.2. LC-MS/MS Analysis 203

9.3. Results 203

9.4. Discussion 204

9.4.1. The identification of disaccharide in LC-MS/MS 204

9.4.2. The quantitative analysis of sucrose and trehalose in earth samples by LC-MS/MS 214

9.5. Conclusions 220

10. Overview and future recommendations 221

10.1. The deficiencies of the previous analytical methods 221

10.2. The analytical strategy applied in this work 221

10.3. Future work 226

Appendix 1. FTIR spectra of all the archaeological samples 230

Appendix 2. TGA-DTA-DSC results 255

Appendix 3. TGA-FTIR results 259

Appendix 4. TGA-MS results 264

Appendix 5. MALDI-TOF-MS results 284

Appendix 6. LC-MS/MS results 354

Appendix 7. Introduction of archeological sites 360

Sites in Henan Province 360

Sites in Zhejiang Province 364

Sites in Jiangxi Province 373

Sites in Jiangsu Province 374

Sites in Shaanxi Province 375

Sites in Shanxi Province 375

Sites in Guangxi Zhuang autonomous region 376

Sites in Hebei Province 376

Sites in Beijing 377

Appendix 8. The intensity of *m/z* 1013 and 1121 peaks in the MALDI-TOF-MS spectra of the modern earth samples 379

Reference 381

Abbreviations and Acronyms

FTIR - Fourier transform infrared spectroscopy

LC-MS/MS - Liquid chromatography-tandem mass spectrometry

LOI - Loss on ignition

LOD - Limit of detection

LOQ - Limit of quantification

MALDI-TOF-MS - Matrix assisted laser desorption ionization-time of flight-mass spectrometry

Py-GC-MS - Pyrolysis-Gas chromatography-Mass Spectrometry

TGA-DSC-DTA - Thermogravimetric analysis-differential scanning calorimetry-differential thermal analysis

TGA-FTIR - Thermogravimetric analysis-Fourier transform infrared spectroscopy

TGA-MS - Thermogravimetric analysis-mass spectrometry

1. Introduction

Earth, wood, brick and stone were widely used by ancient Chinese peoples as the main construction materials (Liang, 1998; Liang, 2011). China also has a long history of using natural organic materials in ancient sites. The earliest record of using these materials in construction was blood being applied as an additive in the waterproof coating on the ground of palace in Xianyang, Shaanxi province in the Qin dynasty (221-207 BCE) (Xing, 1995).

The organic materials were usually applied as additional materials for particular purposes, such as binding, thickening, waterproofing etc. In “Tiangong Kaiwu” (“天工开物” in Chinese), a technological encyclopaedia written by Yingxing Song (1587-1666 CE) in 1637, sticky rice (the sticky rice powder had been boiled in water. No more details were provided by the author. He used the word "糯米粳". Grains should be contained in the mixture) mixed with earth and lime was a typical material applied in the construction of tombs and artificial pools (Song, 2008). Sticky rice was also mentioned by Shenglong Ma (the Ming dynasty, the year of birth and death is unknown) to be added into earth and lime in city wall building (Ma, 1939).

There are many questions to be answered in this area. For example, the spatial and temporal distributions of these organic materials are unknown, as well as their application in different building types. By analysing these organic materials, we can

learn how these buildings were constructed and attempt to answer these questions. Furthermore, this research may also be of great importance to the conservation and reconstruction of ancient sites.

After conducting a literature review (Chapter 2.3) concerning previous research on the application and analysis of organics in Chinese construction materials, 92.7% of published data before 2016 has been obtained by “spot tests” – that is, an analytical method based on a simple chemical reaction. The spot tests are not sensitive and specific enough to identify organic components reliably. Moreover, blank tests to detect the organics in base materials (such as earth) were absent in these references. Thus, methods with higher sensitivity and specificity, such as chromatography and mass spectrometry, should be applied for the identification.

Thus, my research will be divided into two objectives: 1. developing a new analytical strategy including pretreatment, sample screening (including blank tests), extraction of organics and identification at the molecular level (including blank tests); 2. this new strategy will be applied to archaeological samples to build a more complete map of the use of organics in the construction of ancient sites. My research will focus on the identification of starch and disaccharides. Consequently, the regional and chronological characteristics of organic components used in construction materials in ancient China can be studied.

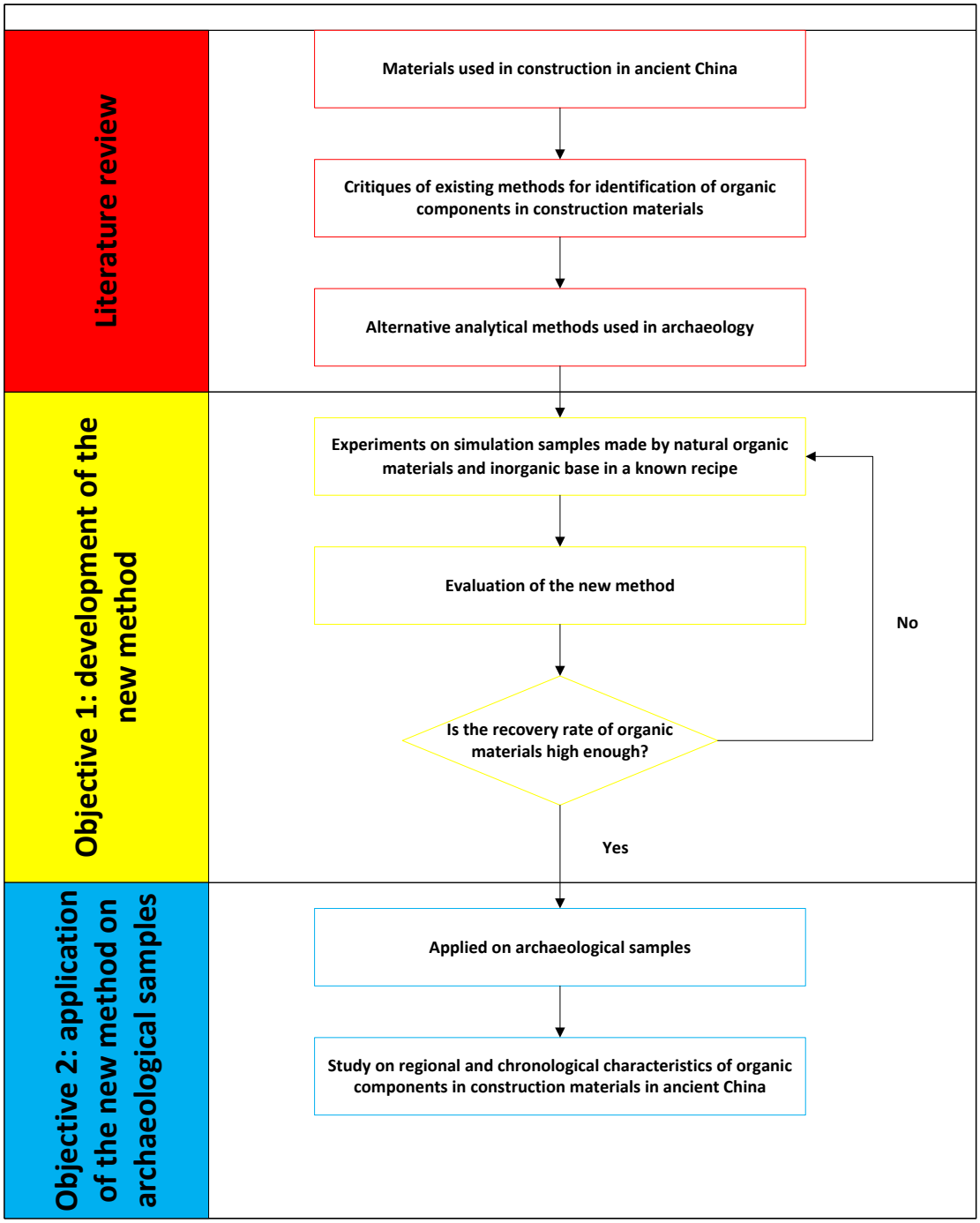


Fig 1-1. Illustration of the research project

8 analytical methods have been used in this thesis for the development of the new method: the iodine-starch test, Fourier transform infrared spectroscopy (FTIR), loss on ignition (LOI), thermogravimetric analysis -differential scanning calorimetry-

differential thermal analysis (TGA-DSC-DTA), thermogravimetric analysis-Fourier transform infrared spectroscopy (TGA-FTIR), thermogravimetric analysis- mass spectrometry (TGA-MS), matrix assisted laser desorption ionization-time of flight-mass spectrometry (MALDI-TOF-MS) and liquid chromatography-tandem mass spectrometry (LC-MS/MS).

2. Background

2.1. Traditional building materials in China

“Five materials would be applied together in construction”, which was mentioned in “the Principles of Constructions” (“营造法式” in Chinese) by Jie Li (1035-1110 CE), showed that earth, wood (including grass and bamboo), brick, stone and tile were widely used by ancient Chinese people for construction (Liang, 1998; Liang, 2011). These materials always contributed to the main parts of ancient sites, such as the foundations and walls.

Earth-based materials have been used in ancient architectures since Neolithic times in 4 types (Hodder, 2006; Hodder, 2012; Khan and Lemmen, 2014; Artioli and Secco, 2016; Artioli et al., 2019):

1. As a coating on the surface of the interior and exterior walls;
2. As materials for the consolidation and smoothing of the floor;
3. As mud bricks;
4. As mortars between stones and bricks.

Besides these 4 types, earth was also directly used in ancient Chinese architecture (the details can be found in Chapters 2.2.2.1-2.2.2.4, pp. 14-24). The occurrence and development of earth buildings are closely linked to the development of human society in ancient China (Zhang et al., 2008). Earth was usually collected from the nearby environment of those sites (Zhang et al., 2008) and mainly applied in the

construction of walls and foundations in the form of rammed earth (Du, 2009). In the north part of ancient China, especially the Loess Plateau region, earth-based materials were mainly based on loess (Artioli et al., 2019). Lime was the most widely used additive in earth-based materials (Yang et al., 2009). The lime plaster, which was made of calcified nodules (extracted from loess and ground up), was usually used on the surface of the ground and walls of the house in ancient sites (Henan Institute of Cultural Relics and Archaeology, 2019; Li, 2016b; Anyang Team of Institute of Archaeology in Chinese Academy of Social Sciences, 1985). The lime mortar was a mixture of loess and lime (Fang et al., 2014), which was used as the binding material between the bricks. While another material, tabia (also known as "Sanhetu"), which has a very similar composition to the lime mortar, was sometimes directly applied as the construction material of the walls and foundations (Liu and Tan, 2016). In addition to earth and lime, sand was applied in tabia in some cases (Luo, 1963; Liang, 2017). Ceramic powder was also mentioned to be used in the construction of a Ming dynasty tomb (tomb occupant is still unknown) in Xindu, Sichuan province (Lai, 1957). However, this claim about the use of ceramic powder relies solely on local anecdotes, and no analytical or archaeological evidence has been provided to support it.

Wood is another important material in Chinese architecture history. It was used to build the frameworks of the architecture, such as pillars and beams (Yang, 2019). In the Liangzhu Bianjiashan site (Zhao, 2012), the Qianshanyang site (Zhejiang Cultural

Relics Management Committee, 1960), the Taosi site (Wang, 2011a), etc., wood remains were found as some parts of the ancient architectures. Other plant materials, such as grass and bamboo, were also widely applied in construction (Institute of Natural Science History of Chinese Academy of Sciences, 2000; Yang, 2010; The Archaeological Team of Chengdu City and The Pixian Museum, 2001; Yang, 2016).

Stone has been used as a construction material for more than 4000 years in China in Shandong, Sichuan, Liaoning, Shanxi, Inner Mongolia and Gansu provinces, (Shandong Institute of Cultural Relics and Archaeology and Cultural Relics Research Office of Liaocheng Cultural Bureau, 1997; Liang and Jia, 2017; Shandong Archaeology Team of Chinese Academy of Social Sciences et al., 2015; Chengdu Cultural Relics and Archaeology Team, 2002). However, the stone was applied together with earth in all above sites. Bricks and tiles were widely found to be used in the Zhouyuan site of the Western Zhou Dynasty (1046-771 BCE) in Fufeng, Baoji, Shaanxi province (Liu, 1993; Zhang et al., 2006). Although some archaeologists (Liu, 2006; Zhan et al., 2006) have claimed that the manufacture of bricks and tiles may be much earlier, more evidence is still needed (Cao and Cao, 2016).

Many natural organic materials were also applied in building materials to create an organic-inorganic construction system. In “Tiangong Kaiwu”, a famous work in the Ming dynasty (1637 CE) recording ancient techniques, sticky rice (which had been boiled in water), as well as Tung oil (extracted from the seeds of *Vernicia fordii*) and

juice of *Actinidia chinensis*, was widely applied in construction (Song, 2008). The addition of these natural organic materials is believed to make the structure “lightly and solidly, never to be destroyed” (“轻筑坚固，永不隳坏” in classical Chinese (Song, 2008)). The application of sticky rice can also be found in other ancient documentary sources (Ma, 1939). Blood was mentioned to be applied in the construction of the palace for waterproofing in Xianyang, Shaanxi province in the Qin dynasty (221-207 BCE) (Xing, 1995).

2.2. Construction of earthen sites in China

2.2.1. The history of ancient earthen sites in China

Earthen sites are archaeological sites in which significant structural components are made of earthen materials. The earthen site has a long history in China. Around 80% of the ancient sites are earthen sites (Wang, 2009). The earthen sites can be divided into ancient cities, tombs, palaces, workshops, temples, and other civil or military facilities according to their functions (Tian, 2004). The distribution of some earthen sites is shown in Fig 2-1.

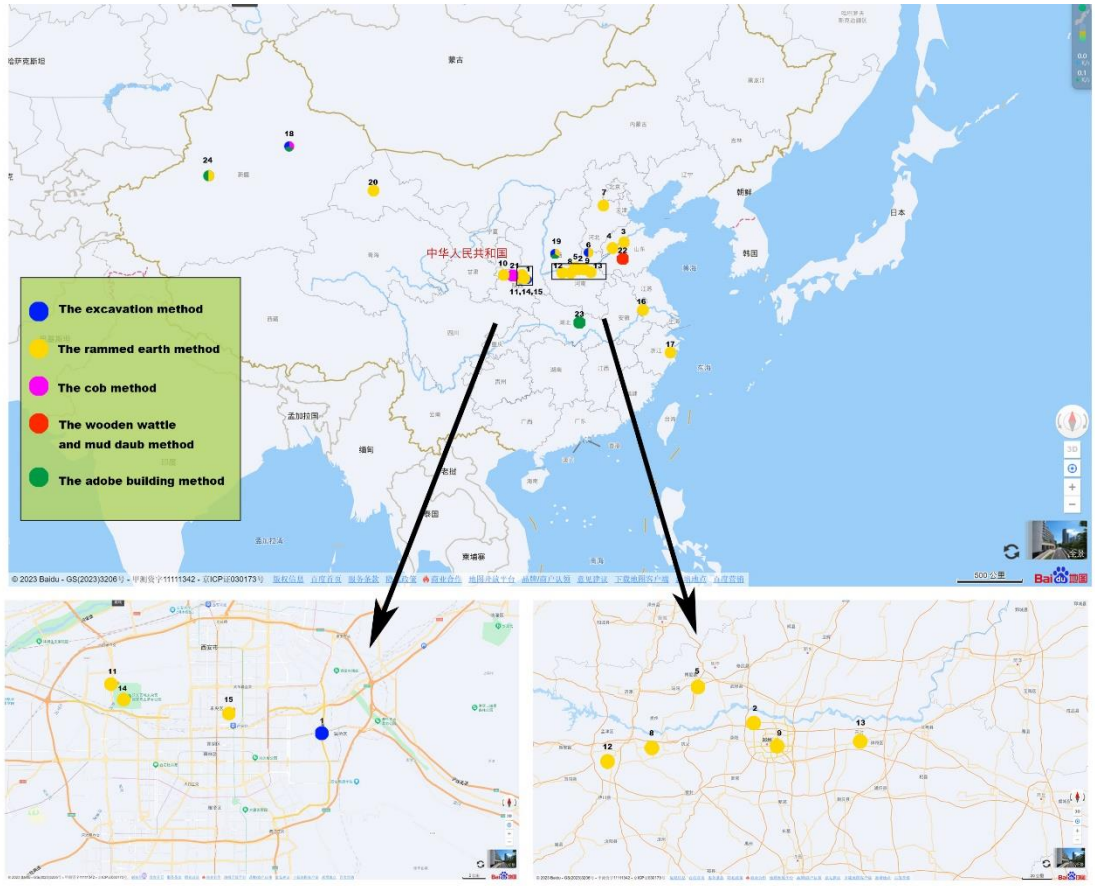


Fig 2-1. The distribution of earthen sites mentioned in Chapter 2.2 and their building techniques (the description of all the building techniques can be found in Chapter 2.2.2, region around Xi'an and Zhengzhou are enlarged): 1. The Banpo site; 2. The Xishan city; 3. The Chengziya site; 4. The Jiaochangpu site; 5. The Xijincheng site; 6. The Yinxu site; 7. The Yan Xiadu site; 8. The Yanshi Shangcheng site; 9. The Zhengzhou Shangcheng site; 10. The Qin Yongcheng site; 11. The Zhichengmen city gate of the Chang'an city site; 12. The Luoyang city walls constructed during the Sui and Tang dynasties; 13. The exterior city walls of the Dongjing city constructed during the Northern Song dynasty; 14. The Weiyang palace in the Western Han Chang'an city site; 15. The Daming palace in the Tang Chang'an city site; 16. The Nanjing city walls constructed during the Ming dynasty; 17. The Taizhou city walls

constructed during the Ming and Qing dynasties; 18. The Jiaohe ancient city site; 19. The Taosi site; 20. The Suoyang city site; 21. The Western Zhou site in Fengchu village; 22. The Yinjia city site; 23. The Menbanwan site; 24. The Tonggusibaxi ancient city site

The underground caves, semi-underground caves and houses in the Banpo site constructed around 6000 years ago are the earliest earthen sites found in China (Yan, 2016). During the prehistory period of China, earthen houses, as well as other small earthen architectures such as tombs, could be widely found in ancient sites (Liu, 1965; Han, 1976; Jiang, 1983; Peng et al., 2004). The construction of earthen city walls started in the middle of the Neolithic Period (Li, 2016a). The earliest earthen city wall found in central China is the Xishan city (3300-2800 BCE) in Zhengzhou, Henan province, belonging to the Yangshao culture (Qian, 1999). Earthen city walls can also be found in the Longshan culture, for example, the Chengziya site (An, 1992; Shandong Institute of Cultural Relics and Archaeology and School of Archaeology Culture and Museum of Peking University, 2019), the Jiaochangpu site (Shandong Archaeology Team of Chinese Academy of Social Sciences et al., 2005), the Xijincheng site (Wang and Wang, 2010) etc. According to incomplete statistics, around 50 Neolithic Period ancient cities, all of which were based on earthen city walls, were found in China from 1949 to 1996, covering a large area of the middle and lower reaches of the Yellow River, the middle reaches of the Yangtze River, Sichuan Basin and Inner Mongolia (Zhang and Yin, 1997). Other large earthen

buildings, such as mounds (Du, 2019) and palaces (Zhao and Xu, 2020), can also be found in sites in the same period.

When the time came to the Shang dynasty (1600-1046 BCE) and the Zhou dynasty (1046-256 BCE), earthen architectures with different functions started to be present in cities in an organized way (Liu, 2003). The Yanshi Shangcheng site (Duan et al., 1984), the Zhengzhou Shangcheng site (Henan Museum and Zhengzhou Museum, 1977), the Yinxu site (Liu, 1980), the Yan Xiadu site (Huang, 1962), the Qin Yongcheng site (Xu and Sun, 1963) are typical earthen sites during this period. Earthen city walls, palaces, houses, workshops, tombs and ancestral temples can be found in these sites. In "Kaogongji" ("考工记" in Chinese), a technological encyclopedia written in the Chunqiu (770-476 BCE) and the Warring States Periods (475-221 BCE), some statements about city planning were given. For example, the construction of the capital city was recorded as: "The construction of the capital city should be a square shape with a side length of 9 li (distance unit, 300 paces), and each side has three gates" ("匠人营国，方九里，旁三门" in classical Chinese) (Ji, 2001); "There are 9 north-south and 9 east-west avenues in the capital city. Each north-south avenue accommodates 9 parallel lanes for carriages. The ancestral temple is located to the left of the royal palace, the altar of state to the right, the imperial court to the front and the market to the back. The market and court are square shapes with a side length of 100 paces" ("国中九经九纬，经途九轨，左祖右社，面朝后市，市朝一夫" in classical Chinese) (Ji, 2001).

From the Qin dynasty (221-207 BCE) to the Song dynasty (960-1279 CE), wooden frame structures gradually took the place of earthen-wooden mixed frame structures in the construction of many palaces and large houses (Fu, 2009). However, earth was still applied in the construction of different building types (Li, 2011). In this period, city walls were always constructed using rammed earth, for example, the Zhichengmen city gate of the Chang'an city site constructed during the Western Han dynasty (202 BCE-8 CE) (Zhang et al., 2009), the Luoyang city walls constructed during the Sui and Tang dynasties (581-907 CE) (Chen, 1961), the exterior city walls of the Dongjing city constructed during the Northern Song dynasty (960-1127 CE) (Qiu and Sun, 1992) etc. Wood and bricks were also applied as the frameworks and coatings in the construction of earthen city walls (Fu, 2009). In the construction of palaces and other large buildings, earthen structures were mainly applied to form a solid foundation, for example, the Weiyang palace in the Western Han Chang'an city site (Liu et al., 1993) and the Daming palace in the Tang Chang'an city site (Ma, 1961; Ma, 1987). Earthen walls could also be found in some palaces, especially before the Tang dynasty (618-907 CE) (Fu, 2009). Construction techniques of all types of architectures before and during the Northern Song dynasty were recorded in "the Principles of Constructions" ("营造法式" in Chinese) by Jie Li (1035-1110 CE). The height, shape and size of buildings (mainly living places and tombs) for the Emperor, nobleman and commoner were severely restricted. Any deviation from the prescribed size would be regarded as a crime (Yang, 1981).

Bricks and stone started to be applied widely in the construction of the architectures on the ground from the Yuan dynasty (1271-1368 CE), which might be related to the change of the ruler's architectural concept, the inflow of foreign religion and craftsmen, fire prevention, defence and other practical purposes (Pan, 2009). Since then, most city walls consisted of a core of earth and stone blocks, which were strengthened by some binding materials and later faced with bricks (Jiang, 2013); for example, the Nanjing city walls constructed during the Ming dynasty (1368-1644 CE) (Wu, 2005), the Taizhou city walls constructed during the Ming and Qing dynasties (1368-1912 CE) (Guo, 2013) etc. From the Yuan dynasties to the Qing dynasties (1271-1912 CE), earth was mainly applied as: 1. supporting materials, such as the core materials of the city walls; 2. binding materials, such as the lime mortar; 3. the raw materials of the bricks and tiles (Pan, 2009). Architectures using earth as the main material could still be found in some parts of China. A series of military forts with gun emplacements were constructed in the Qing dynasty along the coastal line. The building material of these forts was tabia ("Sanhetu") (Li et al., 2008; Zhang et al., 2012; Huang, 2017). Earth was also applied in civil buildings. For example, Tulou ("土楼" in Chinese), a house which is mainly made of earth, was a building type widely distributed in Fujian province (Cai, 1995).

2.2.2. The construction of ancient earthen sites in China

There are 5 main techniques in the construction of ancient earthen sites in China: the excavation method, the rammed earth method, the cob method, the wooden wattle and mud daub method and the adobe building method (Zhang et al., 2008). Different techniques were used together on the same sites. For example, the excavated, cob and adobe building methods were applied together in the construction of Jiaohe ancient city (around 2000 years ago) in Turpan, Xinjiang Uygur Autonomous Region (Shao, 2007; Zhang et al., 2008). The excavated, rammed earth and wooden wattle and mud daub methods were applied in the Taosi site (around 2000 BCE) in Linfen, Shanxi province (Wang, 2011b).

Table 2-1. Construction techniques and their example

Construction technique	Chinese name	Date from	Example
The excavation method	挖余法	Around 6000 years ago	Jiaohe ancient city, Turpan, Xinjiang (Shao, 2007)
The rammed earth method	夯土法	Around 5000 years ago	Suoyang city, Guazhou, Gansu province (Li, 1999)
The cob method	垛泥法	Around 3000 years ago	Fengchu village, Qishan, Shaanxi province (Zhang et al., 2008)

The wooden wattle and mud daub method	木骨泥墙法	Around 6000 years ago	Yinjia city, Sishui, Shandong province (Cui, 1994)
The adobe building method	土坯砌筑法	Around 5000 years ago	Jiaohe ancient city, Turpan, Xinjiang (Zhang et al., 2008)

2.2.2.1. The excavation method

The excavation method is a construction technique largely based on the original topography. It excavates natural materials (mainly soil) either from the vertical earth wall of the mountain or constructed ramp or directly into the ground for extra space. The most widely found ancient earthen building type is the cave. This construction technique was mainly applied in the Loess Plateau and the northwest region (Zhang et al., 2008).

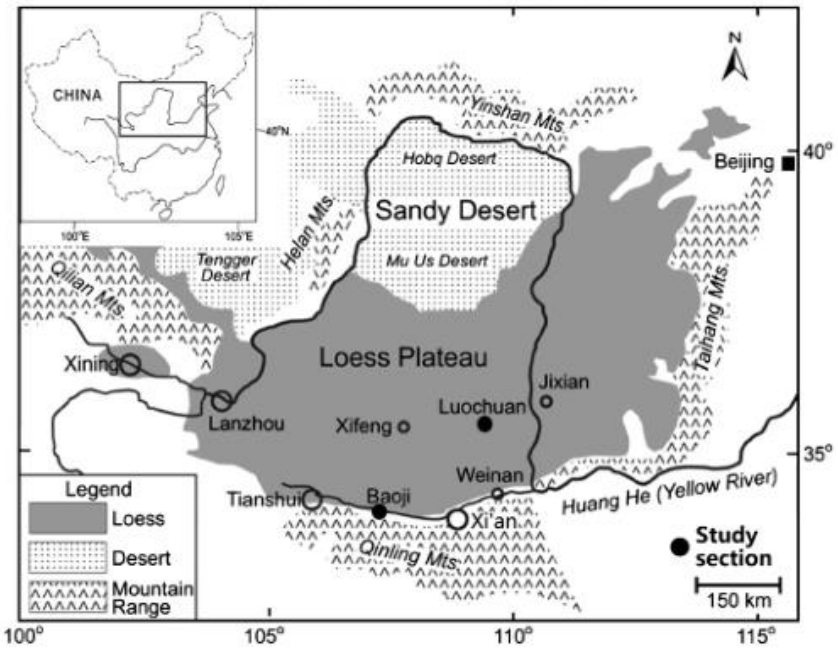


Fig 2-2. A map of the extent of the Loess Plateau (Wang et al., 2013)

In the Taosi site, Xiangfen, Shanxi province, two kinds of earthen buildings constructed by the excavation method were found: loess cave dwelling and semi-underground cave (Wang, 2011b). The cave dwelling was excavated from the side of the mountain. In some cave dwellings, a hole for the central wooden pillar could be found. The pillar might be used to hold the top of the earthen cave. Gateways with steps and slopes could also be found inside some cave dwellings. The living area of the cave dwelling is generally round and about 3 metres in diameter (Gao and Li, 1986). The plaster could sometimes be found on these walls. The semi-underground cave, which is partly dug into the ground with the upper parts and roof constructed above, is the most widely found house type in the Taosi site. The living area ranging from 7 to 22 square metres is usually square with round corners and is oval in only 1

case. Plaster could also be found on the internal walls of semi-underground caves. In some cases, the plasters were mixed with grass and mud (Xie, 2007).

Jiaohe ancient city, Turpan, Xinjiang was another site constructed through the excavation method. The layout of the whole city had been planned on the ground before the construction process. Then the earth was dug out from the surrounding area to form the city walls (Zhang et al., 2008). Most buildings inside the ancient city including streets, houses, courtyards and caves were also constructed by the excavation method (Shao, 2007).

The caves on the Loess Plateau are also typical earthen buildings constructed by the excavation method. For example, the Diyin courtyard, a kind of traditional earthen building in Shanxi, Shaanxi and Henan provinces, was constructed by ancient people (Du, 2009). The first record of the Diyin courtyard could be dated back to 1139 CE. The ancient people dug out an underground space 30 to 40 metres long, 40 metres wide and 10 metres deep. This square area would serve as an open-air yard; then the caves were cut into the vertical walls as living space. Figure 2-3 shows the profile of a Diyin courtyard.

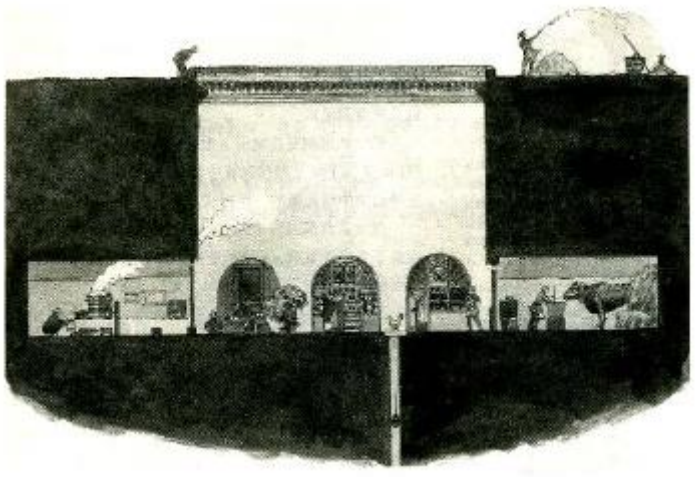


Fig 2-3. The profile of a Diyin courtyard (Du, 2009)

The construction process of the excavation method implies that the majority of the remaining parts of the earth into which the structure is excavated are kept in the original state. Thus, organic binding materials are most likely found in applied plaster layers.

2.2.2.2. The rammed earth method

The rammed earth method was applied using ramming tools to make the earth compact and firm through external force. It is one of the most widely used earthen architecture construction methods in ancient China (Zhang et al., 2008). In some cases, organic binding materials were applied to consolidate the rammed earth (Song, 2008). For example, the sticky rice is added into the earth to make tabia ("sanhetu"). It will be applied in all parts of a building, or some significant parts of a building.

In some rammed earthen sites, mainly large city walls, a ditch was excavated before the city walls were constructed. Other sites, mainly city foundations and some city walls, were directly constructed on the levelled ground (Zhang et al., 2008). The ditch is generally 2 metres deep but sometimes can be 5 metres deep (Zhang and Yin, 1997). Its width is the same as or close to the width of the city wall, and in some cases smaller. Earth was then filled into the ditch and compacted in layers to give a solid foundation beneath the wall. The process started from the bottom of the ditch and ended with the completion of the whole city wall. Generally, the external and internal surfaces of the city wall formed a slope, making its profile an isosceles trapezoid. The profile of a city wall described in "the Principles of Constructions" ("营造法式" in Chinese) by Jie Li (1035-1110 CE) (Li, 2011) in the Song dynasty is shown in Figure 2-4. The standard height of the city wall is 12.4 metres. The width of the top is 12.4 metres and that of the bottom is 18.6 metres. X (can either be a positive or negative number) is the adjustment of height made to the standard size. The width should also be adjusted by the principle shown in Figure 2-4.

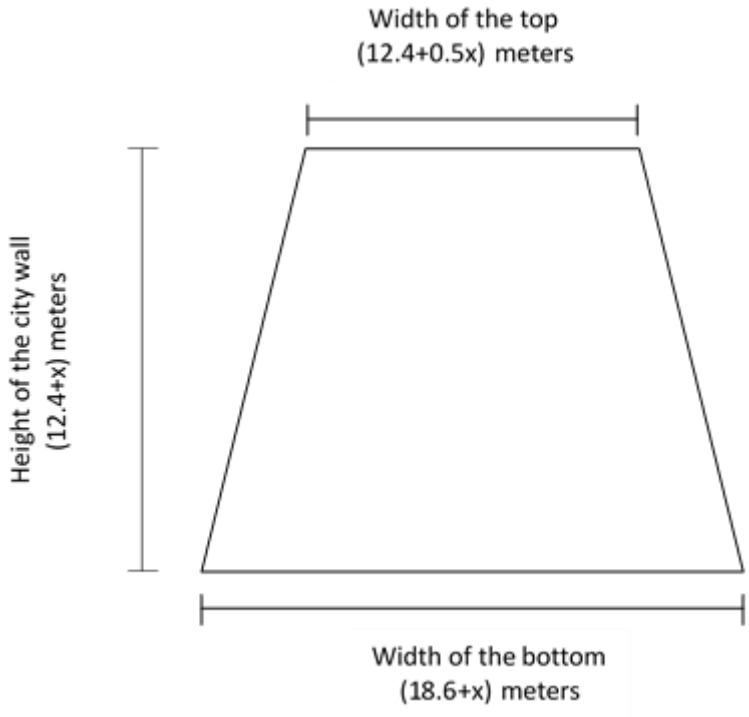


Fig 2-4. The profile of the main body of city wall (1:400), x = 10

Before the construction process of the main body of earthen city walls, either with or without a ditch, a wooden framework was built with wooden pillars and boards. Then the earth was filled into the framework and rammed by a wooden (sometimes iron or stone) ramming pestle (Li, 2015). Sometimes water was also added to shape the earth. When the earth filled up the wooden framework, another framework was built on the top or the side of the first one and the process was repeated. Previous frameworks were removed after the new framework was filled up (Zhang et al., 2008). A diagram that illustrates the construction process, Figure 2-5, is shown below. This rammed-in-frameworks earth ("版筑夯土" in Chinese) technique was found first applied in the construction of Xishan city (3300-2800 BCE) in Zhengzhou, Henan Province. The frameworks applied were around 1.5-3.5 metres in length, 1.1-1.5 metres in width and

0.3-0.6 metres in height (Qian, 1999). In other earthen city walls, especially most of those built in the Neolithic Age (Zhang and Yin, 1997), the rammed-in-frameworks earth technique was not applied - the earth was directly piled and rammed on the top of the ditch or the ground in layers. For example, the ancient city of the Longshan Culture in the Chengziya site, Jinan, Shandong province, was first constructed around 4560 years ago. Then the city wall was re-constructed several times over 1000 years by piling and ramming earth on the top of previous buildings (Cui, 1994).

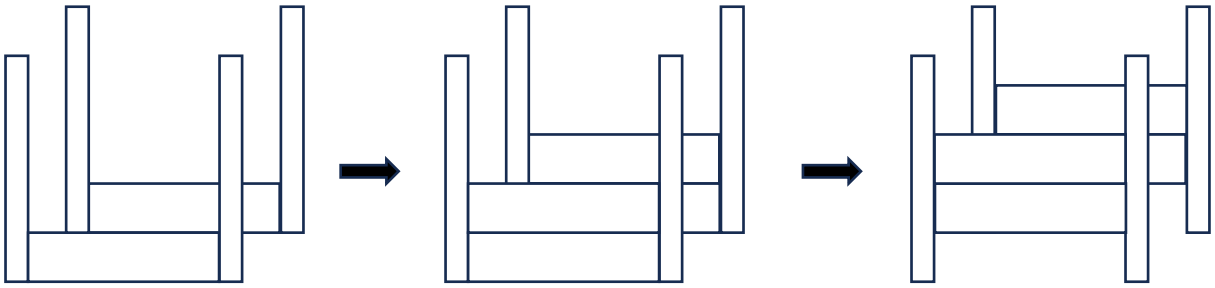


Fig 2-5. The construction process of rammed-in-frameworks earth technique

Besides city walls and large buildings, the rammed earth method was also applied in the construction of some houses. Tulou ("土楼" in Chinese), a kind of round or square earthen building widely found in the Fujian area since the Ming dynasty (Xie, 2004), was constructed by the rammed earth method. Before the construction of a Tulou, its shape and structure were planned on the ground. A pit was excavated according to the

plan. If the height of Tulou is below 3 floors, the pit should be 0.3-0.6 metres deep (Xie, 2004). The pit was then filled with stones, gravel and cobblestones. After that, the earth was added and rammed to form the foundation. The earth applied in the construction of Tulou was a mixture of earth, lime, sand, sticky rice, sugar and egg white (Cai, 1995). In Tulou near the river, the lime mortar was also added. The rammed-in-frameworks earth technique was applied to construct walls (Zhang et al., 2008). The frameworks applied were around 1.5-2 metres in length and 0.4 metres in height. Bamboo and wood were also applied inside the earthen wall for reinforcement (Xie, 2004).

2.2.2.3. The cob method

The cob method is a construction technique of stacking lime mud mixed with sand, straw and water to build walls. It is widely applied in Kashgar, Kuqa and Taxkorgan areas in Xinjiang (Pei et al., 2019).

The earliest cob earthen building in China is found in a quadrangle site constructed in the early Western Zhou dynasty in Fengchu village, Qishan, Shaanxi province (Zhang et al., 2008). A mixture of mud and grass was stacked on the ground in layers and before the construction of each layer, the last layer had to be dried naturally and compressed. The remaining walls in the site were around 0.21 metres in thickness and the lime mortar plasters on both sides of the walls were around 2-2.5 centimetres in

thickness (Fu, 1981).

The cob method was also applied in Jiaohe ancient city. All the cob earthen walls in the site were constructed in layers of around 0.5-0.9 metres in thickness. Each layer consists of mud stacks of 0.45-0.6 metres in length, and there is no obvious trace of conscious connections between two adjacent stacks in the same layer. After the construction of the walls, mud plasters of around 5 centimetres were applied on the surface (Sun, 2006). The vertical sections to show the structure of stacks and the profile of cob earthen walls are shown in Figures 2-6 and 2-7.

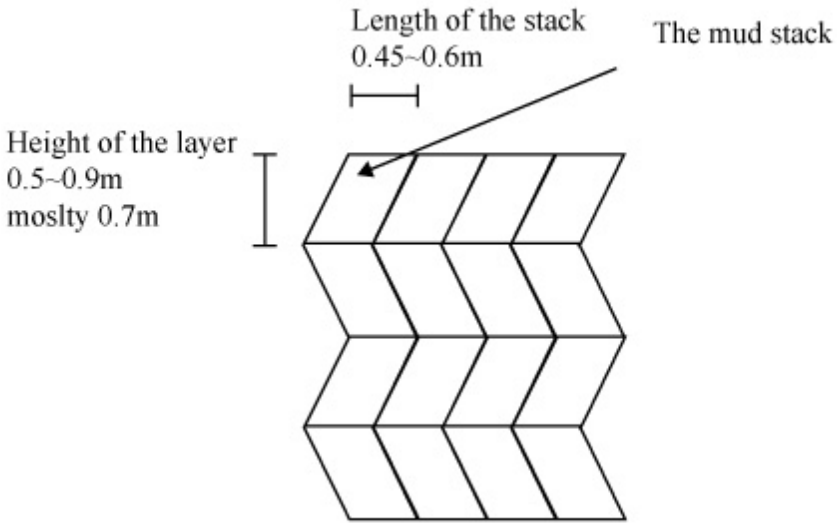


Fig 2-6. The structure of stacks on the surface of cob earthen walls (1:62.5)

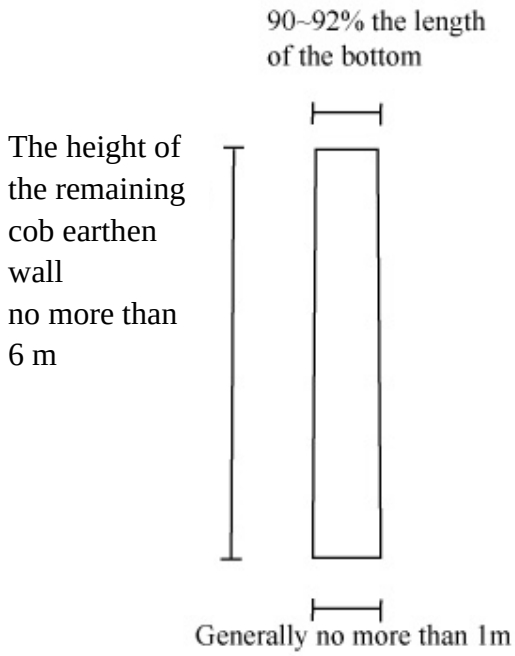


Fig 2-7. The profile of cob earthen walls (1:100)

2.2.2.4. The wooden wattle and mud daub method

The wall made of the wooden wattle and mud daub (“木骨泥墙” in Chinese) method is another earthen building type. It was applied in more than 10 houses in Yinjia city (around 4000 years ago), Sishui, Shandong province (Cui, 1994). A row of wooden pillars was set in a pre-constructed ditch which is 0.3-0.6 metres in depth. The woven grass was applied to connect the pillars into a network. Then the wooden framework was daubed with mud mixed with grass on both the external and internal sides. Sometimes the mud was heated after being applied to the walls. In one square house named F129 which is 27.5 square metres in area, 48 pillars were applied (Cui, 1994).

This type of earthen wall has a low load-bearing capacity and cannot be used as a load-bearing wall. Thus, it is not widely applied in ancient earthen buildings in China (Zhang et al., 2008).

In addition, the application of the cob method and the wooden wattle and mud daub method could be found in the construction of sculptures and wall paintings, especially in grottoes and temples. In the construction of Buddhist statues in Mogao Grottoes, a wooden frame wrapped with local grass and reed would be made before the coarse mud (a mixture of earth and wheat straw) was applied to acquire an approximate shape. Then the fine mud (a mixture of earth and sand, with fibre or cotton) would be used to make the surface of the statue. After that, colours would be applied on the surface of the statue as the final step (Cai, 2005). Yungang Grottoes used a similar technique in the construction of Buddhist statues. Some statues in Yungang Grottoes were based on the wooden or tile framework, while others were based on the stone body of the statues remains (Qin, 2010).

2.2.2.5. The adobe building method

The adobe is an important construction material based on earth and additional materials such as straw or dung. Raw materials are mixed and shaped in the mould and then sun-dried to form the adobe. Then the adobe bricks are used to build the architectures. In different regions, there are different techniques of adobe production

due to the local custom and earth composition. 3 main adobe types which were widely applied in ancient China are (i) the handmade adobe (“手模坯” in Chinese), (ii) the rammed adobe (“杵打坯” in Chinese) and (iii) the wet processed adobe (“水制坯” in Chinese) (Zhang et al., 2008). In the production process of the handmade adobe, the mould was filled with the earth and then the adobe surface was smoothed by hand. While in the production of the rammed adobe, the earth was rammed by the stone pestle in the mould to improve its strength. The production of the wet processed adobe is quite different. The earth was added to water until it came to the right consistency before the adobe production. After the earth turned to a plastic state, adobe bricks were cut and naturally dried.

The adobe building method was applied in a house in the western part of an ancient city belonging to the Qujialing Culture in the Menbanwan site (around 5000 years ago), Yingcheng, Hubei province. The house covers an area of 115.5 square metres, and the remaining walls are between 1.5 and 2.2 metres in height (Li, 2000). After the house was abandoned, it was buried in the west part of the ancient city, and thus, the house had been preserved well when it was found. The adobe bricks applied in the construction are around 35-44 centimetres in length, 17-25 centimetres in width and 5-7 centimetres in thickness. The earthen walls made of adobe bricks are generally 0.4-0.5 metres and no more than 0.6 metres in thickness (Li, 2000). Yellow and white plaster containing rice straw and husk was found on the internal and external surfaces of the adobe walls.

Adobe bricks were also used in Tonggusibaxi ancient city (the Tang dynasty), Aksu, Xinjiang. The city walls in the site were constructed with rammed earth and adobe building techniques. The remaining city walls are around 6.5 metres in height and 3 metres in thickness. Two sizes of adobe were used: 45 centimetres in length, 24 centimetres in width, 10 centimetres in thickness and 35 centimetres in length, 10 centimetres in width, 7 centimetres in thickness (Xu, 2014).

Instead of being made into adobe bricks, the raw earth was cut into blocks and directly applied in earth architecture construction in some dry regions. This kind of earth bulk has high requirements on the strength of the earth and could not be applied for the construction of load-bearing walls. Thus, it was seldom applied in earthen constructions in ancient China (Zhang et al., 2008).

2.3. The organic materials used in ancient sites in China

After a review of the recent works studying Chinese earthen building materials, a total of 47 articles published between 1934-2022 mention the use of natural organic materials in the construction of archaeological sites in ancient China. Amongst these articles, 23 use documentary evidence, for example, annals of local history, folklore, techniques still applied, or cited from other articles, to support their conclusions. 24 articles tried to use analytical data to draw their conclusions. Although none of these

articles mentioned blank tests on raw earth (which may be related to the difficulty of distinguishing the raw materials used in the site), their results still need to be discussed in this chapter since they show some possible examples of organics application. 218 cases from 142 sites are mentioned in these 47 articles (the term "case" is used to count the number of different organic materials used: for example, if 10 samples have been collected from a site, of which 2 are said to contain sticky rice, 6 to contain blood and all of them contain sugar, then there are 3 cases from this site).

Table 2-2. References mentioning the application of organic materials in construction in ancient China, the number of sites and case number involved in each reference and type of evidence they used to prove the existence of organics

Reference	Site number mentioned in the article	Case number	Comment (blank tests missing in all analytical data)
(Zhang et al., 2015)	1	1(the same with that in (Zhang, 2014))	Coomassie brilliant blue method & enzyme-linked immunosorbent assay
(Li et al., 2012)	4	4(1 is the same with that in (Wu, 2005))	I_2-starch test & FTIR
(Liu et al., 2016a)	4	4	FTIR
(Xing, 1995)	1	1	Documentary evidence used
(Liu, 1934)	1	2	Documentary evidence used
(Zhou et al., 2010)	1	2(1 is the same with that in (Zhou, 2009))	I_2-starch test, haemochromogen crystal test & elemental analysis
(Zeng et al., 2010)	1	1	Micro FTIR & energy dispersive X-ray spectroscopy
(Zhou, 2009)	5	7(1 is the same with that in (Zhou et al., 2010), 2 are the same with those in (Wang et al., 2012))	Haemochromogen crystal test & I_2-starch test

(Zhang, 2014)	17	33(1 is the same with that in (Zhang et al., 2015), 18 are the same with those in (Li and Zhang, 2019))	Phenolphthalin, Coomassie brilliant blue method, NaOH-H_2O_2 test, I_2-starch test, Benedict's solution & enzyme-linked immunosorbent assay
(Yang et al., 2008)	1	1	I_2-starch test & FTIR
(Zeng et al., 2007)	1	1	FTIR
(Miao et al., 1981)	1	4	I_2-starch test, FTIR & scanning electron microscopy
(Rocco Mazzeo et al., 2005)	1	3	Pyrolysis–gas chromatography –mass spectrometry & microscopy
(Bonaduce et al., 2008)	1	1(the same with that in (Hu et al., 2015))	Gas chromatography –mass spectrometry
(Hu et al., 2015)	1	1(the same with that in (Bonaduce et al., 2008))	Immunofluorescence microscopy
(Fu, 2010)	1	3	Documentary evidence used
(Li, 1996)	1	1	Documentary evidence used
(Luo, 1960)	1	1	Documentary evidence used
(De'an Museum, 1994)	1	1	Documentary evidence used
(Shen et al., 2006)	1	2	Documentary evidence used
(Ai, 1999)	1	2	Documentary evidence used
(Cheng, 2007)	1	1	Documentary evidence used
(Wu, 2005)	1	3(1 is the same with that in (Li et al., 2012))	Documentary evidence used
(He, 1999)	1	1	Documentary evidence used
(Xie, 2009)	1	3	Documentary evidence used
(Zheng, 2000)	1	1	Documentary evidence used
(Chen, 2000)	1	1	Documentary evidence used
(Peng, 1995)	1	1	Documentary evidence used
(Wang et al., 2012)	1	2(2 are the same with those in (Zhou, 2009))	I_2-starch test, haemochromogen crystal test & elemental analysis
(Cai, 2001)	1	1	Documentary evidence used
(Wang, 2001)	1	1	Documentary evidence used
(Wei, 2009)	1	2	Documentary evidence used
(Yu and Chen, 2004)	1	1	Documentary evidence used
(Zhao, 2007)	1	1	Documentary evidence used

(Li and Deng, 2005)	1	1	Documentary evidence used
(Cai, 1995)	1	2	Documentary evidence used
(Li and Zhang, 2019)	96	129(18 are the same with those in (Zhang, 2014))	Phenolphthalin, Coomassie brilliant blue method, I_2-starch test & Benedict's solution
(Liu et al., 2016b)	6	6(2 are the same with those in (Li and Zhang, 2019) and (Li, 2019), 1 is the same with that in (Wu, 2005), 2 are the same with those in (Zhang, 2014), 1 is the same with that in (Zhang, 2014), (Li and Zhang, 2019), (Li, 2019) and (Shan et al., 2022))	I_2-starch test, FTIR & scanning electron microscopy
(Zheng et al., 2016)	7	7(2 are the same with those in (Zhang et al., 2020b))	I_2-starch test
(Zhang et al., 2020b)	3	3(2 are the same with those in (Zheng et al., 2016))	I_2-starch test
(Shan et al., 2022)	2	2(1 is the same with that in (Zhang, 2014), (Li and Zhang, 2019), (Li, 2019) and (Liu et al., 2016b))	I_2-starch test, FTIR & scanning electron microscopy
(Zhou, 2016)	1	2(2 are the same with those in (Li and Zhang, 2019) and (Li, 2019))	Coomassie brilliant blue method, FTIR & scanning electron microscopy
(Zhang et al., 2020a)	2	3	FTIR & scanning electron microscopy
(Liu et al., 2016c)	1	1	FTIR
(Li, 2019)	96	129(all data is from (Li and Zhang, 2019))	Documentary evidence used
(Zheng et al., 2014)	1	1	FTIR & scanning electron microscopy
(Wei et al., 2013)	4	4(2 are the same with those in (Li and Zhang, 2019) and (Li, 2019))	FTIR & scanning electron microscopy

Many chemical reactions can be used to detect organic materials in samples by the colour change of solution or precipitate production. Analysis methods based on these

“spot tests” are widely reported in the literature cited here. More sophisticated analytical methods are also used to analyse different natural organic materials in ancient sites in China. Methods using different experimental instruments are mentioned in the literature (Table 2-2).

2.3.1. Starch (sticky rice and flour)

In “Tiangong Kaiwu”, sticky rice (rice is boiled in water until the grains disintegrate, the soup with the rice grains is applied) mixed with earth and lime was a typical material applied in the construction of tombs and artificial pools (Song, 2008). The sticky rice was also mentioned by Shenglong Ma (the Ming dynasty, the year of birth and death is unknown) to be added into earth and lime in city wall building (Ma, 1939). The application of sticky rice and flour in ancient sites has also been mentioned in many articles based on documentary evidence (Fu, 2010; Li, 1996; Luo, 1960; De'an Museum, 1994; Shen et al., 2006; Ai, 1999; Cheng, 2007; Wu, 2005; He, 1999; Xie, 2009; Zheng, 2000; Chen, 2000; Peng, 1995; Cai, 2001; Wang, 2001; Wei, 2009; Yu and Chen, 2004; Zhao, 2007; Li and Deng, 2005; Cai, 1995; Liu, 1934; Ma, 1939; Li, 2019). Sticky rice, as well as flour, has also been claimed to be found in construction materials by the identification of starch using analytical methods (Li et al., 2012; Liu et al., 2016a; Yang et al., 2008; Zeng et al., 2007; Zhou et al., 2010;

Zhou, 2009; Wang et al., 2012; Liu et al., 2016b; Zheng et al., 2016; Zhang et al., 2020a; Shan et al., 2022; Zhou, 2016; Zhang et al., 2020b; Liu et al., 2016c; Zheng et al., 2014; Wei et al., 2013). Starch has been identified by the spot test and other analytical methods in construction materials taken from ancient Chinese sites (Zhang, 2014; Miao et al., 1981). In total, there are 84 cases of using starch, sticky rice or flour. Amongst them, 59 (including 51 starch, 5 sticky rice (based on assumptions: these tests can only detect starch and lack blank tests) and 3 flour (similarly identified)) are based on analytical data. So far, no rice grains have been found microscopically in building materials in ancient China, since reviewed references (Liu et al., 2016b; Shan et al., 2022; Zhou, 2016; Zhang et al., 2020a; Zheng et al., 2014; Wei et al., 2013) focus on the structure transformation of limestone.

The iodine-starch test is a method used to detect the presence of starch (Jeffery et al., 1989). When a starch-containing sample is treated with an iodine solution, it undergoes a color change to blue or purple, indicating the formation of a polyiodide starch complex. Zhang (2014) and Miao et al. (1981) used this method to identify starch. The iodine-starch test is also used to prove the existence of flour (the term "flour" used in the literature cited here is just a generic term for ground grain) (Zhou et al., 2010; Zhou, 2009; Wang et al., 2012) and sticky rice (Li et al., 2012; Yang et al., 2008). The iodine-starch test cannot show the origin of the starch in these samples. However, this test has been used to prove the existence of flour and sticky rice, which is impossible. Experiments with higher specificity (chromatography and mass

spectrometry) should be carried out to support their conclusions. Additionally, the soil particles may influence the colour change of iodine-starch test, which means that this method is not suitable for neither soil nor tabia samples (Zhang, 2014).

FTIR (Fourier transform infrared spectroscopy) is a technique used to obtain an infrared absorption spectrum of the material. Molecules will absorb frequencies that are characteristic of their structure. Thus, compounds can be identified by their characteristic peaks in an infrared spectrum. By using FTIR, starch was found in ancient samples (Li et al., 2012; Liu et al., 2016a; Yang et al., 2008; Zeng et al., 2007; Miao et al., 1981). The problem is that FTIR cannot identify specific components—it simply identifies the presence of specific functional groups. Samples from ancient sites are always mixed with soil and other substances, and FTIR cannot achieve a good result in such a complex organic-inorganic mixture. The absorbance peaks of other substances, for example, quartz, which is quite normal in earth samples, may cover the peaks for starch (Zhang, 2014), and in most cases, the concentration of starch may be too low to give clear absorbance peaks.

SEM (scanning electron microscopy), a type of electron microscope that produces images of a sample by scanning it with a focused beam of electrons, can be used to observe the microstructure of samples. Miao et al. (1981) used SEM to show the existence of starch in pagodas of the Shaolin temple (1121-1561 CE) in Zhengzhou, Henan and portrait brick in the Dengxian tomb (the Northern and Southern Dynasties,

420-589 CE) in Nanyang, Henan. However, there is an absence of detailed information given in this reference. Zheng and Wang (2013) used SEM to find 4 suspected residual starch granules in mortar collected from Gubeikou, the Great Wall, Mount Panlong, Miyun, Beijing. However, they noted that the detected starch might be heavily degraded and structurally damaged, potentially affecting the SEM results. Notably, their study did not include tests on environmental samples. Other works (Liu et al., 2016b; Shan et al., 2022; Zhou, 2016; Zhang et al., 2020a; Zheng et al., 2014; Wei et al., 2013) identified the starch by the structure transformation of limestone. But none of them conducted tests on modern samples to prove the transformation.

In summary, the existing methods can only be used to identify starch, not its source (rice, flour, etc.). Moreover, blank tests on raw earth had not been run on all these tests, which means all the existing analytical data is doubtful. The regional distribution of all the claimed cases is shown in Figure 2-8.

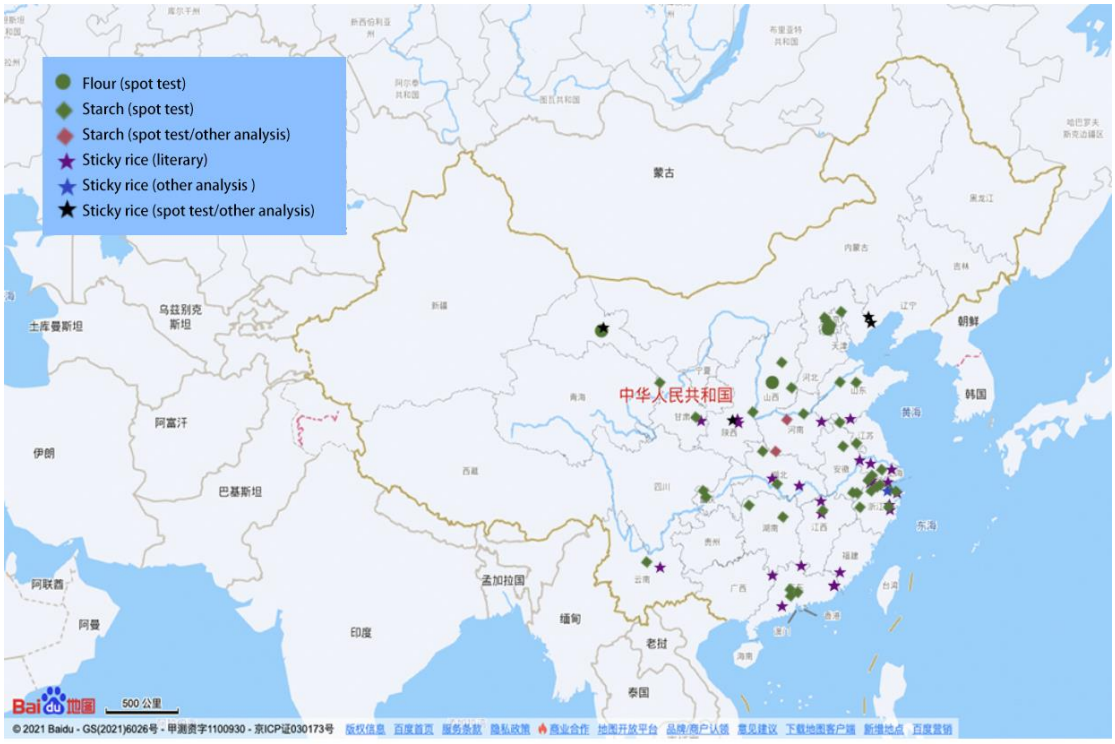


Fig 2-8. Claimed examples of the use of starch, sticky rice or flour

2.3.2. Sugar

Sugar has been identified in construction materials taken from ancient Chinese sites (Zhang, 2014), as well as mentioned in references based on documentary evidence (Fu, 2010; Shen et al., 2006; Xie, 2009; Cai, 1995). In total, there are 18 cases of using sugar. Amongst them, 14 are based on analytical data.

Benedict's solution, containing copper(II) sulfate, sodium citrate and sodium carbonate (Zhang, 2014), is used to detect reducing sugars in samples. The reaction

will produce a brick-red precipitate. This occurs because reducing sugars reduce copper(II) ions to copper(I) oxide, which forms the precipitate. Zhang (2014) found sugar in ancient samples from 6 different sites by using Benedict's solution. However, the term 'sugar' should be used with caution as Benedict's solution only reacts with reducing sugars, such as glucose and fructose, and not with non-reducing sugars like sucrose. He also commented in his dissertation that the colour of the soil might disrupt the result. Whether the brick-red precipitate is a product of the reaction between Benedict's solution and sugar or with small particles from the soil is still a problem to be resolved. Additionally, false positives might occur due to natural sugars present in the soil, while false negatives might arise if materials added to the construction, such as sucrose, are present but not detected by Benedict's solution. Sucrose is often mentioned in the literature as an additive in construction materials (Fu, 2010; Shen et al., 2006; Xie, 2009; Cai, 1995), highlighting the need for developing specific methods to detect sucrose. Furthermore, it is crucial to perform blank tests to differentiate between sugars that are naturally occurring in the soil and those that have been artificially added.

The absence of blank tests in existing analytical methods may lead to doubtful analytical data. The regional distribution of all the cases is shown in Figure 2-9.

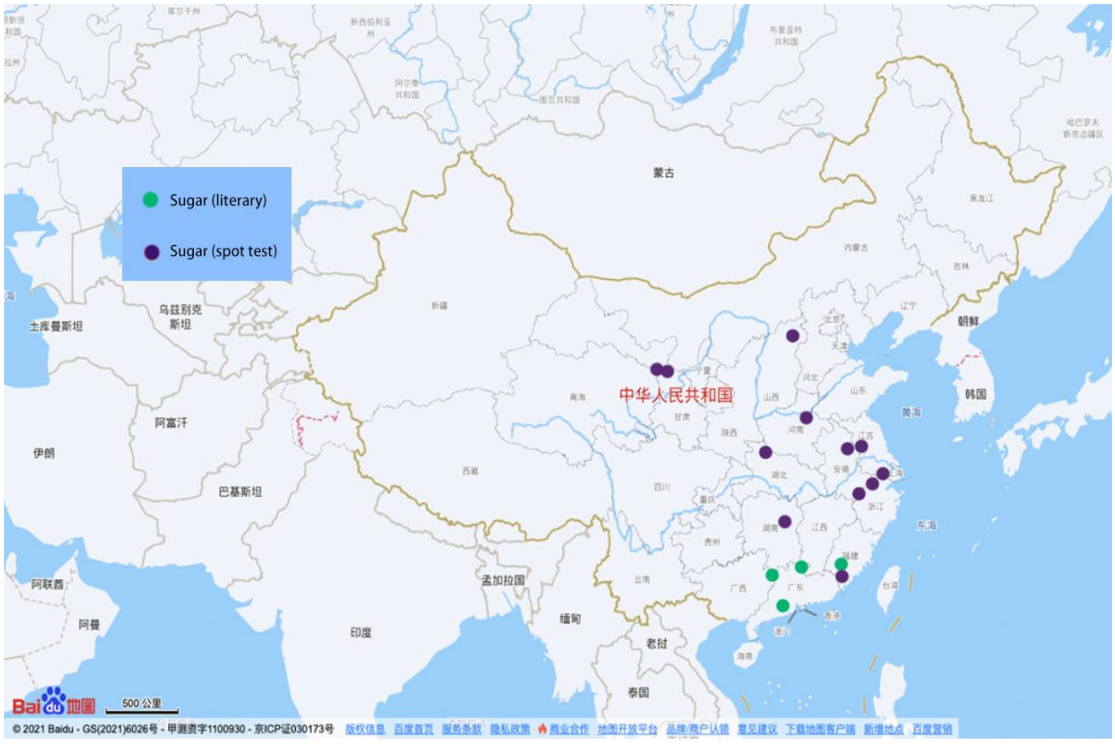


Fig 2-9. Cases of using sugar in ancient China, including: 14 based on analytical data and 4 based on documentary evidence

2.3.3. Protein

Egg white was applied in construction in ancient China (Fu, 2010; Ai, 1999; Xie, 2009; Wei, 2009). Protein has been identified in construction materials taken from ancient Chinese sites (Li and Zhang, 2019). The identification of egg white has also been made on ancient Chinese construction materials (Zhang et al., 2015; Zhang, 2014; Bonaduce et al., 2008; Hu et al., 2015). In total, there are 33 cases of using protein and egg white. Amongst them, 29 (including 20 protein and 9 egg white) are

based on analytical data.

The Coomassie brilliant blue method uses Coomassie brilliant blue reagent to detect protein. They react together in an acidic solution, and the colour of the solution will change from brown to blue. This colour change is due to the interaction between the Coomassie dye anion and the positively charged ammonium groups ($NH_3{}^+$) on protein residues (Sedmak and Grossberg, 1977). This method was also used to analyse egg white (Zhang et al., 2015; Zhang, 2014). The limitation of this method is that other kinds of protein in the samples will also cause the same reaction. Additionally, it is a reaction based on colour change and the colour of the sediment would interfere with the results (Zhang et al., 2015).

ELISA (enzyme-linked immunosorbent assay) is a precise and sensitive quantitative method for analysing antigens. It uses an enzyme-labelled antibody to react with the antibody-antigen compound in the solid phase. Another chemical, which will change colour when it comes in contact with the enzyme, is added. The amount of antigen detected can then be quantified because the depth of colour change is proportional to the amount of antibody-antigen complex produced (Child and Pollard, 1995). Zhang et al. (2015) and Zhang (2014) used ELISA to identify egg white in ancient samples. Among 12 ancient mortar samples (the detail is shown in Table 2-3 below) in which protein had been identified by the Coomassie brilliant blue method, Zhang (2014) found that none of these samples showed the existence of egg white. Besides the

possibility of other proteins, he raised another possible explanation that ELISA could not be conducted with calcium hydroxide since it would change the structure of proteins and lead to a negative result. Moreover, the degradation of proteins in samples may also affect the results of ELISA.

Table 2-3. The details of the ancient mortar samples in which protein had been identified by the Coomassie brilliant blue method in the article of Zhang (2014)

Site	Location	Province	Sample number
Sanxing Bridge	Chenzhou	Hunan	1
The city wall of Zhongdu of the Ming dynasty	Fengyang	Anhui	2
Former Residence of Feng Guorui	Tianshui	Gansu	1
Xiaofeng city wall	Huzhou	Zhejiang	1
Ancheng city wall	Huzhou	Zhejiang	2
The tomb of Shi Songzhi	Yuyao	Zhejiang	1
Liuhe Pagoda	Hangzhou	Zhejiang	1

The north wall of Kaifeng	Kaifeng	Henan	2
The Great Wall	Yanqing	Beijing	1

The absence of blank tests in existing analytical methods may lead to doubtful analytical data. The regional distribution of all the cases is shown in Figure 2-10.

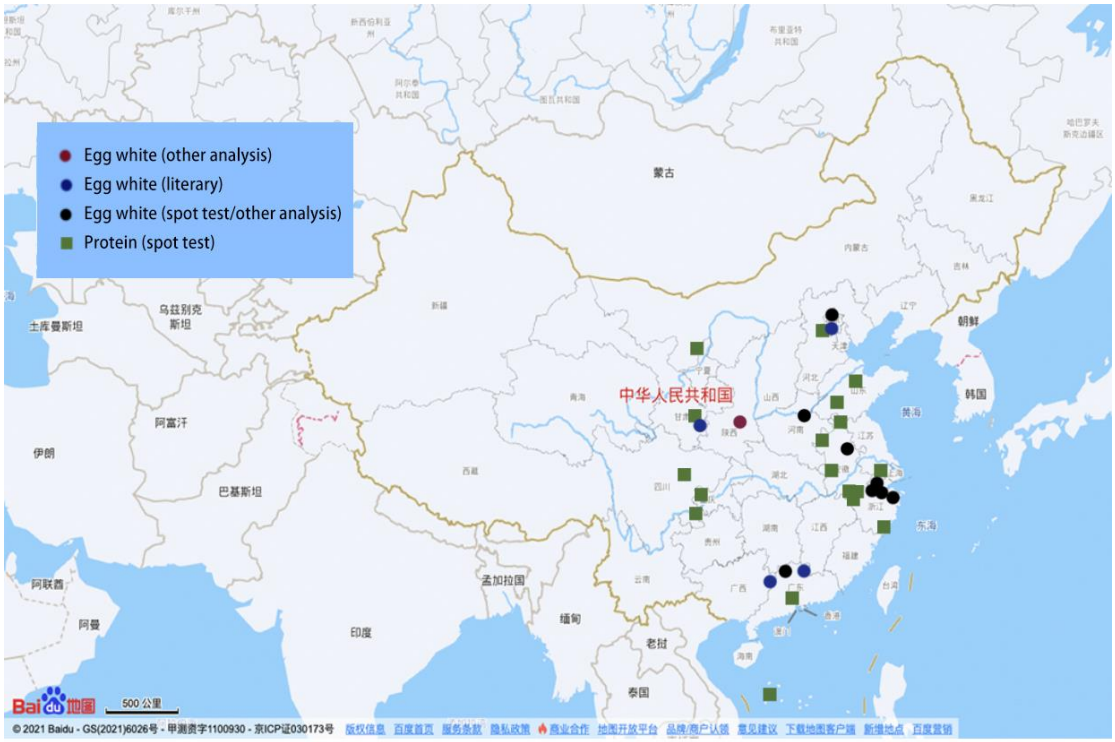


Fig 2-10. Cases of using protein in ancient China, including: protein, 20 based on analytical data; egg white, 9 based on analytical data and 4 based on documentary evidence

2.3.4. Blood (pig blood)

Blood was applied in construction from the 3rd century BCE, which was the Qin dynasty (888-207 BCE, the Qin kingdom period (888-221 BCE) is also included here) (Xing, 1995). Blood has been identified in construction materials taken from ancient Chinese sites by analytical methods (Zhou, 2009; Zhang, 2014). The identification of pig blood has also been mentioned in some references (Zhou et al., 2010; Wang et al., 2012). In total, there are 10 cases of using blood or pig blood. Amongst them, 8 (including 7 blood and 1 pig blood) are based on analytical data.

The Haemochromogen crystal test uses Takayama solution, which consists of sodium hydroxide (10% in 3 mL), pyridine (3 mL), saturated solution of glucose (3 mL) and distilled water (7 mL) for the analysis of blood (Kerr and Mason, 1926). In the presence of blood, salmon-pink crystals will appear under the microscope. Wang et al. (2012) and Zhou (2009) found pig blood in samples from the Summer Palace. The same experiments were also carried out on samples from Zishou temple, Taifu temple (Zhou, 2009) and Mongolia's Bogda Khan Palace Museum (the Yuan dynasty) (Zhou et al., 2010), and blood or pig blood was found in them. However, the Haemochromogen crystal test cannot be used for the identification of the origin of the blood, and thus, the identification of 'pig blood' is not a reliable result.

Another method used for the testing of blood is the Kastle–Meyer test (Glaister,

1926). When the phenolphthalin reagent (containing phenolphthalin and potassium hydroxide) is added with hydrogen peroxide solution into samples containing blood, it will turn red. This test is based on the fact that the haem group of haemoglobin possesses peroxidase-like activity, which catalyses the breakdown of hydrogen peroxide. The oxidising species formed in this reaction can then react with phenolphthalin to produce a visible colour change (Winchester and Wansbrough, 2013). Zhang (2014) used this method to identify blood in ancient samples from Yuzhen Palace in Wudang, Hubei province.

In most cases using the Takayama solution, an obvious haemochromogen crystal reaction cannot be observed. The reaction was so weak that Zhou (2009) demonstrated that there might be blood in the Bogda Khan Palace Museum sample. He also mentioned that, amongst samples from the Summer Palace in Beijing, 4 contained blood, 2 might have contained blood, 1 did not, and 8 gave no apparent results. That shows the uncertainty of the haemochromogen crystal test. The Phenolphthalin test had the same problem in Zhang's experiment (2014). Additionally, the catalytic properties of the Kastle–Meyer test are not specific to blood and can be interfered with by various substances, such as plant and animal peroxidases, oxidising chemicals, and metals like copper and iron (Winchester and Wansbrough, 2013).

Elemental analysis, which is used to calculate the content of different elements in

samples, is also mentioned in the literature for the analysis of pig blood. The content of nitrogen is measured and converted into the content of protein. The content of protein from blood is calculated in the sample after protein from flour has been subtracted. Zhou et al. (2010) and Wang et al. (2012) used this method to measure pig blood in ancient samples. They calculated the approximate content of pig blood by the content of nitrogen, and it was an average value from the literature. So, the content was also an estimated value. Meanwhile, the origin of nitrogen could not be identified as blood or pig blood.

In some cases, the Haemochromogen crystal test and the phenolphthalein test may show limitations due to the low content of organics in archaeological samples, which can result in subtle reaction phenomena and produce negative results (Zhou, 2009; Zhang, 2014). Elemental analysis cannot determine the origin of the nitrogen. The authors (Zhou et al., 2010; Wang et al., 2012) relied on un-referenced citations, rather than specific literature on the construction of the building where the archaeological samples were collected, to support their conclusion. Therefore, their conclusion may be subject to some uncertainty. Furthermore, all these methods above cannot identify the origin of blood. Further experiments might be carried out to identify blood as well as the blood source. Besides, the absence of blank tests in existing analytical methods may also lead to misleading analytical data. The regional distribution of all the cases is shown in Figure 2-11.



Fig 2-11. Cases of using blood and pig blood in ancient China, including: blood, 7 based on analytical data and 2 based on documentary evidence; pig blood, 1 based on analytical data

2.3.5. Lipid

Lipid (including Tung oil (extracted from the seeds of *Vernicia fordii*) and drying oil (extracted from plants)) has been identified in construction materials taken from ancient Chinese sites (Zhang, 2014). It can be from different materials, such as drying oil or Tung oil, which has been mentioned in other references (Zeng et al., 2010; Wu, 2005). In total, there are 52 cases of using lipids. The regional distribution of these

cases is shown in Figure 2-12. Amongst them, 51 (including 1 Tung oil) are based on analytical data.

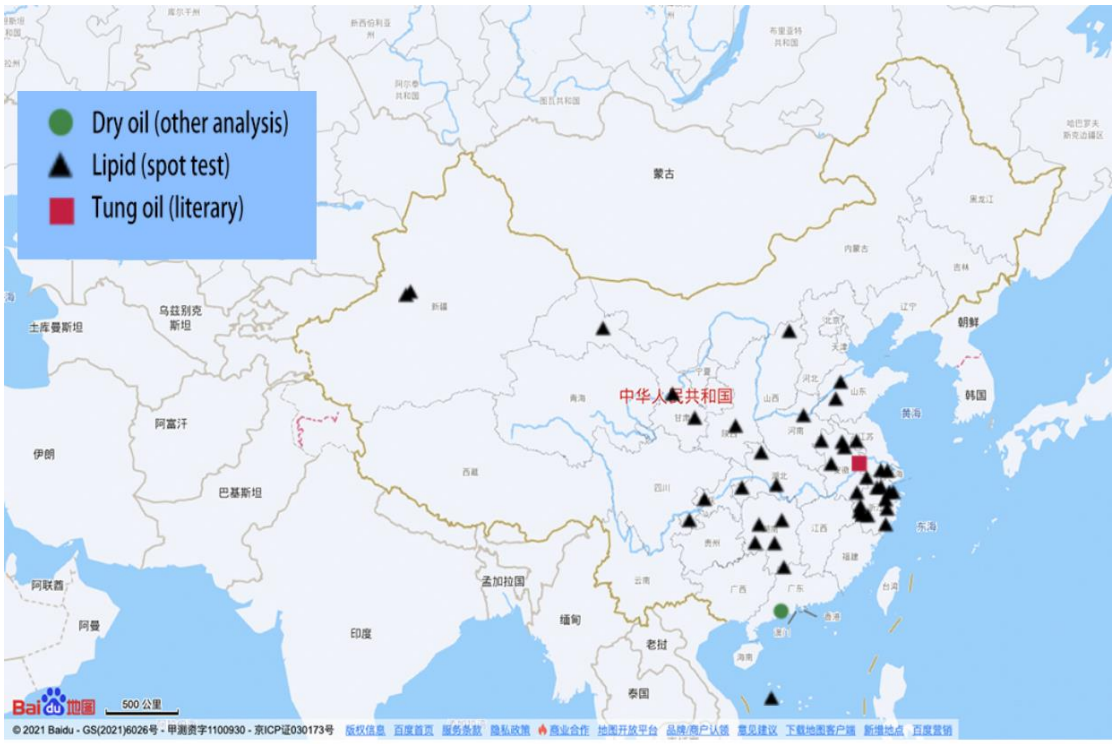


Fig 2-12. Cases of using lipid in ancient China, including: lipid, 50 based on analytical data; Tung oil, 1 based on documentary evidence; drying oil, 1 based on analytical data

The sodium hydroxide - hydrogen peroxide test is used for the analysis of lipids in ancient samples (Zhang, 2014). After the lipid is saponified by sodium hydroxide, it will react with hydrogen peroxide and form characteristic bubbles. This method could not be used to identify the specific species of lipid. Meanwhile, lipids will decompose

because of environmental factors. Thus, there may not be many lipids in ancient samples. The reactions of these samples were too weak when compared with those of simulated samples.

2.3.6. Other natural organic materials

Animal glue (Rocco Mazzeo et al., 2004; Zeng et al., 2010), siccative oil (Rocco Mazzeo et al., 2004), cotton fibre (Rocco Mazzeo et al., 2004), and juice of *Actinidia chinensis* (Wu, 2005) have only been mentioned in 1 or 2 references. There are 5 cases (1 for each, 2 for animal glue). The regional distribution of these cases is shown in Figure 2-13. Amongst them, animal glue, siccative oil and cotton fibre are based on analytical data.

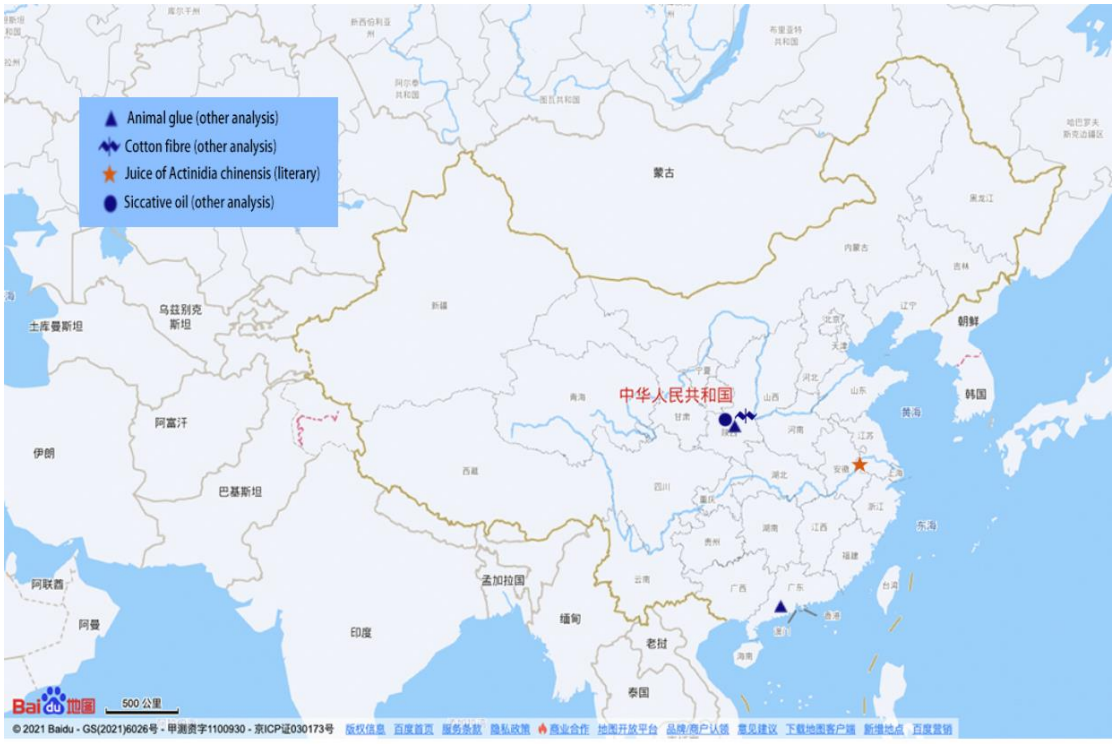


Fig 2-13. Cases of using other natural organic materials in ancient China, including: animal glue, 2 based on analytical data; siccative oil, 1 based on analytical data; cotton fibre, 1 based on analytical data; juice of *Actinidia chinensis*, 1 based on documentary evidence

Rocco Mazzeo et al. used the optical microscope for the identification of cotton fibre (Rocco Mazzeo et al., 2004). By microscopic observation, they compared fabric strips in ancient samples with standard cotton fibres and confirmed the existence of cotton fibres. In the same sample, they also identified the possible application of animal glue and siccative oil using Py-GC-MS (Pyrolysis-Gas chromatography-Mass Spectrometry). Unfortunately, the authors did not provide any details about the detection of animal glue (Rocco Mazzeo et al., 2004). For the detection of siccative

oil, the dimethyl esters of azelaic acid and suberic acid were selected as the biomarkers. The authors pointed out that the oil is most likely Tung oil based on documentary evidence, as there is neither scientific nor historical evidence of the use of other type of siccative oil, such as linseed oil, in ancient China. However, they also suggested that the evidence is not sufficient to conclusively identify Tung oil. Thus, this case is not definitively included among Tung oil cases (Rocco Mazzeo et al., 2004).

Zeng et al. (2010) used FTIR and elemental analysis to analyse ancient samples from Kaiping Diaolou. They drew the conclusion that there might be drying oil or animal glue in the samples. Unfortunately, the results may be insufficient to support this conclusion. Zeng et al. (2010) identified the existence of organic compounds by the high content of carbon and oxygen in the elemental analysis. However, calcium carbonate is also present in the samples, which could account for these two elements. They further suggested the existence of drying oil and animal glue based on the peaks at about 2980, 2928, and 2870 cm^{-1} (assigned to the asymmetric and symmetric CH_2 stretching modes, respectively), at 1790 cm^{-1} (assigned to the carbonyl stretching mode of the ester group), and 1620 cm^{-1} (Amide I) in FTIR. However, as discussed in Chapter 2.3.1, FTIR cannot be applied to conclusively identify specific components in a complex system.

In summary, considering the low sensitivity and specificity of spot tests and FTIR, as

well as the absence of blank tests on raw earth, none of the analytical methods applied in the reviewed literature between 1934-2022 is reliable. Hence, more rigorous tests must be applied to blank, modern and archaeological samples to identify organics in construction materials.

2.4. Organics in natural loess

Besides the artificial addition of organic materials, some organics may be contained in natural loess, which can also be found in the earth used to construct ancient sites. Thus, before identifying added organic materials, a review of the contents and components of organics in the natural earth is of great importance. Meanwhile, it also shows the necessity of running blank tests on natural loess.

2.4.1. The genesis and distribution of loess

Loess is a terrestrial clastic sediment, composed predominantly of silt-size particles (Pye, 1995). Generally, it has a homogenous and porous structure and consists primarily of quartz and felspar particles (Li et al., 2020b). Additionally, variable amounts of clay minerals (5-20%) and carbonates (1-20%) may also be present in loess (Pye, 1995).

The development of loess formation theories has evolved from early classifications that divided loess into glacial loess and desert loess, to later theories acknowledging multiple origins (Li et al., 2020b; Muhs et al., 2014). Glacial loess originates from mountain or continental glaciers, formed by glacial grinding against bedrock (Smalley, 1966; Muhs et al., 2014). The outwash deposits, which are transported away from the ice sheet in meltwater, become the primary source of the glacial loess (Smalley and Derbyshire, 1990). Desert loess, initially thought to come directly from deserts (Smalley and Vita-Finzi, 1968), was later found to be supplied by surrounding mountains through fluvial transport (Smalley and Krinsley, 1978; Muhs, 2013; Smalley et al., 2014). Thus, the term "mountain loess" was then applied to replace desert loess (Smalley and Derbyshire, 1990). Muhs et al. (2014) found that volcanic ash is also one of the major sources of loess in some areas. Additionally, they suggested that the loess in certain regions had multiple origins, including both glacial and non-glacial sources.

Various transport forms, including aeolian (Pye, 1995) and fluvial (Smalley, 1995) transport, are involved from the source area where original particles are produced, to the loess accumulation zones. Li et al. (2020b) summarized the formation of loess into 3 modes: 1) continental glacier provenance-river transport mode; 2) mountain provenance-river transport mode; 3) Mountain provenance-river transport-desert transition mode.

The total estimated area of loess regions worldwide is approximately 8.61 million square kilometres, covering around 6% of the total land area. Major regions include North America (1.51 million square kilometres), South America (0.46 million square kilometres), Europe (1.71 million square kilometres), Asia (4.72 million square kilometres), Africa (0.08 million square kilometres), and Oceania (0.13 million square kilometres). Significant loess coverage is found in countries like China, Russia, the USA, Argentina, and Ukraine (Li et al., 2020b). In China, loess and loess-like soils are widely distributed in the northern part. Their total distribution area is approximately 0.63 million square kilometres, about 6.3% of the country's land surface (Lin and Liang, 1980).

2.4.2. Sources of organic matter in loess

According to the formation process of the loess, the organic matter is carried within the original particles by far and middle distance aeolian transport to the sedimentary locations. Additionally, it is affected by the post-sedimentary illuviation processes and post-sedimentary “contamination” (Zech and Zech, 2018). The latter may come from the decaying remains of animals and vegetation through a series of biochemical reactions and primarily exists in clay and silt fractions (Li and Pang, 2014). A detailed review of the content and types of organic matter in loess will be discussed in Chapters 2.4.3 and 2.4.4.

2.4.3. The organic matter content in loess in China

The organic matter content in loess has been investigated by many scientists. Diao and Wen (1988) analysed 110 samples from 34 spots in Shanxi, Shaanxi and Gansu provinces. The organic matter content of these samples ranges from 0.179% to 0.883% and averages 0.390%. Another research carried out by Zhao et al. (2017) using a Total Organic Carbon instrument (manufactured by Elementar corporation, Germany, with an error of less than 0.05%) shows that the organic matter content of 110 samples collected from 5 spots in the Chinese Loess Plateau ranges from 0.04% to 0.44%.

The spatial studies on the organic matter in loess on the Chinese Loess Plateau have also been carried out by analysing the soil organic carbon content with a TOC instrument. The soil organic carbon contents range from 0.23% to 4.24% (1.45 $g \cdot cm^{-3}$ was applied as the soil density for calculation) in the depth of 0-20 cm and the average is 1.56%. The soil organic carbon contents of the eastern parts of the Chinese Loess Plateau are higher than those of the central and western parts (Xu et al., 2003). Another study showed that when the depth came to 0-100cm, the soil organic carbon contents of samples of different types ranged from 0.08% to 0.16% (1.45 $g \cdot cm^{-3}$ was applied as the soil density for calculation) (Han et al., 2010).

A framework of the Loess Critical Zone (which is located in the intersection of

bedrock, groundwater, pedosphere, atmosphere and biosphere) presented by Yang et al. (2024) provides a comprehensive study based on a series of studies on the organic carbon content of the loess in China. The organic content ranges from 0.23% (Li et al., 2021) to 8.62% (Ni, 2013) (1.45 $g \cdot cm^{-3}$ was applied as the soil density for calculation). Based on samples collected from 5 main loess observation stations on China's Loess Plateau: Shenmu, Suide, Ansai, Guyuan, and Changwu, another comprehensive study suggested that the loess organic content, after removing visible organic materials such as plant roots, is from 0.08% to 0.31%, with an average of 0.17% (Yao et al., 2023).

The content of soil organic carbon is affected by time, depth, land use, soil texture, and soil water content (Wang et al., 2016). The soil organic carbon was significantly lower under shrubland than under cropland and grassland in the 0-200 cm soil layer. However, the overall vertical distributions of soil organic carbon were similar among the 3 land use types. The contents were higher in the 0-500 cm soil layer than in the 0-100 cm layer under cropland, grassland, and shrubland. There were also higher soil organic carbon contents in loamy than in sandy soils in each 100 cm thick soil layer. The soil organic carbon contents were lower at mid-slope than at upper and lower slope positions, although the contents were similar on slopes with shaded and sunlit aspects.

These studies provide a baseline understanding of the organic matter content in loess,

which is essential before the analysis of organic matter in earth samples from the ancient sites.

2.4.4. The composition of organic matter in loess in China

The accumulation and transformation of organic material in soil formation are variable and influenced by the composition of parent materials, climatic conditions, ecosystem development rate, and land use management practices (Abakumov et al., 2013). Although extracting organic matter molecules from soil has been quite challenging and made it particularly difficult to analyse the small molecular compounds in soil (Li et al., 2018), various analytical approaches have been used to study the chemical composition of organic matter in loess.

Organic matter in loess can be classified based on operational definitions, which are determined by specific extraction and analysis procedures rather than distinct chemical structures. The large and recognizable remains of plant, animal, and soil organisms that can be separated from soils by hand picking and sieving techniques are referred to as particulate organic matter (Paul, 2007, p. 32). Different types of humic substances are fractionated by dispersion of soil in a strong base followed by acidification. The non-extractable fraction is termed humin. The dispersible fraction precipitated at low pH (<2) is known as humic acid. The dissolved fraction not affected by pH is termed fulvic acid (Paul, 2007, p. 332). It is crucial to understand

that these definitions are based on extraction methods and do not represent chemically distinct structures. The chemical compositions of loess collected from Yunwu Mountain, Guyuan city, Ningxia Hui Autonomous Region, China were studied (Cheng and An, 2015). Carbon fractions had a similar increasing trend during natural vegetation restoration. The concentrations of particulate organic carbon, fulvic acid carbon, and humic acid carbon accounted for 24.5%–49.1%, 5.8%–9.1%, and 4.6%–6.1% of total carbon.

Organic matter in loess can also be classified based on its chemical composition, which considers specific types of organic molecules present in the soil. This method provides a detailed understanding of the different forms of carbon in soil. For example, the prime source of amino acids in the soil is microbial in origin. The bulk of these compounds occurs as peptides in the structures of mucoproteins, mucopeptides, and teichoic acids present in the cells and cell walls of microorganisms (Curry et al., 1994). Oches and McCoy (2001) used the amino acid racemization technique to detect amino acids in loess sediments and applied it to study the chronostratigraphy and paleoclimatic questions in loess samples. Shen et al. (2017) studied the distribution of *n*-alkanes in Miocene loess in Qinan, western Chinese Loess Plateau. They demonstrated that *n*-alkanes in loess samples from Qinan range from C_{14} to C_{35}. Amongst them, the relative content of short-chain *n*-alkanes (C_{14}–C_{20}) is significantly greater than that of long-chain *n*-alkanes (C_{26}–C_{35}). The content of medium-chain *n*-alkanes (C_{21}–C_{25}) in all samples is lower than the others.

Based on a quick review of the content and composition of organics in natural loess, a baseline considering the background organic matter in natural loess should be built to help any study of Chinese earth-based building material. In the review of Yang et al. (2024), 8.62% is the maximum of TOC in natural loess. However, this is a calculation value from the soil organic carbon density at a depth of 0-100 cm, using 1.45 $g \cdot cm^{-3}$ as the soil bulk density for the calculation. Therefore, an average value of 1.56% (Xu et al., 2003) and 0.17% (without particulate organic carbon)(Yao et al., 2023) should be considered as the limit of the baseline. This value could be used for the screening of archaeological samples. Various organic compounds, such as amino acids, alkanes, saccharides etc., can be found in natural loess, which means that blank tests are crucial in the development of new analytical methods to avoid the detection of these compounds from the raw earth.

3. Materials

3.1. Modern samples

Modern samples were prepared with known organic content to assess the accuracy of different methods. The modern samples were made using loess from the Changping District, Beijing, China. The loess was homogenised and baked at 450℃ for 13 hours to remove all the original organics (the weight had kept stable after 13 hours) before mixing with the organics (starch from different sources and cellulose) to avoid contamination. Water, which would interfere with the result of LOI and FTIR, was also removed in this process. All modern samples were homogenised and then kept in closed glass tubes. Unbaked loess samples were also used for blank tests. No water is added in M series samples (details can be found in Table 3-1) and no heating or boiling steps were applied to avoid influence to the sticky rice. In T series (details can be found in Table 3-2, pp. 75-76), which in later part of this chapter, sticky rice juice (boiled in water and with grains) was applied to make modern samples, as in some of the ancient literature described

Details of the modern samples are shown in Table 3-1.

Table 3-1. Detail of the modern samples

Sample	Organic content (weight percentage)	The source of the organic
M1	0.090	sticky rice powder produced by Foo Lung Ching Kee Company (Hong Kong)
M2	0.94	
M3	2.8	
M4	7.1	
M5	19	
M6	30	
M7	52	
WS1	2	Wheat starch powder produced by Xingwang Food Co., Ltd., Foshan, Guangdong province
WS2	2	Wheat starch powder produced by Liangrun Whole Grain Food Co., Ltd., Xinxiang, Henan province
WS3	2	Wheat starch powder produced by Zhenlemen

		Food Co., Ltd., Kunshan, Jiangsu province
SPS1	2	Sweet potato starch powder produced by Tengda Chunfeng Agricultural and Sideline Products Processing Factory, Junlian, Yibin, Sichuan province
SPS2	2	Sweet potato starch powder produced by Yang Weiming Food Store, Qingfu Town, Gaoxian County, Yibin, Sichuan province
CS1	2	Corn starch powder produced by Aijin Characteristic Agriculture

		Development Co., Ltd., Jiangxi province
CS2	2	Corn starch powder produced by Ganzhiyuan Sugar Industry Co., Ltd., Nanjing, Jiangsu province
RF1	2	Rice flour powder produced by Cho Heng Rice Vermicelli Factory Co., Ltd., Bangkok, Thailand
RF2	2	Rice flour powder produced by Enmiao Food Co., Ltd., Henan province
C1	2	Cellulose
C2	5	
C3	10	

In addition to the modern earth samples made by directly mixing baked loess and sticky rice powder, modern tabia (mentioned in Chapter 2.1) samples have also been prepared. Although the content of the sticky rice or sticky rice juice added is not mentioned in ancient references, some sources provide the ratio of loess, sand, and lime. In the text of "Tiangong Kaiwu", the proportion of the tabia is described as: "Mix one part lime with two parts of river sand and loess" ("灰一分入河沙、黄土三分" in classical Chinese) (Song, 2008). No more details are provided about the ratio of sand and loess. Thus, the modern tabia proportion was decided as: the same weight of lime, sand and loess. However, different dynasties, regions or applications may have different ratios. According to the other reference (Wang, 1936) describing the official construction techniques of stone bridges in the Qing dynasty: "Lime soil refers to a mixture of lime and loess, also known as tabia. The lime soil is mixed in a ratio of 40% lime to 60% loess" ("灰土即石灰与黄土之混合，或谓‘三合土’；灰土按四六掺合，石灰四成，黄土六成" in classical Chinese), the ratio of lime to loess in tabia used for stone bridges during the Qing dynasty was 2:3, with no sand included. Therefore, 3 types of tabia were prepared with the ratio of the calcium oxide (used to replace lime for the stability of ratio), loess (collected from the Changping District, Beijing, China) and silicon dioxide (used to replace sand for the stability of ratio) 1:1:1, 2:3:0 and 3:2:1 (this set of proportion is used for comparison): water was added into sticky rice powder produced by Foo Lung Ching Kee Company (Hong Kong). The juice was boiled and stirred to gelatinize the sticky rice. Once cooled to the room temperature, the rice juice was added into the mixture of loess, calcium

oxide and silicon dioxide. Additional water was then added until the surface of the mixture was completely covered. The mixture was kept stirring to ensure homogenisation, and then dried in the air to obtain a powder. Details of the modern tabia samples are shown in Table 3-2.

Table 3-2. Detail of the modern tabia samples

Sample	Ratio of the calcium oxide, loess and silicon dioxide (weight)	Sticky rice content (weight percentage)
T1	1:1:1	2
T2	1:1:1	5
T3	1:1:1	10
T4	2:3:0	2
T5	2:3:0	5
T6	2:3:0	10
T7	3:2:1	2
T8	3:2:1	5
T9	3:2:1	10
T10	1:1:1	0.2
T11	1:1:1	0.02
T12	2:3:0	0.2

T13	2:3:0	0.02
T14	3:2:1	0.2
T15	3:2:1	0.02
T16	1:1:1	0.032
T17	2:3:0	0.032
T18	3:2:1	0.032
T19	1:1:1	0.016
T20	2:3:0	0.016
T21	3:2:1	0.016
T22	1:1:1	0.008
T23	2:3:0	0.008
T24	3:2:1	0.008
T25	1:1:1	0.004
T26	2:3:0	0.004
T27	3:2:1	0.004
T28	1:1:1	0.002
T29	2:3:0	0.002
T30	3:2:1	0.002

3.2. Archaeological samples

Archaeological samples were collected from different ancient sites in Henan, Zhejiang, Hebei, Shaanxi, Shanxi, Jiangsu, Jiangxi Provinces, the Guangxi Zhuang autonomous region and Beijing in China. The distribution of those sites is shown in Figure 3-1, and the construction periods for these sites are shown in Figure 3-2. The introduction to these sites can be found in 3.3.

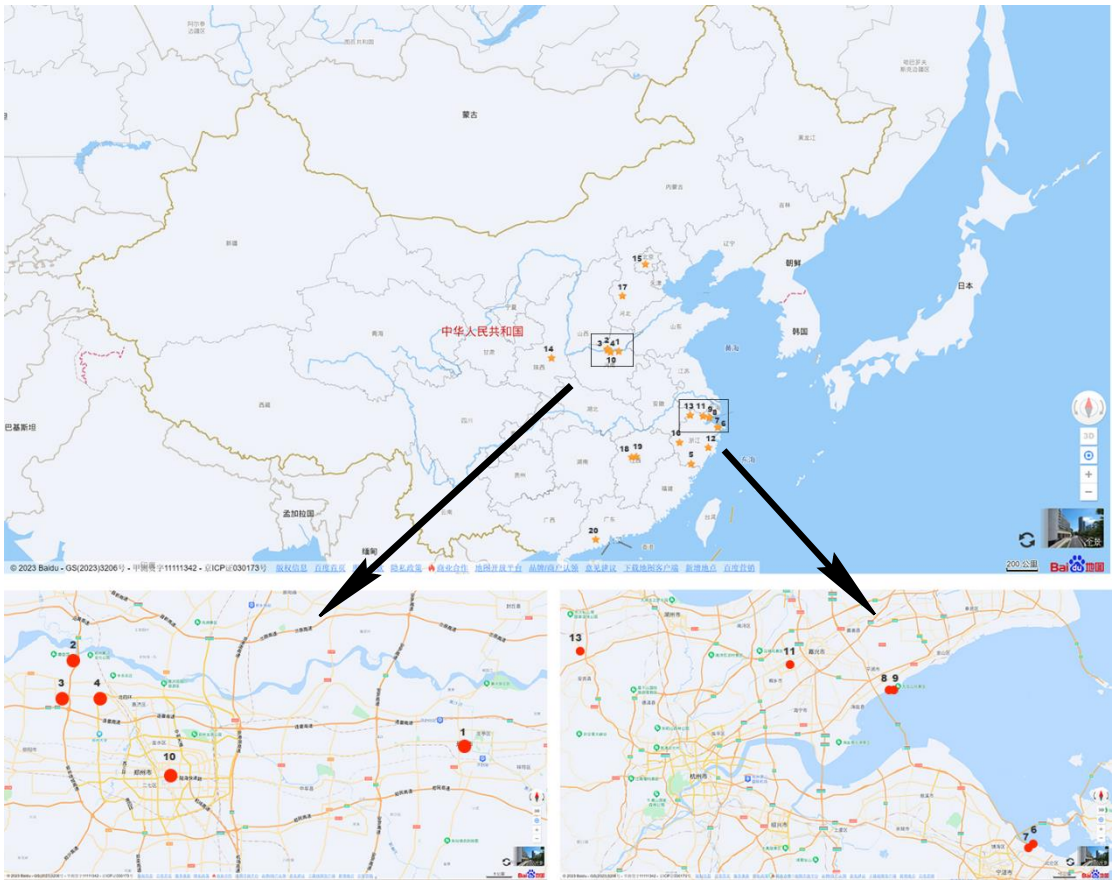


Fig 3-1. The distribution of collected ancient sites (details of these sites are in Table 3-3 in numerical order, pp. 79-83)

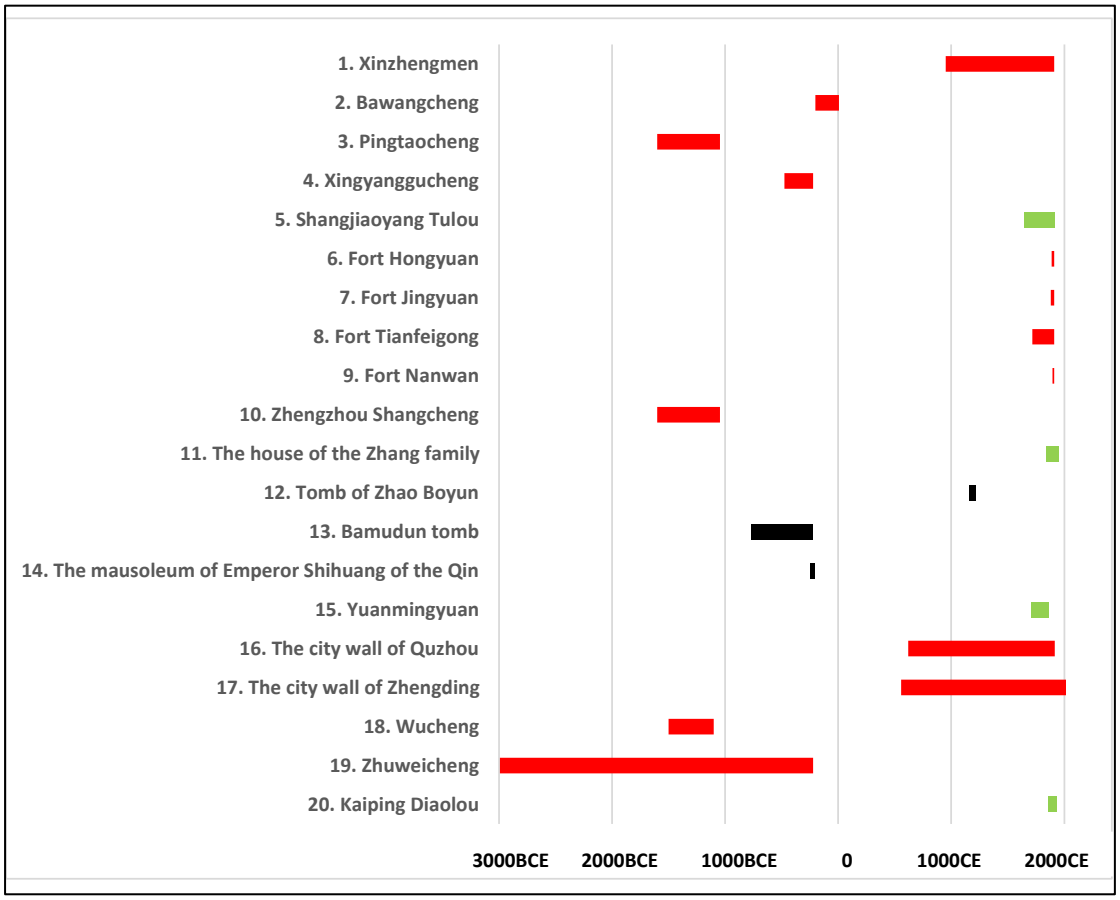


Fig 3-2. The construction period of the sites from which samples have been collected (red ones are military buildings; green ones are buildings for living; black ones are buildings for burial)

All the samples were taken directly from ancient sites or provided by archaeologists, put into plastic sealed bags, labelled and transported to Oxford under the licence to import, move and keep prohibited soil for chemical and physical analysis (licence No. 123959/334532/0). (Some samples have not been transported to Oxford, they were directly analysed in China).

Some samples were used in the development of the new analytical protocol. Their

details are listed in Table 3-3.

Table 3-3. Detail of the archaeological samples

Number	Site	Area	Sample	Description
1	Xinzhengmen	Luoyang, Henan province	XZM1	Rammed earth
			XZM2	Rammed earth
			XZM3	Rammed earth
			XZM4	Rammed earth
			XZM5	Sediment from the Northern Song dynasty (960-1127 CE)
			XZM6	Sediment from the Jin kingdom (1115-1234 CE)
			XZM7	Sediment from the Yuan dynasty (1271-1368 CE)
			XZM8	Sediment from the Ming dynasty (1368-1644 CE)
2	Bawangcheng	Zhengzhou, Henan province	BWC1	Rammed earth on the bottom
			BWC2	Rammed earth on the bottom
			BWC3	Rammed earth on the bottom
			BWC4	Rammed earth
			BWC5	Rammed earth
			BWC6	Rammed earth
			BWC7	Rammed earth on the top
			BWC8	Rammed earth on the top

			BWC9	Rammed earth on the top
3	Pingtaocheng	Zhengzhou, Henan province	PTC1	Rammed earth from the east wall
			PTC2	Rammed earth from the east wall
			PTC3	Rammed earth from the north wall
			PTC4	Rammed earth from the north wall
			PTC5	Rammed earth from the north wall
			PTC6	Rammed earth from the north wall
			PTC7	Rammed earth from the north wall
			PTC8	Rammed earth from the north wall
4	Xingyanggucheng	Zhengzhou, Henan province	XYGC1	Rammed earth
			XYGC2	Rammed earth
			XYGC3	Rammed earth
			XYGC4	Rammed earth
			XYGC5	Rammed earth
			XYGC6	Rammed earth
			XYGC7	Sediment on the bottom
5	Shangjiaoyang Tulou	Wenzhou, Zhejiang province	SJYTL1	Tabia on the surface of internal wall
			SJYTL2	Tabia on the surface of internal wall

			SJYTL3	Tabia on the surface of internal wall
			SJYTL4	Tabia on the surface of external wall
			SJYTL5	Tabia on the surface of external wall
6	Fort Hongyuan	Ningbo, Zhejiang province	HYPT1	Tabia
			HYPT-B1	Earth from the mound on which the Fort Hongyuan site is located
			HYPT-B2	Earth from the mound on which the Fort Hongyuan site is located
			HYPT-B3	Earth from the mound on which the Fort Hongyuan site is located
7	Fort Jingyuan	Ningbo, Zhejiang province	JYPT1	Tabia
			JYPT2	Tabia
			JYPT-B1	Earth from the mound on which the Fort Jingyuan site is located
			JYPT-B2	Earth from the mound on which the Fort Jingyuan site is located
			JYPT-B3	Earth from the mound on which the Fort Jingyuan site is located
8	Fort Tianfeigong	Pinghu,	TFGPT1	Tabia

		Zhejiang province	TFGPT-B1	Earth collected from the mound near the Fort Tianfeigong site
9	Fort Nanwan	Pinghu, Zhejiang province	NWPT-B1	Earth collected from the mound near the Fort Nanwan site
			NWPT-B2	Earth collected from the mound near the Fort Nanwan site
10	Zhengzhou Shangcheng	Zhengzhou, Henan province	ZZSC1	Rammed earth on the top
			ZZSC2	Rammed earth on the top
			ZZSC3	Rammed earth on the top
11	The house of the Zhang family	Jiaxin, Zhejiang province	HNZZ1	Tabia
12	Tomb of Zhao Boyun	Taizhou, Zhejiang province	ZBYM1	Tabia
			ZBYM2	Tabia
			ZBYM3	Dark green and black resin-like
13	Bamudun tomb	Huzhou, Zhejiang province	BMD1	Earth from burial cave
			BMD2	Earth from burial cave
			BMD3	Rammed earth on the top
14	The mausoleum of Emperor Shihuang of the Qin	Xi’an, Shaanxi province	QL1	Rammed earth from the wall on the ground
15	Yuanmingyuan	Beijing	YMY1	Rammed earth
16	The city wall of Quzhou	Quzhou, Zhejiang province	QZCQ1	Lime mortar
17	The city wall of Zhengding	Shijiazhuang, Hebei province	ZDBM1	Lime mortar

18	Wucheng	Zhangshu, Jiangxi province	WC1	Rammed earth on the top
			WC2	Rammed earth in the middle
			WC3	Rammed earth on the bottom
			WC4	Rammed earth on the bottom
			WC5	Earth on the bottom
19	Zhuweicheng	Zhangshu, Jiangxi province	ZWC1	Rammed earth on the top
			ZWC2	Rammed earth on the top
			ZWC3	Rammed earth on the top
			ZWC4	Rammed earth on the bottom
			ZWC5	Rammed earth on the bottom
20	Kaiping Diaolou	Kaiping, Guangdong province	XAL	Tabia collected from Xi’an Lou
			XAL-B1	Earth collected from near Xi’an Lou
			CAL	Tabia collected from Chang’an Lou
			CAL-B1	Earth collected from near Chang’an Lou
			SRL	Tabia collected from Shiru Lou
			SRL-B1	Earth collected from near Shiru Lou
			ZLL	Tabia collected from Zulong Lou
			ZLL-B1	Earth collected from near Zulong Lou

3.3. Artificially aged samples

The degradation of starch may have a possible influence on the identification of the starch in soil samples. Therefore, degraded samples were prepared by being heated in the oven at 50℃, each heating cycle lasts for 12h. Sample details are shown in Table 3-4.

Table 3-4. Details of the aged samples (sample details of T1-9 can be found in Table 3-2, pp. 75-76)

Sample	Original sample	Heating time
AT1A	T1	120 h
AT1B	T1	240 h
AT1C	T1	360 h
AT2A	T2	120 h
AT2B	T2	240 h
AT2C	T2	360 h
AT3A	T3	120 h
AT3B	T3	240 h
AT3C	T3	360 h
AT4A	T4	120 h
AT4B	T4	240 h

AT4C	T4	360 h
AT5A	T5	120 h
AT5B	T5	240 h
AT5C	T5	360 h
AT6A	T6	120 h
AT6B	T6	240 h
AT6C	T6	360 h
AT7A	T7	120 h
AT7B	T7	240 h
AT7C	T7	360 h
AT8A	T8	120 h
AT8B	T8	240 h
AT8C	T8	360 h
AT9A	T9	120 h
AT9B	T9	240 h
AT9C	T9	360 h

The tests conducted on all the samples are shown in Table 3-5.

Table 3-5. Tests conducted on all the samples (The iodine-starch test, FTIR and LOI were conducted in Oxford. Other tests were conducted in China)

	Sample	The iodine-starch test	FTIR	TGA-DSC-DTA	LOI	TGA-FTIR	TGA-MS	MALDI-TOF-MS	LC-MS/MS
Modern sample	M1	✓	✓		✓	✓	✓		
	M2	✓	✓		✓	✓	✓		
	M3	✓	✓		✓	✓	✓	✓	
	M4	✓	✓	✓	✓	✓	✓		
	M5	✓							
	M6	✓		✓					
	M7	✓							
	WS1							✓	
	WS2							✓	
	WS3							✓	
	SPS1							✓	
	SPS2							✓	
	CS1							✓	
	CS2							✓	
	RF1							✓	
	RF2							✓	
	C1							✓	
	C2							✓	
	C3							✓	
	T1							✓	
	T2							✓	
	T3							✓	
	T4							✓	
	T5							✓	
	T6							✓	
	T7							✓	
	T8							✓	
	T9							✓	
	T10							✓	
	T11							✓	
	T12							✓	
	T13							✓	
	T14							✓	
	T15							✓	
	T16							✓	

	T17										✓	
	T18										✓	
	T19										✓	
	T20										✓	
	T21										✓	
	T22										✓	
	T23										✓	
	T24										✓	
	T25										✓	
	T26										✓	
	T27										✓	
	T28										✓	
	T29										✓	
	T30										✓	
Archaeological sample	XZM1		✓			✓					✓	
	XZM2		✓			✓					✓	
	XZM3		✓			✓					✓	
	XZM4		✓			✓					✓	
	XZM5		✓			✓					✓	
	XZM6		✓			✓					✓	
	XZM7	✓	✓	✓		✓	✓		✓		✓	
	XZM8		✓			✓					✓	
	BWC1		✓			✓					✓	
	BWC2		✓			✓					✓	
	BWC3		✓			✓					✓	
	BWC4		✓			✓					✓	
	BWC5		✓			✓					✓	
	BWC6		✓			✓					✓	
	BWC7		✓			✓					✓	
	BWC8		✓			✓					✓	
	BWC9		✓			✓						
	PTC1		✓			✓					✓	
	PTC2		✓			✓					✓	
	PTC3		✓			✓					✓	
	PTC4		✓			✓					✓	
	PTC5		✓			✓					✓	
	PTC6		✓			✓					✓	
	PTC7		✓			✓					✓	
	PTC8		✓			✓					✓	
	XYGC1		✓			✓					✓	
	XYGC2		✓			✓					✓	
	XYGC3		✓			✓					✓	
	XYGC4		✓			✓					✓	

XYGC5		✓		✓			✓
XYGC6		✓		✓			✓
XYGC7		✓		✓			✓
SJYTL1		✓		✓			✓
SJYTL2		✓		✓			
SJYTL3		✓	✓	✓	✓	✓	✓
SJYTL4		✓		✓			✓
SJYTL5		✓		✓			✓
HYPT1	✓	✓	✓	✓	✓	✓	✓
HYPT-B1							✓
HYPT-B2							✓
HYPT-B3							✓
JYPT1		✓		✓			
JYPT2		✓		✓			
JYPT-B1							✓
JYPT-B2							✓
JYPT-B3							✓
TFGPT1							✓
TFGPT-B1							✓
NWPT-B1							✓
NWPT-B2							✓
ZZSC1		✓		✓			✓
ZZSC2		✓		✓			✓
ZZSC3		✓		✓			✓
HNZZ1		✓		✓			✓
ZBYM1		✓		✓			
ZBYM2		✓		✓			
ZBYM3		✓		✓			
BMD1		✓		✓			✓
BMD2		✓		✓			✓
BMD3		✓		✓			✓
QL1							✓
YMY1							✓
QZCQ1							✓
ZDBM1							✓
WC1							✓
WC2							✓
WC3							✓
WC4							✓
WC5							✓

	ZWC1	✓	
	ZWC2	✓	
	ZWC3	✓	
	ZWC4	✓	
	ZWC5	✓	
	XAL		✓
	XAL-B1		✓
	CAL		✓
	CAL-B1		✓
	SRL		✓
	SRL-B1		✓
	ZLL		✓
	ZLL-B1		✓
Artificially aged sample	AT1A	✓	
	AT1B	✓	
	AT1C	✓	
	AT2A	✓	
	AT2B	✓	
	AT2C	✓	
	AT3A	✓	
	AT3B	✓	
	AT3C	✓	
	AT4A	✓	
	AT4B	✓	
	AT4C	✓	
	AT5A	✓	
	AT5B	✓	
	AT5C	✓	
	AT6A	✓	
	AT6B	✓	
	AT6C	✓	
	AT7A	✓	
	AT7B	✓	
	AT7C	✓	
	AT8A	✓	
	AT8B	✓	
	AT8C	✓	
	AT9A	✓	
	AT9B	✓	
	AT9C	✓	

4. The iodine-starch test

Although the iodine-starch test is a commonly referenced analytical method for identifying starch in archaeological studies, as discussed in Chapter 2.3.1, its specificity remains questionable. This chapter will examine its applicability in the screening step, which aims to identify earth samples containing sufficient organics for further analysis and does not require high specificity. Zhang (2014) reports a relatively low detection limit of 0.033% for starch in modern samples composed of sticky rice and calcium hydroxide. The potential of this method for analysing earth samples with low starch content will be explored in this chapter to assess its feasibility for the screening process.

4.1. Samples

The iodine-starch test was applied to sticky rice powder, modern (n = 7) and 2 archaeological samples . Details can be found in Chapter 3 (pp. 54-83).

4.2. Methods

The iodine-starch test (Jeffery et al., 1989) is based on the colour change that occurs during the reaction between starch and iodine. Starches can be separated into two major components: amylose and amylopectin. Amylose turns blue, while amylopectin turns purple when they react with iodine. Amylopectin accounts for over 98% of the

starch content in sticky rice (Fuller and Castillo, 2015). Therefore, the method applied in this chapter is based on the same test run on lime mortar samples by Zhang (2014) to detect the amylopectin. It was used for the development of the screening step. 0.2 g of material to be tested was ground into powder, mixed with 5 mL water, and heated in a water bath at 100℃ for 10-20 min with agitation. The suspension formed was cooled to room temperature before the supernatant was separated. Then the pH of the supernatant was adjusted to 6.0-7.0 with acetic acid. The iodine–KI (potassium iodide) reagent was made by dissolving 1.0 g iodine in 100 mL water in the presence of 3.0 g KI. The iodine–KI reagent was dropped into the supernatant with agitation. If there is amylopectin in the sample, a purple colour is observed. The colour change was then measured by colorimetry from the wavelength of 460 nm to 800 nm. The iodine-starch test was run by the author in Research Laboratory for Archaeology and the History of Art, University of Oxford. The colorimetry test was run on the BMG Labtech PHERAstar Plus by Shuang Liu, a DPhil candidate in Chemical Biology, the Schofield group, Department of Chemistry, University of Oxford.

4.3. Results

The results of the iodine-starch test are shown below.

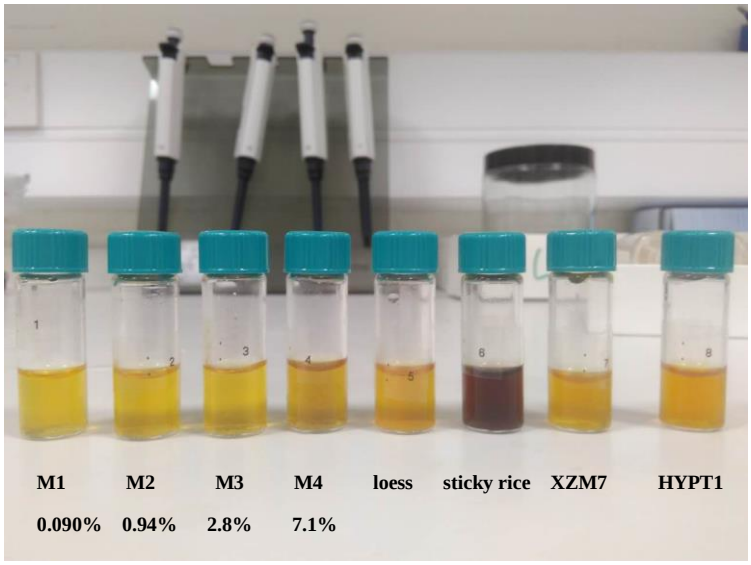


Fig 4-1. The iodine-starch test result, from left to right: M1, M2, M3, M4, loess, sticky rice, XZM7, HYPT1 (sample details can be found in Chapter 3.1, pp. 54-60 and Table 3-3, pp. 79-83)

None of the modern and archaeological samples turned purple. Only the sticky rice sample turned dark purple after the iodine–KI reagent was added.

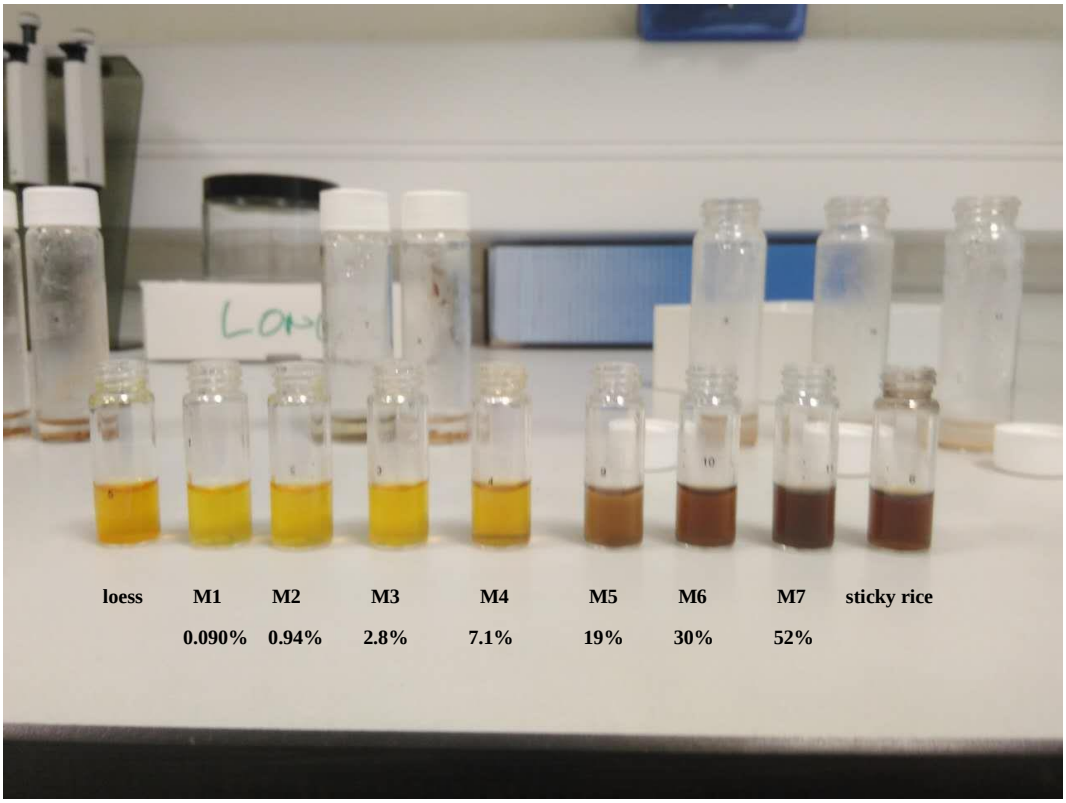


Fig 4-2. Additional iodine-starch test result, from left to right: loess, 7 modern samples (M1-M7, sample details can be found in Chapter 3.1, pp. 54-60), sticky rice

As shown in Figure 4-2, M5 turned to light purple, while M6 and M7 turned to dark purple after the iodine-starch test, indicating the existence of amylopectin.

The iodine-starch test was also run on modern earth samples (the preparation details can be found in Chapter 3.1, pp. 54-60) with sticky rice content of 0%, 2%, 4%, 6%, 8%, 10%, 12%, 14%, 16%, 18%, 20% and 100%. The colour was measured by colorimetry, which shows the result in Figure 4-3.

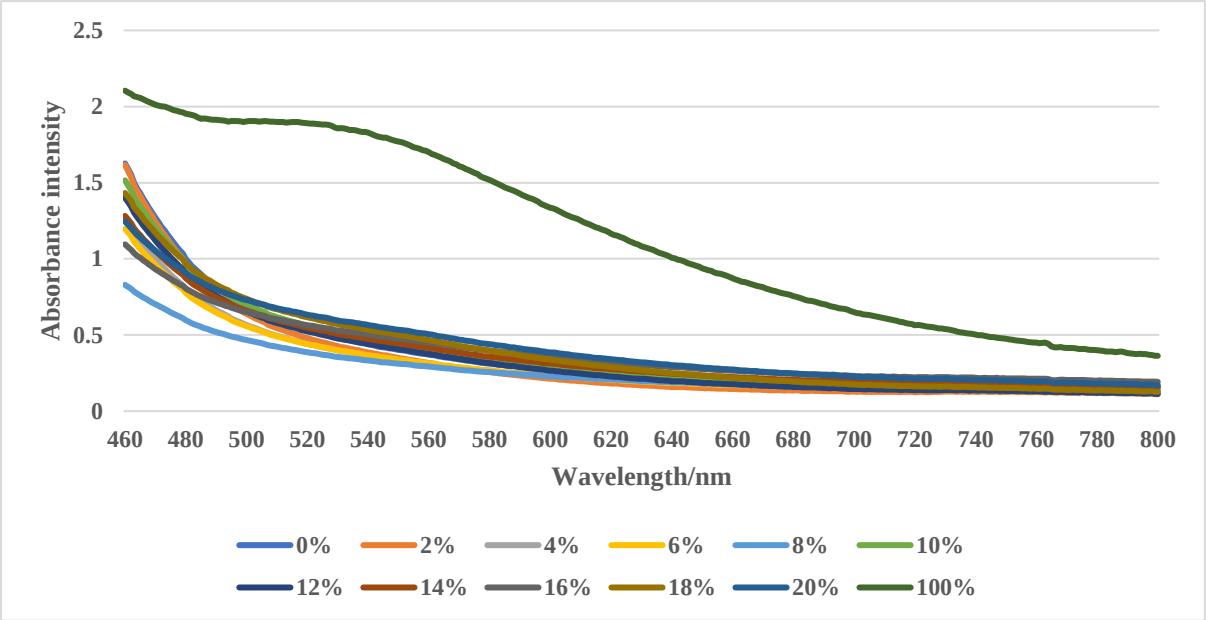


Fig 4-3. Absorbance intensity from 460 nm to 800 nm of modern samples after the iodine-starch test

There is an absorption peak caused by the iodine-starch test of amylopectin around 530 nm in the curve of the pure sticky rice sample (Yan, 2016). However, the absorption peak is not apparent in the curves of other modern samples, especially in samples with low sticky rice content.

4.4. Discussion

The iodine-starch test failed to obtain a positive result in earth samples with a sticky rice content of no more than 7.1%. Due to the difficulty of visually judging the colour change, colorimetry was employed to observe the presence of a peak at 530 nm, corresponding to the absorbance of the iodine-amylopectin complex. The observations

indicated that in samples with a sticky rice content of less than 20%, no significant peak was detected at 530 nm (as shown in Figure 4-3). To further quantify these results, the absorbance intensity was measured and recorded at 530 nm across all tested modern samples.

Figure 4-4 displays the absorbance intensity at 530 nm for the tested modern samples, which is used to assess the applicability of the iodine-starch test in identifying amylopectin from earth samples.

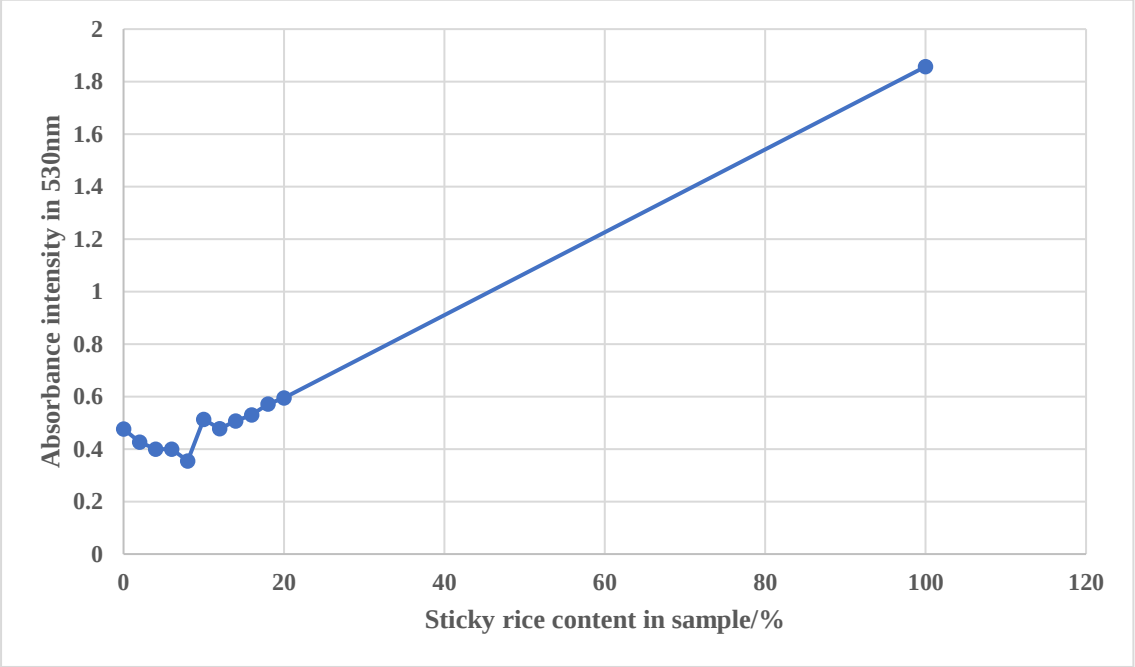


Fig 4-4. Absorbance intensity at 530 nm of modern samples after the iodine-starch test

The colorimetry result in Figure 4-4 shows that the absorbance intensity at 530nm of

modern samples with no more than 10% sticky rice content fluctuates between 0.3551 and 0.5133. When the sticky rice content is more than 10%, the absorbance intensity and the sticky rice content exhibit a linear relation. The linear fitting result is shown in Figure 4-5.

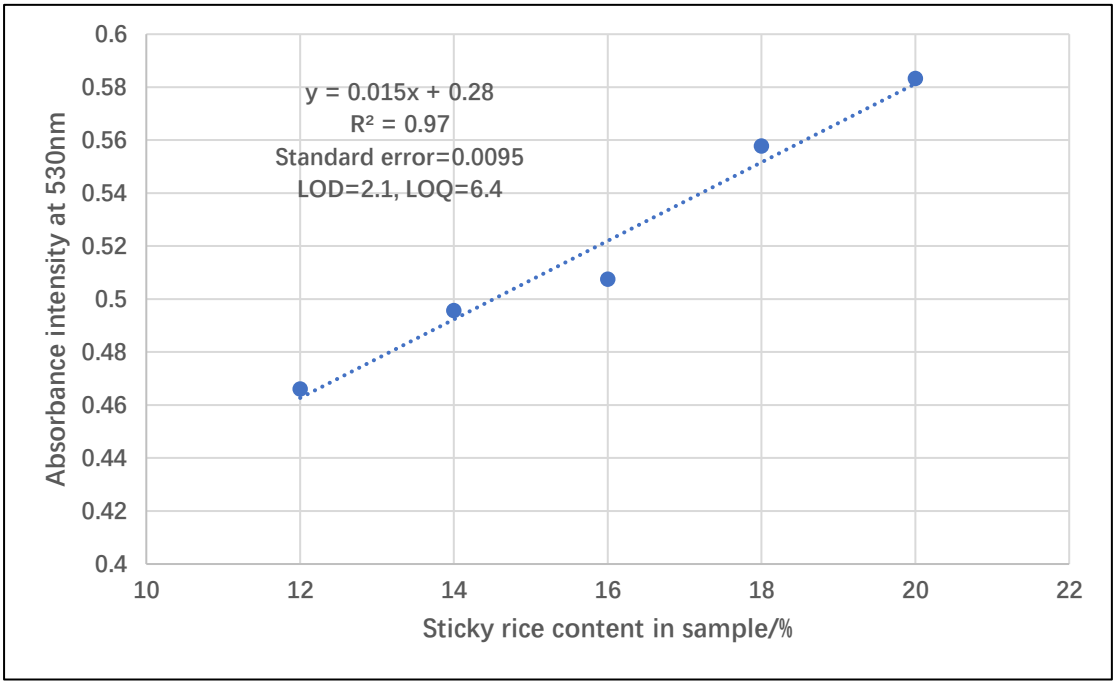


Fig 4-5. The linear fitting result of absorbance intensity at 530 nm of modern samples (sticky rice content 12%-20%) after the iodine-starch test

Although the limit of detection (LOD) and limit of quantification (LOQ) are 2.1% and 6.4% respectively, as calculated in Figure 4-5, the fluctuation of absorbance intensity at 530 nm of tested earth samples with sticky rice content from 0% to 10% would make the iodine-starch test an infeasible method to identify amylopectin from earth samples containing less than 10%. Furthermore, as shown in Figure 4-4, when the

sticky rice content is no less than 18%, the absorbance intensity exceeds the maximum intensity value of samples containing sticky rice from 0% to 10%. Thus, the iodine-starch test cannot achieve a reliable positive result for the earth samples with sticky rice content lower than 18%, which means that it is likely to be ineffective for archaeological samples.

As shown in a case study in Jiangyin, Jiangsu province, the content of added organics in soil samples is around 1%-2% (Meng, 2011). Therefore, the iodine-starch is not a sensitive method for the analysis of amylopectin in soil samples. It could not be used in the screening step.

4.5. Conclusions

Although the iodine-starch test has been widely applied in many previous studies to identify starch (such as sticky rice or flour), it is not suitable for either the screening or identification steps. This is because the test does not produce reliable positive results for samples with sticky rice content below 18%, which is significantly higher than the organic content typically found in archaeological samples.

5. Fourier transform infrared spectroscopy (FTIR)

This study examines the effectiveness of FTIR in detecting starch within earth samples and its potential as a screening tool. FTIR identifies functional groups, but its efficacy can be doubtful in complex mixtures due to interference from substances like quartz, common in soil, which can obscure the characteristic absorbance peaks of organic compounds such as starch (detailed discussion can be found in Chapter 2.3.1). Thus, it is hypothesised that FTIR may not effectively quantify starch content in soil samples.

However, FTIR's rapid and convenient operation could still be useful in preliminary screening to identify soil samples with sufficient organic content, thereby reducing costs and improving the efficiency of subsequent, more detailed analyses.

This chapter aims to validate the practical application of FTIR in soil sample analysis and explore its application in the screening step.

5.1. Samples

The FTIR test (Jeffery et al., 1989) was applied to loess, sticky rice powder, modern (n = 4) and archaeological (n = 50) samples. Details can be found in Chapter 3 (pp. 54-83).

5.2. Methods

All the samples were ground into powder before FTIR and kept in a desiccator. Samples (0.5 g-1.0 g) were directly analysed on a Cary 640 Series FTIR spectrometer with a Pike ATR stage from Agilent Technologies by the author in Research Laboratory for Archaeology and the History of Art, University of Oxford. Spectra were collected from 400 to 4000 cm^{-1} with 64 scans of acquisition with a resolution of 4 cm^{-1}. The removal of background (carbon dioxide) and marking of characteristic peaks were accomplished by Thermo Fisher Scientific Inc. OMNIC 8.2.0.387.

5.3. Results

The FTIR spectra of modern samples M1-M4 (sample details can be found in Table 3-1, pp. 71-73) are shown below. Distinct peaks at around 500, 1000 and 1400 cm^{-1} can be observed in these 4 spectra. Variations among the samples can be observed at around 2800-3000 cm^{-1} and at around 3000-3500 cm^{-1}. A detailed discussion of these findings is presented in Chapter 5.4.

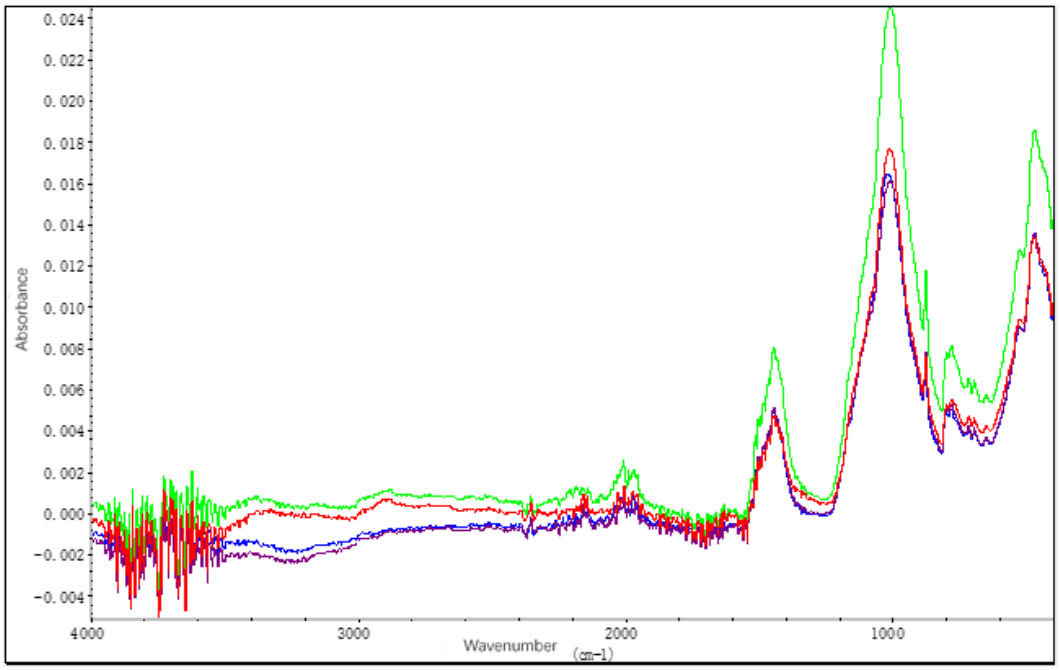


Fig 5-1. FTIR spectra of modern samples: M1 (blue line), M2 (purple line), M3 (green line) and M4 (red line)

All the modern and archaeological sample spectra can be found in appendix 1. The spectra of the loess and sticky rice can be found in Chapter 5.4.1.

5.4. Discussion

5.4.1. The characteristic peaks of the sticky rice in FTIR

Sticky rice and loess samples were used to locate the unique characteristic peaks for distinguishing sticky rice in soil samples. The structure of amylopectin is shown in Figure 5-2. As shown in the spectra of blank samples (sticky rice and loess) in Figure 5-3, there are 5 peaks in the FTIR spectra of sticky rice, which are strong enough to recognise. The peak at around 3000-3500 cm^{-1} is the stretching vibration of the

oxygen-hydrogen (O-H) bond. The peak at around 2800-3000 cm^{-1} is the stretching vibration of the carbon-hydrogen (C-H) bond. The peak at around 900-1100 cm^{-1} is the stretching vibration of the carbon-carbon (C-C) bond. The peaks at around 1000-1200 cm^{-1} are the stretching vibration of the carbon-oxygen (C-O) bond (Liu and Zhang, 2002).

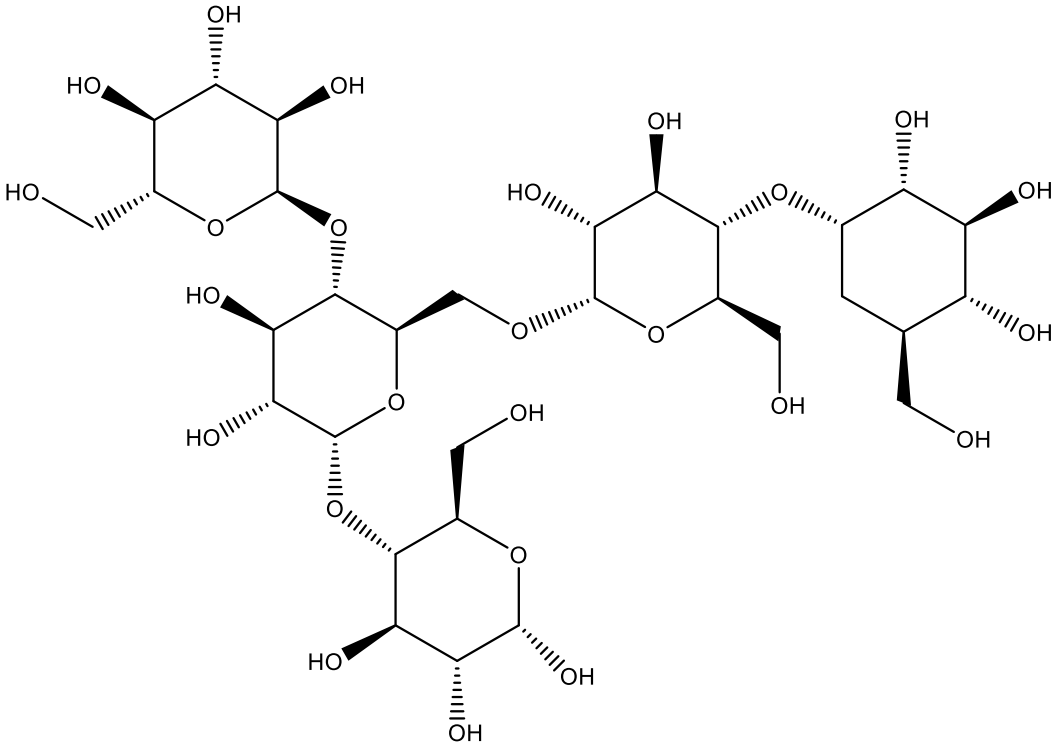


Fig 5-2. Structure of amylopectin

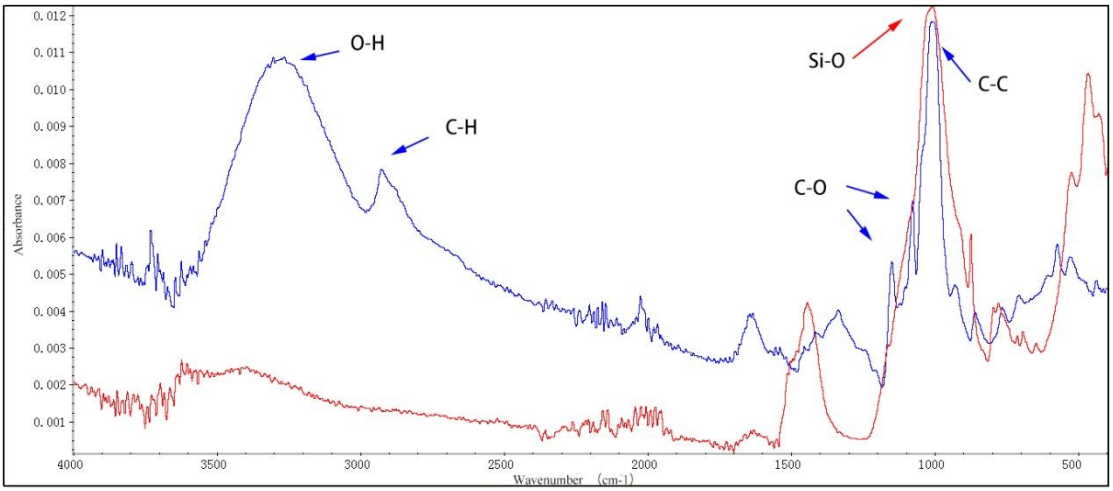


Fig 5-3. FTIR spectra of sticky rice (purple) and loess (red) (sample details can be found in Chapter 3.1, pp. 54-60)

However, the O-H bond of water is also in the same region as that of sticky rice (Liu and Zhang, 2002). Water is quite common and very difficult to remove from soil samples. C-O and C-C peaks at around 1000 cm^{-1} are high and sharp, which are easy to recognise. But in the spectrum of loess, there is also a peak at around 1000 cm^{-1}, which is the stretching vibration of silicon-oxygen (Si-O) bond coming from quartz in soil. The peak will block the peaks of C-C and C-O bonds in sticky rice. Thus, only peaks at around 2800-3000 cm^{-1} can be used for the identification of sticky rice. However, most organic materials have C-H bonds, which produce peaks at around 2800-3000 cm^{-1} into the spectra. Therefore, peaks at around 2800-3000 cm^{-1} can only be used for the identification of organics in soil samples. But it can also be used in the screening step as a simple mark of enough organics for following extraction and identification steps.

The spectrum for BWC1 from the Bawangcheng site is shown in Figure 5-4. Several peaks at around 2800-3000 cm^{-1} can be found in it. Unlike the sharp peak in the spectrum of sticky rice, these peaks mean there are a lot of peaks in this region. It is very difficult to locate the same peak as in the sticky rice spectrum. The only conclusion that can be drawn is that there are organics in this sample, and they are more diverse than in sticky rice. Thus, this sample can be selected for the next extraction and identification steps.

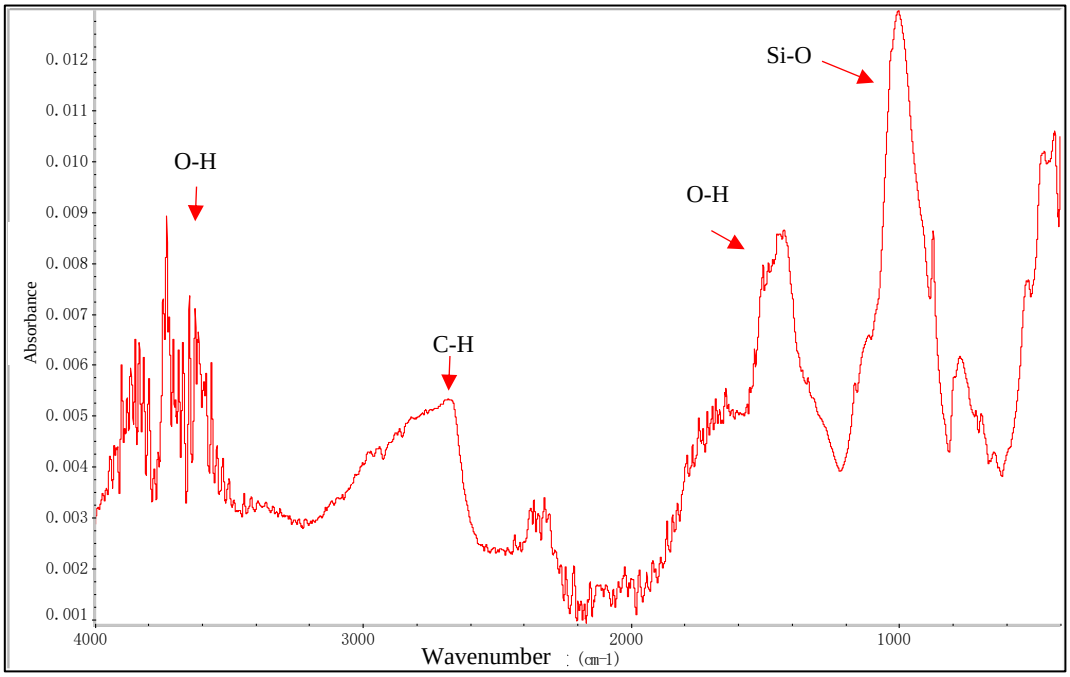


Fig 5-4. FTIR spectrum of BWC1 from Bawangcheng

Figures 5-5, 5-6, 5-7 and 5-8 show the spectra of samples from the Pingtaocheng, Shangjiaoyang Tulou, Xingyangguchengand Xinzhengmen sites. Peaks can also be found around 2800-3000 cm^{-1}, which means that there are enough organics in these

samples for later steps.

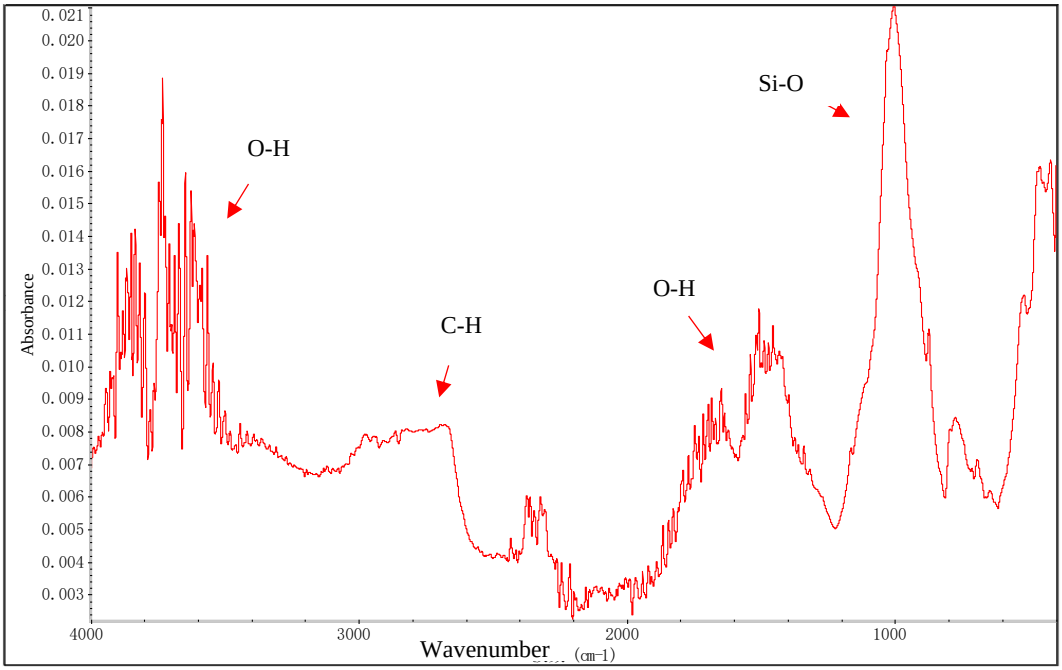


Fig 5-5. FTIR spectrum of PTC3 from Pingtaocheng

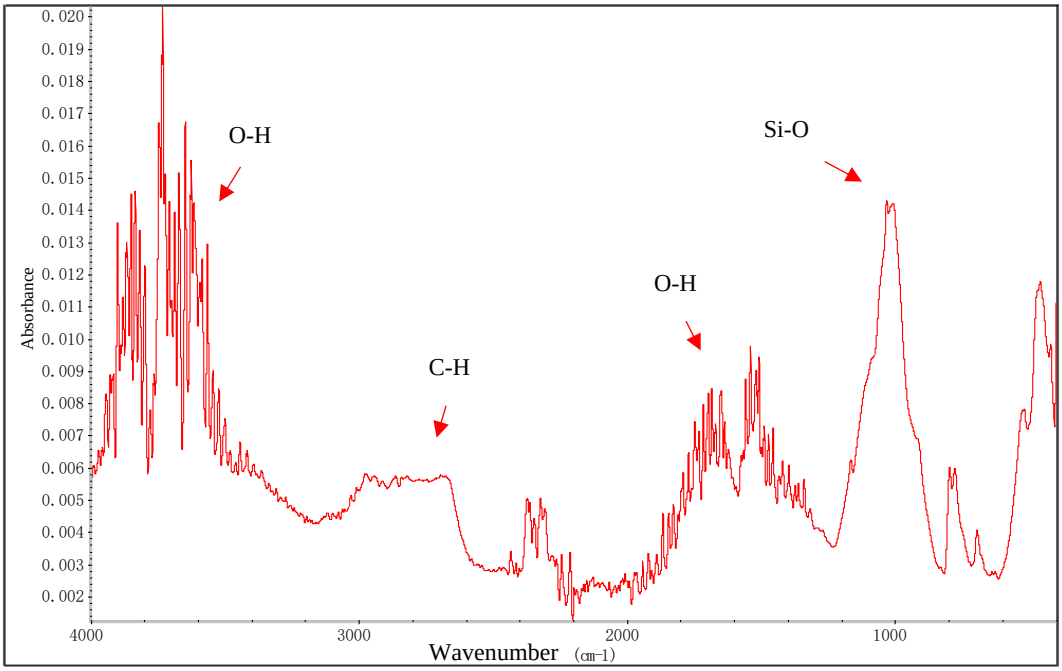


Fig 5-6. FTIR spectrum of SJYTL1 from Shangjiaoyang Tulou

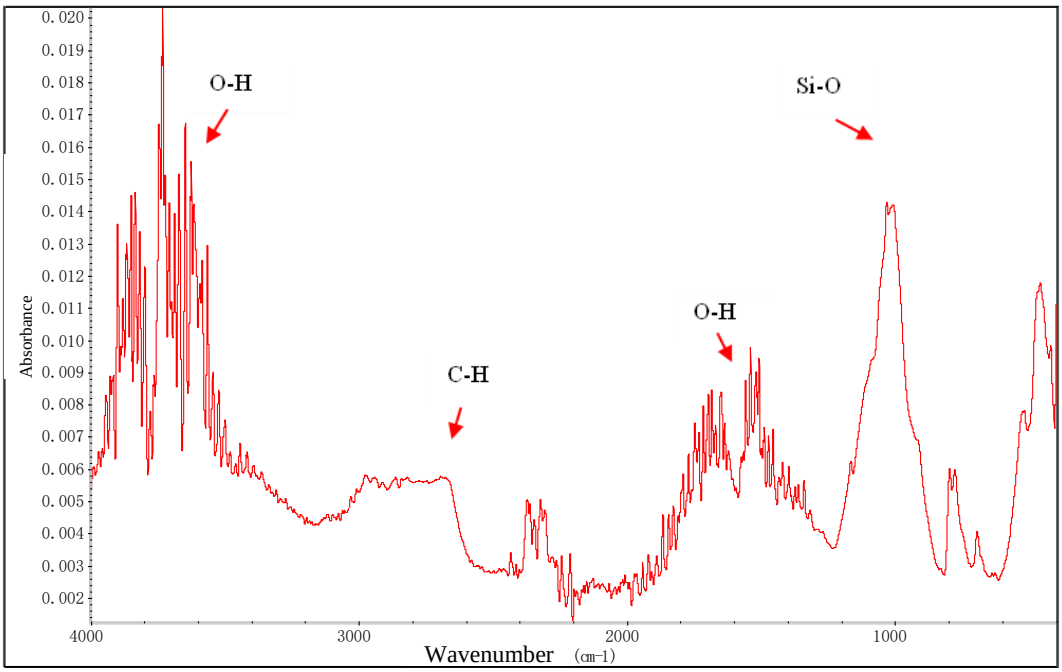


Fig 5-7. FTIR spectrum of XYGC1 from Xingyangguchengg

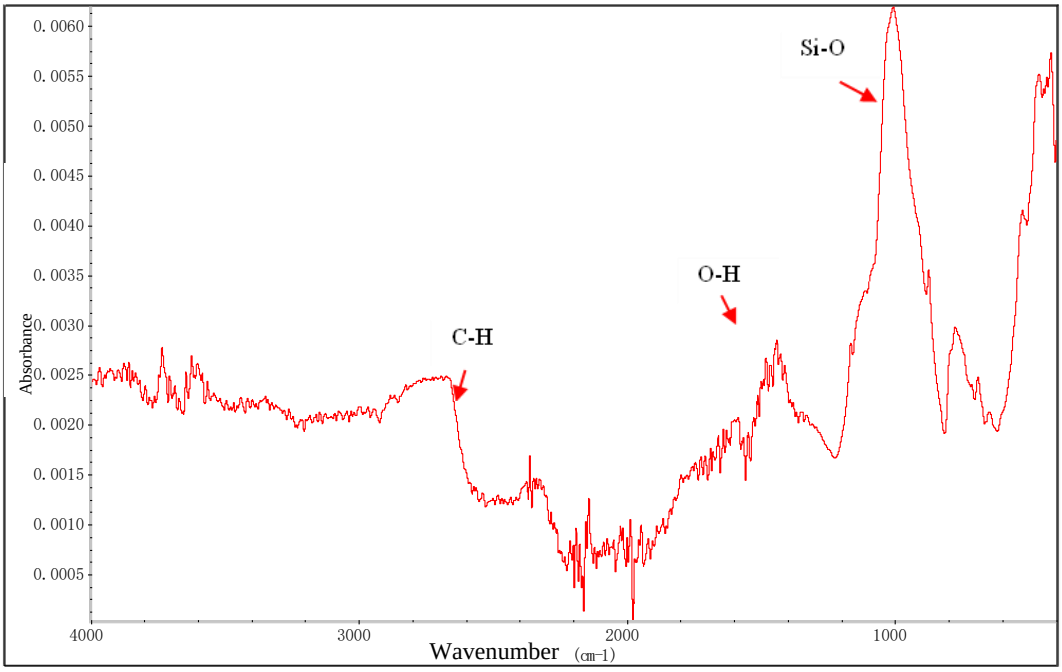


Fig 5-8. FTIR spectrum of XZM1 from Xinzhengmen

Figure 5-9 shows the spectra of samples from the tomb of Zhao Boyun. Peaks can be found around 2800-3000 cm^{-1} in every spectrum. Sample ZBYM3 (the red line shown in Figure 5-9, sample details can be found in Table 3-3, pp. 79-83) is a resin-like sample. The peaks for inorganics, especially the Si-O bond near 1000 cm^{-1}, can hardly be found in its spectrum. The implication is that this sample contains a high amount of organics, which may be the raw materials added into construction materials.

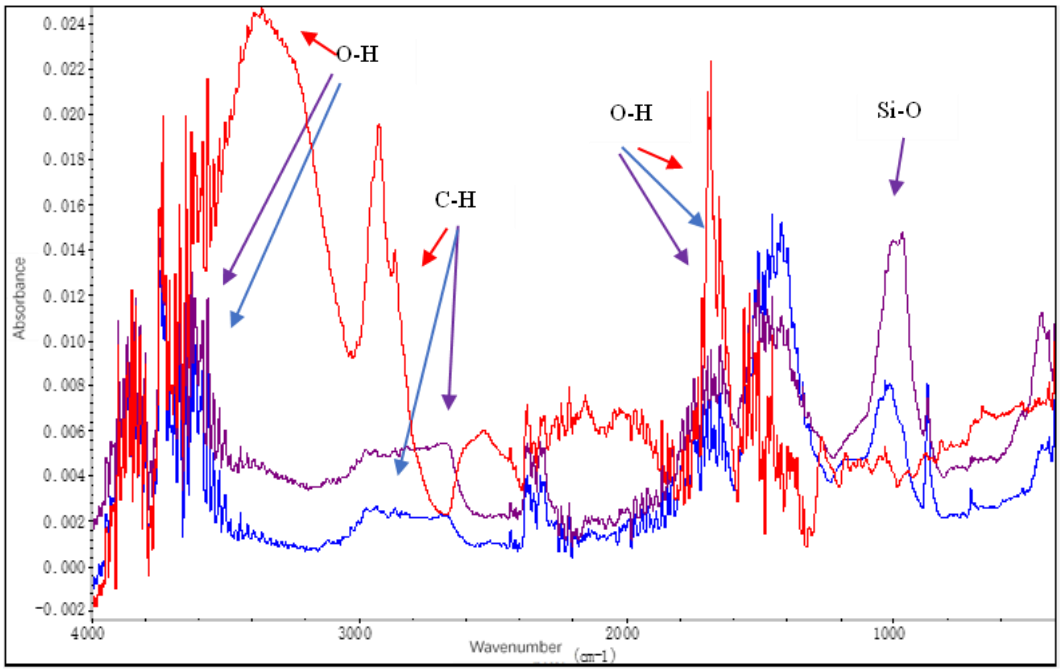


Fig 5-9. FTIR spectra of ZBYM1-3 (red, blue and purple lines, sample details can be found in Table 3-3, pp. 79-83) from the tomb of Zhao Boyun

Though not so many samples were collected at the above sites, spectra of samples from the house of the Zhang family, Fort Jingyuan and Fort Hongyuan still indicate the existence of organics in these samples, as shown in Figure 5-10.

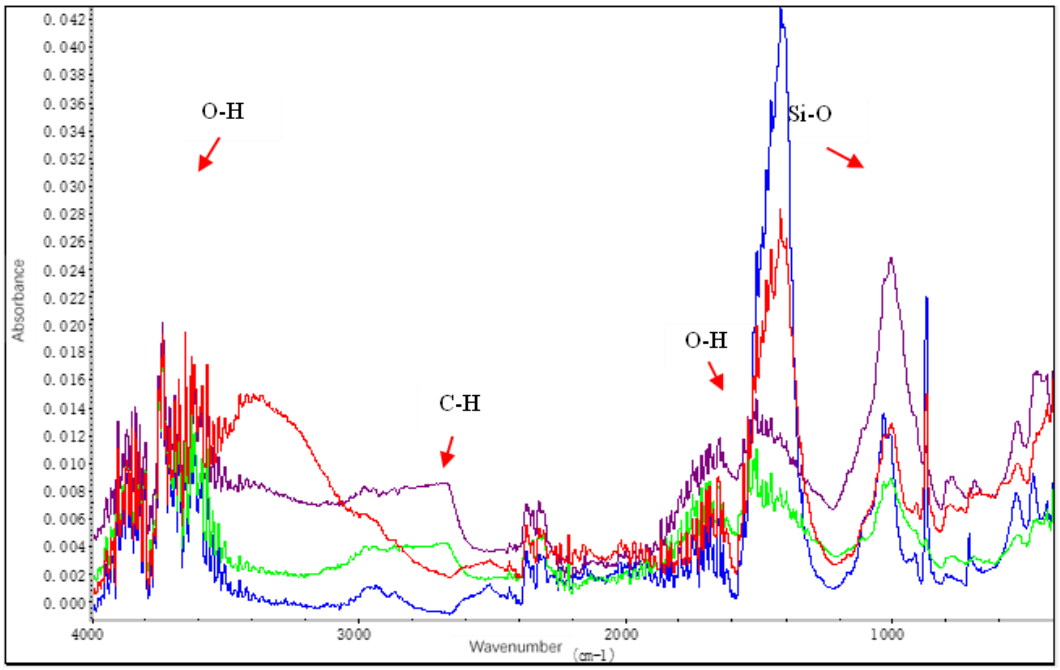


Fig 5-10. FTIR spectra of HNZZ1, JYPT1 and HYPT1 from the house of the Zhang family (blue line), Fort Jingyuan (red and green lines) and Fort Hongyuan (purple line) (sample details can be found in Table 3-3, pp. 79-83)

In the spectrum of HNZZ1 (the blue line in Figure 5-10) and JYPT2 (the red line in Figure 5-10), there are several peaks at around 1400-1500 cm^{-1}, which are the bending vibration of the CH bond (Liu and Zhang, 2002). That means the organics in these 2 samples are different from the others, which may be due to the application of different materials or the different degradation processes.

5.4.2. The detection limit of FTIR

To determine the detection limit of FTIR for organic content in soil samples, 4 modern samples (M1-M4) with varying concentrations of sticky rice (0.090%, 0.94%,

2.8%, and 7.1%, respectively) were analysed. The focus was on the 2800-3000 cm^{-1} range, where characteristic peaks for organics, including starch, are typically observed.

For each sample, the absorbance of the peak at around 2800-3000 cm^{-1}, noise level, and signal-to-noise ratio are shown in Table 5-1. The noise level was determined in the 2600-2700 cm^{-1} range, and the signal-to-noise ratio was calculated by dividing the peak absorbance by the noise level.

Table 5-1. Detection of organics in soil samples using FTIR

Sticky rice content (weight percentage)	Absorbance	Noise level	Signal-to-Noise Ratio
0.090%	-1.07e-3	2.50e-5	-42.7
0.94%	-1.29e-3	4.42e-5	-29.1
2.8%	5.45e-4	4.35e-5	12.5
7.1%	1.2e-5	7.62e-5	0.157

The results indicate that the signal of organics is more evident in the 2.8% sample, while the other samples have lower or negative signal-to-noise ratios, suggesting that the detection may be interrupted by noise or measurement errors. For M3 (sticky rice content 2.8%) and M4 (sticky rice content 7.1%), the signal-to-noise ratios were 12.5

and 0.157, respectively. The lower signal-to-noise ratio for the 7.1% sample compared to the 2.8% sample might be due to measurement variability. However, for M1 (sticky rice content 0.090%) and M2 (sticky rice content 0.94%), the signal-to-noise ratios were negative, indicating that the organic content in these soil samples is too low to be reliably detected by FTIR. Thus, the detection limit of FTIR for sticky rice in soil samples appears to be around 2.8%, as this is the concentration where the signal-to-noise ratio exceeds 10. This makes FTIR a much more sensitive method for screening earth samples containing enough organics for subsequent analyses than the iodine-starch test.

5.4.3. Shortcomings of FTIR

Figures 5-11 and 5-12 are the spectra for 3 samples from the Bamudun tomb and 3 from the Zhengzhou Shangcheng site. In every spectrum, there are peaks at approximately 2600-4000 cm^{-1} and 1600 cm^{-1}, which are the peaks for water (Liu and Zhang, 2002). The peaks at around 2600-4000 cm^{-1} are so high and broad that the peaks for identifying organics around 2800-3000 cm^{-1} cannot be found on the spectra. Because of the high water content in these samples, the water peaks cannot be removed, even after being kept in a desiccator.

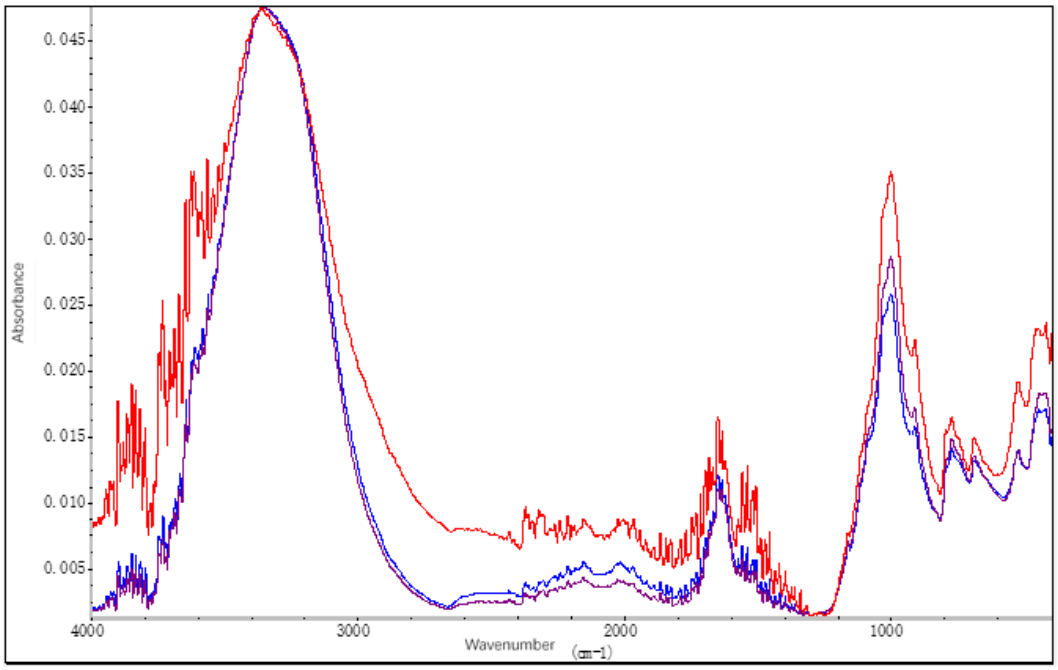


Fig 5-11. FTIR spectra of archaeological samples from the Bamudun tomb: BMD1 (blue line), BMD2 (purple line), BMD3 (red line)

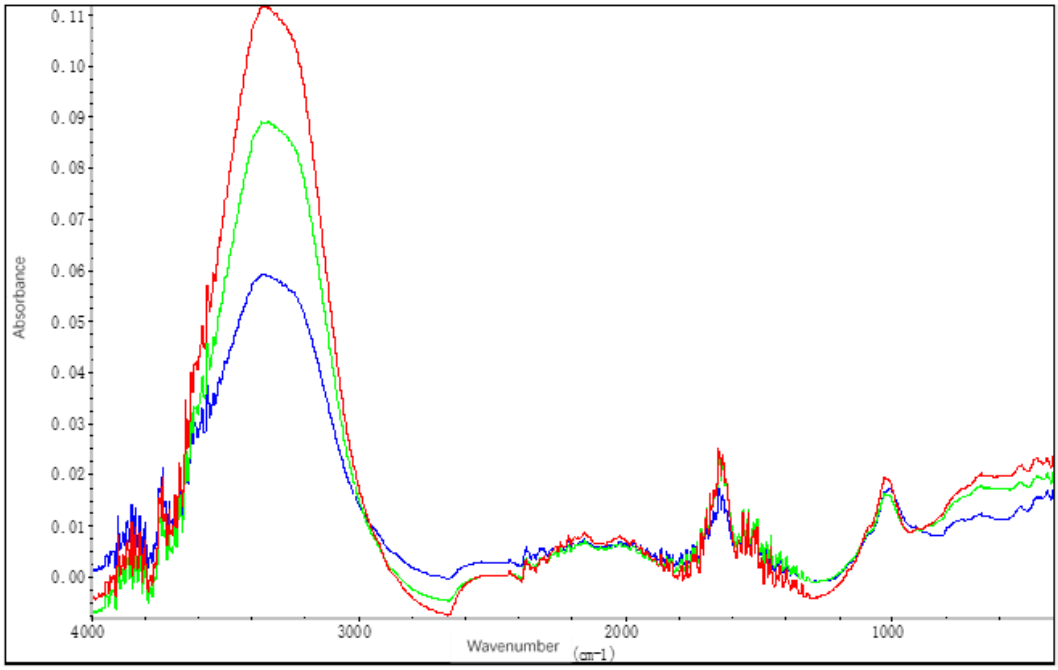


Fig 5-12. FTIR spectra of archaeological samples from Zhengzhou Shangcheng: ZZSC1 (blue line), ZZSC2 (red line), ZZSC3 (green line)

Therefore, peaks at around 2800-3000 cm^{-1} are challenging to differentiate from the existence of significant water peaks. Thus, wet samples must be dried before FTIR. However, the drying process needs to be very carefully done, or some organics may be lost. This topic will be discussed in Chapter 6.4.3.

FTIR can be used to screen samples with enough organics, but it cannot be applied for quantitative analysis without additional methods. According to the Lambert-Beer law, the peak height in the FTIR spectra are generally proportional to the concentration of the corresponding components. However, as shown in Table 5-1, the peak height around 2800-3000 cm^{-1} in the spectra of modern samples do not follow the expected order based on the sticky rice content. Specifically, the absorbance values follow the order M3 > M4 > M1 > M2, while the actual sticky rice content follows the order M4 > M3 > M2 > M1. This discrepancy indicates that the peak height around 2800-3000 cm^{-1} cannot accurately represent the sticky rice content in the samples. This may be due to factors such as overlapping peaks from other organic compounds (e.g. water) or measurement variability. FTIR's application in the deconvolution of mixtures by manual analysis is limited due to these factors. Therefore, for quantitative results, other methods such as LOI should be applied to these samples.

5.5. Conclusions

Although the FTIR test has been widely applied in many previous studies to identify

starch (such as sticky rice or flour), it is not suitable to identify starch in earth samples due to the existence of quartz. Moreover, FTIR is not a sufficiently specific and reliable analysis method to identify organics in a complex system. Therefore, FTIR cannot be used in the identification step. However, it could be a quick and effective method in the screening step to screen for the samples which may contain organics. Samples that exhibit pronounced peaks at around 2800-3000cm^{-1} will be selected for further analysis in later steps. “Wet samples” (archaeological samples that have high water peaks in the FTIR spectra) will also be selected.

6. Sequential loss on ignition (LOI) and thermogravimetric analysis -differential scanning calorimetry-differential thermal analysis (TGA-DSC-DTA)

LOI, a method of weighing the sample before and after ignition and determining the weight percent loss by difference (Dean, 1974), was used for the development of the screening step. A crucial aspect of this method is deciding the temperature at which complete decomposition of organic matter in earth samples occurs. To address this challenge, TGA-DSC-DTA, a combination of thermal analysis techniques of assessing material properties under varying temperatures (Wunderlich, 1990), was applied. The choice of TGA-DSC-DTA was driven by its ability to provide precise information on the thermal behaviour of materials, allowing for the accurate determination of the appropriate temperatures for LOI. By employing these techniques, a deeper understanding of the decomposition process was expected. Earth samples containing sufficient organics could then be screened for further analysis.

6.1. Samples

The TGA-DSC-DTA test was applied to unbaked loess, baked loess, 2 modern earth samples, M4 and M6, and 3 archaeological samples, HYPT1, SJYTL3 and XZM7. Details can be found in Chapter 3 (pp. 54-83). The unbaked loess was selected to understand the natural loess content, while the baked loess served as a background study since all modern samples were made from baked loess. Modern samples were used to explore detection limits, and archaeological samples were chosen to observe

the application of TGA-DSC-DTA in archaeological contexts. Considering the complexity and high cost of the tests, only 3 samples from different sites were selected.

The LOI test was applied to the same modern and archaeological samples as those used in the FTIR test, as listed in Chapter 5.1, to ensure consistency in the screening process. Further details of these samples can be found in Chapter 3 (pp. 54-83).

6.2. Methods

10 mg sample was measured and tested in Peking University, Beijing by a Q600 SDT TGA-DSC-DTA tester from room temperature to 800℃ with a ramp rate of 10 $K \cdot min^{-1}$. The atmosphere was air, and the flow rate was 100 $mL \cdot min^{-1}$. The TGA-DSC-DTA tests were run by Fei Zhang, a technician in the Analytical Instrumentation Centre, College of Chemistry and Molecular Engineering, Peking University.

The LOI method is based on the procedure described by Dean (1974) and the research conducted by Wang et al. (2011). I ran the tests in Research Laboratory for Archaeology and the History of Art, University of Oxford.

1. All the samples were ground into powder and kept in a desiccator before LOI. A clean ceramic crucible was dried in an oven at 450℃ for 1 hour. After cooling to

room temperature in a desiccator, it was weighed precisely by a digital analytical balance (0.001 g), and the value was recorded as W_1.

2. Around 2 g sample was added into the crucible and weighed, and the value was recorded as W_2. Then the sample and crucible were heated in a muffle furnace at 100℃ for 1 hour. After cooling to room temperature in a desiccator, the sample and crucible were weighed, and the value was recorded as W_3.

3. The sample and crucible were returned to the muffle furnace and heated to 450℃ for 2 hours. The sample and crucible were weighed again after cooling to room temperature in a desiccator, and the value was recorded as W_4.

For the modern experimental samples, the loess had already been baked at 100℃ to constant weight (13 hours). Thus, only steps 1 and 3 were applied.

The loss on ignition was then calculated by:

$$LOI100 = \frac{W_2 - W_3}{W_2 - W_1} \times 100\%$$

$$LOI450 = \frac{W_3 - W_4}{W_2 - W_1} \times 100\%$$

W_1 is the weight of the crucible. W_2 is the weight of the crucible and sample before

heating. W_3 is the weight of the crucible and sample after heating to 100℃. W_4 is the weight of the crucible and sample after heating to 450℃. $LOI100$ is the loss on ignition at 100℃. $LOI450$ is the loss on ignition at 450℃.

6.3. Results

The results of the TGA-DTA-DSC tests are shown in appendix 2, and further discussion about these results can be found in Chapter 6.4.1.

The LOI results of the modern earth samples are shown in Table 6-1.

Table 6-1. LOI result of modern samples (sample details can be found in Table 3-1, pp. 71-73)

Sample	Sticky rice content (weight percentage)	LOI450 (weight percentage)
M1	0.090%	0.675%
M2	0.94%	0.917%
M3	2.8%	2.999%
M4	7.1%	6.911%

The results of archaeological samples are shown in Table 6-2.

Table 6-2. LOI result of archaeological samples (sample details can be found in Table 3-3, pp. 79-83)

Sample	LOI100	LOI450
XZM1	0.748%	0.951%
XZM2	1.107%	2.049%
XZM3	0.779%	1.143%
XZM4	1.605%	2.354%
XZM5	1.176%	1.934%
XZM6	0.828%	2.030%
XZM7	1.433%	5.709%
XZM8	1.461%	2.428%
BWC1	0.859%	2.509%
BWC2	0.827%	1.113%
BWC3	1.124%	1.154%
BWC4	1.029%	1.708%
BWC5	0.663%	1.166%
BWC6	0.812%	1.359%
BWC7	0.970%	2.110%
BWC8	0.948%	1.415%
BWC9	0.996%	1.092%
PTC1	1.496%	1.916%

PTC2	1.581%	2.070%
PTC3	1.561%	1.607%
PTC4	1.492%	2.262%
PTC5	1.929%	2.063%
PTC6	1.710%	1.821%
PTC7	1.611%	2.016%
PTC8	1.406%	1.895%
XYGC1	13.309%	2.341%
XYGC2	1.679%	2.606%
XYGC3	1.701%	2.622%
XYGC4	1.887%	3.181%
XYGC5	1.744%	2.166%
XYGC6	1.726%	2.164%
XYGC7	1.595%	1.979%
SJYTL1	2.748%	3.496%
SJYTL2	1.224%	3.564%
SJYTL3	1.655%	4.115%
SJYTL4	0.597%	2.240%
SJYTL5	0.899%	2.900%
HYPT1	2.354%	6.724%
JYPT1	1.709%	5.033%

JYPT2	1.207%	10.863%
ZZSC1	0.883%	1.401%
ZZSC2	0.625%	1.371%
ZZSC3	0.838%	1.059%
HNZZ1	0.887%	4.322%
ZBYM1	1.938%	6.158%
ZBYM2	3.280%	8.094%
ZBYM3	1.139%	96.681%
BMD1	1.847%	3.036%
BMD2	1.837%	2.980%
BMD3	2.007%	3.981%

6.4. Discussion

6.4.1. TGA-DTA-DSC and LOI

In Figure 6-1, there is a weight loss between around 630℃ to 700℃ in the TGA curve of the baked loess, as well as a peak at around 690℃ in the DTA and DSC curves. It is the decomposition temperature of calcium carbonate in TGA (Li and Pang, 2014). This weight loss or peak can also be found in unbaked soil, M4 and M6 (which are shown in Figures 6-2, 6-3 and 6-4), all of which have the same loess components. For HYPT1, the weight loss between around 630℃ to 700℃ and peak

on the heat flow curve around 690℃ still exist, indicating calcium carbonate may also be in this sample. XZM7 and SJYTL are pretty different. There are two possible explanations: 1) there is no calcium carbonate in these samples; 2) some other materials shift the decomposition temperature of calcium carbonate in TGA.

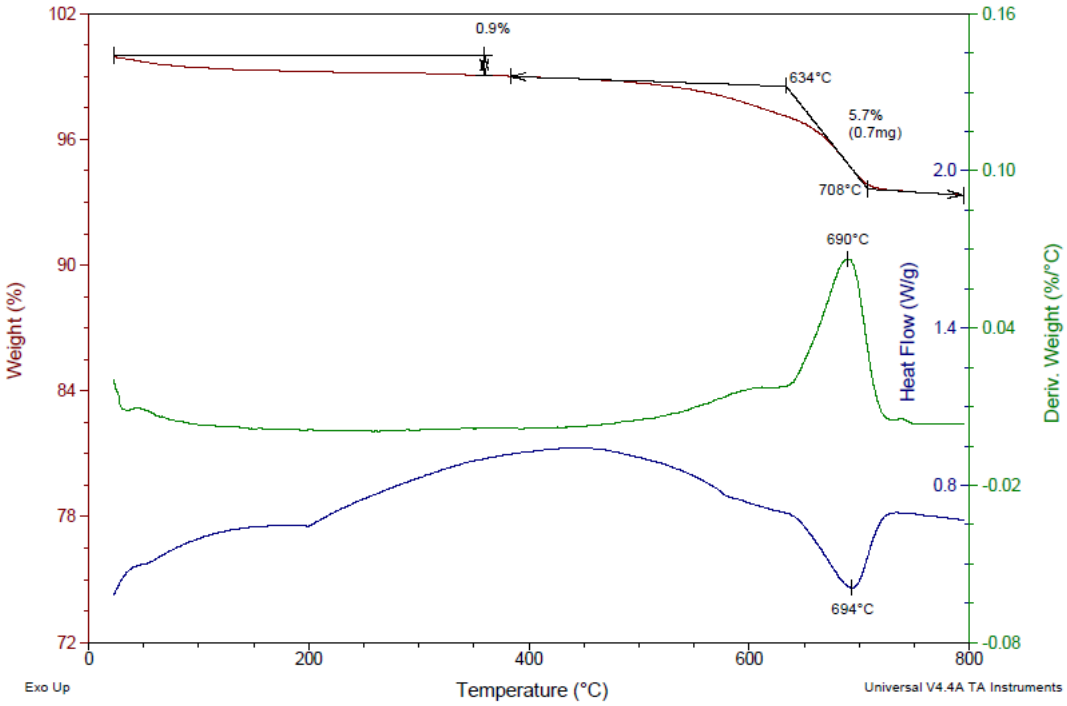


Fig 6-1. TGA-DTA-DSC result of baked loess: the red line is TGA, the green line is DTA, and the blue line is DSC. Sample details can be found in Chapter 3.1 (pp. 54-60)

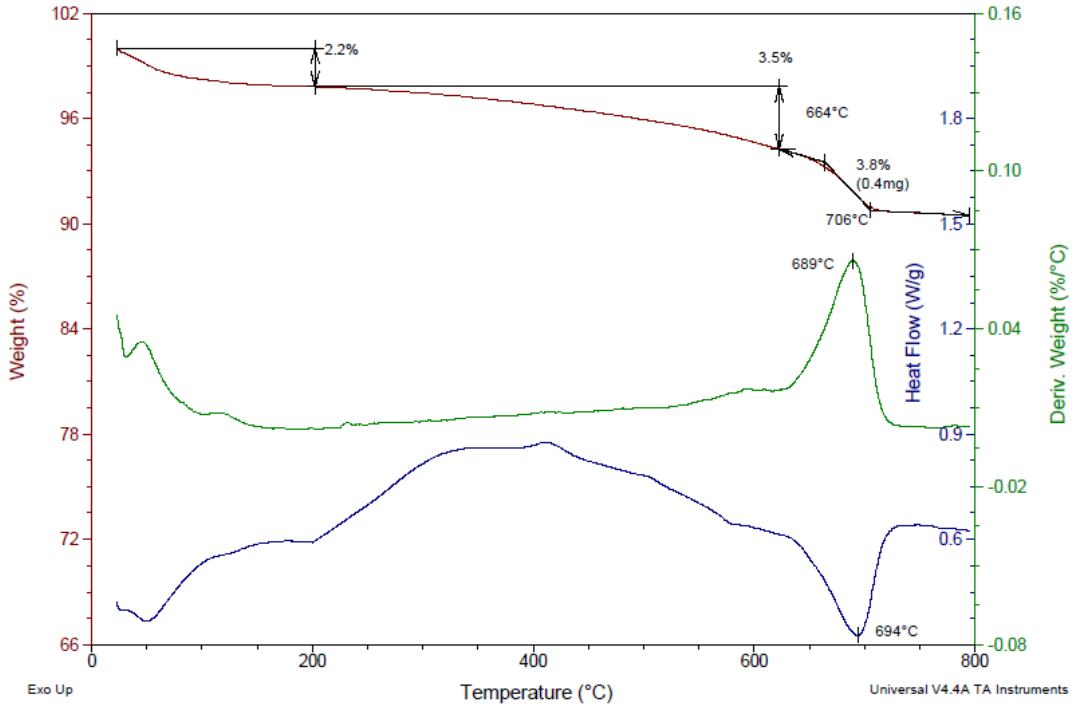


Fig 6-2. TGA-DTA-DSC result of unbaked loess: the red line is TGA, the green line is DTA, and the blue line is DSC. Sample details can be found in Chapter 3.1 (pp. 54-60)

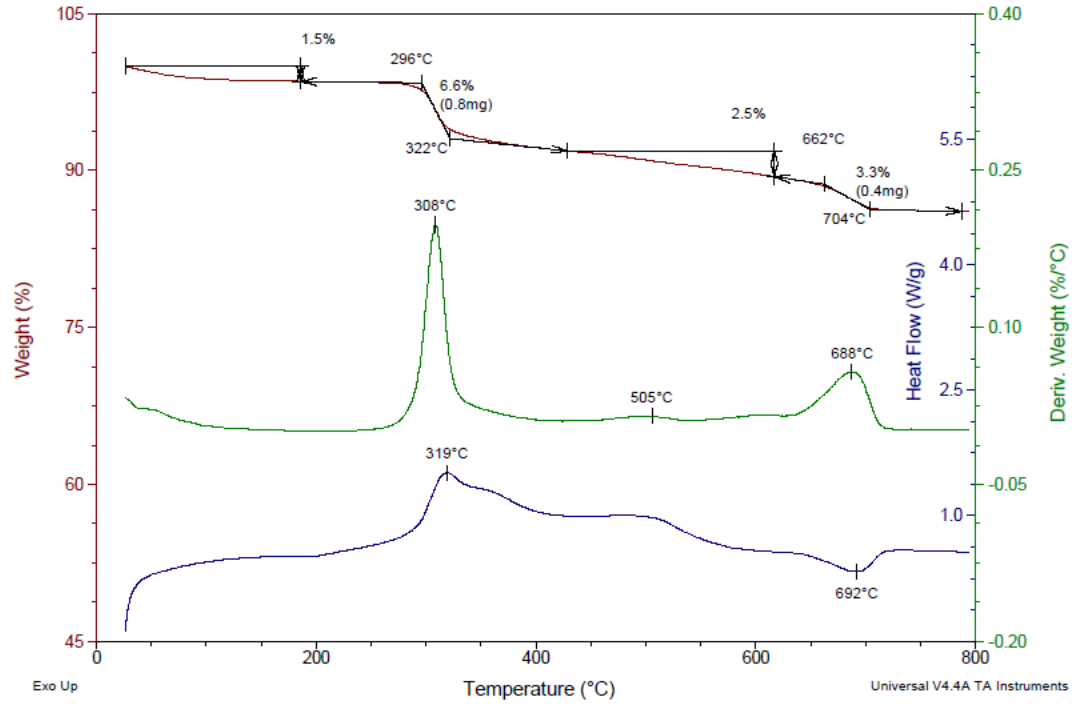


Fig 6-3. TGA-DTA-DSC result of M4: the red line is TGA, the green line is DTA, and the blue line is DSC. Sample details can be found in Table 3-1 (pp. 71-73)

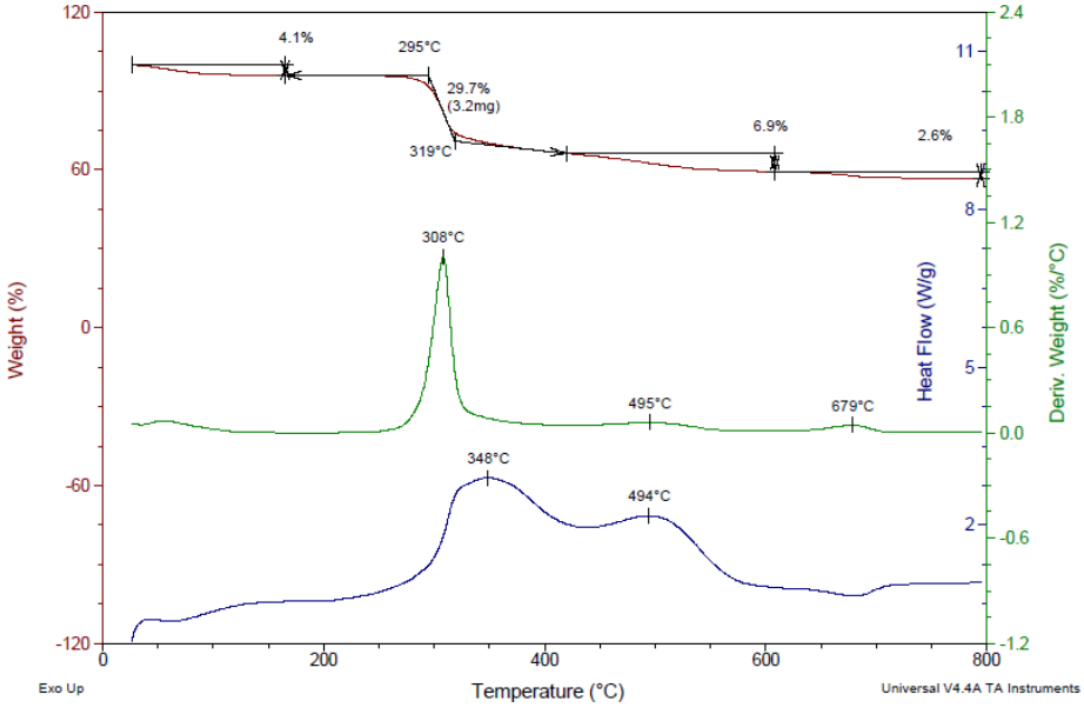


Fig 6-4. TGA-DTA-DSC result of M6: the red line is TGA, the green line is DTA, and the blue line is DSC. Sample details can be found in Table 3-1 (pp. 71-73)

According to the weight loss shown in Figures 6-3 and 6-4, the weight loss caused by the decomposition of sticky rice predominantly occurs between approximately 300℃ to 450℃ (for M4, some part of the organic loss is under 200℃). The sticky rice contents in M4 and M6 are 7.1% and 29%, which are approximately equal to the weight loss, 6.6% and 29.7% in Figures 6-3 and 6-4. The conclusion can be drawn that the main part of the sticky rice loss in TGA occurs at around 300℃ to 450℃, and others are at under 200℃. Moreover, as shown in Figures 6-1, 6-2, 6-3 and 6-4, there are weight losses between around 450℃ to 600℃ in baked loess, unbaked loess, M4 and M6, which cannot be the weight loss caused by the decomposition of sticky rice. Thus, the weight loss of modern samples under 800℃ can be divided into 4 stages: 1) below 200℃, mainly due to the evaporation of water and a small part of organics; 2) approximately 300℃ to 450℃, mainly due to the decomposition of sticky rice; 3) between about 450℃ to 600℃, mainly due to the decomposition of other components in loess (not calcium carbonate); 4) between around 630℃ to 700℃, mainly due to the decomposition of calcium carbonate.

Different from the TGA results of modern samples and loess, weight loss curves for the archaeological samples do not have a pronounced weight loss in a narrow temperature region. They decrease gradually from 200℃ to 600℃, meaning that they may have more diverse organic components than sticky rice.

According to the TGA results, 100℃ and 450℃ could be fixed for the heating cycle of LOI for rammed earth samples. Compared with LOI, TGA shows the whole process of heating samples. If combined with FTIR or MS, TGA may give far more information than LOI. However, LOI is much more operable and cost-effective than TGA. Although LOI can only offer a narrower data scope compared to TGA, it is a more effective and economical method to measure the organic content in samples in the screening step.

6.4.2. The detection limit of LOI

The recovery rate of LOI on modern samples (LOI data can be found in Table 6-2) has been calculated. The result is shown in Table 6-3.

Table 6-3. The recovery rate of LOI on modern samples

	Sticky rice content (weight percentage)	LOI450	Recovery rate
M1	0.090%	0.68%	756%
M2	0.94%	0.92%	98%
M3	2.8%	3.0%	107%
M4	7.1%	6.9%	97%

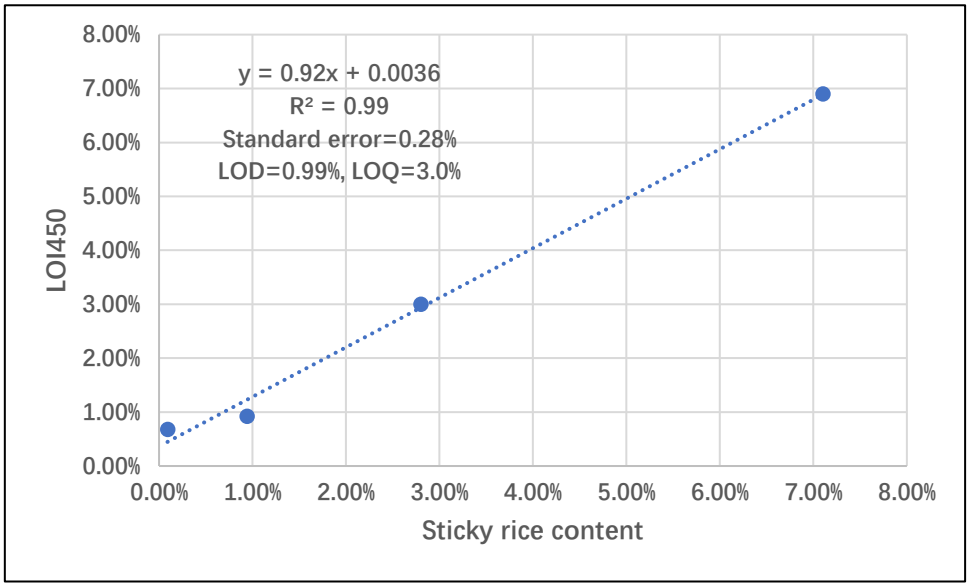


Fig 6-5. The linear fitting result of LOI on modern samples

As shown in Figure 6-5, the LOD and LOQ for LOI are 0.99% (compared to 2.8% for FTIR) and 3.0% respectively, indicating that LOI is a better method for quantitative analysis than FTIR in the screening step.

6.4.3. Shortcomings of LOI

Compared with modern samples made of baked loess and organic materials, archaeological samples are quite different. Some of them may contain much water, even after they were kept in the desiccator before the test, as shown in Figures 5-11 and 5-12. A heating cycle has been run at 100℃ to remove water. However, organics may be lost from some samples in this heating cycle. As shown below in Figure 6-6, these are the FTIR spectra of SJYTL3 (one sample from the Shangjiaoyang Tulou site) before LOI, after the heating cycle at 100℃ and after the heating cycle at 450℃.

The peaks at around 2800-3000 cm^{-1} for the organics have been partially (100℃) and completely (450℃) removed together with the water peaks at about 2600-4000 cm^{-1}.

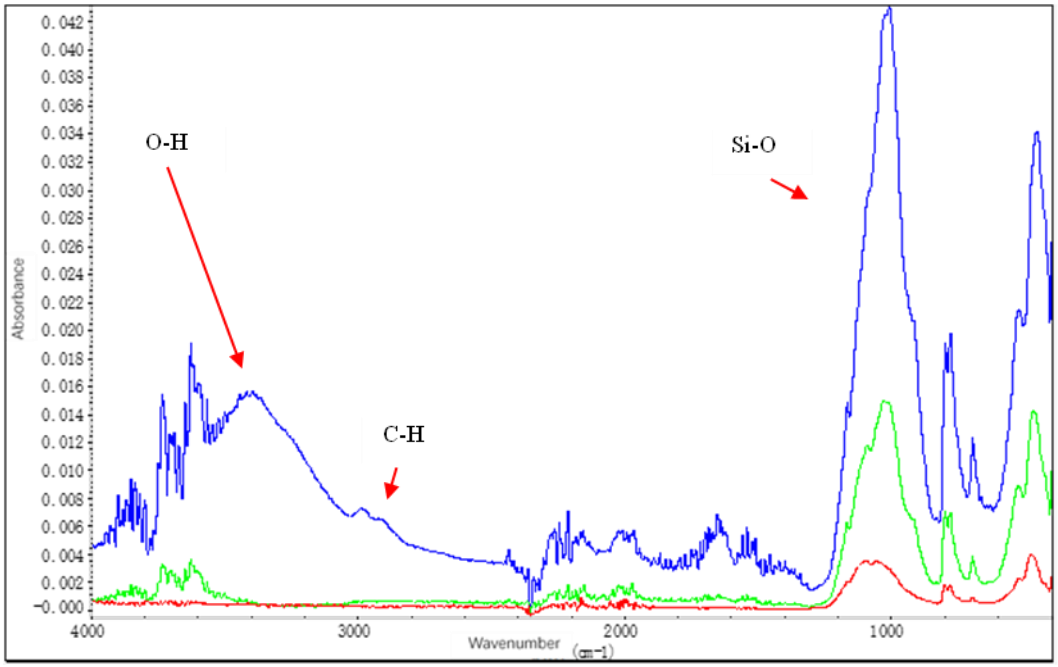


Fig 6-6. FTIR spectra of SJYTL3 in the LOI: before LOI test (blue line), after being heated at 100℃ (green line) and after being heated at 450℃ (red line)

Thus, LOI100 should also be taken into consideration in the screening step. Samples with high LOI100 values but low LOI450 values may also contain many organics. FTIR results could help solve this problem. “Wet samples” (samples with peaks at around 2800-3000cm^{-1} blocked by water peaks in FTIR spectra, for example, samples in Figures 5-11 and 5-12) will also be selected in the screening step.

6.5. Conclusions

LOI can be applied to estimate the organic content in earth samples. Although it cannot be used to identify the molecular structure of the organics in samples, it serves as a quick and effective method during the screening step to filter out samples that may contain organics. One advantage it has over FTIR is that LOI450 can be applied to detect the organics in earth samples without the interference of water. If LOI450 is higher than 0.99%, which is the detection limit of LOI, there may be a significant amount of organics in the samples. However, for samples with an organic content lower than 0.99%, the results from FTIR should be taken into consideration.

TGA-DTA-DSC, although superior to FTIR and LOI in terms of performance, are complex and expensive. Therefore, FTIR and LOI offer a reasonable alternative. However, TGA-DTA-DSC can be used to determine the appropriate temperature to apply in the LOI tests. 100℃ and 450℃ are suitable temperatures for the removal of water and organics, respectively, in LOI tests for rammed earth samples. Since a small amount of organic material was found to be burnt before reaching 100℃, LOI100 and LOI450 should be applied together in the screening step.

7. Thermogravimetric analysis-Fourier transform infrared spectroscopy (TGA-FTIR) and Thermogravimetric analysis- mass spectrometry (TGA-MS)

Compared with LOI, TGA covers the whole process of thermal decomposition in earth samples. More details, predominantly the weight loss at each temperature stage, can be obtained from the TGA tests. When coupled with other analytical methods, TGA may be applied in the identification step. The potential of using TGA-FTIR and TGA-MS is explored in this chapter. TGA-FTIR transports gases released from TGA to FTIR for identification. Similarly, TGA-MS transports the gases into a quadrupole mass spectrometer (Darribère, 2009). The selected ion monitoring mode is applied in TGA-MS to focus on specific ion masses. If specific molecules can be identified in the modern samples, they may be applied as biomarkers of the sticky rice or starch in earth samples. If the specificity and sensitivity can be confirmed, TGA-FTIR and TGA-MS will be ideal methods for the identification step.

7.1. Samples

The TGA-FTIR and TGA-MS tests were applied to sticky rice powder, unbaked loess, baked loess, 4 modern earth samples, M1 to M4, and 3 archaeological samples, HYPT1, SJYTL3 and XZM7. Details can be found in Chapter 3 (pp. 54-83). The loess and modern samples were selected to explore the specificity and sensitivity, while the archaeological samples were chosen to observe the application of TGA-FTIR and TGA-MS in archaeological contexts. Considering the complexity and high

cost of the tests, and for consistency with TGA, the same 3 archaeological samples were selected.

7.2. Methods

40mg sample was measured and tested by a Perkin Elmer TG-FTIR-MS tester from room temperature to 600℃ with the ramp rate of 20 $\mathrm{K \cdot min^{-1}}$. The atmosphere was nitrogen, and the flow rate was 45 $\mathrm{mL \cdot min^{-1}}$. The emitted gases were transported to a FRONTIER FTIR spectrometer at a flow rate of 70 $\mathrm{mL \cdot min^{-1}}$. The temperatures of transporting lines and the FTIR test zone were 280℃. Spectra were collected from 450 to 4000 $\mathrm{cm^{-1}}$ with a resolution of 8 $\mathrm{cm^{-1}}$. Then the gases were transported to a Clarus SQ8T quadrupole mass spectrometer at a flow rate of 70 $\mathrm{mL \cdot min^{-1}}$. The temperature of the ion source (EI) was 230℃, and the electron ionisation energy was 70 eV. The TGA-FTIR and TGA-MS tests were run by the author and Fei Zhang, a technician in the Analytical Instrumentation Centre, College of Chemistry and Molecular Engineering, Peking University.

7.3. Results and discussion

7.3.1. The potential of TGA-FTIR in the identification step

The potential of TGA, combined with FTIR, was explored to develop the identification step. If all the thermal decomposition products emitted in TGA can be

identified by FTIR or MS, more information about the earth samples could be obtained.

An example of TGA-FTIR result is shown below.

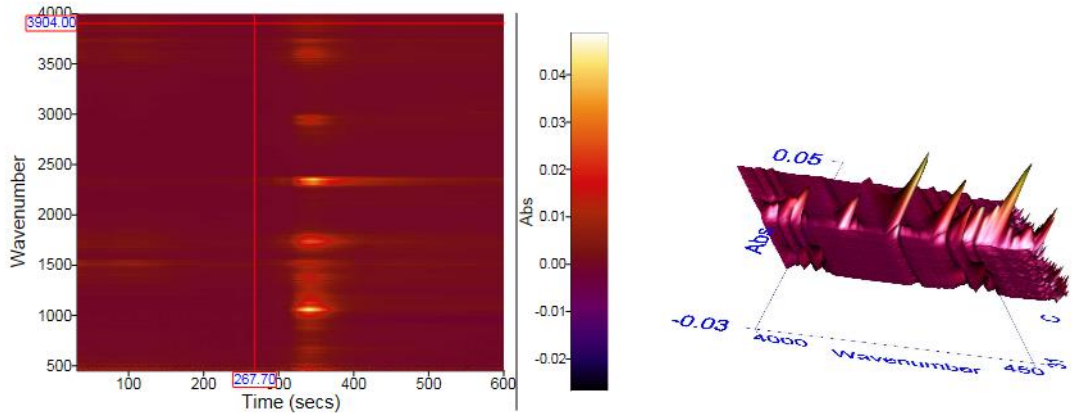


Fig 7-1. FTIR profile of the sticky rice with the change of temperature (sample details can be found in Chapter 3.1, pp. 54-60): The left part shows the FTIR profile of the thermal decomposition products of the sticky rice as the temperature changes. "Time" refers to the moment when the emitted gases enter the FTIR testing zone. The relationship between temperature and time is given by the equation: $Temperature(℃) = 0.82 \times time(s) + 51$. The colour shows the intensity of FTIR absorbance. A brighter colour (bright yellow) indicates higher absorbance intensity, while a darker colour (dark purple) indicates lower intensity. The right part presents a three-dimensional representation of the FTIR spectra of the sticky rice during the heating process. The X-axis represents time, indicating when the emitted gases reach the FTIR testing zone. The Y-axis denotes the wavelength, and the Z-axis corresponds to the FTIR absorbance intensity, replacing the colour gradient used in the left figure

As shown in Fig 7-1, the active signals of this TGA-FTIR spectrum are from 100 and 350s (133 and 338℃), representing that the gases from the decomposition products of sticky rice are mainly released at these two temperatures. The FTIR spectra of the

escaping gases at 133 and 338℃ (extracted from right part of Figure 7-1, X-coordinate at around 100 and 350s) from the sticky rice powder are shown in Figures 7-2 and 7-3.

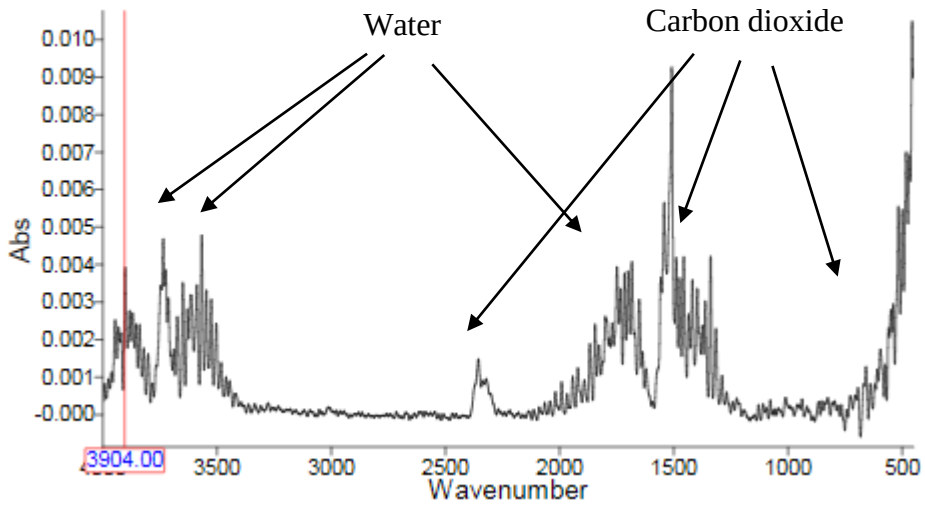


Fig 7-2. FTIR spectrum of the escaping gases at 133℃ from the sticky rice sample

As shown in Figure 7-2, the peaks at approximately 1600 cm^{-1} are from the bending vibration of the oxygen-hydrogen (O-H) bond in water. The peaks at about 3650 and 3750 cm^{-1} are from the stretching vibration of the oxygen-hydrogen (O-H) bond in water. The peaks at around 660 cm^{-1} are from the bending vibration of carbon dioxide, while the peaks at approximately 1340 and 2350 cm^{-1} are from the stretching vibration of carbon dioxide (Silverstein, 2005). That indicates that the escaping gases of 133℃ are water and carbon dioxide.

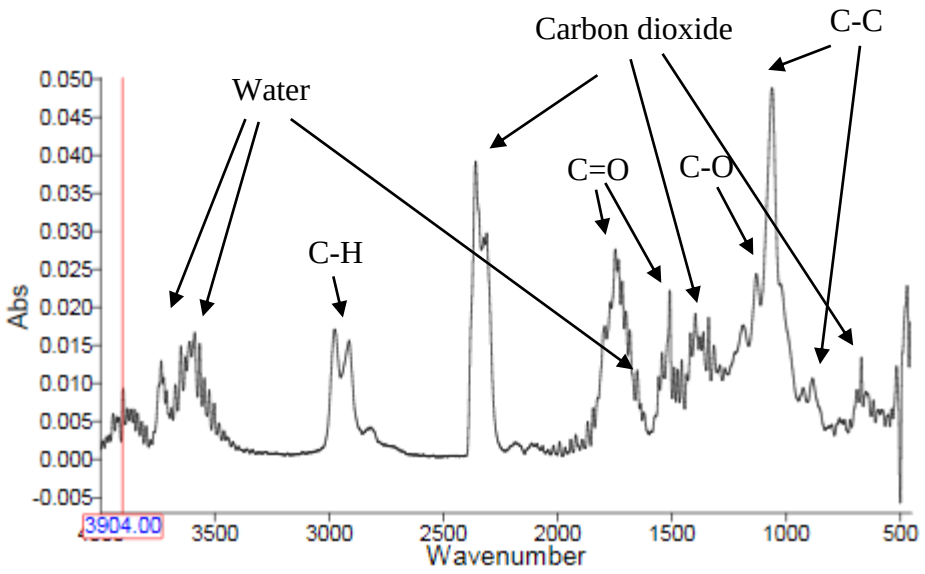


Fig 7-3. FTIR spectrum of the escaping gases at 338℃ from the sticky rice sample

As shown in Figure 7-3, the FTIR spectrum of the gases escaping at 338℃ from the sticky rice sample reveals several peaks. The peaks at approximately 2900 cm^{-1} are from the stretching vibration of the carbon-hydrogen (C-H) bond. The peaks at around 900-1100 cm^{-1} are from the stretching vibration of the carbon-carbon (C-C) bond. The peaks at around 1000-1200 cm^{-1} are from the stretching vibration of the carbon-oxygen (C-O) bond. The peaks at about 1500-1800 cm^{-1} are from the stretching vibration of the carbon-oxygen double (C=O) bond (Liu and Zhang, 2002). These signals could be from a variety of organic compounds. In a previous study on the TGA-FTIR result of starch (Liu et al., 2010), the maximum decomposition rate was at 333℃, which is quite similar to 338℃ in this study. The authors suggested that the gaseous products could include methane, ethylene, and formaldehyde. Additionally, water and carbon dioxide signals are still detectable in the spectrum. However,

identifying these organic compounds with FTIR still presents a challenge.

The results of all the TGA-FTIR tests are shown in Table 7-1.

Table 7-1. The results of all the TGA-FTIR tests (the complete results can be found in Appendix 3)

Sample		Description	Result
Sticky rice powder		Produced by Foo Lung Ching Kee Company (Hong Kong)	Water and carbon dioxide at 133℃; Water, carbon dioxide and a variety of organic compounds at 338℃
Loess		Loess collected from the Changping District, Beijing	Water and carbon dioxide at 103℃; Carbon dioxide at 330 and 594℃
Baked Loess		Baked at 450℃ for 13 hours	Water at 133℃; Carbon dioxide (trace amount) at 342 and 599℃
Modern sample	M1	Sticky rice content 0.090% (weight	Water and carbon dioxide (slight amount) at 100℃;

		percentage)	Carbon dioxide (slight amount) at 408℃
	M2	Sticky rice content 0.94% (weight percentage)	Carbon dioxide at 340℃
	M3	Sticky rice content 2.8% (weight percentage)	Water and carbon dioxide at 88℃; Water at 150℃; Water, carbon dioxide and a variety of organic compounds at 339℃
	M4	Sticky rice content 7.1% (weight percentage)	Water and carbon dioxide at 96℃; Water, carbon dioxide and a variety of organic compounds at 337℃
Archaeological sample	HYPT1	Tabia collected from the Fort Hongyuan site, Ningbo, Zhejiang province	Water and carbon dioxide at 158 and 330℃; Carbon dioxide at 291℃
	SJYTL3	Tabia collected from the	Water at 105℃;

	Shangjiaoyang Tulou site, Wenzhou, Zhejiang province	Water and carbon dioxide at 338℃
XZM7	Sediment collected from the Xinzhengmen site, Luoyang, Henan province	Water at 166℃; Carbon dioxide at 383℃

The escaping gases from the unbaked and baked loess samples are mainly water and carbon dioxide. Carbon dioxide was still escaping from the baked loess sample during the low-temperature period, which might be related to the adsorption of water and carbon dioxide from the atmosphere after all the organics were removed. However, the trace amount of carbon dioxide released at 342 and 599℃ indicating that the main part of the organics in loess has already been removed by the heating process.

Only in the profiles of M3 and M4 can a noticeable difference with loess samples be observed. The only compound that had been identified in the decomposition products of M2 was carbon dioxide, which could also be found in the escaping gases of unbaked and baked loess. Thus, TGA-FTIR failed to distinguish the sticky rice from M2, indicating that the method did not produce a diagnostic response at 0.94%. Consequently, the detecting limit of this method lies between 0.94% and 2.84%.

The FTIR spectra of the escaping gases at around 338℃ from M3 and M4 (Figures 7-4 and 7-5) share the same characteristic peak positions as those in the spectrum from sticky rice (shown in Figure 7-3). This suggests that the gases released from M3 and M4 at this temperature might have a composition similar to that of sticky rice. While it is true that TGA-FTIR cannot identify escaping gases at the molecular level, it was employed because it targets the escaping gases, where the organic signals are relatively simple and more pronounced. Compared to direct FTIR analysis of the sample, where the composition is more complex and high levels of inorganic components can obscure organic signals, TGA-FTIR allows for clearer detection of organic compounds. However, to identify the specific molecular structures of the escaping gases, additional analytical methods would be required.

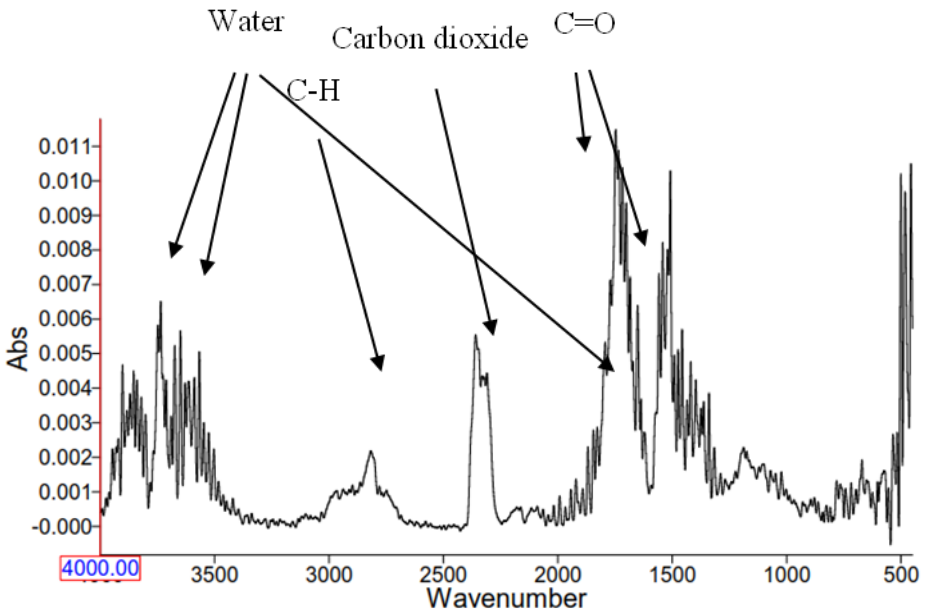


Fig 7-4. The FTIR spectrum of the escaping gases at around 338℃ extracted from the TGA-FTIR result of M3

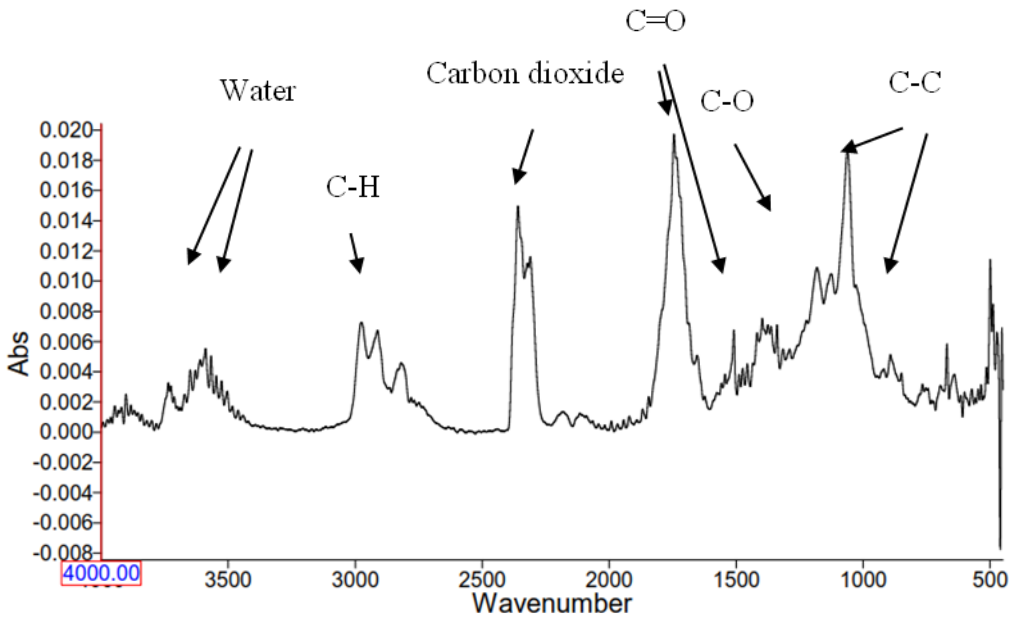


Fig 7-5. The FTIR spectrum of the escaping gases at around 338℃ extracted from the TGA-FTIR result of M4

No pronounced difference from the loess samples could be observed from the FTIR profiles of the archaeological samples, which indicated that the presence of sticky rice in these samples cannot be identified by TGA-FTIR. Either sticky rice does not exist in these samples, or the sticky rice content in these samples is lower than 0.94%.

Although escaping gases at similar temperatures to sticky rice decomposition can be found in the TGA-FTIR spectra of 2 selected archaeological samples (HYPT1 at 330℃, SJYTL3 at 338℃), the similar peaks to those in Figure 7-3 cannot be observed in the FTIR spectra of these gases from all 3 archaeological samples. This makes identifying sticky rice in the earth samples a challenge. It therefore suggests that

TGA-FTIR might not be a suitable or sensitive method for this identification step.

7.3.2. The potential of TGA-MS in the identification step

The potential of TGA, combined with MS (the experimental details can be found in Chapter 7.2), was explored to develop the identification step.

Part of the TGA-MS result of the sticky rice is shown in Figure 7-6. From the bottom to the top, there are the curves of the intensity change during the heating process for total ion chromatogram, *m/z* = 17, 18 and 44.

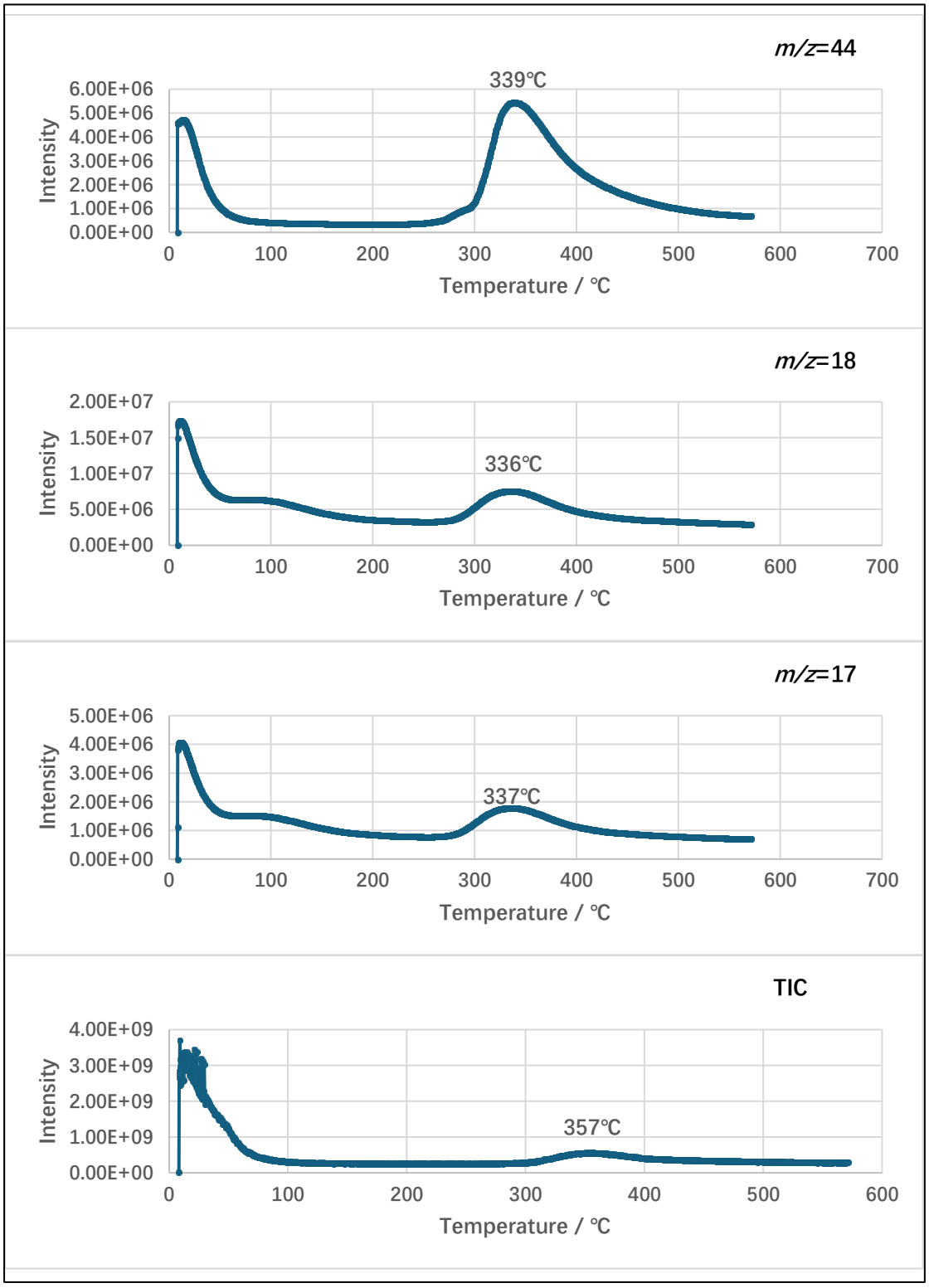
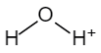
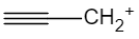
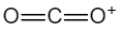
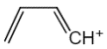
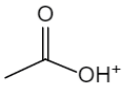
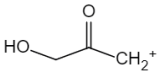
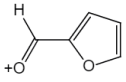
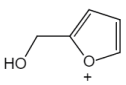
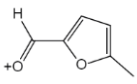


Fig 7-6. Part of the TGA-MS result of the sticky rice (sample details can be found in Chapter 3.1, pp. 54-60, the complete results can be found in Appendix 4)

In TGA-MS, the selected ion monitoring mode is used, where representative *m/z* values are selected according to the possible pyrolysis products of amylopectin. A series of organic compounds, such as furfural, 2-furanmethanol, 5-methylfurfural, acetic acid and hydroxyacetone, have been reported to be obtained in the pyrolysis process of polysaccharides. These compounds originated from the pyrolysis of the glucose structure (Patwardhan et al., 2009). The main *m/z* values of these compounds in the mass spectrum, according to the database (database: replib, Fine, TSCA, RTECS, EPA, HODOC, NIH, EINECS, IRDB. Contributor for furfural, 2-furanmethanol and 5-methylfurfural: NIST Mass Spectrometry Data Center; for acetic acid: Chemical Concepts; for hydroxyacetone: SODA AROMATIC CO., LTD.; used with permission, courtesy of Funatsu Laboratory, University of Tokyo. The copyright is reserved by Funatsu Laboratory), as well as those from water and carbon dioxide (Darribère, 2009), are listed in Table 7-2. The fragment ions of the pyrolysis amylopectin were individually monitored throughout the heating process by these *m/z* value.

Table 7-2. The possible identification of the fragments

Fragment ions (*m/z*)	Fragment formula	Fragment structure	Possible parent compound
17	OH^+		Water
18	H_2O^+		Water
39	$C_3H_3^+$		Furfural or 2-Furanmethanol
44	CO_2^+		Carbon dioxide
53	$C_4H_5^+$		5-Methylfurfural or 2-Furanmethanol
60	$C_2H_4O_2^+$		Acetic acid
67	$C_4H_3O^+$		Furfural
73	$C_3H_5O_2^+$		Hydroxyacetone
96	$C_5H_4O_2^+$		Furfural
98	$C_5H_6O_2^+$		2-Furanmethanol
110	$C_6H_6O_2^+$		5-Methylfurfural

The intensity of these fragment ions reached the maximum around 336 to 367℃, representing the pyrolysis temperature of the sticky rice.

The results of all the TGA-MS tests are shown in Table 7-3.

Table 7-3. The results of all the TGA-MS tests (the complete results can be found in Appendix 4)

Sample		Description	Fragment ions found in the TGA-MS result (*m/z*)
Sticky rice powder		Produced by Foo Lung Ching Kee Company (Hong Kong)	(17, 18, 39, 44, 53, 60, 67, 73, 96, 98, 110) at around 336 to 367℃
Loess		Loess collected from the Changping District, Beijing	-
Baked Loess		Baked at 450℃ for 13 hours	-
Modern sample	M1	Sticky rice content 0.090% (weight percentage)	-
	M2	Sticky rice content	(53, 60, 67, 73, 96, 98, 110)

		0.94% (weight percentage)	at around 336 to 367℃
	M3	Sticky rice content 2.8% (weight percentage)	(53, 60, 67, 73, 96, 98, 110) at around 336 to 367℃
	M4	Sticky rice content 7.1% (weight percentage)	(39, 53, 60, 67, 73, 96, 98, 110) at around 336 to 367℃
Archaeological sample	HYPT1	Tabia collected from the Fort Hongyuan site, Ningbo, Zhejiang province	(53, 67, 96, 110) at around 167℃, (53, 96, 110) at around 336 to 367℃, (53, 67, 96, 98, 110) at around 470℃
	SJYTL3	Tabia collected from the Shangjiaoyang Tulou site, Wenzhou, Zhejiang province	(53, 67, 96, 98, 110) at around 470℃
	XZM7	Sediment collected from the Xinzhengmen site, Luoyang, Henan province	(60, 73, 96, 110) at around 336 to 367℃, (53, 67, 96, 98, 110) at around 470℃

Almost no fragments ions were found between 336 and 367℃, meaning the organics

in the natural loess will not disrupt the results of TGA-MS for the identification. Although there were still some tiny peaks from around 360 and 400℃ in the result of unbaked loess, they were too weak to be distinguished from the background signals.

Pronounced peaks between 336 and 367℃ were found in the TGA-MS results (*m/z* = 53, 60, 67, 73, 96, 98, and 110) of modern samples, except for M1. The detection limit of TGA-MS is below 0.94%, which is lower than those of FTIR and LOI. Nevertheless, it is worth mentioning that the specificity of TGA-MS in identifying sticky rice in earth samples still needs to be verified through more tests on modern samples containing other added organics. In previous work, the TGA-MS tests were applied to detect poly(ethylene terephthalate) microplastics in soil samples. The *m/z* = 105 and 154 signals at around 300-650℃ were confirmed to be reliable indicators for poly(ethylene terephthalate) (David et al., 2018). The *m/z* values (53, 60, 67, 73, 96, 98, and 110) applied in this study may originate from furfural, 2-furanmethanol, 5-methylfurfural, acetic acid, and hydroxyacetone. However, these compounds have also been found in the pyrolysis products of several monosaccharides, disaccharides, and polysaccharides, including cellulose and maize starch (Patwardhan et al., 2009). This overlap may affect the specificity of TGA-MS in identifying amylopectin in soil samples. Future work could address this issue by: 1) elucidating the pyrolysis process of amylopectin combined with kinetic models, a method that has already been applied to soil humic substances (Li et al., 2020a); and 2) conducting more tests on modern samples containing different saccharides to evaluate the feasibility of applying the

pyrolysis temperature to distinguish those saccharides.

Peaks between 336 and 367℃ could be found in the TGA-MS result of HYPT1 (*m/z* = 53, 96 and 110), indicating the possible existence of the pyrolysis products of the sticky rice. No peaks were found in *m/z* = 60 and 73, while many in other positions were found. It should be related to the degradation of organics or the existence of other materials, which should also be taken into consideration. These peaks could be divided into two parts: around 167℃ in *m/z* = 53, 67, 96 and 110; around 470℃ in *m/z* = 53, 67, 96, 98 and 110, indicating the possible existence of two or two groups of organics materials in this sample.

Although no apparent peaks between 336 and 367℃ could be found in SJYTL3, peaks at around 470℃ in *m/z* = 53, 67, 96, 98 and 110 could still be found.

In the TGA-MS result of XZM7, peaks between 336 and 367℃ could be found in *m/z* = 60, 73, 96 and 110, while peaks at around 470℃ in *m/z* = 53, 67, 96, 98 and 110 could still be found, which is quite similar to the result of HYPT1. The only difference is that peaks at around 167℃ could not be found.

In summary, 3 kinds or groups of organics not shown in loess samples have been found in archaeological samples: A. pyrolysis temperature around 167℃; B. pyrolysis temperature around 350℃ (possibly amylopectin); C. pyrolysis temperature around

470℃. Types A and C may be from the degradation of the sticky rice or organics from other sources (for example, other added organics or organics transported from the environment after the construction). Types A, B and C were found in HYPT1, types B and C were found in XZM7, while only type C was found in SJYTL3. The application of TGA-MS in identifying organics in earth samples could be an essential part of future work (after DPhil and with enough funding for the tests).

7.5. Conclusions

The application of TGA-FTIR and TGA-MS in the identification step has been explored in this chapter. However, due to the high expense of these two tests, only a few modern earth and archaeological samples could be analysed, which might limit the generalizability of the findings.

Escaping gases at similar temperature to the sticky rice decomposition (approximately 330℃) were captured in the TGA-FTIR tests of 2 archaeological samples (HYPT1 and SJYTL3), while in XZM7, no escaping gases were found at similar temperature. However, most of the characteristic peaks in the FTIR spectrum of sticky rice thermal decomposition products at about 330℃ cannot be found in archaeological samples. Therefore, TGA-FTIR is not an ideal analysis method in the identification step.

3 kinds or groups of organics have been found in archaeological samples in the TGA-

MS tests. These compounds are not present in the spectra of loess or baked loess, indicating that these organics may be artificially added. The same compounds as the thermal decomposition products of sticky rice between 336 and 367℃ were found in HYPT1 and XZM7, which suggests the possible existence of sticky rice in these 2 archaeological samples.

8. Matrix assisted laser desorption ionization-time of flight-mass spectrometry (MALDI-TOF-MS)

8.1. Samples

MALDI-TOF-MS is a technique widely used to analyse large biomolecules such as proteins, peptides, and polysaccharides. It embeds the analyte in a matrix that aids in its laser-induced desorption and ionization, and measures the *m/z* value of these ionized fragments by the time of flight (Caprioli, 1997). The MALDI-TOF-MS test was applied to loess, baked loess, modern (including aged modern samples, n = 70) and archaeological samples (n = 67). Details can be found in Chapter 3 (pp. 54-83).

8.2. Methods

MALDI-TOF-MS was used to analyse the organic materials in earth samples in the identification step. The analysis protocol was first applied to modern earth and tabia samples to determine the sensitivity and specificity of the protocol. Then, the MALDI-TOF-MS tests were applied to archaeological samples to detect the existence of organics. The analytical protocol mainly includes the identification of polysaccharide.

The MALDI-TOF-MS method is based on and modified (discussed in Chapter 8.3.3) from the procedure described by Zheng and Wang (2013). A simplify illustration of the protocol is shown in Figure 8-1.

1. Around 0.05 g earth sample was ground and added into a 1.5 mL vial (vial I) with 500 μL water.

2. 500 μL 1 M HCl (hydrochloric acid) was added into vial I. After no bubbles were generated, vial I was centrifuged at 3000 r.p.m for 2 min. The supernatant was then removed. This step was repeated 3 times until the reaction of all calcium carbonate was complete.

3. Vial I was added with 500 μL water and centrifuged at 3000 r.p.m for 2 min. The precipitate was kept, and this step was repeated until the pH of the supernatant to around 7.

4. Vial I was added with 500 μL water and centrifuged at 3000 r.p.m for 2 min. 100 μL supernatant was transferred into another vial (vial II) to confirm that no character signals were introduced by the protocol.

5. A buffer exchange was conducted on the α-amylase solution with 50 mM ammonium acetate solution in centrifuge tubes equipped with filtration membranes of 30 kDa molecular weight cut-off. The tubes were centrifuged at 12000 r.p.m for 12min for 5 times.

6. 2 μM α-amylase after buffer exchange was added into vial I, and the vibration was applied. After being heated at 50℃ for 15 min, vial I was added with 4 μL 1% FA/water and centrifuged at 3000 r.p.m for 2 min.

7. 50 μL supernatant was transferred to another vial (vial III) and evaporated to dryness. 50 μL TA solution (ACN/water = 1:1, 0.1% TFA) with the internal standard (agar heptose, $C_{42}H_{66}O_{33}$, 4 μg/mL) was added for re-dissolution to get a sample solution.

8. The sample solution was applied with 2,5-DHB (2,5-Dihydroxybenzoic acid, $C_7H_6O_4$) at the ratio of 1:1 onto the target plate and then vacuum dried. The MALDI-TOF-MS analysis was performed on a Bruker rapifleX^{TM} MALDI-TOF mass spectrometer, with the mass spectrometry collection parameters set at a laser energy of 60% and 1000 shots. MS spectra were acquired in the range from *m/z* 800 to 2400. The data was processed using FlexAnalysis 4.0. The methodology was developed by the author. All the tests were conducted under the direction of the author, with assistance from Xiaopeng Yao, Hulingxiao Chai, and Xiang Xu at the Institute of Cell Analysis, Shenzhen Bay Laboratory. Due to pandemic restrictions, the author was unable to physically be present in Shenzhen but remotely oversaw the entire testing process.

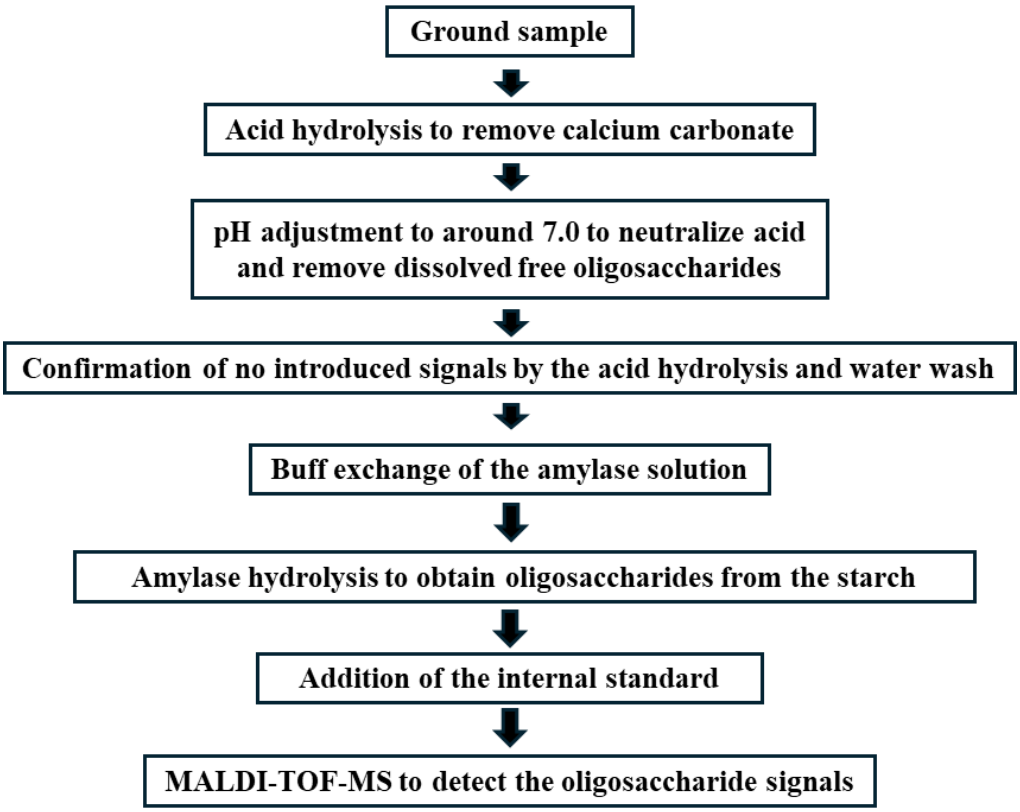


Fig 8-1. A simplify illustration of the MALDI-TOF-MS protocol

8.3. Results and discussion

8.3.1. The identification of starch in MALDI-TOF-MS

The MALDI-TOF-MS tests were applied to modern and archaeological samples to identify sticky rice by detecting the starch molecules. The MALDI-TOF-MS spectra of sticky rice powder (produced by Foo Lung Ching Kee Company (Hong Kong) and also applied in the preparation of the modern samples) and modern sample M3 (sample details can be found in Table 3-1, pp. 71-73) are shown in Figures 8-2 and 8-3.

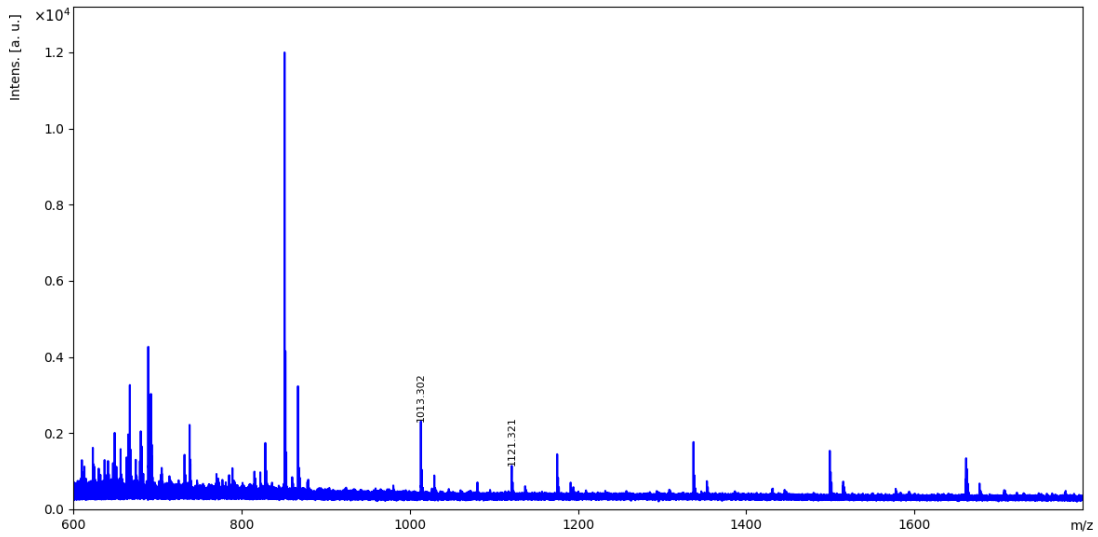


Fig 8-2. The MALDI-TOF-MS spectrum of sticky rice powder

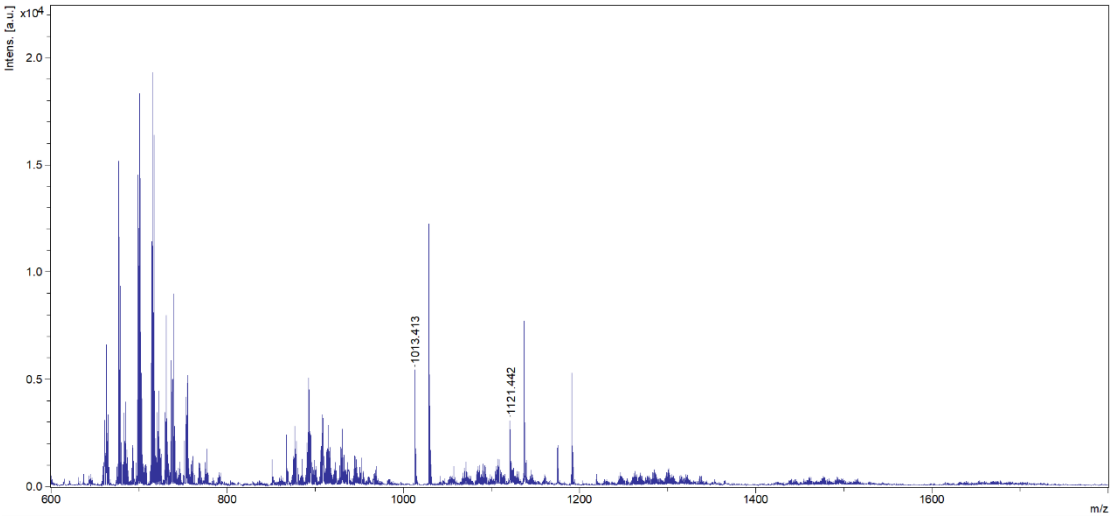


Fig 8-3. The MALDI-TOF-MS spectrum of M3

Agar heptose was applied as the internal standard and its molecular structure is shown below.

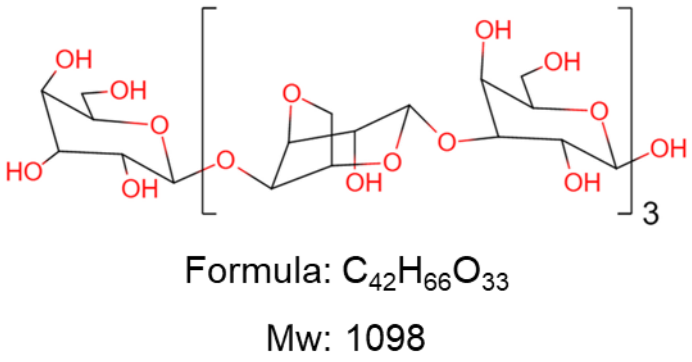


Fig 8-4. The molecular structure of agar heptose

As the presence of Na^+ and K^+ seems inevitable in the earth samples, the fragments of the target saccharide and internal standard form sodium and potassium adduct ions, which were shown on the mass spectra. The peak at around *m/z* 1121 is exactly from the sodium adduct ion of the internal standard, and the peak at around *m/z* 1013 present in the spectra of both sticky rice powder and M3 is likely from the sodium adduct ion of a hexasaccharide ($C_{36}H_{62}O_{31}$), which should be one of the decomposition products of the sticky rice after enzyme hydrolysis.

The MALDI-TOF-MS tests were also run on the natural and baked loess samples.

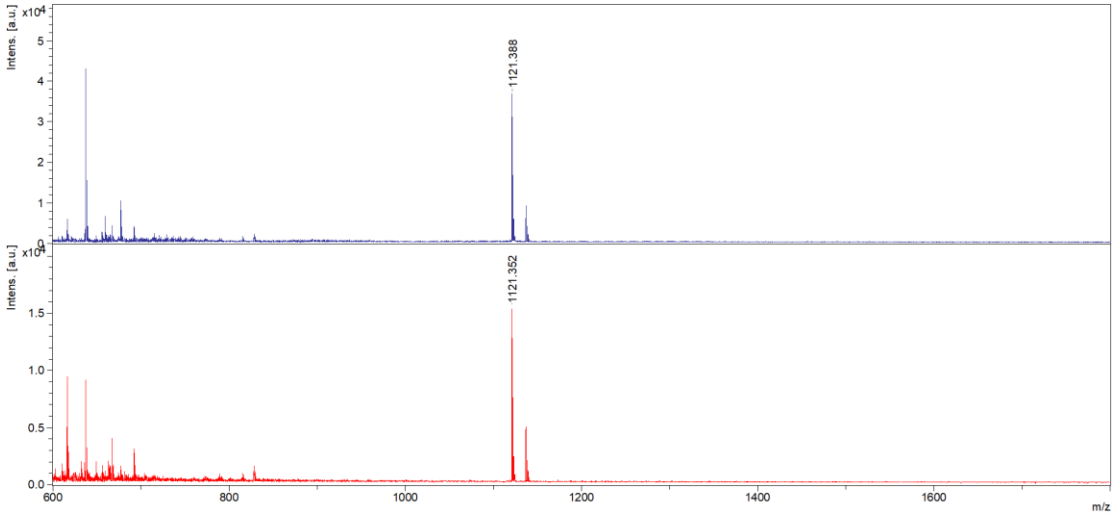


Fig 8-5. The MALDI-TOF-MS spectra of the natural loess (the blue line is the result without enzyme hydrolysis and the red line is after enzyme hydrolysis)

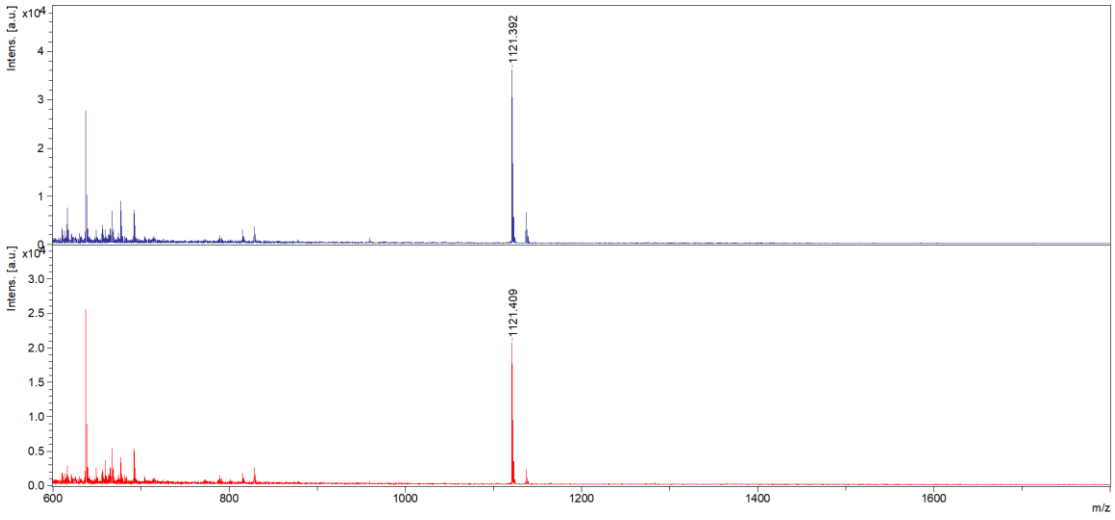


Fig 8-6. The MALDI-TOF-MS spectra of the baked loess (the blue line is the result without enzyme hydrolysis and the red line is after enzyme hydrolysis)

According to the results, only the peaks at around *m/z* 1121, which are the signal of the internal standard, were found in the spectra. The peak at around 1013 was too weak that it could hardly be observed. The area near 1013 in the MALDI-TOF-MS

spectrum of the loess is enlarged and shown below. 3 modern samples were also shown for comparison.

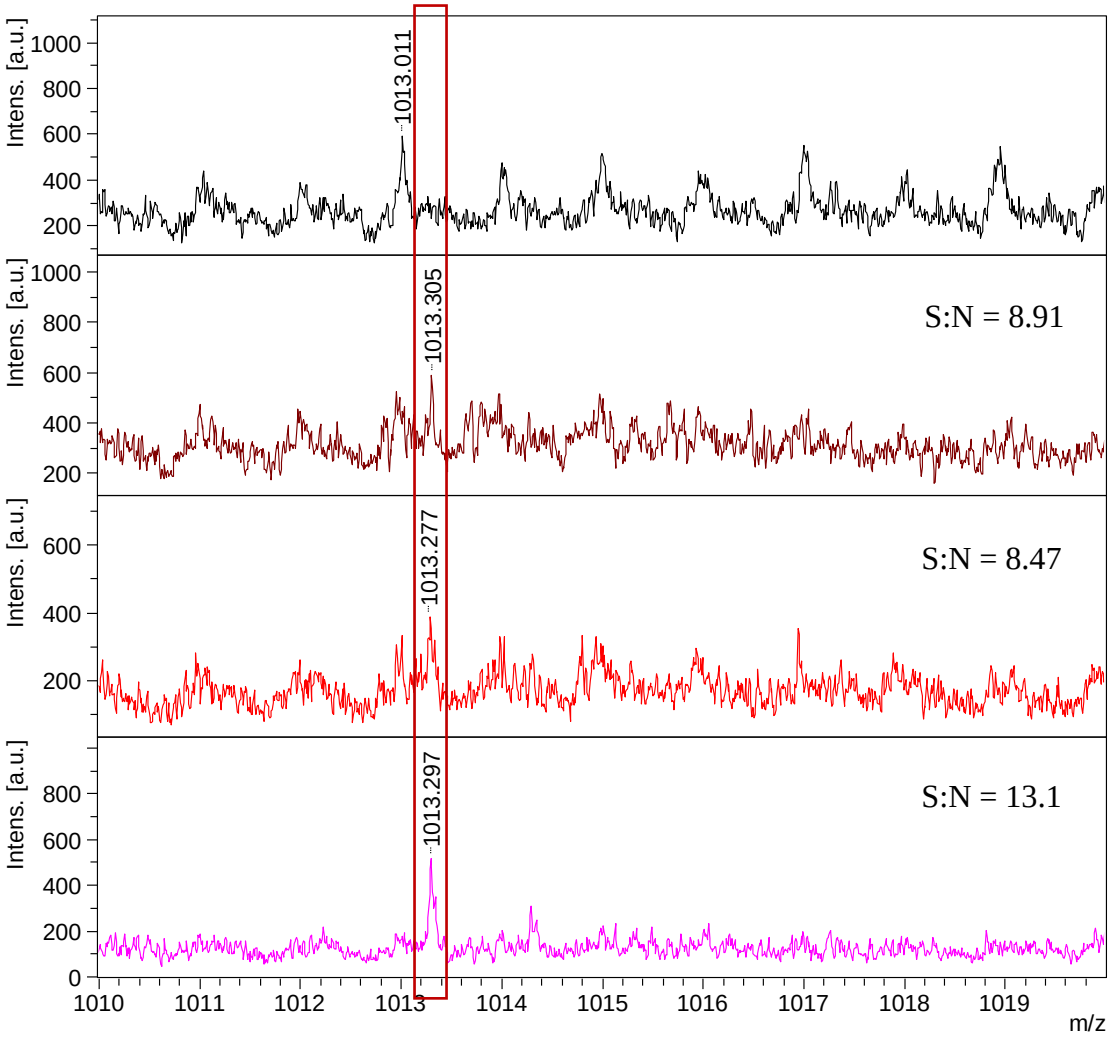


Fig 8-7. The area near *m/z* 1013 in the MALDI-TOF-MS spectra (from top to bottom: loess, T30 (0.002% sticky rice content), T27 (0.004% sticky rice content), T24 (0.008% sticky rice content))

As shown in Figure 8-7, the peak at around *m/z* 1013 in the spectrum of loess is slightly different from the peaks in the spectra of modern samples. This kind of peak

can also be observed in some archaeological samples. An example is shown in Figure 8-8.

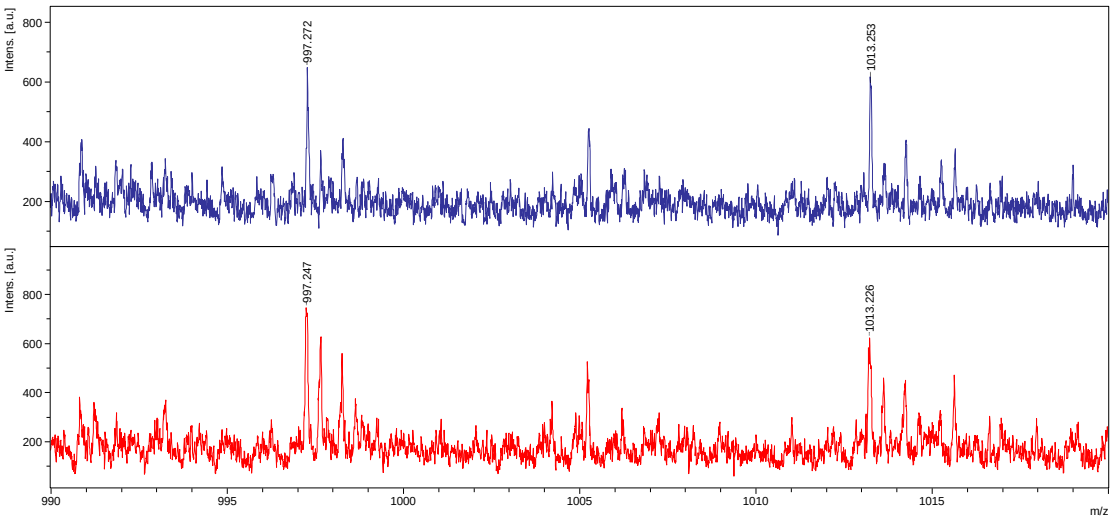


Fig 8-8. The area near *m/z* 1013 in the MALDI-TOF-MS spectra of WC3 (sample details can be found in Table 3-3, pp. 79-83. The blue line is before enzyme hydrolysis and the red line is after enzyme hydrolysis)

Peaks at around *m/z* 997 could also be observed, indicating that the peaks at around *m/z* 1013 in these spectra are not from the sodium adduct ion of a hexasaccharide, but are from the potassium adduct ions of other molecules (997 = 1013-39+23). The peaks at around *m/z* 997 cannot be observed in the MALDI-TOF-MS spectra of all the modern samples. Moreover, the peaks at around *m/z* 997 and 1013 can be found before and after the enzyme hydrolysis. It can be inferred that the peaks are from the loess, but not from the sticky rice. Therefore, the existence of peaks at around *m/z* 997 in the MALDI-TOF-MS spectra means that the peaks at around *m/z* 1013 may be the

“fake” indicator for the sticky rice.

The calculation has also been applied to rule out the “fake” molecular markers. Due to slight variations in peak positions among different MALDI-TOF-MS spectra, the peak at approximately *m/z* 1121, serving as the internal standard, is used to calibrate the peak value at around 1013. Below are the calibrated values of the peaks around 1013 for a series of related samples.

Table 8-1. The calibrated values of the peaks at around *m/z* 1013 and 1121 in the MALDI-TOF-MS spectra (The calibrated value of the 1013 peak = 1013 peak value + theoretical value of 1121 peak - experimental value of 1121 peak)

	1013 peak value	1121 peak (internal standard)		The calibrated value of the 1013 peak
		Theoretical value	Experimental value	
WC3 Shot 1	1013.253	1121.338	1121.310	1013.281
WC3 Shot 2	1013.226	1121.338	1121.273	1013.291
T16	1013.305	1121.338	1121.315	1013.328
T17	1013.263	1121.338	1121.286	1013.315
T18	1013.299	1121.338	1121.310	1013.327

T19	1013.323	1121.338	1121.325	1013.336
T20	1013.283	1121.338	1121.293	1013.328
T21	1013.314	1121.338	1121.331	1013.321

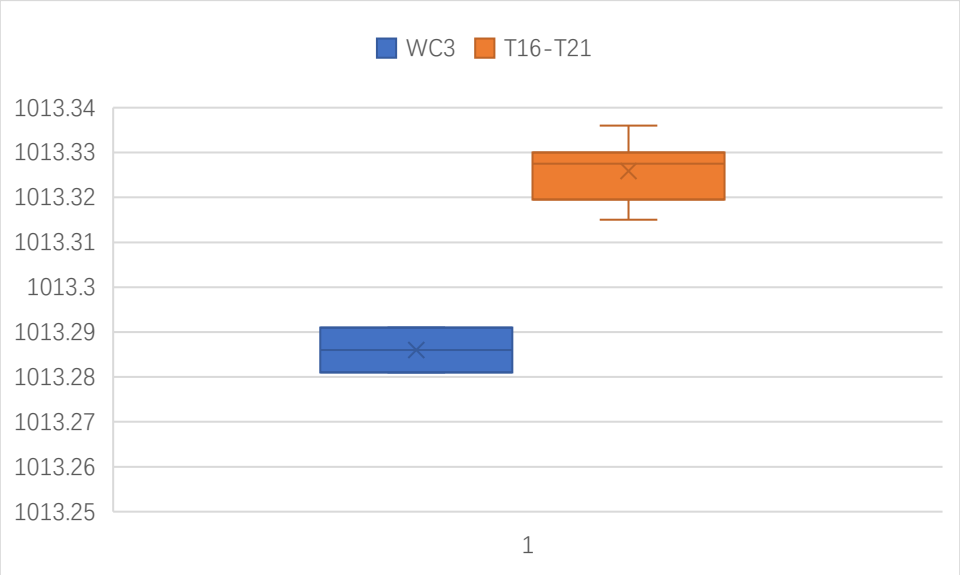


Fig 8-9. The calibrated values of the peaks at around *m/z* 1013 in the MALDI-TOF-MS spectra of WC3 and modern samples (T16-T21, sample details can be found in Table 3-2, pp. 75-76)

As shown in the Table 8-1 and Figure 8-9, the difference between the calibrated peaks at around *m/z* 1013 in the MALDI-TOF-MS spectra of WC3 and modern samples is quite significant. Specifically, the calibrated modern sample peak is *m/z* 1013.325 ± 0.008 (the theoretical value of the hexasaccharide signal is 1013.317), while that in WC3 is no more than 1013.300. Although these two types of 1013 peaks are in

similar positions, they are different signals. This provides additional evidence that the peaks at around *m/z* 1013 in the spectra of the loess, WC3, and some other archaeological samples are "fake" indicators for sticky rice. Thus, the existence of the sticky rice in samples can only be confirmed if: 1) there are no peaks at around *m/z* 997; 2) the calibrated characteristic peak is *m/z* 1013.325 ± 0.008.

The specificity of the MALDI-TOF-MS protocol for saccharide has also been evaluated on modern samples containing different kinds of starch: wheat starch (WS1, WS2 and WS3), sweet potato starch (SPS1 and SPS2), corn starch (CS1 and CS2), rice flour (RF1 and RF2) and sticky rice (M3). The contents of starch in samples are around 2%, and the sample details can be found in Table 3-1 (pp. 71-73).

The MALDI-TOF-MS results of all the starch samples can be found in Appendix 5. An example is shown in Figure 8-10.

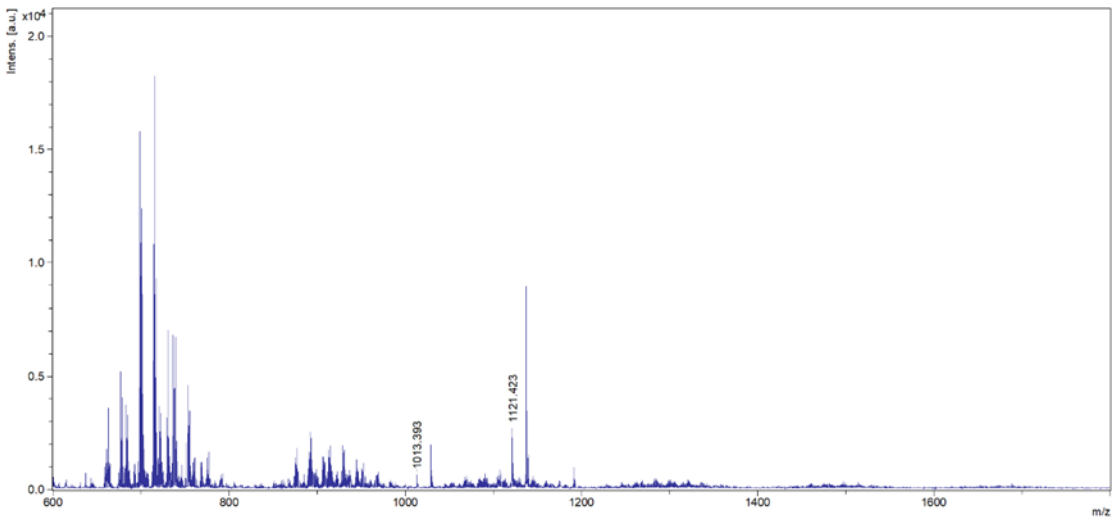


Fig 8-10. MALDI-TOF-MS result of CS1

The starch indicator peak could be found in all the modern samples containing different kinds of starch except for WS1. The signal at around *m/z* 1013 was too weak to be shown on the mass spectrum of WS1. The peaks at around *m/z* 1029 and 1137 were marked as the potassium adduct ions of the hexasaccharide (which was also identified in starch) and the internal standard.

Therefore, the peak at *m/z* 1013.325 ± 0.008 in MALDI-TOF-MS spectra can be used to identify starch, but not sticky rice in earth samples. Nonetheless, identifying starch in these samples remains crucial, as it confirms the artificial addition of organics in construction materials. In subsequent chapters, the term “starch” will describe the natural organic material applied in construction materials, rather than “sticky rice.”

The MALDI-TOF-MS tests were also applied to archaeological samples. Peaks at around *m/z* 1013 were detected in 2 samples: HYPT1 and TFGPT1. The spectra are shown in Figures 8-11 and 8-12.

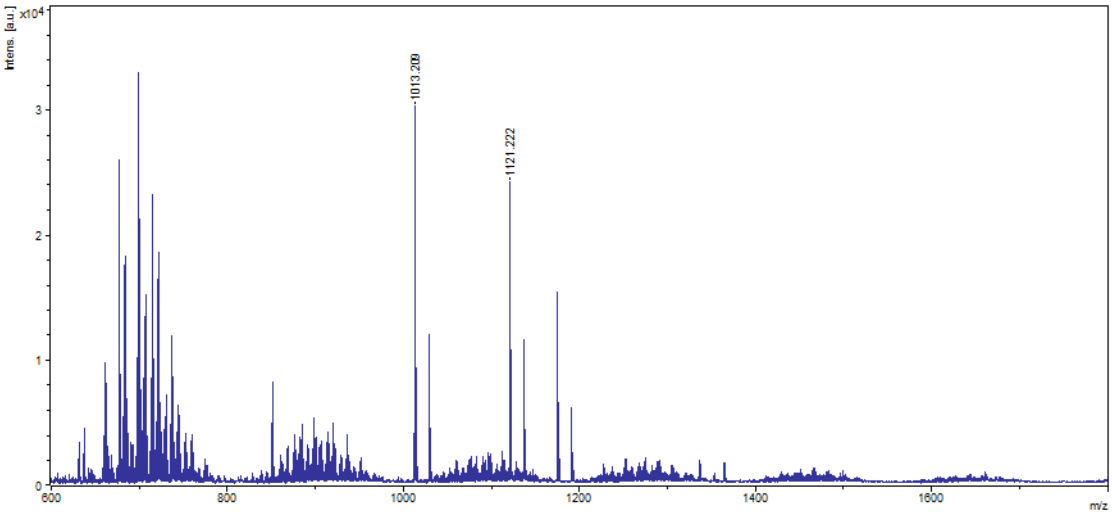


Fig 8-11. MALDI-TOF-MS result of HYPT1

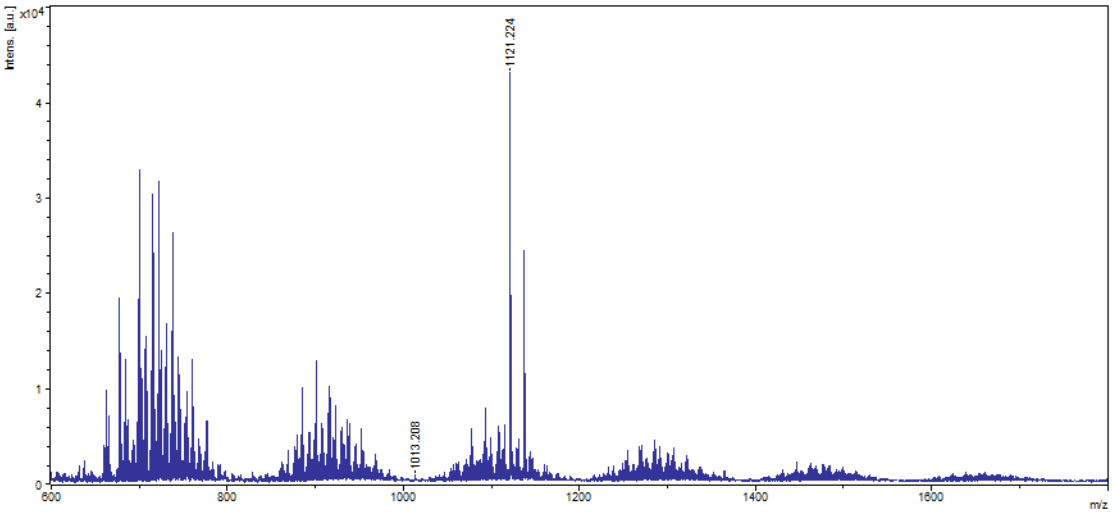


Fig 8-12. MALDI-TOF-MS result of TFGPT1

No peaks at around *m/z* 997 can be found in the spectra, and the calibrated

characteristic peak value (1013 peak value + 1121.338 - 1121 peak value) of HYPT1 and TFGPT1 are 1013.325 and 1013.322, which are the signal of starch indicator (1013.325 ± 0.008). Therefore, starch was identified in HYPT1 and TFGPT1.

To trace the origin of the starch in the archaeological samples HYPT1 and TFGPT1, 9 earth samples were collected from the surrounding environment of the 2 sites (Fort Hongyuan for HYPT1 and Fort Tianfeigong for TFGPT1). These samples were then analysed using MALDI-TOF-MS. Amongst them, HYPT-B1, HYPT-B2 and HYPT-B3 were directly collected from the Fort Hongyuan site. JYPT-B1, JYPT-B2 and JYPT-B3 came from the Fort Jingyuan, located quite close to the Fort Hongyuan site, for comparison. TFGPT-B1 was directly collected from the Fort Tianfeigong site. NWPT-B1 and NWPT-B2 came from the Fort Nanwan site, located quite close to the Fort Tianfeigong site, which were also included for comparison purposes. The MALDI-TOF-MS results of these background samples are shown in Figures 8-13-8-21.

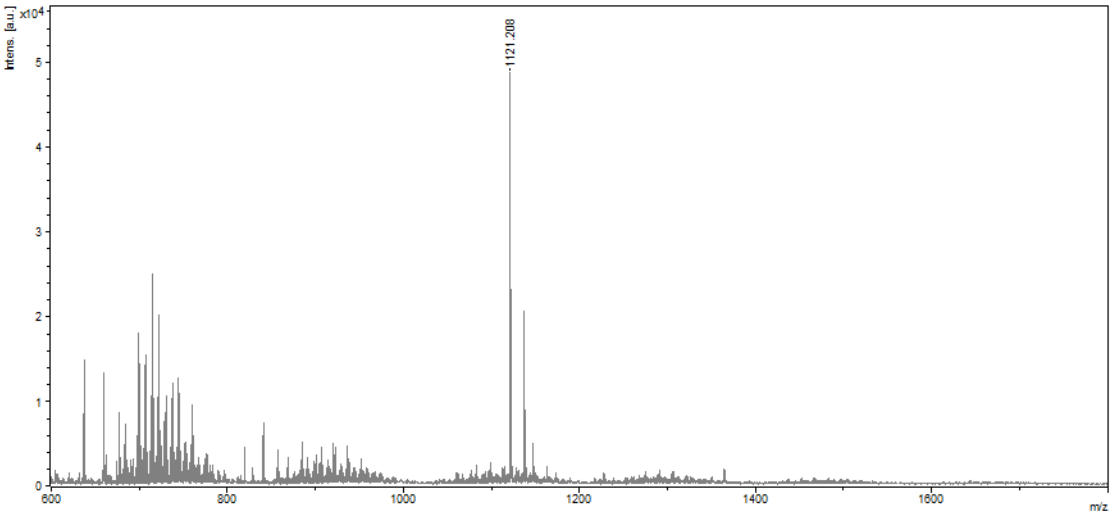


Fig 8-13. MALDI-TOF-MS result of HYPT-B1

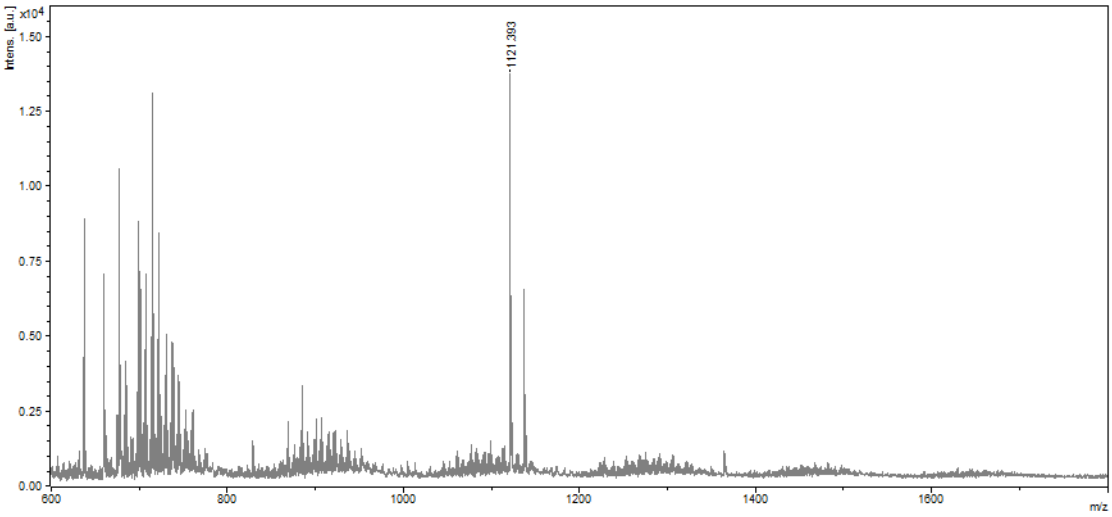


Fig 8-14. MALDI-TOF-MS result of HYPT-B2

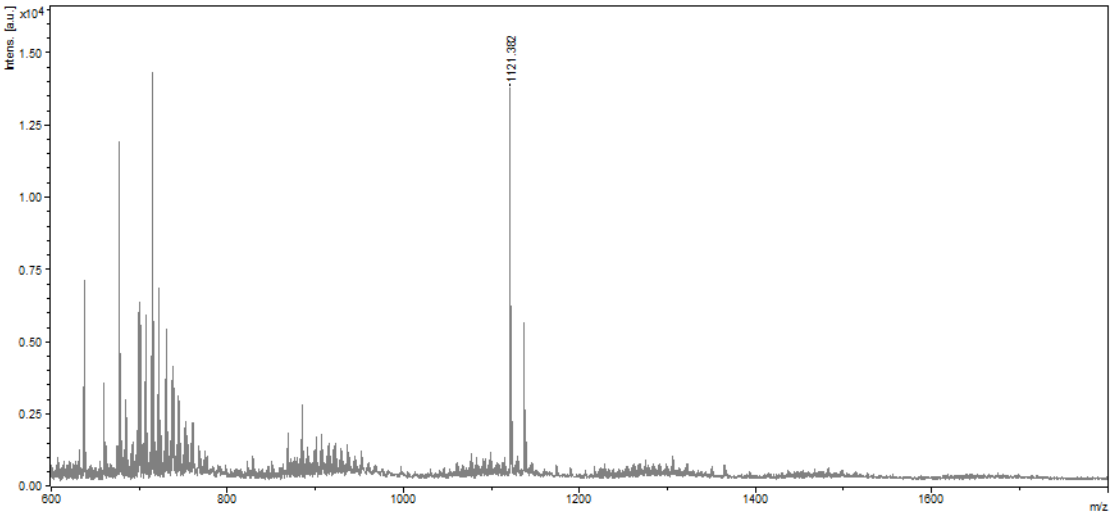


Fig 8-15. MALDI-TOF-MS result of HYPT-B3

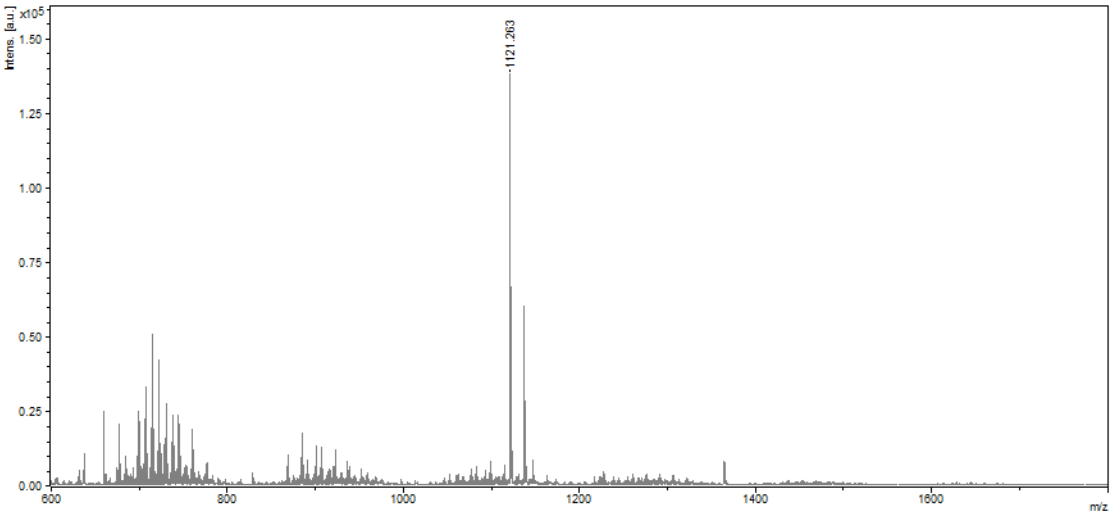


Fig 8-16. MALDI-TOF-MS result of JYPT-B1

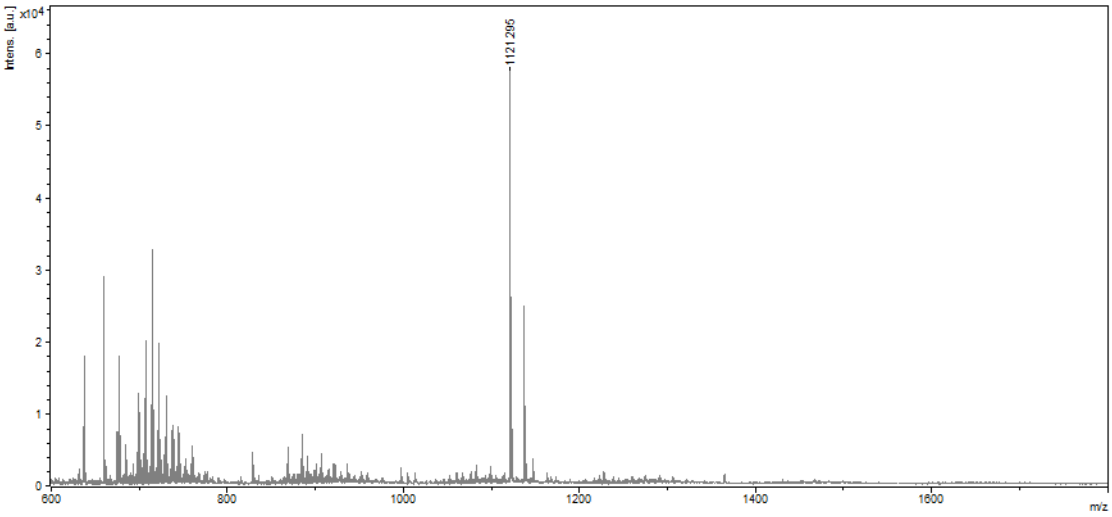


Fig 8-17. MALDI-TOF-MS result of JYPT-B2

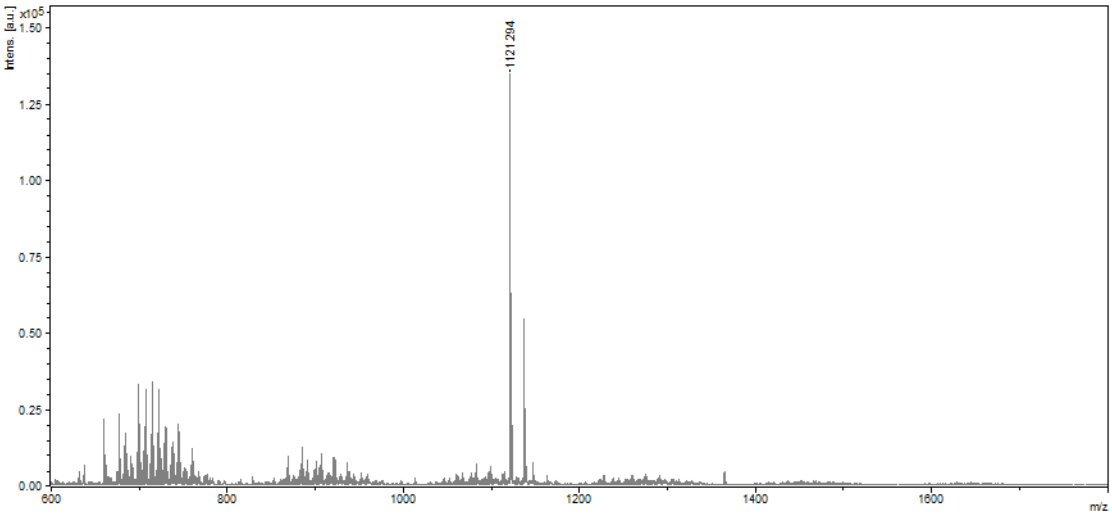


Fig 8-18. MALDI-TOF-MS result of JYPT-B3

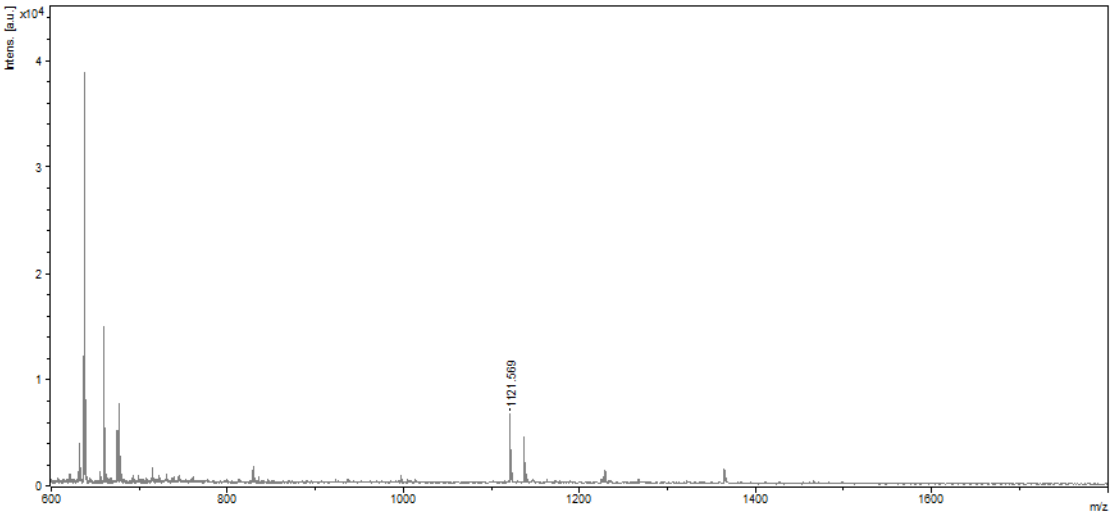


Fig 8-19. MALDI-TOF-MS result of TFGPT-B1

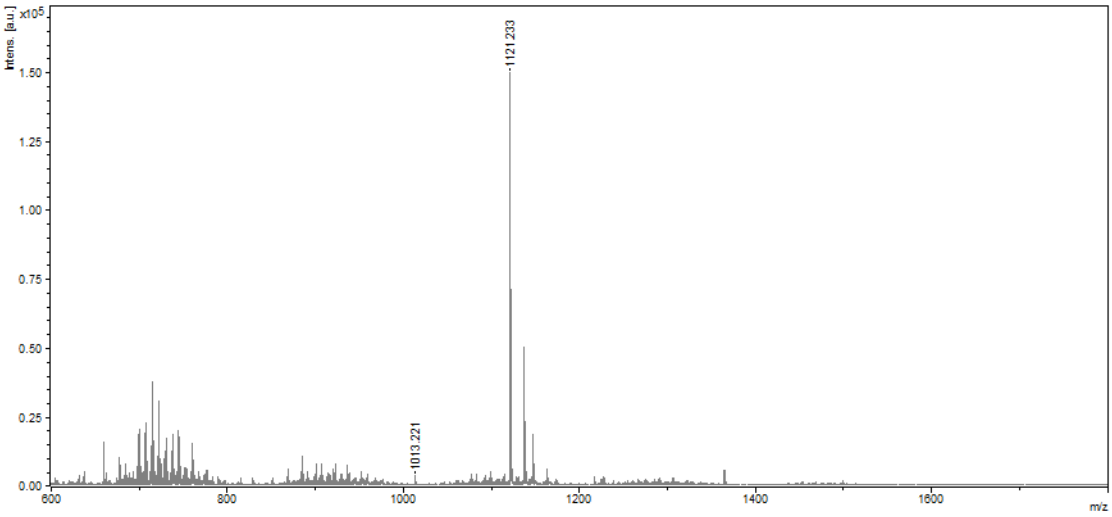


Fig 8-20. MALDI-TOF-MS result of NWPT-B1

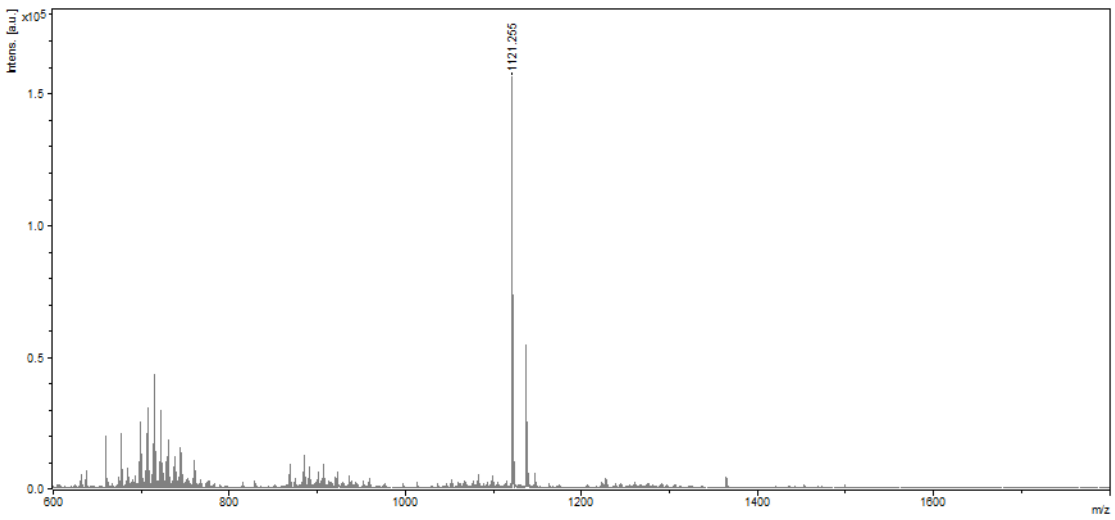


Fig 8-21. MALDI-TOF-MS result of NWPT-B2

As shown in Figures 8-13, 8-14 and 8-15, the *m/z* 1013 peak cannot be observed in the MALDI-TOF-MS spectra of all background sample of HYPT1, indicating that starch does not exist in the surrounding environment of the Fort Hongyuan site. Thus, the conclusion can be drawn that the starch in HYPT1 is artificially added. However, the *m/z* 1013 peak in the TFGPT1 spectrum is so faint that it's hardly observable (shown in Figure 8-12). Additionally, this starch indicator is also present in the NWPT-B1 spectrum (shown in Figure 8-20). Therefore, the possibility that the starch in TFGPT1 originates from the background cannot be ruled out. Further tests are required on samples from the Fort Tianfeigong site to pinpoint the source of the starch in TFGPT1.

8.3.2. The detection limit of MALDI-TOF-MS

The MALDI-TOF-MS tests were also run on modern tabia samples containing different content of starch to test the detection limit of this analytical method. The intensity of the peaks at around *m/z* 1013 and 1121 in the mass spectra for the starch and internal standard is shown in Appendix 8. The ratios of the two peaks for the 9 shots of the same sample have been calculated. Their averages and standard deviations are shown in Table 8-2.

Table 8-2. Calculation results from the MALDI-TOF-MS spectra of modern earth samples (each sample tested 9 times in parallel)

	Average	Standard deviation
T1	0.563	0.032
T2	0.902	0.041
T3	2.148	0.062
T4	7.820	0.456
T5	25.447	1.416
T6	37.794	1.549
T7	5.466	0.136
T8	20.673	1.175
T9	116.500	5.892
T10	0.159	0.009

T11	0.133	0.010
T12	0.765	0.032
T13	0.072	0.004
T14	0.327	0.050
T15	0.150	0.009
T16	0.079	0.009
T17	0.081	0.007
T18	0.461	0.053
T19	0.070	0.004
T20	0.096	0.009
T21	0.064	0.005
T22	0.026	0.006
T23	0.063	0.007
T24	0.062	0.008
T25	-	-
T26	0.039	0.006
T27	0.044	0.008
T28	-	-
T29	0.031	0.004
T30	0.022	0.003

The intensity ratio of each type of tabia sample is shown in Tables 8-3, 8-4 and 8-5.

Table 8-3. The intensity ratio of the “111” tabia samples (CaO, loess and SiO_2 are 1:1:1 in mass)

Sample	The starch content (weight percentage)	The ratio of the intensity at around 1013 and 1021
T1	2%	0.563
T2	5%	0.902
T3	10%	2.148
T10	0.2%	0.159
T11	0.02%	0.133
T16	0.032%	0.079
T19	0.016%	0.070
T22	0.008%	0.026
T25	0.004%	-
T28	0.002%	-

Table 8-4. The intensity ratio of the “321” tabia samples (CaO, loess and SiO_2 are 3:2:1 in mass)

Sample	The starch content (weight percentage)	The ratio of the intensity at around 1013 and 1021
T7	2%	5.466
T8	5%	20.673
T9	10%	116.500
T14	0.2%	0.327
T15	0.02%	0.150
T18	0.032%	0.461
T21	0.016%	0.064
T24	0.008%	0.062
T27	0.004%	0.044
T30	0.002%	0.022

Table 8-5. The intensity ratio of the “230” tabia samples (CaO, loess and SiO_2 are 2:3:0 in mass)

Sample	The starch content (weight percentage)	The ratio of the intensity at around 1013 and 1021
T4	2%	7.820
T5	5%	25.447
T6	10%	37.794
T12	0.2%	0.765
T13	0.02%	0.072
T17	0.032%	0.081
T20	0.016%	0.096
T23	0.008%	0.063
T26	0.004%	0.039
T29	0.002%	0.031

The linear fitting result between the intensity ratio and starch content is shown below.

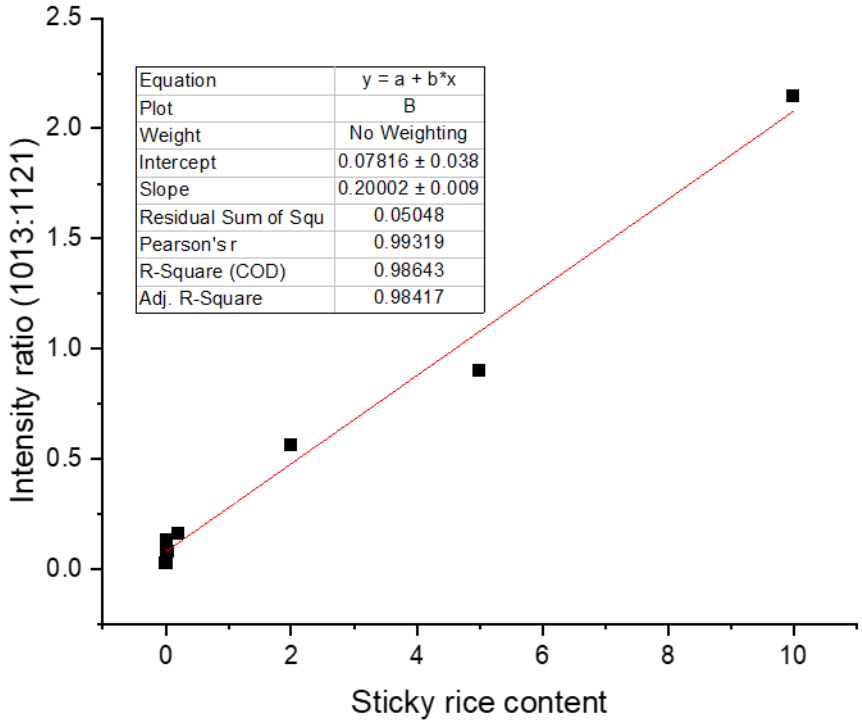


Fig 8-22. The linear fitting result of “111” tabia samples (the red line is the fitting line)

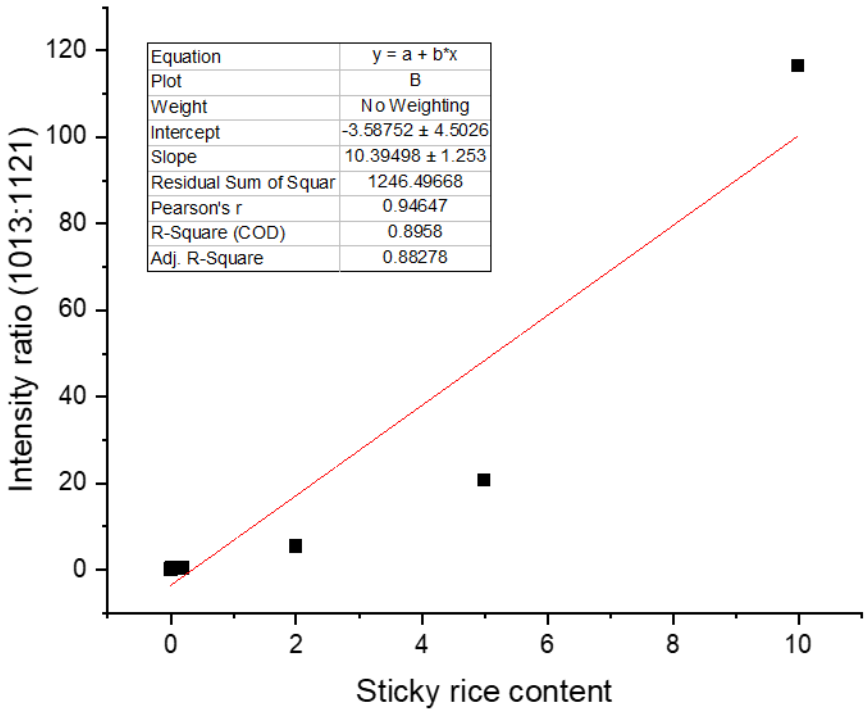


Fig 8-23. The linear fitting result of “321” tabia samples (the red line is the fitting line)

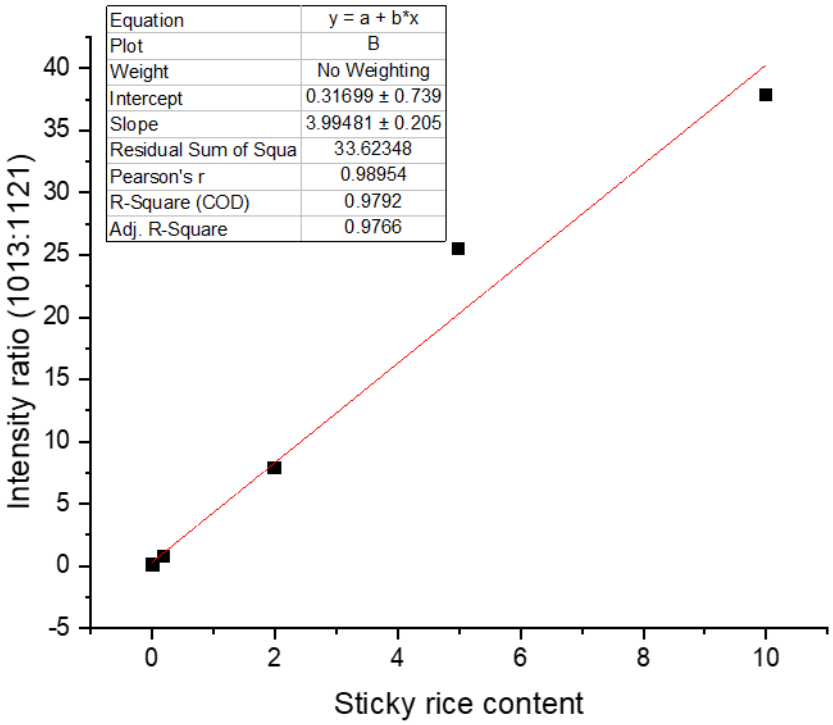


Fig 8-24. The linear fitting result of “230” tabia samples (the red line is the fitting line)

The linear fitting results of 3 types of tabia samples show that the ratio of the intensity at around *m/z* 1013 and 1121 in the MALDI-TOF-MS spectra of “111” and “230” tabia samples has a solid linear relation with the starch content added in advance, which indicates that the MALDI-TOF-MS tests can be applied for quantitative analysis in these two types of tabia. However, the linear relation is influenced by the inorganic composition of the earth sample. For the “321” tabia samples, the linear relation is not so solid. This may be a crucial part of the future work.

The area near *m/z* 1013 and 1121 in the MALDI-TOF-MS spectra is enlarged and shown below to confirm the detection limit.

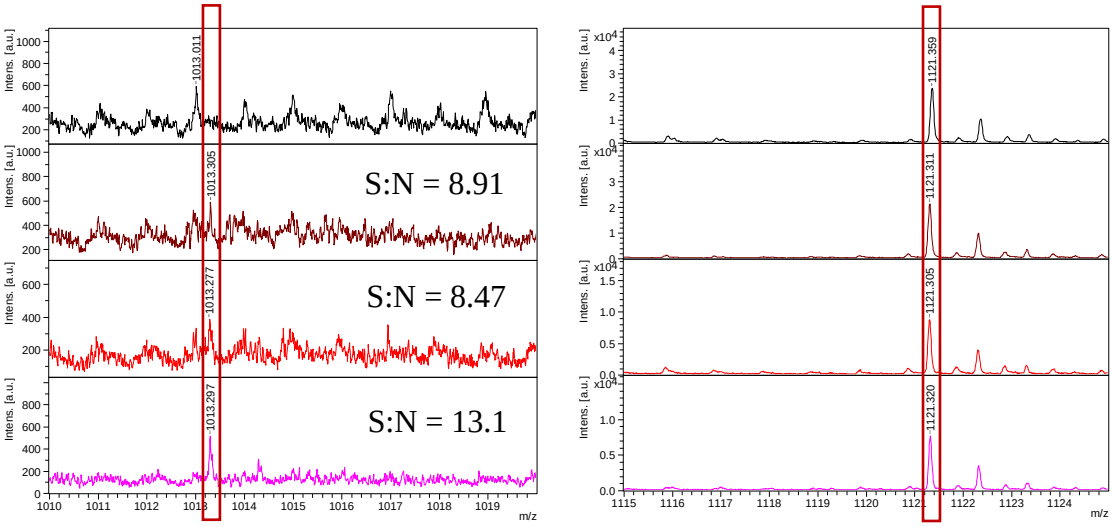


Fig 8-25. The area near *m/z* 1013 and 1121 in the MALDI-TOF-MS spectra (from top to bottom: loess, T30 (0.002% starch content), T27 (0.004% starch content), T24 (0.008% starch content))

The intensity of the peaks around *m/z* 1013 in the MALDI-TOF-MS spectra of T27 and T30 is challenging to distinguish from the background signals ($signal: noise \leq 10$), while the peak in T24 is significant enough for identification ($signal: noise \geq 10$). Thus, the detection limit of the MALDI-TOF-MS for the identification of starch in earth samples is 0.008% (m/m).

8.3.3. Optimisation of the extraction process

Initially, water was applied as the solvent for the extraction of starch after the removal of calcium carbonate from earth samples by acid hydrolysis. A series of peaks at the interval of *m/z* 162 can be observed in the MALDI-TOF-MS spectra of the extract, as shown in Fig 8-26.

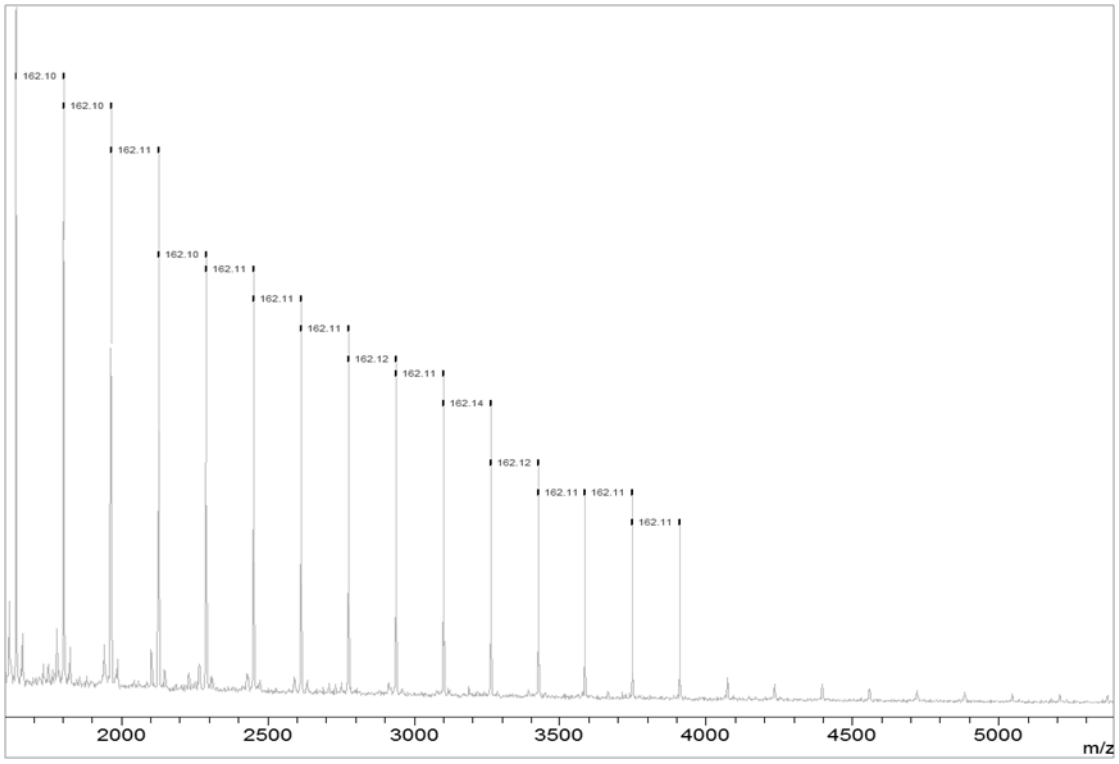


Fig 8-26. The MALDI-TOF-MS spectrum of the water extract of M3 (sample details can be found in Table 3-1, pp. 71-73)

These signals may be from oligosaccharides ($162 = M_{C_6H_{10}O_5}$, a dehydrated monosaccharide), which are the decomposition products of the starch. This pattern can also be observed in some archaeological samples, and 3 examples are shown

below.

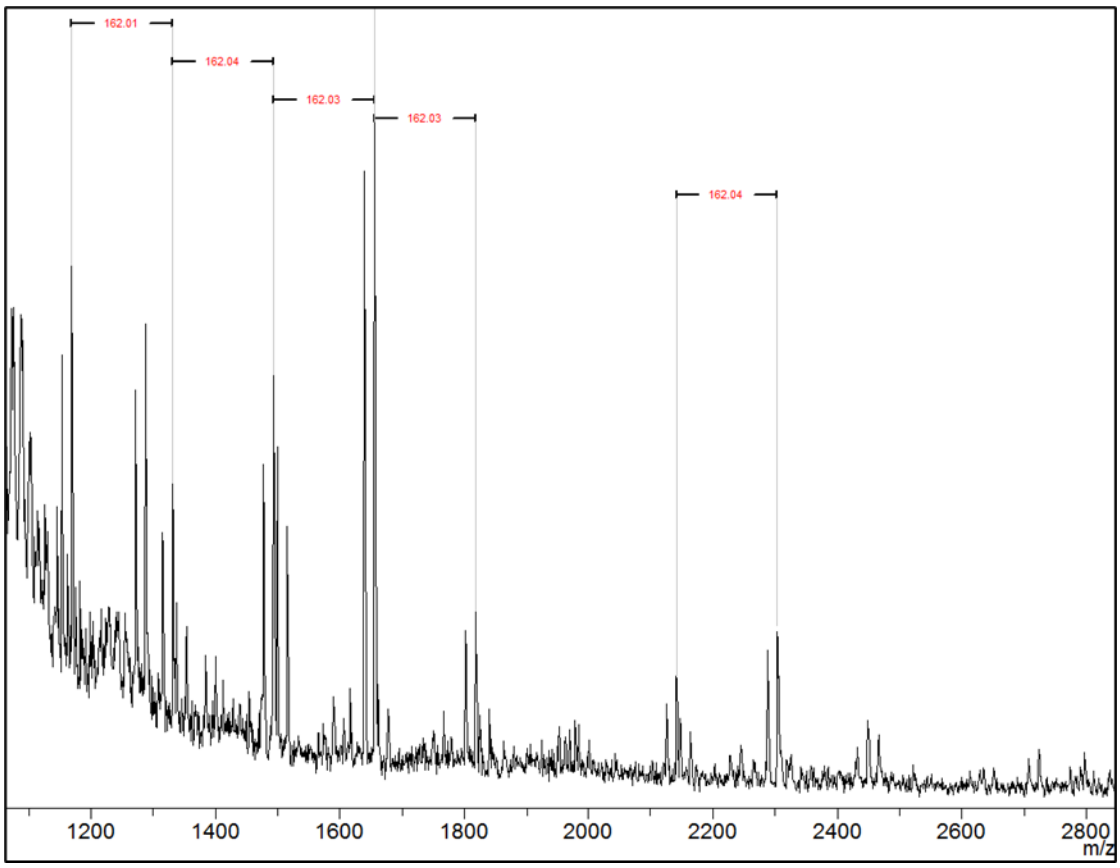


Fig 8-27. The MALDI-TOF-MS spectrum of the water extract of XZM7 (sample details can be found in Table 3-3, pp. 79-83)

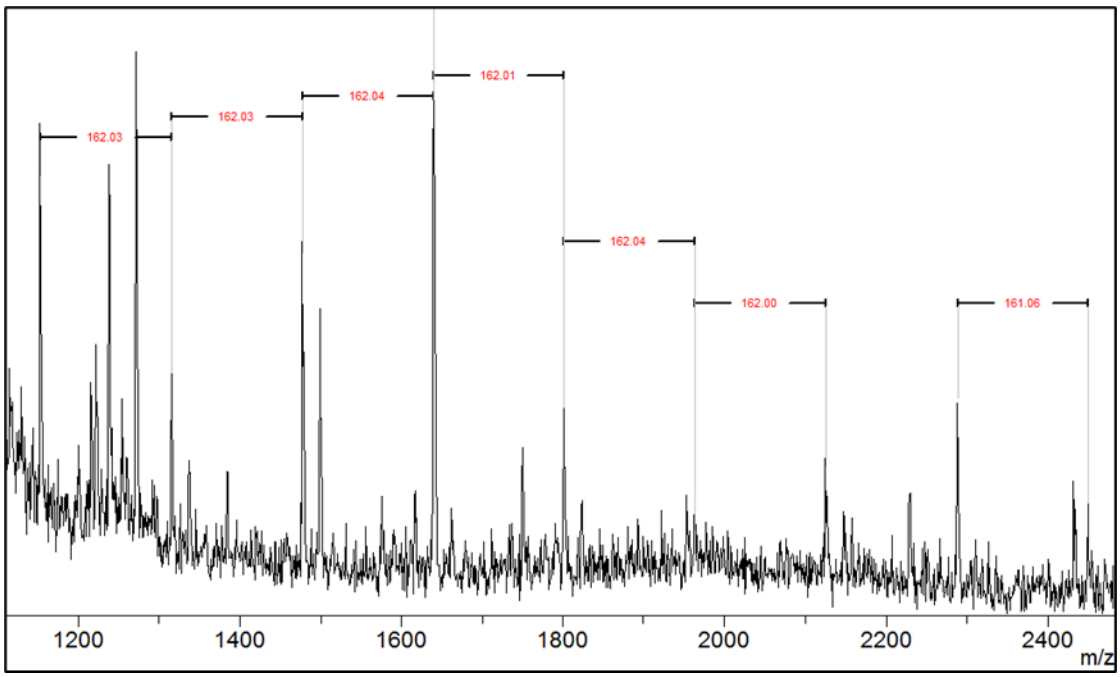


Fig 8-28. The MALDI-TOF-MS spectrum of the water extract of BWC3 (sample details can be found in Table 3-3, pp. 79-83)

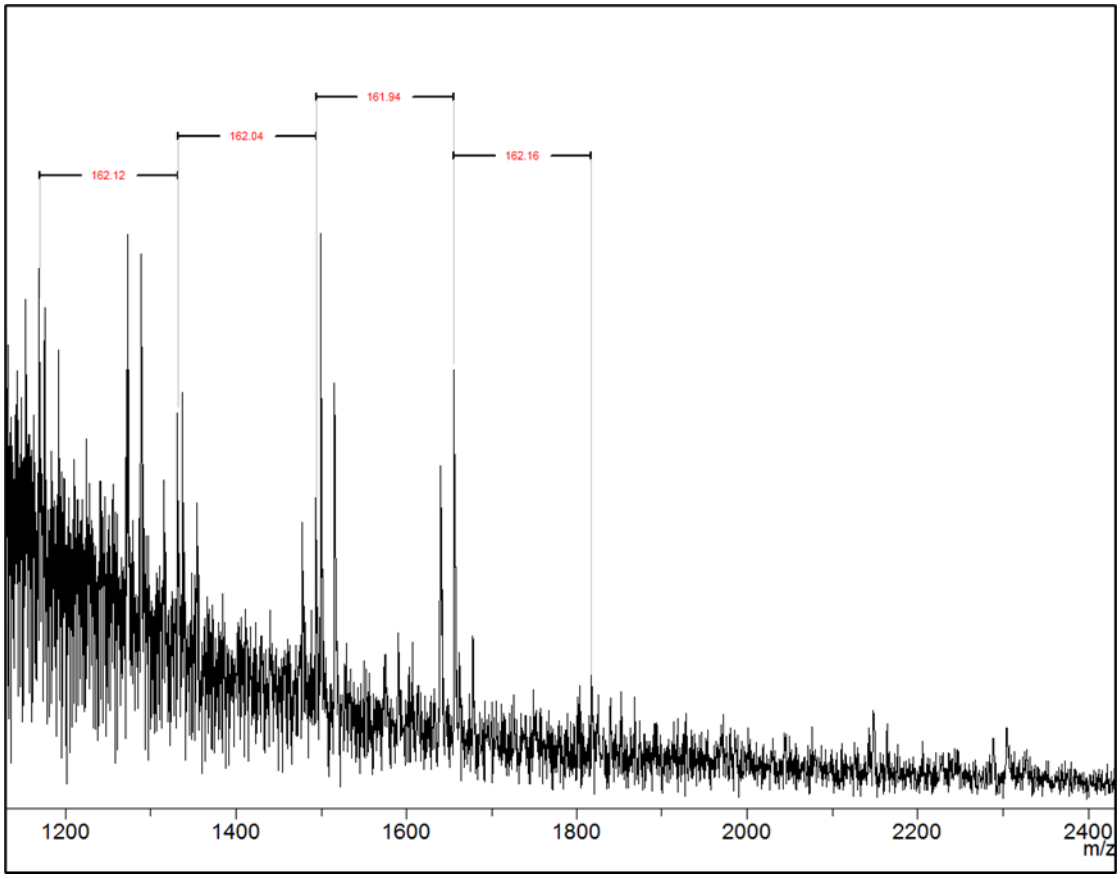


Fig 8-29. The MALDI-TOF-MS spectrum of the water extract of YMY1 (sample details can be found in Table 3-3, pp. 79-83)

However, these oligosaccharides may be the decomposition products of other polysaccharides, such as cellulose, which can be from some plant remains in earth samples. Therefore, the removal of oligosaccharides and the amylase hydrolysis have to be applied in the final protocol to ensure the signals of oligosaccharides are from the starch in earth samples.

The MALDI-TOF-MS tests have been run on T4 (sample details can be found in Table 3-2, pp. 75-76) to evaluate the effect of water wash and enzyme hydrolysis. The

spectra before and after water wash and amylase hydrolysis are shown below.

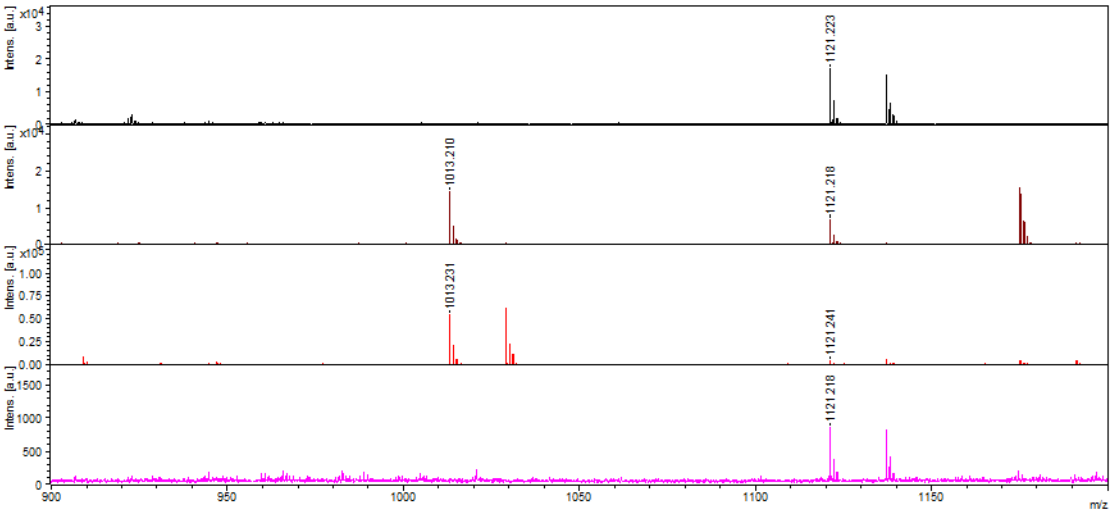


Fig 8-30. The MALDI-TOF-MS spectra of T4 (sample details can be found in Table 3-2, pp. 75-76, from top to bottom: hexasaccharide was added and then water wash was applied, water wash was applied and then hexasaccharide was added, the amylase hydrolysis was applied and no water wash was applied, the amylase hydrolysis and water wash were applied)

As shown in Figure 8-30, the signals for the hexasaccharide at around *m/z* 1013 have been removed by water wash, whether the enzyme hydrolysis has been applied or not. Therefore, water wash and enzyme hydrolysis can ensure that the signals at around *m/z* 1013 and 1029 in the MALDI-TOF-MS spectra are the sodium and potassium adduct ions of the hexasaccharide from the starch in earth samples.

8.3.4. The influence of cellulose in the earth samples

Cellulose could always be found in the loess as the decomposition products of dead plants (Su et al., 2022). Further research has been conducted to verify that the 1013 signals in the MALDI-TOF-MS spectra are exclusively derived from starch and not from cellulose.

The extraction of cellulose was performed by mixing 10 mg of cellulose with 500 μL of water. The supernatant was then obtained by centrifuging the mixture at 3000 r.p.m for 2 min. The solution mixed with the matrix (2,5-DHB) at the ratio of 1:1 was then analysed by MALDI-TOF-MS. Several signals can be observable in the spectrum, including the hexasaccharide peak at around *m/z* 1013, which was utilised in previous chapters to identify starch. These signals may interfere with the identification of starch in the MALDI-TOF-MS tests. The isotope labelling method (Hanson, 2019) was applied to trace the origin of these oligosaccharides. Oxygen-18 water was applied to the extraction of cellulose instead of water. If a 2-Da shift in the position of the starch indicator is observed within the MALDI-TOF-MS spectra, it serves as an indication that oxygen-18 is present in the oligosaccharides, thereby suggesting that these oligosaccharides originate from the hydrolysis of cellulose in the extraction process. The results are shown below.

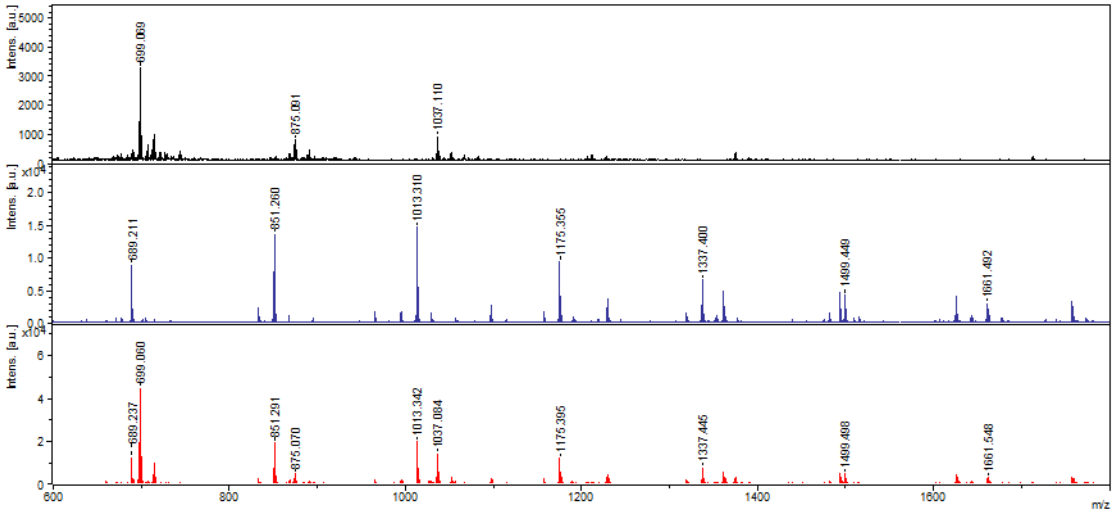


Fig 8-31. The MALDI-TOF-MS spectra of cellulose extraction (from top to bottom: the matrix, water extraction of cellulose, oxygen-18 water extraction of cellulose)

Cellulose is not soluble in water, and the *m/z* values of the peaks (which are not shown in the spectrum of the matrix) in the spectrum are the molecular weight of the adduct ions of oligosaccharides. The origin of these peaks is shown in Table 8-6.

Table 8-6. the origin of the peaks in the spectrum of cellulose extraction

Peaks	Adduct ions	The formula of the saccharide	Degree of polymerization
689.211	Na^+	$C_{24}H_{42}O_{21}$	4
851.260	Na^+	$C_{30}H_{52}O_{26}$	5
1013.310	Na^+	$C_{36}H_{62}O_{31}$	6
1175.355	Na^+	$C_{42}H_{72}O_{36}$	7
1337.400	Na^+	$C_{48}H_{82}O_{41}$	8
1499.449	Na^+	$C_{54}H_{92}O_{46}$	9
1661.492	Na^+	$C_{60}H_{102}O_{51}$	10

There is no difference (a 2-Da shift of the peak position) between the position of the peaks in the spectra of water and oxygen-18 water extraction of cellulose, indicating that the oligosaccharides in the MALDI-TOF-MS spectra of cellulose extraction are not from the hydrolysis products of cellulose with water. Therefore, some oligosaccharides, as the decomposition products of the cellulose, can be observed in the MALDI-TOF-MS spectra of cellulose extraction. These oligosaccharides (mainly the hexasaccharide) will not affect the results, since the hexasaccharide is removed by the water wash step (discussed in Chapter 8.3.3) before the enzyme hydrolysis.

However, some signals of oligosaccharides were produced in the enzyme hydrolysis step (cellulase was applied instead of amylase), including the *m/z* 1013 peak, as

shown in Figure 8-32.

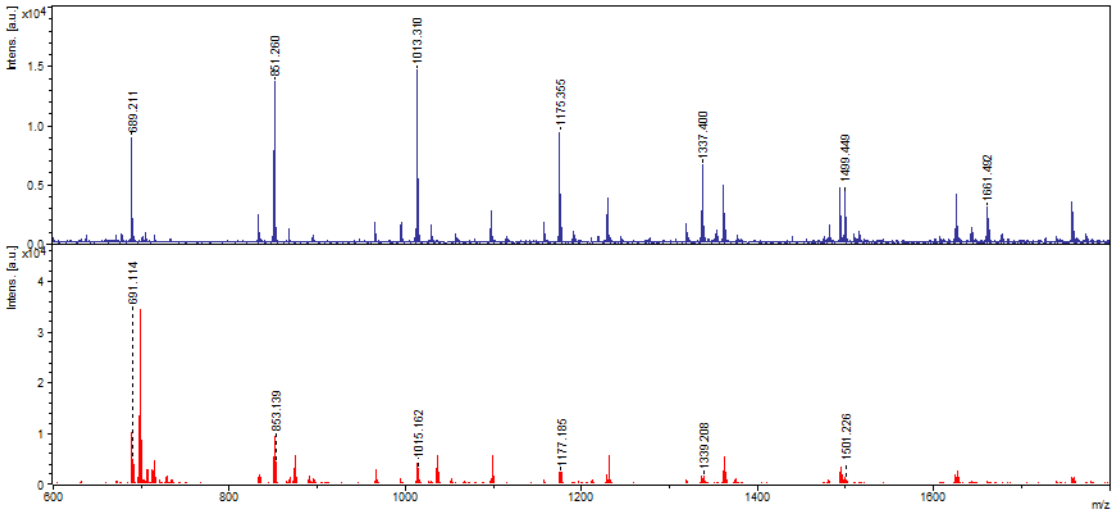


Fig 8-32. The MALDI-TOF-MS spectra of cellulose extraction before and after cellulase hydrolysis (from top to bottom: oxygen-18 water extraction of cellulose, after cellulase hydrolysis in oxygen-18 water)

A 2-Da shift of the peak position can be observed in the MALDI-TOF-MS spectra before and after the cellulase hydrolysis, indicating that some oligosaccharides were produced in the cellulase hydrolysis.

The influence of cellulose on the low molecular weight region of the MALDI-TOF-MS spectra in the enzyme hydrolysis step has been studied. The results are shown below. To display the low molecular weight region, the anion mode was applied in the MALDI-TOF-MS tests with NEDC (N-(1-Naphthyl) ethylenediamine dihydrochloride, $C_{12}H_{16}Cl_2N_2$) as the matrix.

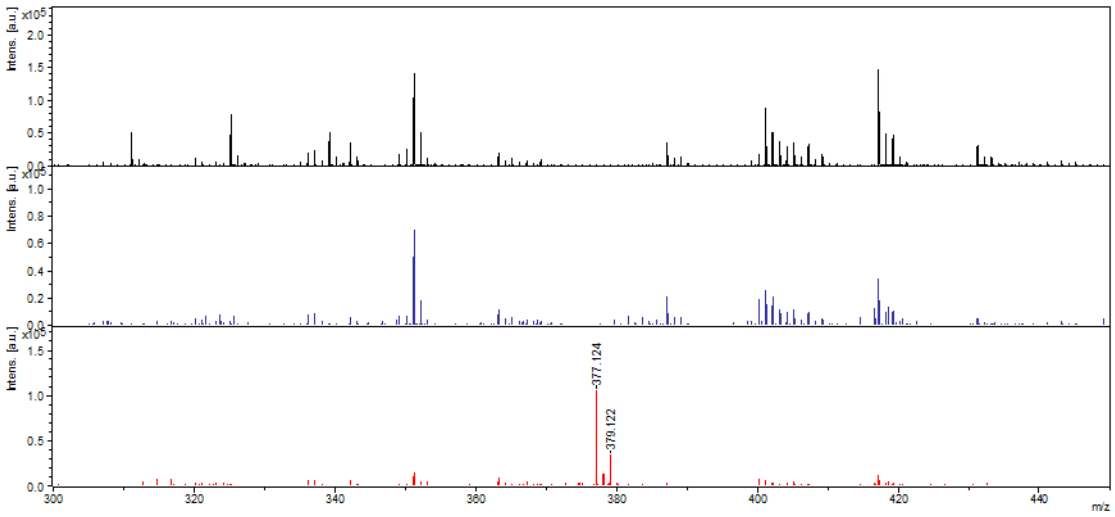


Fig 8-33. The MALDI-TOF-MS spectra of cellulose extraction (from top to bottom: before enzyme hydrolysis, after amylase hydrolysis, after cellulase hydrolysis)

In the low molecular weight region of the spectrum of cellulose extraction after cellulase hydrolysis, the peak around *m/z* 377 can be observed as the signal of the chloride adduct ion of cellobiose ($C_{12}H_{22}O_{11}$, 377 = 35+342), which is the main decomposition product of the cellulose after cellulase hydrolysis.

The influence of cellulase on the enzyme hydrolysis of the starch has also been studied for comparison. The results are shown below.

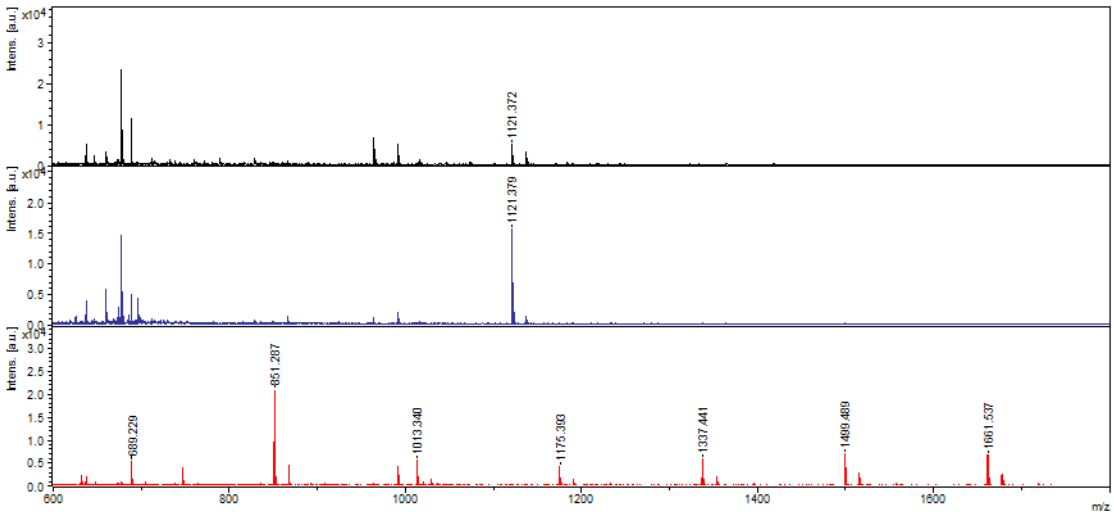


Fig 8-34. The MALDI-TOF-MS spectra of starch extraction (from top to bottom: before enzyme hydrolysis, after cellulase hydrolysis, after amylase hydrolysis)

As shown in Figure 8-34, there is no significant difference between the spectra before and after the cellulase hydrolysis, which serves as the further evidence of the specificity of amylase and cellulase.

Earth samples containing cellulose were prepared to evaluate the impact of cellulose on the identification of starch in earth samples. Information of these samples is shown in Table 8-7. Other details can be found in Table 3-1 (pp. 71-73).

Table 8-7. Details of the modern earth samples containing cellulose

Sample	Cellulose content (weight percentage)
C1	2%
C2	5%
C3	10%

These cellulose-earth samples were run by the same saccharide protocol as the modern and archaeological samples (all samples were taken 3 shots). The results are shown below.

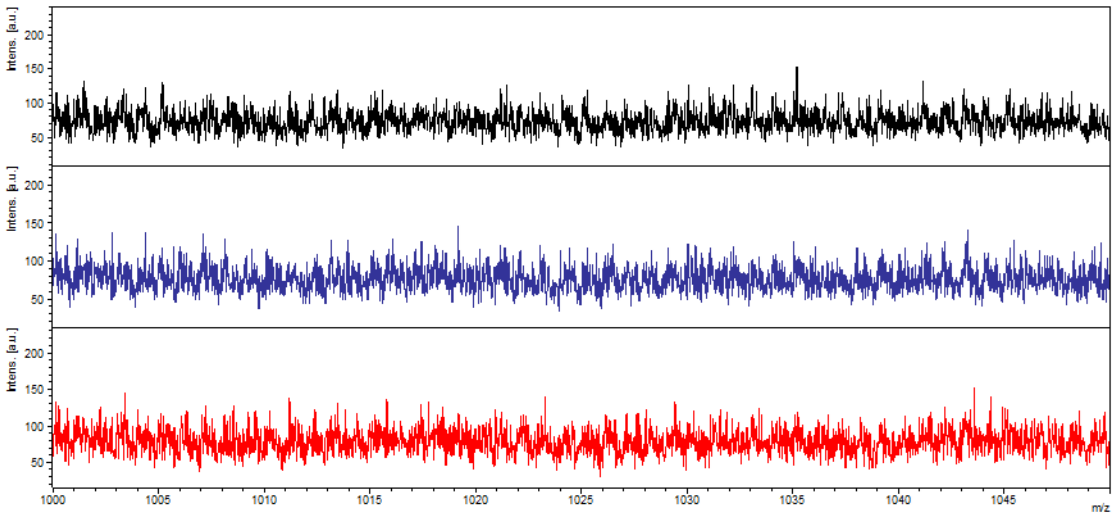


Fig 8-35. The MALDI-TOF-MS results of C1 (3 shots, and the region between *m/z* 1000-1050 is enlarged)

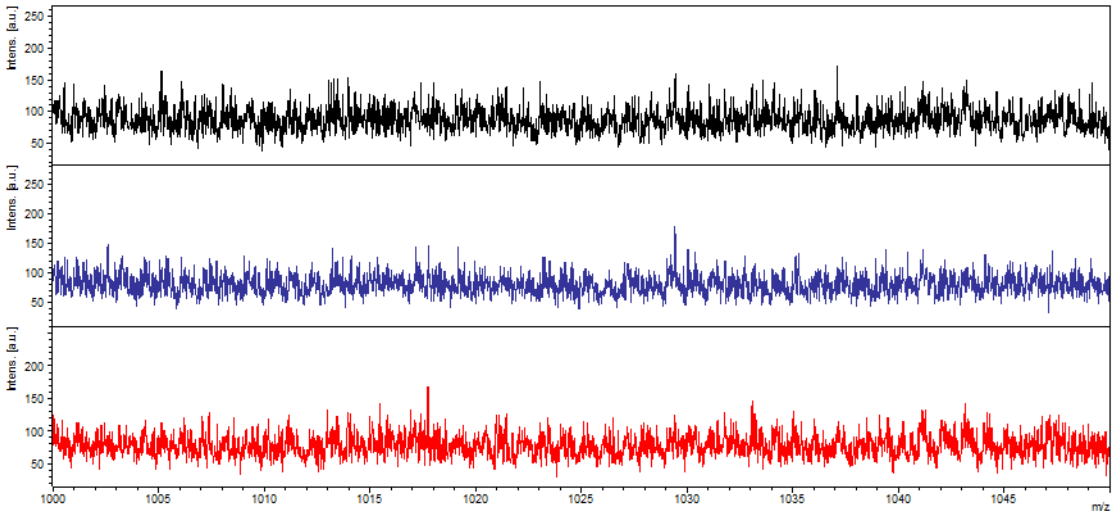


Fig 8-36. The MALDI-TOF-MS results of C2 (3 shots, and the region between *m/z* 1000-1050 is enlarged)

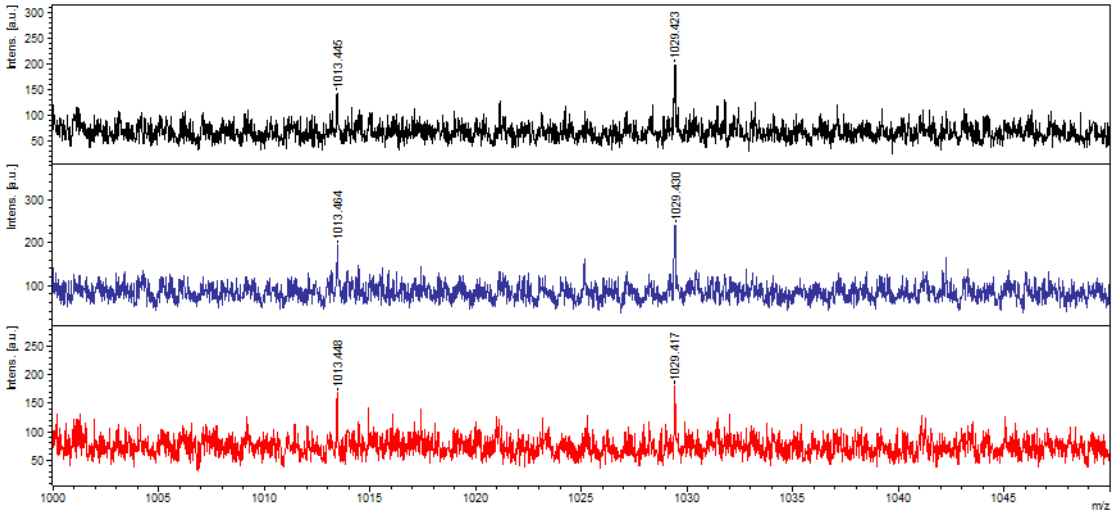


Fig 8-37. The MALDI-TOF-MS results of C3 (3 shots, and the region between *m/z* 1000-1050 is enlarged)

In the spectra of C1 and C2, peaks at *m/z* 1013 cannot be observed, indicating that the hexasaccharide generated initially in cellulose has been removed by the wash step. In the spectrum of C3, extremely weak signals can be observed around *m/z* 1013 and

1029, which are the sodium and potassium adduct ions of the hexasaccharide. However, 10% is relatively high for the weight content of cellulose in the natural loess. In the meantime, the low-intensity signals (even 10% content) will hardly have an impact on the identification of starch in earth samples.

8.3.5. Degradation of starch in earth samples

The degradation of starch may generate a variation on the peak at around *m/z* 1013, which will have a possible influence on the identification of the starch in soil samples. Therefore, degraded samples were prepared by being heated in the oven at 50℃, each heating cycle lasts for 12h. Information of these samples is shown in Table 8-8. Other details can be found in Table 3-4 (pp. 84-85).

Table 8-8. Details of the aged samples (sample details of T1-9 can be found in Table 3-2, pp. 75-76)

Sample	Original sample	Heating time
AT1A	T1	120 h
AT1B	T1	240 h
AT1C	T1	360 h
AT2A	T2	120 h
AT2B	T2	240 h
AT2C	T2	360 h

AT3A	T3	120 h
AT3B	T3	240 h
AT3C	T3	360 h
AT4A	T4	120 h
AT4B	T4	240 h
AT4C	T4	360 h
AT5A	T5	120 h
AT5B	T5	240 h
AT5C	T5	360 h
AT6A	T6	120 h
AT6B	T6	240 h
AT6C	T6	360 h
AT7A	T7	120 h
AT7B	T7	240 h
AT7C	T7	360 h
AT8A	T8	120 h
AT8B	T8	240 h
AT8C	T8	360 h
AT9A	T9	120 h
AT9B	T9	240 h
AT9C	T9	360 h

In the aging process, the alteration in weight of each sample over time (every 12h, weighed after the samples had cooled down) was assessed, and the results are presented below.

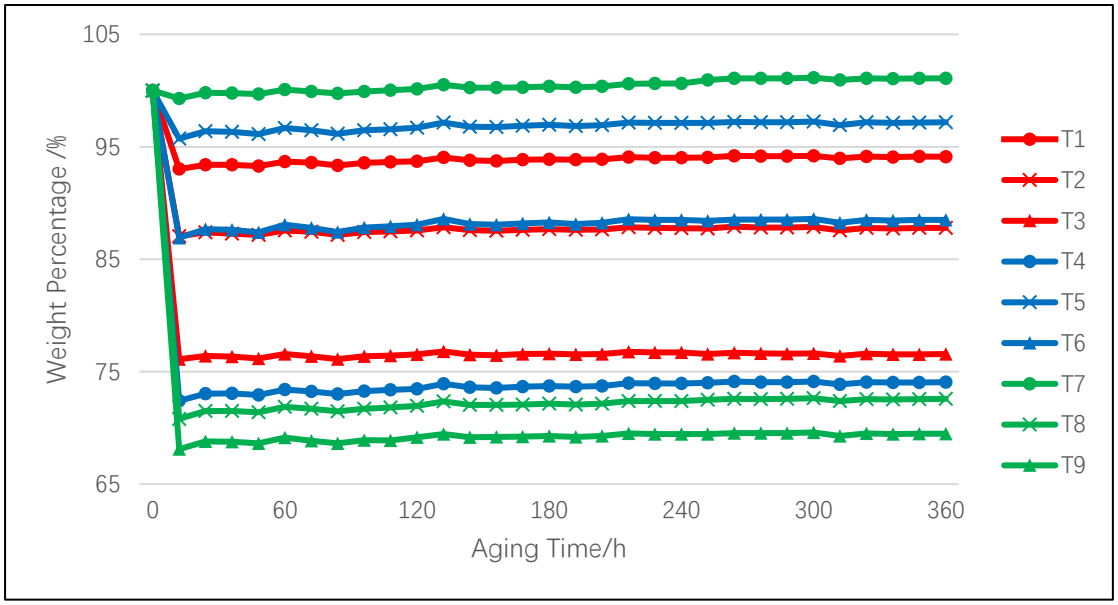


Fig 8-38. The alteration in weight of T1-T9 (sample details can be found in Table 3-2, pp. 75-76) over time

For all the samples, the most significant weight loss of the entire heating process occurred in the first 12-hour cycle. The amount of the weight loss in this period seems to be relevant to the content of starch for the “111” (T1-3) and “321” (T7-9) tabia samples. The decrease in weight of the heated samples is: T1<T2<T3, and T7<T8<T9; while the starch content is: T1 (2%)<T2 (5%)<T3 (10%), and T7 (2%)<T8 (5%)<T9 (10%). A possible explanation is that the weight loss is due to the degradation of the starch, such as dehydration. Thus, higher starch content in the tabia

samples resulted in greater weight loss upon heating. However, apart from the positive correlation between the weight loss and the starch content of "111" and "321" tabia samples, the results of "230" samples display a distinct pattern. The decrease in weight of the heated samples is: T5<T6<T4; while the starch content is: T4 (2%)<T5 (5%)<T6 (10%), indicating that the thermal decomposition of the starch in the tabia samples is complicated.

The MALDI-TOF-MS tests were run on all the aged samples. The intensity ratios of the peaks at around *m/z* 1013 and 1121 for the 9 shots of the same sample and their averages have also been calculated and are shown in Table 8-9.

Table 8-9. The ratio of the intensity at around *m/z* 1013 and 1121 in the MALDI-TOF-MS spectra of the aged tabia samples

	Shot 1	Shot 2	Shot 3	Shot 4	Shot 5	Shot 6	Shot 7	Shot 8	Shot 9	Average
AT1A	0.266	0.312	0.339	0.323	0.326	0.320	0.271	0.238	0.295	0.299
AT1B	0.184	0.251	0.204	0.249	0.218	0.243	0.275	0.280	0.234	0.238
AT1C	0.525	0.505	0.443	0.529	0.520	0.549	0.537	0.596	0.570	0.531
AT2A	0.290	0.256	0.286	0.261	0.324	0.318	0.287	0.301	0.289	0.290
AT2B	0.165	0.184	0.179	0.187	0.163	0.165	0.170	0.180	0.167	0.173
AT2C	0.296	0.276	0.255	0.290	0.321	0.302	0.306	0.282	0.240	0.285
AT3A	0.260	0.317	0.286	0.284	0.273	0.287	0.266	0.251	0.245	0.274

AT3B	0.363	0.336	0.320	0.342	0.369	0.380	0.303	0.377	0.351	0.349
AT3C	0.370	0.376	0.342	0.418	0.359	0.392	0.353	0.362	0.321	0.366
AT4A	1.30	1.06	1.14	1.40	1.39	1.36	1.16	1.16	1.15	1.23
AT4B	1.79	1.81	1.79	3.88	3.27	2.31	3.38	2.95	3.44	2.74
AT4C	2.94	2.89	2.94	3.29	2.84	3.40	2.86	2.97	2.85	3.00
AT5A	2.44	2.98	2.02	2.19	2.67	2.30	2.72	2.63	2.48	2.49
AT5B	2.83	2.74	3.50	2.41	2.81	2.72	2.25	2.26	1.94	2.61
AT5C	3.27	3.26	3.35	3.62	3.41	3.38	3.39	3.09	3.59	3.37
AT6A	63.7	59.8	43.2	42.0	45.0	52.8	47.9	48.8	57.6	51.2
AT6B	46.3	46.7	44.5	31.9	35.1	43.9	32.6	26.8	25.3	37.0
AT6C	81.5	77.0	65.9	82.7	80.4	75.0	74.9	91.1	72.0	77.8
AT7A	2.16	2.28	2.39	2.26	2.05	1.91	1.42	1.75	1.82	2.00
AT7B	1.83	1.94	1.89	1.77	1.69	1.83	1.85	1.81	1.79	1.82
AT7C	2.52	2.62	2.55	2.64	2.50	2.41	2.56	2.45	2.58	2.54
AT8A	5.53	4.57	5.11	4.74	3.81	4.10	5.10	4.59	4.25	4.64
AT8B	13.0	12.0	11.3	10.7	11.6	10.7	14.9	13.3	13.7	12.4
AT8C	10.2	11.0	11.0	11.8	10.8	10.3	11.2	11.7	10.5	10.9
AT9A	37.4	36.2	38.6	37.0	37.9	35.5	39.3	44.6	33.2	37.7
AT9B	17.5	20.3	17.8	14.5	16.1	14.0	24.7	19.3	17.1	17.9
AT9C	25.5	26.4	25.4	27.3	26.1	27.0	28.9	28.9	26.1	26.9

The alteration in the intensity ratio through time between the peaks at around *m/z* 1013 and 1121 in the MALDI-TOF-MS spectra of "111", "230" and "321" tabia samples is shown in Figures 8-39, 8-40 and 8-41. The intensity ratios of T1-9 are also shown in the figures as the data of 0 h.

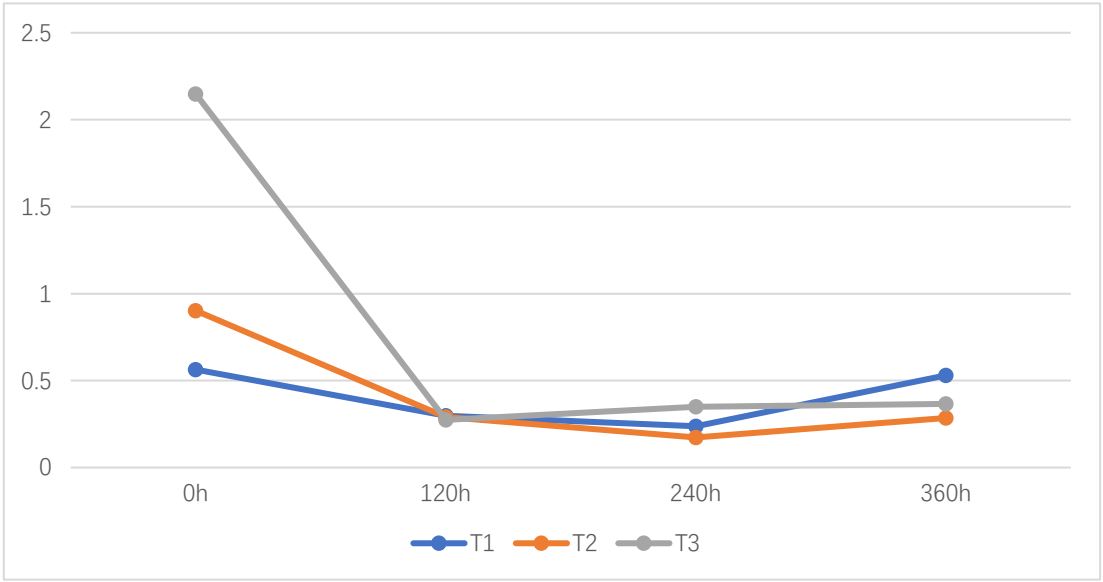


Fig 8-39. The alteration in the intensity ratio through time between the peaks at around *m/z* 1013 and 1121 in the MALDI-TOF-MS spectra of "111" tabia samples (AT1A, AT1B and AT1C are shown in the line of T1; AT2A, AT2B and AT2C are shown in the line of T2; AT3A, AT3B and AT3C are shown in the line of T3)

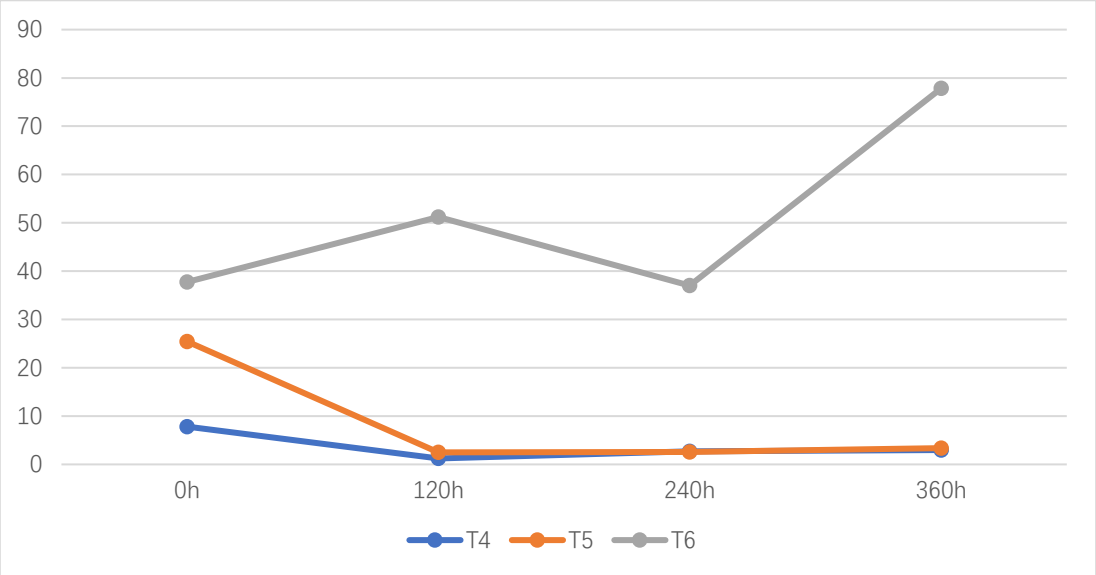


Fig 8-40. The alteration in the intensity ratio through time between the peaks at around *m/z* 1013 and 1121 in the MALDI-TOF-MS spectra of "230" tabia samples (AT4A, AT4B and AT4C are shown in the line of T4; AT5A, AT5B and AT5C are shown in the line of T5; AT6A, AT6B and AT6C are shown in the line of T6)

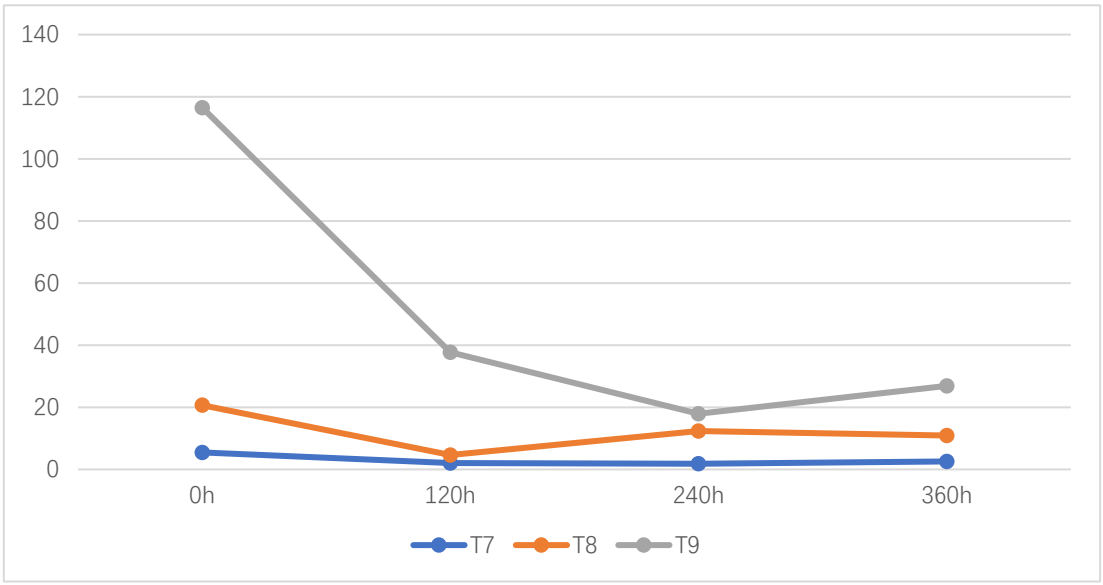


Fig 8-41. The alteration in the intensity ratio through time between the peaks at around *m/z* 1013 and 1121 in the MALDI-TOF-MS spectra of "321" tabia samples (AT7A, AT7B and AT7C are shown in the line of T7; AT8A, AT8B and AT8C are shown in the line of T8; AT9A, AT9B and AT9C are shown in the line of T9)

The intensity ratio of the peaks at around *m/z* 1013 and 1121 decreases in the spectra of most degraded earth samples compared to that of their original samples, indicating that a slighter amount of hexasaccharide was produced after the enzyme hydrolysis due to the degradation of starch. However, the degraded samples of T6 show a distinctive trend, with an increase in the intensity ratio. This suggests that there is a greater amount of hexasaccharide in the enzyme hydrolysis products of the aged starch present in the degraded samples of T6. It seems that the degradation of the starch in earth is a very complicated process. Further tests have to be run to learn this subject, for example, more degradation conditions, shorter time interval or longer degradation time, in the future. Moreover, as shown in Figure 8-38, the weight of the

heated samples after 12 h remained relatively constant. However, Figures 8-39, 8-40, and 8-41 show that the variation of intensity ratio of *m/z* 1013 and 1121 peaks in their MALDI-TOF-MS spectra is not the same pattern except for T7, of which the intensity ratio remains relatively constant after 120 h. This reveals that the compounds in the earth samples transformed though the weight kept consistently steady after heating.

8.5. Conclusions

A new MALDI-TOF-MS protocol was developed on modern earth samples to identify the starch. Following the release and removal of free oligosaccharides through acid hydrolysis and water wash, amylase hydrolysis was conducted on the remaining residues. As a result, any oligosaccharides identified in subsequent steps can be attributed to the presence of starch. The peak (after calibration) at *m/z* 1013.325 ± 0.008, which is the signal of the sodium adduct ion of a hexasaccharide, serves as the indicator for the starch. In some cases, this peak can be "fake" marker for starch if there is a peak at around *m/z* 997, or the characteristic peak is lower than 1013.300. This protocol was then applied to archaeological samples. Starch was identified in 2 samples: HYPT1 (from the Fort Hongyuan site) and TFGPT1 (from the Fort Tianfeigong site). In all the environmental samples of HYPT1, starch cannot be found, which indicates that the starch in HYPT1 was artificially added. In 1 of the 3 environmental samples of TFGPT1, trace amount of starch was detected, meaning that the artificial addition of starch in TFGPT1 is still to be confirmed by further test.

The new protocol was also applied to modern samples containing different kinds of starch (wheat starch, sweet potato starch, corn starch, rice flour and sticky rice). The indicators can be found in samples containing all kinds of starch. Therefore, the MALDI-TOF-MS cannot be used to identify the species of starch.

The ratio of the intensity between approximately *m/z* 1013 and 1121 (internal standard) can be used to calculate the content of starch in earth samples. The detection limit of the MALDI-TOF-MS tests to identify starch in earth samples is 0.008% (m/m).

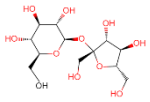
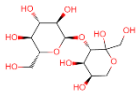
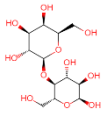
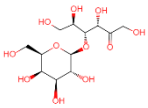
The influence of cellulose and starch degradation on the identification of starch in earth samples was also evaluated by tests on modern and aged modern samples. The existence of cellulose will not affect the MALDI-TOF-MS tests. However, the degradation of starch is very complicated. More aging conditions and further tests have to be applied to figure out the whole process.

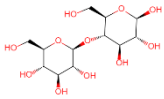
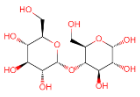
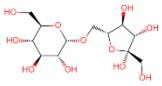
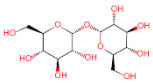
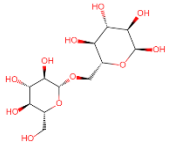
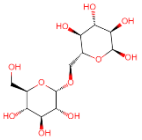
9. Liquid chromatography-tandem mass spectrometry (LC-MS/MS)

9.1. Samples

The LC-MS/MS test was applied to disaccharide standards (n = 10) and archaeological samples (n = 8) to analyse the disaccharide. Information of disaccharide standards is shown in Table 9-1. Other details can be found in Chapter 3 (pp. 54-83).

Table 9-1. Details of the disaccharide standards applied in the LC-MS/MS test

Sample name	Chemical structure	Details
Sucrose		Produced by Beijing Solarbio Science & Technology Co., Ltd.
Turanose		Produced by Shanghai Aladdin Biochemical Technology Co., Ltd.
Lactose		Produced by Shanghai Macklin Biochemical Technology Co., Ltd.
Lactulose		Produced by Shanghai Aladdin Biochemical Technology Co., Ltd.

Cellobiose		Produced by Shanghai Aladdin Biochemical Technology Co., Ltd.
Maltose		Produced by Shanghai Aladdin Biochemical Technology Co., Ltd.
Isomaltulose		Produced by Shanghai Aladdin Biochemical Technology Co., Ltd.
Trehalose		Produced by Shanghai Aladdin Biochemical Technology Co., Ltd.
Gentiobiose		Produced by Shanghai Acmec Biochemical Co., Ltd.
Isomaltose		Produced by Shanghai Acmec Biochemical Co., Ltd.

9.2. Methods

The LC-MS/MS method was collaboratively developed by Xiaopeng Yao (from the Institute of Cell Analysis, Shenzhen Bay Laboratory) and the author. Due to pandemic restrictions, the author was unable to physically be present in Shenzhen. Therefore, the author remotely directed the methodology development process, while Xiaopeng Yao executed the practical aspects of the method under the author's guidance.

9.2.1. Sample preparation

1. The disaccharide standards were dissolved in ultrapure water to produce a stock solution at 10 $mg \cdot mL^{-1}$. This was diluted to different concentrations (100-10000 $ng \cdot mL^{-1}$) before the mass spectrometry analysis (1 μL for each sample).

2. 500 μL of ultrapure water was added to the 50 mg ground archaeological sample. After thorough mixing, the mixture was centrifuged and passed through a 0.22 μm filter.

3. 200 μL of the filtrate was then placed in a vacuum concentrator (Speed Vac SPD1030, Thermo Fisher Scientific, USA) for drying. Before the mass spectrometry analysis, the dried samples were resuspended in 20 μL of ultrapure water.

9.2.2. LC-MS/MS Analysis

The LC-MS/MS analysis was performed using a Triple Quad 5500+ mass spectrometer (SCIEX, USA) equipped with a 1260 Infinity II liquid chromatograph (Agilent, USA). The chromatographic column employed was the Accucore 150 Amide HILIC. The mobile phases used were as follows: Mobile phase A was 0.02% $NH_3 \cdot H_2O$, while mobile phase B was 80% ACN with 0.02% $NH_3 \cdot H_2O$, all delivered at a flow rate of 0.2 $mL \cdot min^{-1}$. The elution gradient was programmed as: 0–0.5 min, 80% phase B; 0.5–15.5 min, 80% to 50% phase B; 15.5–17 min, 50% phase B; 17–18 min, 50% to 80% phase B; and 18–23 min, 80% phase B.

The mass spectrometry parameters were set in negative ion mode, with an *m/z* range of 50–360. The declustering voltage and MS/MS fragmentation energy were optimized using sucrose.

9.3. Results

The results of the LC-MS/MS tests are shown in appendix 6, and further discussion about these results can be found in Chapter 9.4.

9.4. Discussion

9.4.1. The identification of disaccharide in LC-MS/MS

Brown sugar is mentioned in some references (Shen et al., 2006; Chen, 2018; Bai et al., 2021) used in the construction of Kaiping Diaolou. The LC-MS/MS tests were used to identify brown sugar by detecting the sucrose molecules in archaeological samples collected from different architectures in Kaiping.

Initially, the LC-MS/MS tests were conducted on various disaccharide standards to evaluate the method's specificity for sucrose analysis based on retention time. Single ion monitoring was applied to monitor the *m/z* 341 fragment (disaccharide fragment, as shown in Figures 9-10, 9-11 and 9-12). The LC-MS/MS results of 10 standard disaccharide samples are shown below in Figure 9-1.

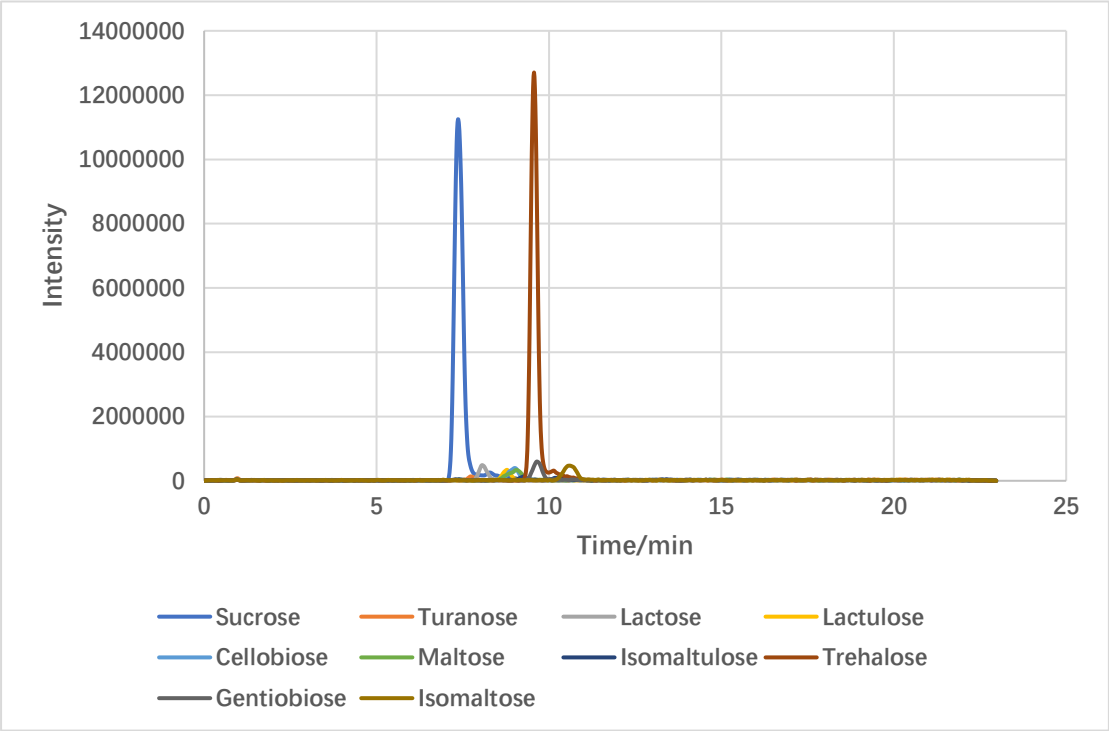


Fig 9-1. The LC-MS/MS results of the standard disaccharides

The intensities of the sucrose and trehalose signals are significantly higher than those of other disaccharides in the LC-MS/MS chromatogram. This phenomenon may be attributed to a combination of factors, including the unique molecular structures of these two disaccharides, their ionization efficiencies, and the detection sensitivities of the mass spectrometer. The retention time of these disaccharides is shown below in Table 9-2.

Table 9-2. The retention time of different disaccharides

Disaccharide	Retention time (min)
Sucrose	7.38
Turanose	7.76
Lactose	8.08
Lactulose	8.77
Cellobiose	8.98
Maltose	9.03
Isomaltulose	9.25 and 10.29
Trehalose	9.57
Gentiobiose	9.66
Isomaltose	10.61

The LC-MS/MS tests were also applied to archaeological samples. The LC results are shown in Figures 9-2 to 9-9.

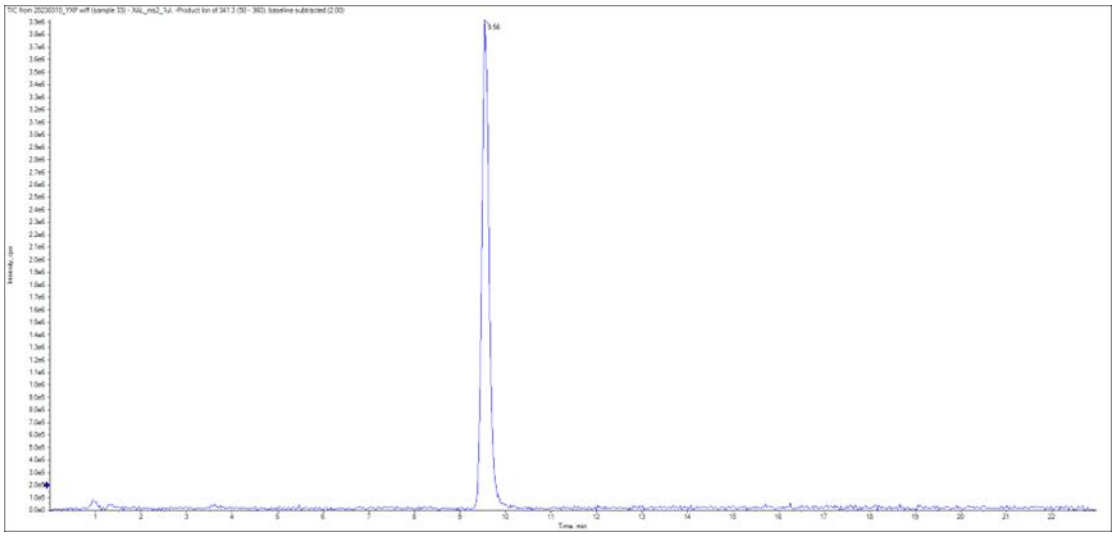


Fig 9-2. The LC result of XAL

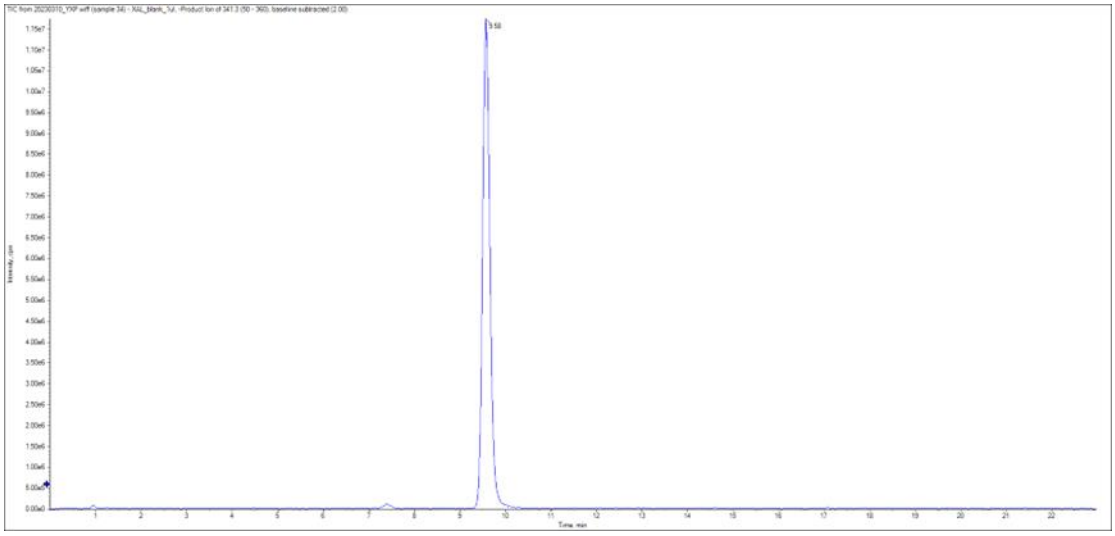


Fig 9-3. The LC result of XAL-B1

As shown in Figures 9-2 and 9-3, a peak at around 9.57 min can be found in the LC chromatogram of XAL and XAL-B1. Additionally, a weak signal at around 7.38 min can be found in XAL-B1.

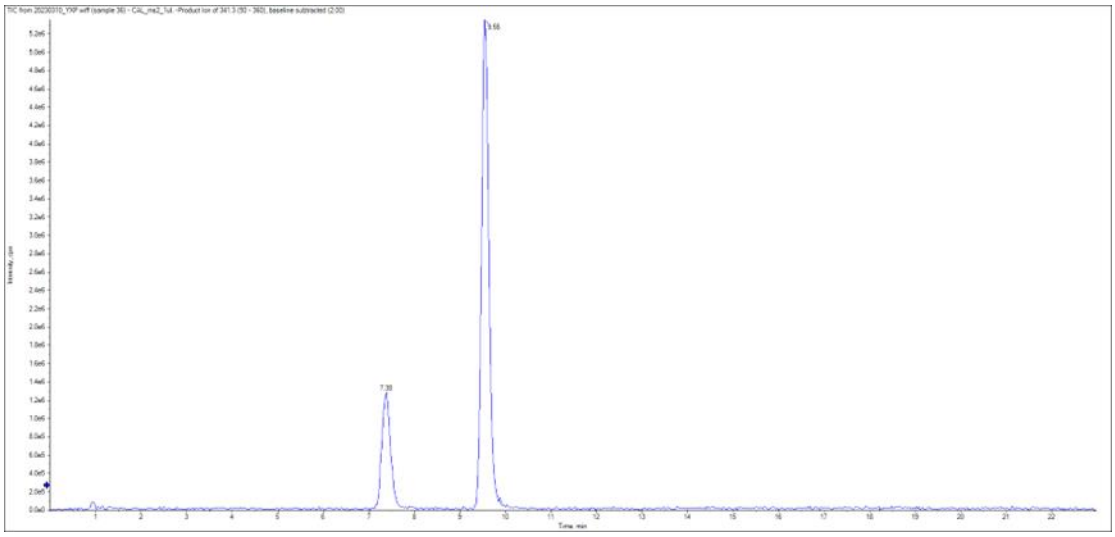


Fig 9-4. The LC result of CAL

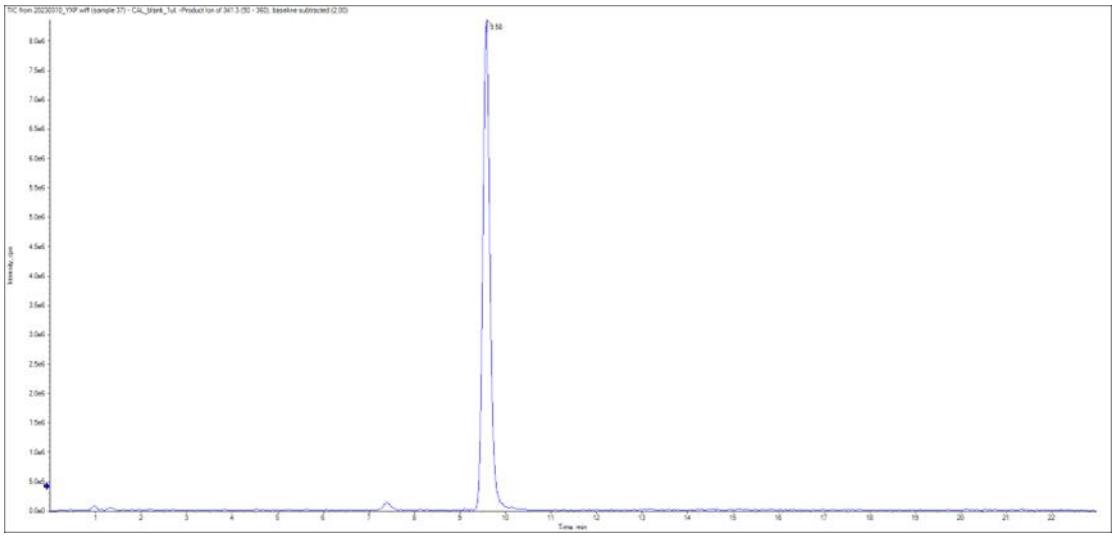


Fig 9-5. The LC result of CAL-B1

As shown in Figures 9-4 and 9-5, two peaks at around 7.38 and 9.57 min can be found in the LC chromatograms of CAL and CAL-B1. Similar to that in XAL-B1, the signal at around 7.38 min in CAL-B1 is very weak.

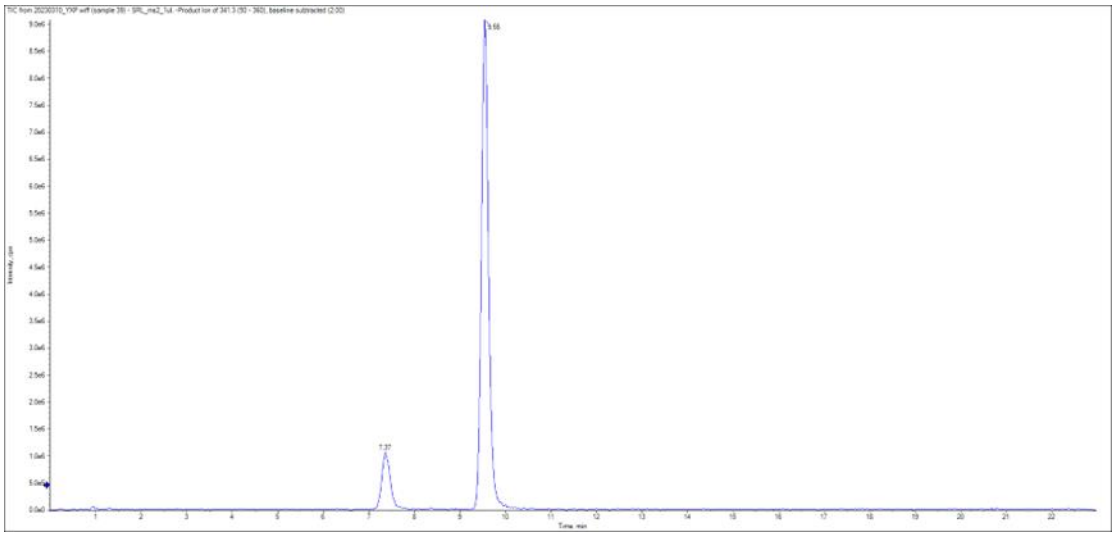


Fig 9-6. The LC result of SRL

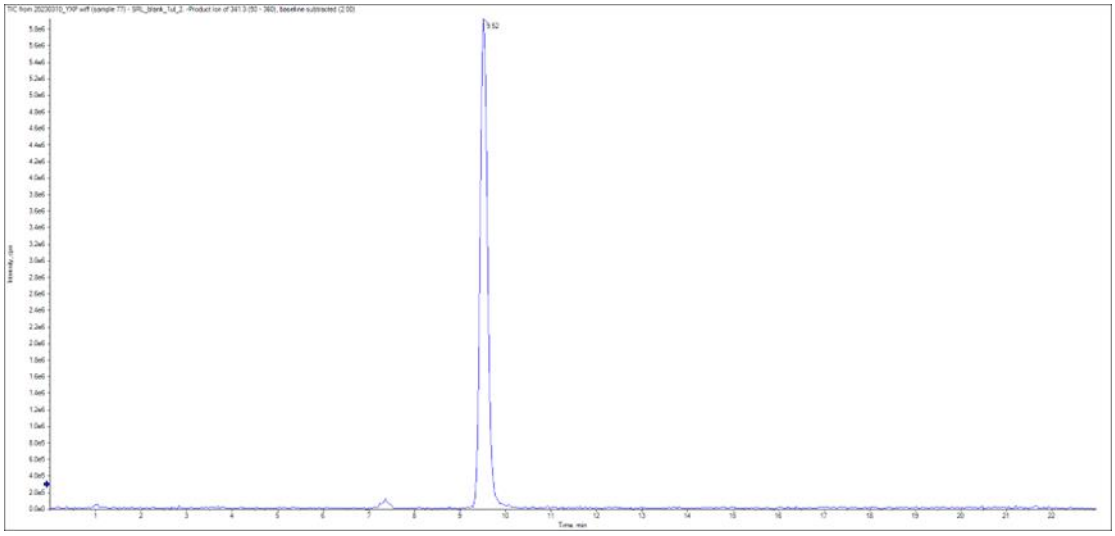


Fig 9-7. The LC result of SRL-B1

As shown in Figures 9-6 and 9-7, two peaks at around 7.38 and 9.57 min can be found in the LC chromatograms of SRL and SRL-B1. Similar to that in XAL-B1, the signal at around 7.38 min in SRL-B1 is very weak.

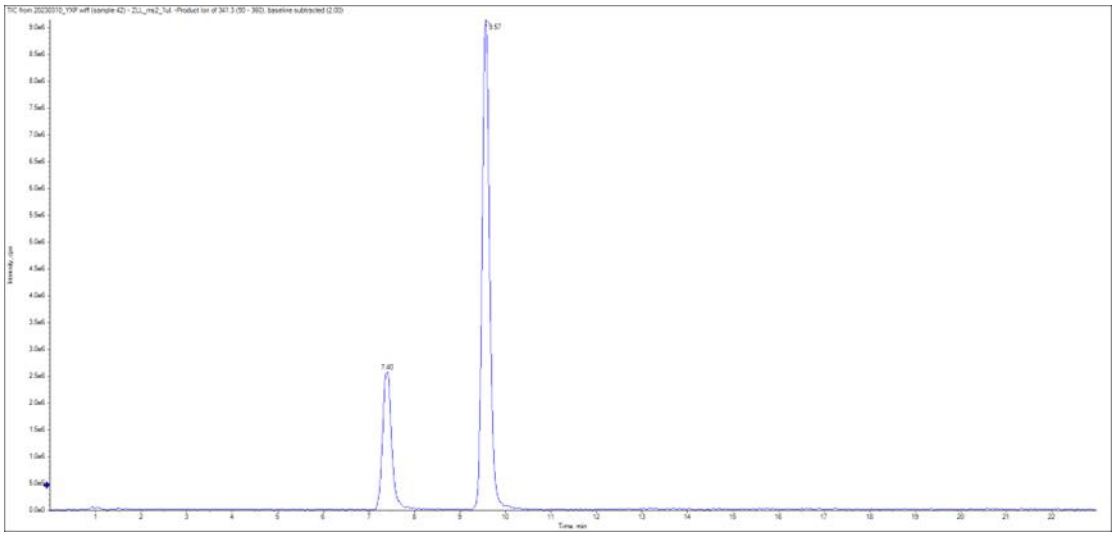


Fig 9-8. The LC result of ZLL

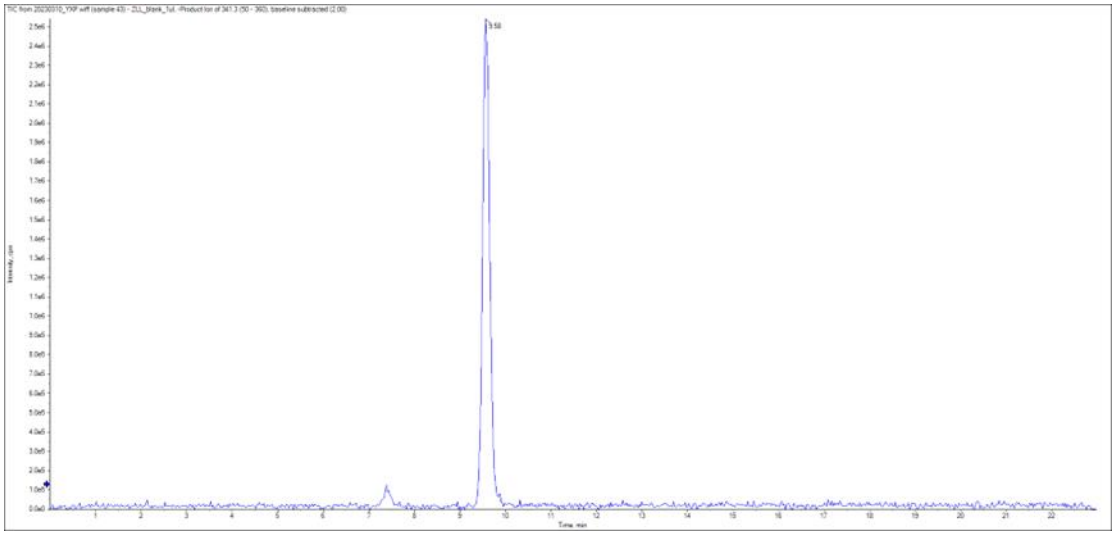


Fig 9-9. The LC result of ZLL-B1

As shown in Figures 9-8 and 9-9, two peaks at around 7.38 and 9.57 min can be found in the LC chromatograms of ZLL and ZLL-B1. Similar to that in XAL-B1, the signal at around 7.38 min in ZLL-B1 is very weak.

To sum up, strong signals of sucrose (retention time at around 7.38 min) are found in 3 archaeological samples: CAL, SRL and ZLL, while weak signals of sucrose are found in XAL-B1, CAL-B1, SRL-B1 and ZLL-B1. This suggests that although small amounts of sucrose might be present in all environmental samples around the Diaolous in Kaiping district, the amount of sucrose in CAL, SRL and ZLL may be significantly higher, which may be relevant to the addition of brown sugar during the construction process. The quantitative analysis can be found in Chapter 9.4.2.

Strong signals at around 9.57 min can be found in all the 8 archaeological samples. These signals may be from trehalose (retention time 9.57 min) and gentiobiose (retention time 9.66 min). MS/MS was applied to distinguish these two disaccharides. The results are shown in Figures 9-10 and 9-11.

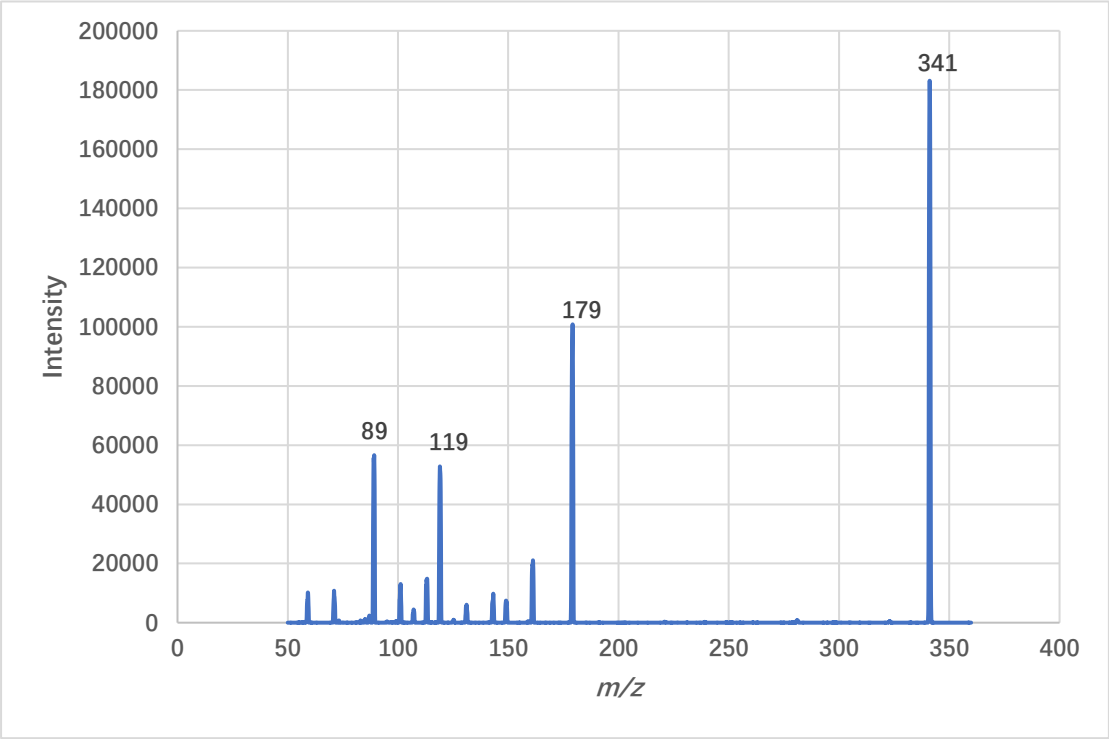


Fig 9-10. The MS/MS result of trehalose

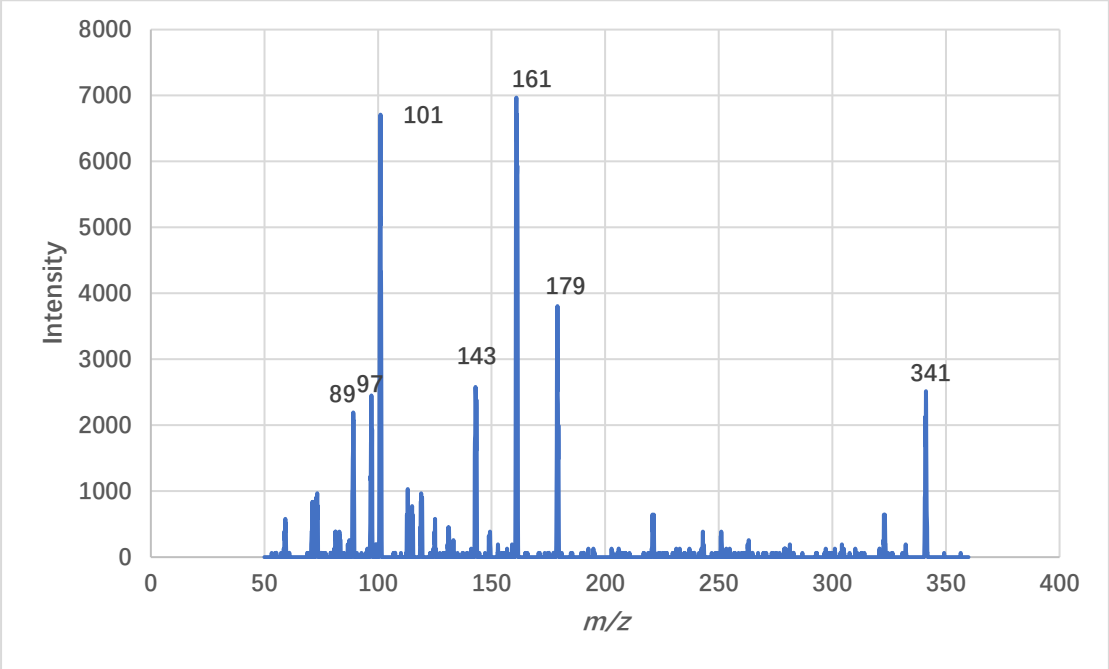


Fig 9-11. The MS/MS result of gentiobiose

Although most of the peak positions of trehalose and gentiobiose are the same due to their similar molecular structure (the same molecular formula $C_{12}H_{22}O_{11}$), the intensity of their peaks displays different patterns. It indicates that LC-MS/MS can be applied to distinguish trehalose and gentiobiose from the earth samples. The signals observed at around 9.57 min in Figures 9-2 to 9-9 are from trehalose. An example is shown in Figure 9-12.

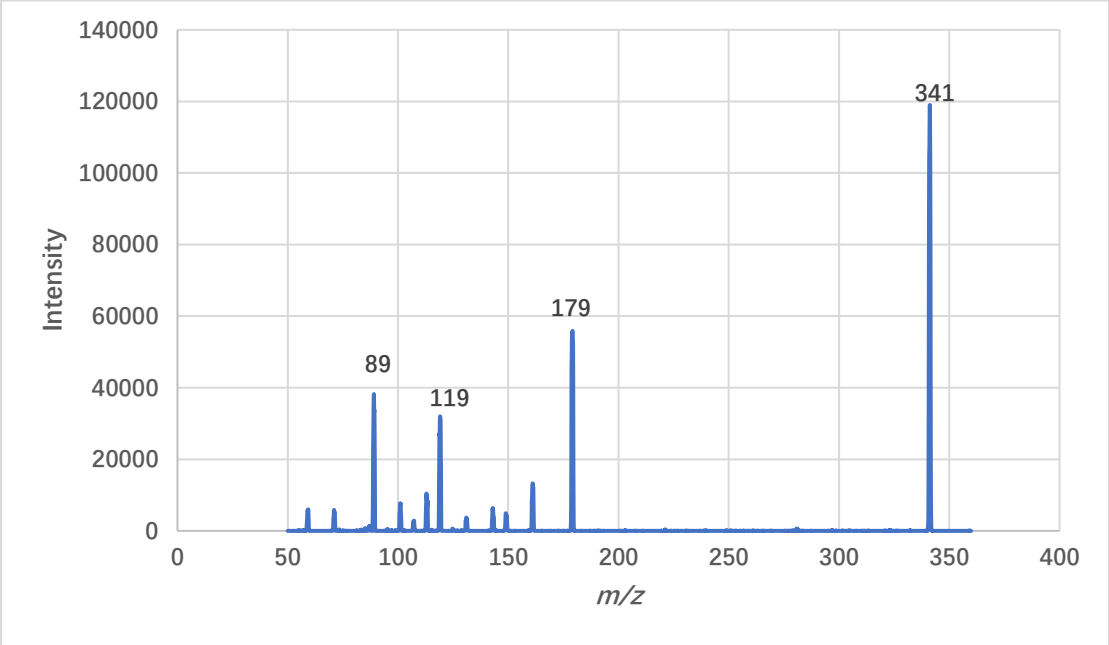


Fig 9-12. The MS/MS result of the compound at around 9.57 min of ZLL

Sucrose is one of the major soluble sugars in plants (Balasubramanian et al., 1972). It is the predominant sugar in the phloem of plants (Bieleski, 1995), and also can be found in the soil near the root tip (Jaeger et al., 1999; Farrar et al., 2003). Trehalose, which is widely found in soya bean plants (Streeter, 1981) and fungi (Thevelein, 1984; Martin et al., 1988; Niederer et al., 1989), also can remain in the soil. A study,

which was conducted by Medeiros et al. (2006) on a ryegrass field located in the Willamette Valley, Oregon, USA from January 2004 to January 2005, demonstrates that trehalose is the most abundant sugar found in the soil samples during the study period, and followed by sucrose. Therefore, the sucrose and trehalose detected from the archaeological samples may be from the natural soil or artificial addition. Quantitative analysis is necessary to be conducted to provide more evidence.

9.4.2. The quantitative analysis of sucrose and trehalose in earth samples by LC-MS/MS

The LC-MS/MS test was initially applied to sucrose and trehalose standards to evaluate its quantitative capability. The results of sucrose are shown in Table 9-3.

Table 9-3. The relation between the peak area at around 7.38 min in the LC chromatograms of sucrose standards and the tested sucrose mass

Sucrose mass	Peak area			
(pg)	1	2	3	Average
100	2.49e6	2.03e6	2.29e6	2.27e6
200	4.37e6	4.36e6	4.31e6	4.35e6
500	1.19e7	1.09e7	1.08e7	1.12e7
1000	2.14e7	2.03e7	2.04e7	2.07e7
2000	4.33e7	3.91e7	3.81e7	4.02e7

5000	1.10e8	1.02e8	1.04e8	1.06e8
10000	1.97e8	1.90e8	1.93e8	1.94e8

The linear fitting result between the peak area at around 7.38 min in the LC chromatograms of sucrose standards and the tested sucrose mass is shown below.

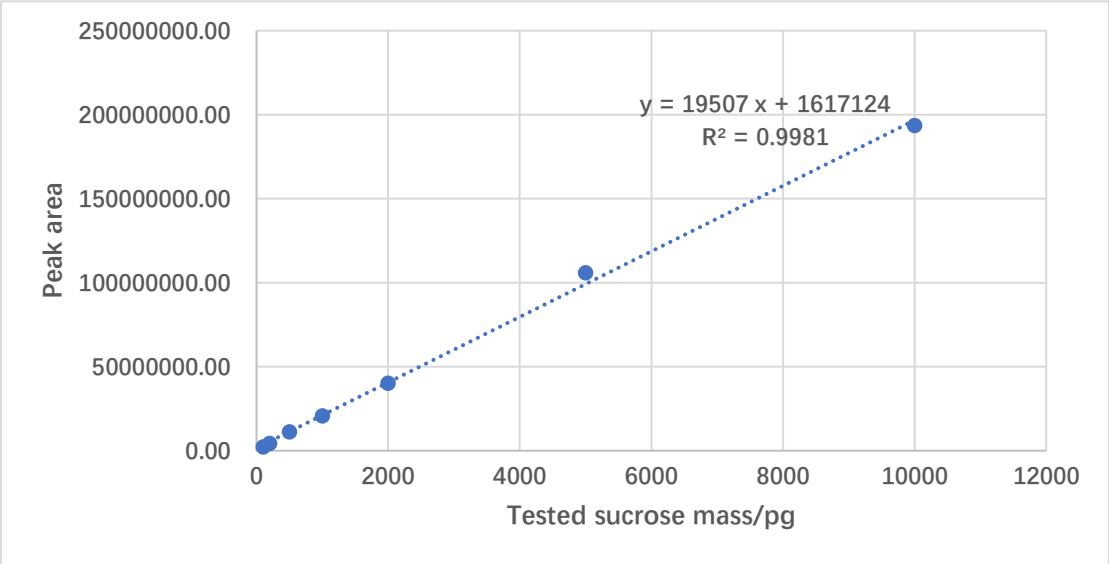


Fig 9-13. The linear fitting result between the peak area at around 7.38 min in the LC chromatograms of sucrose standards and the tested sucrose mass

As shown in Figure 9-13, the peak area at around 7.38 min in the LC chromatograms of sucrose standards has a solid linear relation with the tested sucrose mass, which indicates that the LC tests can be applied for the quantitative analysis of sucrose in earth samples.

The LC results of trehalose are shown in Table 9-4.

Table 9-4. The relation between the peak area at around 9.57 min in the LC chromatograms of trehalose standards and the tested trehalose mass

Trehalose mass (pg)	Peak area			
	1	2	3	Average
100	2.27e6	2.32e6	2.40e6	2.33e6
200	4.72e6	4.43e6	3.91e6	4.36e6
500	1.21e7	1.17e7	1.14e7	1.17e7
1000	2.26e7	2.14e7	2.24e7	2.21e7
2000	4.25e7	4.21e7	4.25e7	4.24e7
5000	9.78e7	9.77e7	9.58e7	9.71e7
10000	1.79e8	1.75e8	1.74e8	1.76e8

The linear fitting result between the peak area at around 9.57 min in the LC chromatograms of trehalose standards and the tested trehalose mass is shown below.

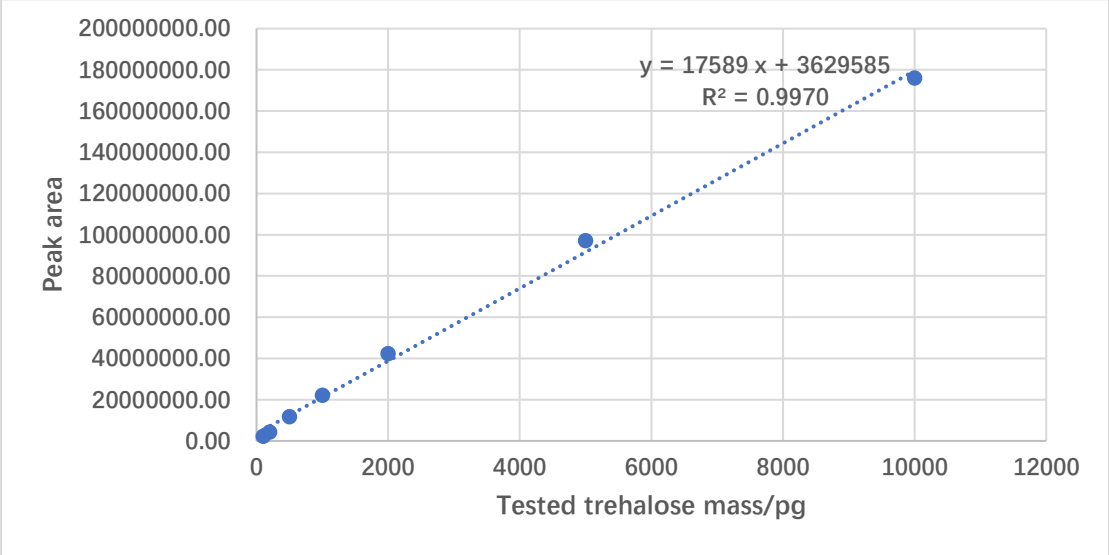


Fig 9-14. The linear fitting result between the peak area at around 9.57 min in the LC chromatograms of trehalose standards and the tested trehalose mass

As shown in Figure 9-14, the peak area at around 9.57 min in the LC chromatograms of trehalose standards has a solid linear relation with the tested trehalose mass, which indicates that the LC tests can be applied for the quantitative analysis of trehalose in earth samples.

The content of sucrose and trehalose in archaeological samples was then calculated by:

$$The\ content\ of\ sucrose = \frac{500}{200} \times \frac{Peak\ area - 1617124}{19507 \times 50} pg \cdot mg^{-1}$$

$$The\ content\ of\ trehalose = \frac{500}{200} \times \frac{Peak\ area - 3629585}{17589 \times 50} pg \cdot mg^{-1}$$

1617124 and 19507 are from Figure 9-13, while 3629585 and 17589 are from Figure 9-14. 500 (μL) is the amount of water added into the sample, and 200 (μL) is the filtrate applied to LC-MS/MS. 50 (mg) is the amount of archaeological sample.

The results are shown in Tables 9-5 and 9-6.

Table 9-5. The content of sucrose in archaeological samples

Sample	Peak area at around 7.38 min	The content of sucrose ($pg \cdot mg^{-1}$)
XAL	-	-
XAL-B1	1.27e6	-0.880
CAL	1.67e7	38.7
CAL-B1	1.54e6	-0.206
SRL	1.40e7	31.7
SRL-B1	1.12e6	-1.27
ZLL	3.54e7	86.7
ZLL-B1	9.74e5	-1.65

Table 9-6. The content of trehalose in archaeological samples

Sample	Peak area at around 9.57 min	The content of trehalose ($pg \cdot mg^{-1}$)
XAL	4.36e7	113.7138439
XAL-B1	1.32e8	365.8347291
CAL	6.07e7	162.3107597
CAL-B1	9.27e7	253.1549779
SRL	1.00e8	274.5420136
SRL-B1	6.84e7	184.0193357
ZLL	1.06e8	290.3465726
ZLL-B1	2.81e7	69.46129931

As shown in Table 9-5, the sucrose contents in CAL, SRL and ZLL are significantly higher than those in their environment samples (the calculation results are below zero due to the low sucrose content), indicating that sucrose in these 3 buildings is artificially added. Sucrose cannot be detected in XAL and its environmental sample XAL-B1. The content of trehalose in all 8 archaeological samples maintains in a similar level (69.46-365.83 $pg \cdot mg^{-1}$). Therefore, the trehalose in archaeological samples is from the natural soil rather than artificially addition.

9.5. Conclusions

The LC-MS/MS test was used to detect disaccharides in both modern and archaeological earth samples. The method was first tested on 9 disaccharide standards. The retention time in LC chromatograms, combined with corresponding MS/MS results, can be used to analyse disaccharides.

Sucrose was detected in CAL, SRL and ZLL, while the sucrose content in XAL and all the environmental samples was too low for detection. Therefore, the sucrose in CAL, SRL and ZLL was artificially added. Trehalose was detected in all the archaeological samples and its content is at the similar level between samples from the ancient buildings and the environment, meaning that the trehalose is from the natural soil.

10. Overview and future recommendations

10.1. The deficiencies of the previous analytical methods

Natural organic materials have been widely used in construction materials in ancient China. Starch, egg white, sugar, blood, lipid and other kinds of materials have been reported in literature. The construction technique can be traced to the State of Qin (888-207 BCE).

From the literature review on the analysis of organics in Chinese construction materials, it becomes evident that a significant majority (92.7%) of prior methods lean heavily on “spot tests” - simple chemical reaction-based analysis. Such tests lack the required sensitivity and specificity for reliable identification of organic components. Additionally, there was a notable absence of blank tests for detecting organics in base materials like earth in these studies. It is, therefore, concluded that more advanced techniques, specifically chromatography and mass spectrometry, are essential for accurate identification in future research.

10.2. The analytical strategy applied in this work

The study aimed to address the challenges of detecting starch and disaccharides in ancient construction through innovative analytical methods, overcoming the limitations of traditional techniques. This represents a significant step forward in

archaeological science, particularly in understanding ancient building practices. 8 analytical methods were applied for the development of the new strategy. Amongst these methods, the iodine-starch test, though applied in many previous references to identify starch (sticky rice or flour), is suitable for neither screening nor identification steps, since the iodine-starch test is not appliable for earth samples containing sticky rice lower than 18%, which is much higher than the organic content in archaeological samples. FTIR and LOI are the most effective methods in the screening step. Samples that have pronounced peaks at around 2800-3000cm^{-1} will be selected for later steps. "Wet samples" (archaeological samples that have high water peaks in the FTIR spectra) will also be included in this step. LOI results are also considered. If LOI450 is higher than 0.99%, which is the detection limit of LOI, there may be enough organics in the samples.

TGA-DTA-DSC, offering more information than FTIR and LOI, can be used to decide the temperature applied in LOI. However, it is not as effective as FTIR and LOI because of its complexity in operation and high expense. Moreover, the potential of TGA to give more information when combined with FTIR and MS was explored. TGA-MS could be applied in the identification step to show the possible existence of sticky rice in HYPT1 and XZM7. It also indicated that there was one or one type of organics in HYPT1, XZM7 and SJYTL3.

In the new MALDI-TOF-MS protocol, a procedure to identify starch was outlined.

Following the elimination of free oligosaccharides using acid hydrolysis and a water wash, the remaining residues were subjected to amylase hydrolysis. This ensures that any oligosaccharides detected subsequently are attributed to the presence of starch. A significant marker for starch is the peak at *m/z* 1013.325 ± 0.008 (after calibration: 1013 peak value + 1121.338 - 1121 peak value). Importantly, this indicator is misleading, when the peaks at around *m/z* 997 are found. Starch was detected in samples HYPT1 and TFGPT1. However, it was absent in 6 environmental samples of HYPT1 and only a trace amount was detected in 1 of the 3 environmental samples of TFGPT1. The MALDI-TOF-MS is an ideal method to identify starch in earth samples with its high specificity and low detection limit of 0.008% (m/m). This method represents a breakthrough in archaeological analysis by addressing the high detection limits of iodine-starch tests and other traditional techniques. Its ability to detect trace amounts of starch in challenging contexts, such as low-organic archaeological samples, marks a significant advancement in the field.

The LC-MS/MS method was employed to detect disaccharides in earth samples. Initial tests were conducted on 9 disaccharide standards. The results suggest that the retention time in LC chromatograms, paired with MS/MS data, serves as an effective means to analyse disaccharides. While sucrose appeared in samples such as CAL, SRL, and ZLL, and was not detected in their environmental samples, its artificial addition is evident. The trehalose content seemed consistent across all ancient samples, potentially indicating its natural soil origins.

Table 10-1. The positive and negative features of each analytical method

Method	Advantages	Disadvantages	Application
Iodine-starch test	Ease of operation and low expense	Very low specificity and sensitivity	Not applicable
FTIR	Ease of operation and low expense	Low specificity and not suitable for wet samples	The screening step
LOI	Ease of operation, high sensitivity and low expense	Low specificity	The screening step
TGA-DTA-DSC	More detailed thermal decomposition information than LOI	High complexity and expense	Providing the suitable temperatures for LOI
TGA-FTIR	More detailed information than FTIR	Low specificity, low sensitivity, high complexity and high expense	Not applicable
TGA-MS	More detailed information than TGA	High complexity and expense	Potential for the identification step
MALDI-TOF-MS	Very high specificity and sensitivity for starch identification	High expense	The identification step of starch
LC-MS/MS	Very high specificity and sensitivity for disaccharides identification	High expense	The identification step of disaccharides

The new analytical strategy for the identification of starch and disaccharides in earth samples is shown in Figure 10-1.

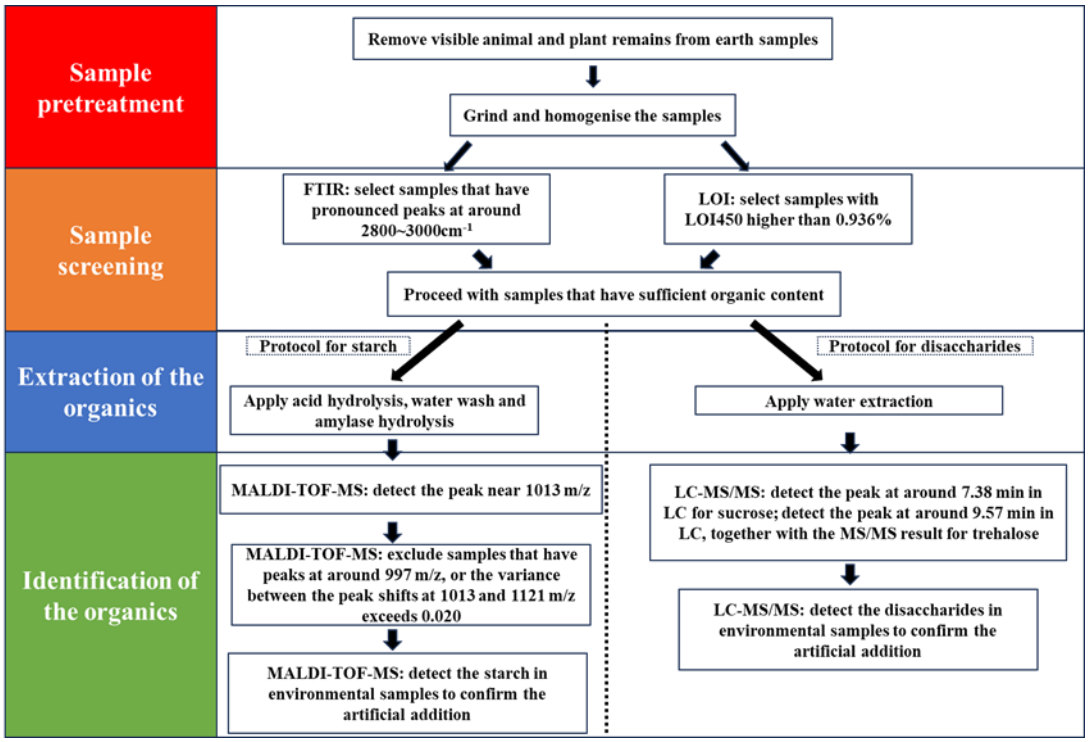


Fig 10-1. Schematic diagram of the new analytical strategy for starch and disaccharides

In the analysis of starch content across 67 archaeological samples, only 2 samples were found to contain starch. This finding contradicts the widespread presence of starch reported in earlier studies, as discussed in Chapter 2. Concerns have been raised about the reliability of the methodologies used in these prior studies in that chapter. This discrepancy highlights the need for more rigorous methodological approaches in archaeological science. By challenging earlier conclusions, this study not only corrects potential misinterpretations but also sets a new standard for future investigations into organic material use in ancient construction. Therefore, it is crucial

to reanalyse their samples using the new protocol. This will provide deeper insights into the application of organic materials in ancient Chinese earthen construction materials. Beyond the reanalysis of earlier samples, this protocol has the potential to transform how archaeological science approaches the study of ancient building materials. By combining high specificity with low detection limits, these methods can be applied to a broader range of contexts, enriching our understanding of ancient construction techniques, resource use, and socio-economic dynamics.

Regarding the analysis of sucrose, some literature sources (Shen et al., 2006; Chen, 2018; Bai et al., 2021), though largely based on local anecdotes, have mentioned the use of brown sugar in the construction of the Kaiping Diaolou. The analysis of 8 archaeological samples (including 4 environmental samples), detected sucrose in 3 of them. This suggests a certain degree of reliability in these folk tales and provides a direction for future sample selection.

10.3. Future work

Several avenues for future research are proposed below. These suggestions are grounded in the existing findings of this study and are designed to address the limitations and expand the scope of this research field.

1) Broader application of the analytical strategy

The newly developed analytical strategy could be applied to archaeological earth samples from a wider range of ancient sites spanning different periods and regions. This would provide a more comprehensive understanding of how natural organic materials were employed in the construction of ancient Chinese earthen buildings. For instance, comparative studies could reveal regional and temporal variations in the use of sticky rice or other natural binders. Such work would test the hypothesis that cultural and environmental factors influenced material selection in ancient construction practices. Future researchers could begin by selecting well-preserved sites with known historical contexts, ensuring the samples are representative of diverse geographic and climatic conditions. Relevant literature on regional construction techniques (Li and Zhang, 2019) should guide site selection and contextual interpretation;

2) Development of TGA-MS as an analytical method

TGA-MS holds significant potential for detecting organic materials in archaeological samples. Preliminary results from this study indicate that starch presence, confirmed via MALDI-TOF-MS (HYPT1), can also be identified using TGA-MS. However, the method requires further refinement. A key hypothesis is that TGA-MS, when optimized, can provide quantitative and qualitative insights into starch degradation products. Future work could focus on standardising the operating parameters, such as heating rates and ionization settings, to enhance sensitivity. Advanced techniques like MS/MS may address current limitations, enabling more precise molecular

identification. Studies like (David et al., 2018; Li et al., 2020a) provide a foundation for developing protocols and interpreting results;

3) Investigating the mechanisms of starch degradation

Understanding the degradation mechanisms of natural organics under various conditions remains critical. Current experiments could be expanded to include more complex degradation environments, such as varying pH, humidity, and microbial activity. A hypothesis to test is that degradation rates are significantly influenced by these factors, leading to different molecular by-products. Future research should adopt a systematic approach, such as factorial experiments, to isolate and evaluate the impact of individual variables. Long-term experiments with shorter sampling intervals could provide a more granular view of the degradation process. Relevant studies on starch degradation (Liu et al., 2019) offer valuable frameworks for designing these experiments;

4) Developing analytical methods with higher specificity

To distinguish sticky rice starch from other types of starch, new analytical techniques with higher specificity need to be developed. A promising direction involves the analysis of plant DNA residues. This approach could test the hypothesis that genetic markers unique to sticky rice can be identified even in highly degraded samples. Techniques like PCR amplification and next-generation sequencing could be employed to extract and analyse these markers. A detailed review of recent

advancements in ancient DNA analysis (Chen and Nedoluzhko, 2023) would help future researchers design effective extraction and amplification protocols;

5) Dating the organics in earth samples

Dating the organic materials embedded in ancient earthen structures is crucial for confirming the artificial addition of these substances during construction. While challenging due to the difficulty in isolating and purifying target molecules, such work could significantly enhance our understanding of construction timelines and techniques. Radiocarbon dating of purified starch residues, or alternative methods such as lipid residue dating, could be explored. The hypothesis is that direct dating of these organics will align with the historical construction dates of the sites. Future researchers might adopt multi-step purification methods to isolate compounds suitable for dating, while also accounting for potential contamination. Some recent research (Hajdas et al., 2024) may offer possible guidance.

Appendix 1. FTIR spectra of all the archaeological samples

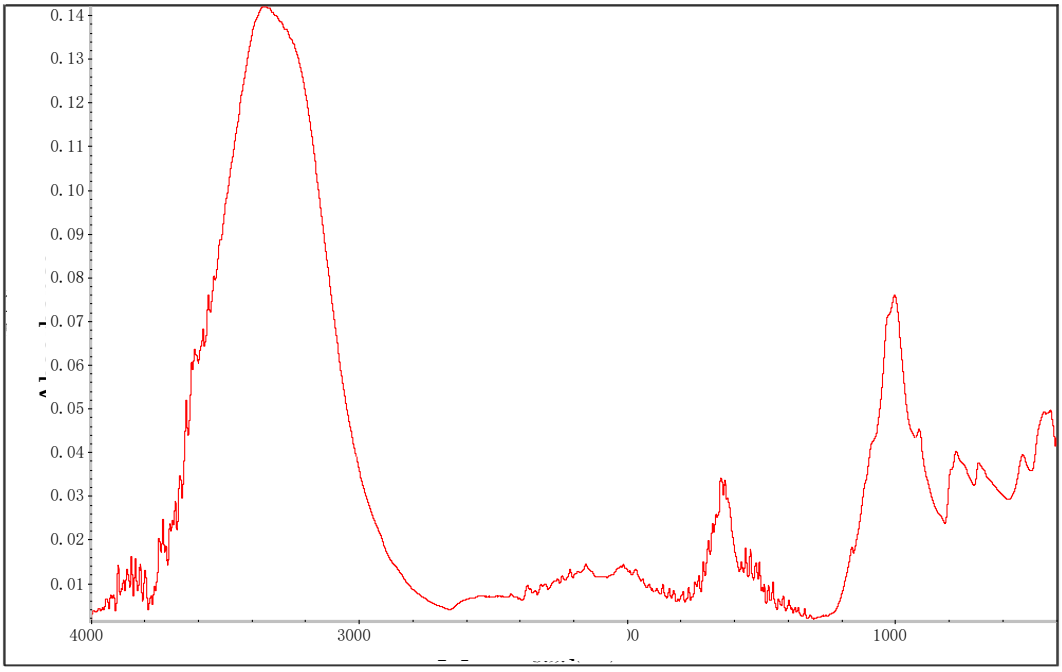


Fig A-1. the FTIR spectrum of BMD1 from the Bamudun site

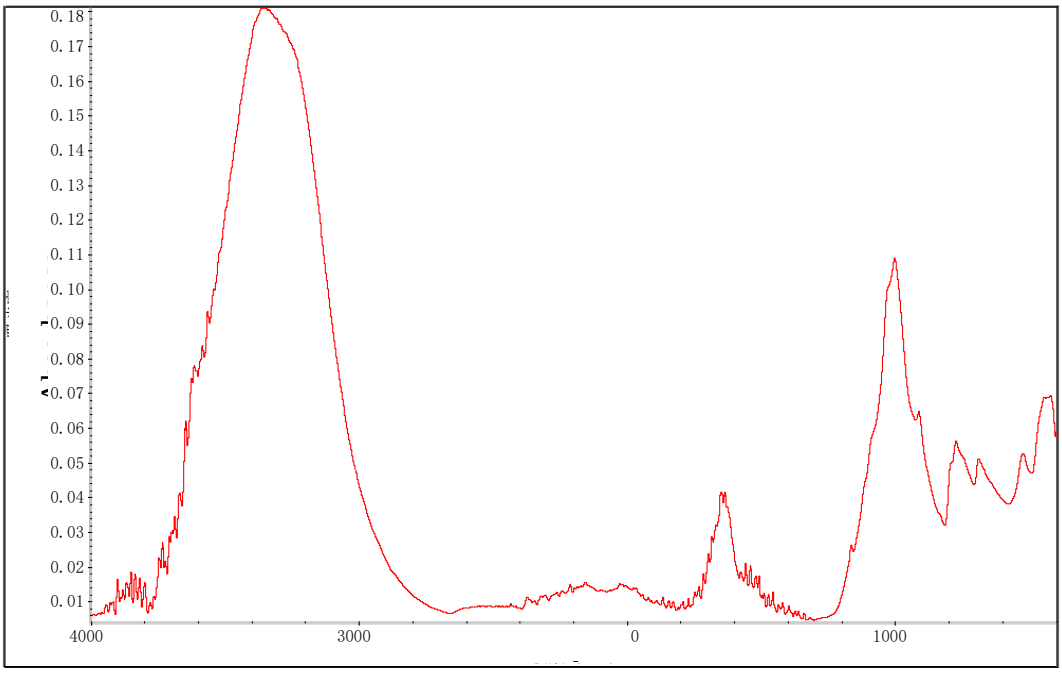


Fig A-2. the FTIR spectrum of BMD2 from the Bamudun site

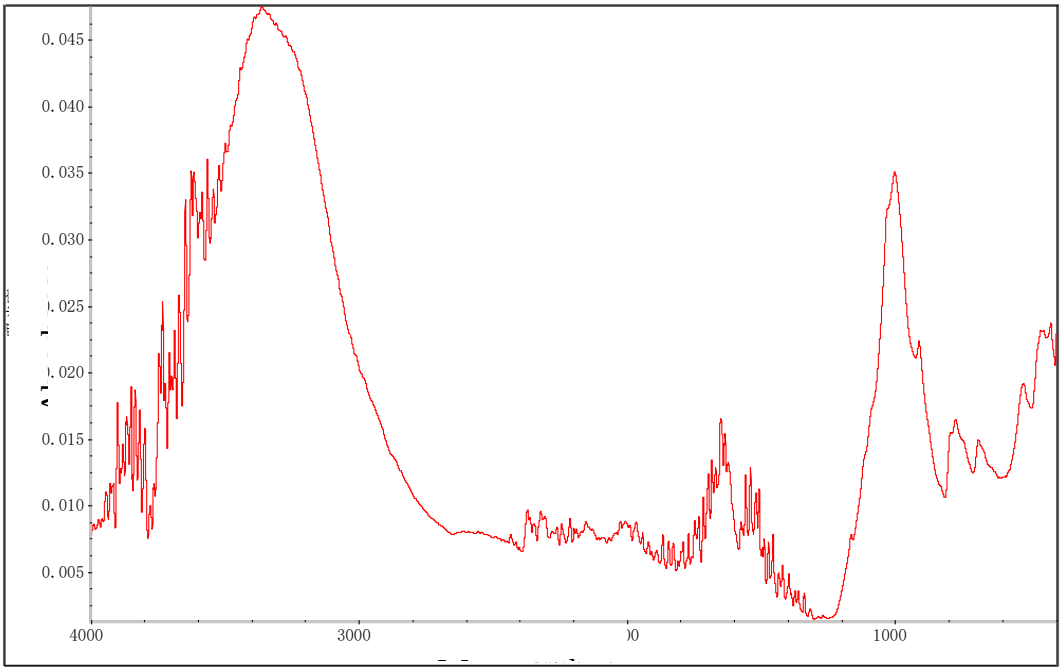


Fig A-3. the FTIR spectrum of BMD3 from the Bamudun site

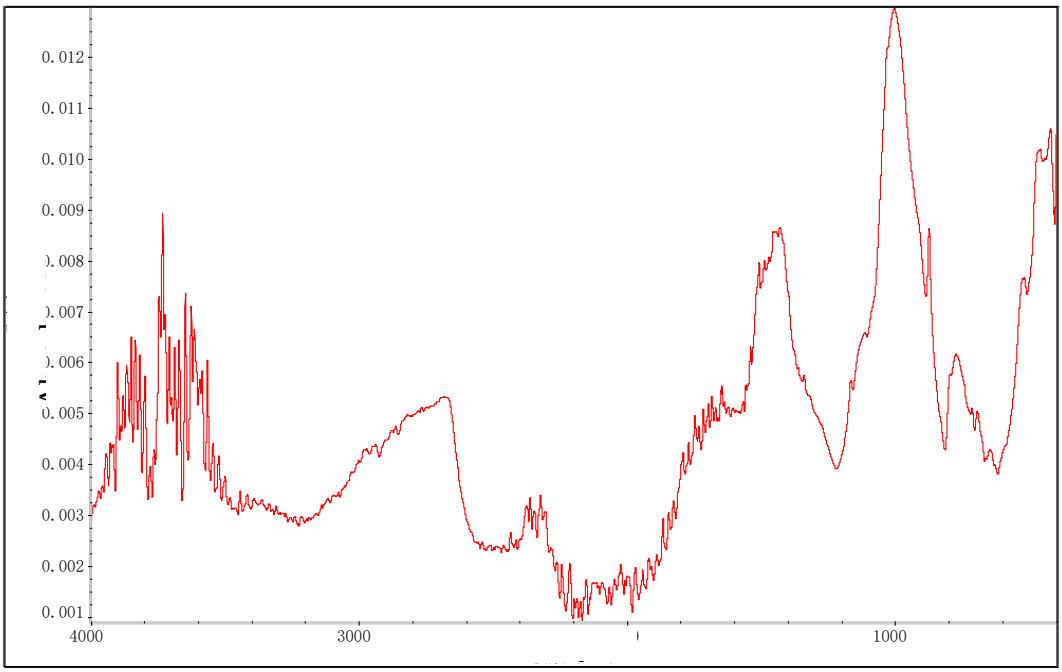


Fig A-4. the FTIR spectrum of BWC1 from the Bawangcheng site

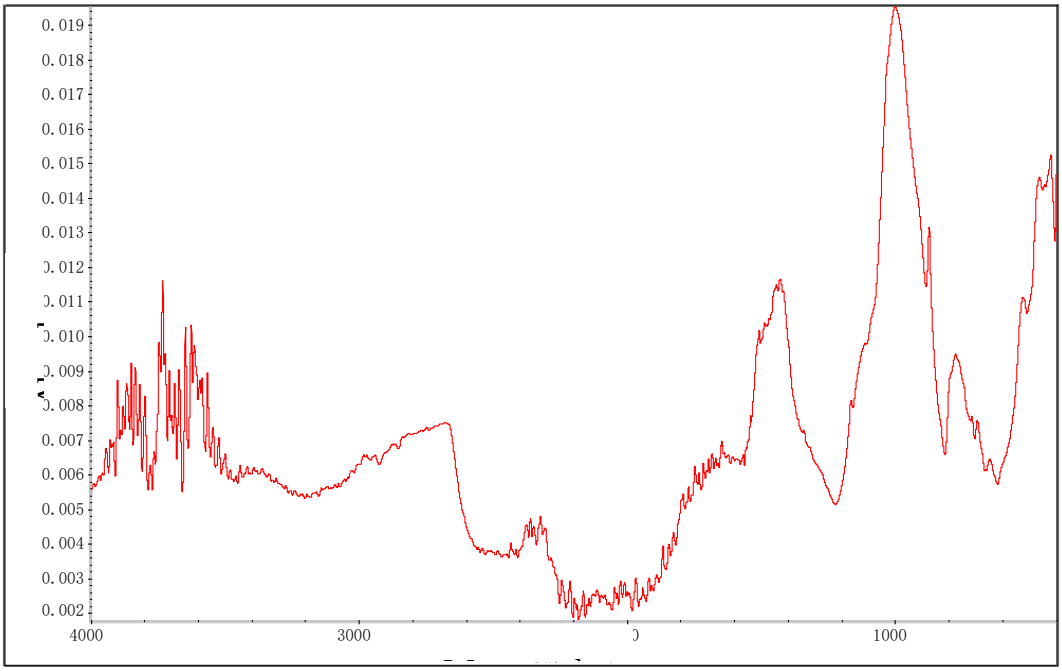


Fig A-5. the FTIR spectrum of BWC2 from the Bawangcheng site

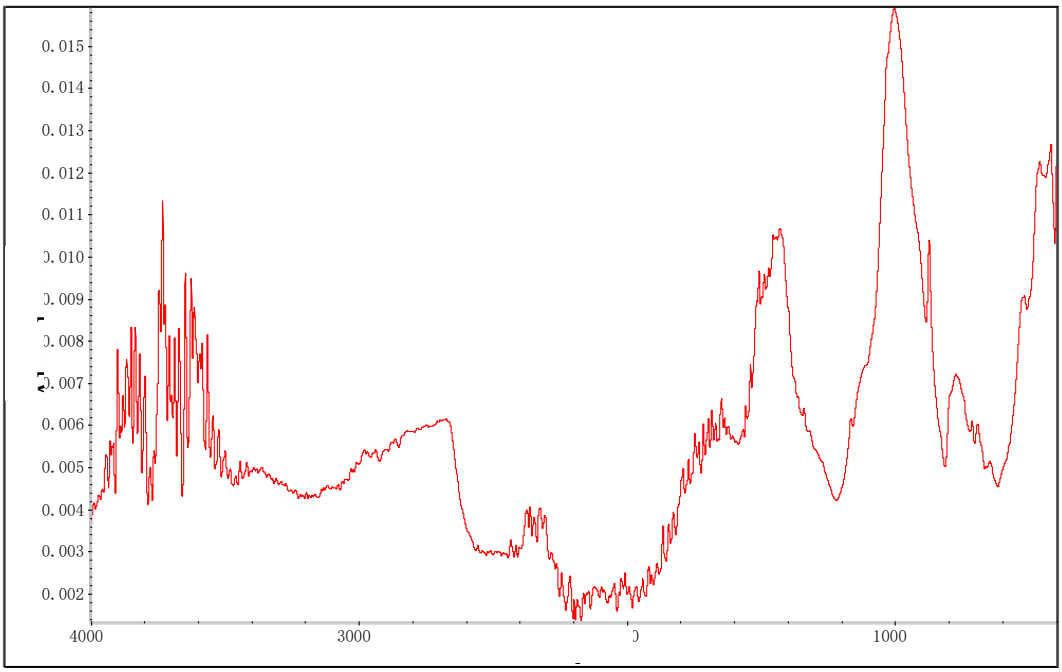


Fig A-6. the FTIR spectrum of BWC3 from the Bawangcheng site

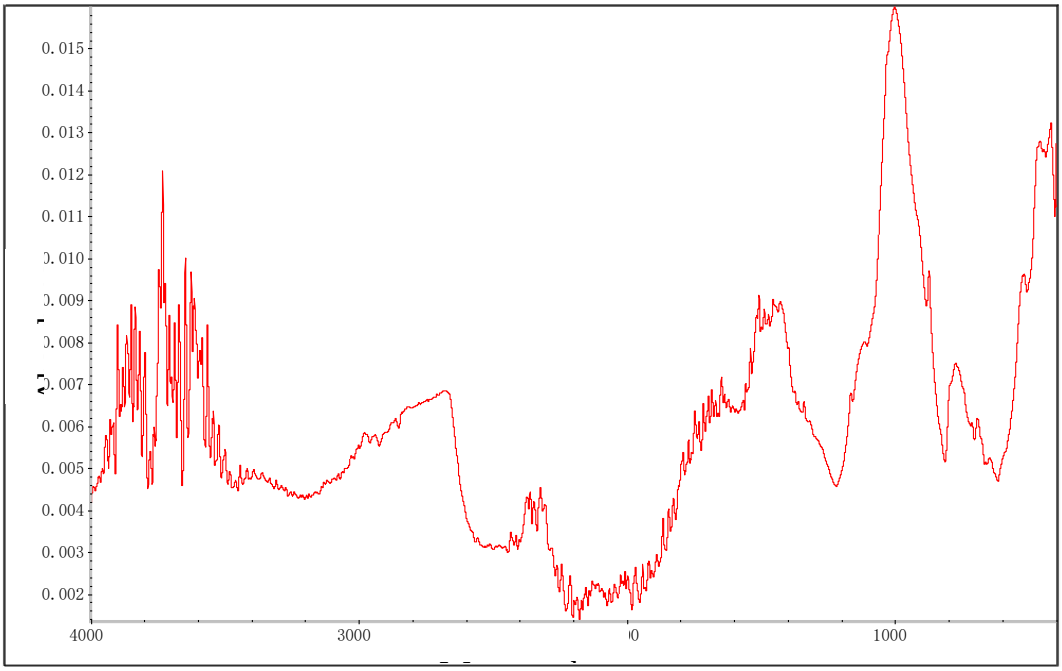


Fig A-7. the FTIR spectrum of BWC4 from the Bawangcheng site

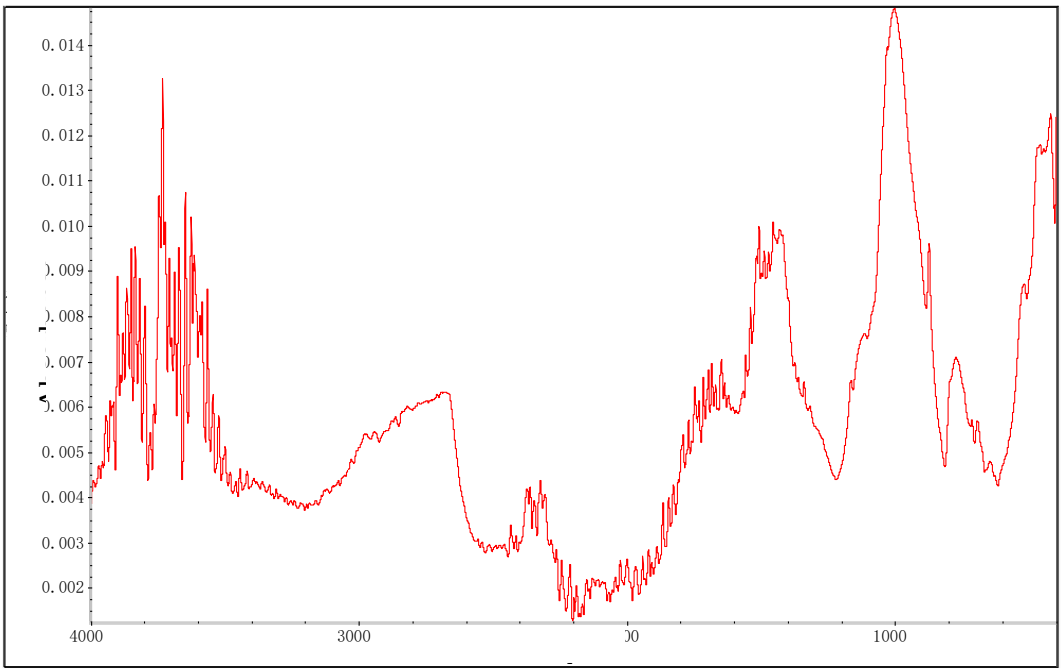


Fig A-8. the FTIR spectrum of BWC5 from the Bawangcheng site

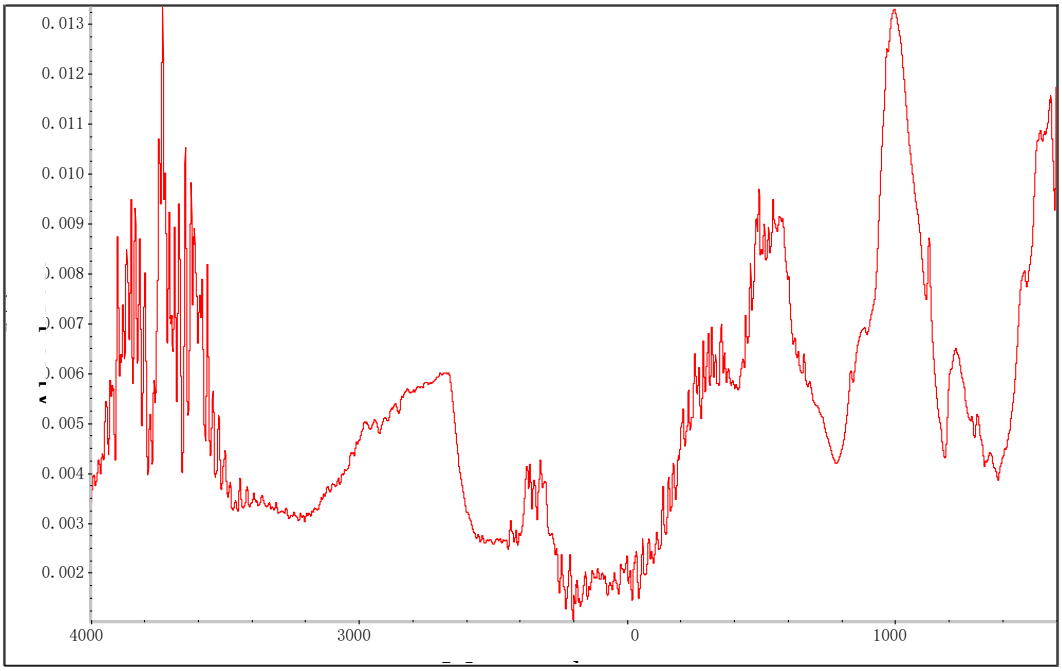


Fig A-9. the FTIR spectrum of BWC6 from the Bawangcheng site

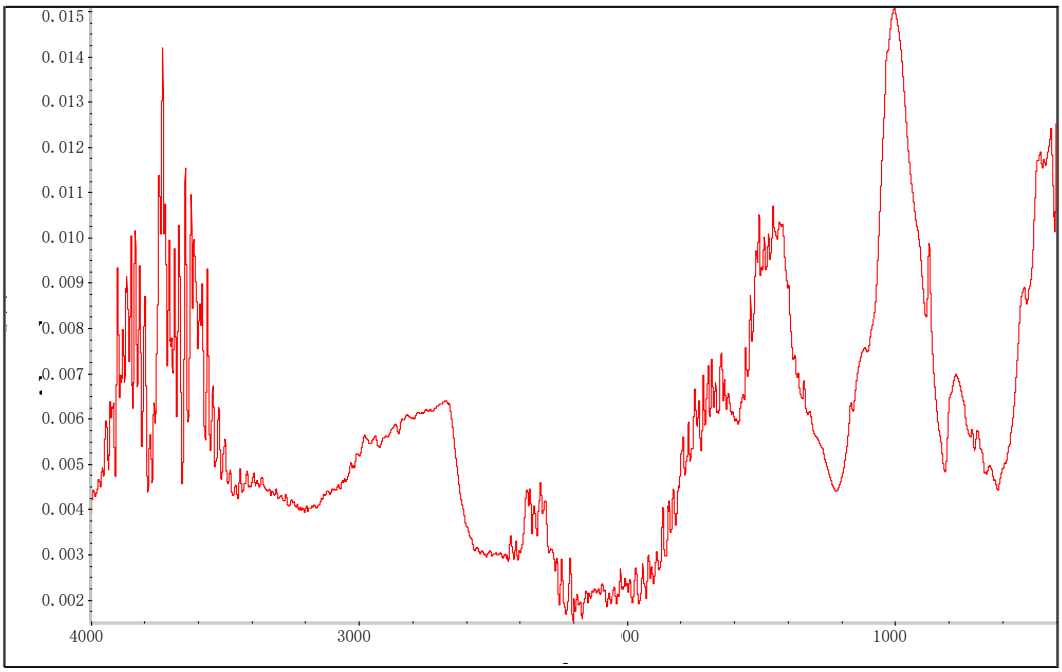


Fig A-10. the FTIR spectrum of BWC7 from the Bawangcheng site

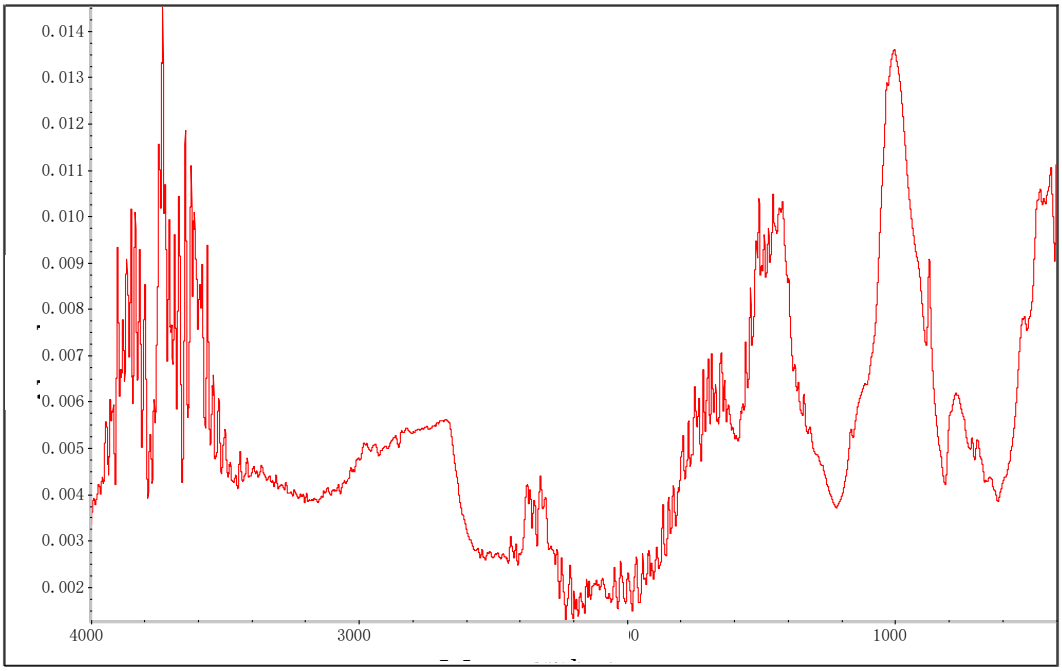


Fig A-11. the FTIR spectrum of BWC8 from the Bawangcheng site

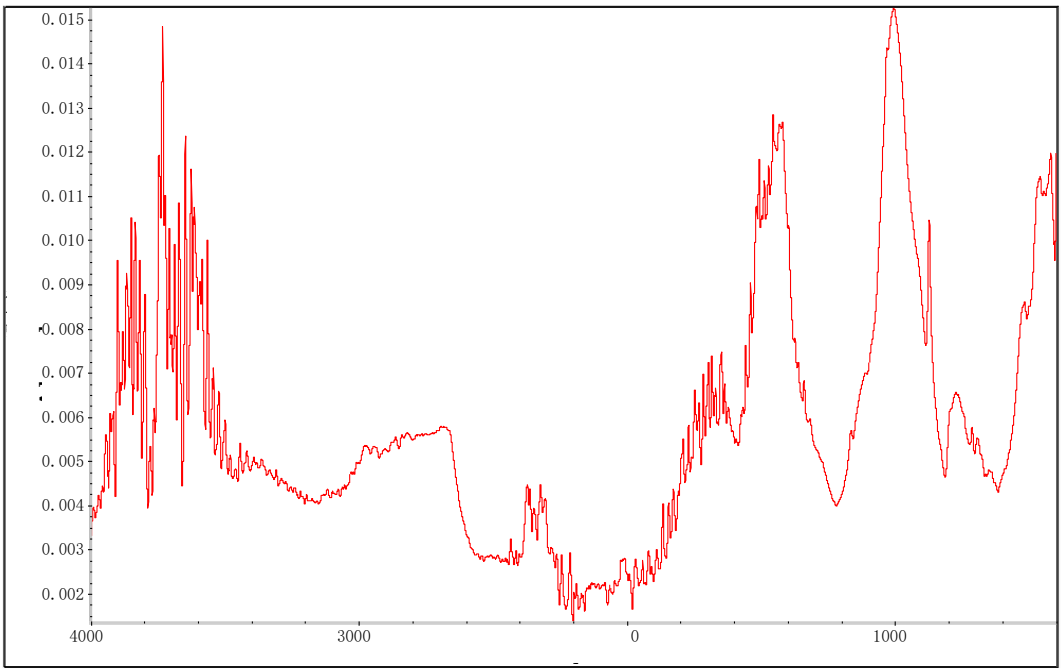


Fig A-12. the FTIR spectrum of BWC9 from the Bawangcheng site

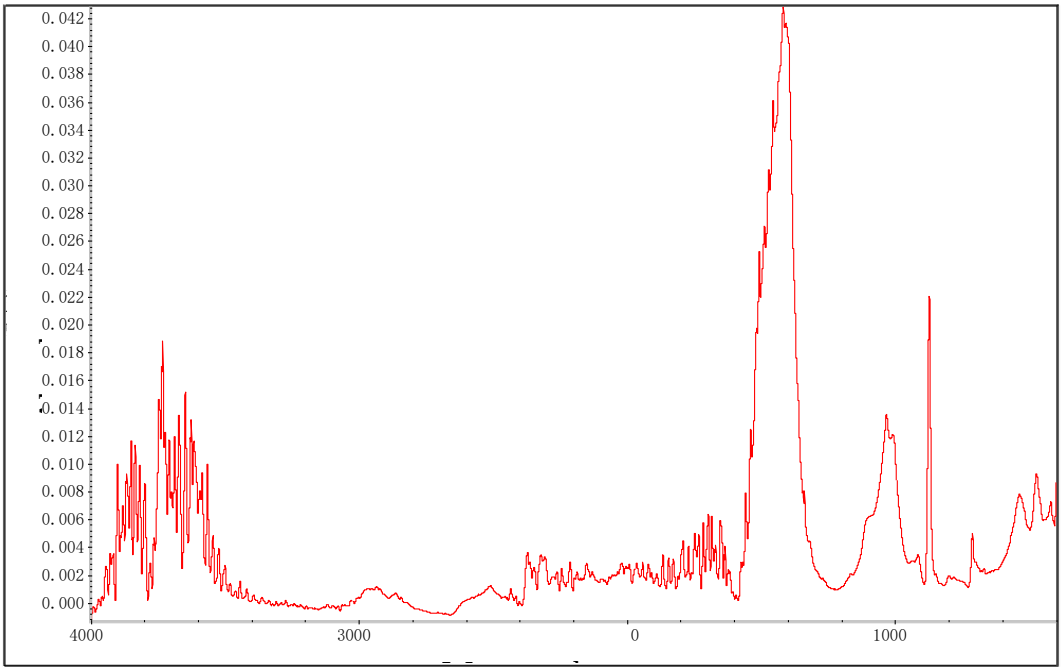


Fig A-13. the FTIR spectrum of HNZZ1 from the house of the Zhang family

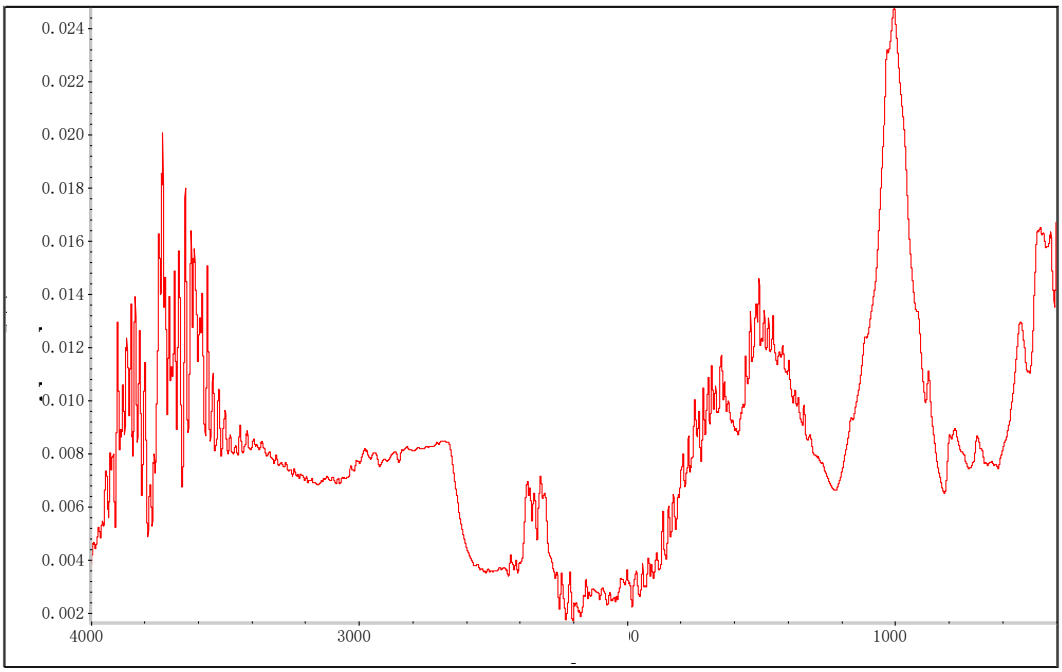


Fig A-14. the FTIR spectrum of HYPT1 from the Fort Hongyuan site

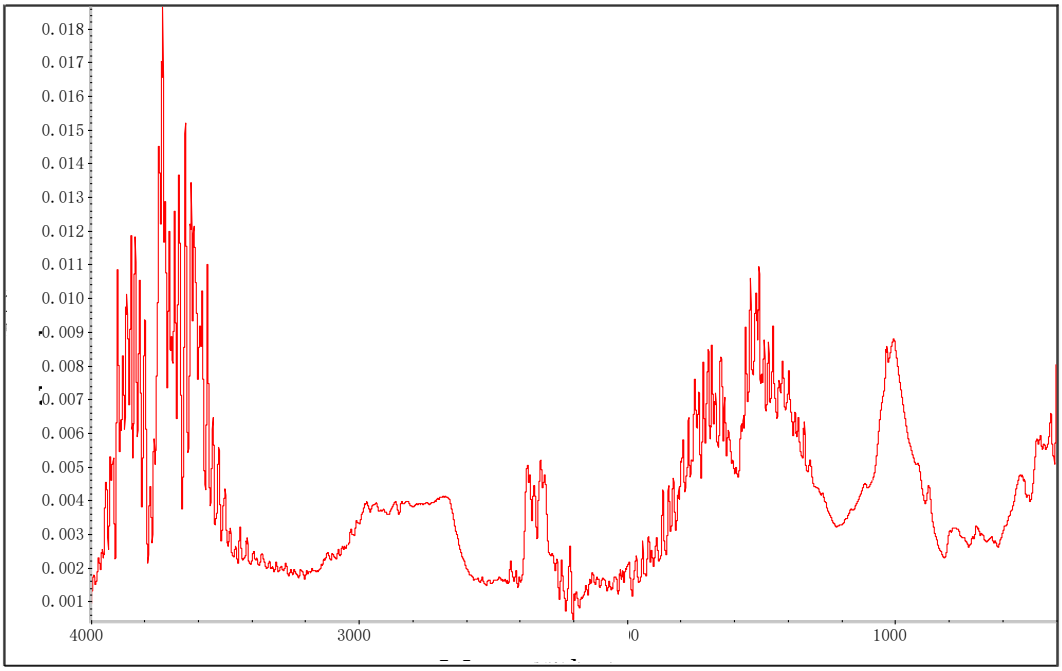


Fig A-15. the FTIR spectrum of JYPT1 from the Fort Jingyuan site

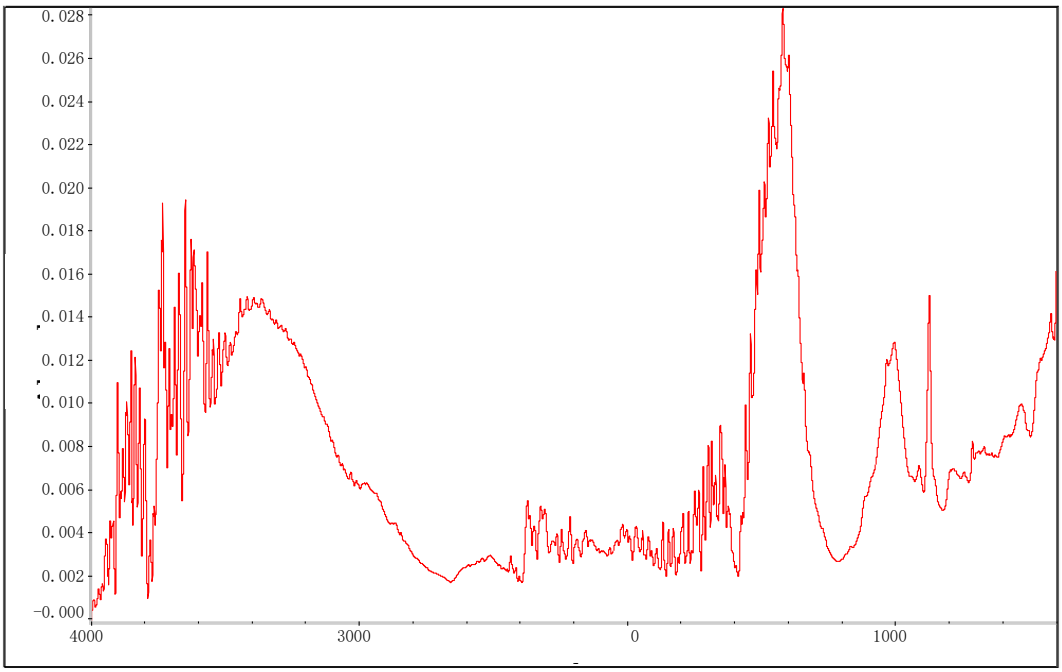


Fig A-16. the FTIR spectrum of JYPT2 from the Fort Jingyuan site

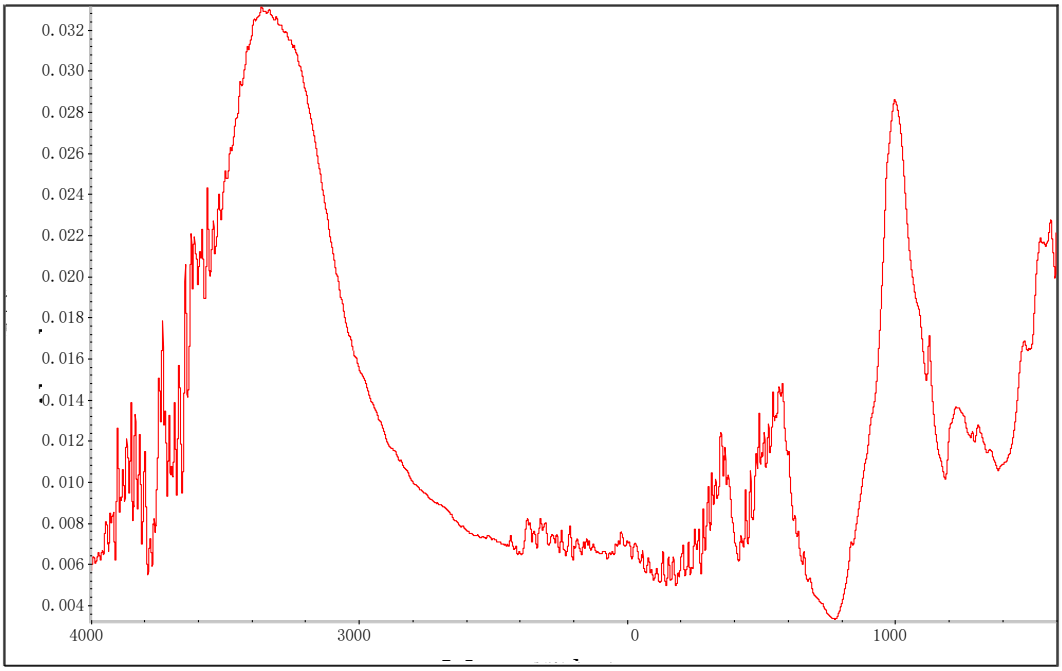


Fig A-17. the FTIR spectrum of PTC1 from the Pingtaocheng site

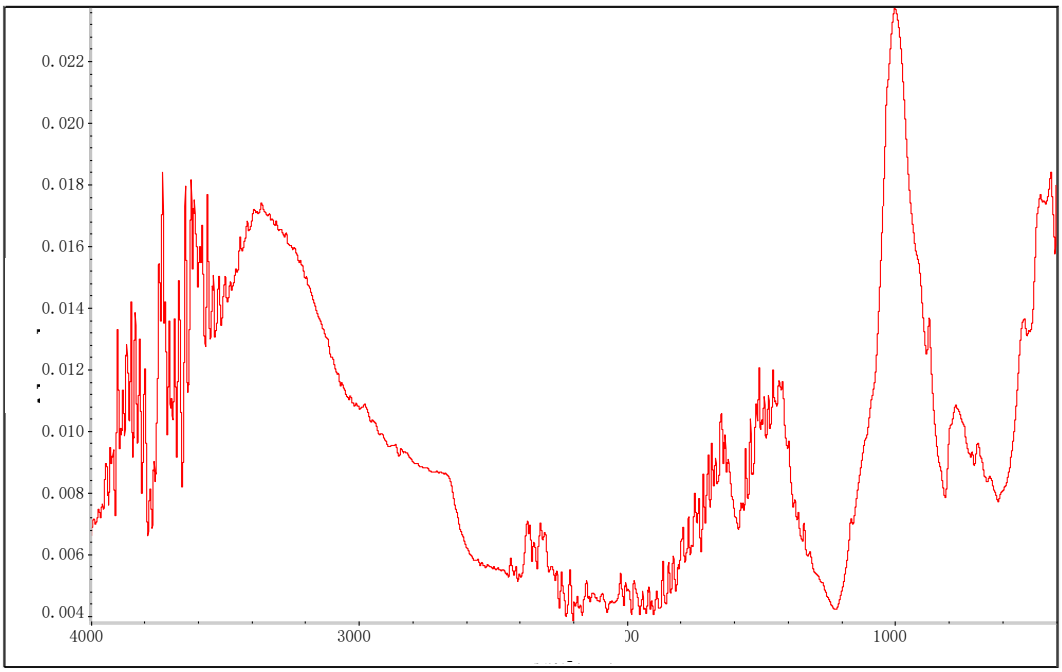


Fig A-18. the FTIR spectrum of PTC2 from the Pingtaocheng site

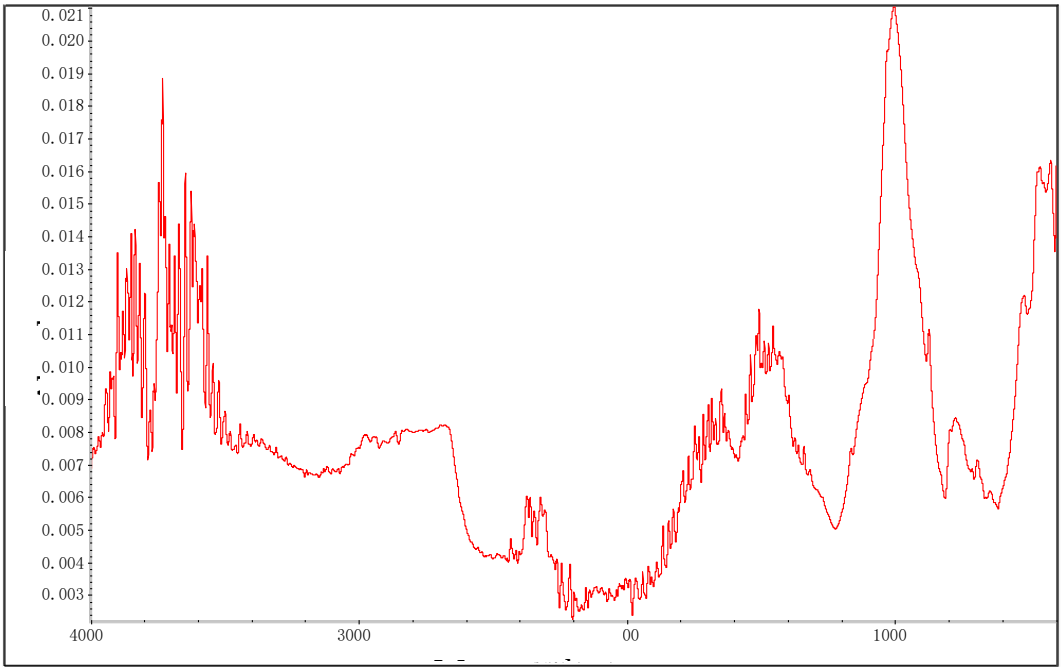


Fig A-19. the FTIR spectrum of PTC3 from the Pingtaocheng site

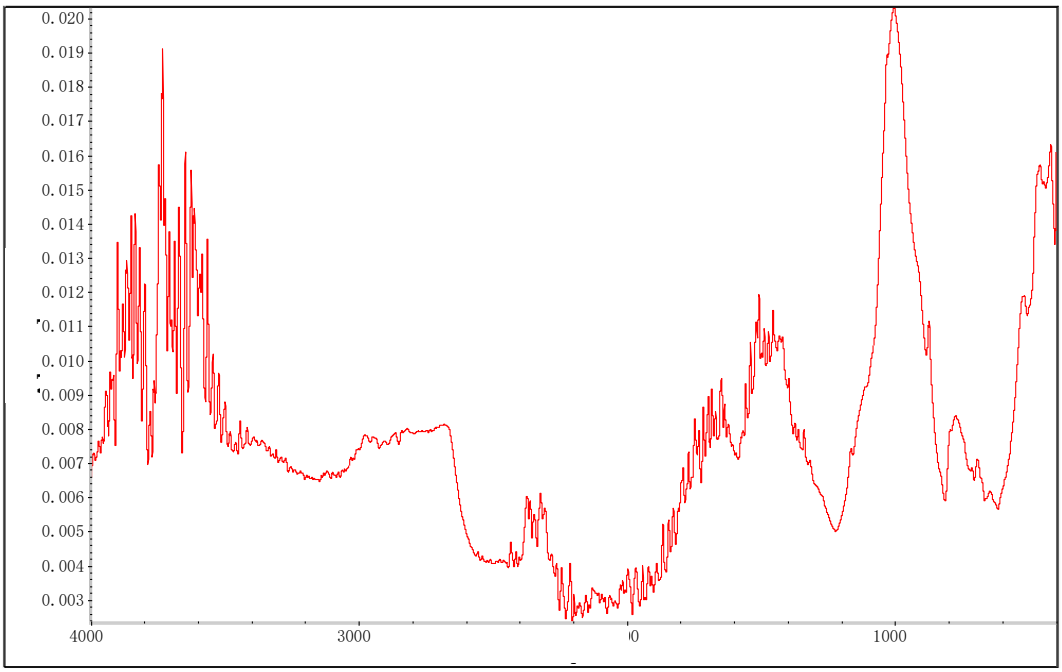


Fig A-20. the FTIR spectrum of PTC4 from the Pingtaocheng site

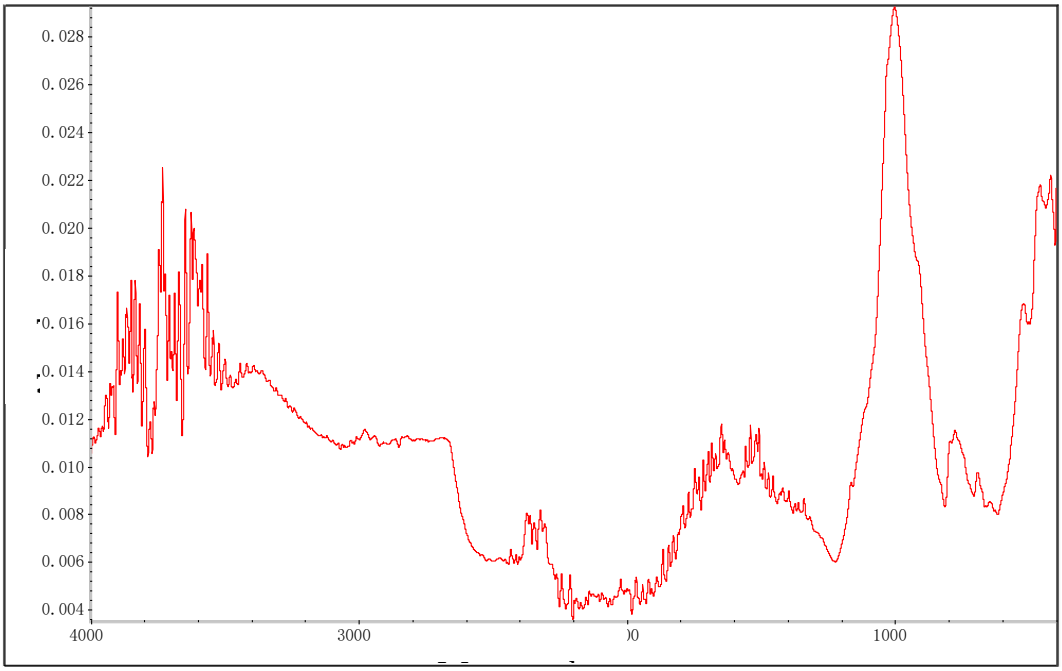


Fig A-21. the FTIR spectrum of PTC5 from the Pingtaocheng site

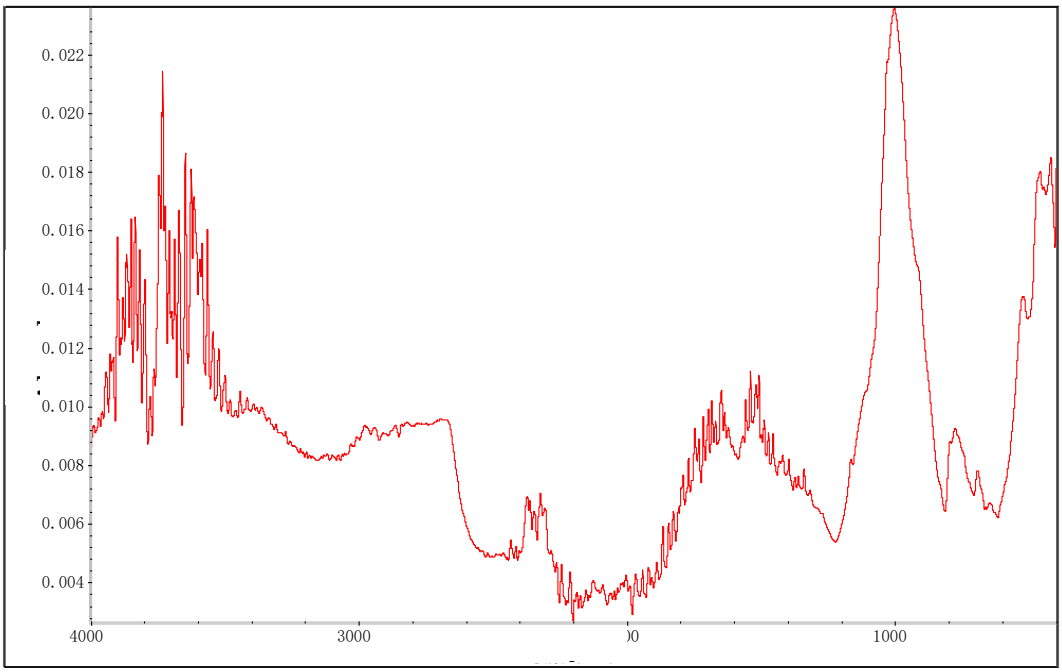


Fig A-22. the FTIR spectrum of PTC6 from the Pingtaocheng site

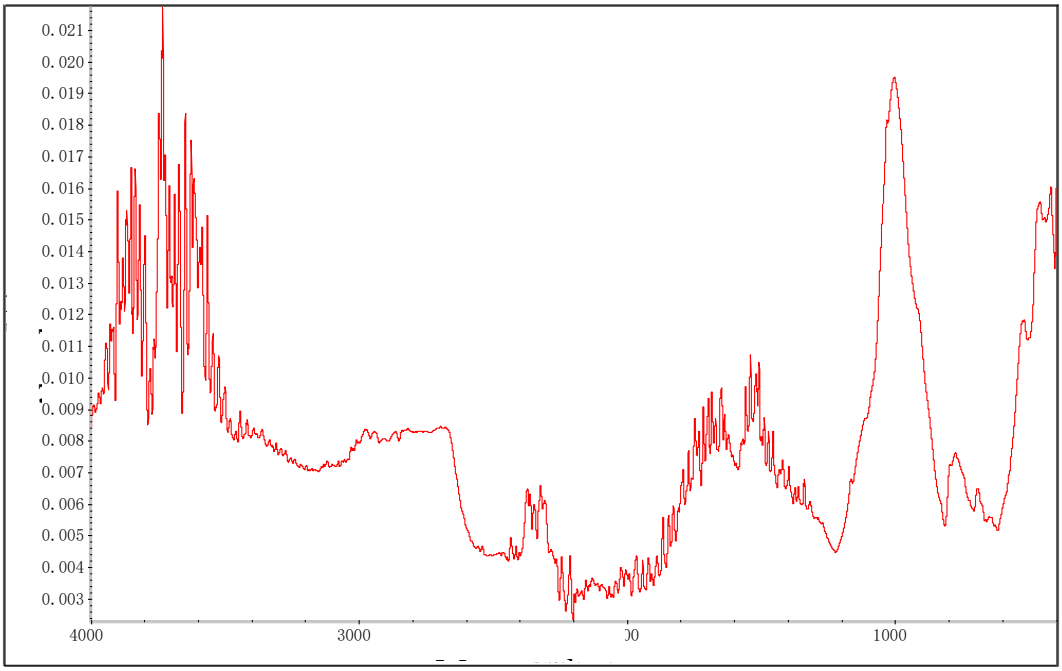


Fig A-23. the FTIR spectrum of PTC7 from the Pingtaocheng site

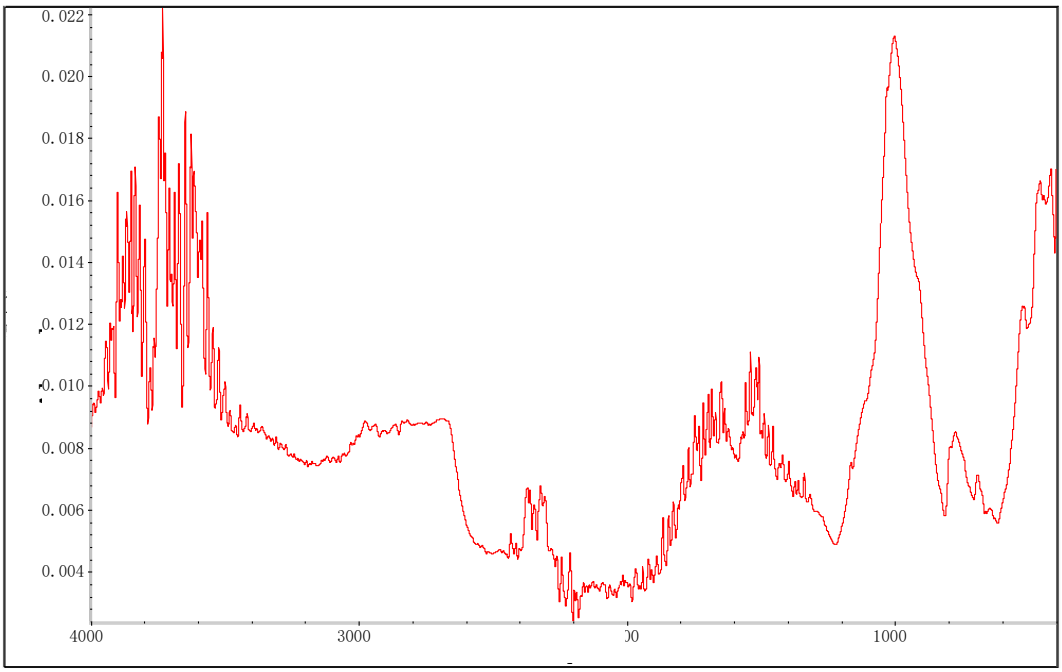


Fig A-24. the FTIR spectrum of PTC8 from the Pingtaocheng site

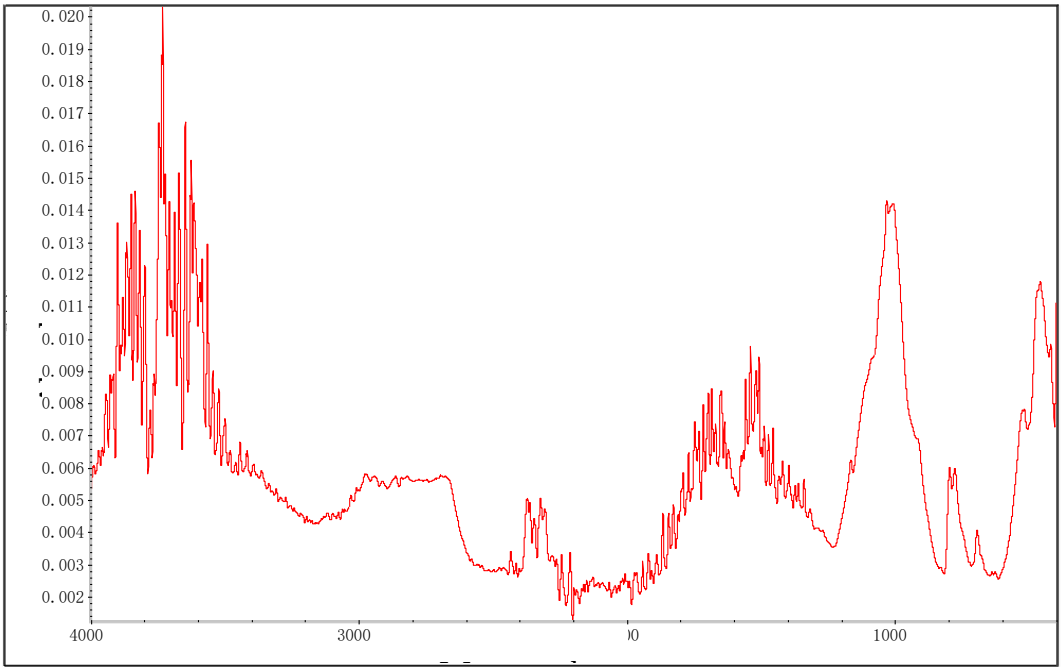


Fig A-25. the FTIR spectrum of SJYTL1 from the Shangjiaoyang Tulou site

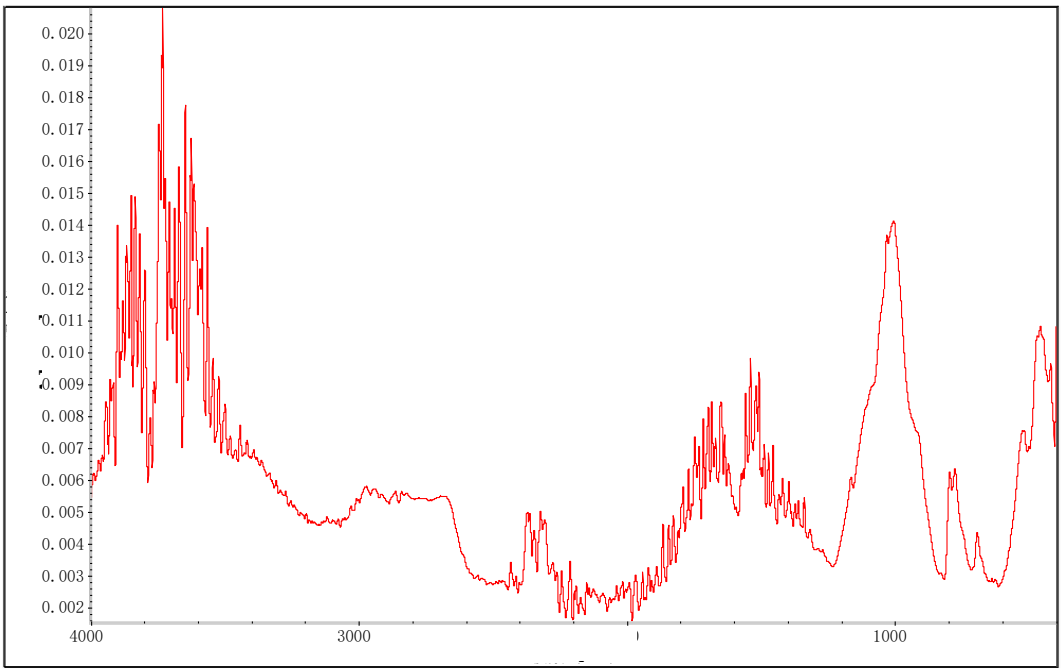


Fig A-26. the FTIR spectrum of SJYTL2 from the Shangjiaoyang Tulou site

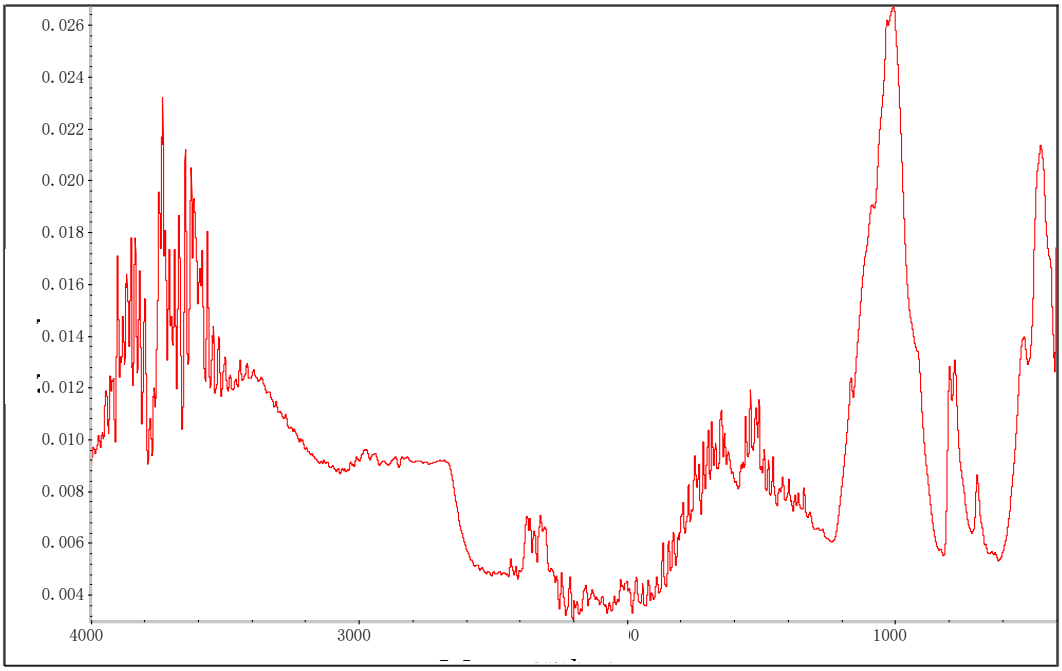


Fig A-27. the FTIR spectrum of SJYTL3 from the Shangjiaoyang Tulou site

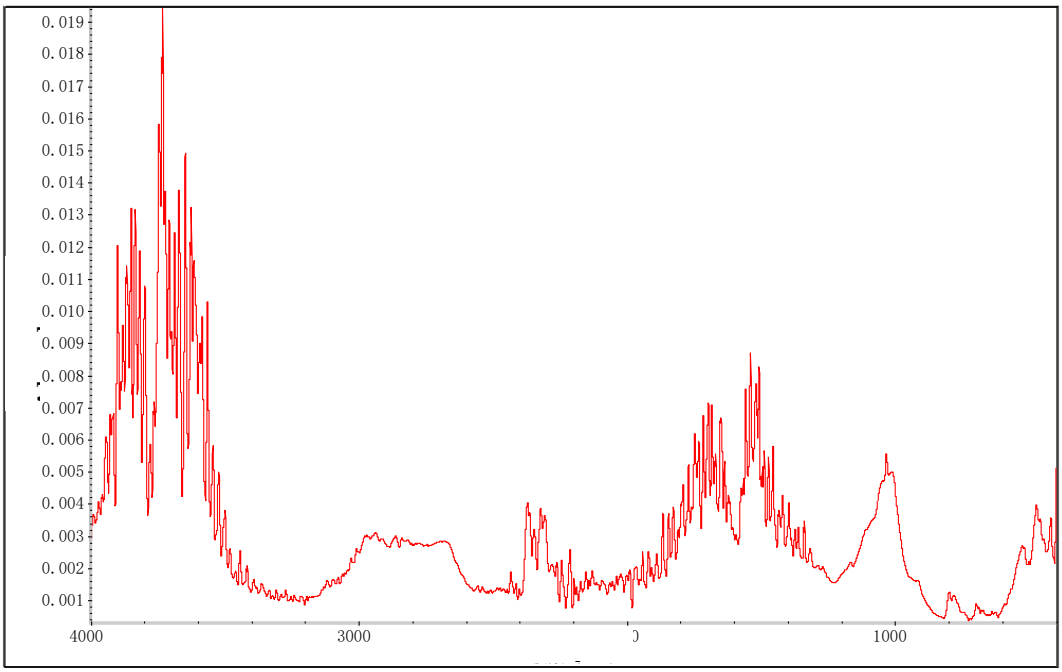


Fig A-28. the FTIR spectrum of SJYTL4 from the Shangjiaoyang Tulou site

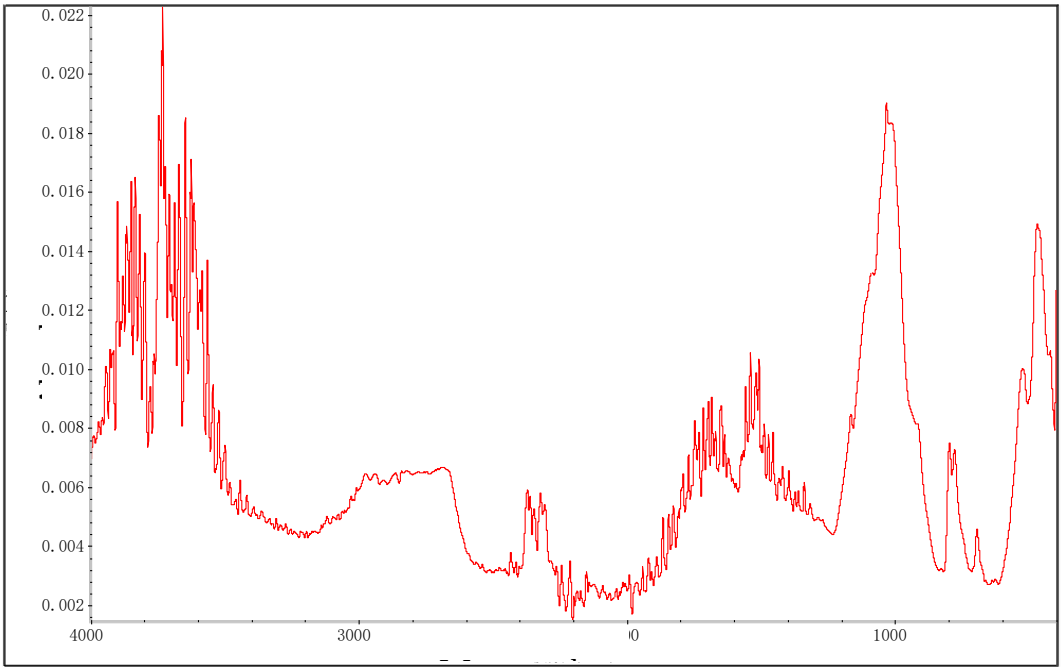


Fig A-29. the FTIR spectrum of SJYTL5 from the Shangjiaoyang Tulou site

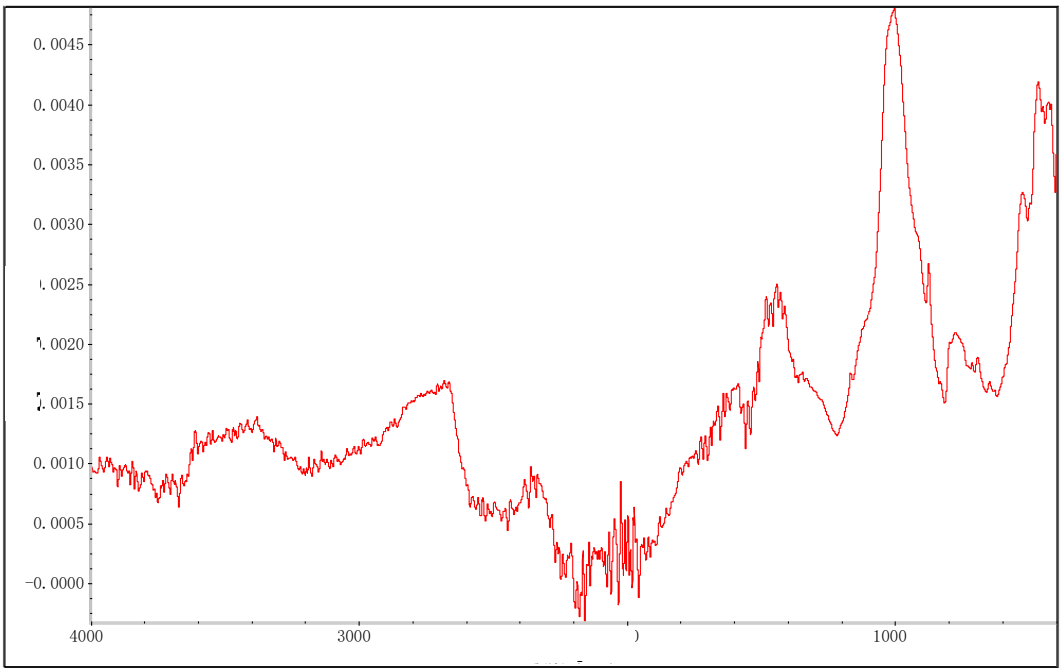


Fig A-30. the FTIR spectrum of XYGC1 from the Xingyangguchengsite

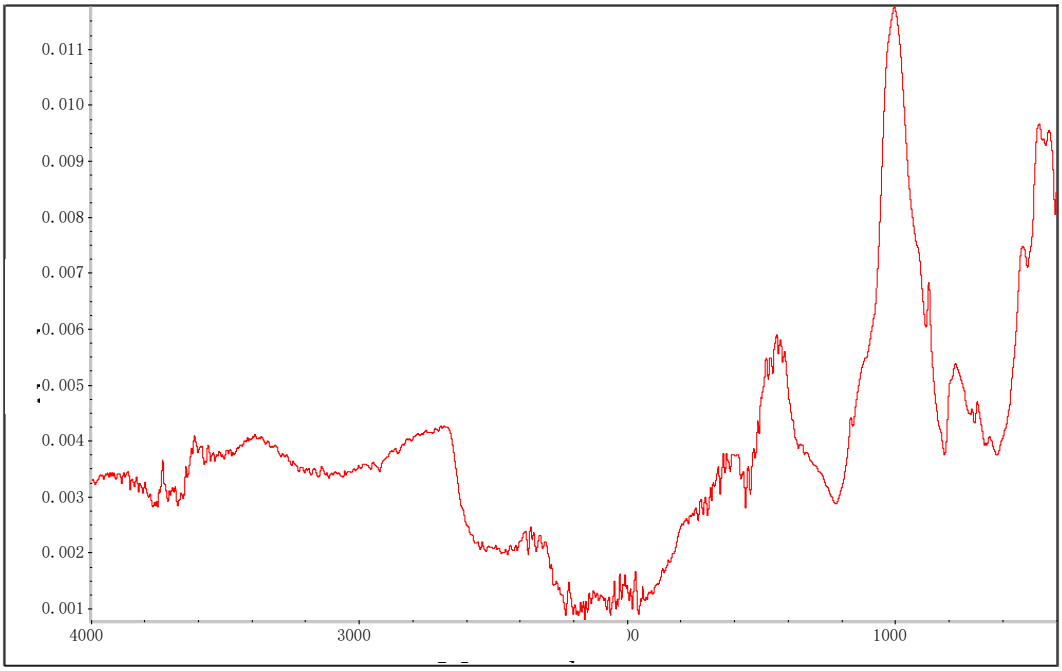


Fig A-31. the FTIR spectrum of XYGC2 from the Xingyanggucheng site

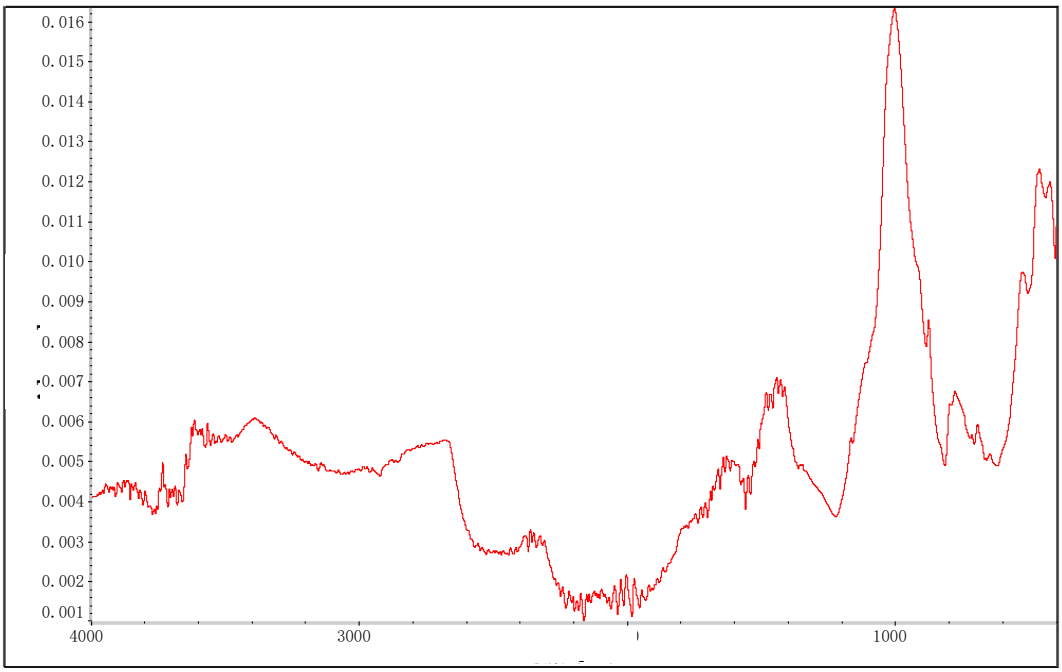


Fig A-32. the FTIR spectrum of XYGC3 from the Xingyanggucheng site

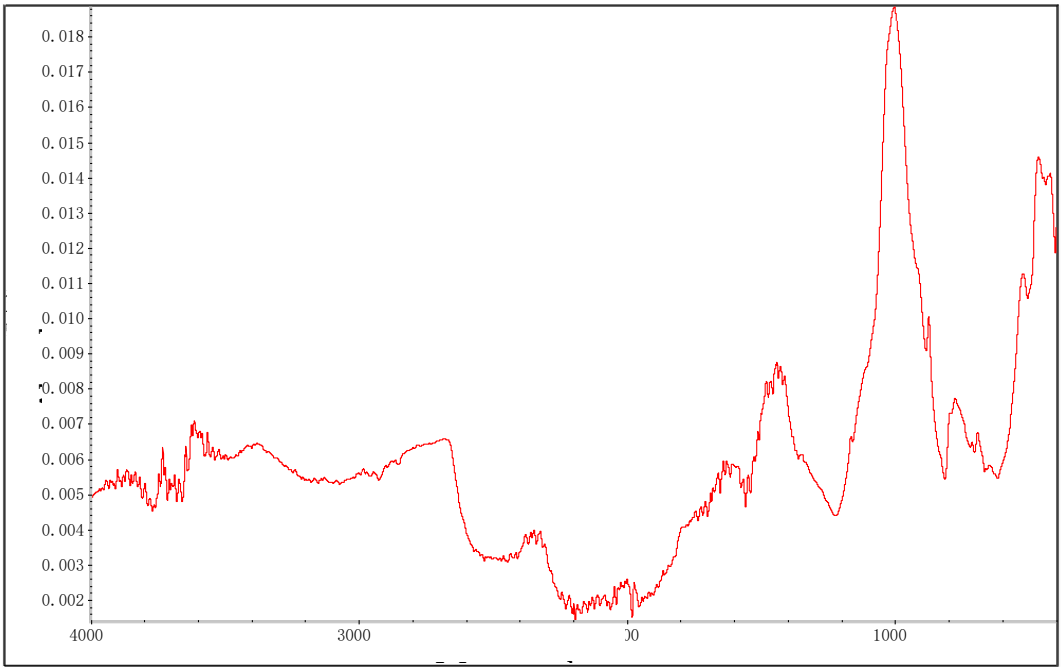


Fig A-33. the FTIR spectrum of XYGC4 from the Xingyangguchenng site

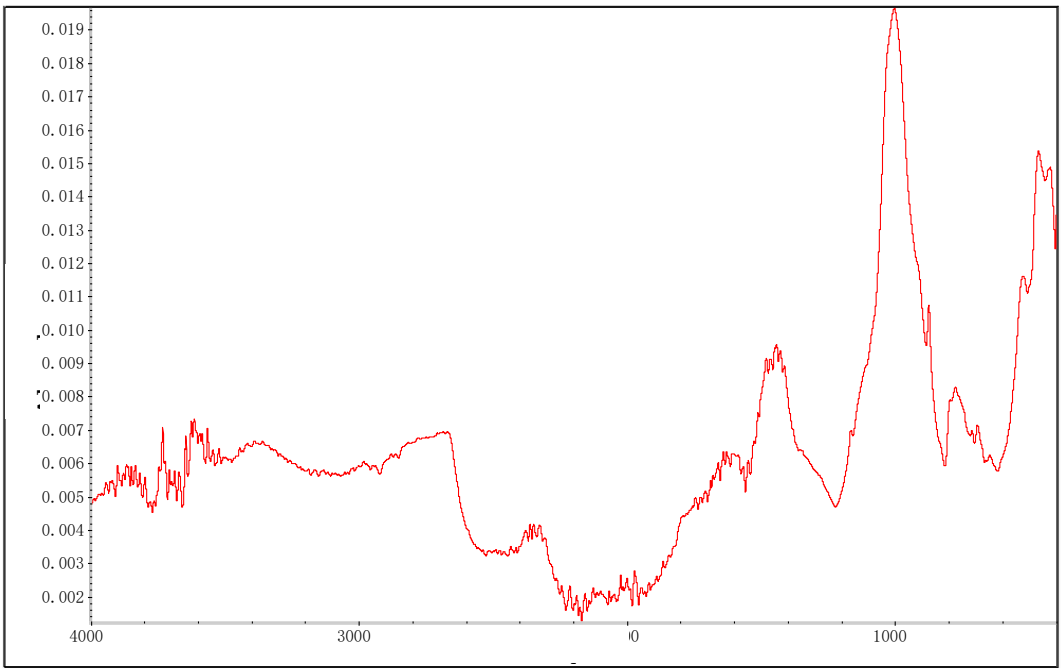


Fig A-34. the FTIR spectrum of XYGC5 from the Xingyangguchenng site

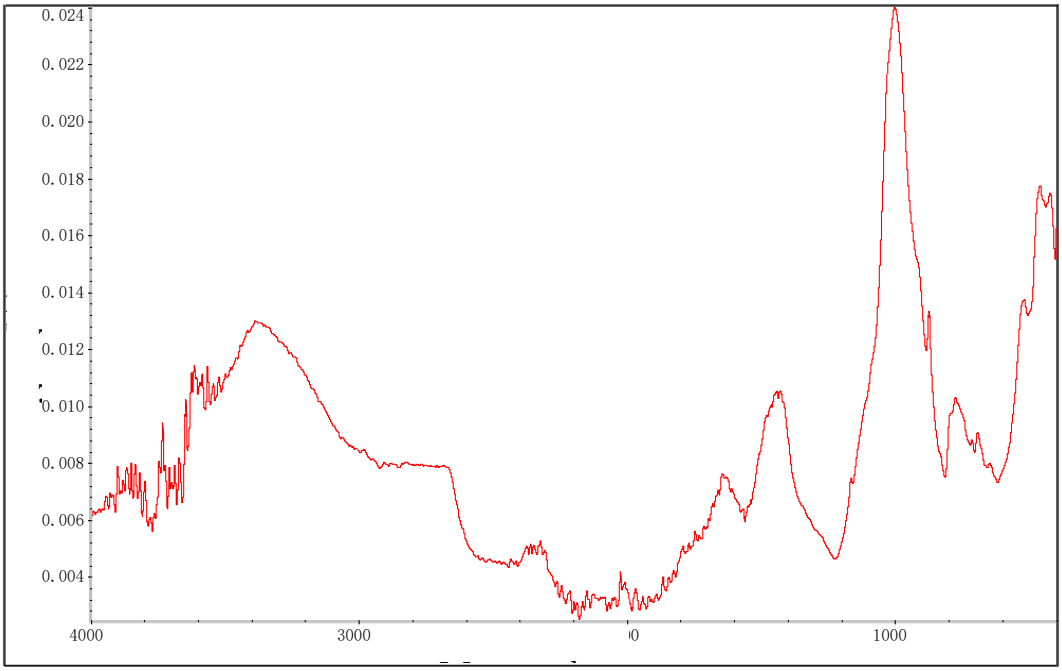


Fig A-35. the FTIR spectrum of XYGC6 from the Xingyanggucheng site

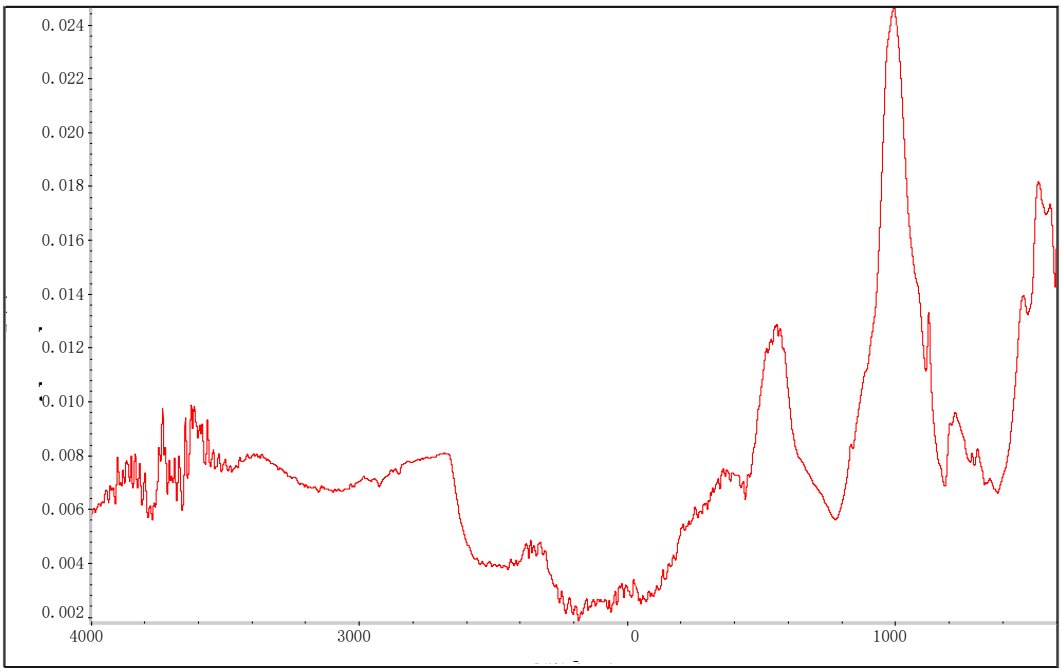


Fig A-36. the FTIR spectrum of XYGC7 from the Xingyanggucheng site

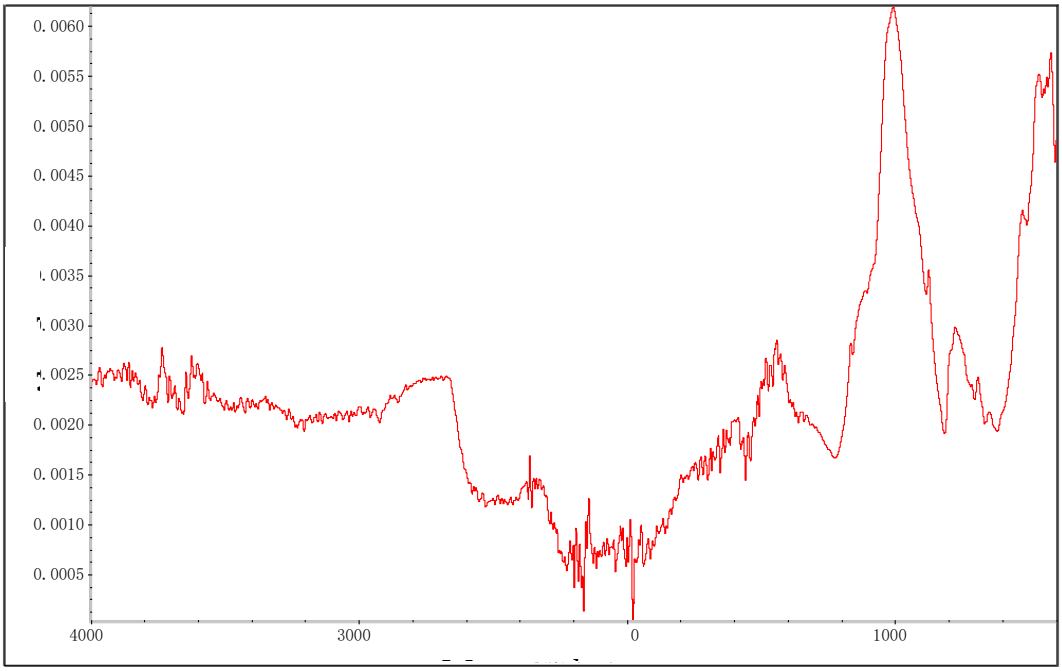


Fig A-37. the FTIR spectrum of XZM1 from the Xinzhengmen site

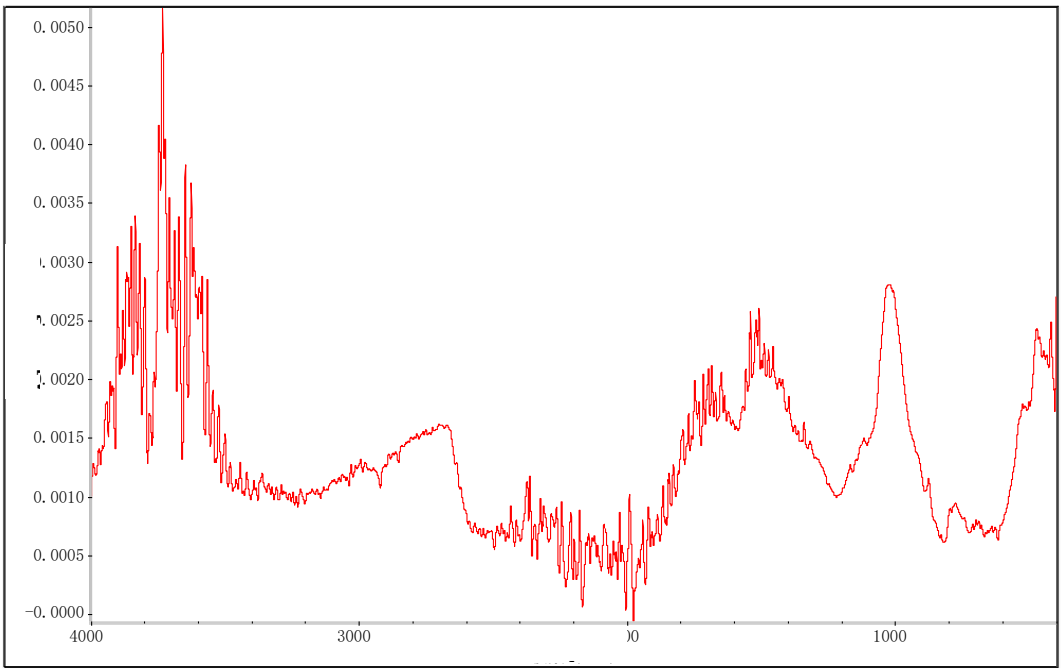


Fig A-38. the FTIR spectrum of XZM2 from the Xinzhengmen site

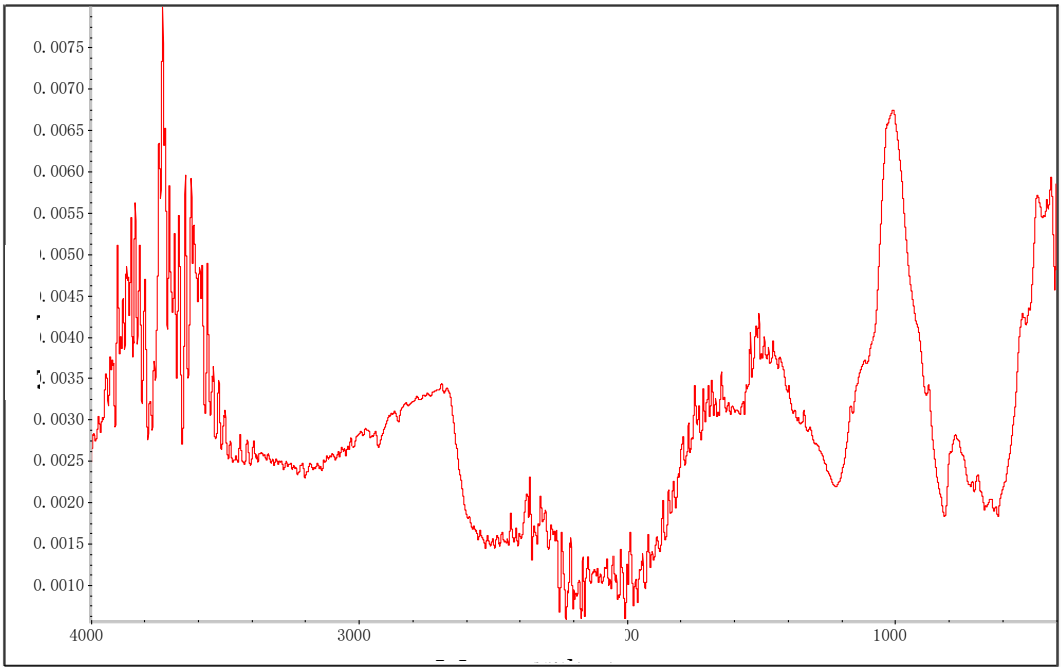


Fig A-39. the FTIR spectrum of XZM3 from the Xinzhengmen site

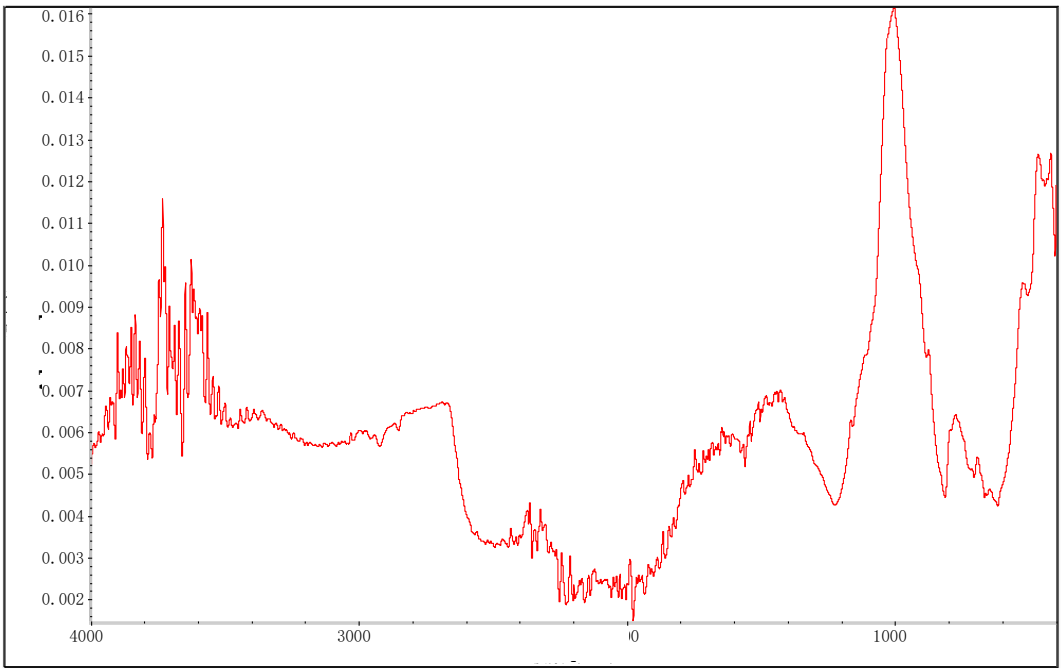


Fig A-40. the FTIR spectrum of XZM4 from the Xinzhengmen site

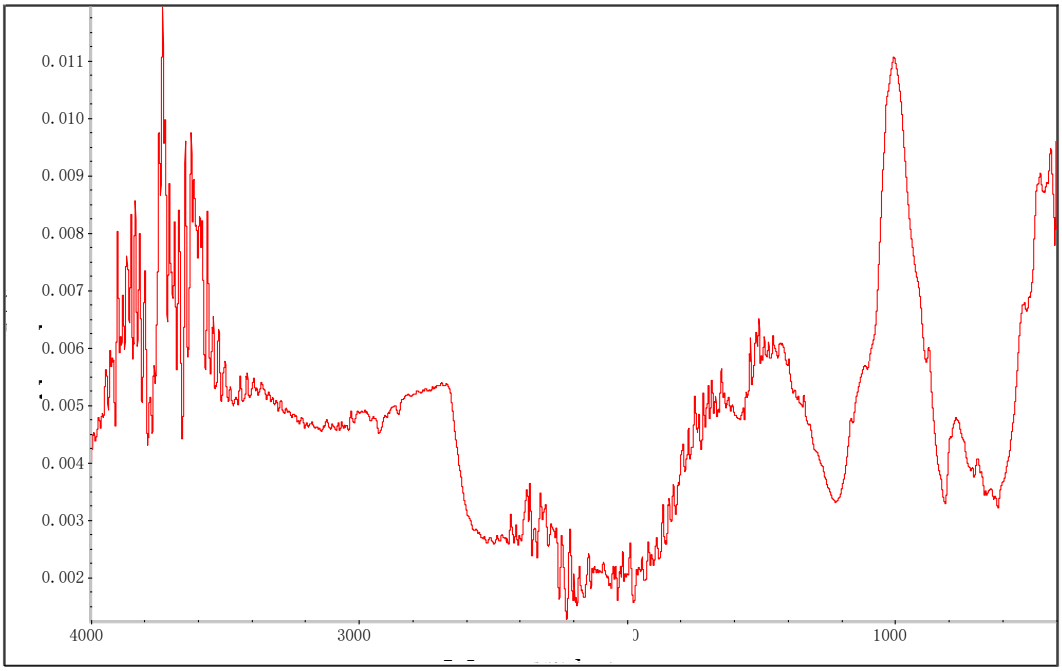


Fig A-41. the FTIR spectrum of XZM5 from the Xinzhengmen site

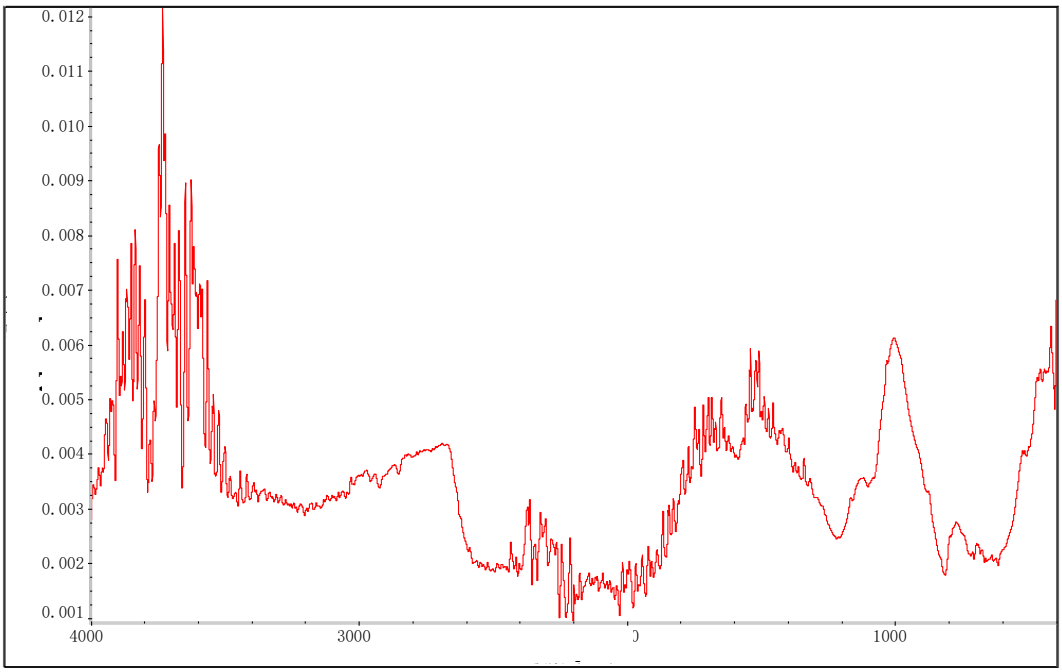


Fig A-42. the FTIR spectrum of XZM6 from the Xinzhengmen site

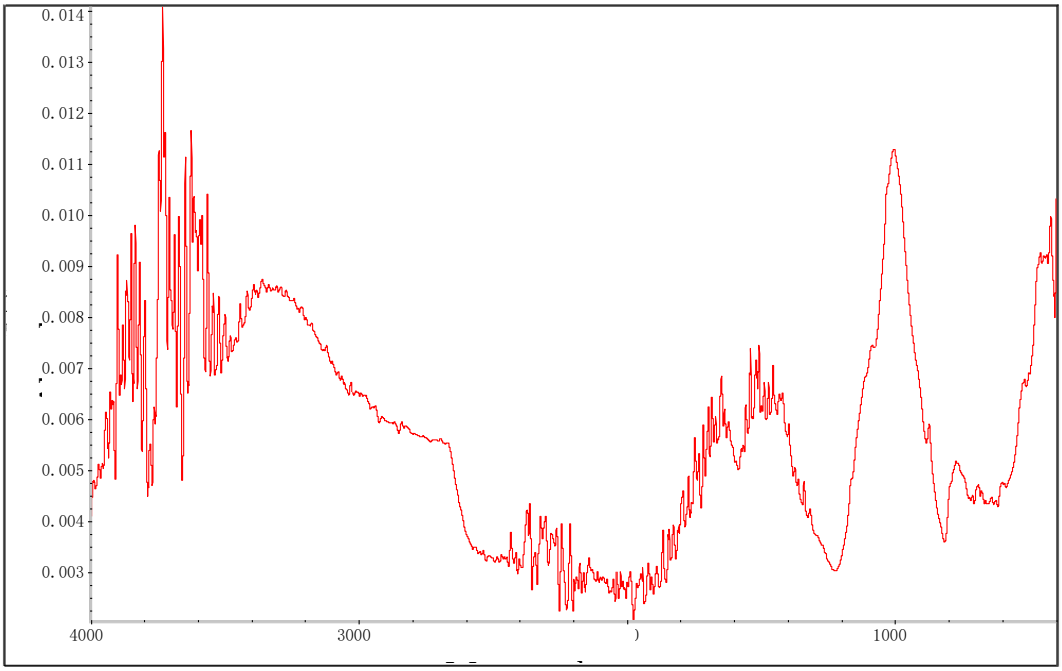


Fig A-43. the FTIR spectrum of XZM7 from the Xinzhengmen site

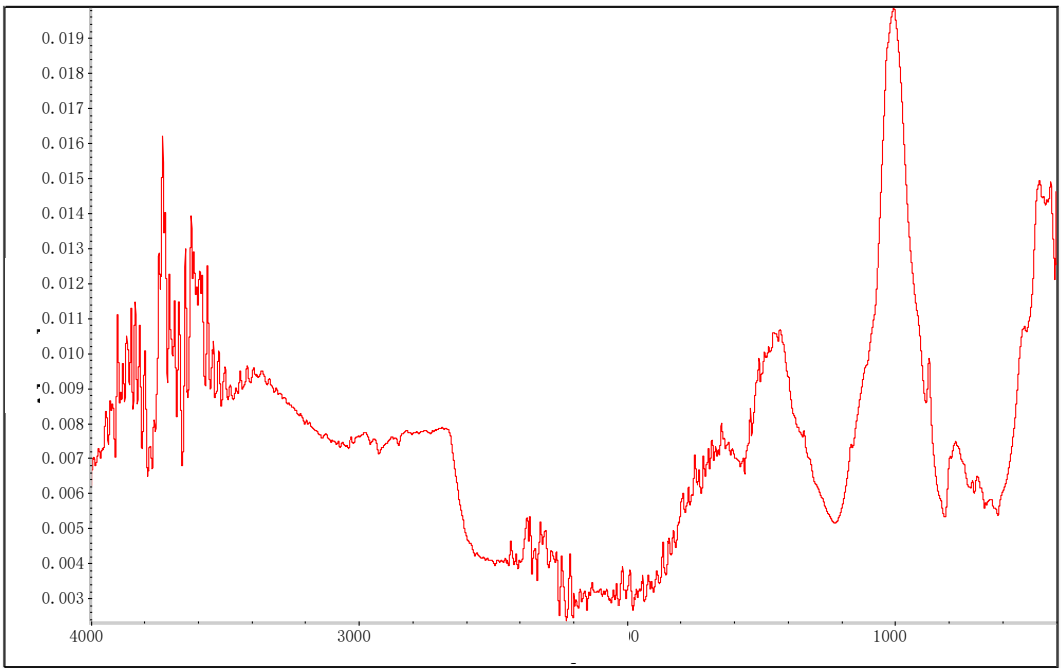


Fig A-44. the FTIR spectrum of XZM8 from the Xinzhengmen site

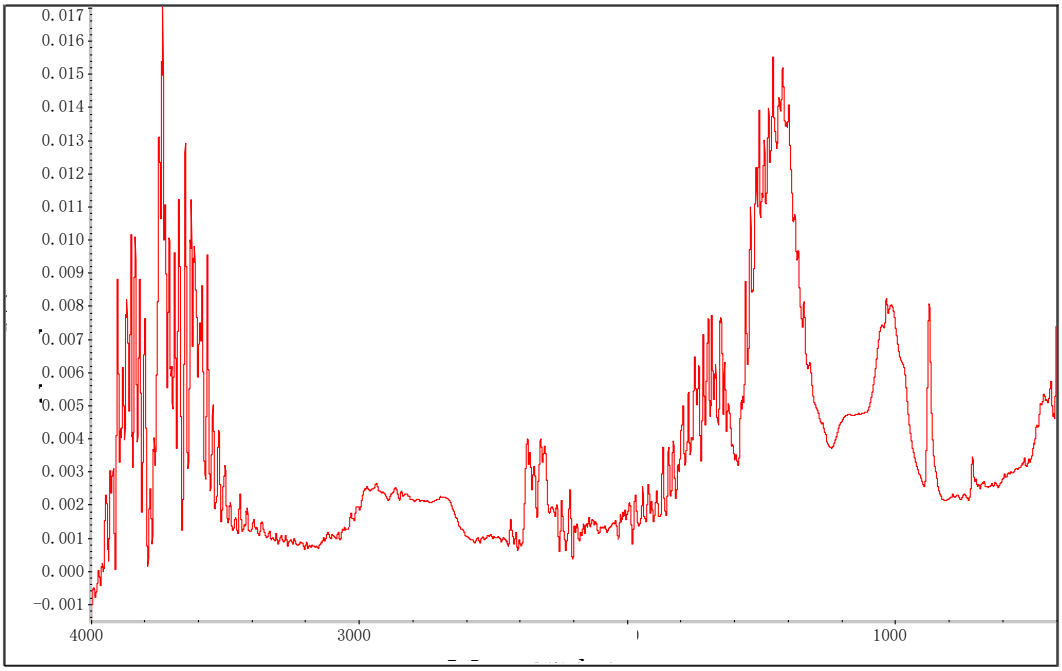


Fig A-45. the FTIR spectrum of ZBYM1 from the tomb of Zhao Boyun

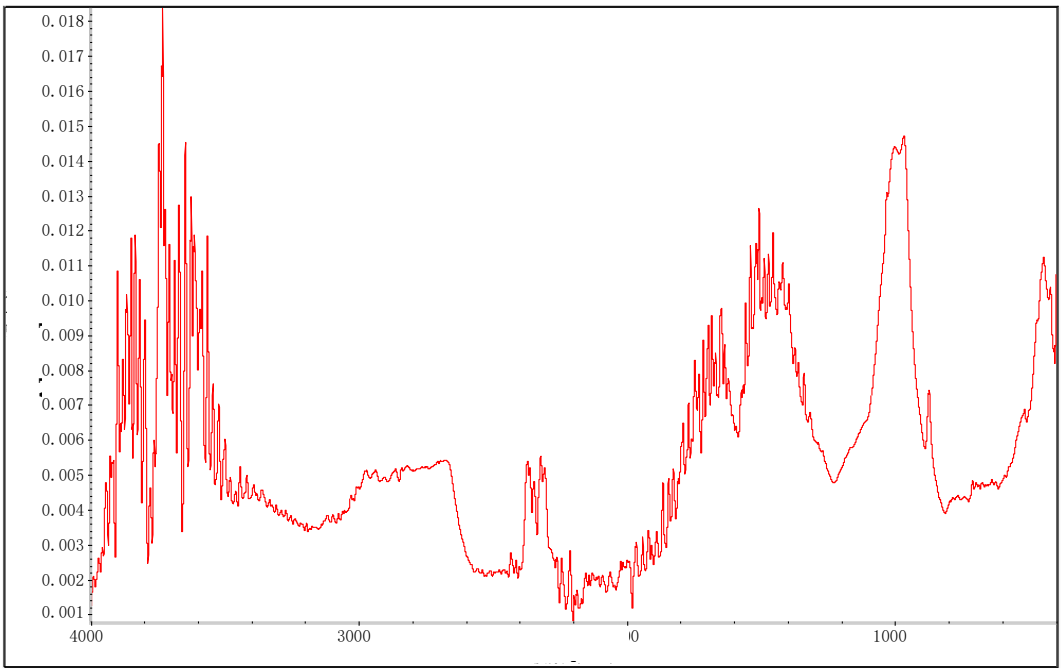


Fig A-46. the FTIR spectrum of ZBYM2 from the tomb of Zhao Boyun

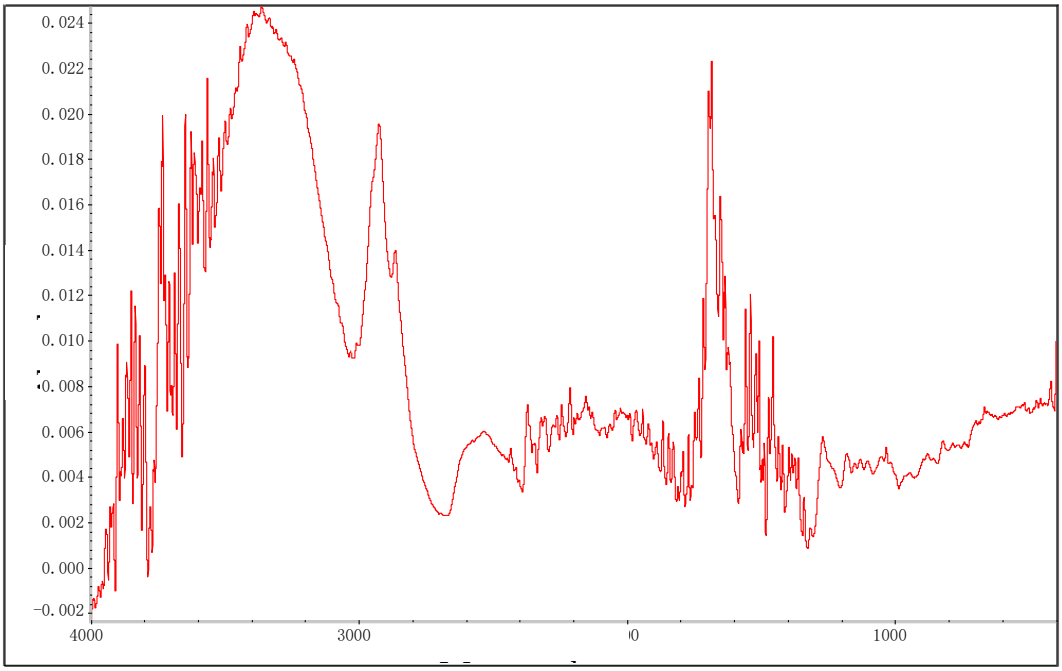


Fig A-47. the FTIR spectrum of ZBYM3 from the tomb of Zhao Boyun

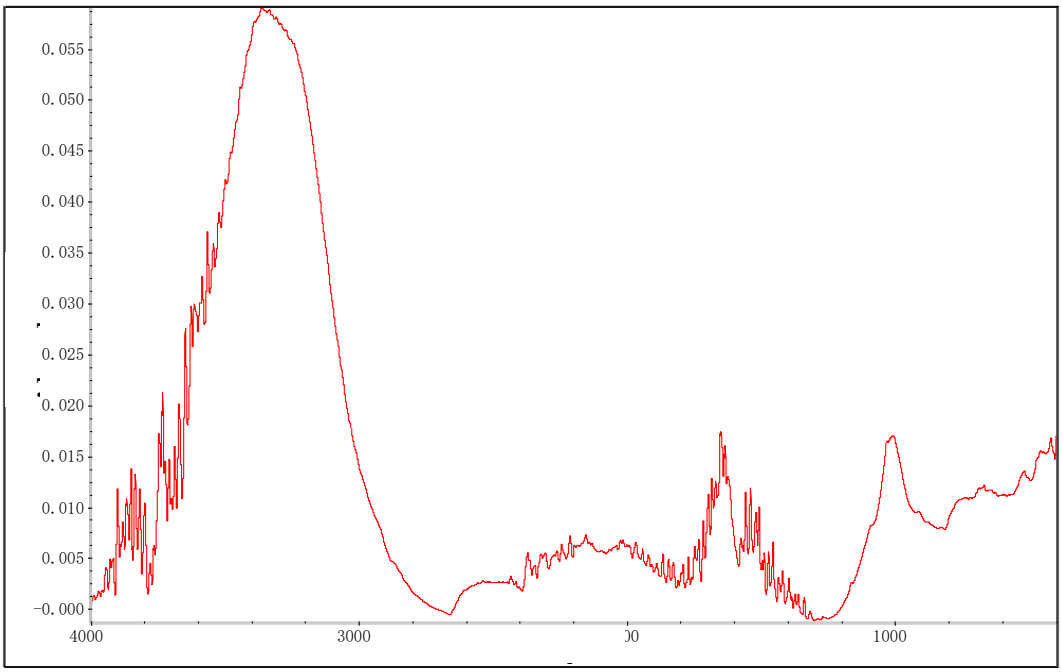


Fig A-48. the FTIR spectrum of ZZSC1 from the Zhengzhou Shangcheng site

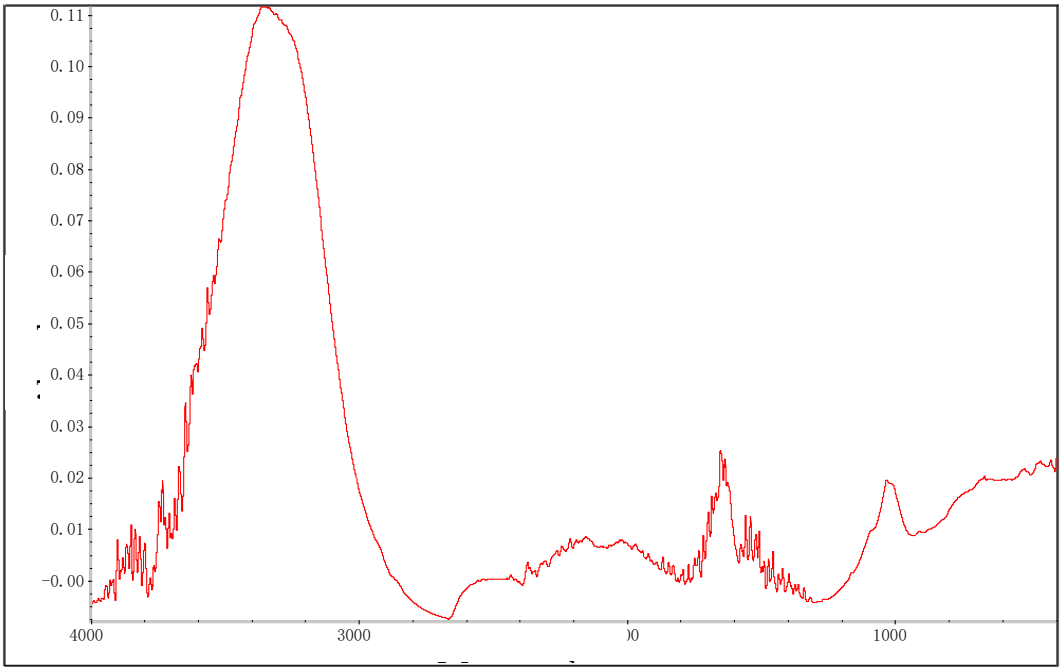


Fig A-49. the FTIR spectrum of ZZSC2 from the Zhengzhou Shangcheng site

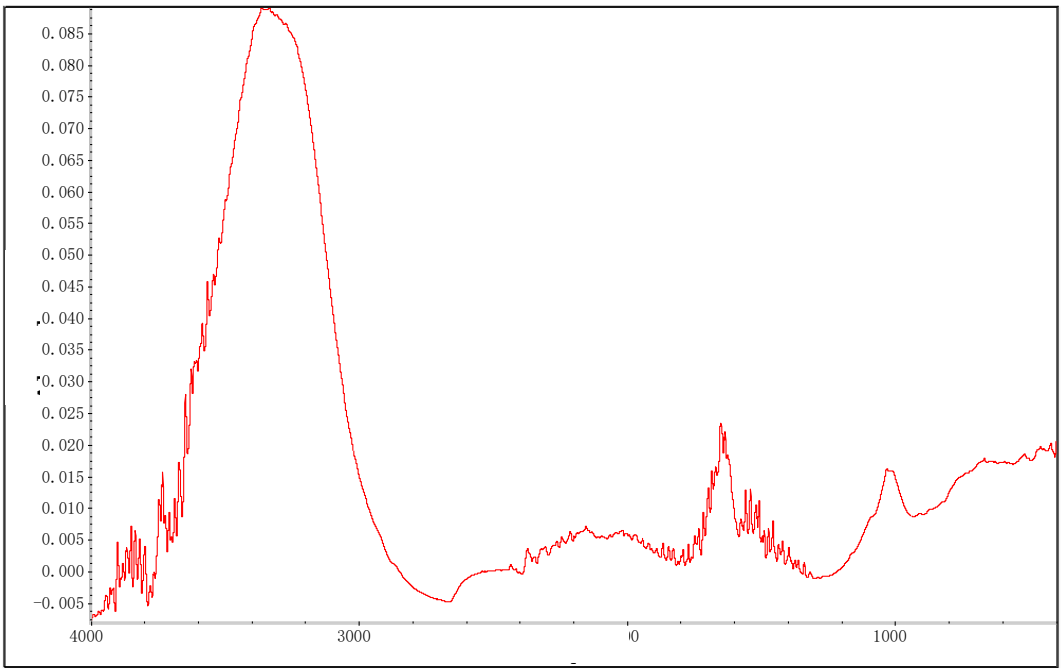


Fig A-50. the FTIR spectrum of ZZSC3 from the Zhengzhou Shangcheng site

Appendix 2. TGA-DTA-DSC results

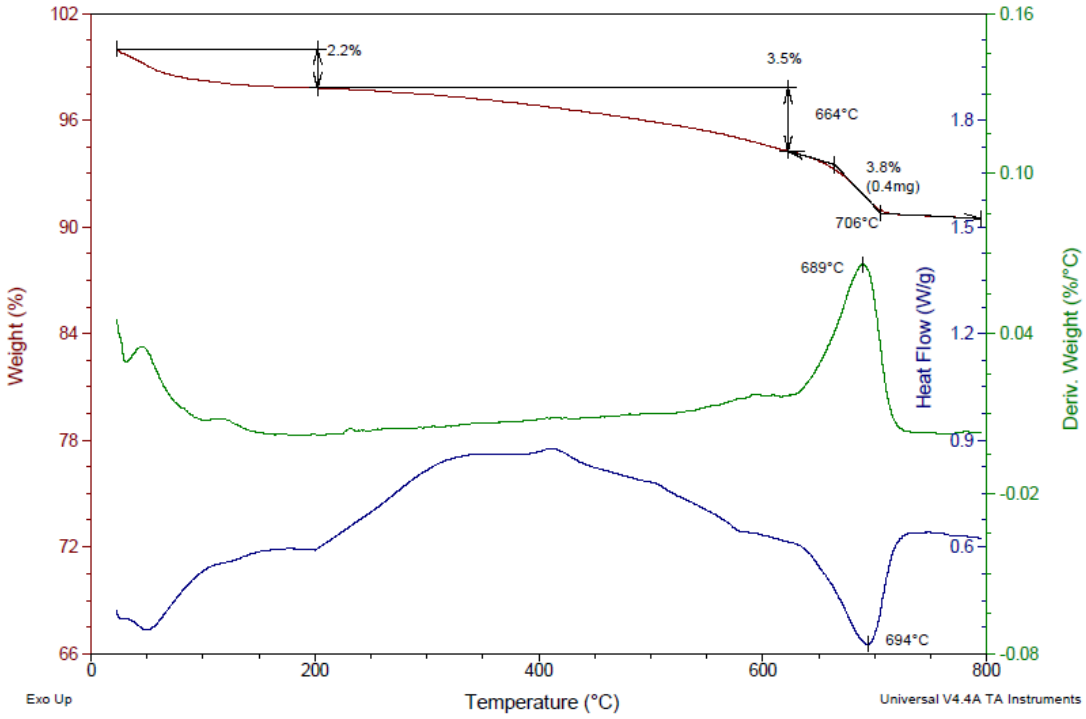


Fig B-1. The TGA-DTA-DSC result of loess

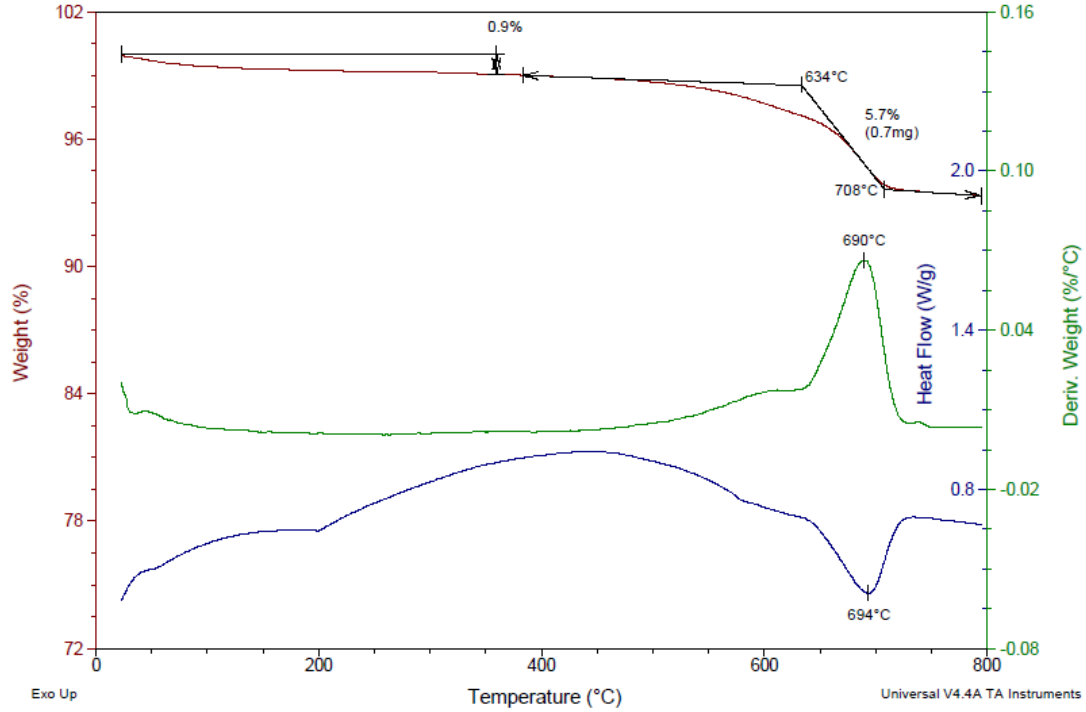


Fig B-2. The TGA-DTA-DSC result of baked loess

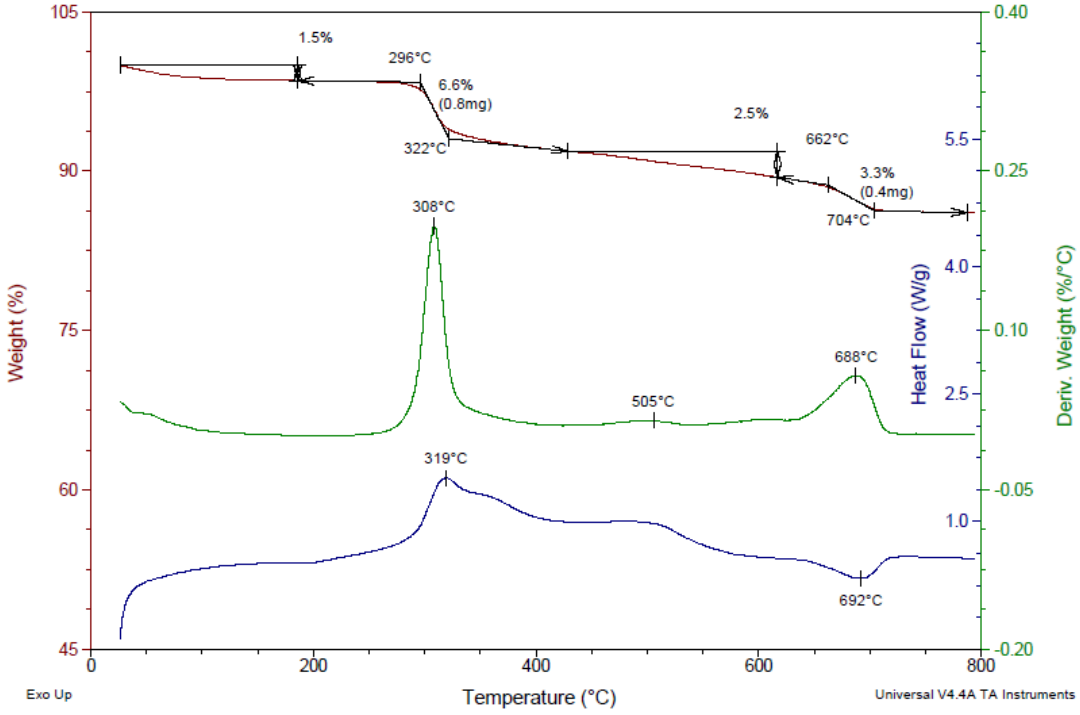


Fig B-3. The TGA-DTA-DSC result of M4

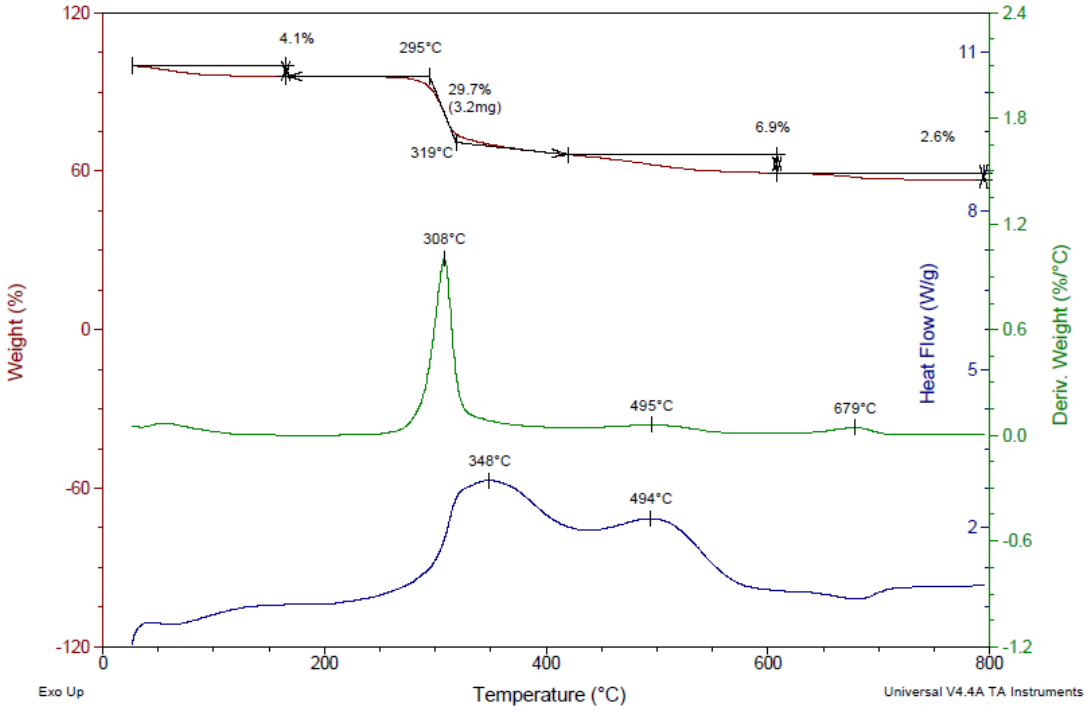


Fig B-4. The TGA-DTA-DSC result of M6

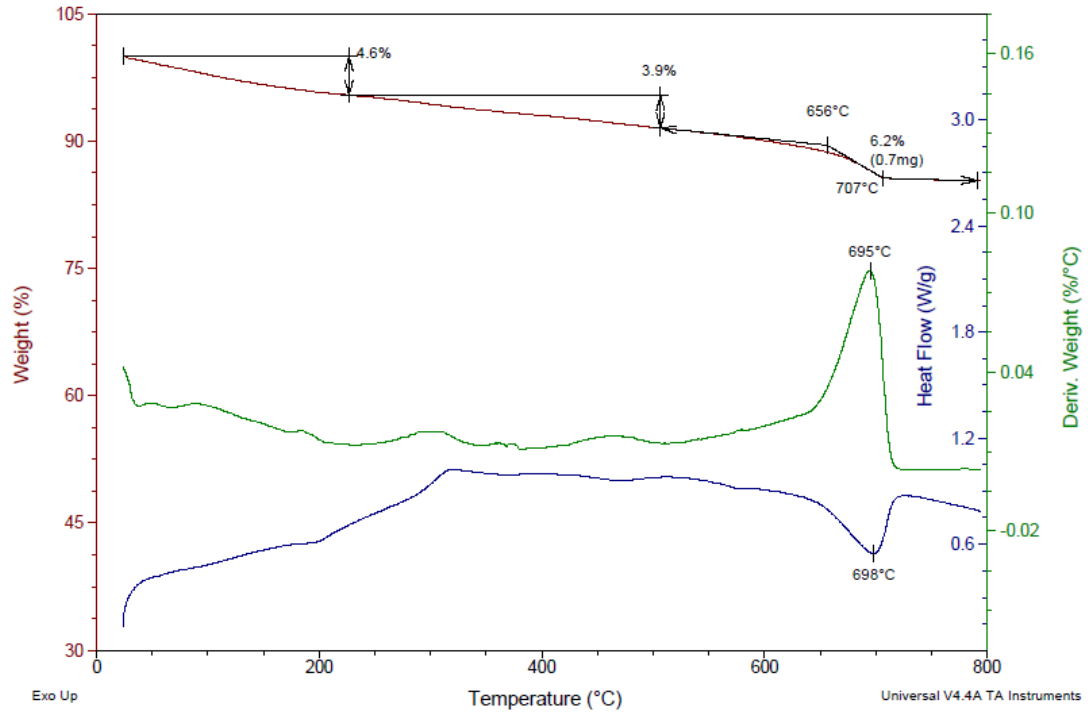


Fig B-5. The TGA-DTA-DSC result of HYPT1

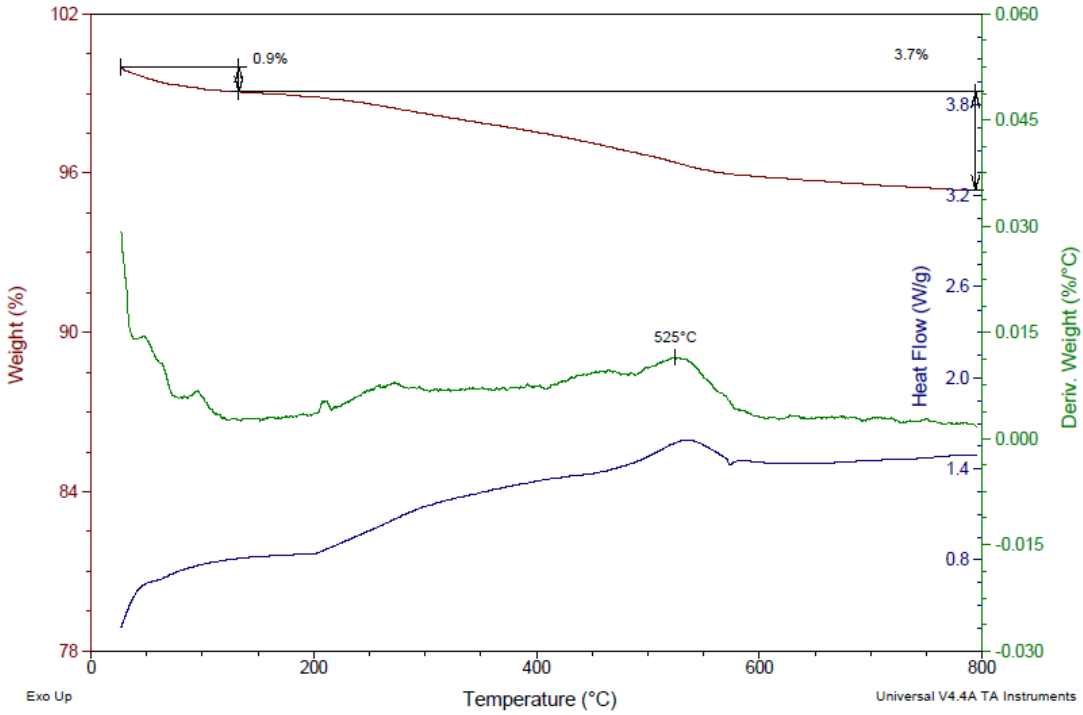


Fig B-6. The TGA-DTA-DSC result of SJYTL3

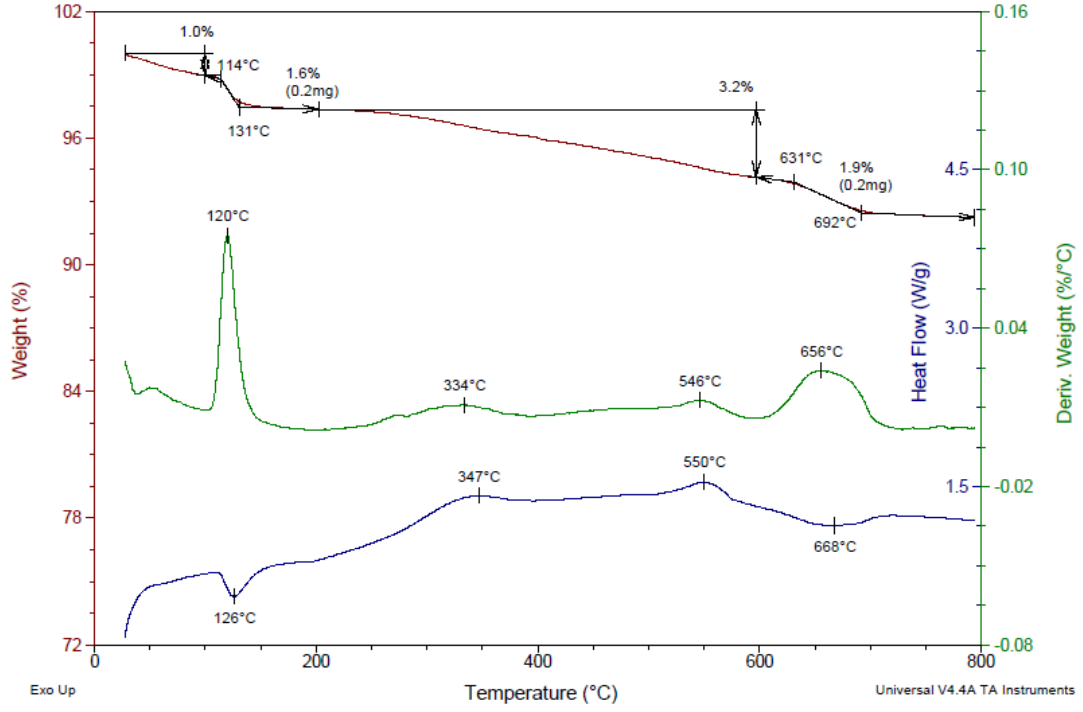


Fig B-7. The TGA-DTA-DSC result of XZM7

Appendix 3. TGA-FTIR results

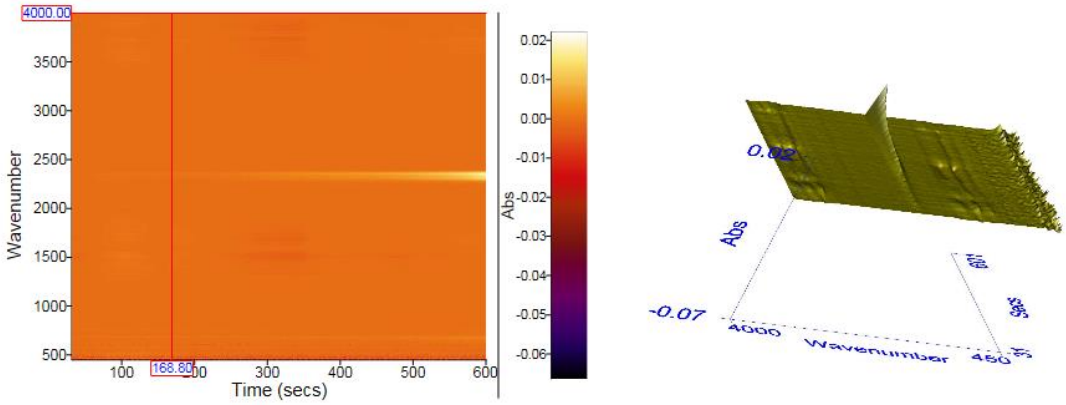


Fig C-1. FTIR profile of the sticky rice with the change of temperature

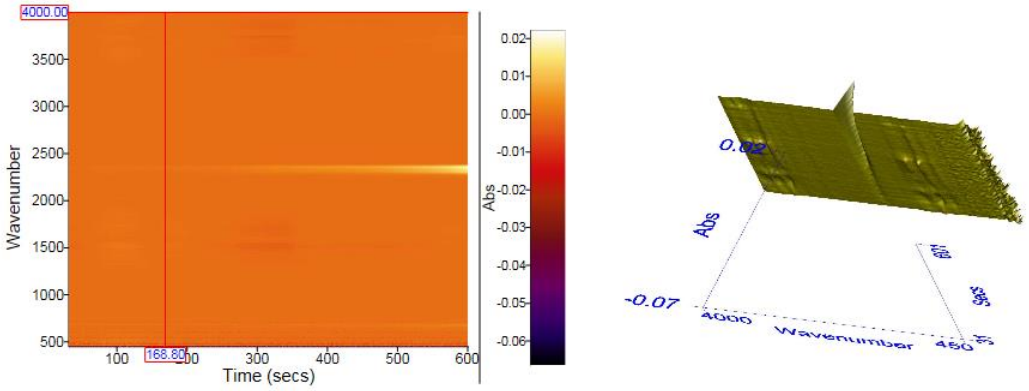


Fig C-2. FTIR profile of the loess with the change of temperature

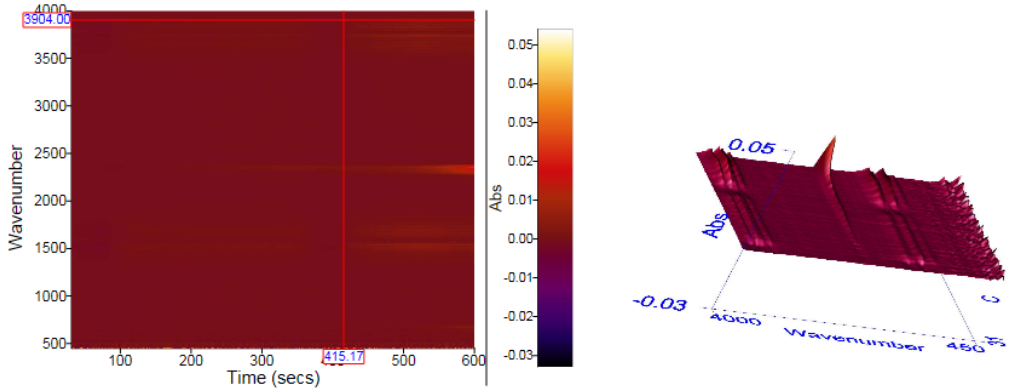


Fig C-3. FTIR profile of the baked loess with the change of temperature

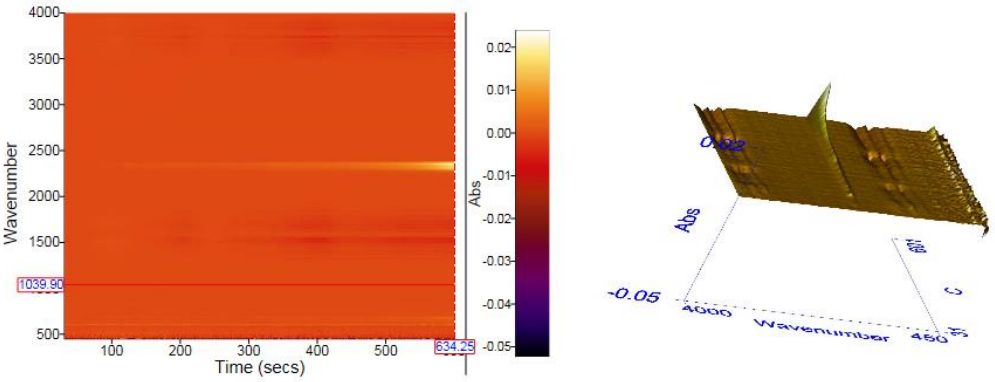


Fig C-4. FTIR profile of M1 with the change of temperature

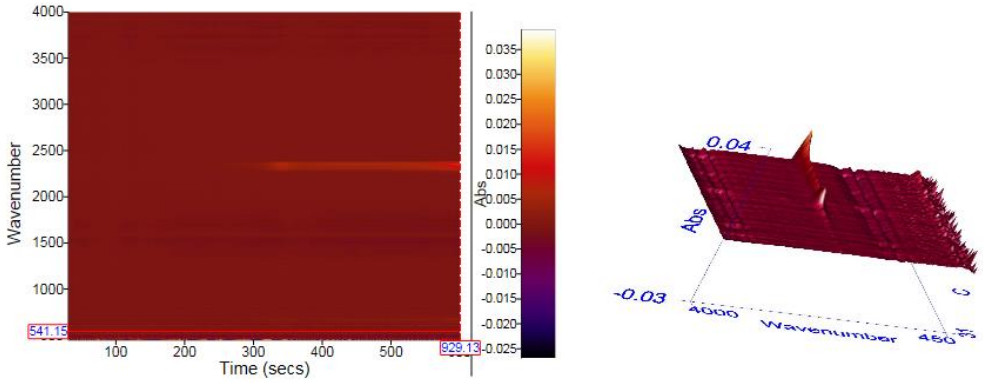


Fig C-5. FTIR profile of M2 with the change of temperature

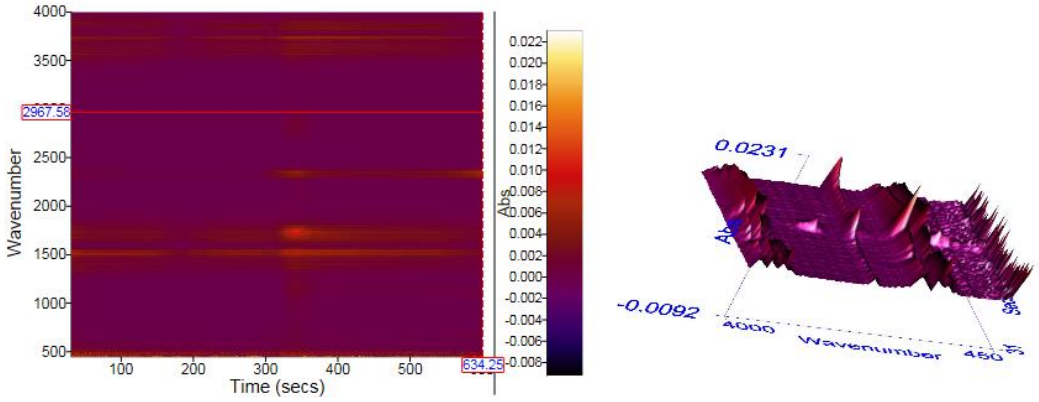


Fig C-6. FTIR profile of M3 with the change of temperature

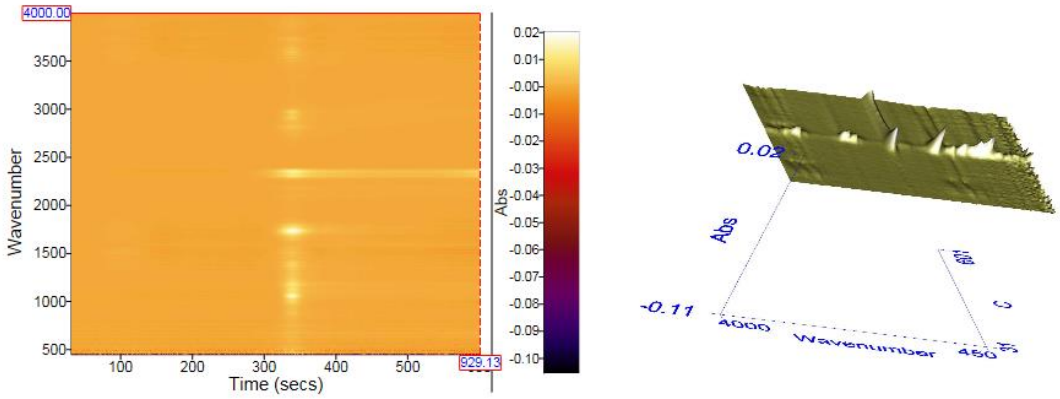


Fig C-7. FTIR profile of M4 with the change of temperature

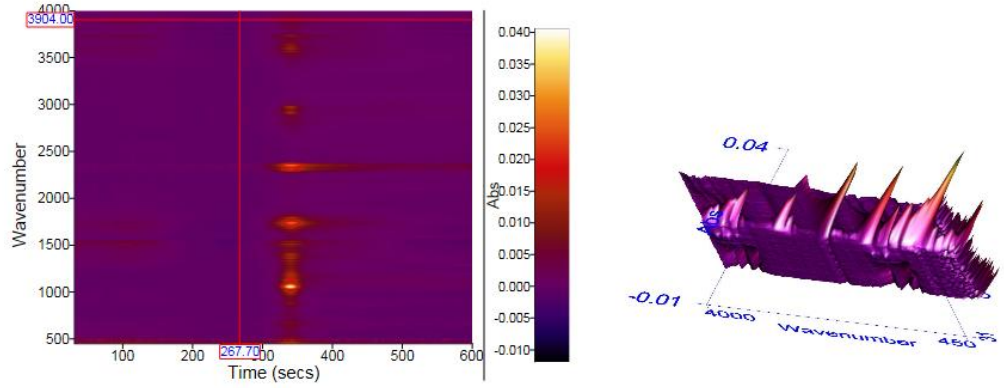


Fig C-8. FTIR profile of M6 with the change of temperature

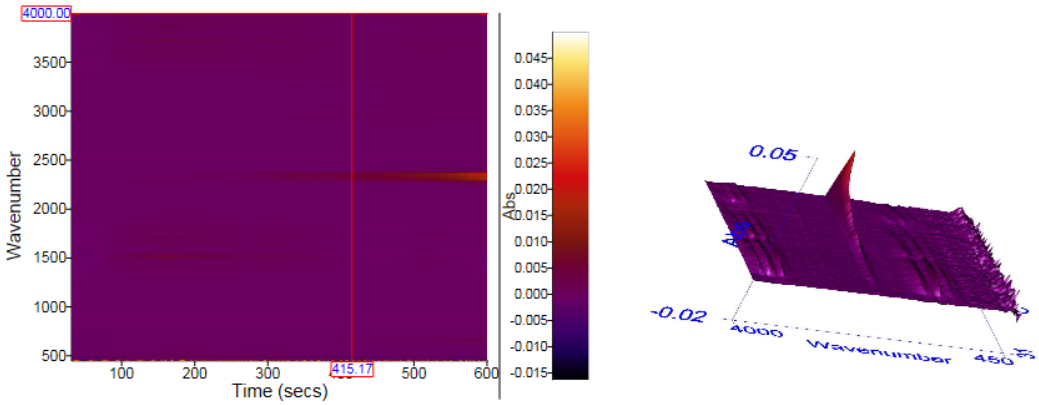


Fig C-9. FTIR profile of HYPT1 with the change of temperature

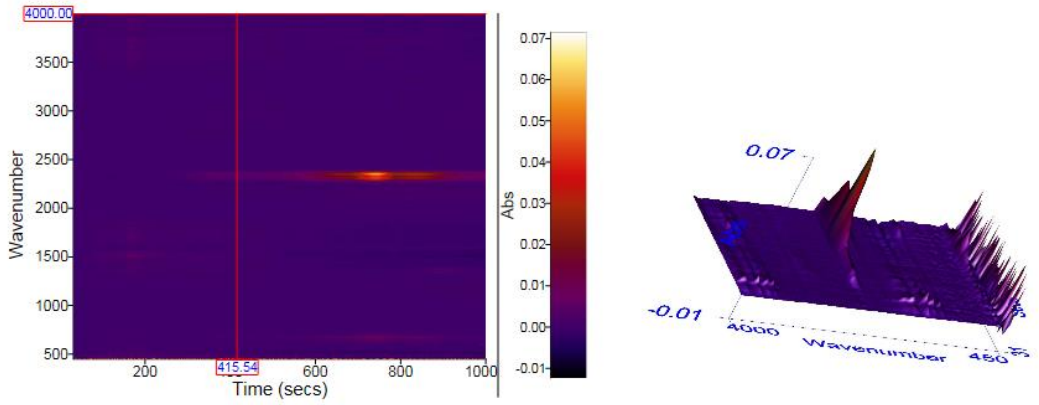


Fig C-10. FTIR profile of XZM7 with the change of temperature

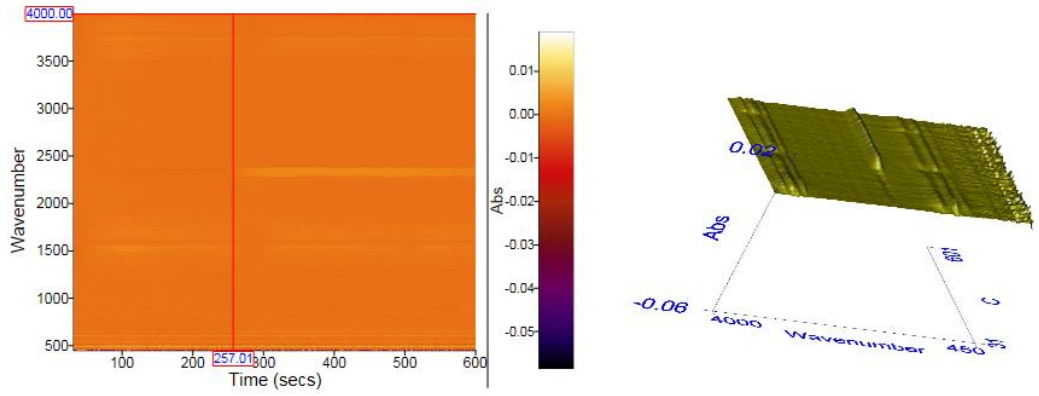
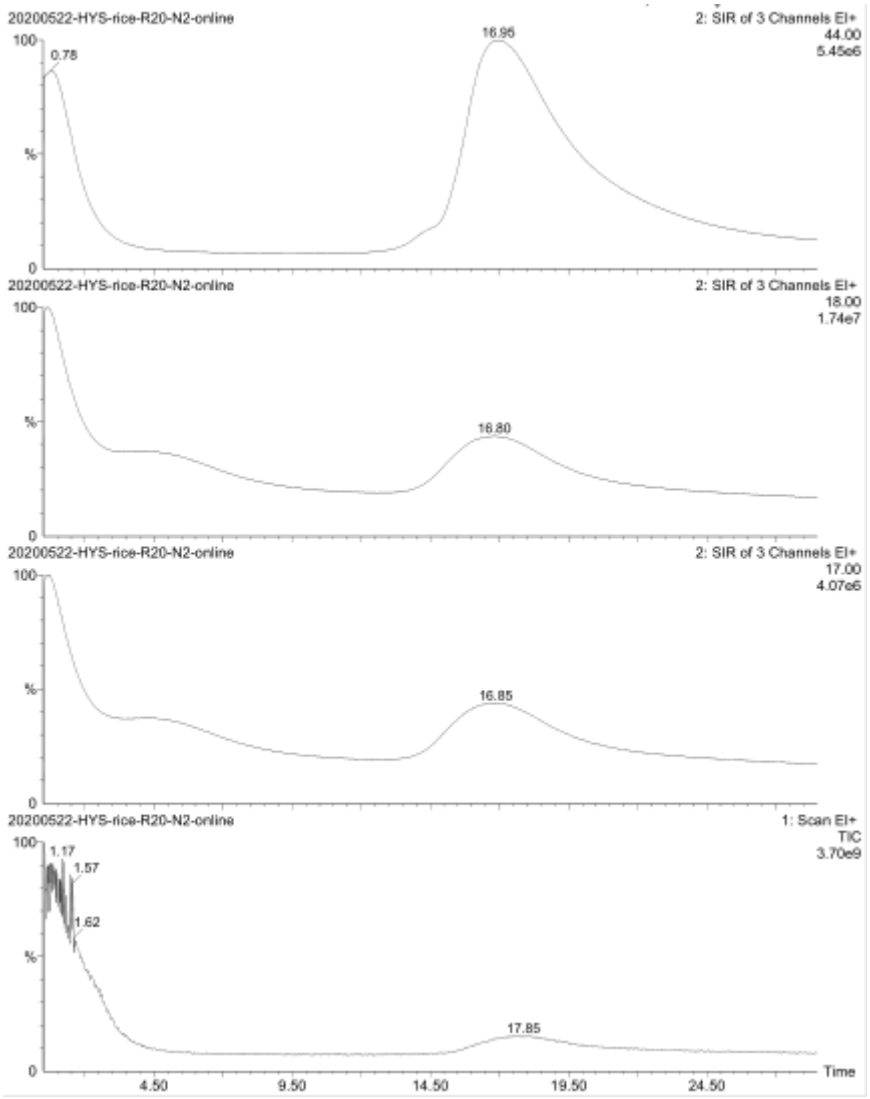


Fig C-11. FTIR profile of SJYTL3 with the change of temperature

Appendix 4. TGA-MS results



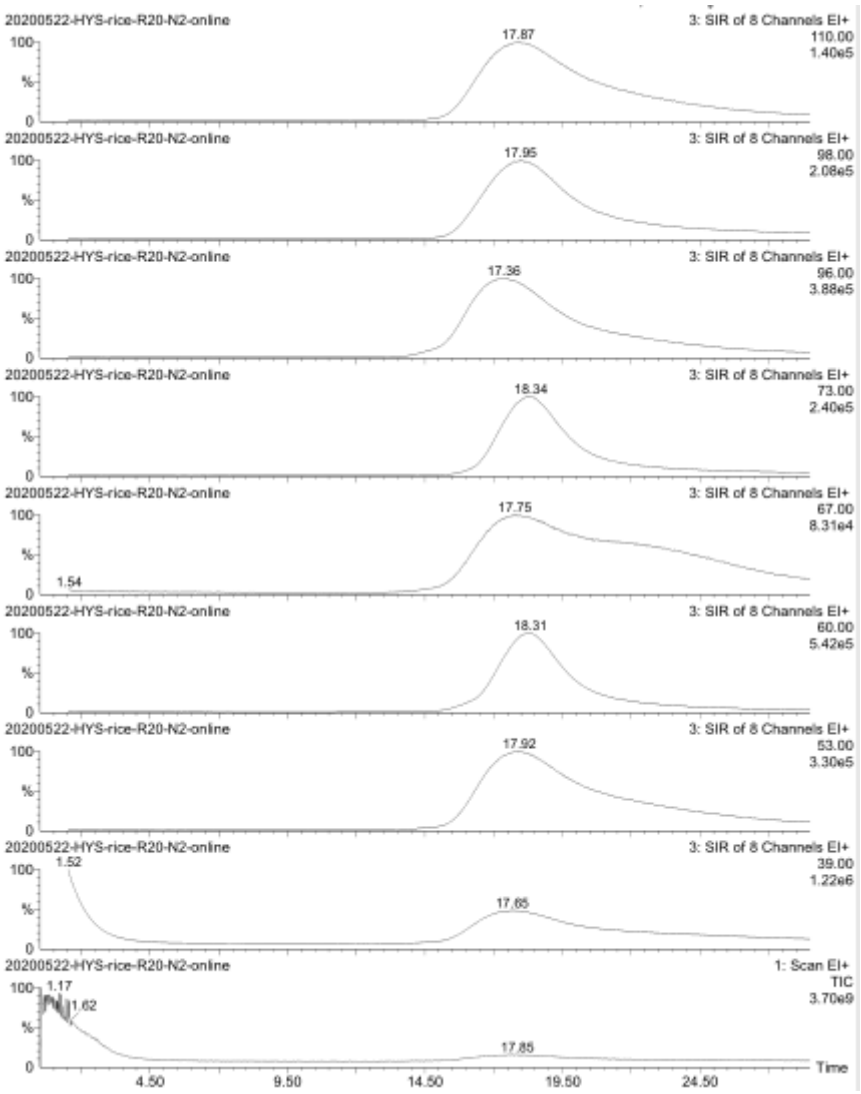
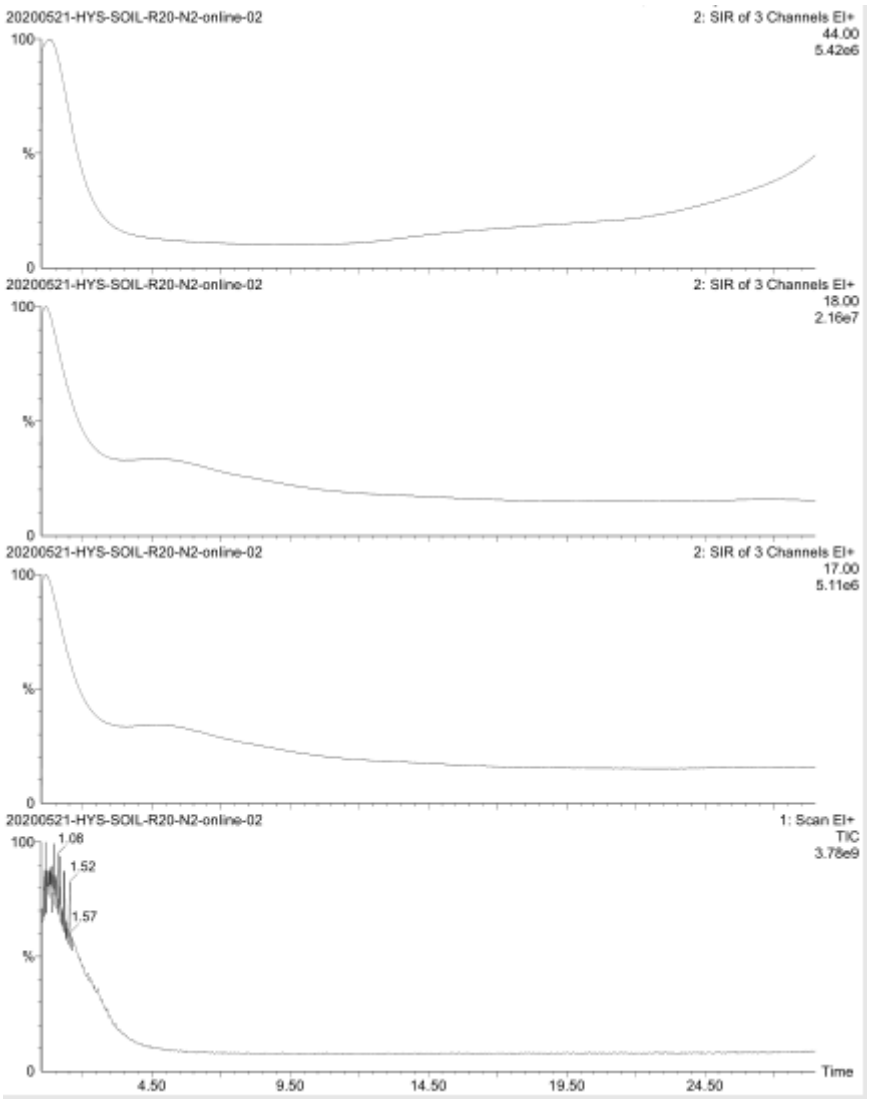


Fig D-1. TGA-MS result of the sticky rice


20200521-HYS-SOIL-R20-N2-online-02
2: SIR of 3 Channels EI+
44.00
5.42e6
100
%
0
20200521-HYS-SOIL-R20-N2-online-02
2: SIR of 3 Channels EI+
18.00
2.16e7
100
%
0
20200521-HYS-SOIL-R20-N2-online-02
2: SIR of 3 Channels EI+
17.00
5.11e6
100
%
0
20200521-HYS-SOIL-R20-N2-online-02
1: Scan EI+
TIC
3.78e9
1.08
1.52
1.57
100
%
0
Time
4.50
9.50
14.50
19.50
24.50

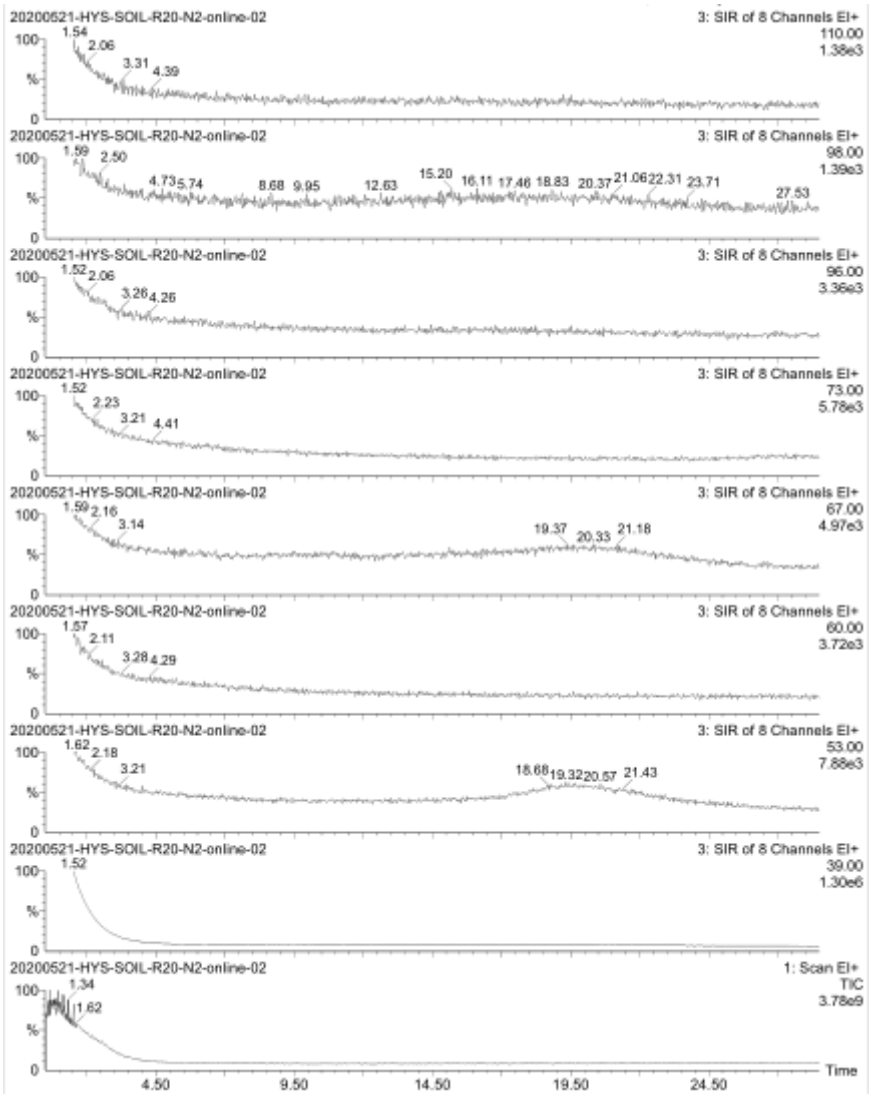
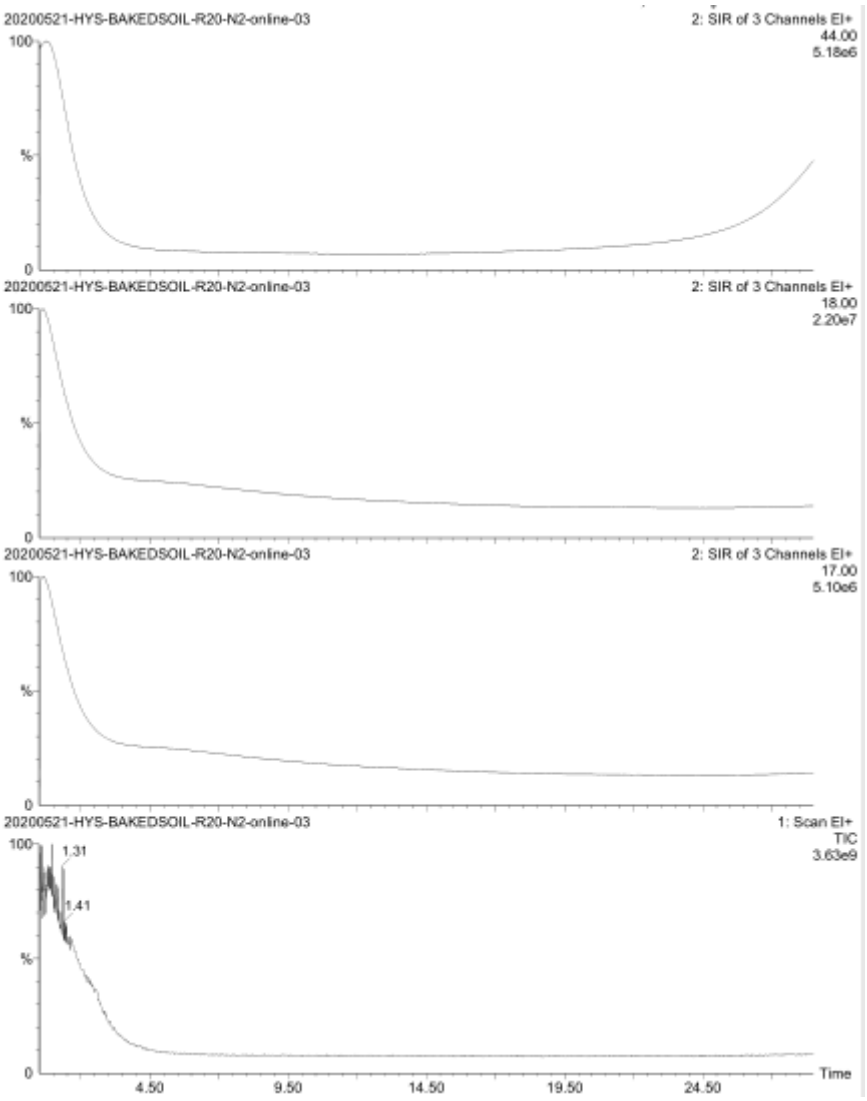


Fig D-2. TGA-MS result of the loess


20200521-HYS-BAKEDSOIL-R20-N2-online-03
2: SIR of 3 Channels EI+
44.00
5.18e6
100
%
0
20200521-HYS-BAKEDSOIL-R20-N2-online-03
2: SIR of 3 Channels EI+
18.00
2.20e7
100
%
0
20200521-HYS-BAKEDSOIL-R20-N2-online-03
2: SIR of 3 Channels EI+
17.00
5.10e6
100
%
0
20200521-HYS-BAKEDSOIL-R20-N2-online-03
1: Scan EI+
TIC
3.63e9
100
1.31
1.41
%
0
Time
4.50
9.50
14.50
19.50
24.50

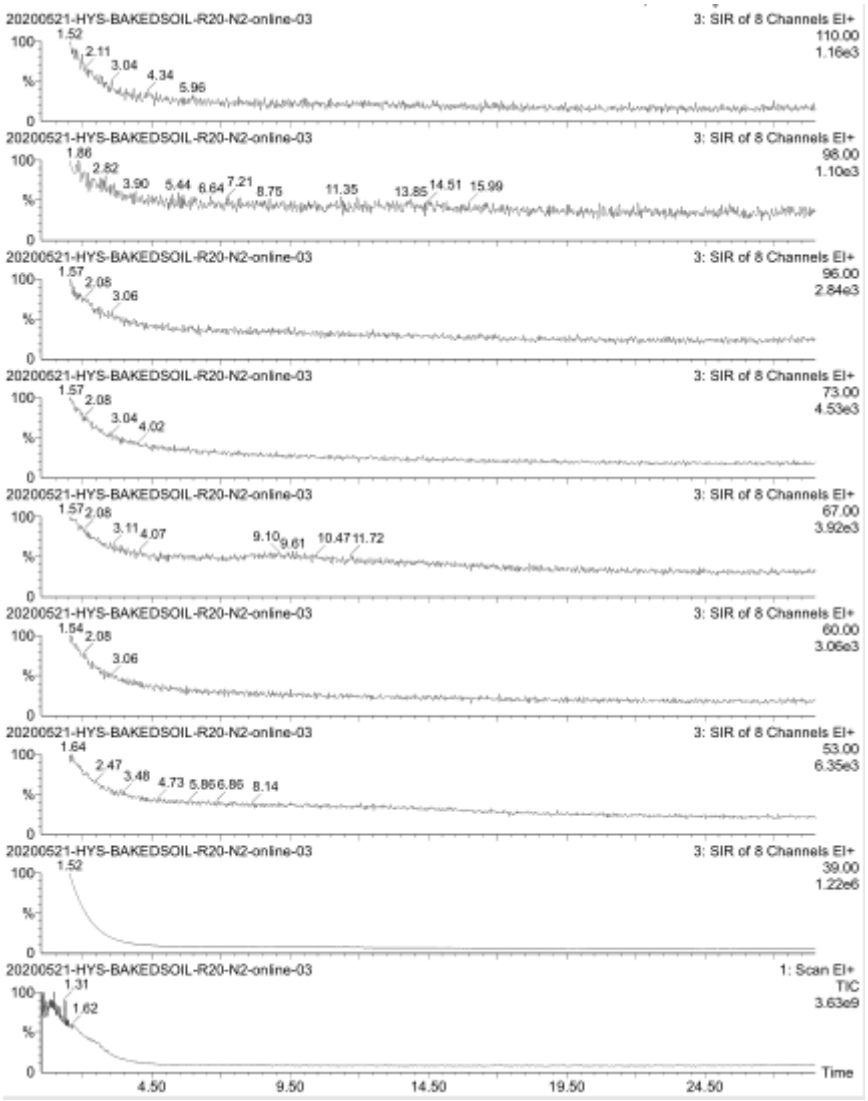
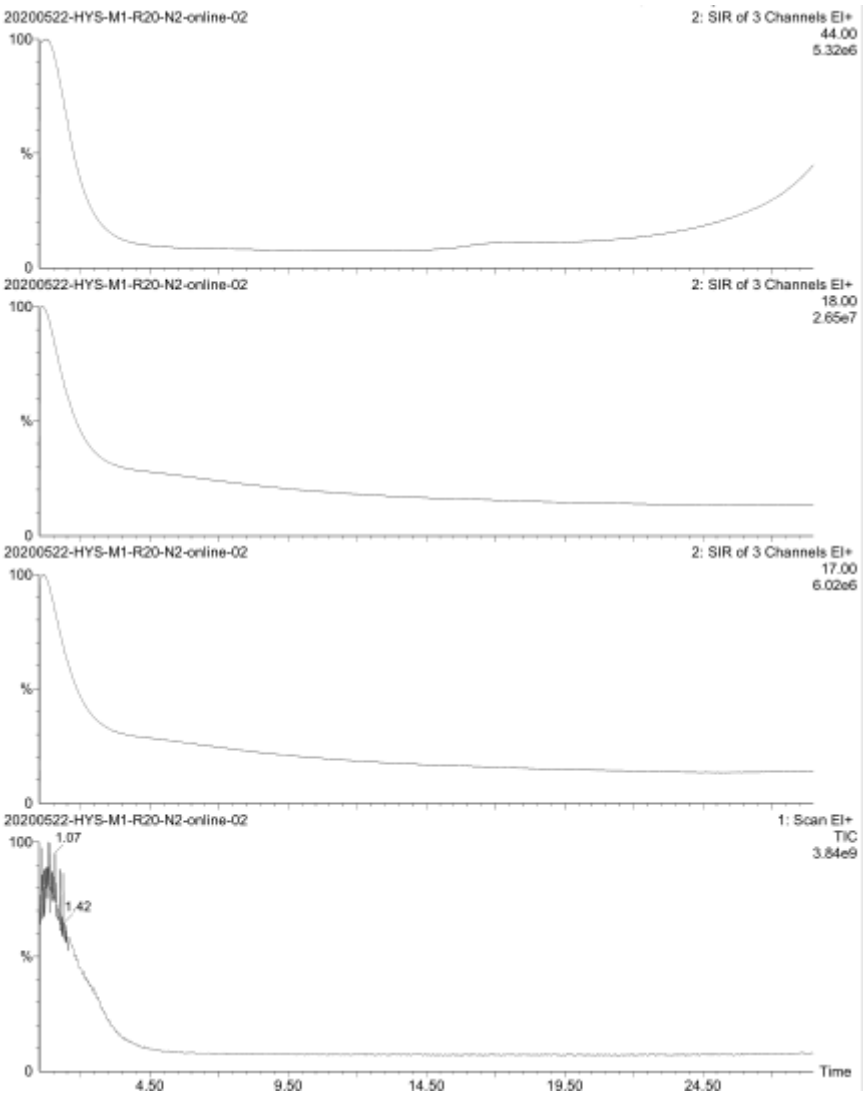


Fig D-3. TGA-MS result of the baked loess


20200522-HYS-M1-R20-N2-online-02
2: SIR of 3 Channels EI+
44.00
5.32e6
100
%
0
20200522-HYS-M1-R20-N2-online-02
2: SIR of 3 Channels EI+
18.00
2.65e7
100
%
0
20200522-HYS-M1-R20-N2-online-02
2: SIR of 3 Channels EI+
17.00
6.02e6
100
%
0
20200522-HYS-M1-R20-N2-online-02
1: Scan EI+
TIC
3.84e9
100
1.07
1.42
%
0
Time
4.50
9.50
14.50
19.50
24.50

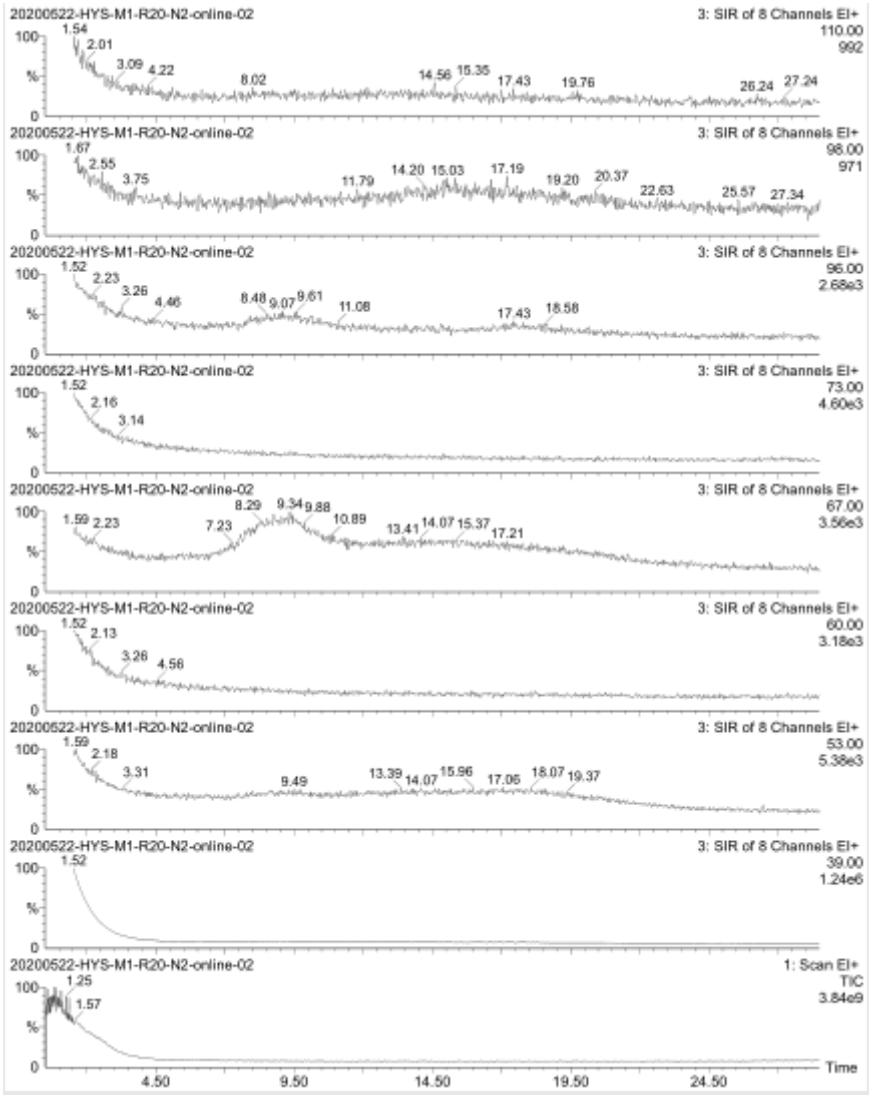
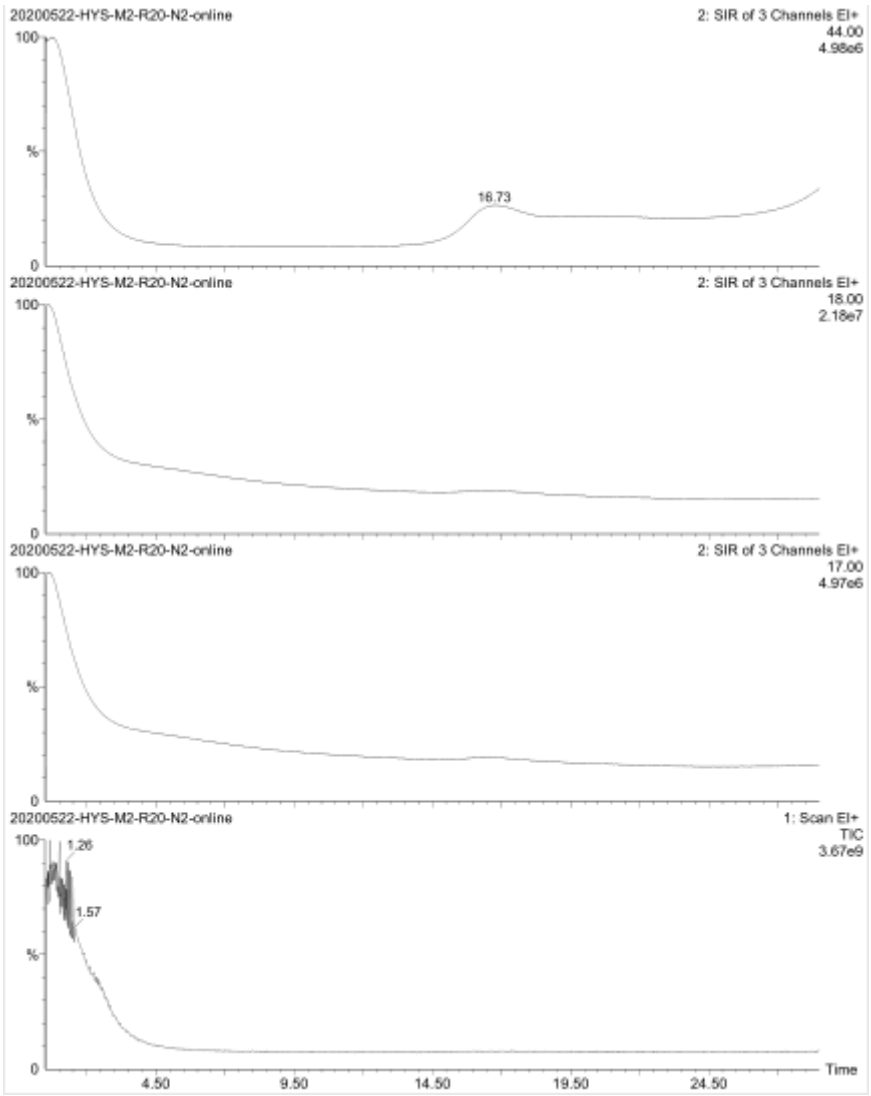


Fig D-4. TGA-MS result of M1


20200522-HYS-M2-R20-N2-online
2: SIR of 3 Channels EI+
44.00
4.98e6
100
%
0
16.73
20200522-HYS-M2-R20-N2-online
2: SIR of 3 Channels EI+
18.00
2.18e7
100
%
0
20200522-HYS-M2-R20-N2-online
2: SIR of 3 Channels EI+
17.00
4.97e6
100
%
0
20200522-HYS-M2-R20-N2-online
1: Scan EI+
TIC
3.67e9
100
1.26
1.57
%
0
Time
4.50
9.50
14.50
19.50
24.50

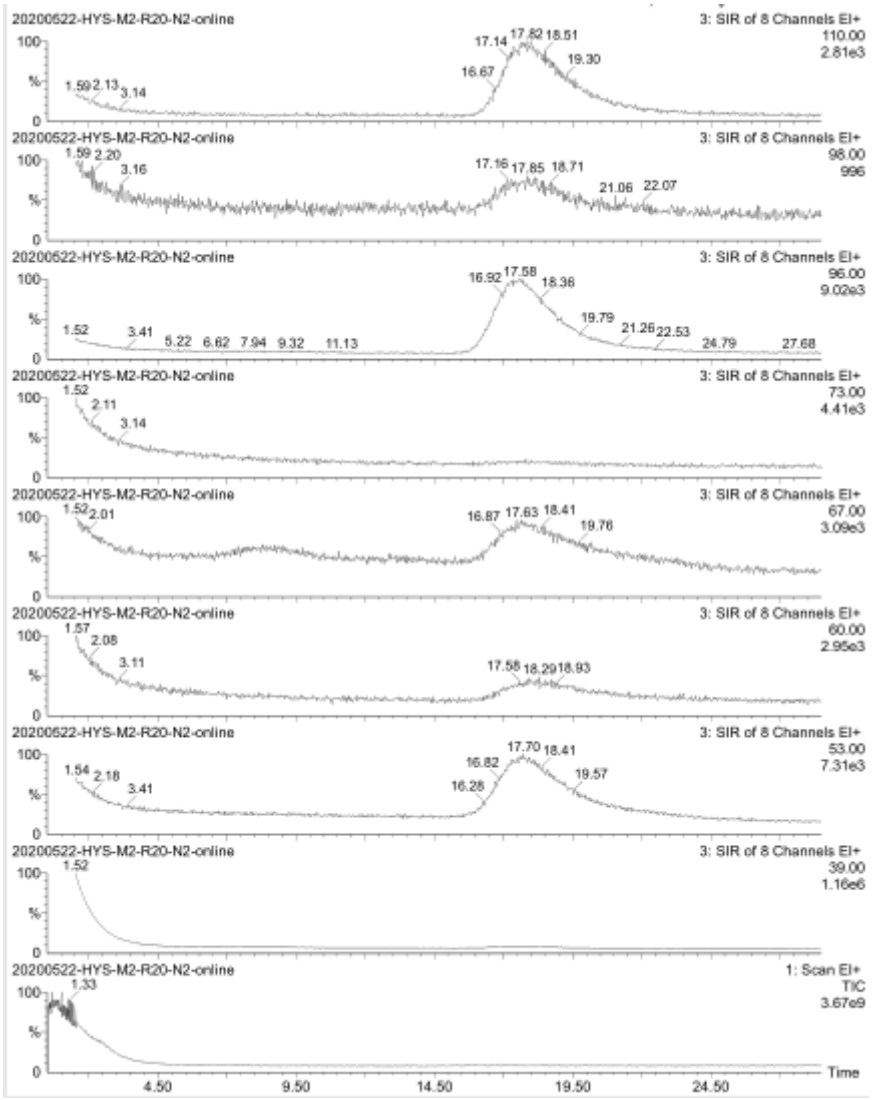
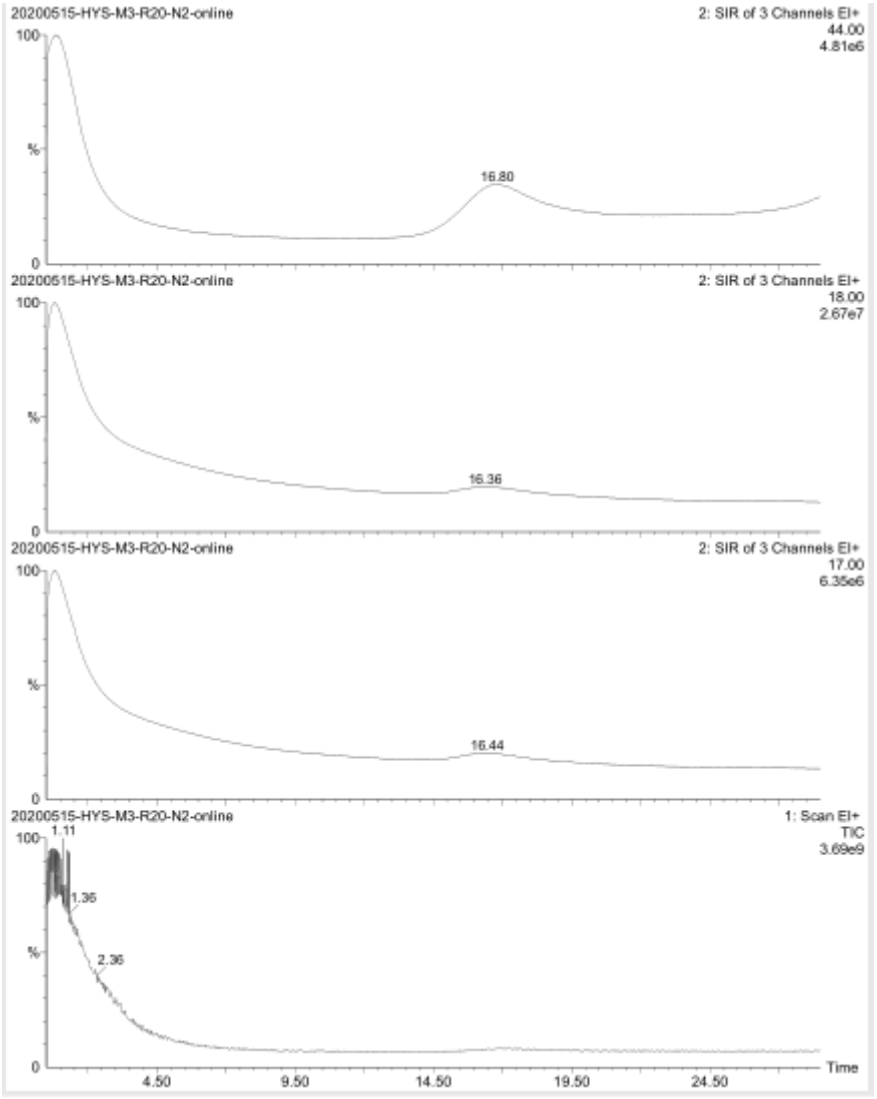


Fig D-5. TGA-MS result of M2


20200515-HYS-M3-R20-N2-online
2: SIR of 3 Channels EI+
44.00
4.81e6
16.80
20200515-HYS-M3-R20-N2-online
2: SIR of 3 Channels EI+
18.00
2.67e7
16.36
20200515-HYS-M3-R20-N2-online
2: SIR of 3 Channels EI+
17.00
6.35e6
16.44
20200515-HYS-M3-R20-N2-online
1: Scan EI+
TIC
3.69e9
1.11
1.35
2.36
100
%
0
4.50
9.50
14.50
19.50
24.50
Time

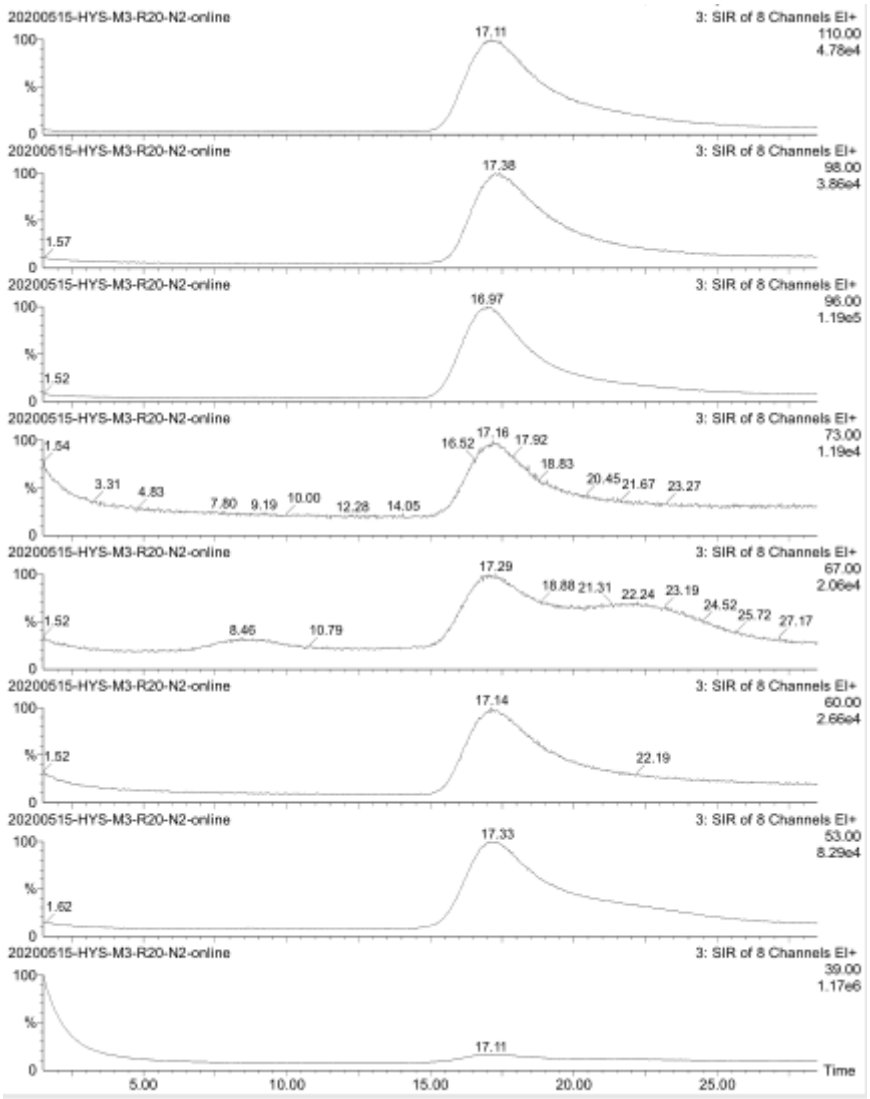
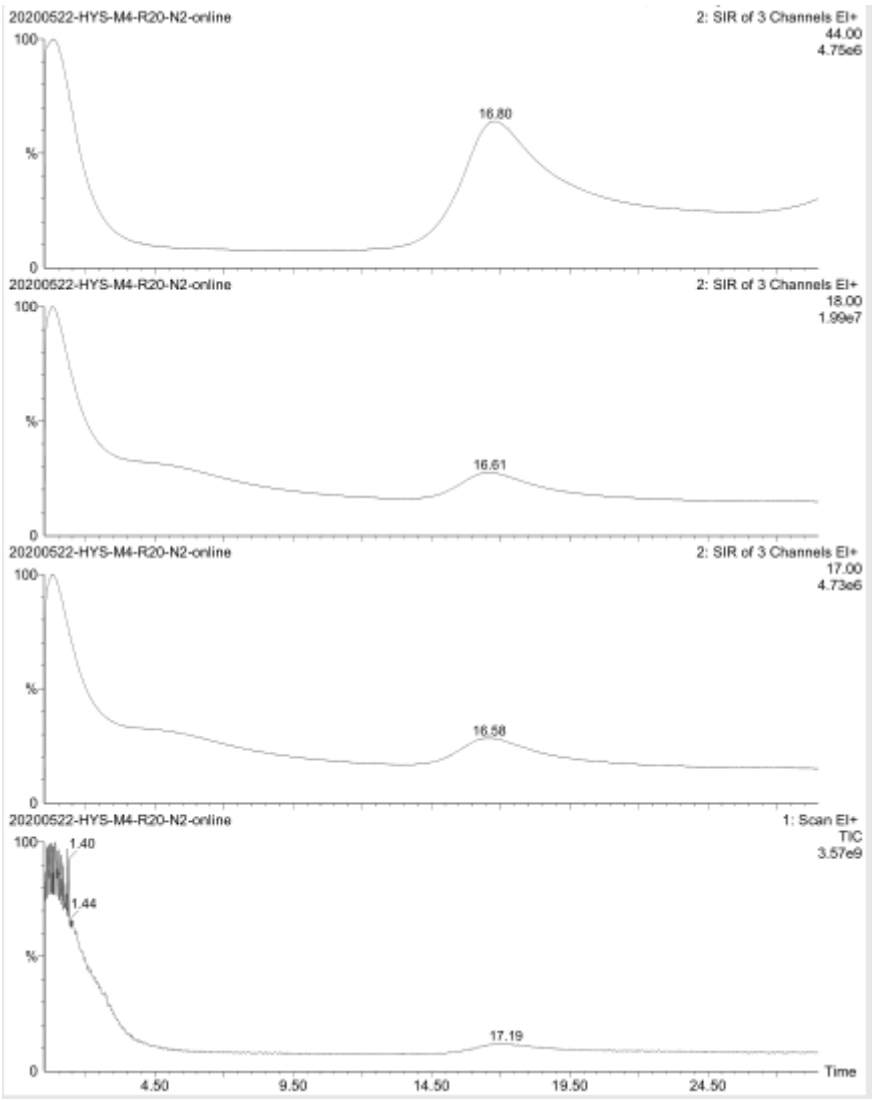


Fig D-6. TGA-MS result of M3


20200522-HYS-M4-R20-N2-online
2: SIR of 3 Channels EI+
44.00
4.75e6
16.80
20200522-HYS-M4-R20-N2-online
2: SIR of 3 Channels EI+
18.00
1.99e7
16.61
20200522-HYS-M4-R20-N2-online
2: SIR of 3 Channels EI+
17.00
4.73e6
16.58
20200522-HYS-M4-R20-N2-online
1: Scan EI+
TIC
3.57e9
1.40
1.44
17.19
100
%
0
4.50
9.50
14.50
19.50
24.50
Time

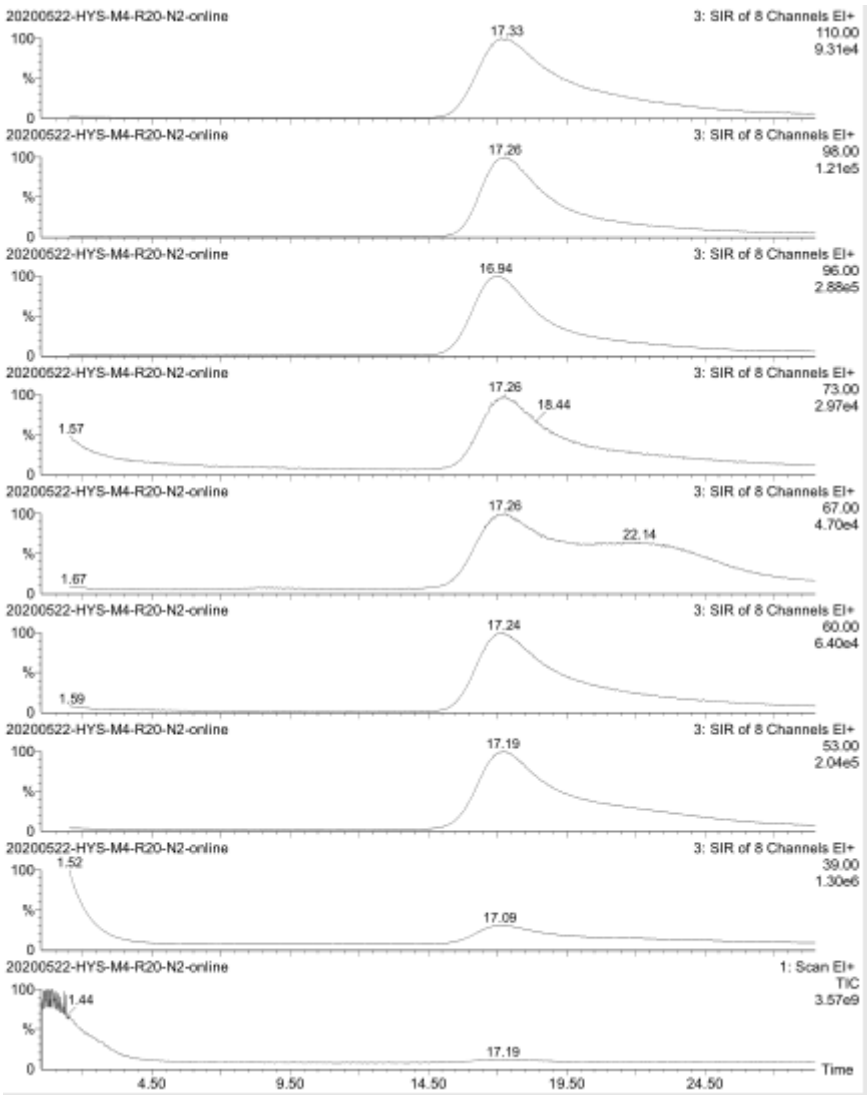
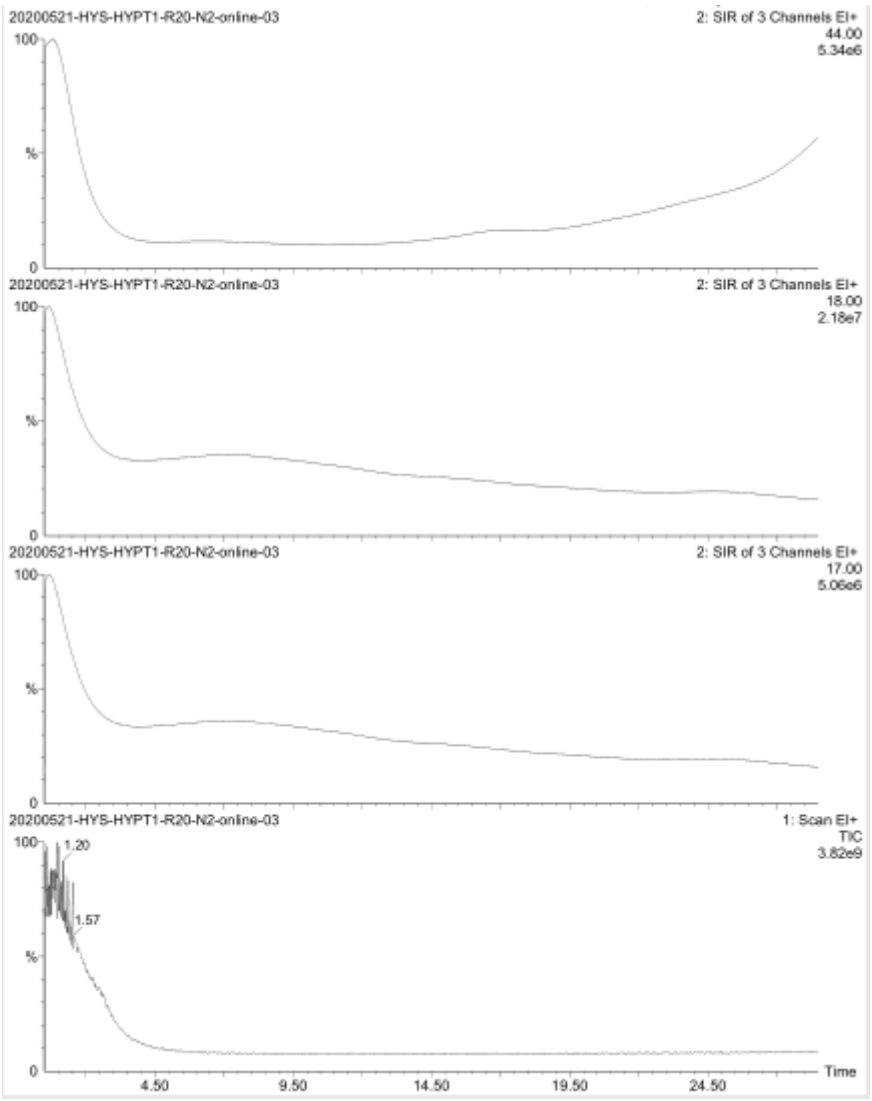


Fig D-7. TGA-MS result of M4


20200521-HYS-HYPT1-R20-N2-online-03
2: SIR of 3 Channels EI+
44.00
5.34e6
100
%
0
20200521-HYS-HYPT1-R20-N2-online-03
2: SIR of 3 Channels EI+
18.00
2.18e7
100
%
0
20200521-HYS-HYPT1-R20-N2-online-03
2: SIR of 3 Channels EI+
17.00
5.06e6
100
%
0
20200521-HYS-HYPT1-R20-N2-online-03
1: Scan EI+
TIC
3.82e9
100
1.20
1.57
%
0
4.50
9.50
14.50
19.50
24.50
Time

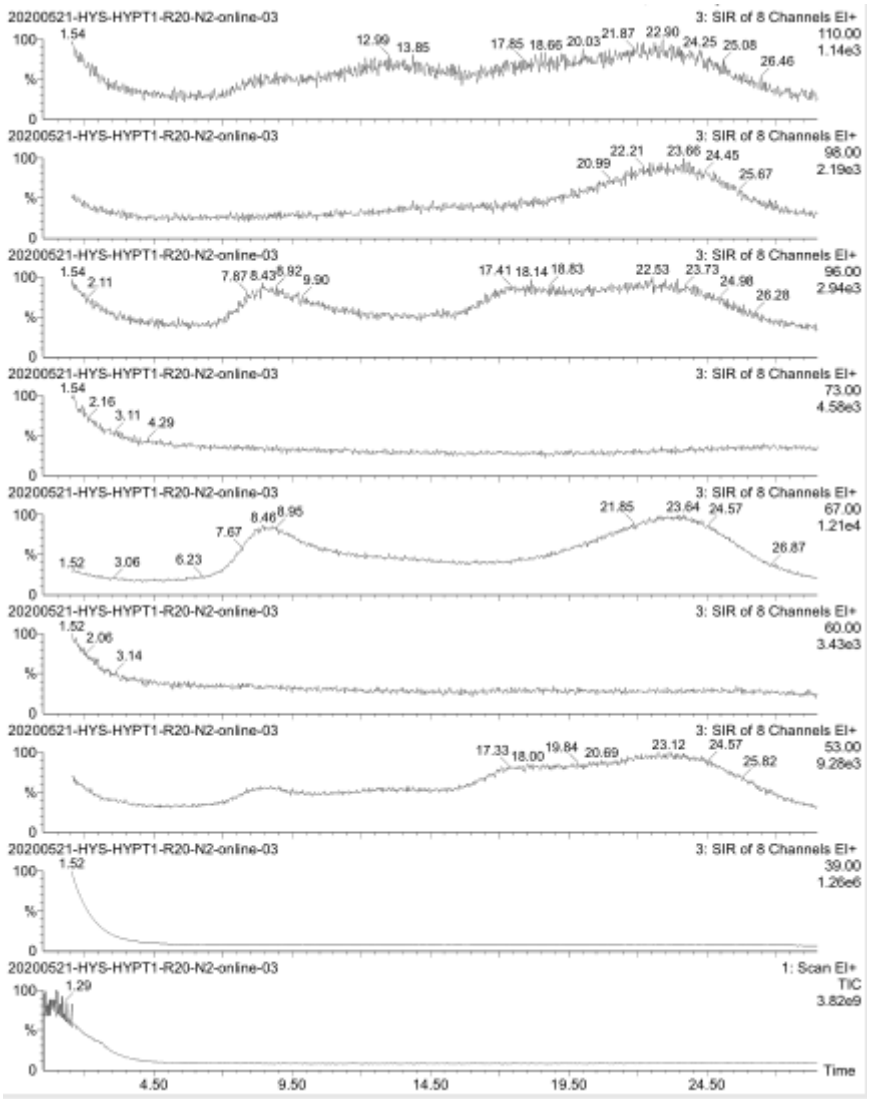
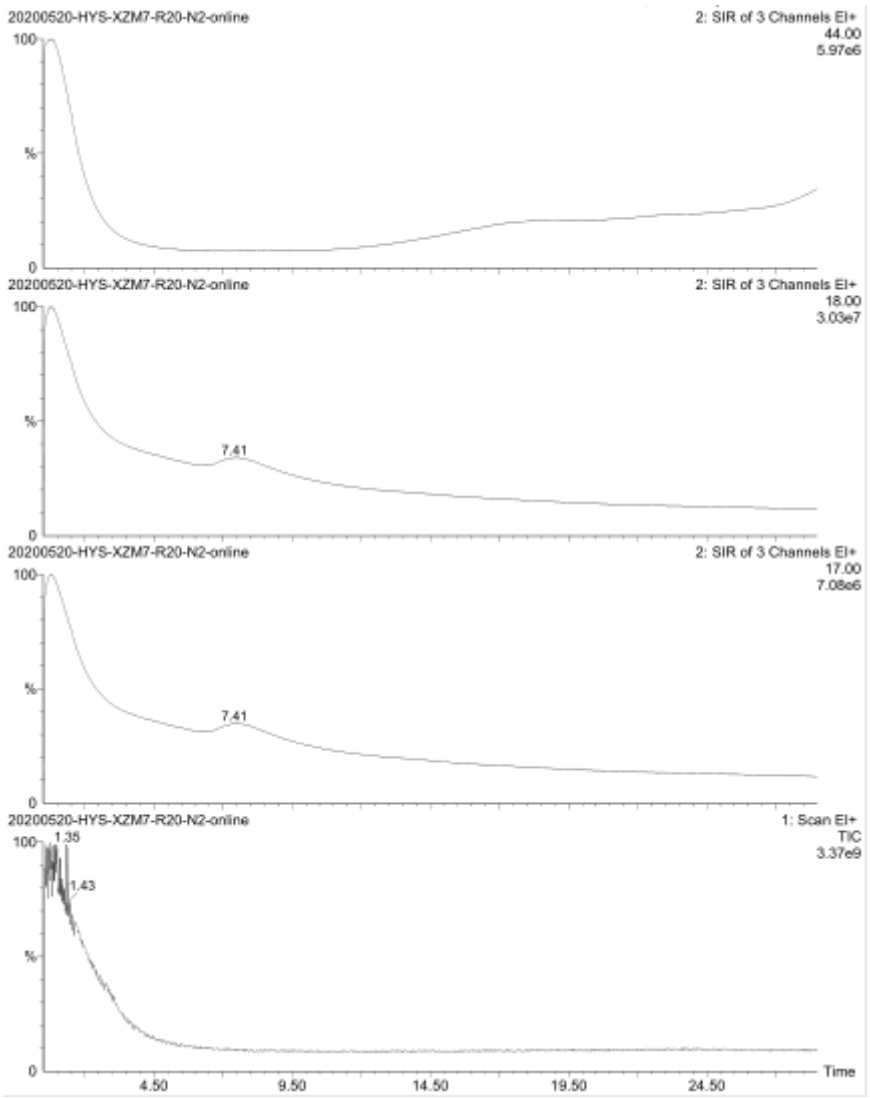


Fig D-8. TGA-MS result of HYPT1


20200520-HYS-XZM7-R20-N2-online
2: SIR of 3 Channels EI+
44.00
5.97e6
100
%
0
20200520-HYS-XZM7-R20-N2-online
2: SIR of 3 Channels EI+
18.00
3.03e7
7.41
20200520-HYS-XZM7-R20-N2-online
2: SIR of 3 Channels EI+
17.00
7.08e6
7.41
20200520-HYS-XZM7-R20-N2-online
1: Scan EI+
TIC
3.37e9
1.35
1.43
4.50
9.50
14.50
19.50
24.50
Time

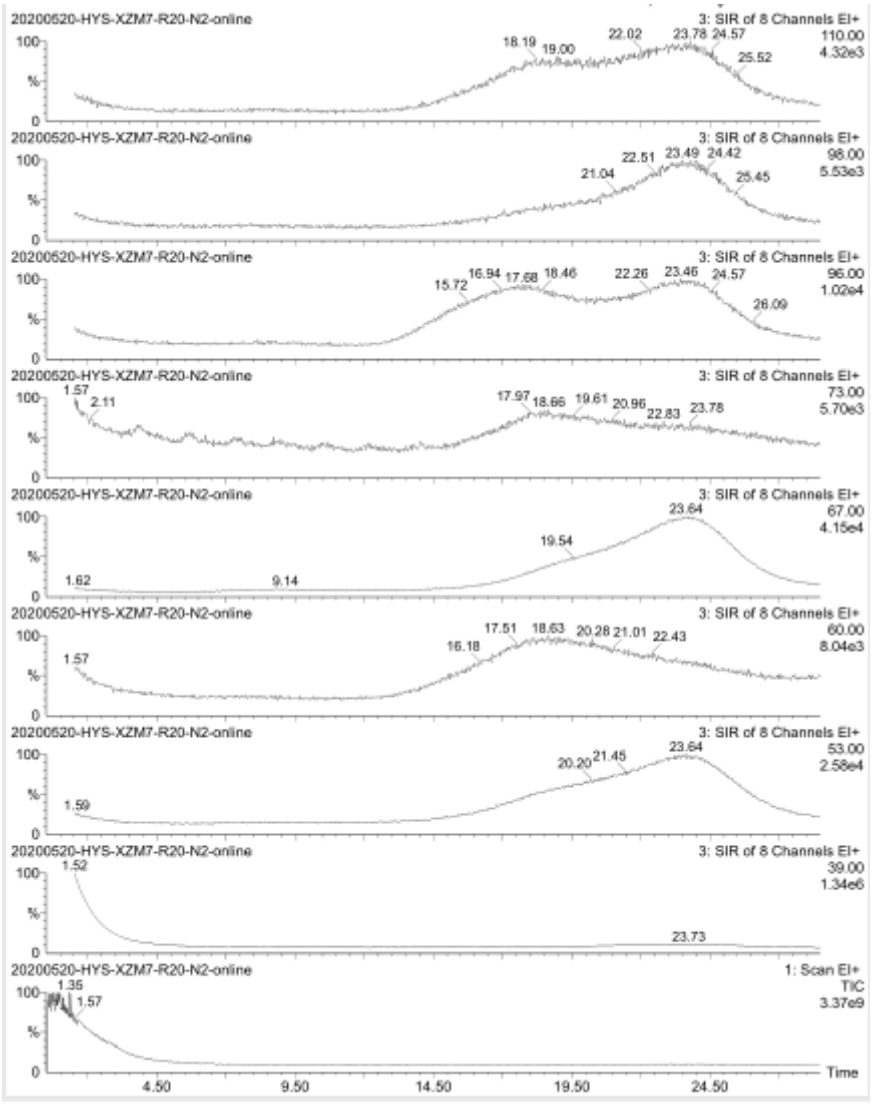
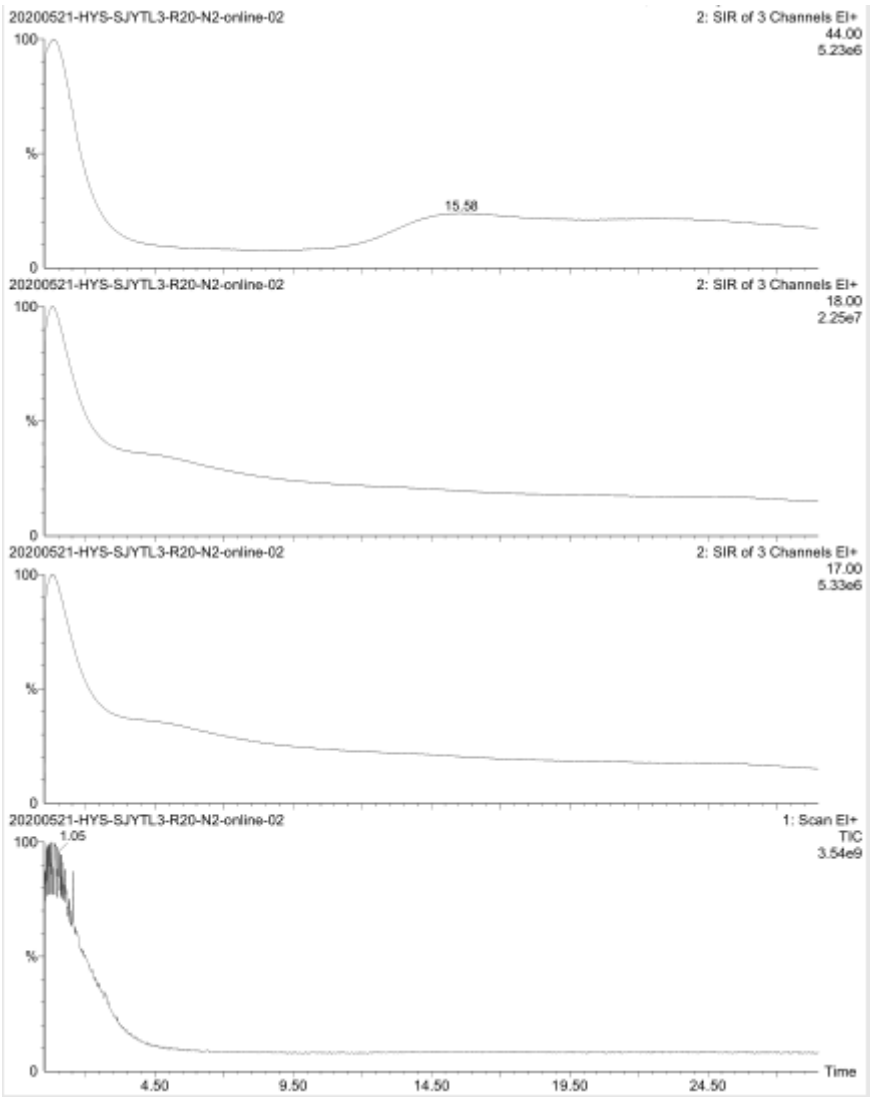


Fig D-9. TGA-MS result of XZM7


20200521-HYS-SJYTL3-R20-N2-online-02
2: SIR of 3 Channels EI+
44.00
5.23e6
100
%
0
15.58
20200521-HYS-SJYTL3-R20-N2-online-02
2: SIR of 3 Channels EI+
18.00
2.25e7
100
%
0
20200521-HYS-SJYTL3-R20-N2-online-02
2: SIR of 3 Channels EI+
17.00
5.33e6
100
%
0
20200521-HYS-SJYTL3-R20-N2-online-02
1: Scan EI+
TIC
3.54e9
100
1.05
%
0
4.50
9.50
14.50
19.50
24.50
Time

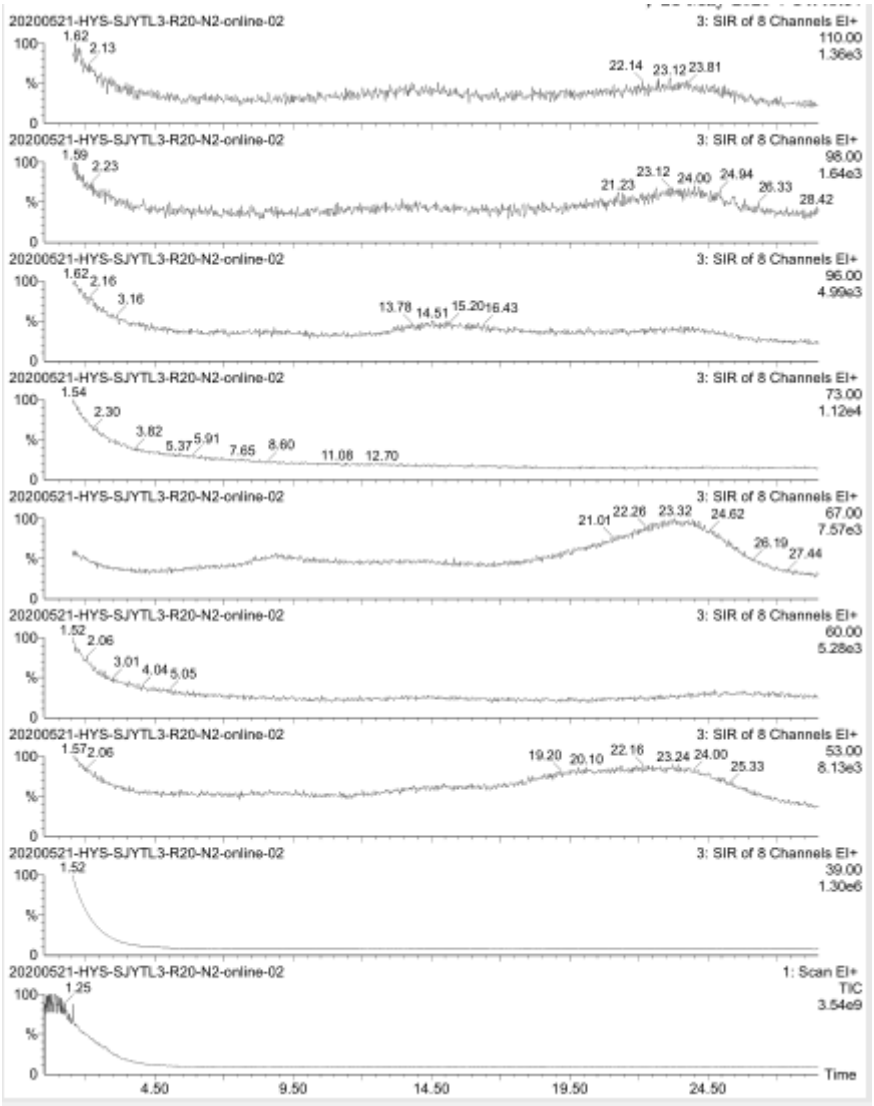


Fig D-10. TGA-MS result of SJYTL3

Appendix 5. MALDI-TOF-MS results

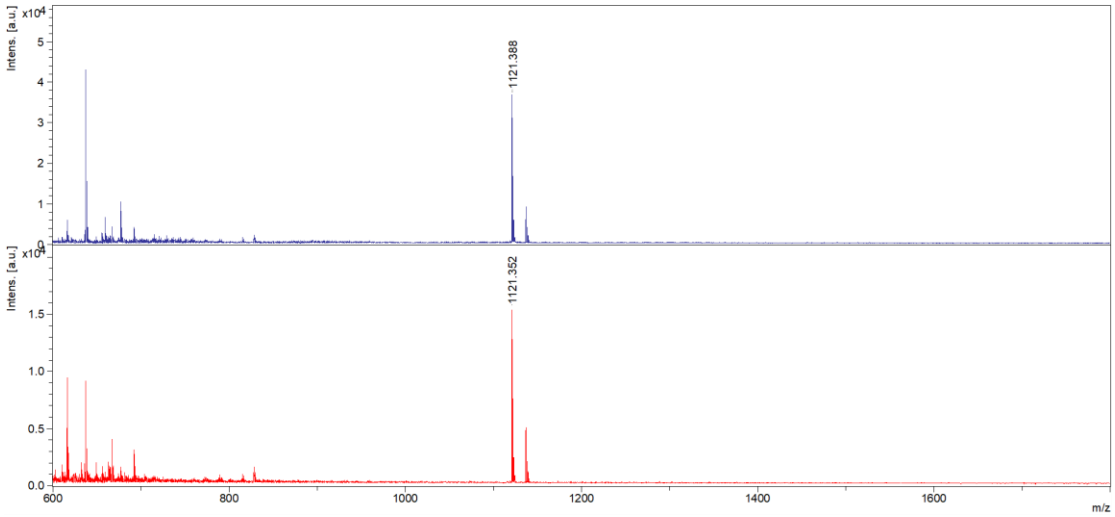


Fig E-1. The MALDI-TOF-MS result of loess (the blue line is the result without enzyme hydrolysis and the red line is after enzyme hydrolysis)

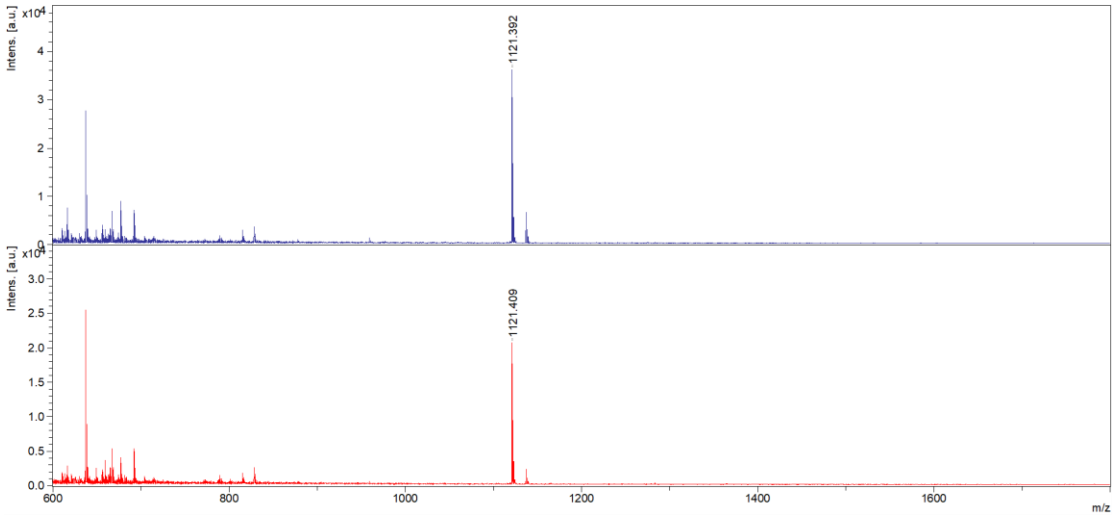


Fig E-2. The MALDI-TOF-MS result of baked loess (the blue line is the result without enzyme hydrolysis and the red line is after enzyme hydrolysis)

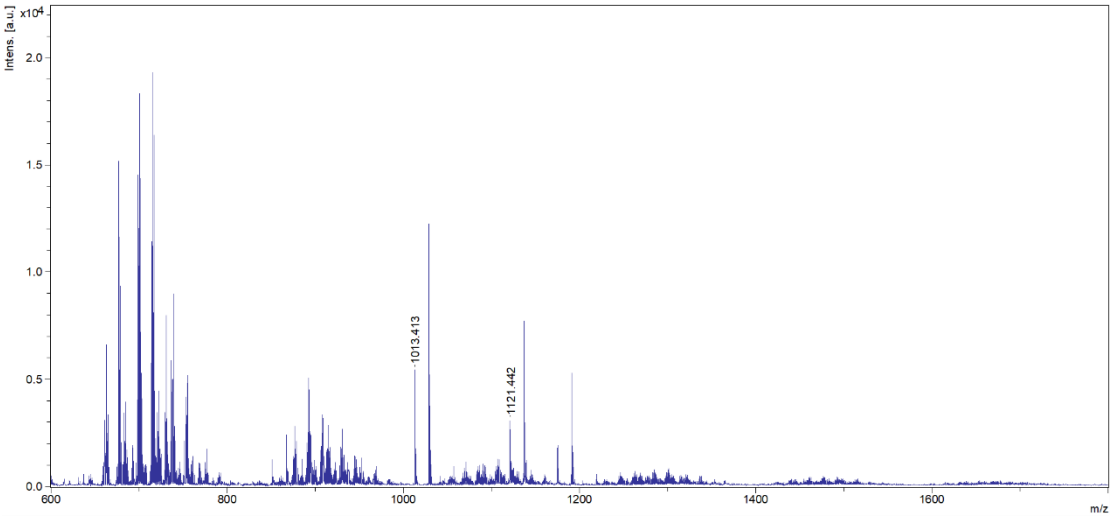


Fig E-3. The MALDI-TOF-MS result of M3

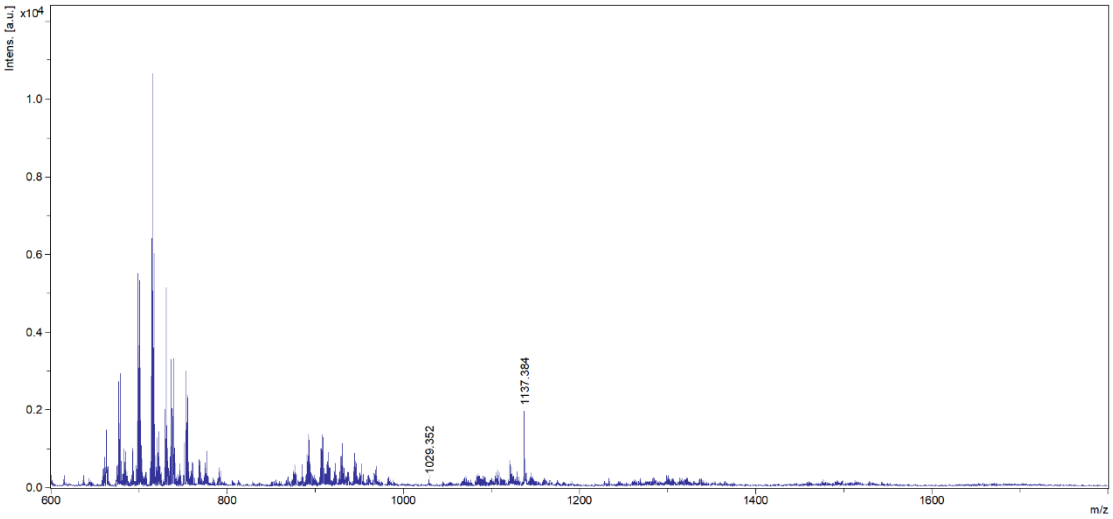


Fig E-4. The MALDI-TOF-MS result of WS1

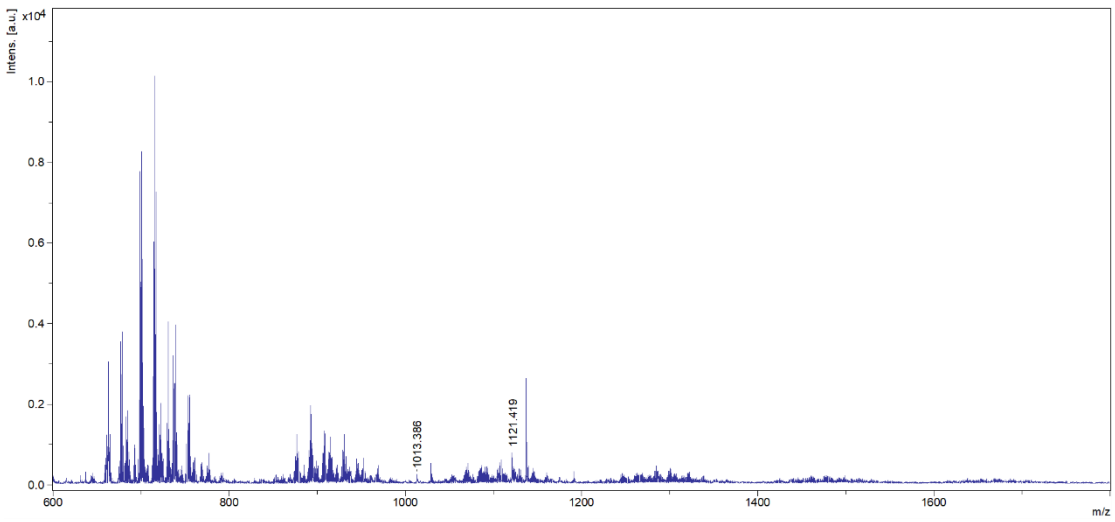


Fig E-5. The MALDI-TOF-MS result of WS2

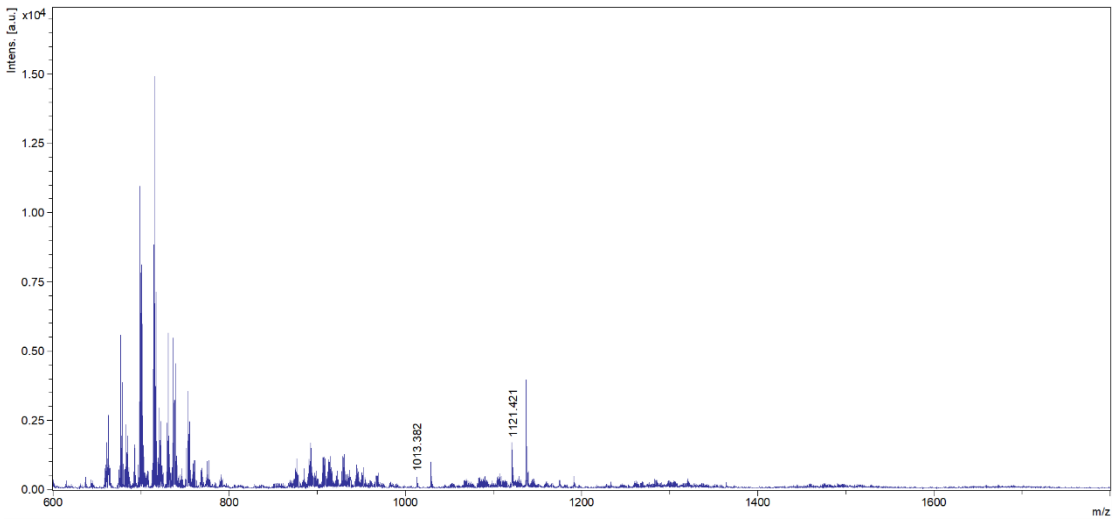


Fig E-6. The MALDI-TOF-MS result of WS3

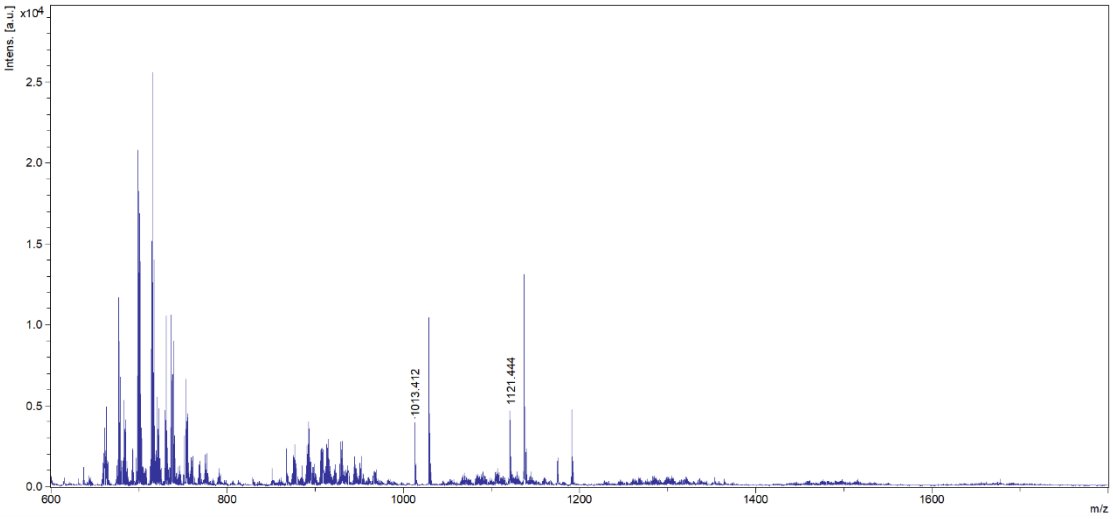


Fig E-7. The MALDI-TOF-MS result of SPS1

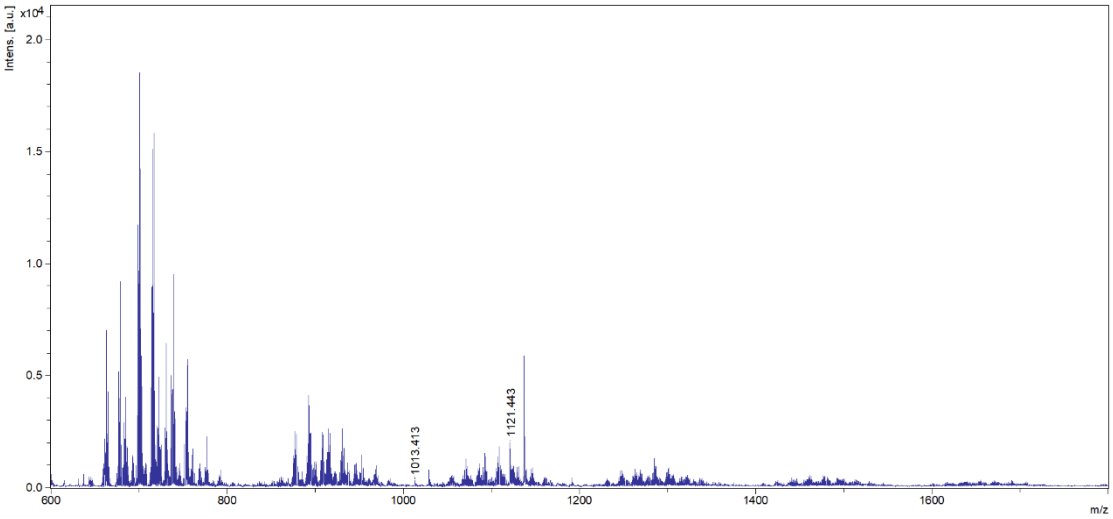


Fig E-8. The MALDI-TOF-MS result of SPS2

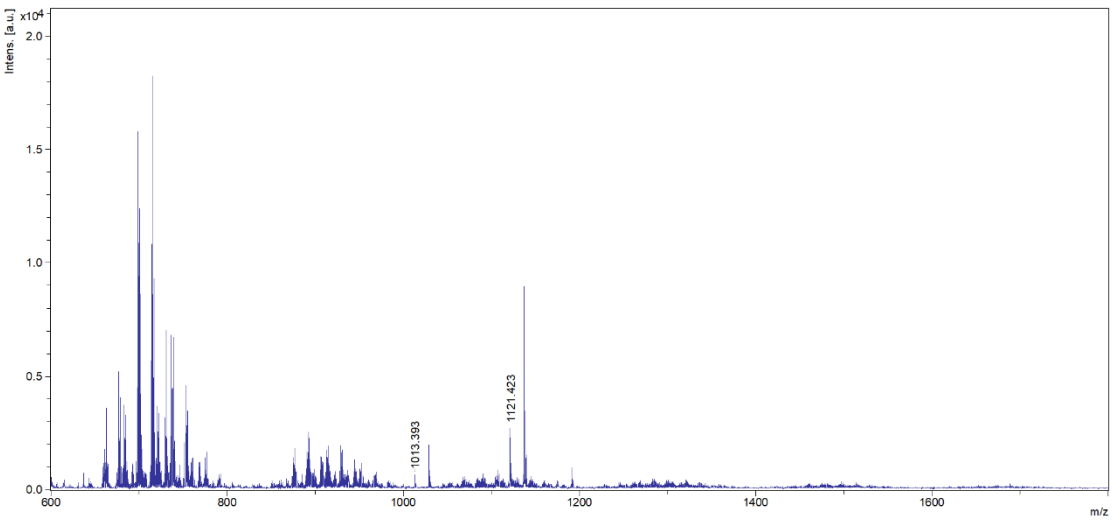


Fig E-9. The MALDI-TOF-MS result of CS1

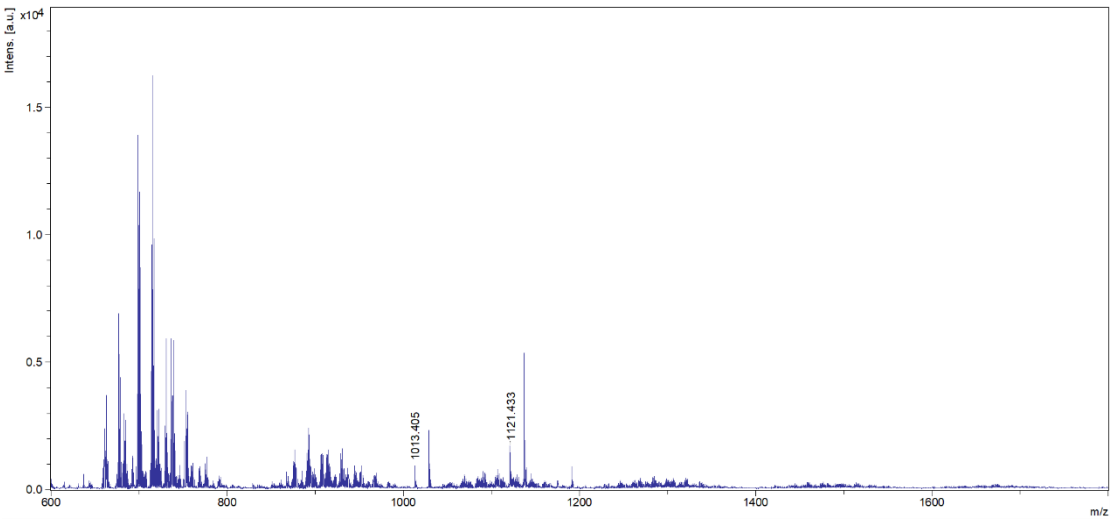


Fig E-10. The MALDI-TOF-MS result of CS2

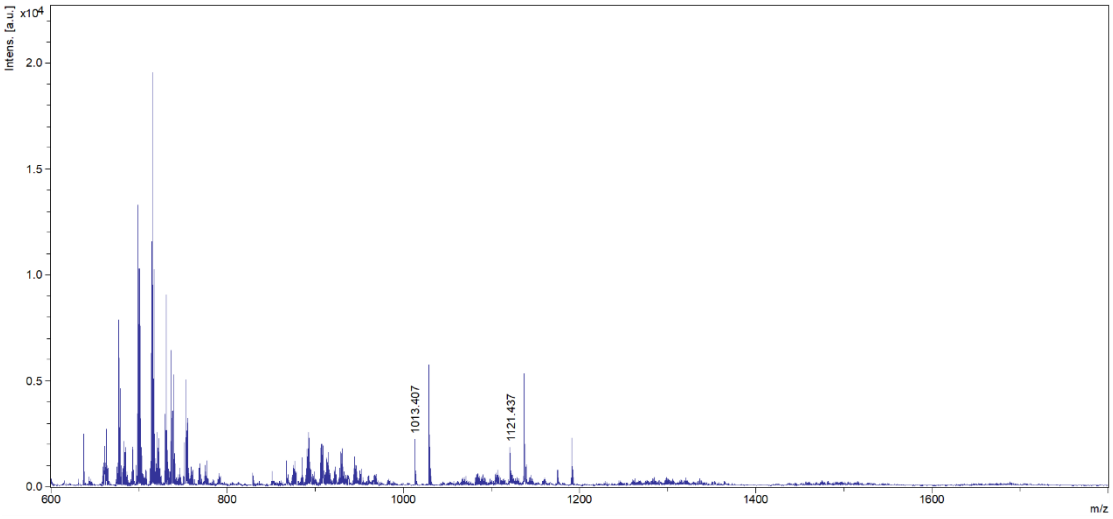


Fig E-11. The MALDI-TOF-MS result of RF1

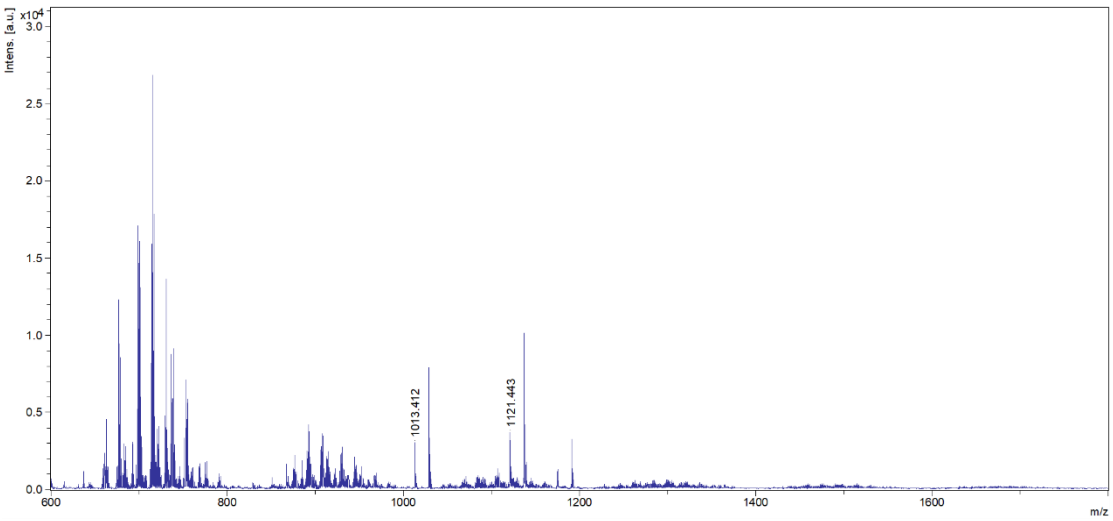


Fig E-12. The MALDI-TOF-MS result of RF2

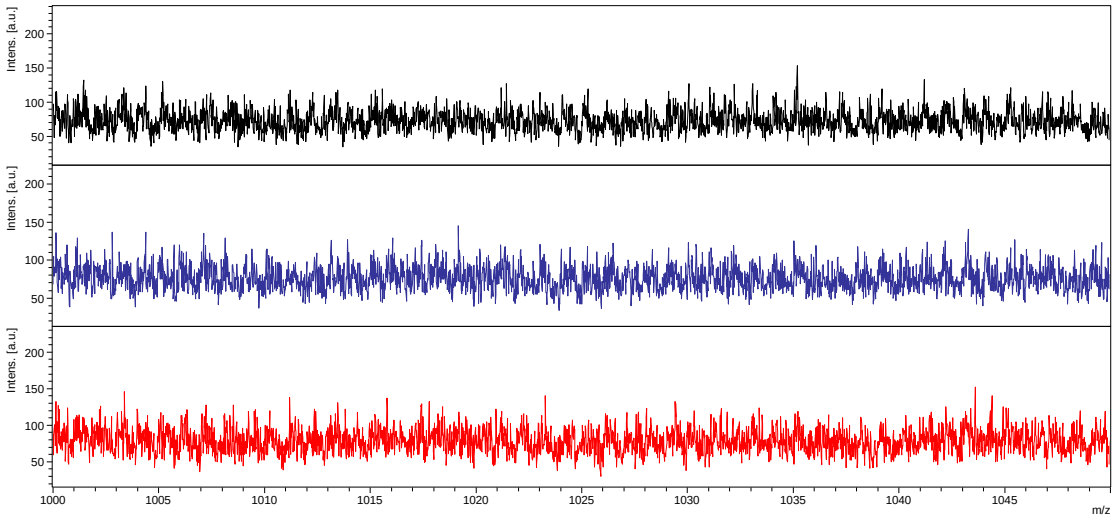


Fig E-13. The MALDI-TOF-MS result of C1

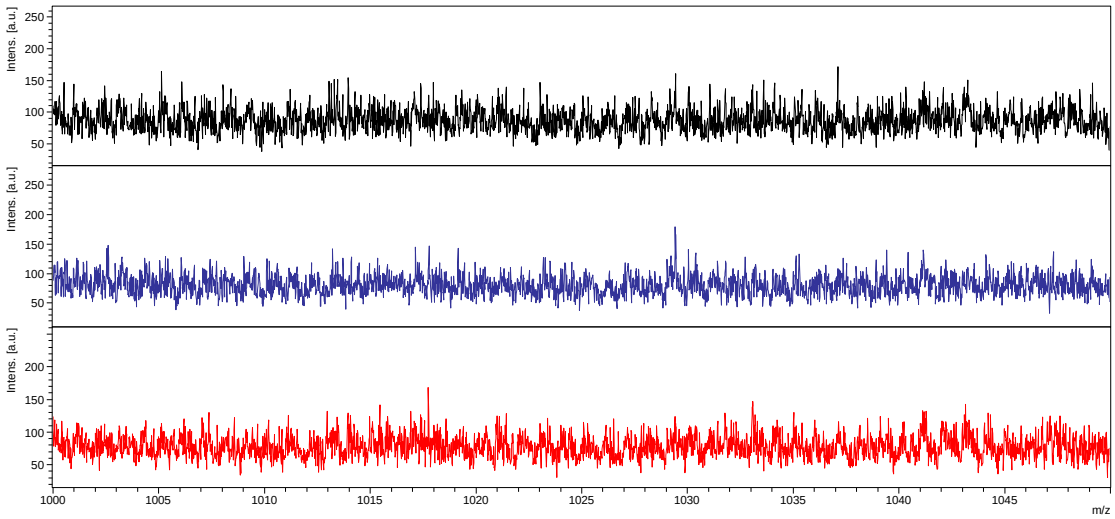


Fig E-14. The MALDI-TOF-MS result of C2

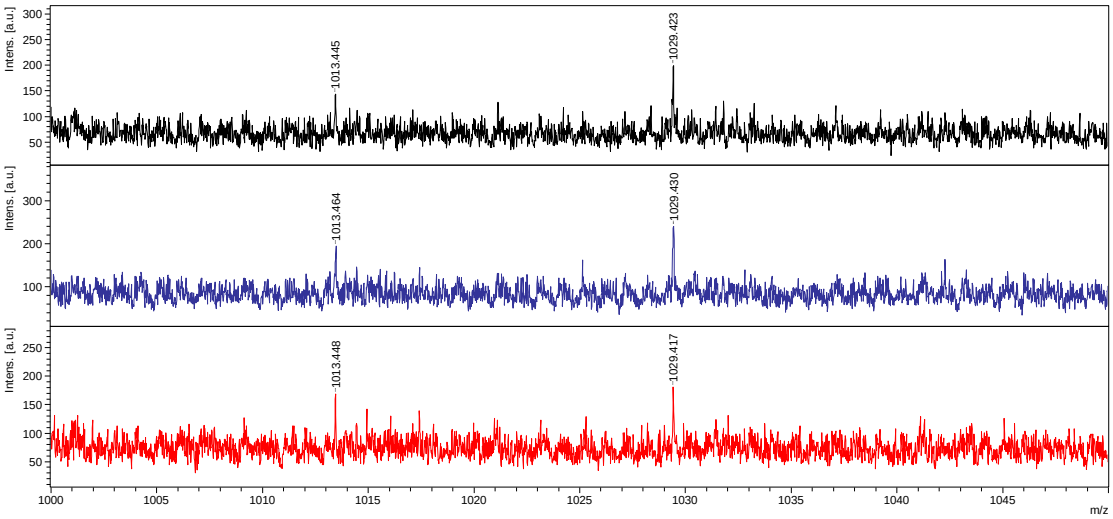


Fig E-15. The MALDI-TOF-MS result of C3

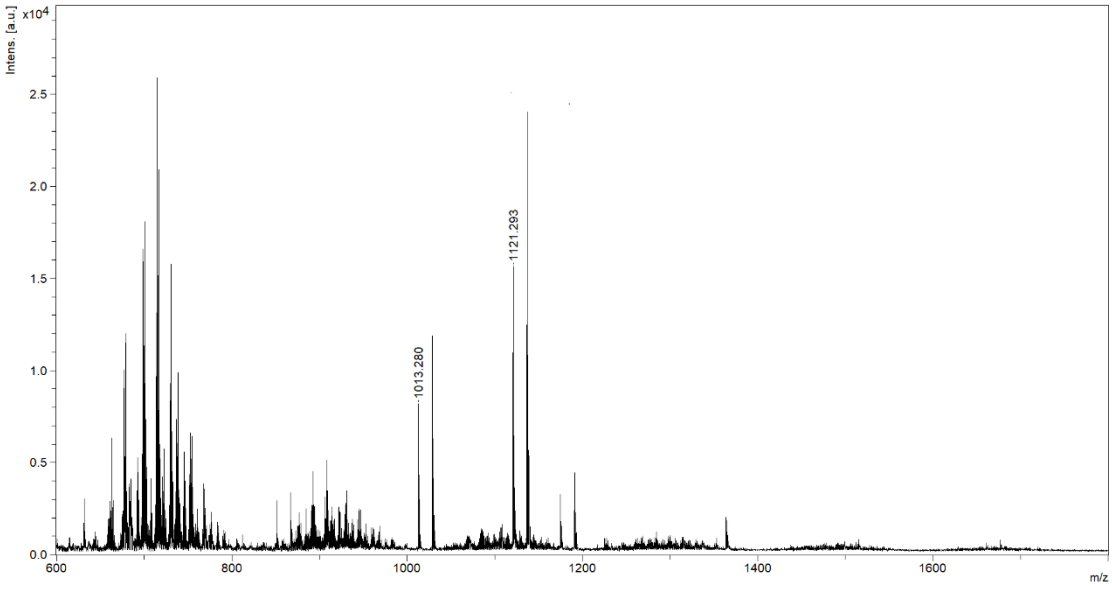


Fig E-16. The MALDI-TOF-MS result of T1

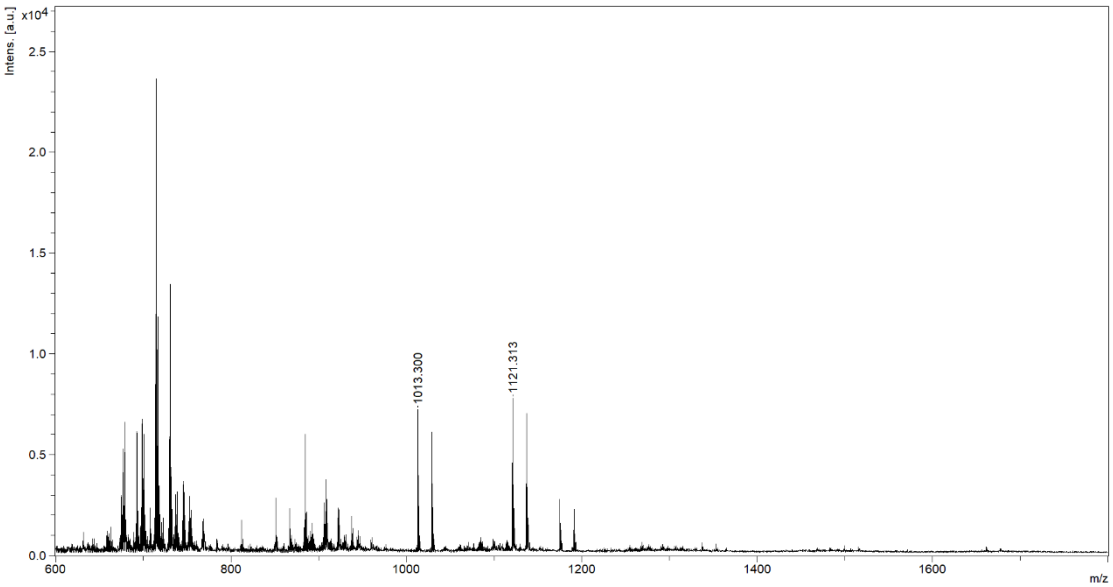


Fig E-17. The MALDI-TOF-MS result of T2

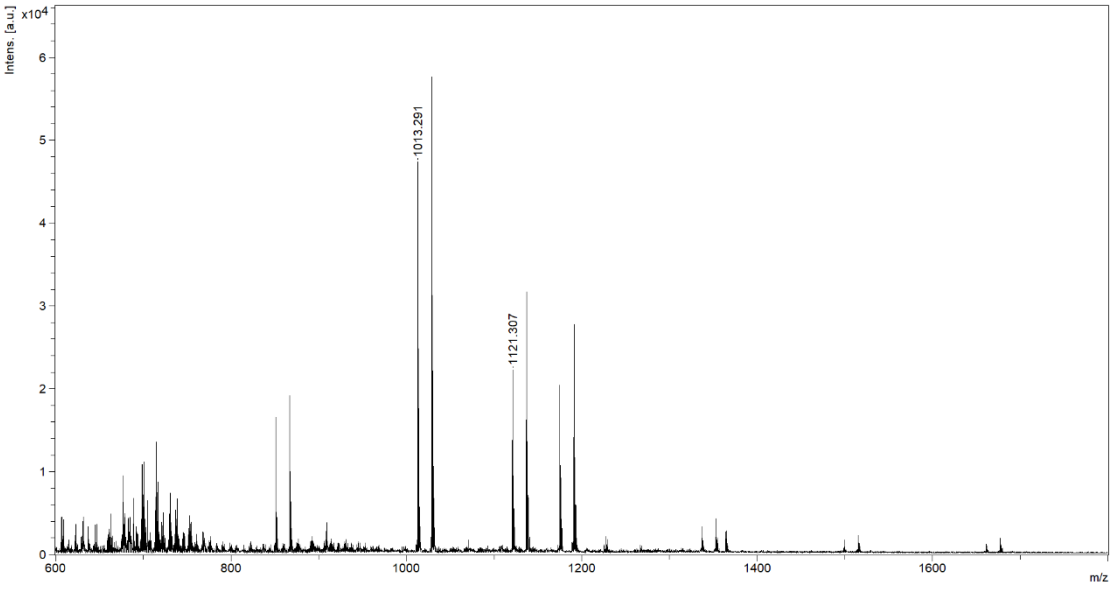


Fig E-18. The MALDI-TOF-MS result of T3

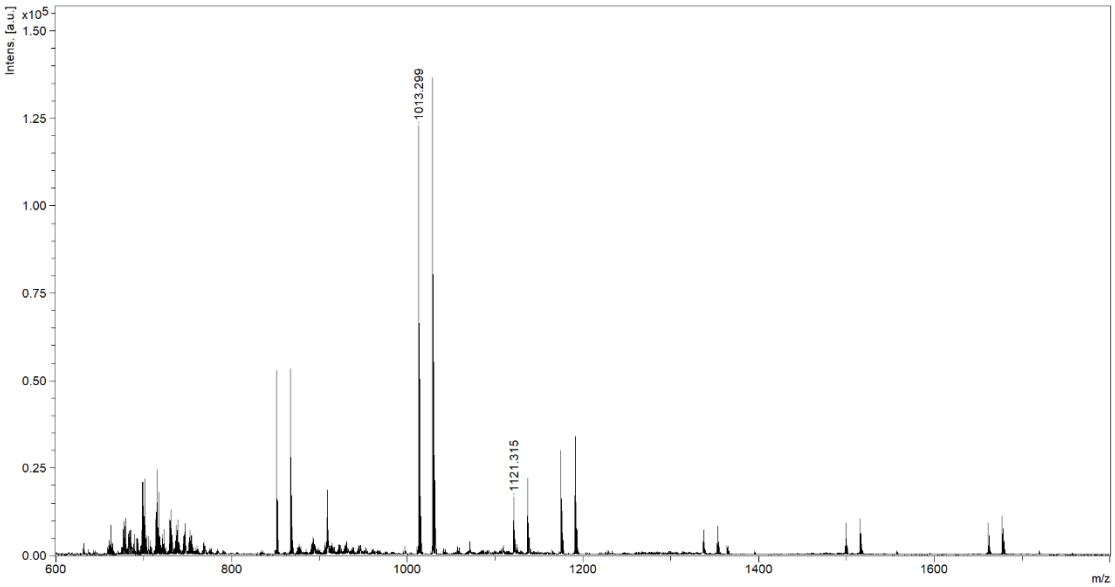


Fig E-19. The MALDI-TOF-MS result of T4

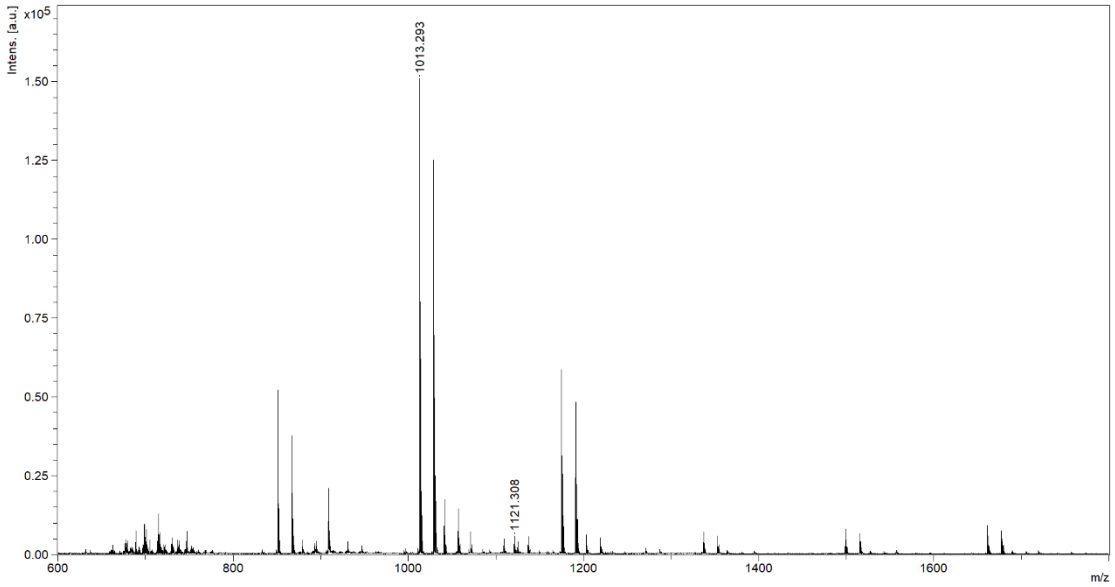


Fig E-20. The MALDI-TOF-MS result of T5

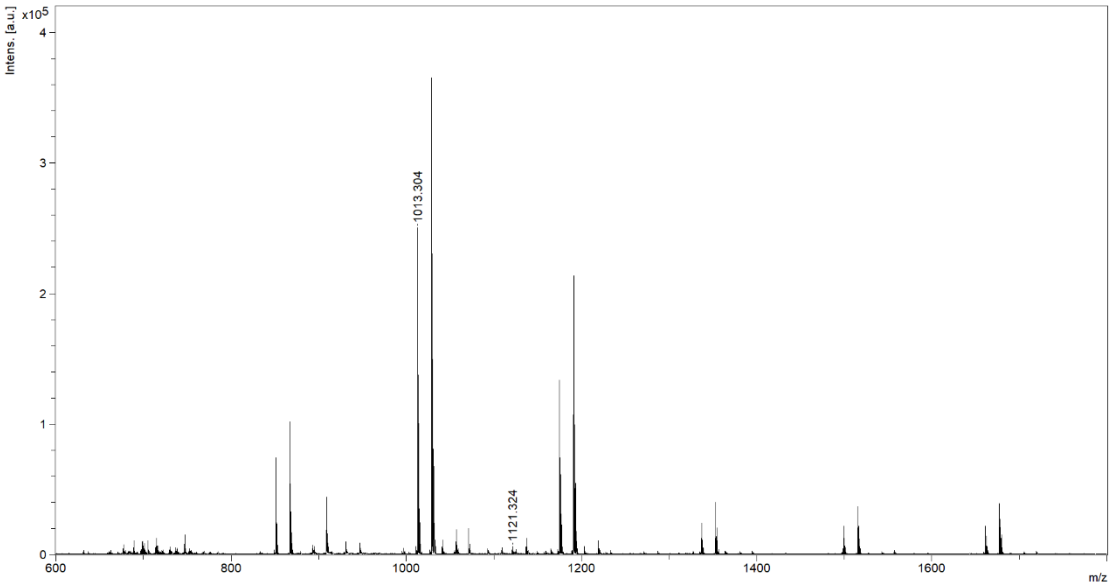


Fig E-21. The MALDI-TOF-MS result of T6

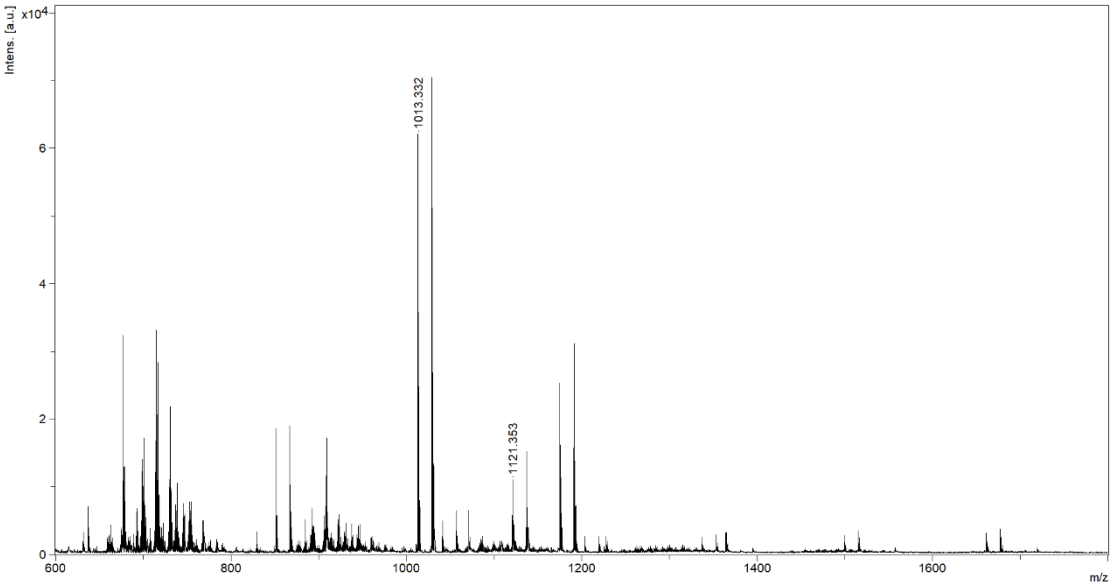


Fig E-22. The MALDI-TOF-MS result of T7

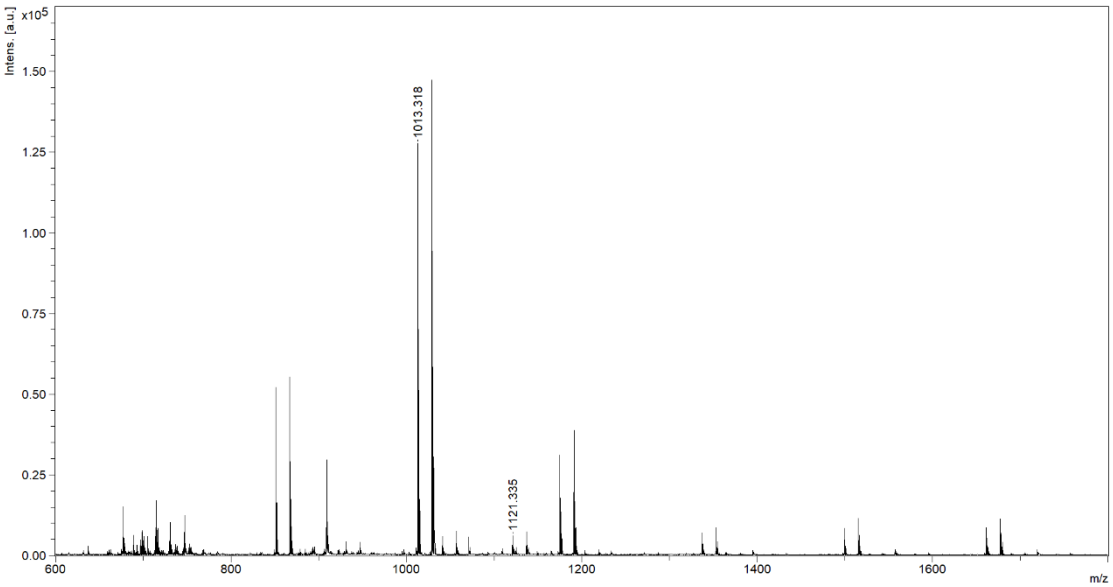


Fig E-23. The MALDI-TOF-MS result of T8

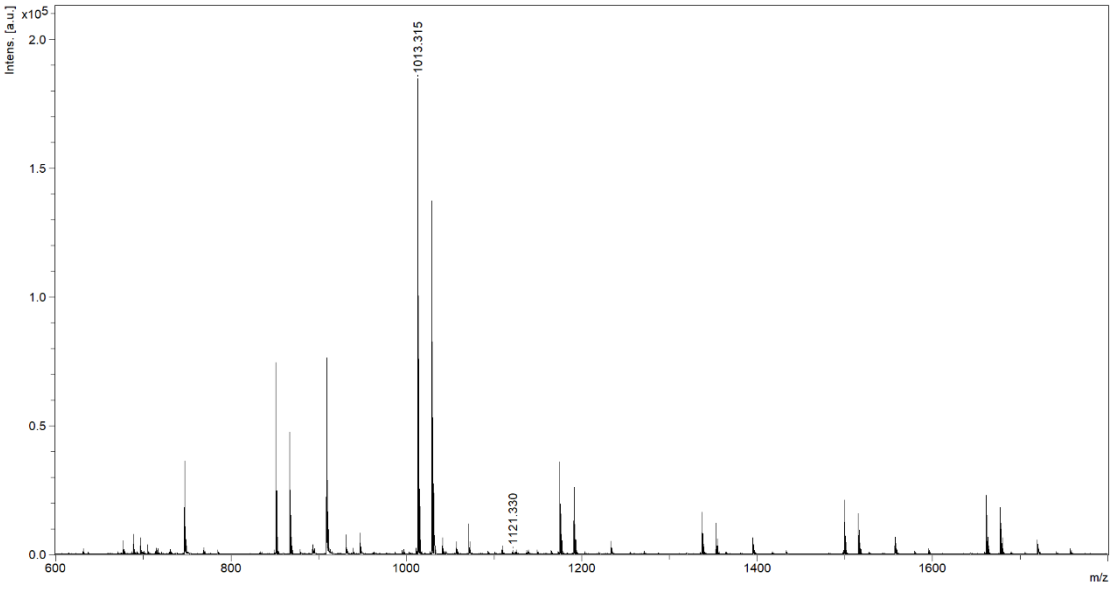


Fig E-24. The MALDI-TOF-MS result of T9

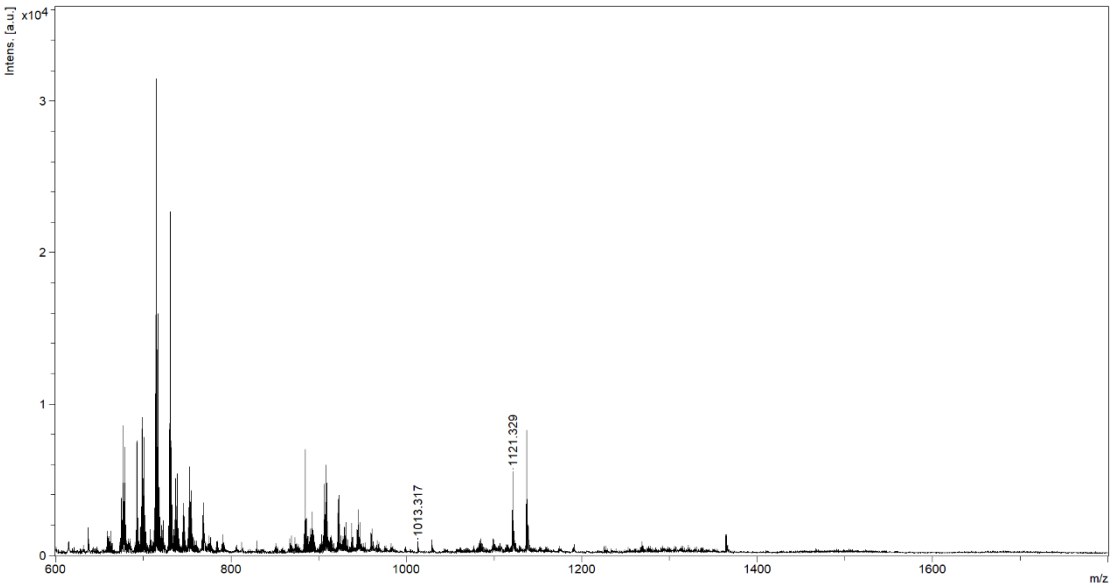


Fig E-25. The MALDI-TOF-MS result of T10

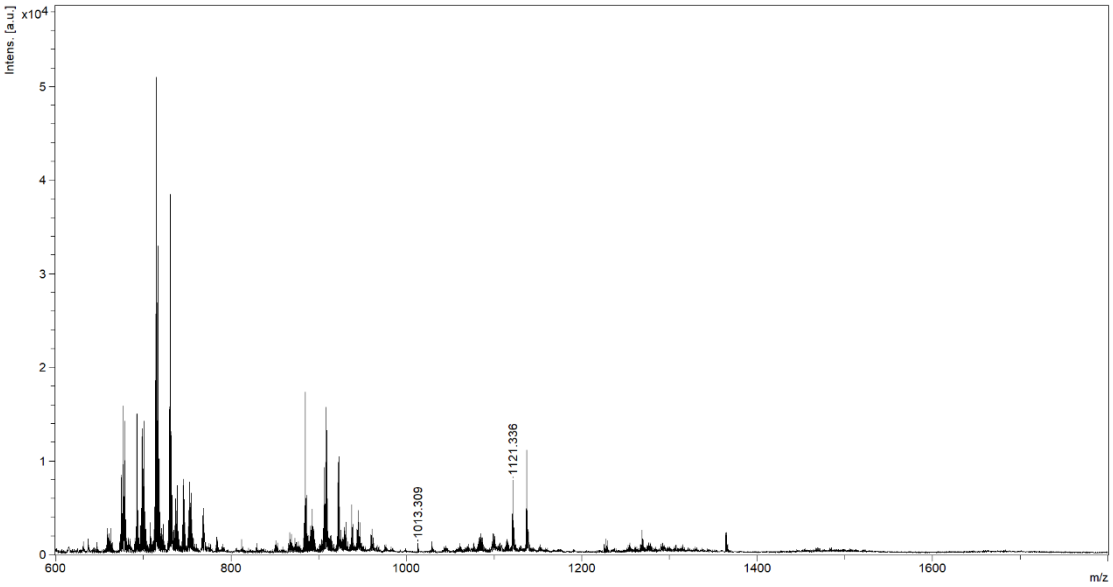


Fig E-26. The MALDI-TOF-MS result of T11

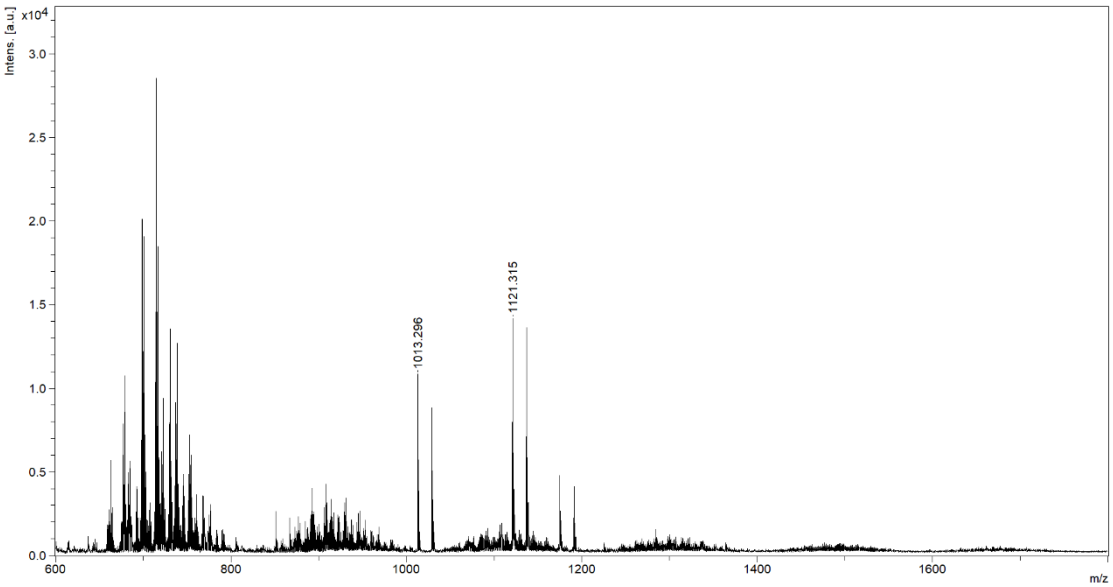


Fig E-27. The MALDI-TOF-MS result of T12

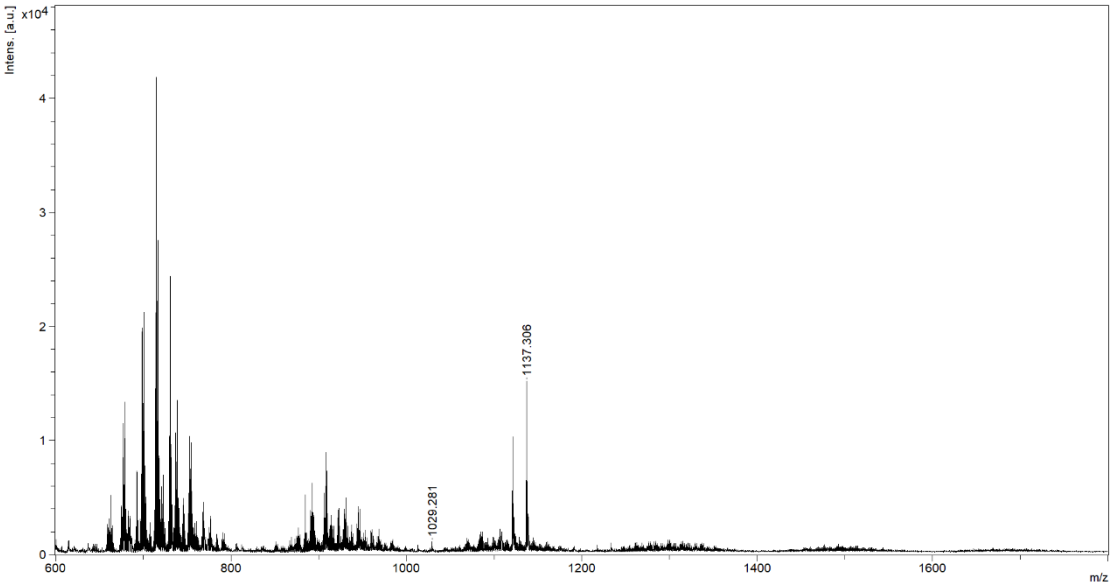


Fig E-28. The MALDI-TOF-MS result of T13

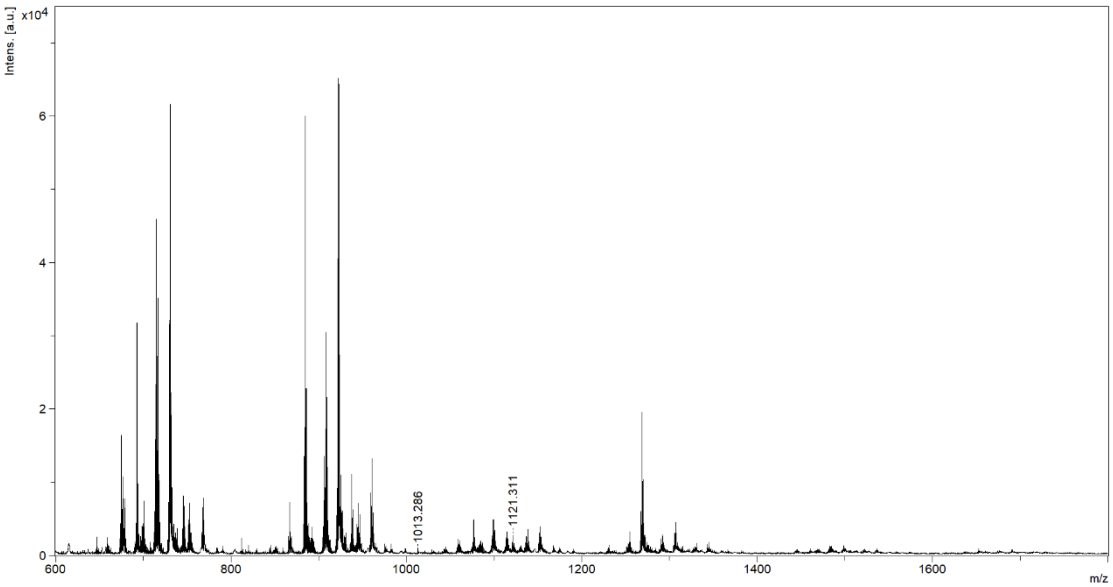


Fig E-29. The MALDI-TOF-MS result of T14

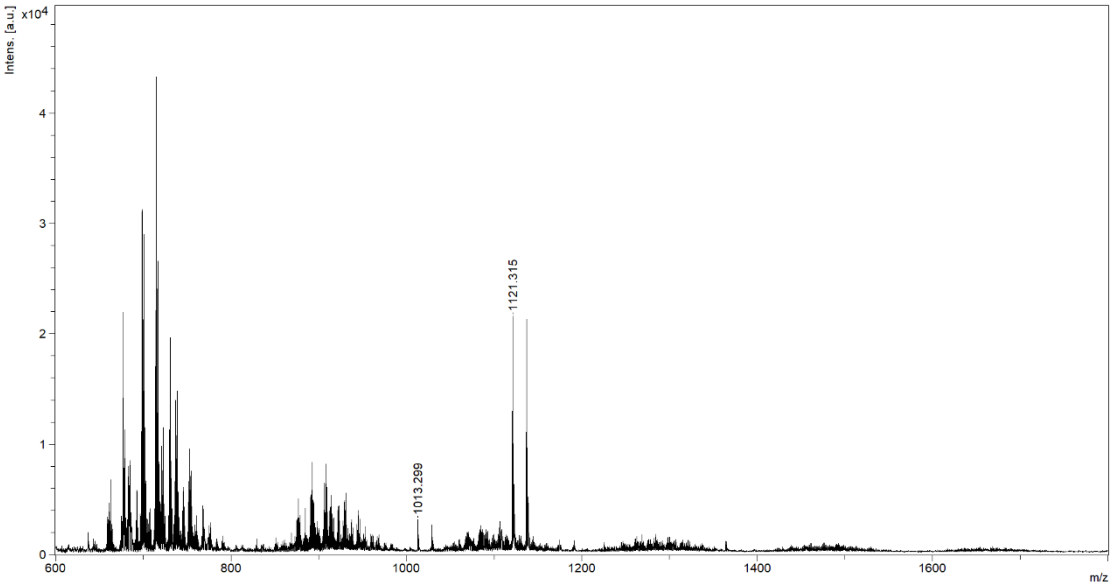


Fig E-30. The MALDI-TOF-MS result of T15

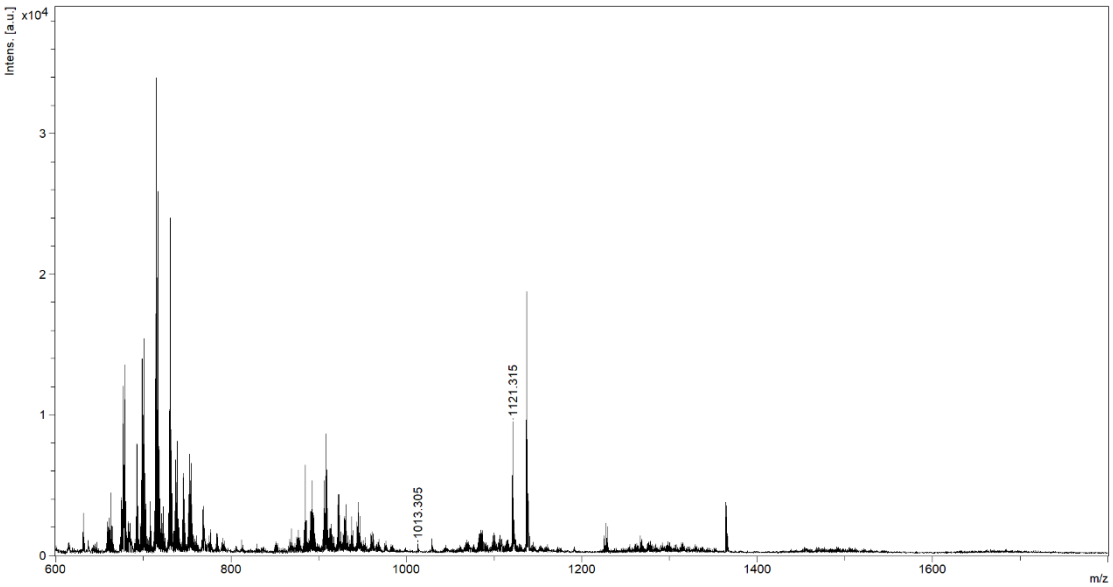


Fig E-31. The MALDI-TOF-MS result of T16

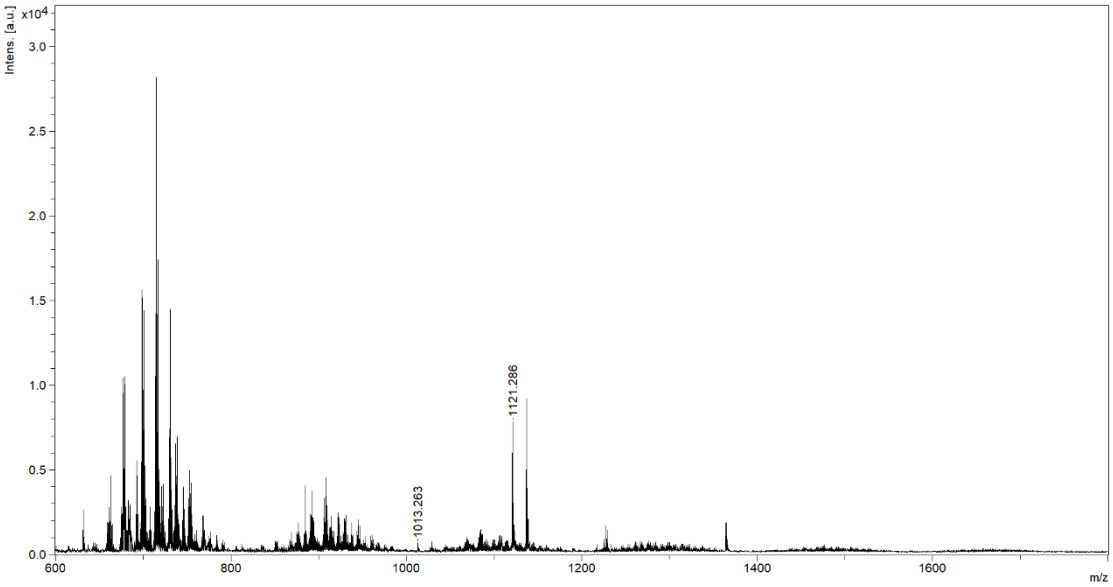


Fig E-32. The MALDI-TOF-MS result of T17

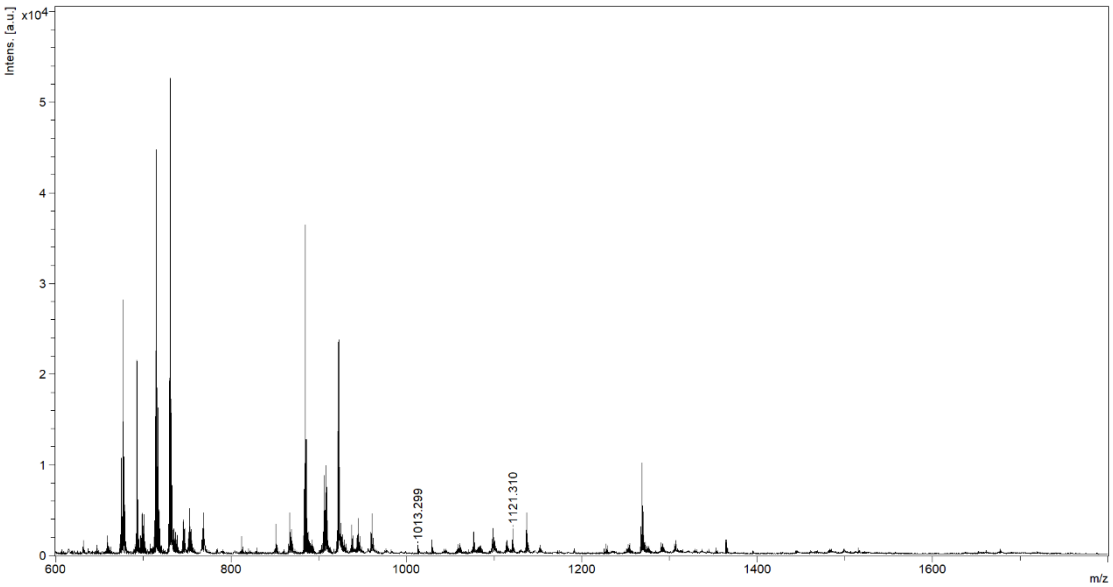


Fig E-33. The MALDI-TOF-MS result of T18

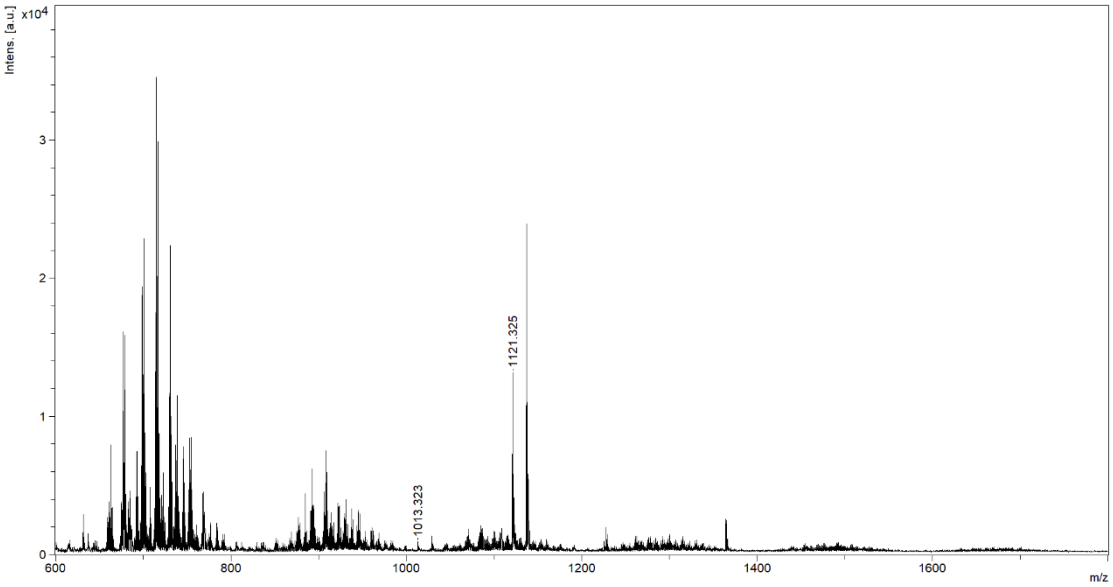


Fig E-34. The MALDI-TOF-MS result of T19

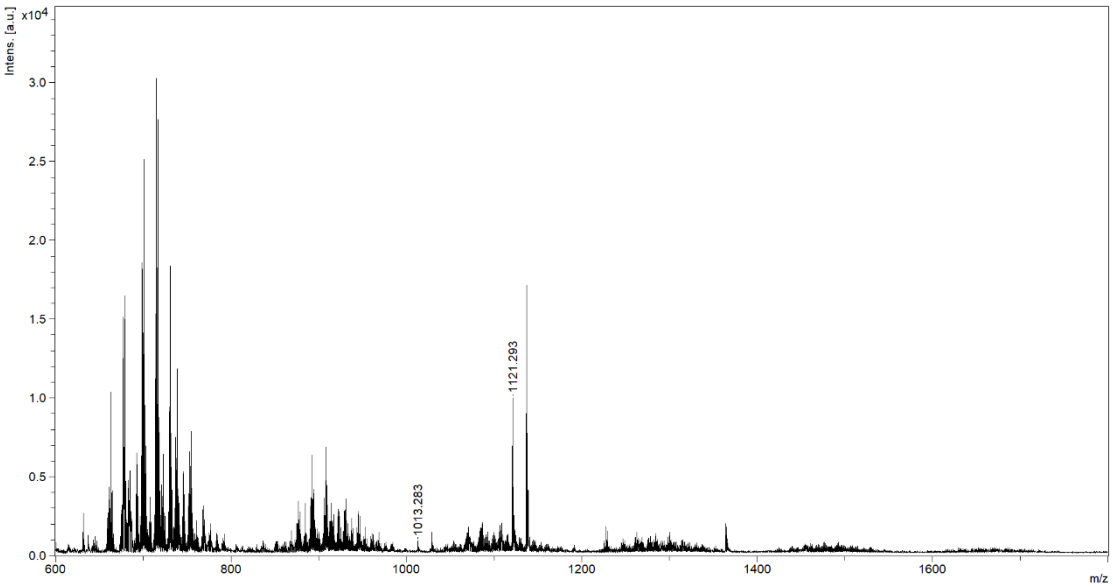


Fig E-35. The MALDI-TOF-MS result of T20

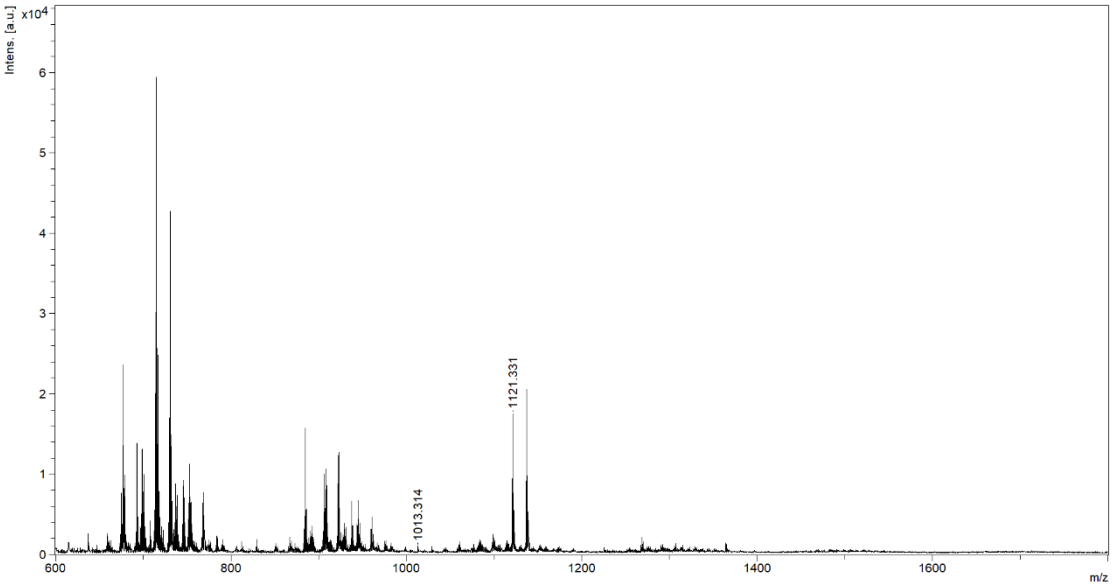


Fig E-36. The MALDI-TOF-MS result of T21

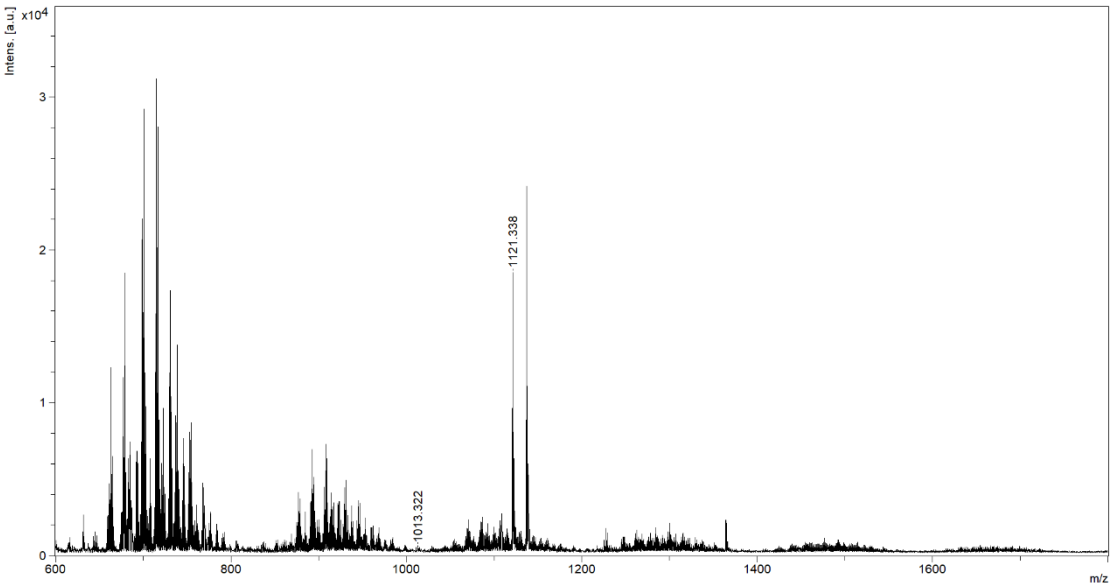


Fig E-37. The MALDI-TOF-MS result of T22

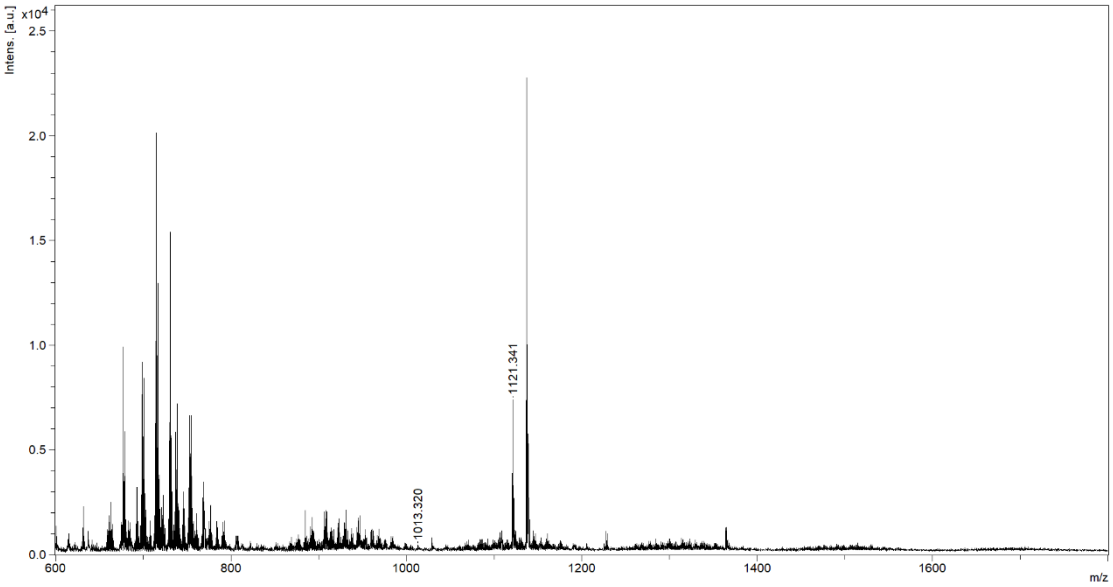


Fig E-38. The MALDI-TOF-MS result of T23

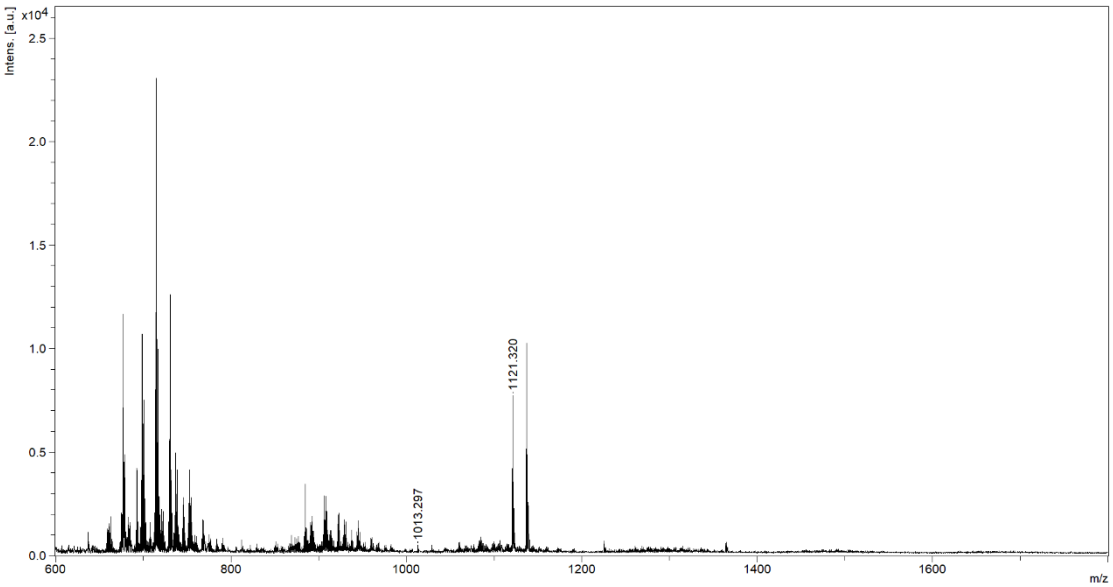


Fig E-39. The MALDI-TOF-MS result of T24

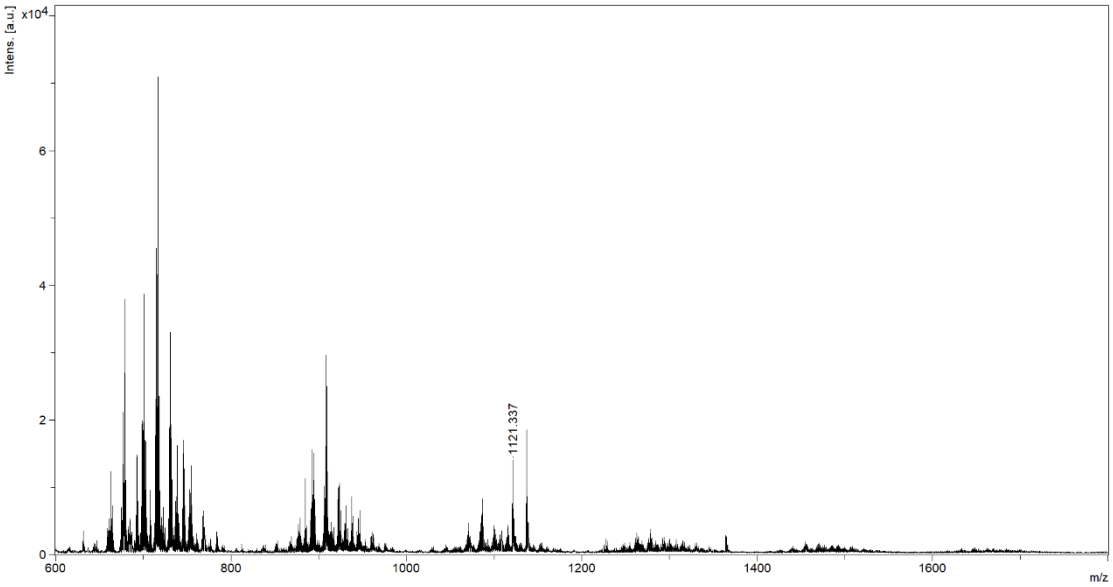


Fig E-40. The MALDI-TOF-MS result of T25

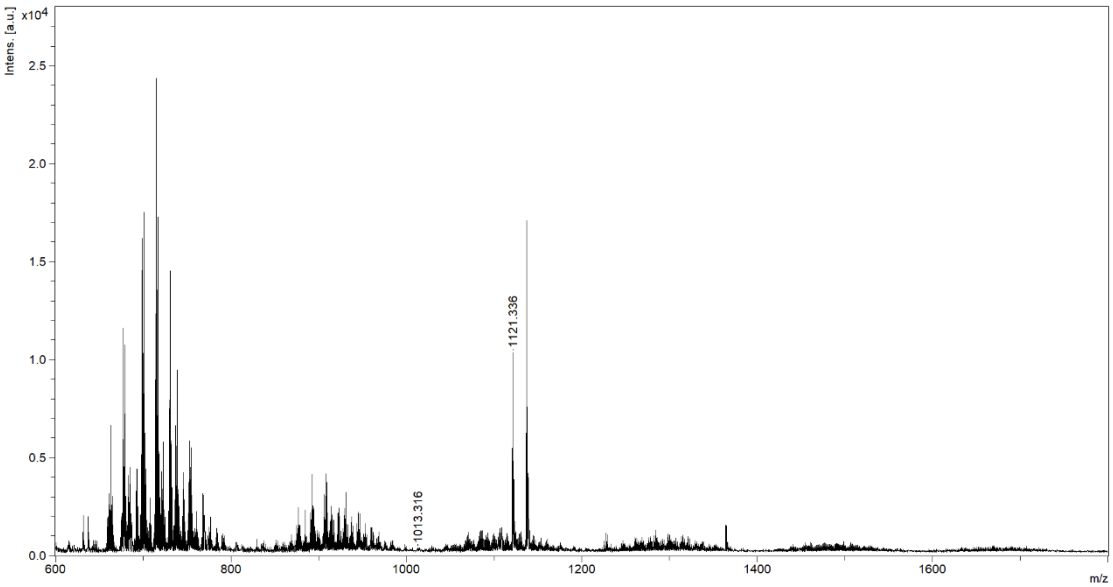


Fig E-41. The MALDI-TOF-MS result of T26

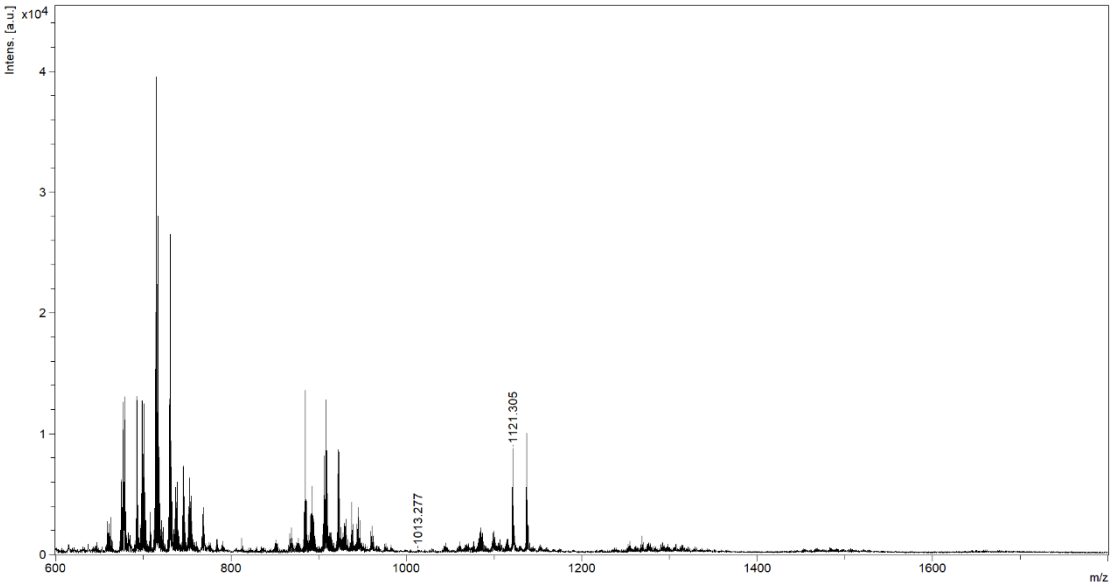


Fig E-42. The MALDI-TOF-MS result of T27

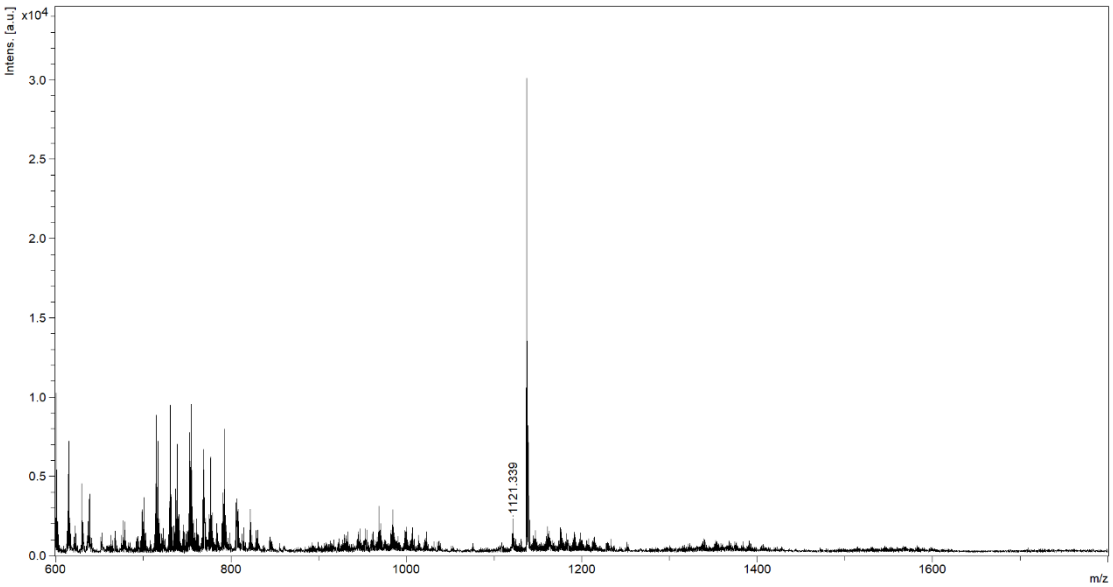


Fig E-43. The MALDI-TOF-MS result of T28

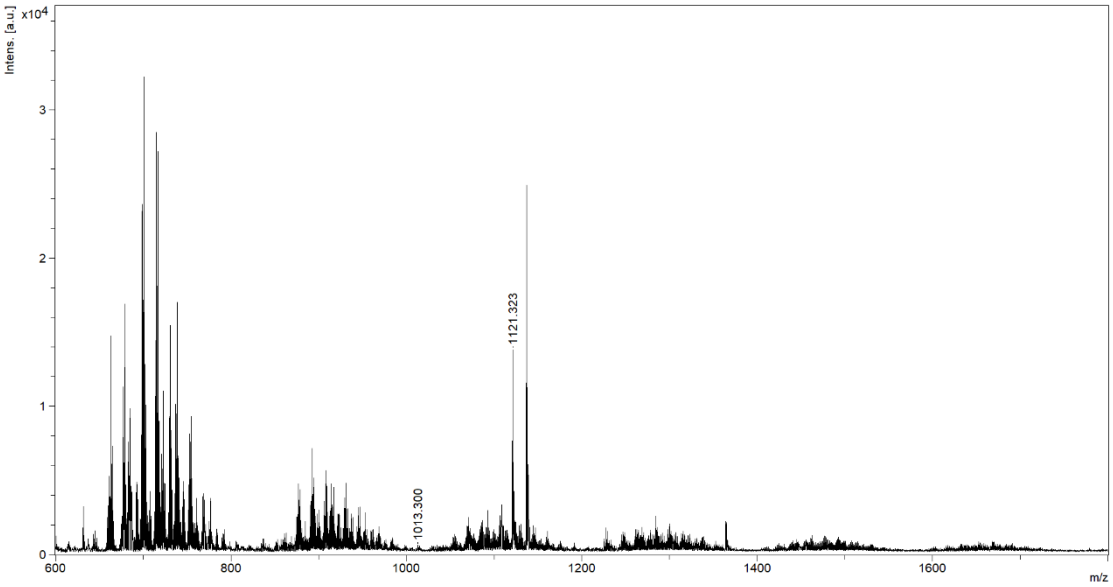


Fig E-44. The MALDI-TOF-MS result of T29

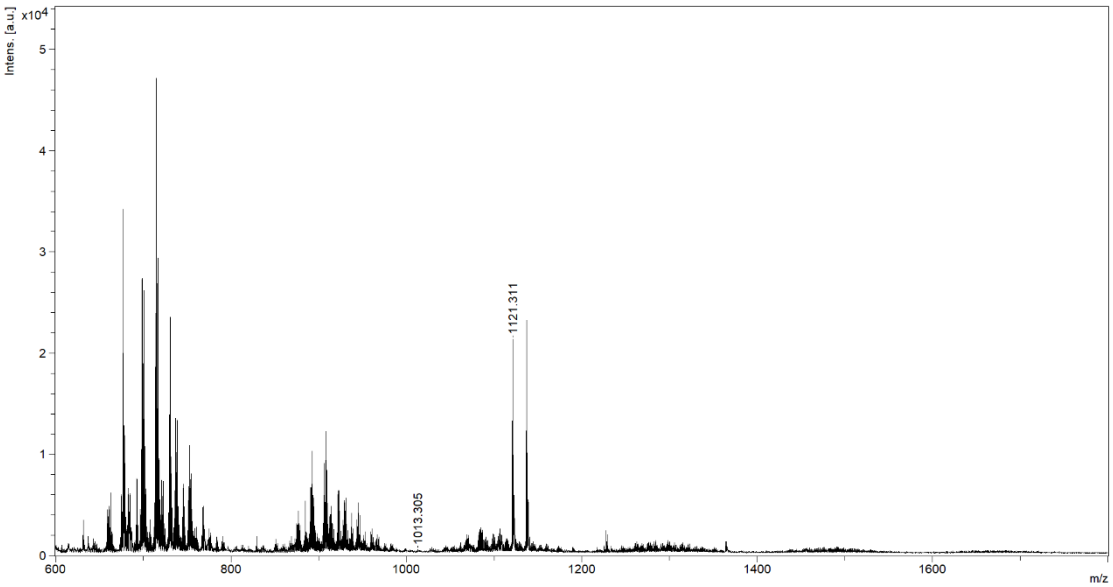


Fig E-45. The MALDI-TOF-MS result of T30

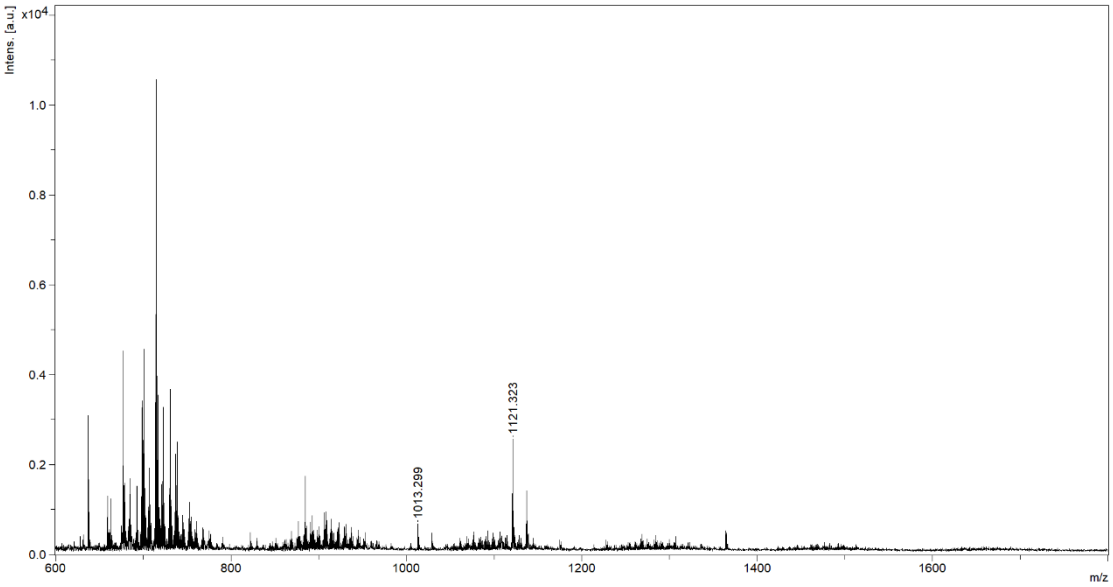


Fig E-46. The MALDI-TOF-MS result of AT1A

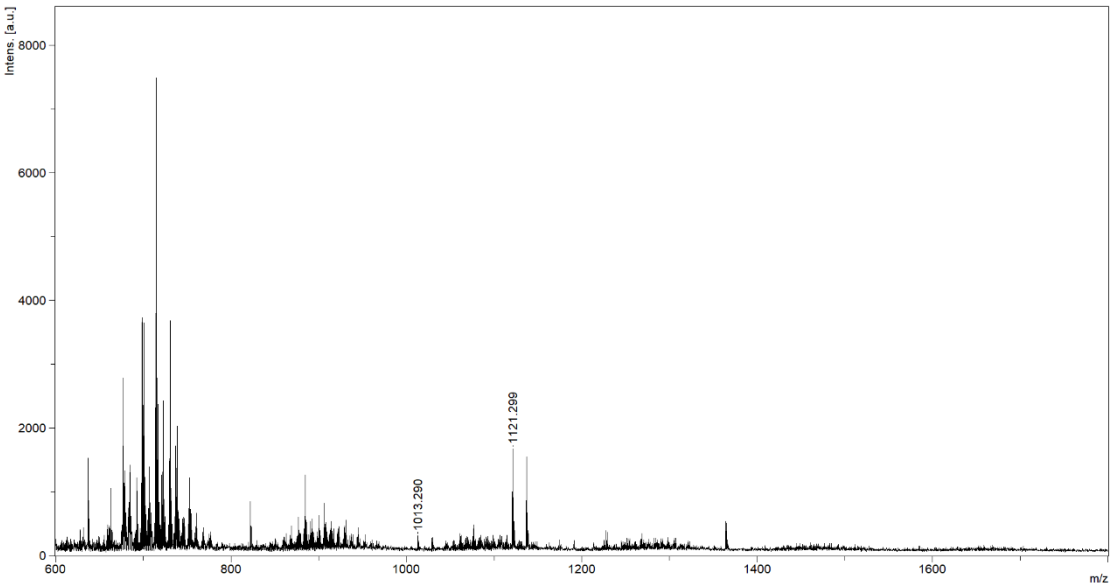


Fig E-47. The MALDI-TOF-MS result of AT1B

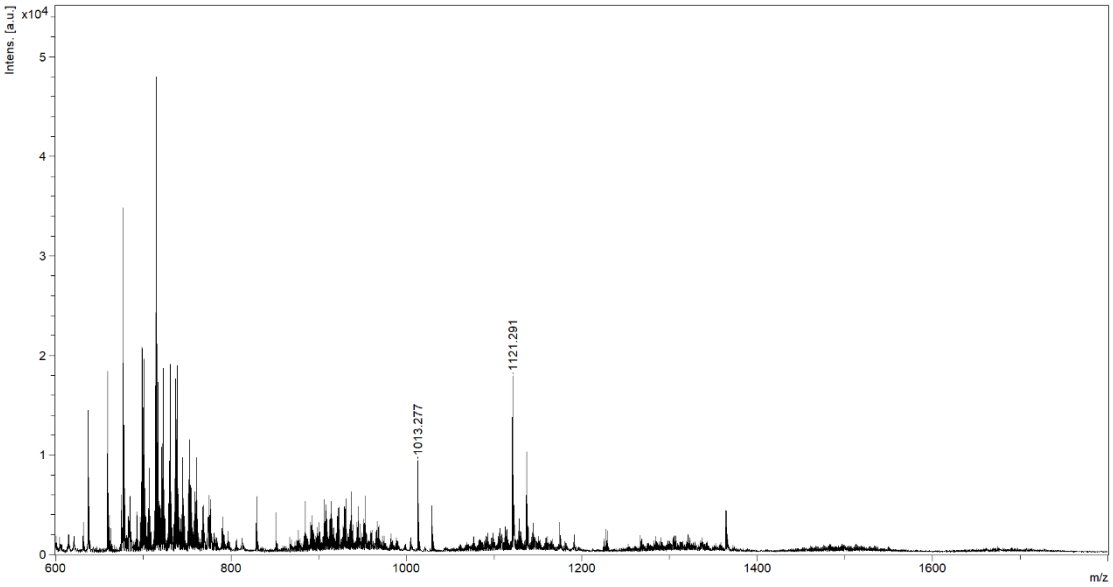


Fig E-48. The MALDI-TOF-MS result of AT1C

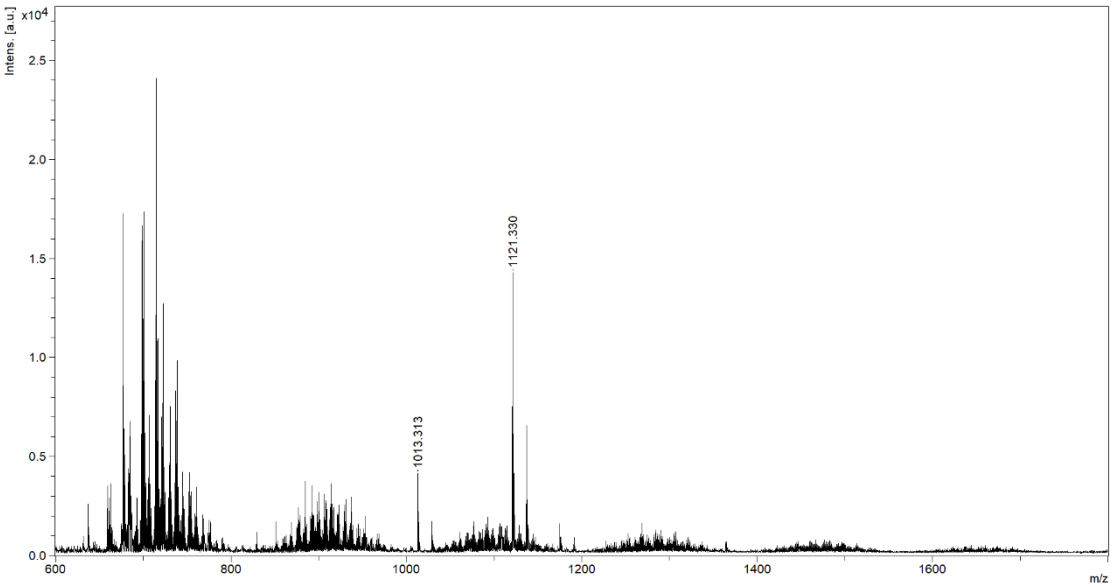


Fig E-49. The MALDI-TOF-MS result of AT2A

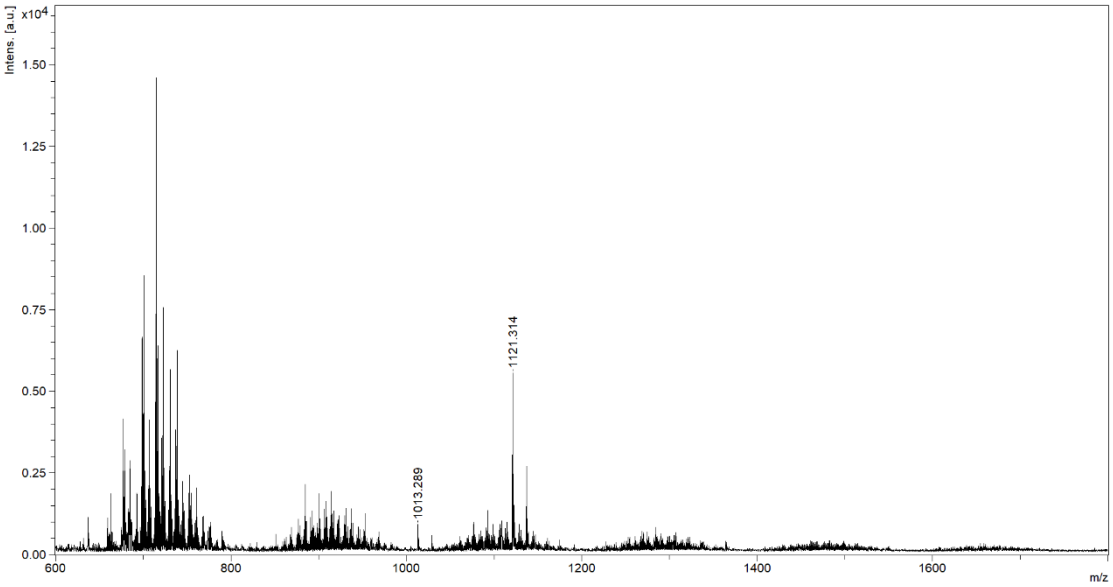


Fig E-50. The MALDI-TOF-MS result of AT2B

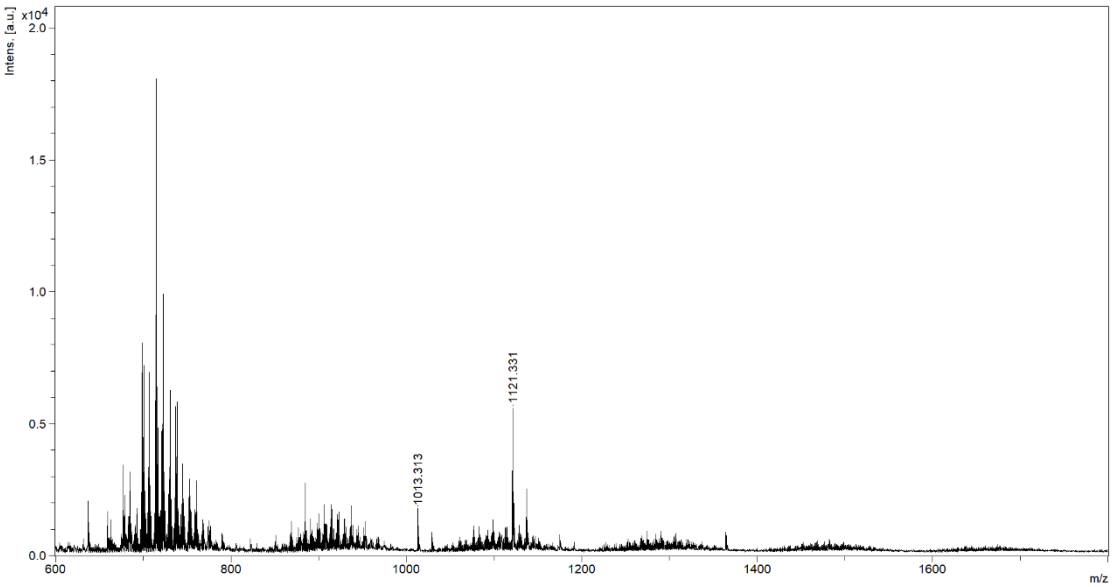


Fig E-51. The MALDI-TOF-MS result of AT2C

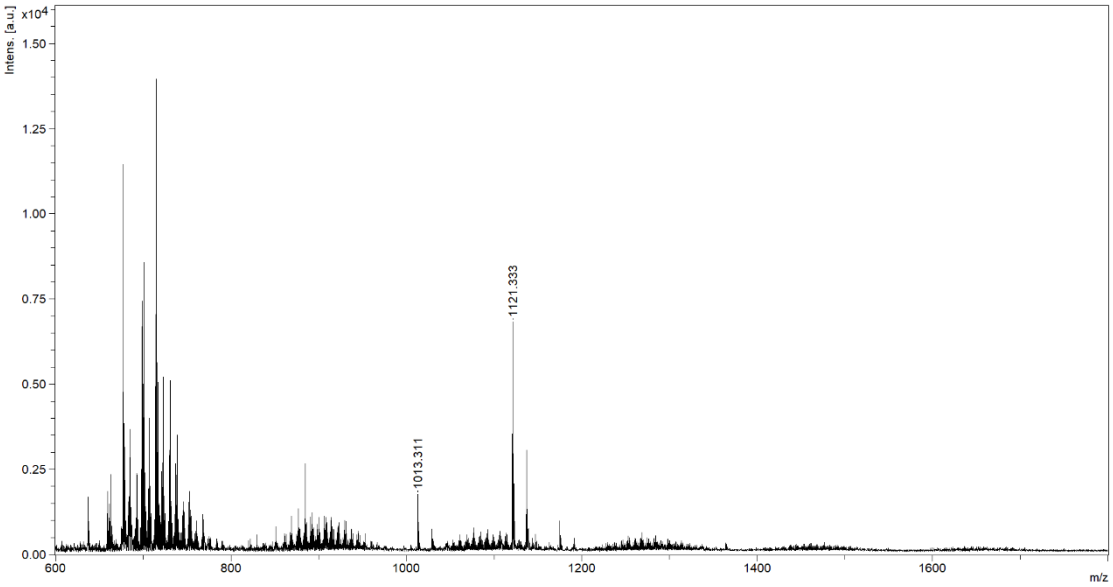


Fig E-52. The MALDI-TOF-MS result of AT3A

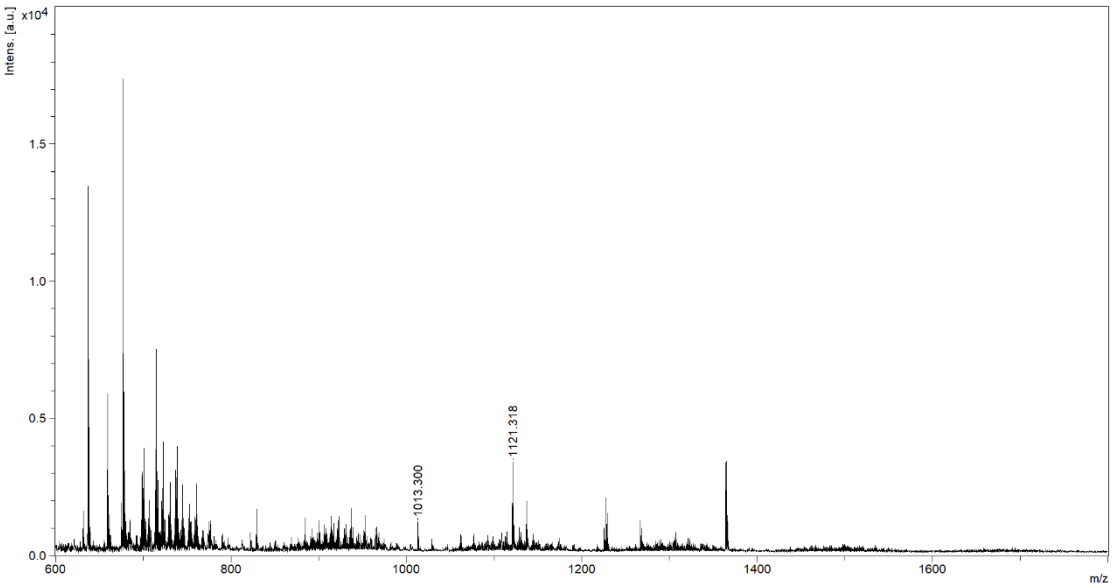


Fig E-53. The MALDI-TOF-MS result of AT3B

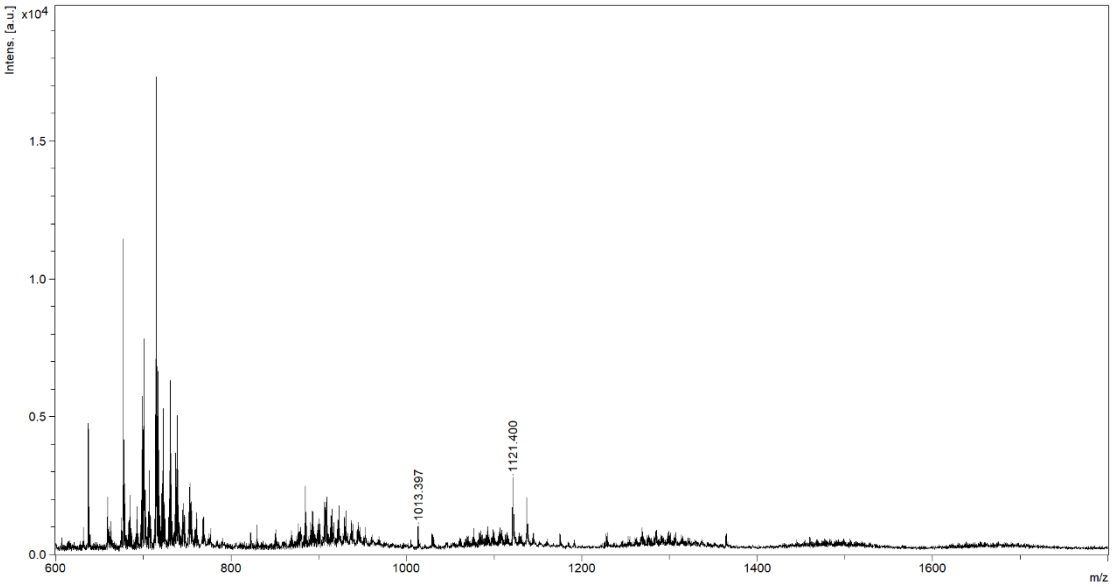


Fig E-54. The MALDI-TOF-MS result of AT3C

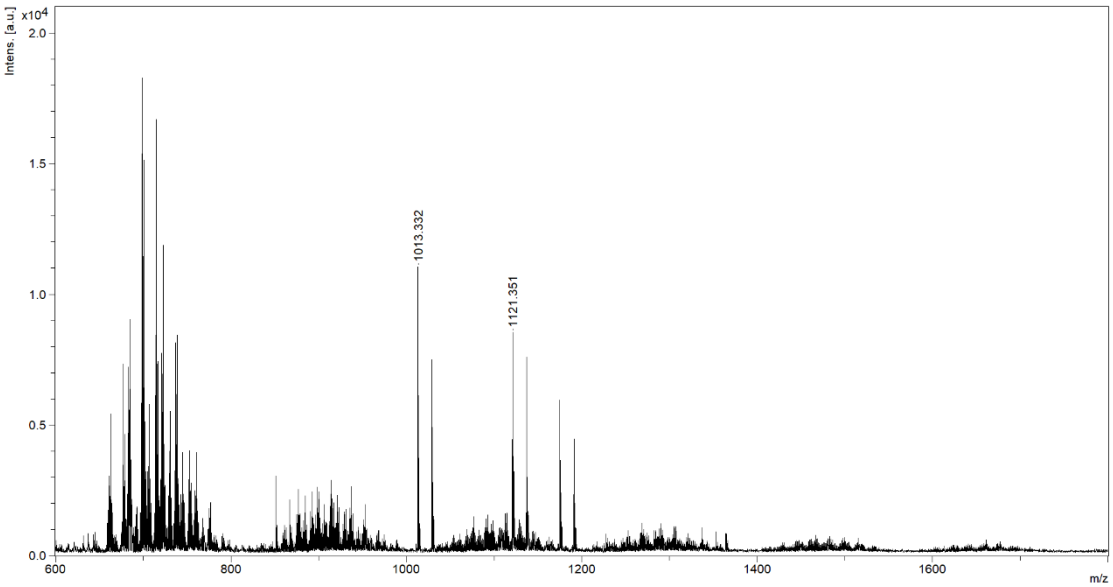


Fig E-55. The MALDI-TOF-MS result of AT4A

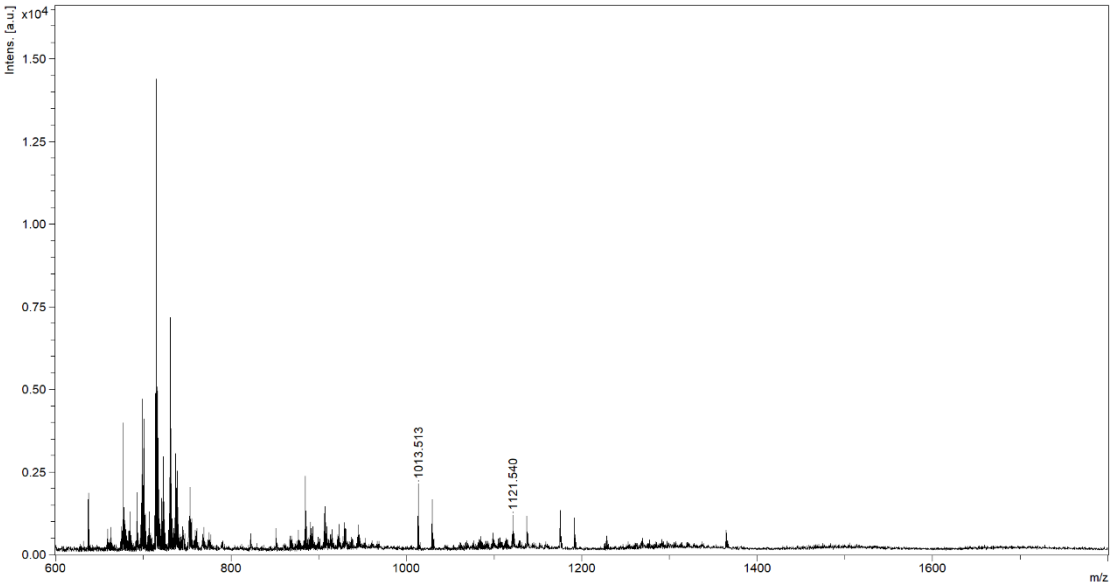


Fig E-56. The MALDI-TOF-MS result of AT4B

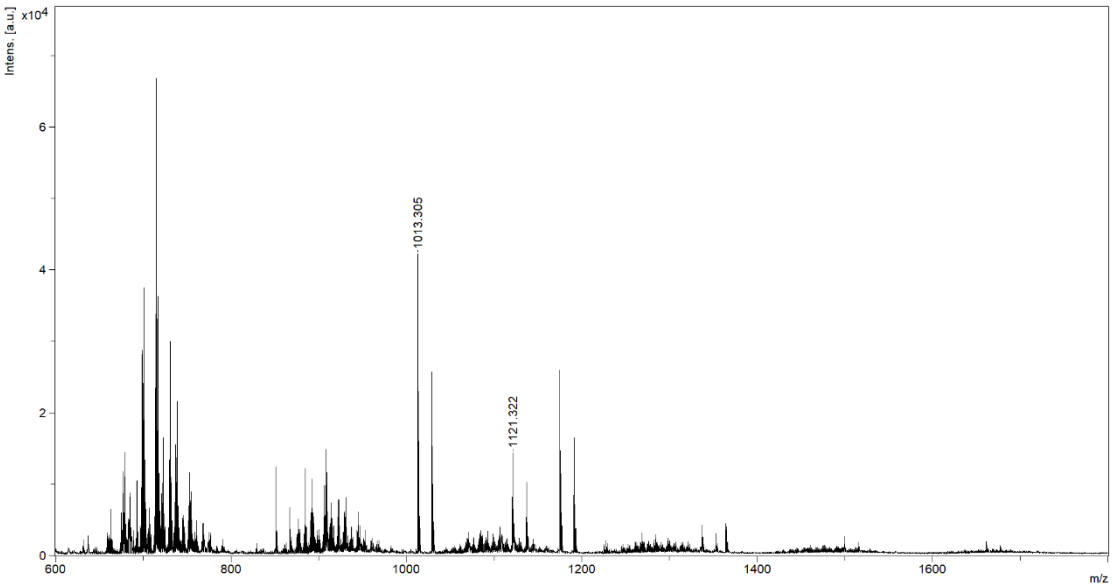


Fig E-57. The MALDI-TOF-MS result of AT4C

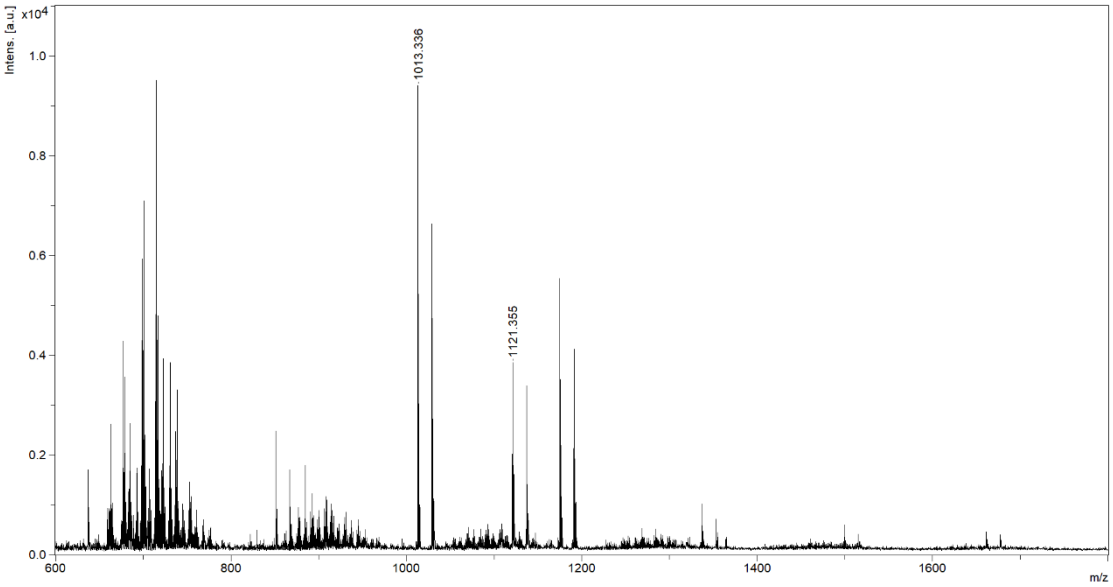


Fig E-58. The MALDI-TOF-MS result of AT5A

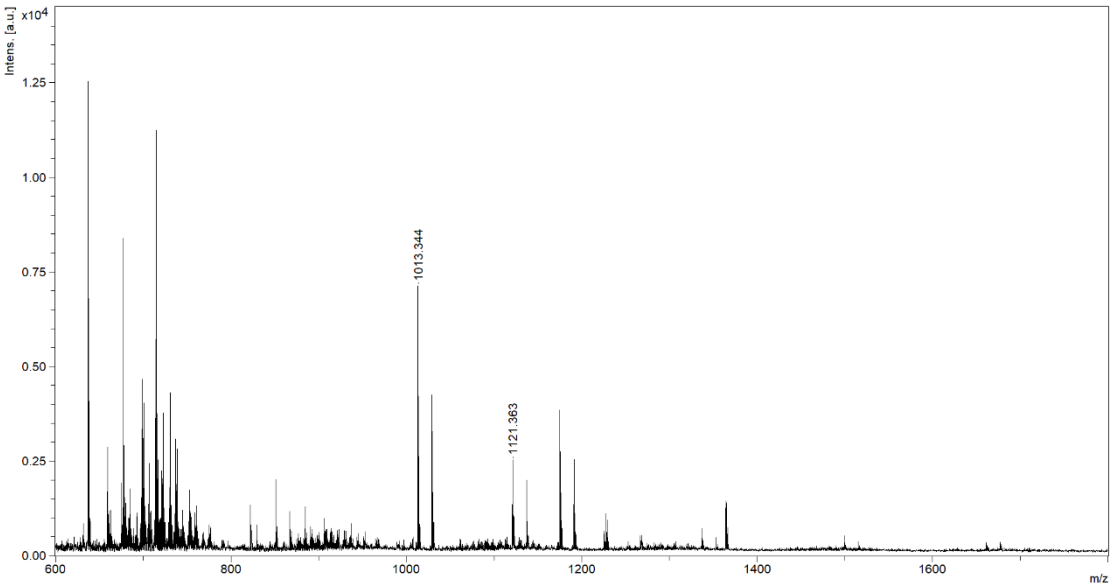


Fig E-59. The MALDI-TOF-MS result of AT5B

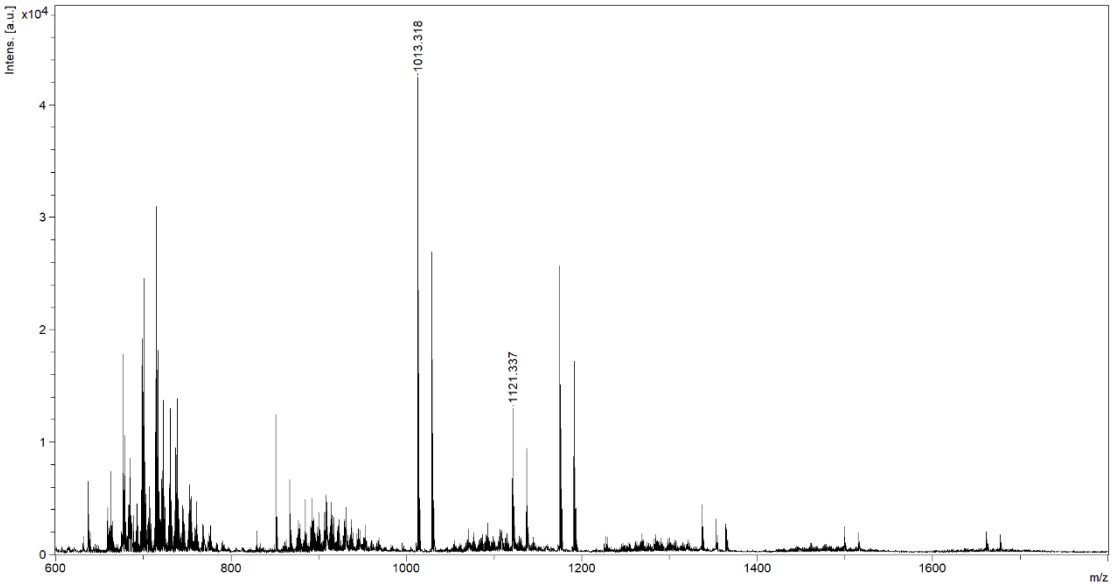


Fig E-60. The MALDI-TOF-MS result of AT5C

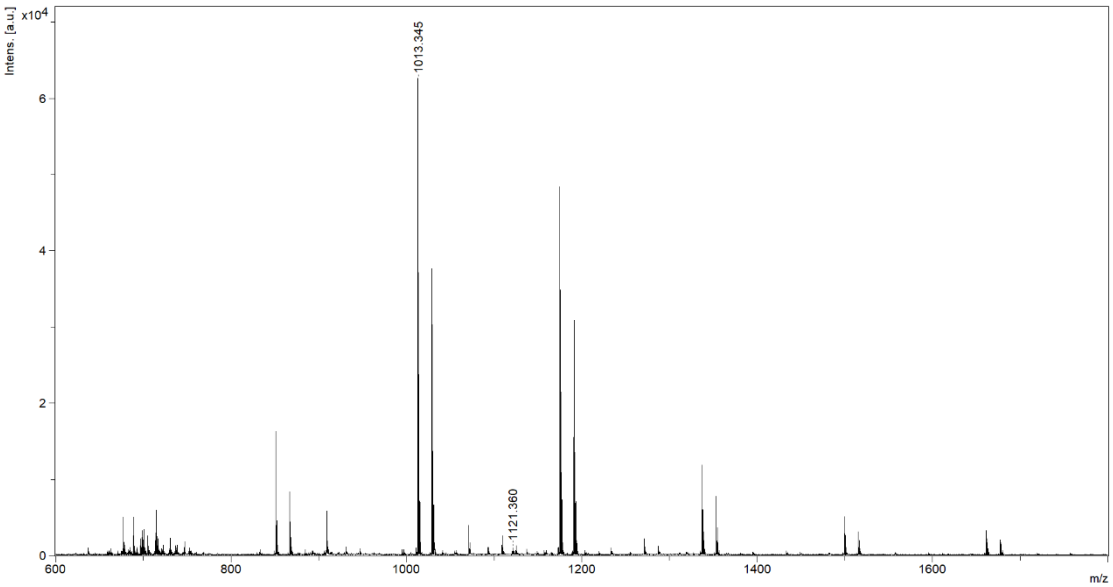


Fig E-61. The MALDI-TOF-MS result of AT6A

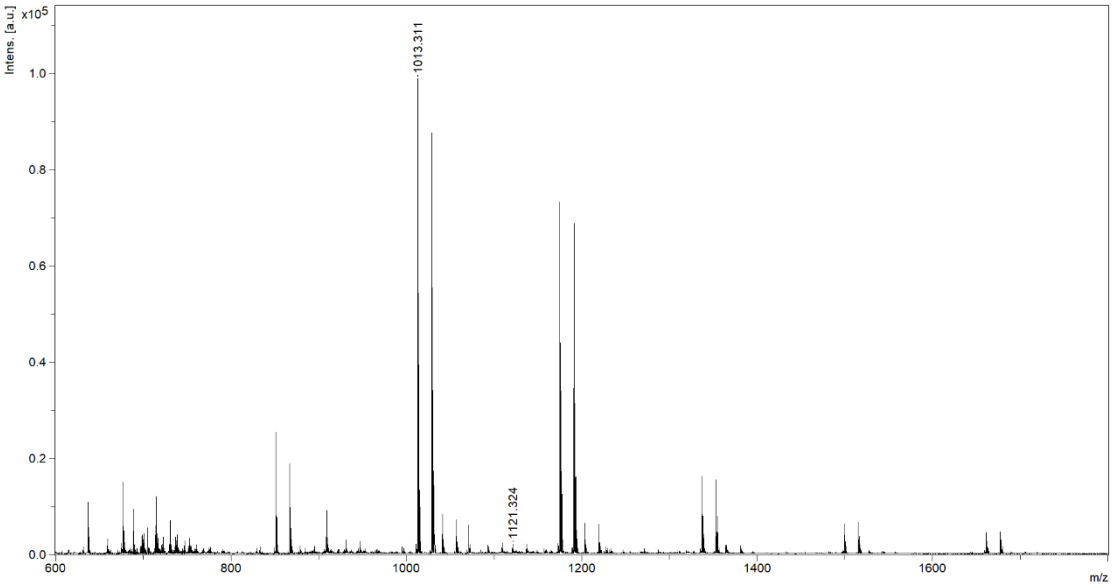


Fig E-62. The MALDI-TOF-MS result of AT6B

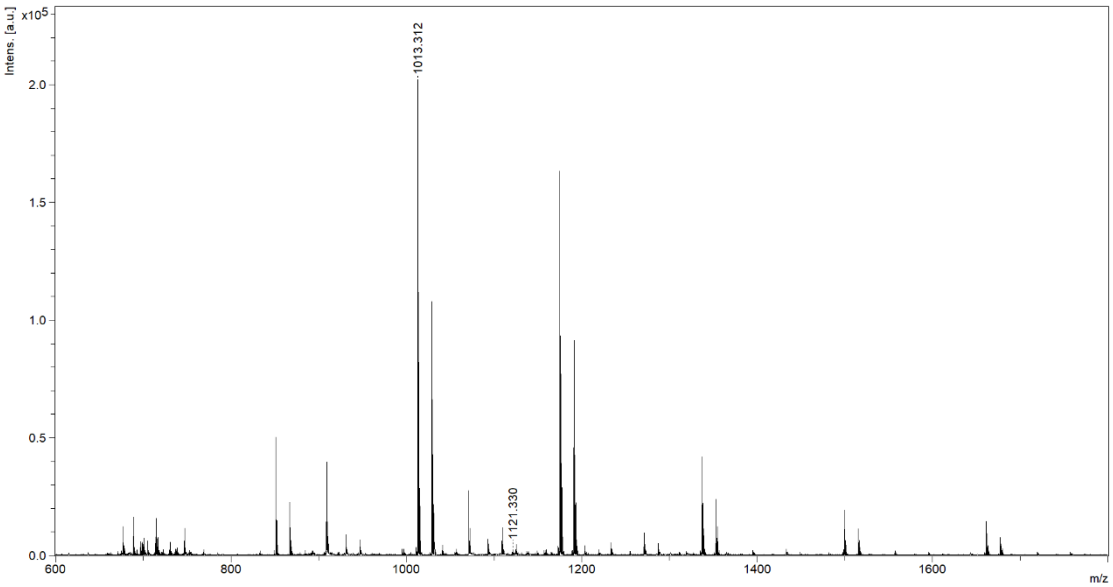


Fig E-63. The MALDI-TOF-MS result of AT6C

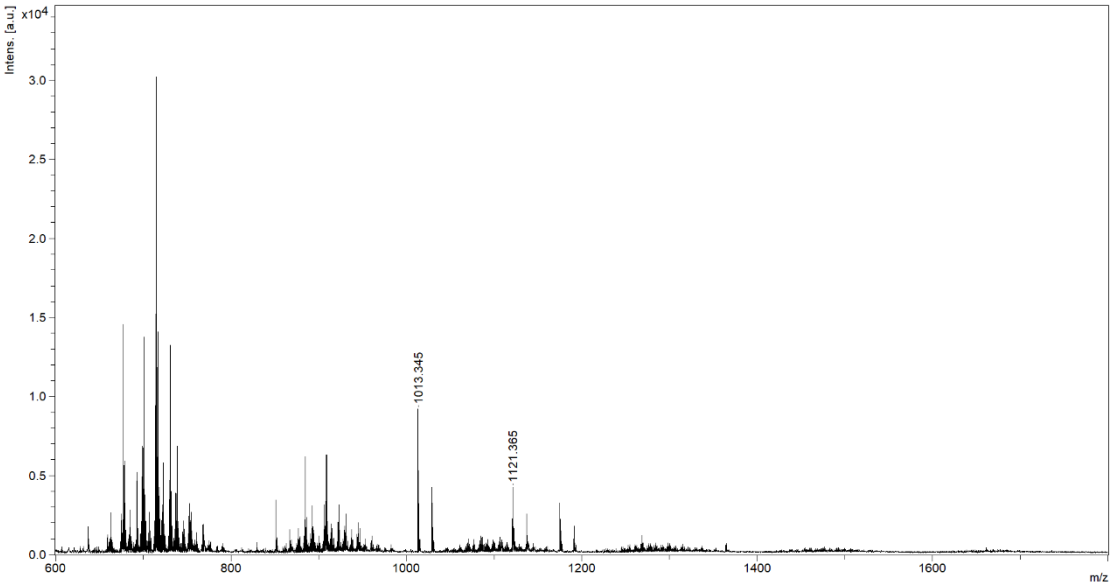


Fig E-64. The MALDI-TOF-MS result of AT7A

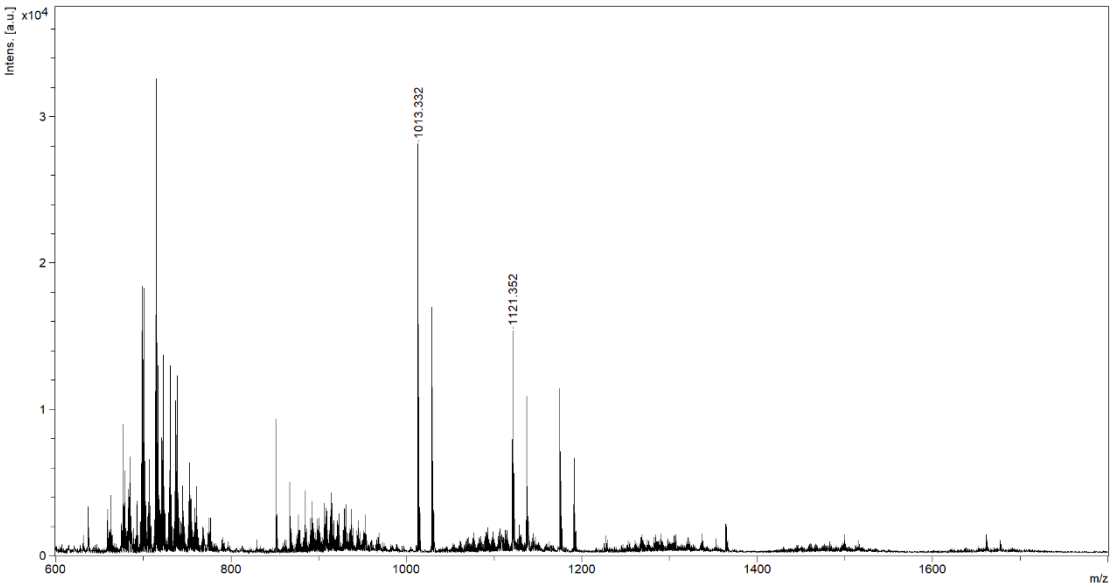


Fig E-65. The MALDI-TOF-MS result of AT7B

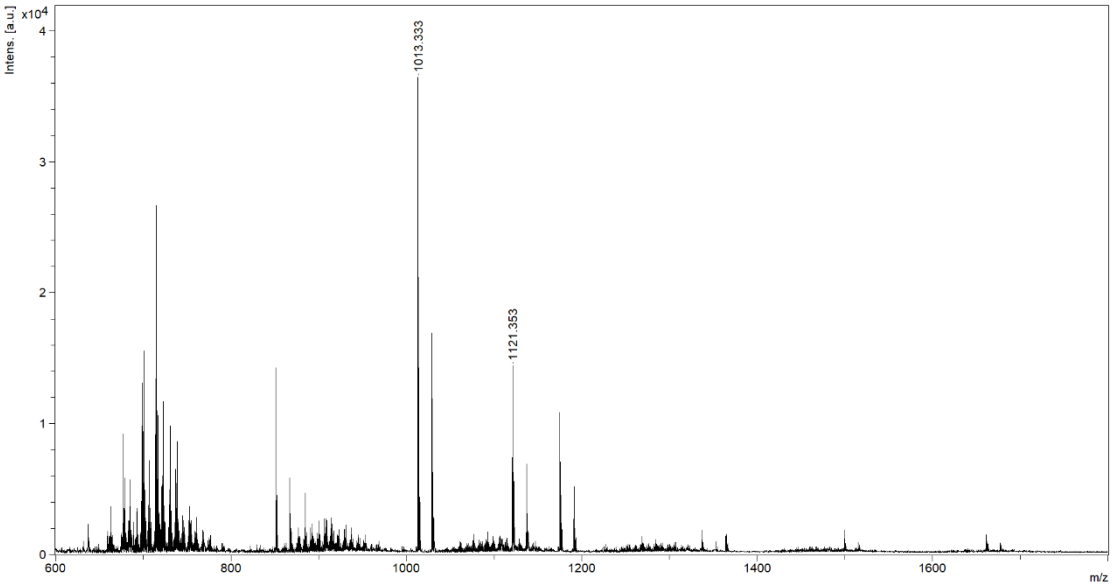


Fig E-66. The MALDI-TOF-MS result of AT7C

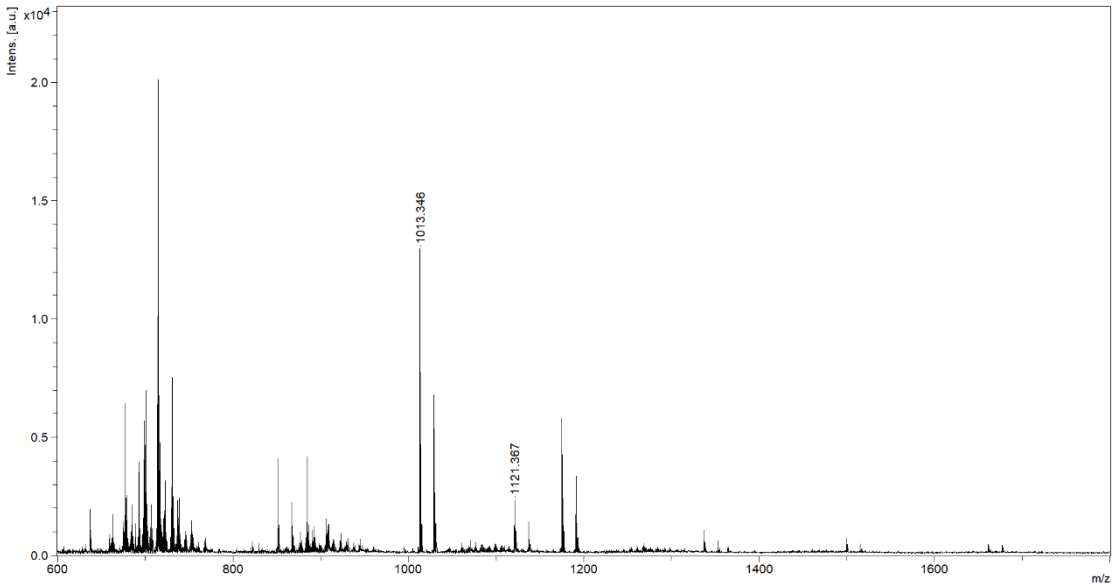


Fig E-67. The MALDI-TOF-MS result of AT8A

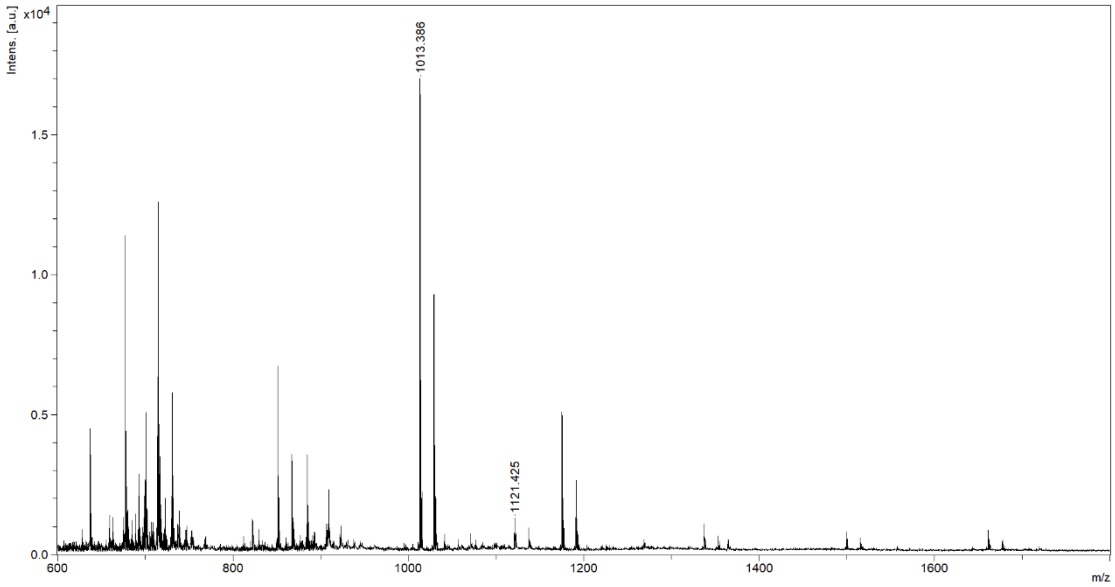


Fig E-68. The MALDI-TOF-MS result of AT8B

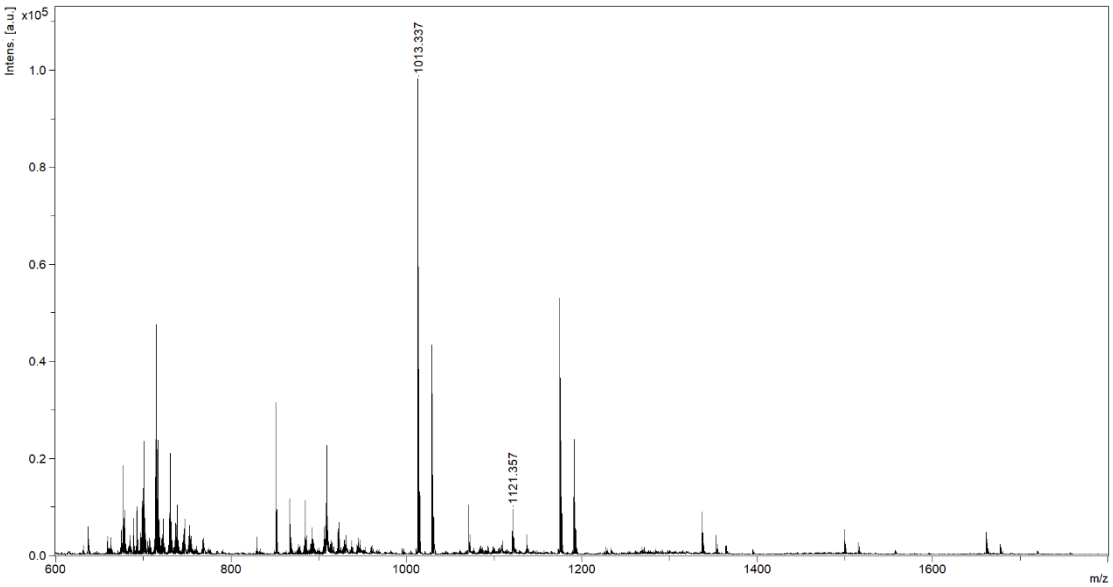


Fig E-69. The MALDI-TOF-MS result of AT8C

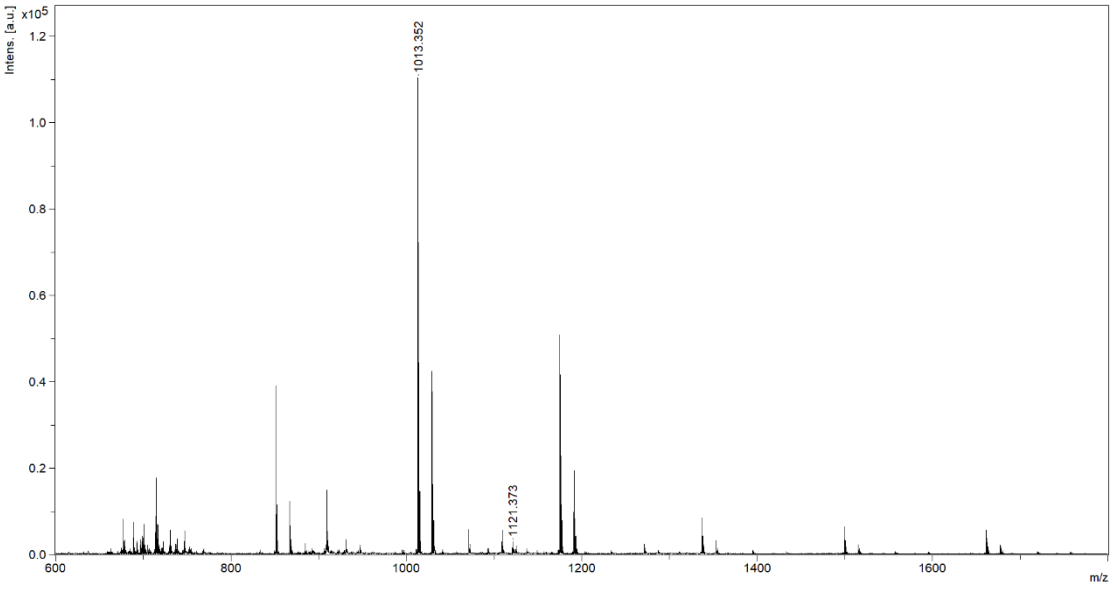


Fig E-70. The MALDI-TOF-MS result of AT9A

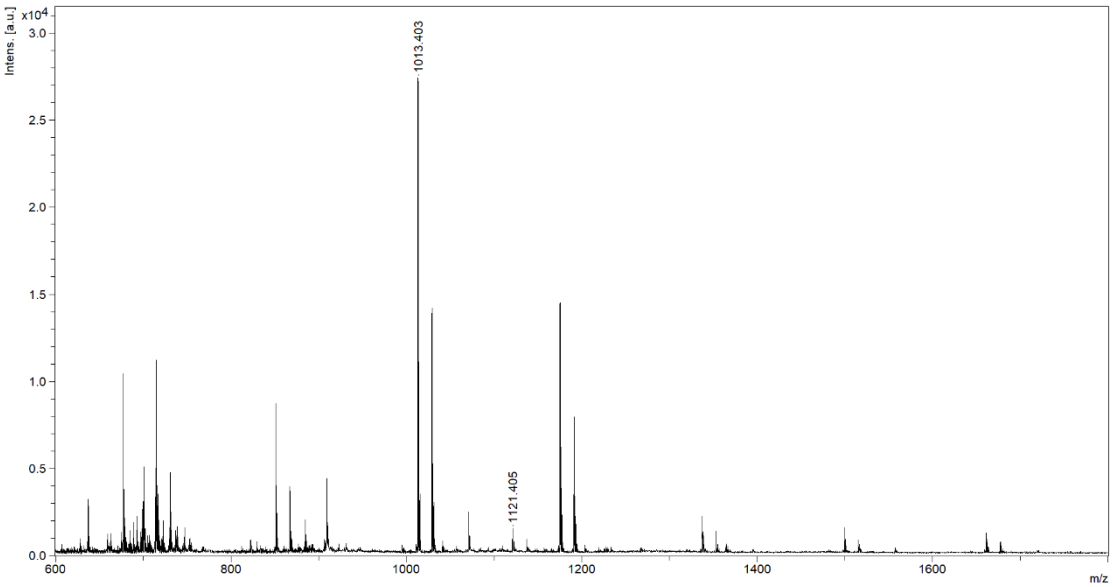


Fig E-71. The MALDI-TOF-MS result of AT9B

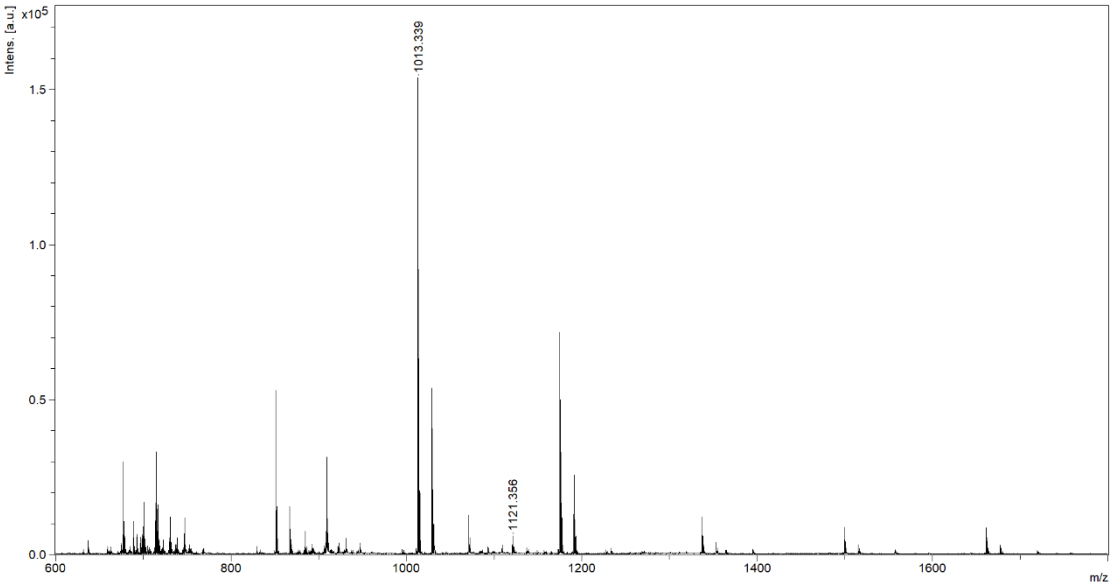


Fig E-72. The MALDI-TOF-MS result of AT9C

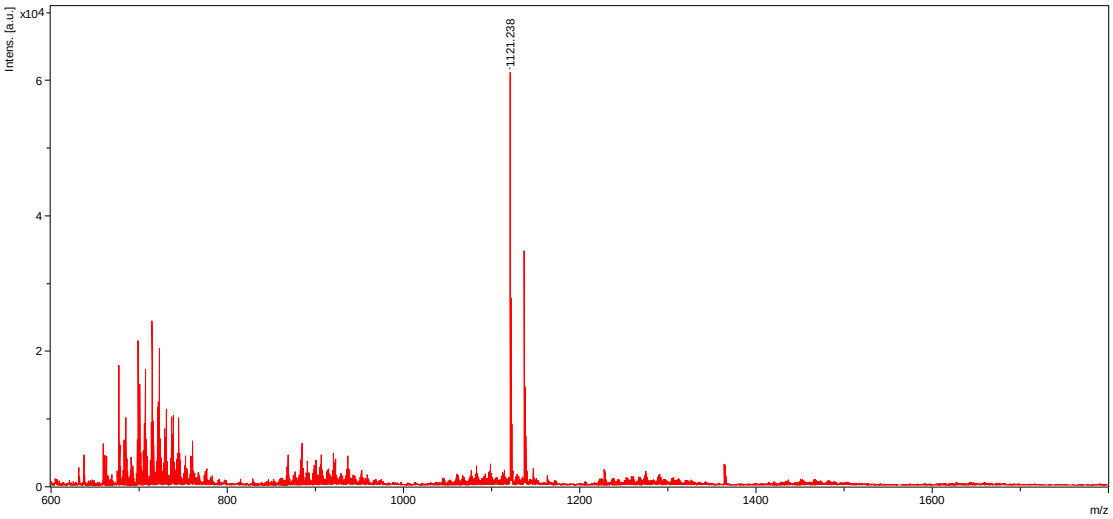


Fig E-73. The MALDI-TOF-MS result of XZM1

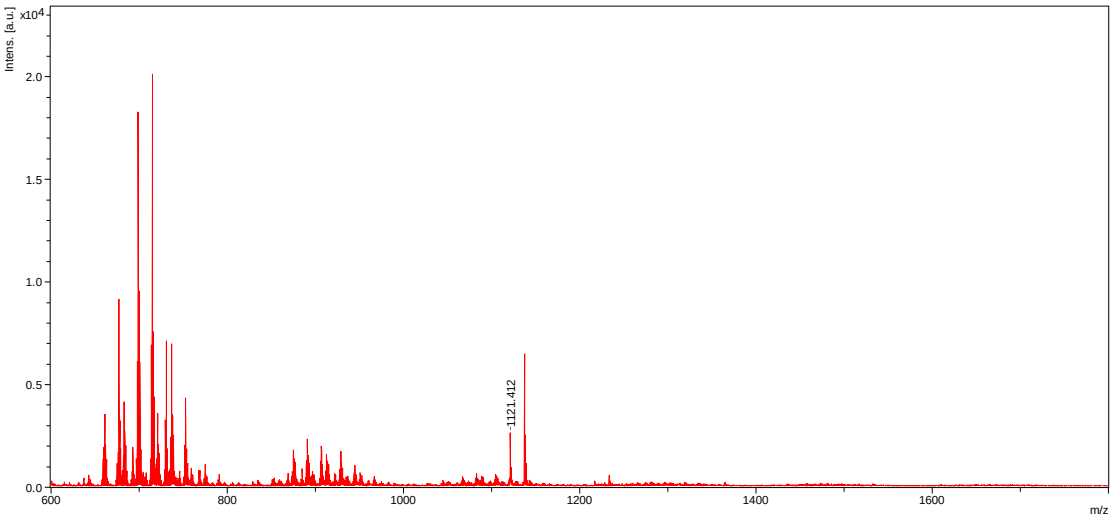


Fig E-74. The MALDI-TOF-MS result of XZM2

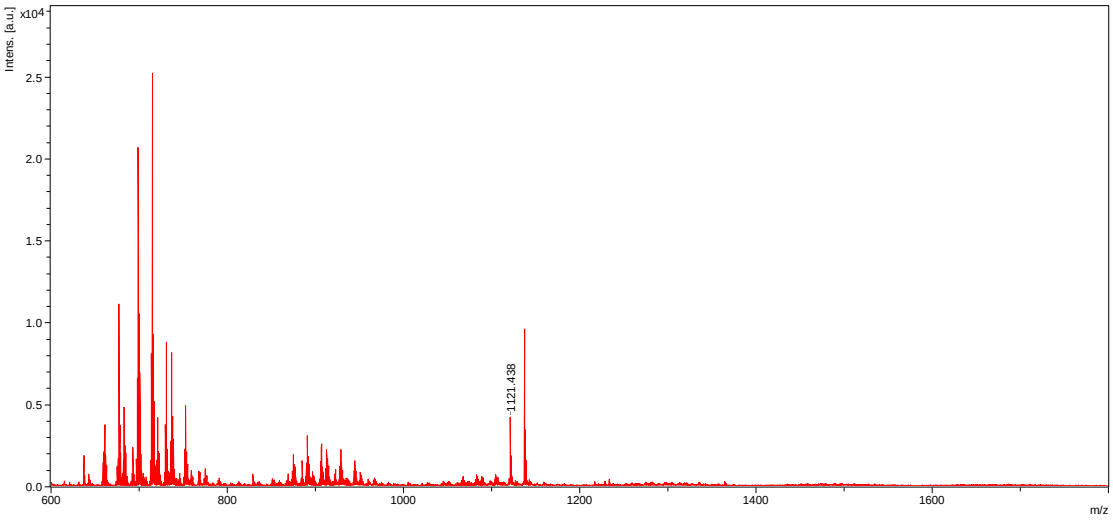


Fig E-75. The MALDI-TOF-MS result of XZM3

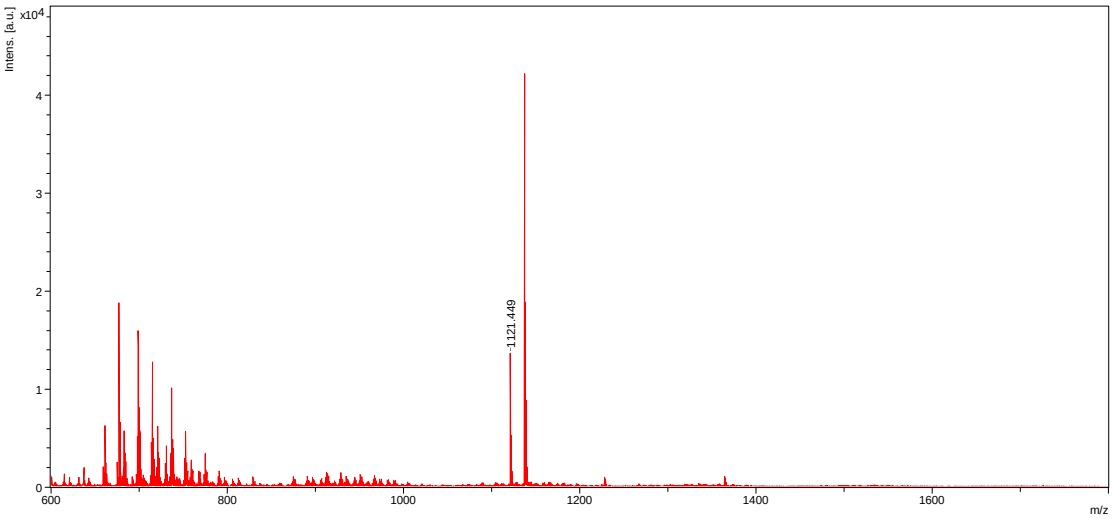


Fig E-76. The MALDI-TOF-MS result of XZM4

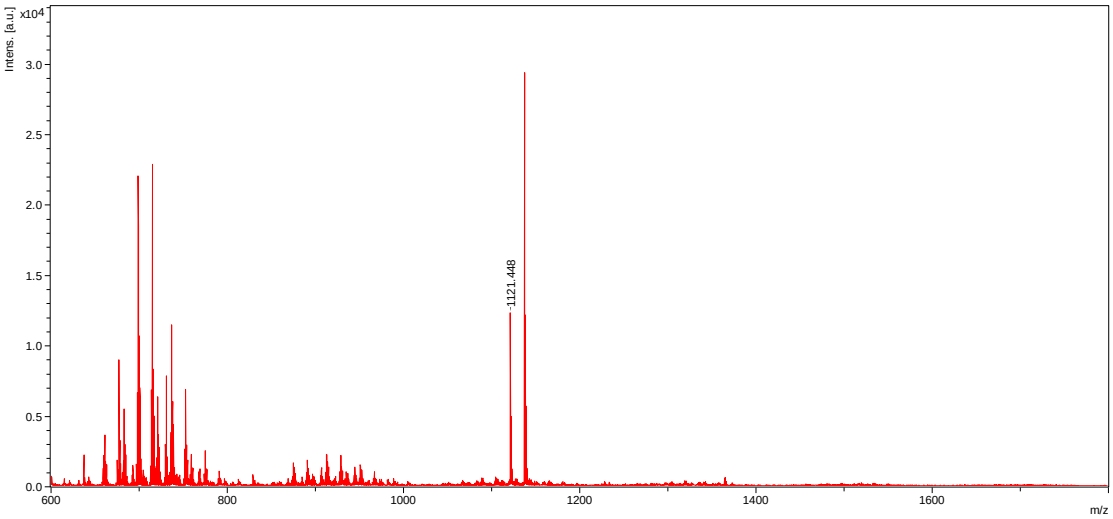


Fig E-77. The MALDI-TOF-MS result of XZM5

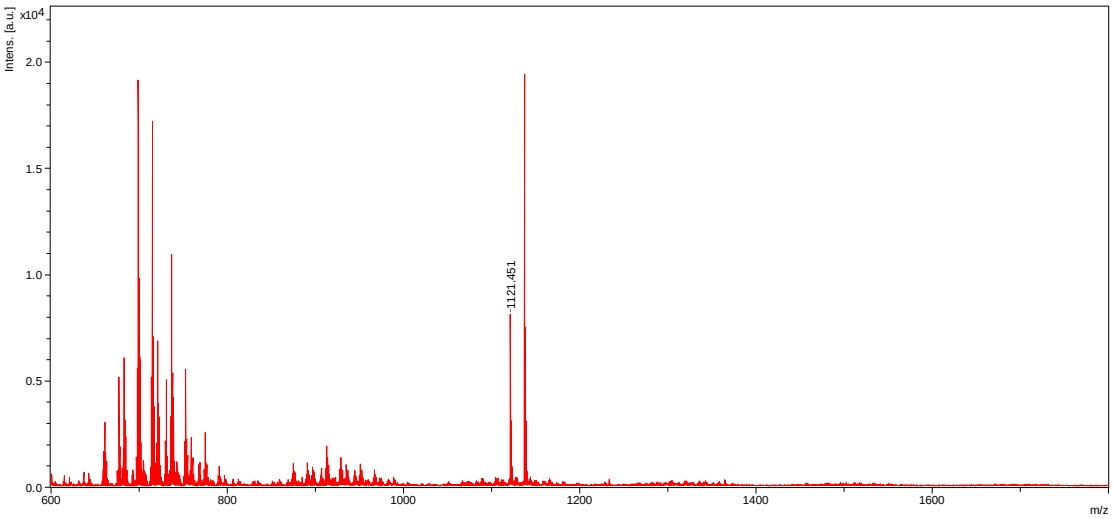


Fig E-78. The MALDI-TOF-MS result of XZM6

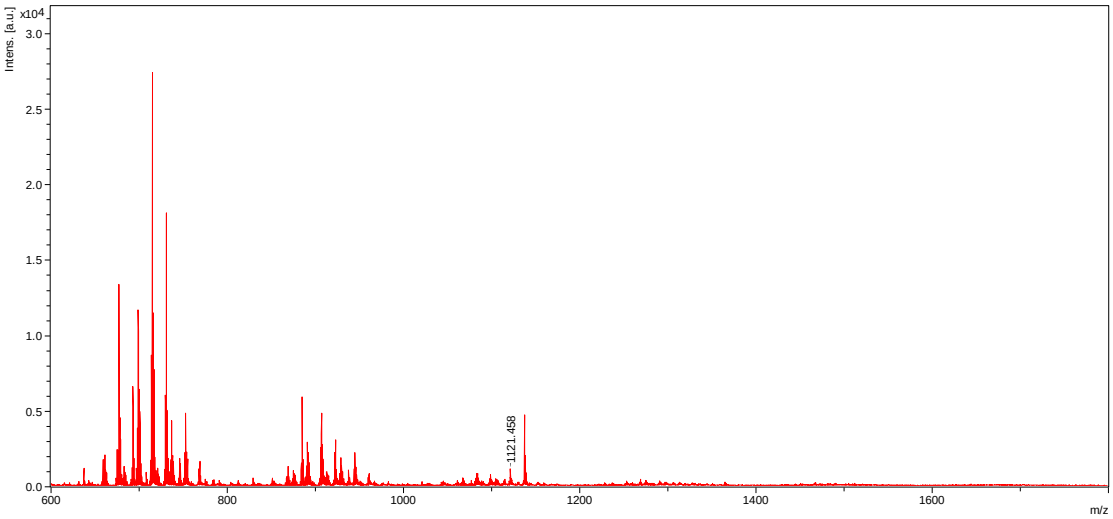


Fig E-79. The MALDI-TOF-MS result of XZM7

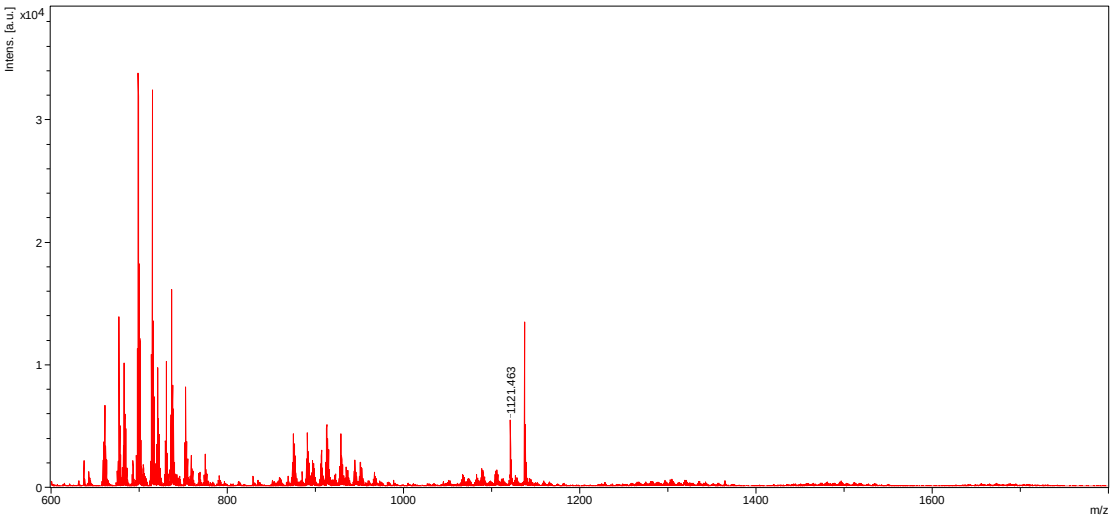


Fig E-80. The MALDI-TOF-MS result of XZM8

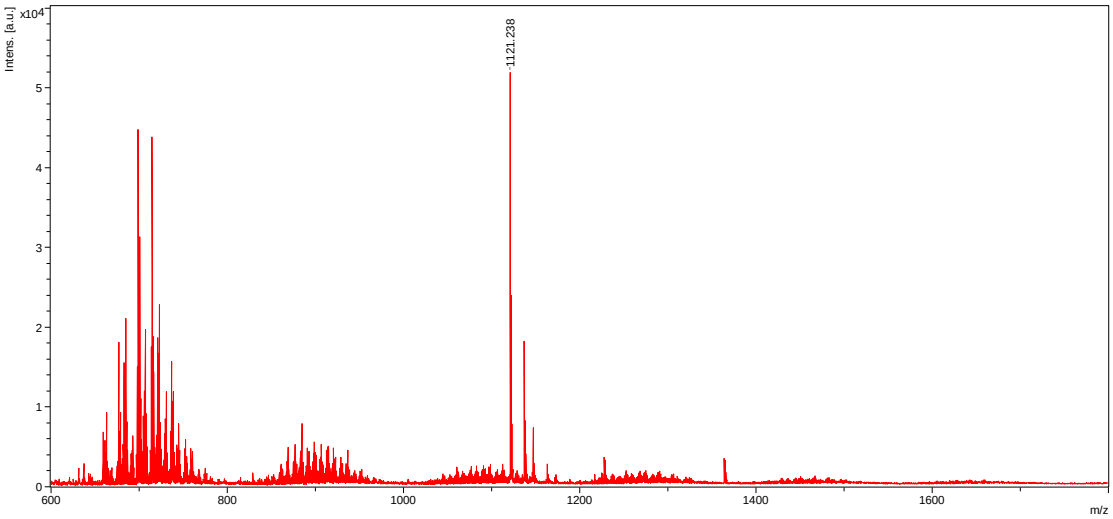


Fig E-81. The MALDI-TOF-MS result of BWC1

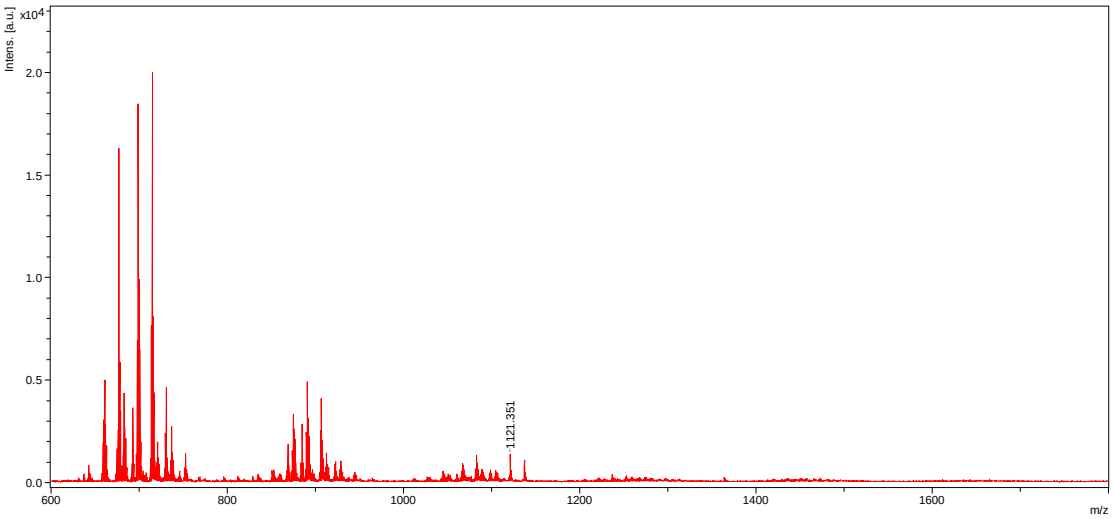


Fig E-82. The MALDI-TOF-MS result of BWC2

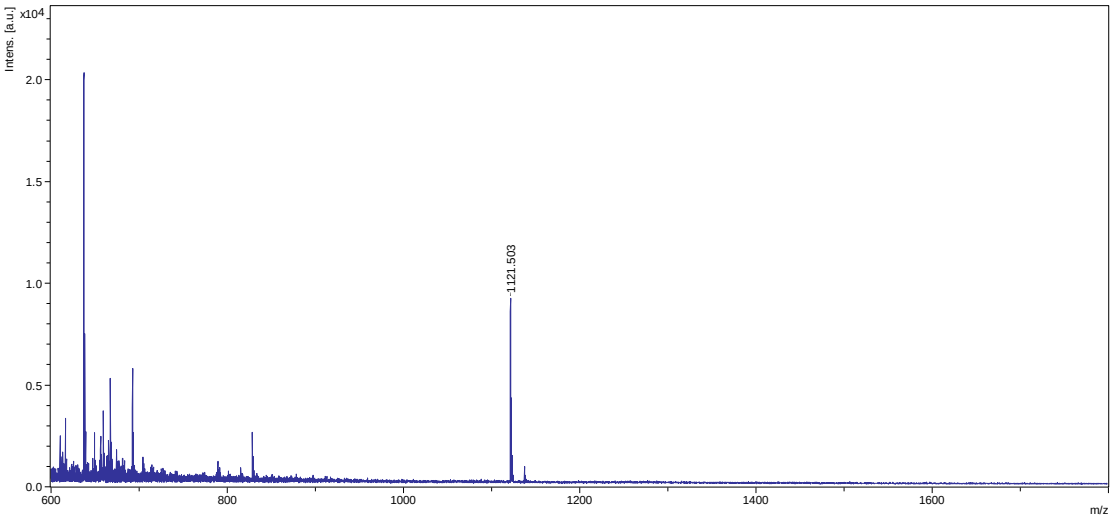


Fig E-83. The MALDI-TOF-MS result of BWC3

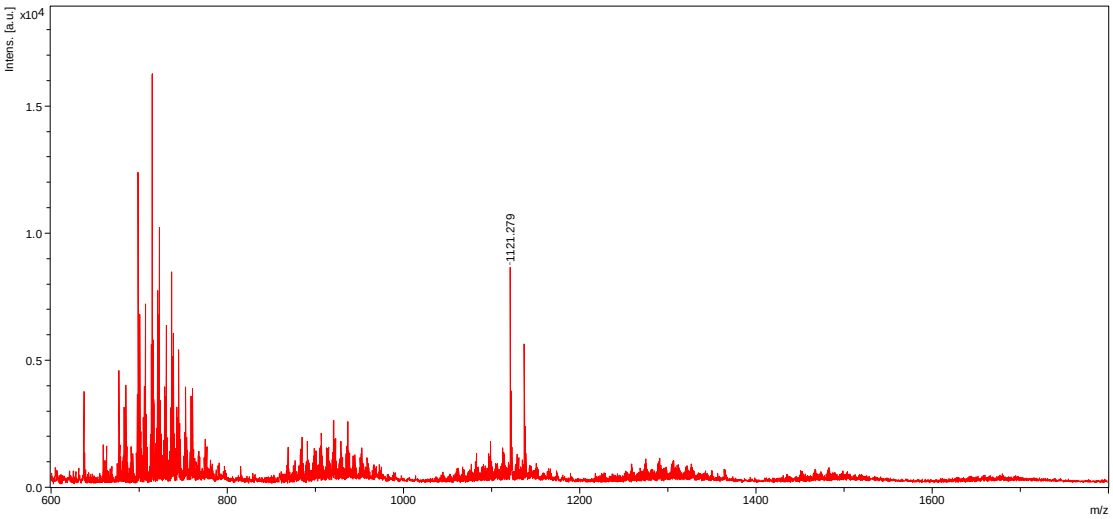


Fig E-84. The MALDI-TOF-MS result of BWC4

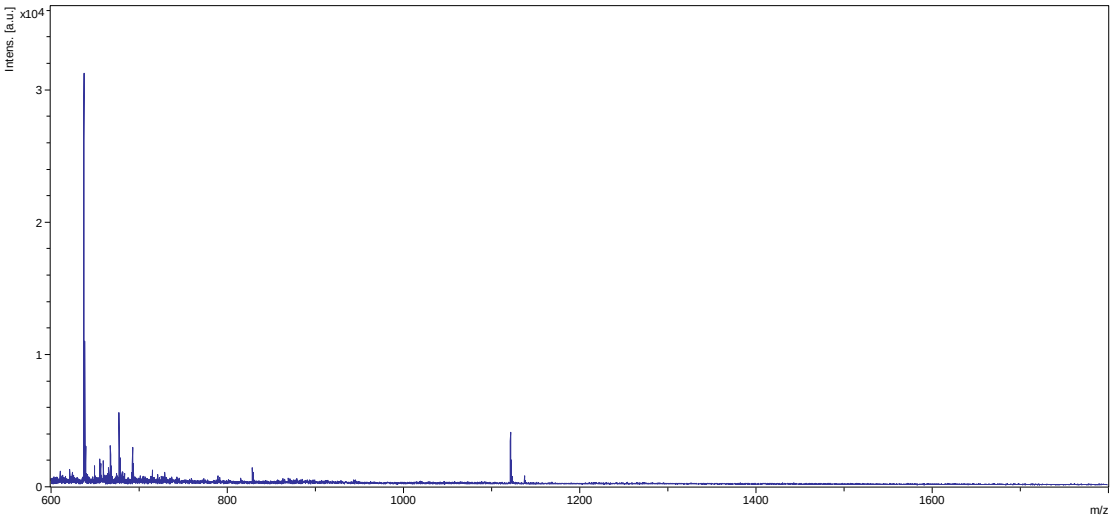


Fig E-85. The MALDI-TOF-MS result of BWC5

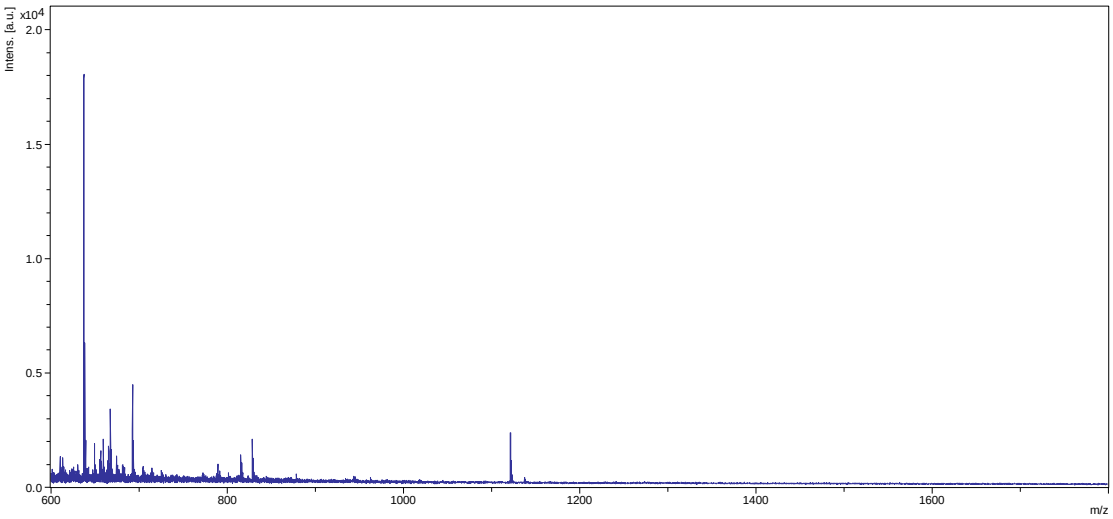


Fig E-86. The MALDI-TOF-MS result of BWC6

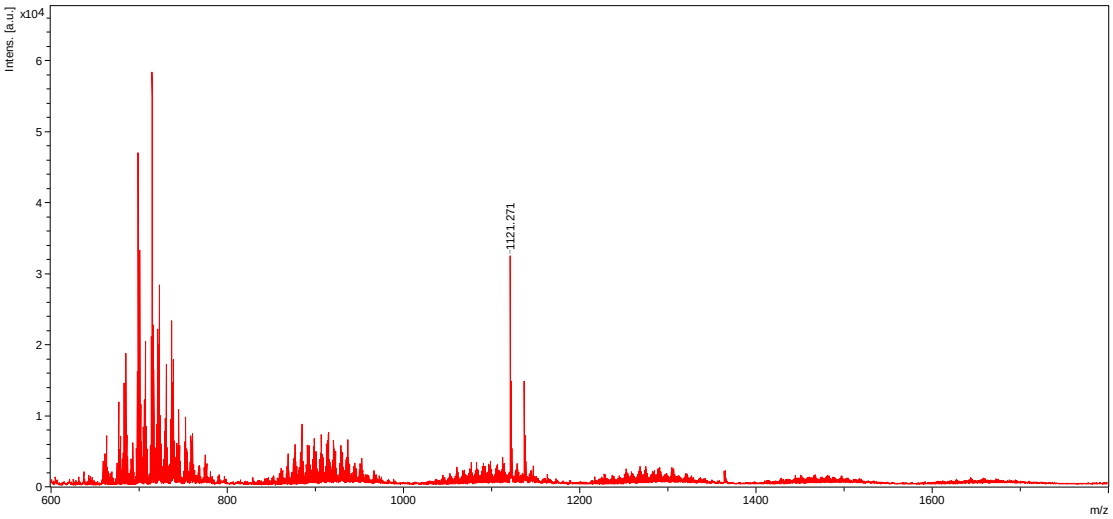


Fig E-87. The MALDI-TOF-MS result of BWC7

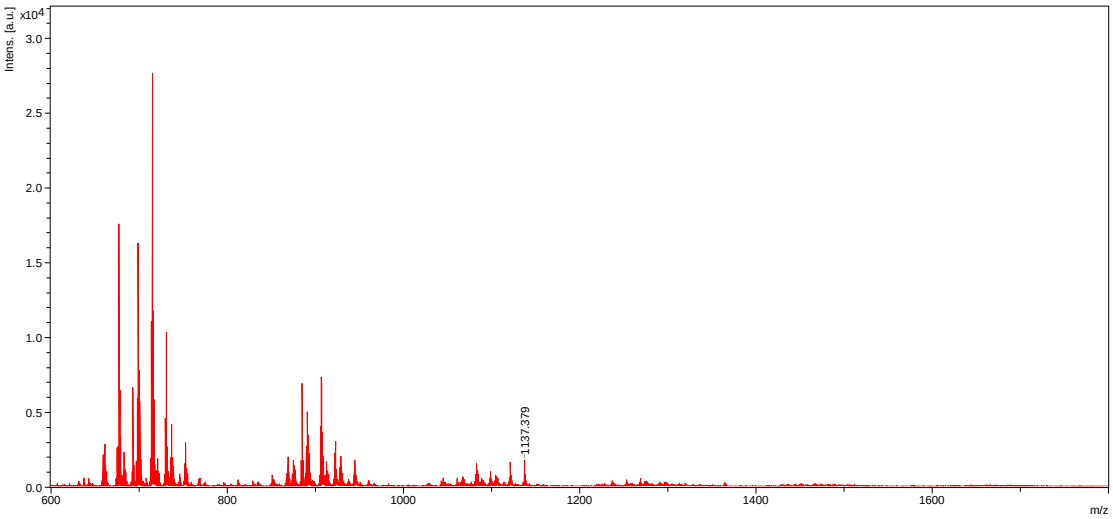


Fig E-88. The MALDI-TOF-MS result of BWC8

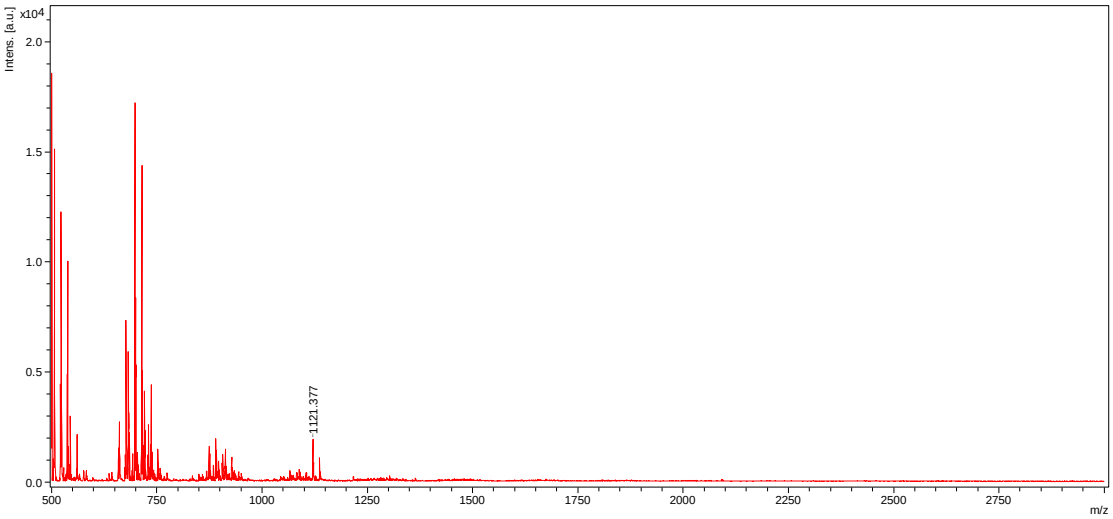


Fig E-89. The MALDI-TOF-MS result of PTC1

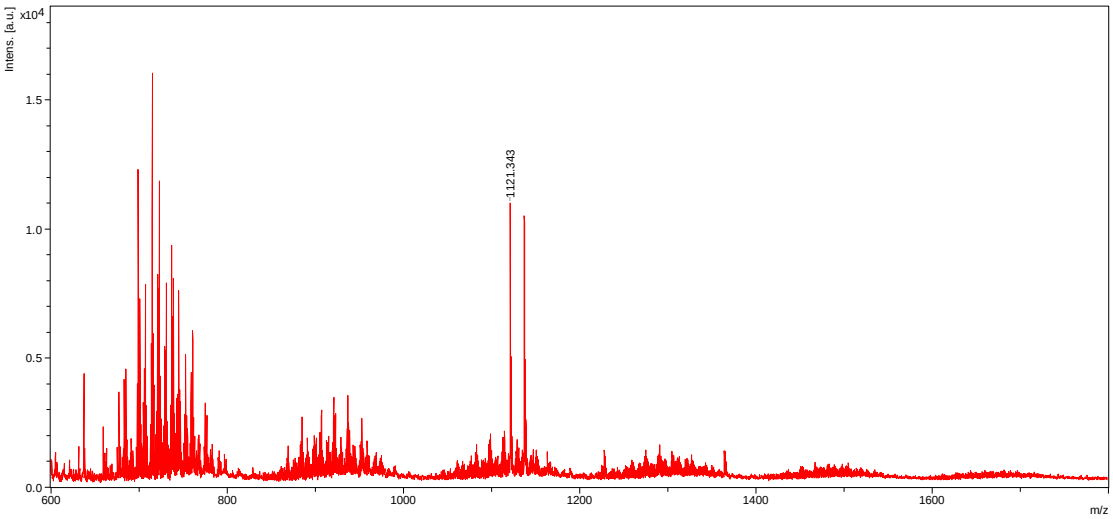


Fig E-90. The MALDI-TOF-MS result of PTC2

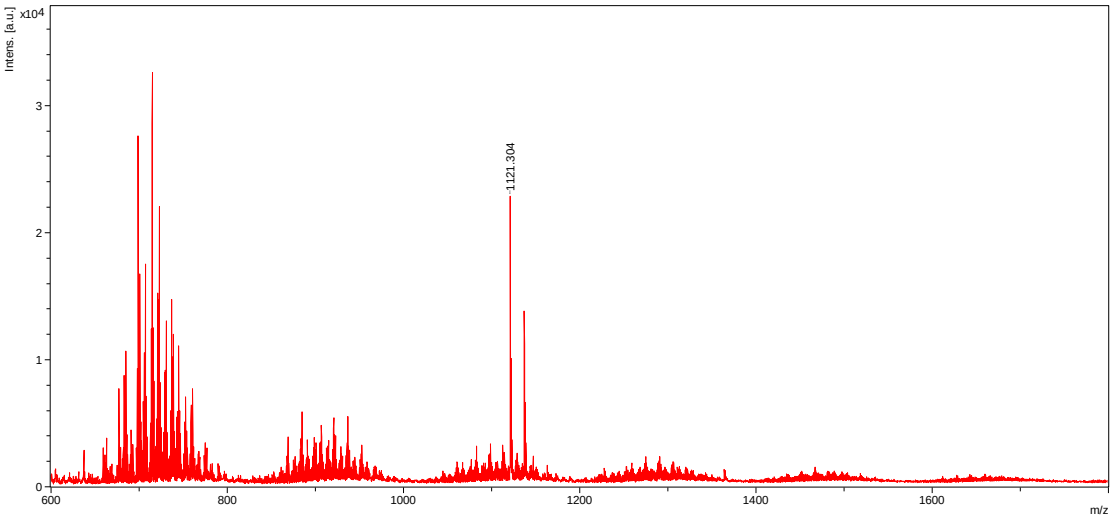


Fig E-91. The MALDI-TOF-MS result of PTC3

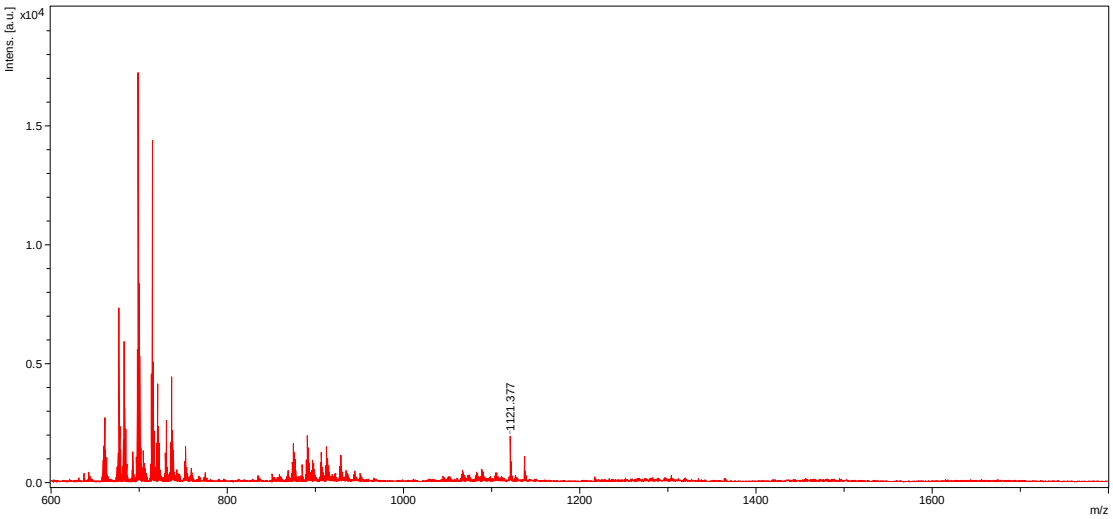


Fig E-92. The MALDI-TOF-MS result of PTC4

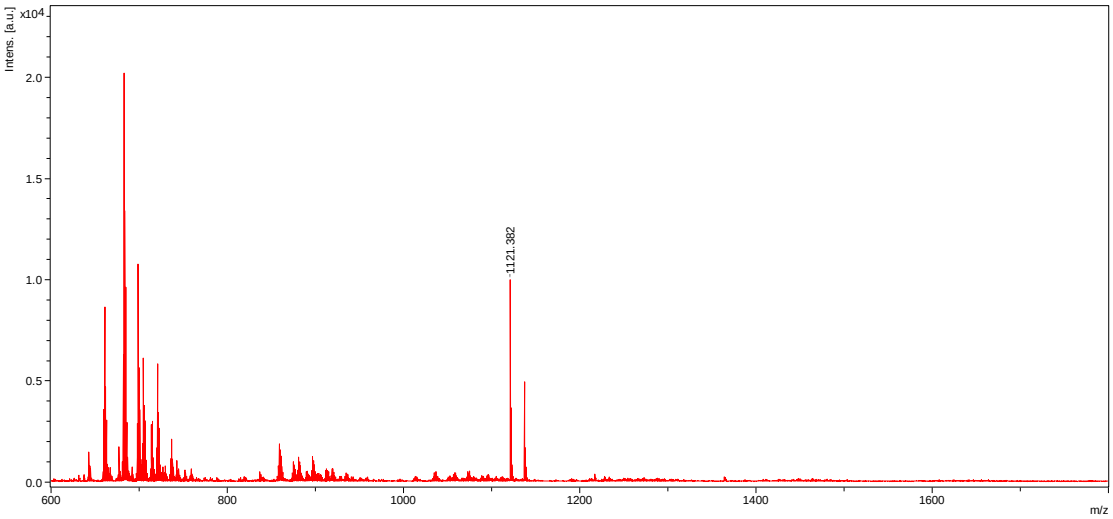


Fig E-93. The MALDI-TOF-MS result of PTC5

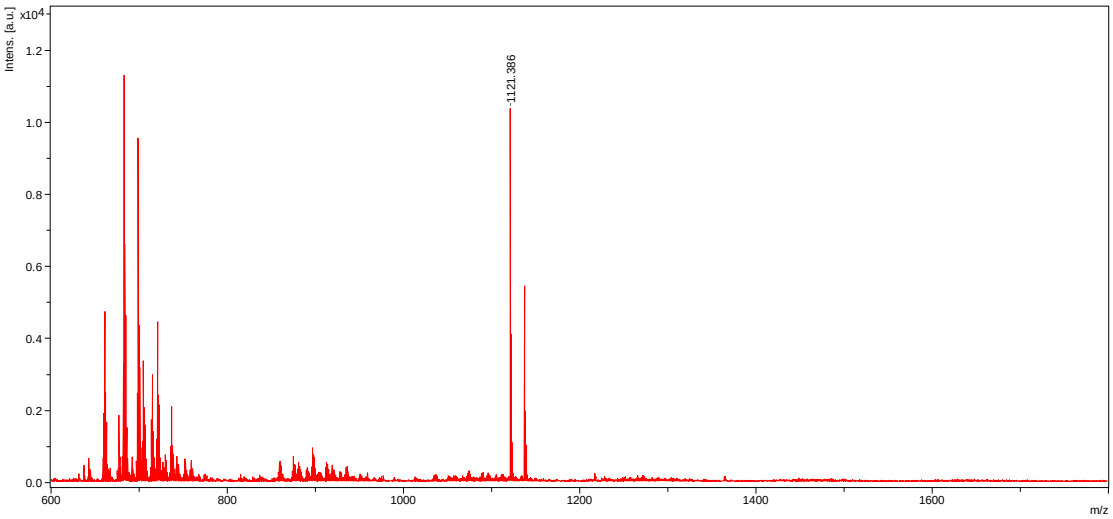


Fig E-94. The MALDI-TOF-MS result of PTC6

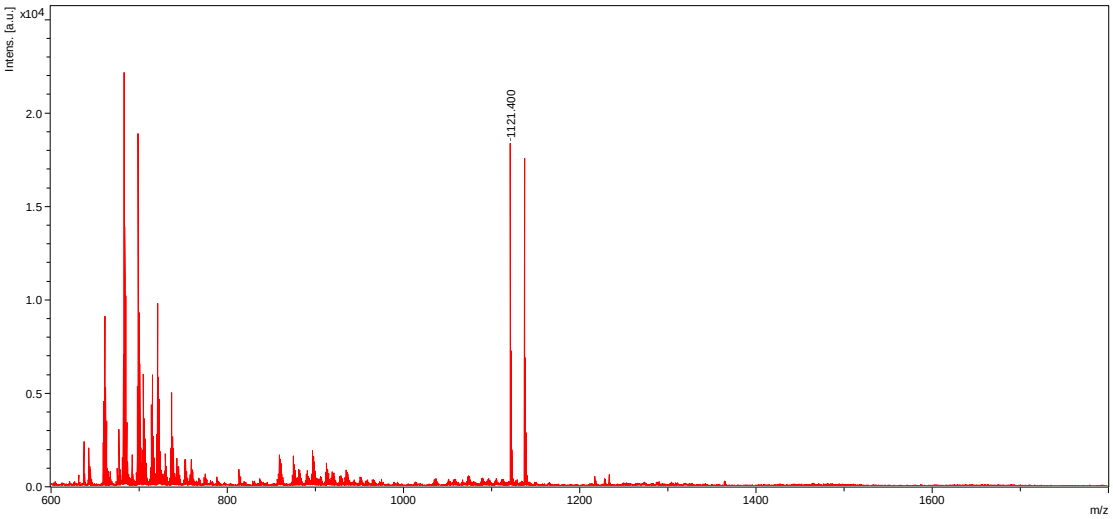


Fig E-95. The MALDI-TOF-MS result of PTC7

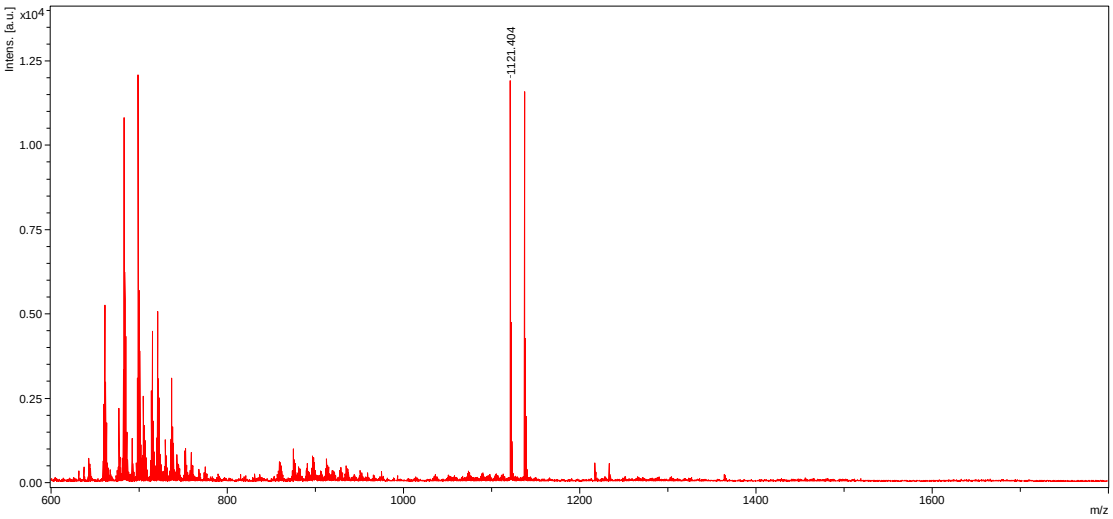


Fig E-96. The MALDI-TOF-MS result of PTC8

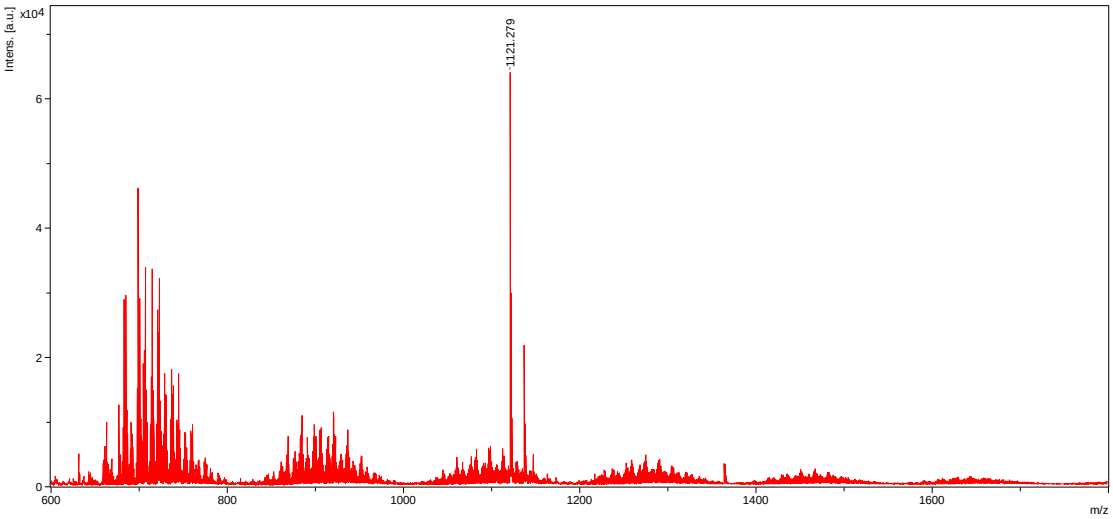


Fig E-97. The MALDI-TOF-MS result of XYGC1

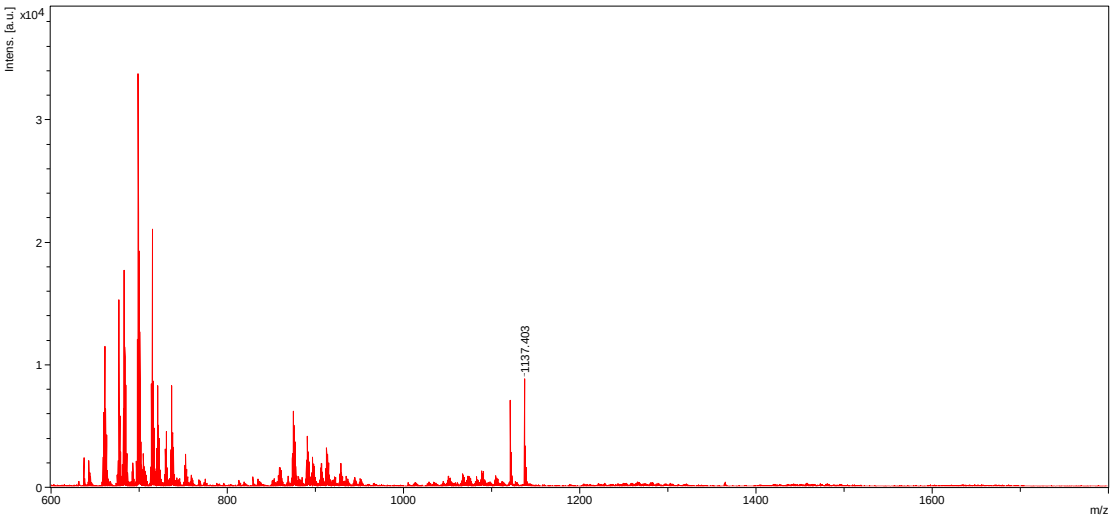


Fig E-98. The MALDI-TOF-MS result of XYGC2

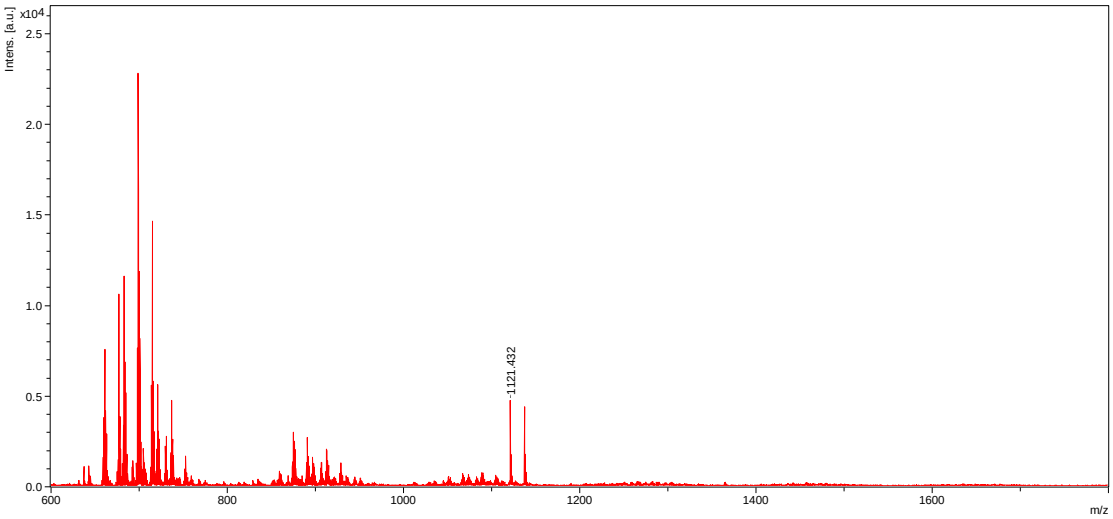


Fig E-99. The MALDI-TOF-MS result of XYGC3

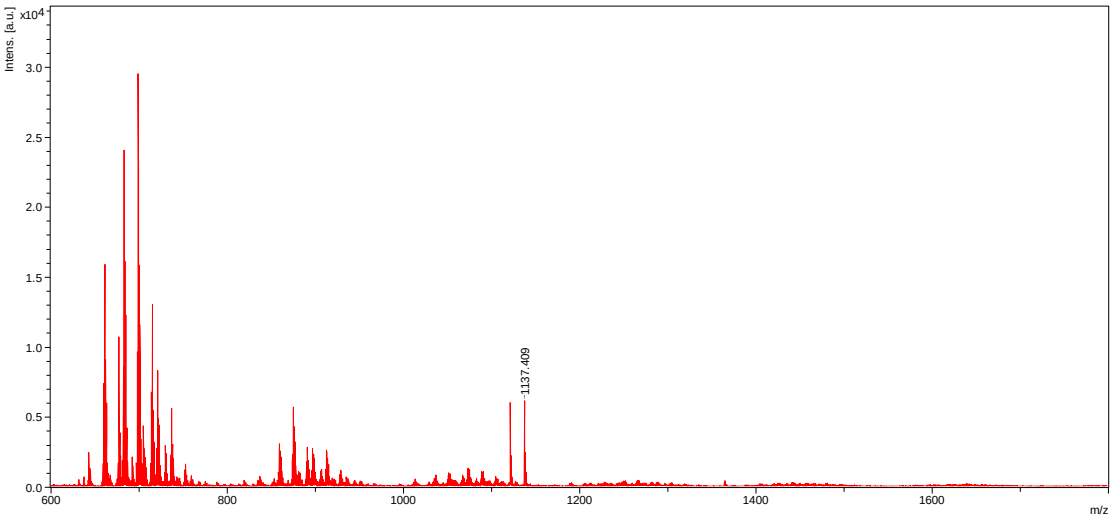


Fig E-100. The MALDI-TOF-MS result of XYGC4

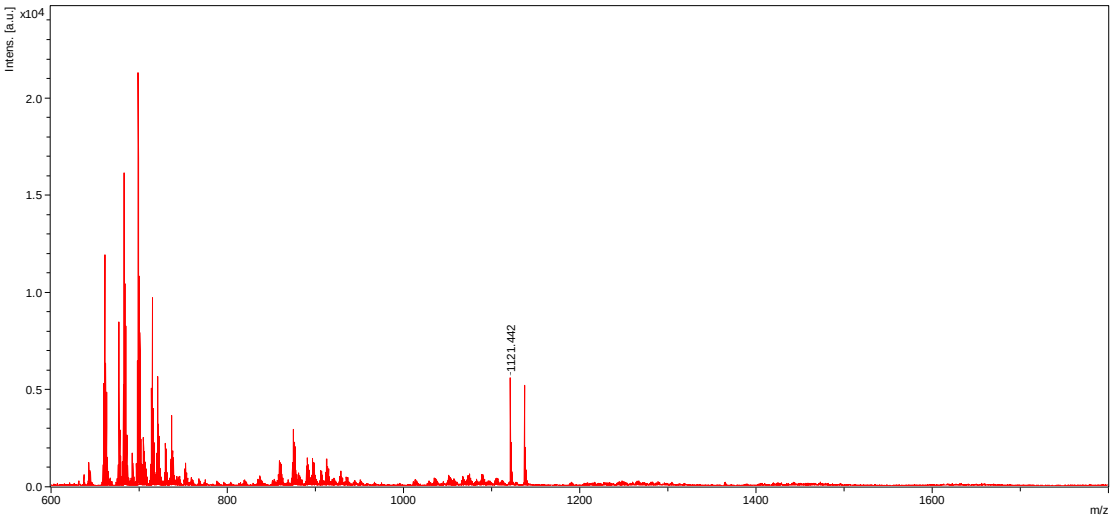


Fig E-101. The MALDI-TOF-MS result of XYGC5

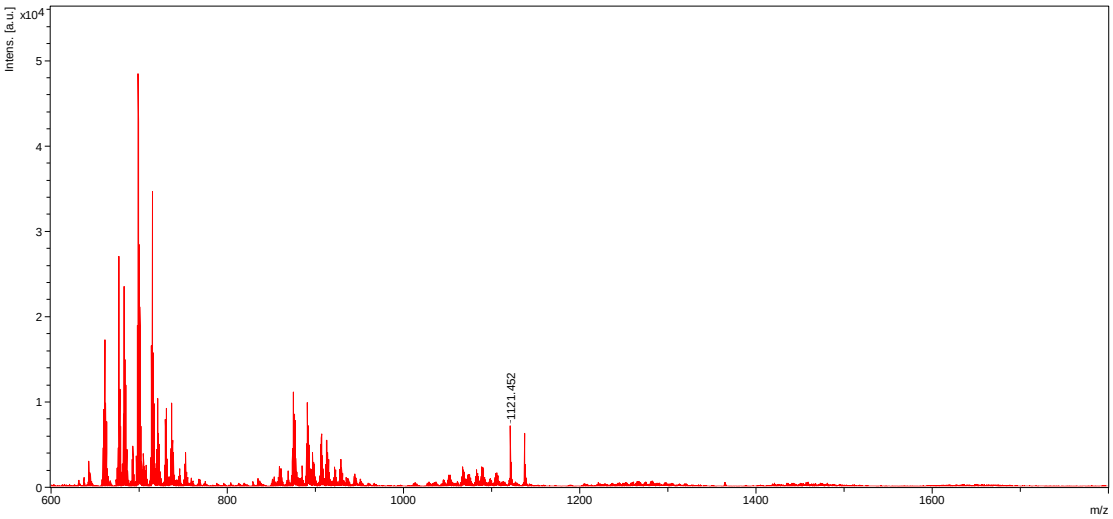


Fig E-102. The MALDI-TOF-MS result of XYGC6

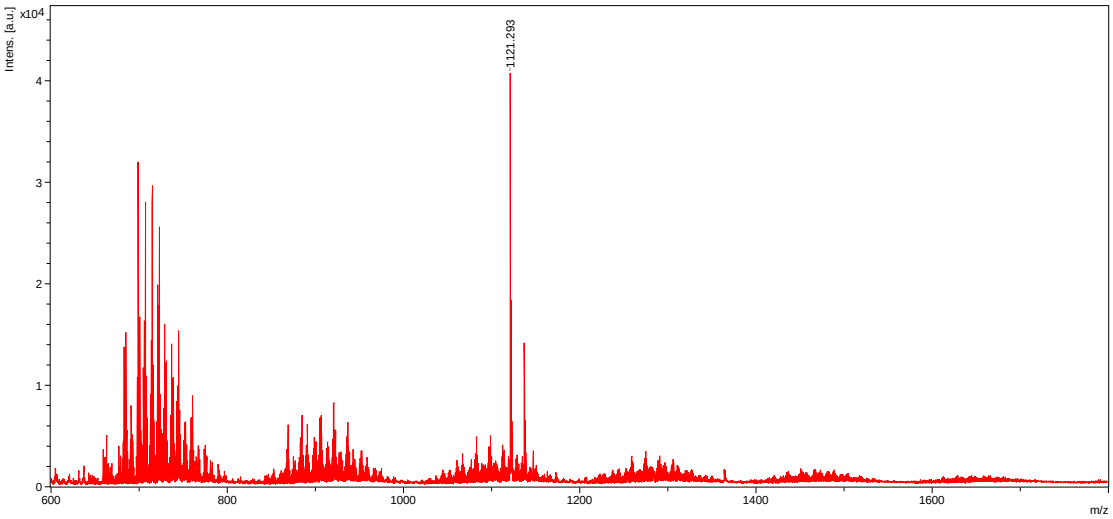


Fig E-103. The MALDI-TOF-MS result of XYGC7

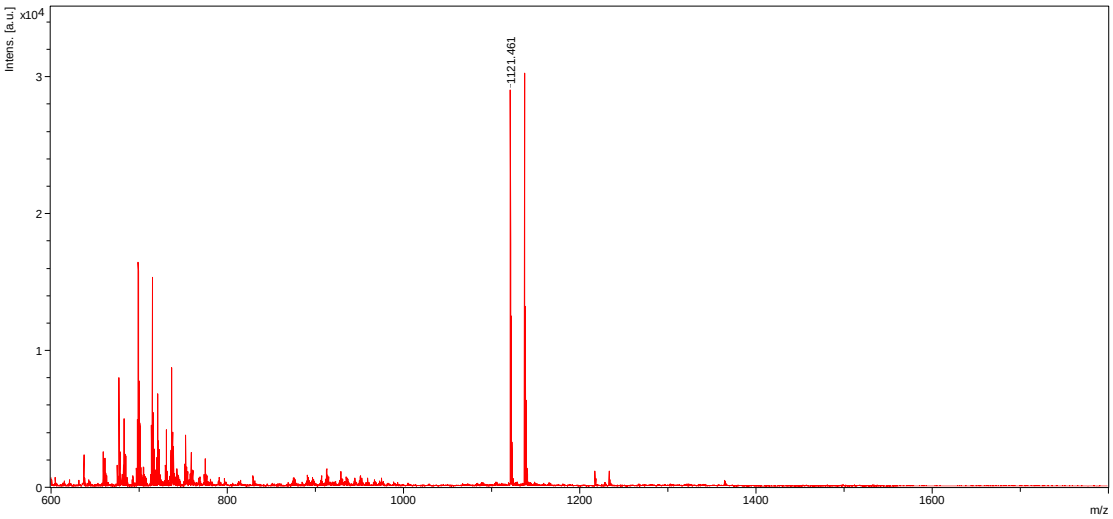


Fig E-104. The MALDI-TOF-MS result of SJYTL1

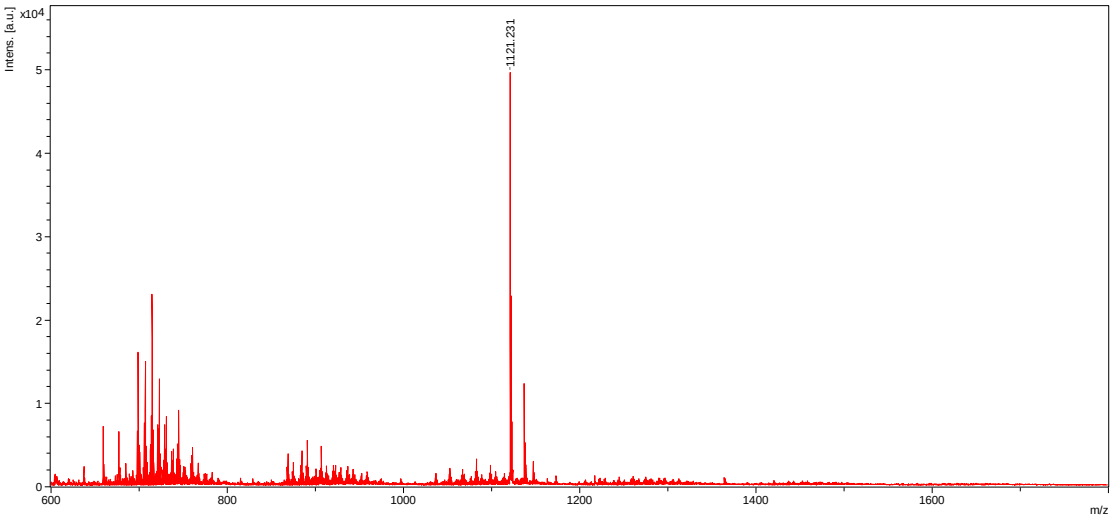


Fig E-105. The MALDI-TOF-MS result of SJYTL3

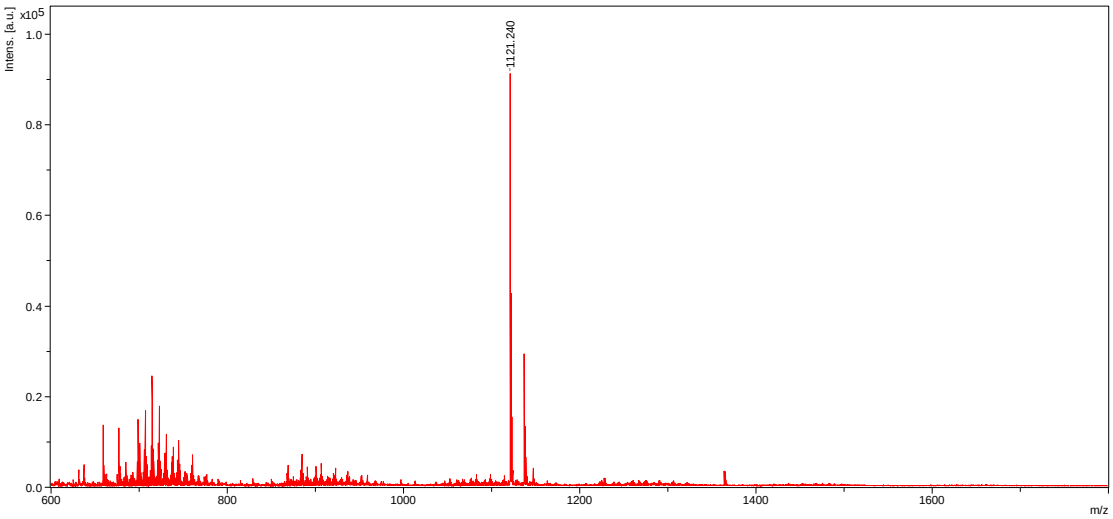


Fig E-106. The MALDI-TOF-MS result of SJYTL4

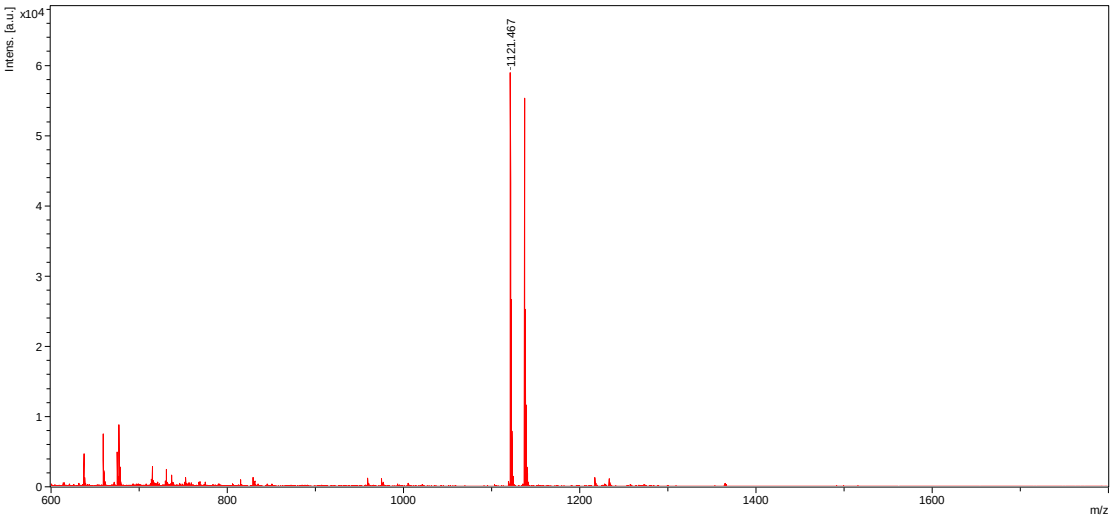


Fig E-107. The MALDI-TOF-MS result of SJYTL5

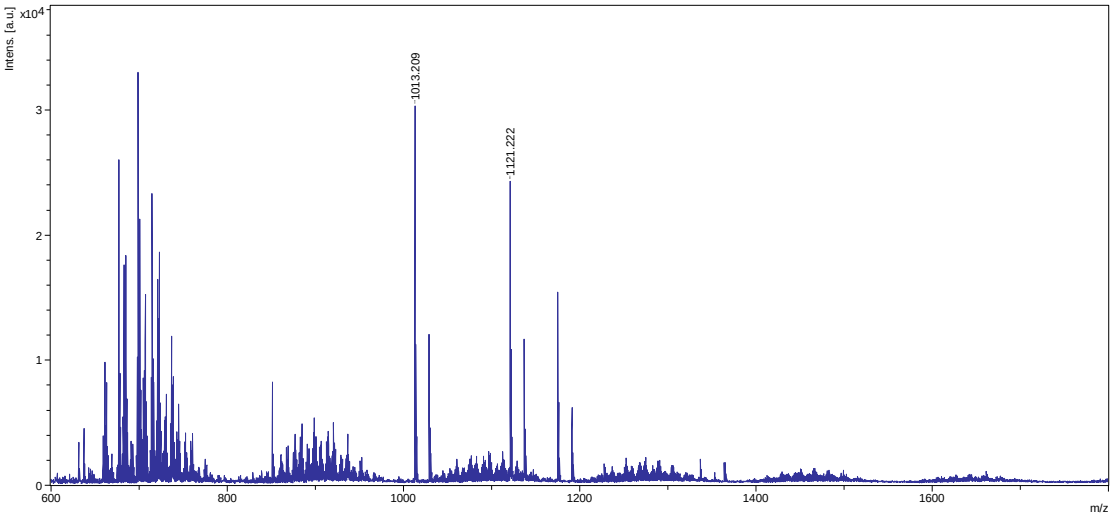


Fig E-108. The MALDI-TOF-MS result of HYPT1

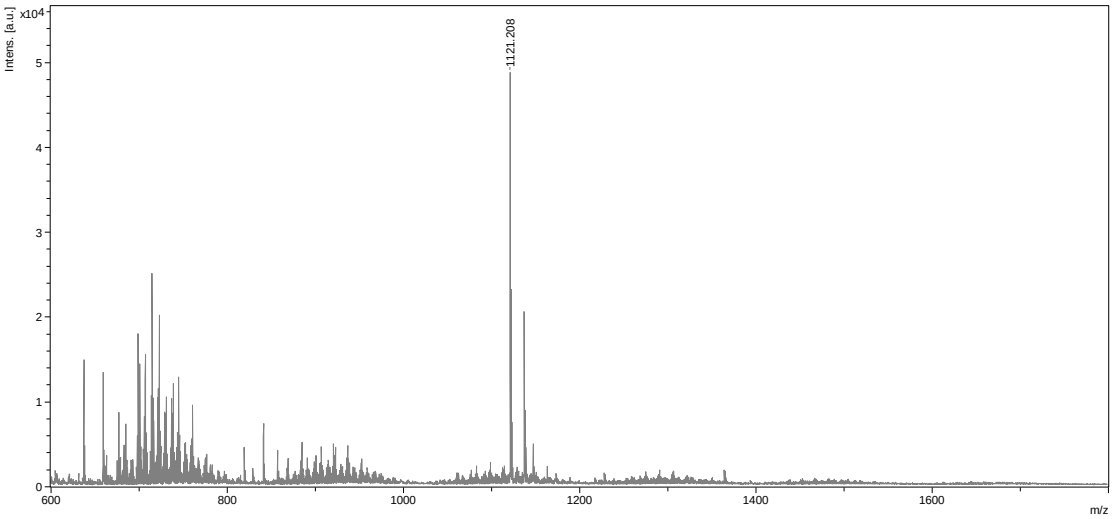


Fig E-109. The MALDI-TOF-MS result of HYPT-B1

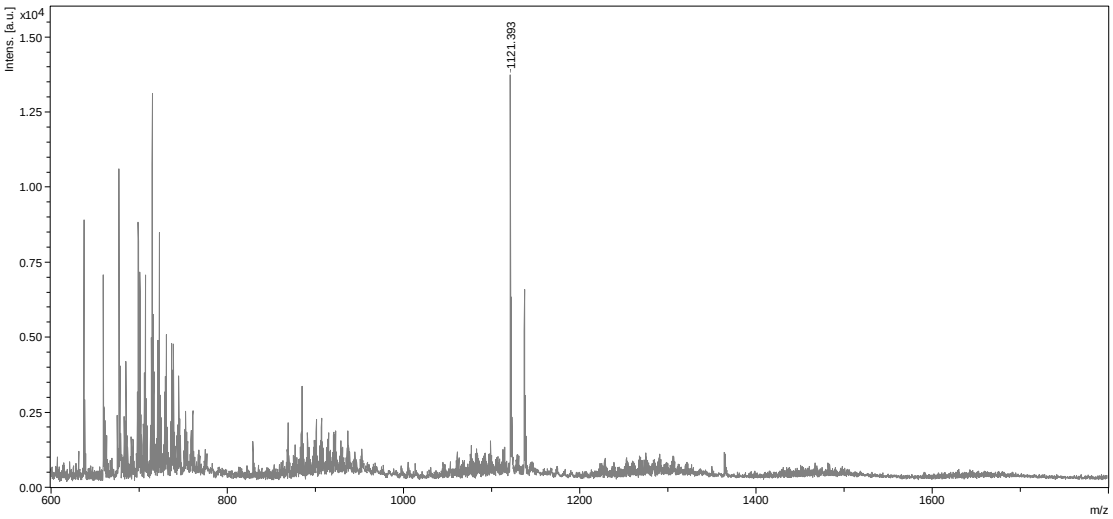


Fig E-110. The MALDI-TOF-MS result of HYPT-B2

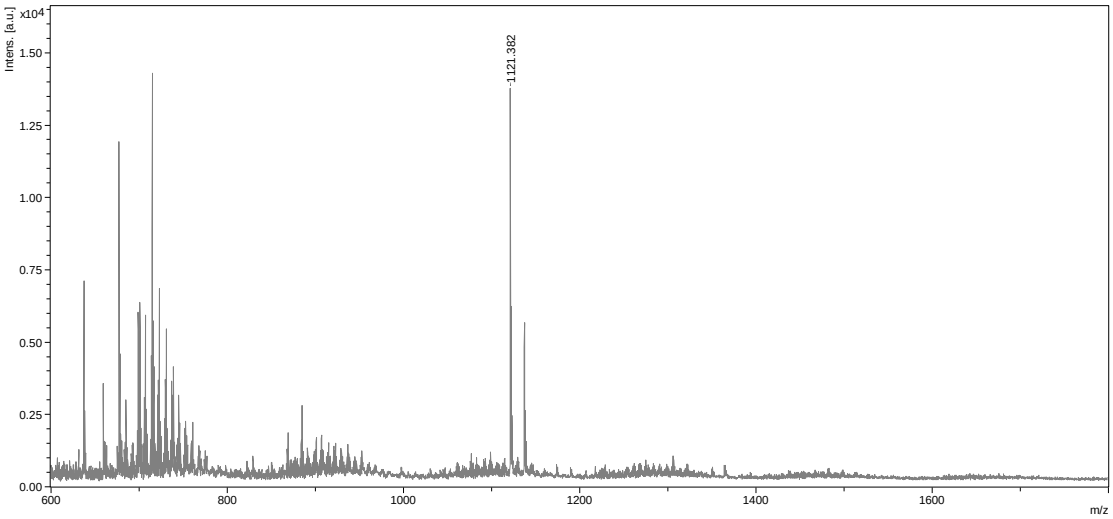


Fig E-111. The MALDI-TOF-MS result of HYPT-B3

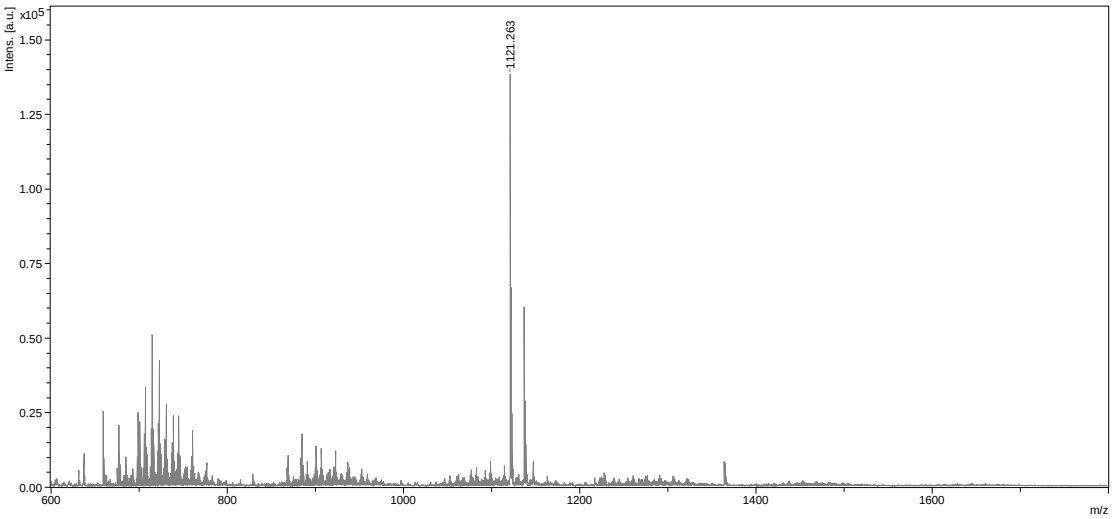


Fig E-112. The MALDI-TOF-MS result of JYPT-B1

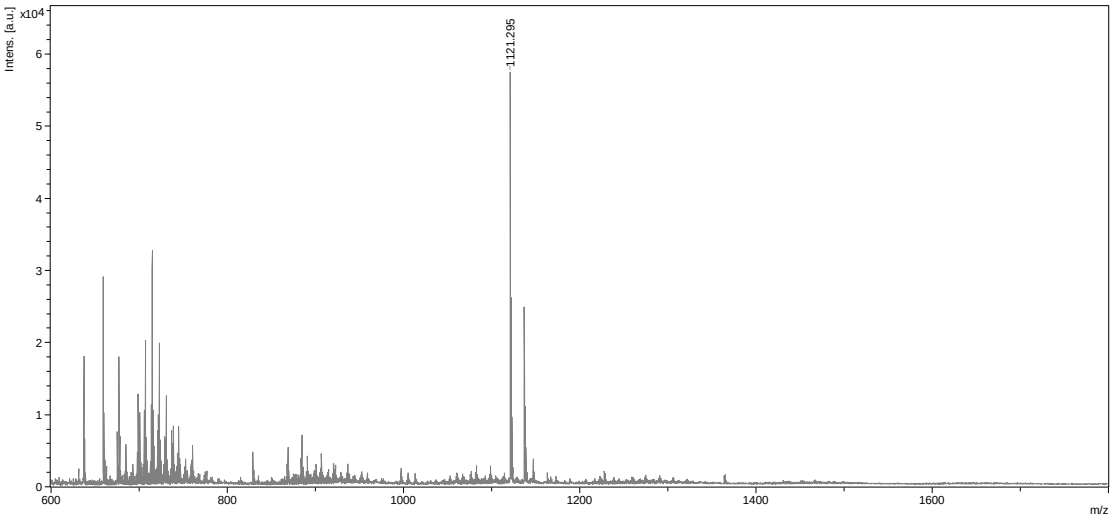


Fig E-113. The MALDI-TOF-MS result of JYPT-B2

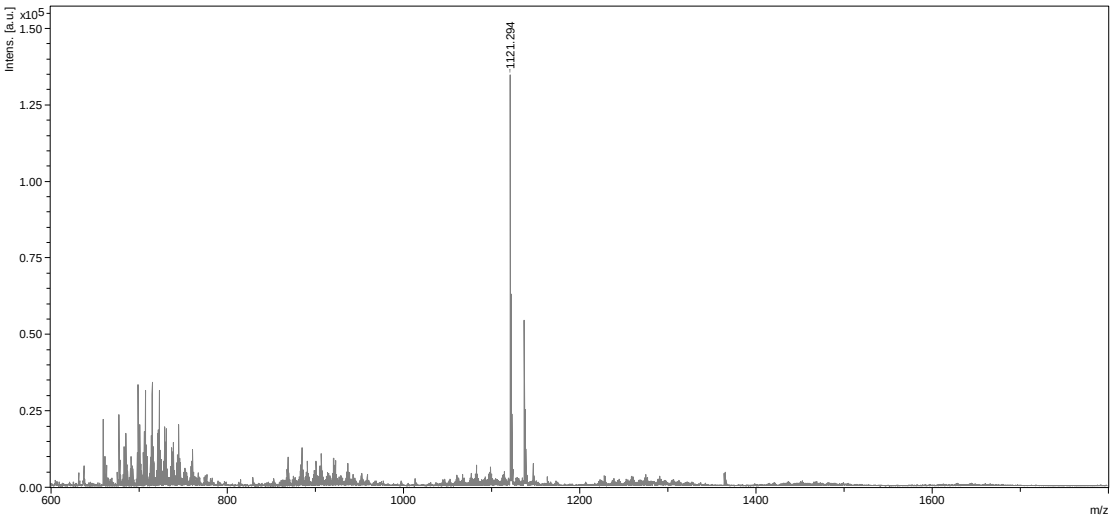


Fig E-114. The MALDI-TOF-MS result of JYPT-B3

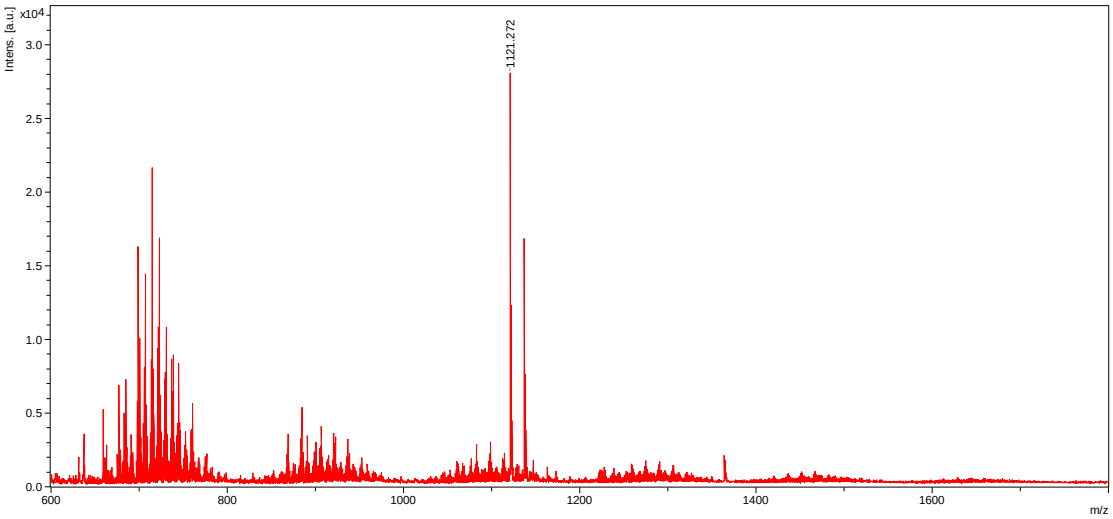


Fig E-115. The MALDI-TOF-MS result of ZZSC1

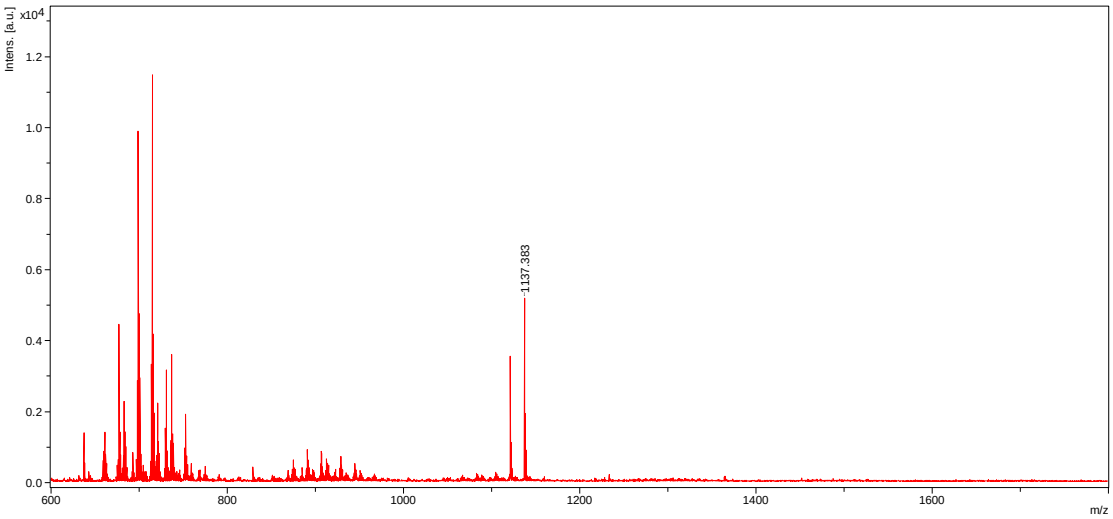


Fig E-116. The MALDI-TOF-MS result of ZZSC2

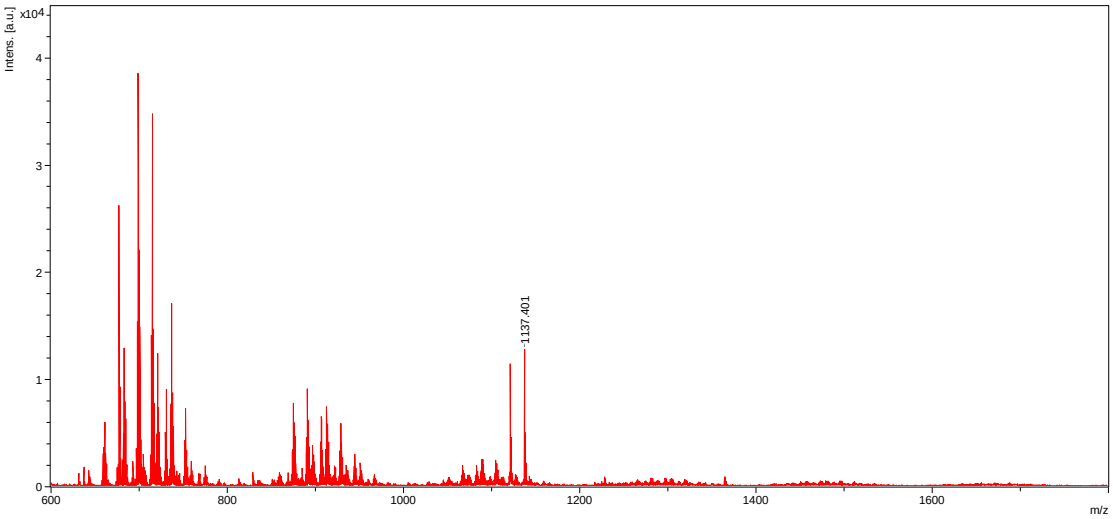


Fig E-117. The MALDI-TOF-MS result of ZZSC3

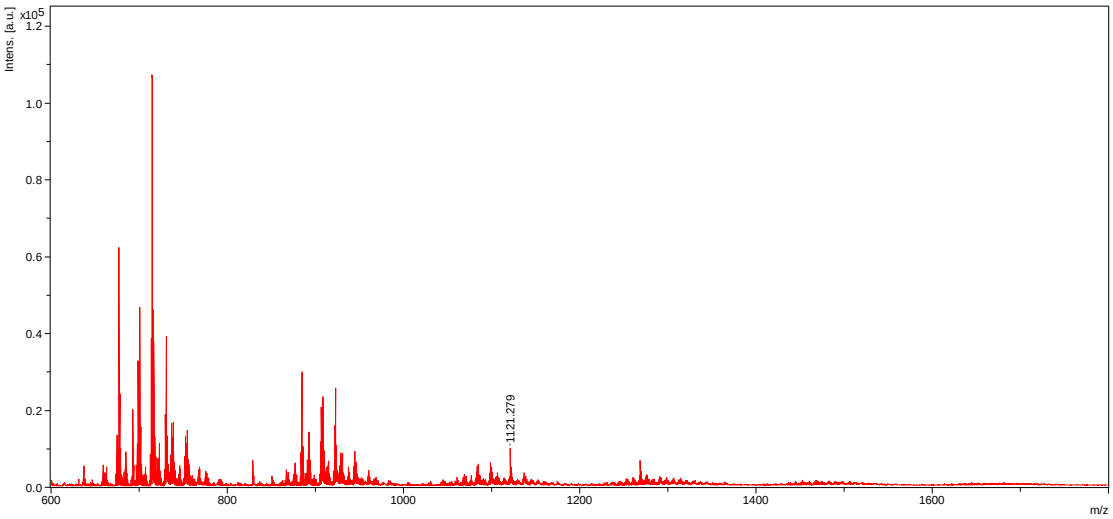


Fig E-118. The MALDI-TOF-MS result of HNZZ1

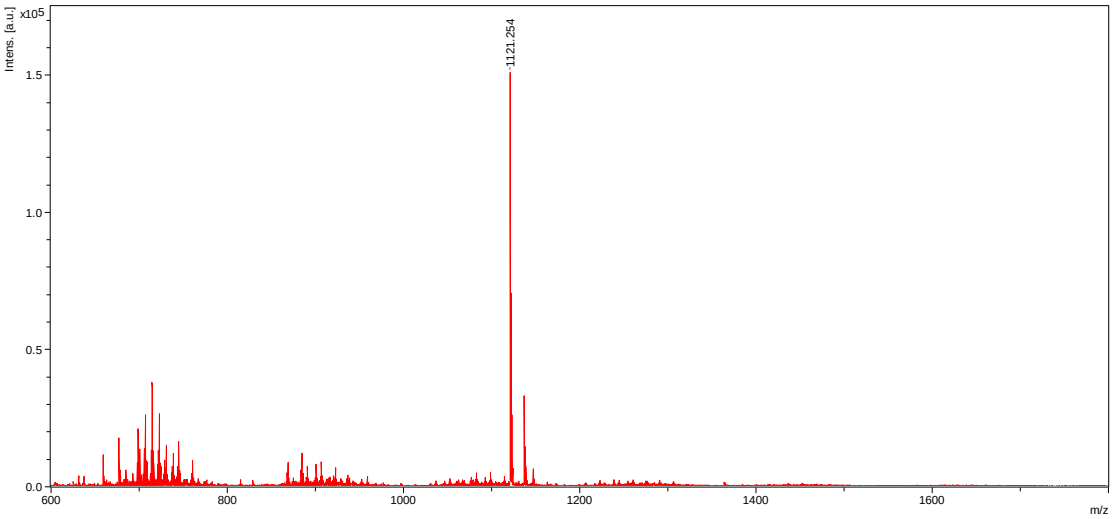


Fig E-119. The MALDI-TOF-MS result of BMD1

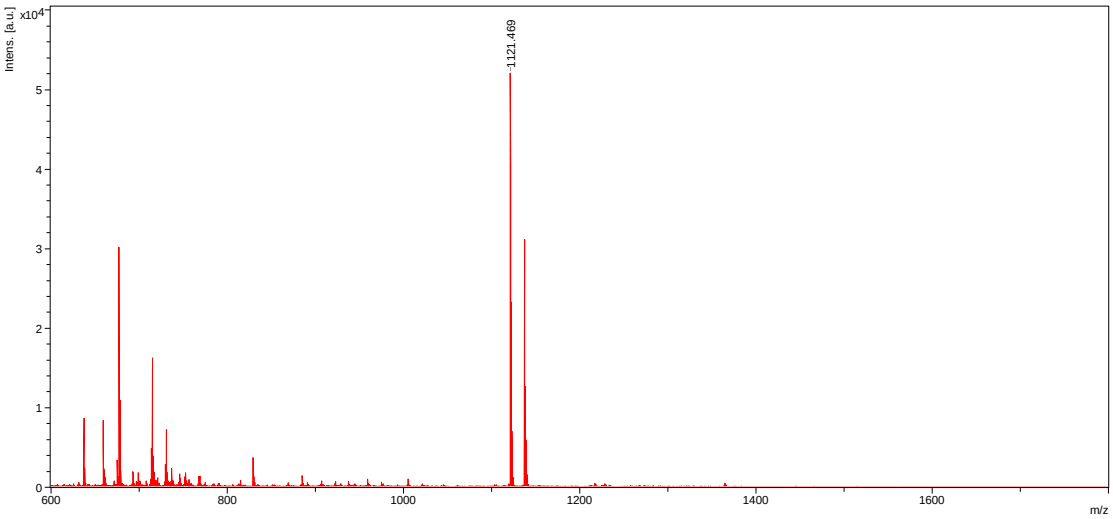


Fig E-120. The MALDI-TOF-MS result of BMD2

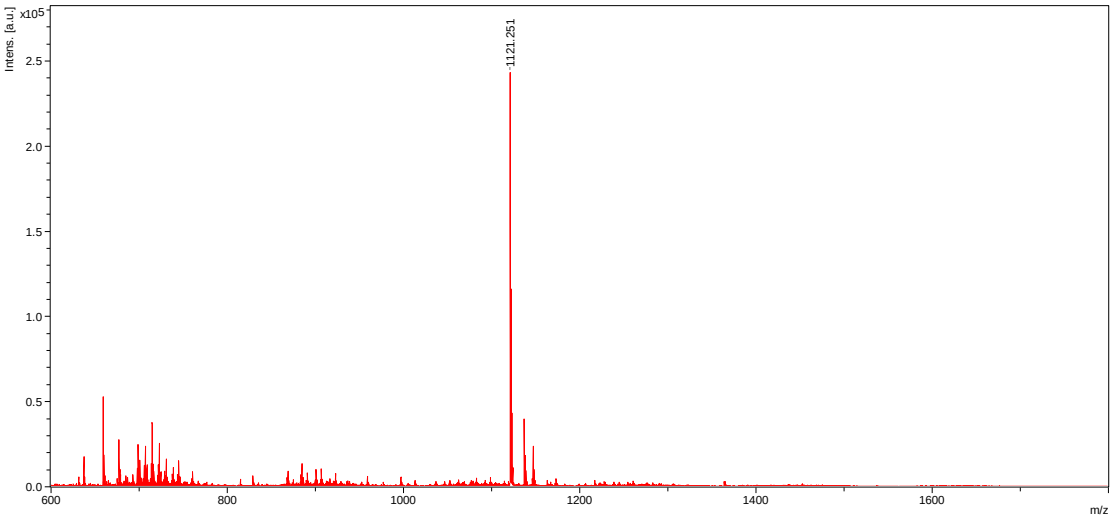


Fig E-121. The MALDI-TOF-MS result of BMD3

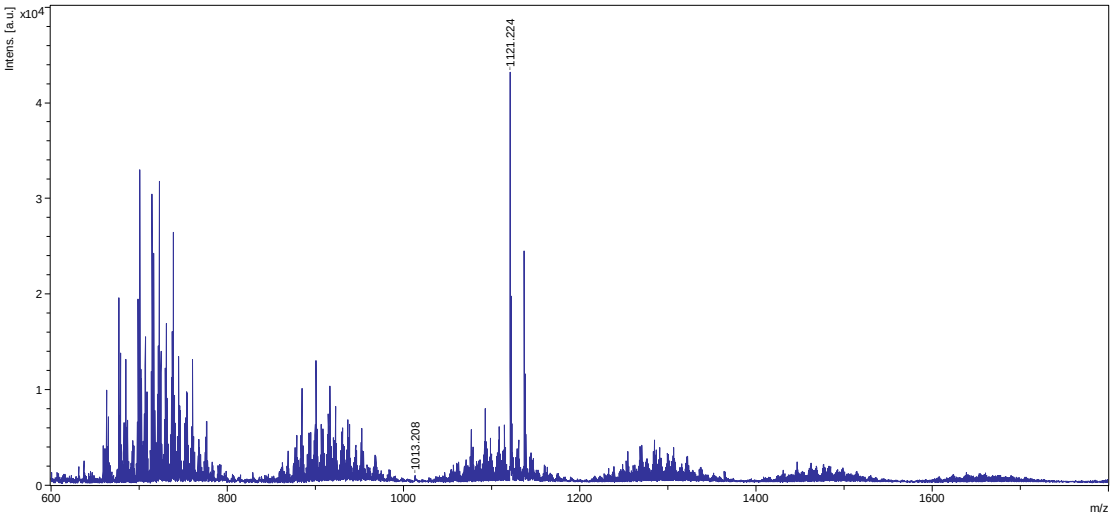


Fig E-122. The MALDI-TOF-MS result of TFGPT1

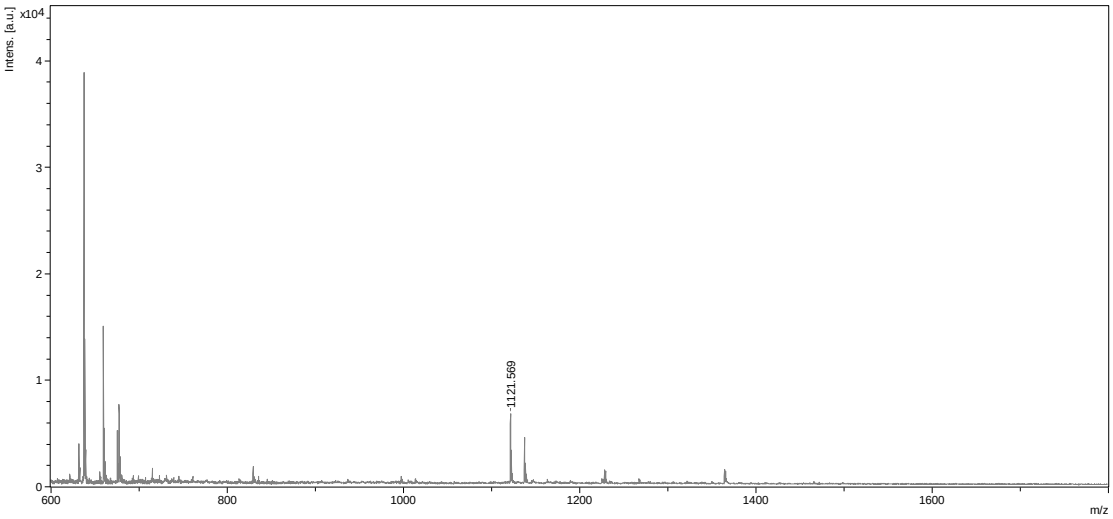


Fig E-123. The MALDI-TOF-MS result of TFGPT-B1

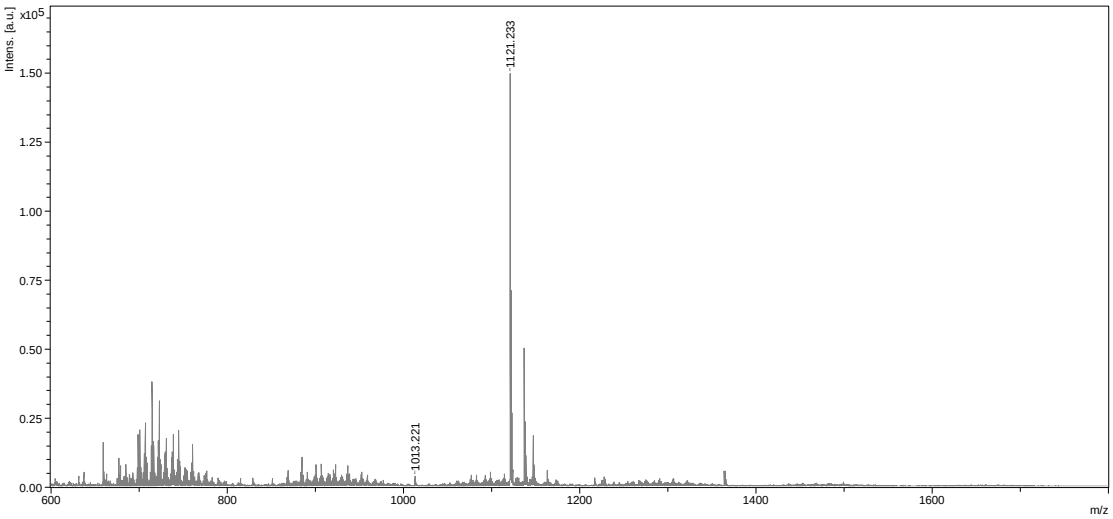


Fig E-124. The MALDI-TOF-MS result of NWPT-B1

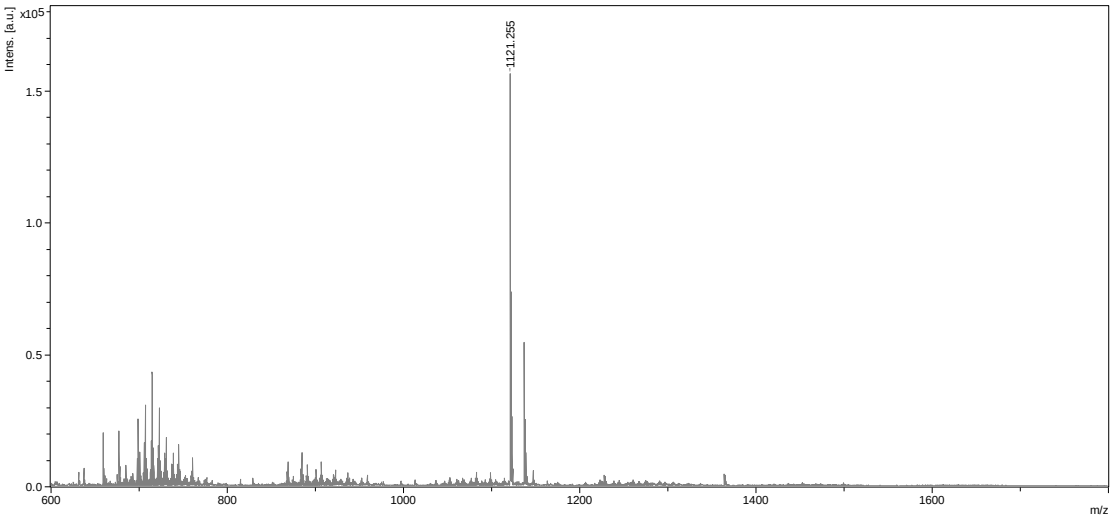


Fig E-125. The MALDI-TOF-MS result of NWPT-B2

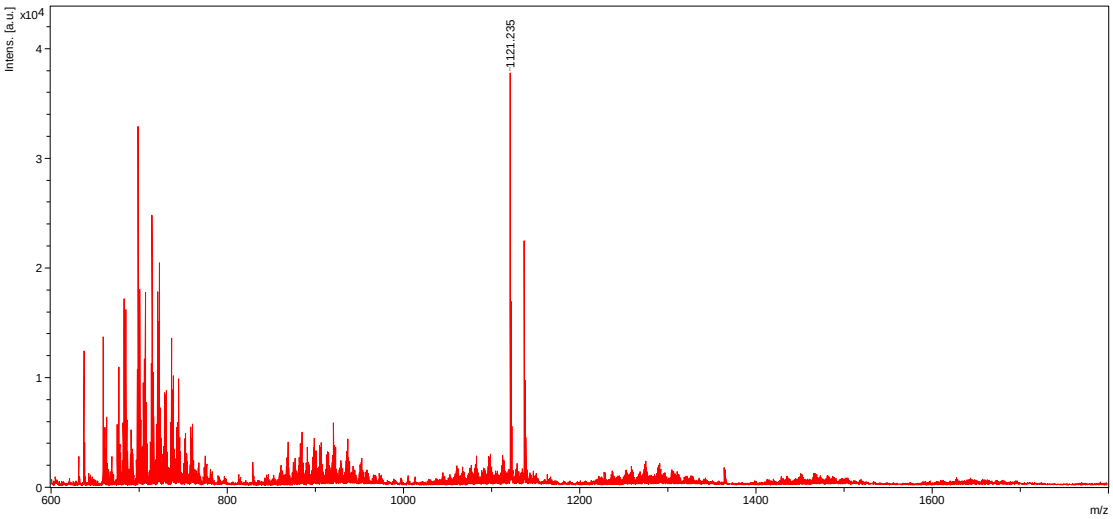


Fig E-126. The MALDI-TOF-MS result of QL1

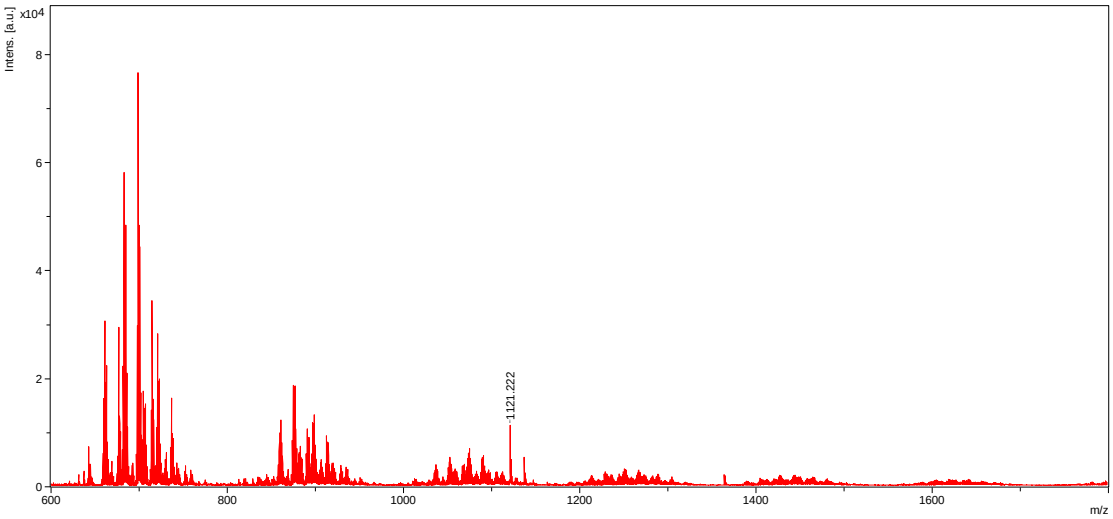


Fig E-127. The MALDI-TOF-MS result of YMY1

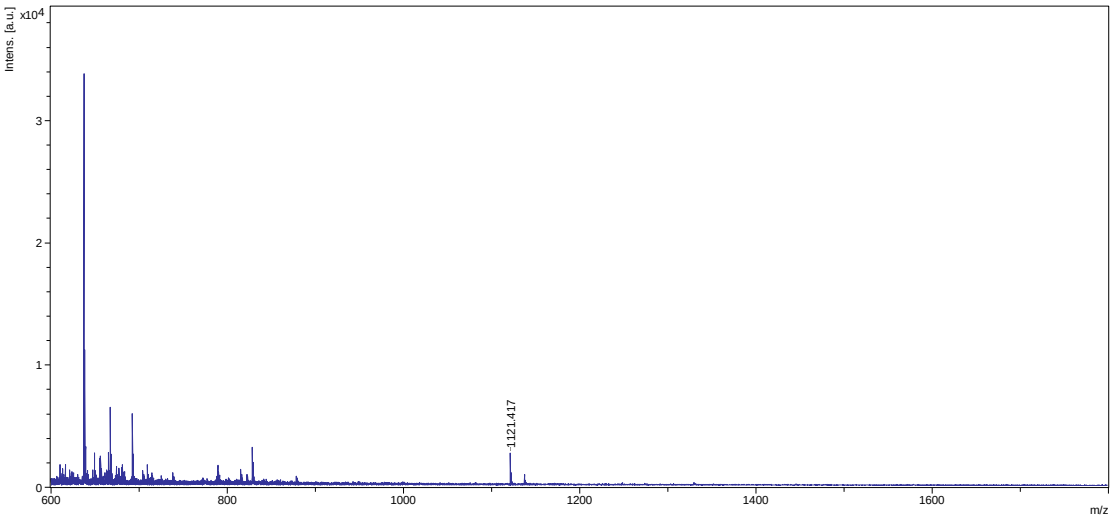


Fig E-128. The MALDI-TOF-MS result of QZCQ1

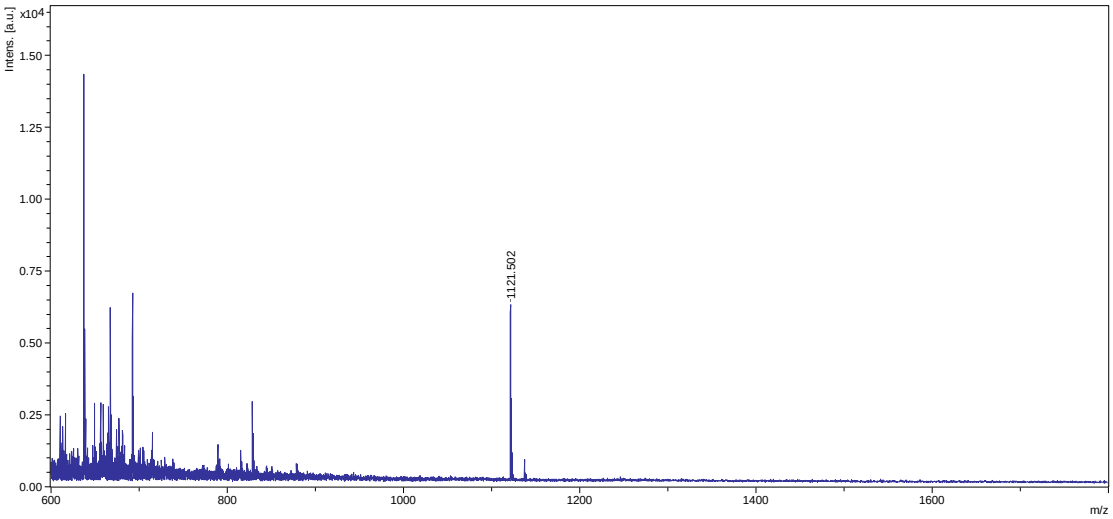


Fig E-129. The MALDI-TOF-MS result of ZDBM1

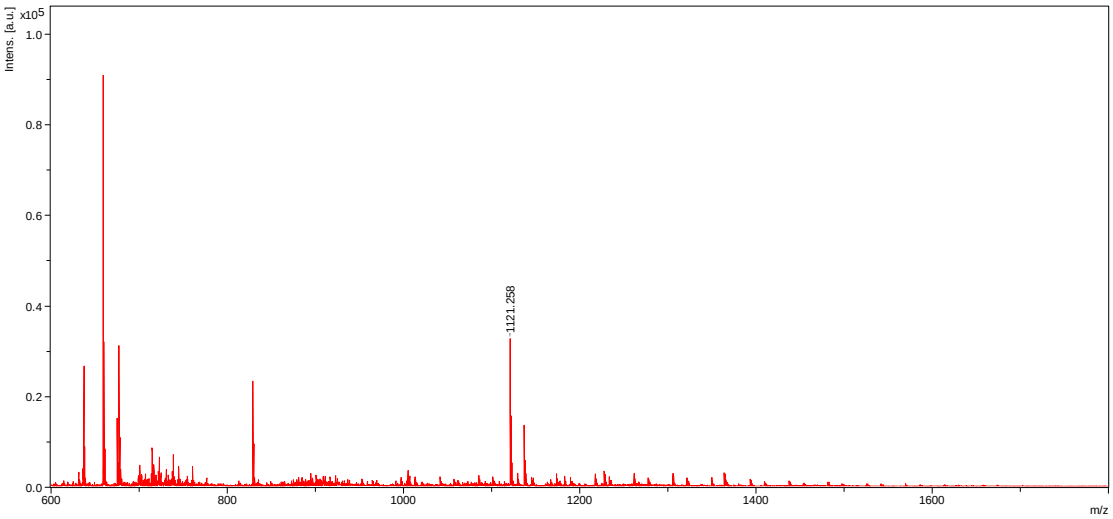


Fig E-130. The MALDI-TOF-MS result of WC1

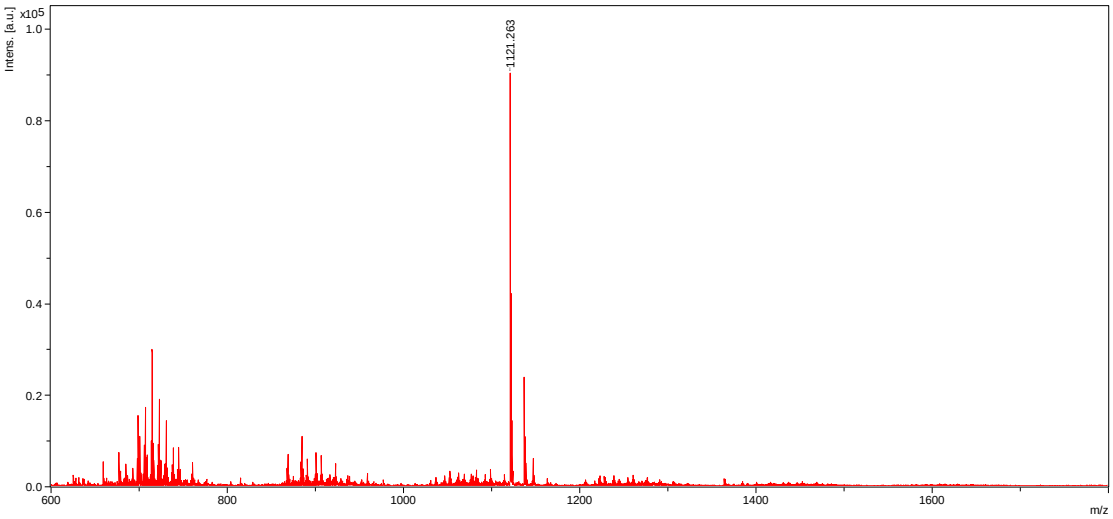


Fig E-131. The MALDI-TOF-MS result of WC2

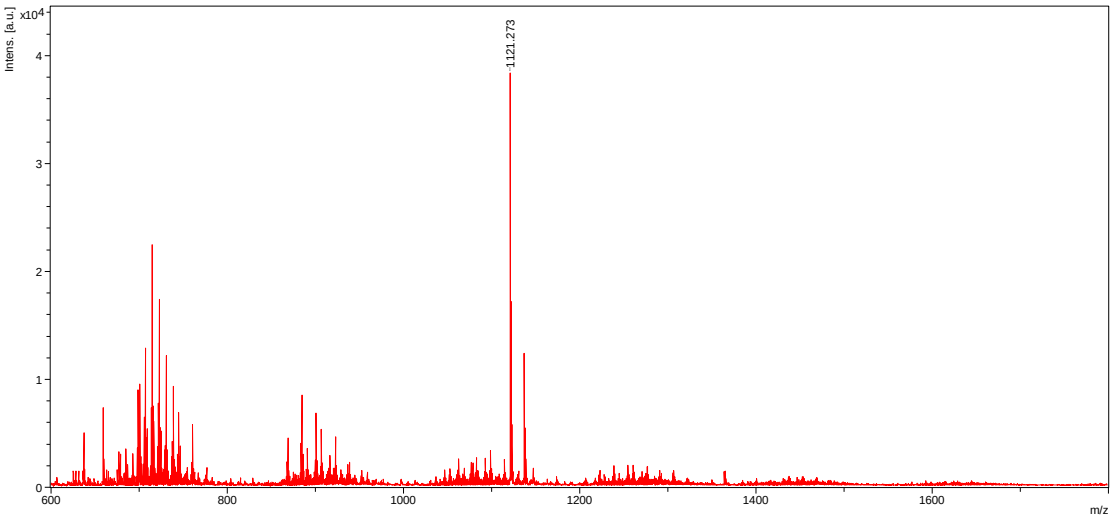


Fig E-132. The MALDI-TOF-MS result of WC3

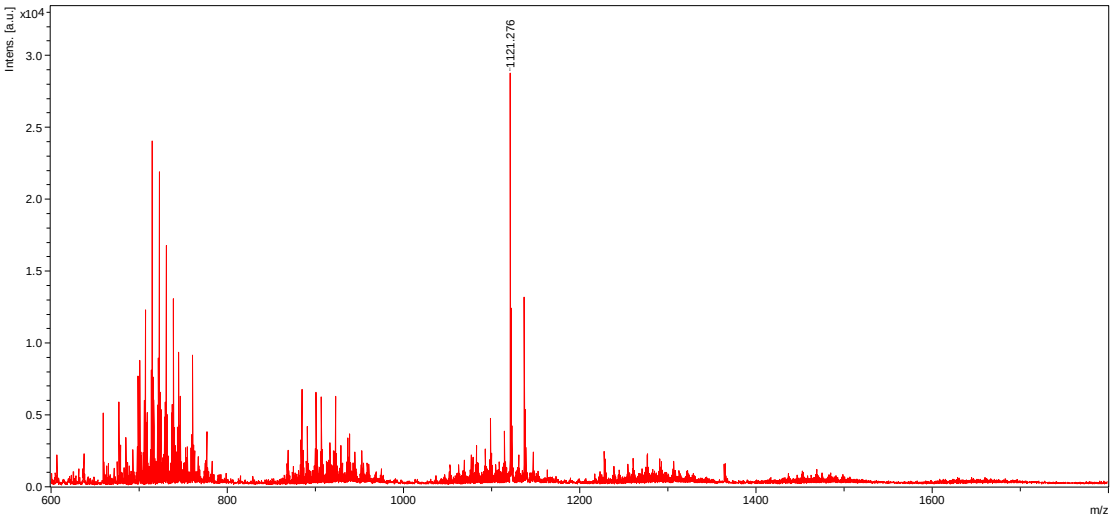


Fig E-133. The MALDI-TOF-MS result of WC4

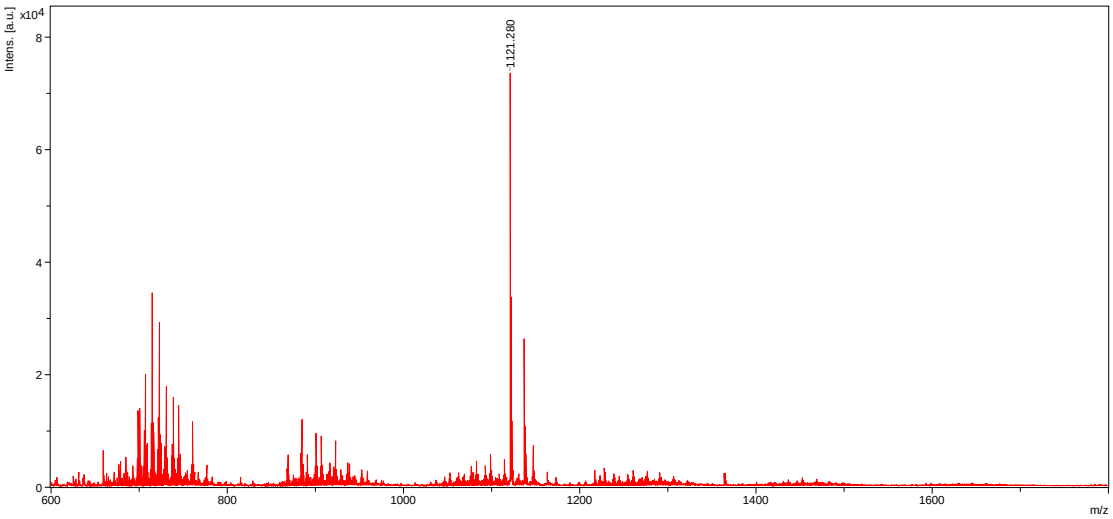


Fig E-134. The MALDI-TOF-MS result of WC5

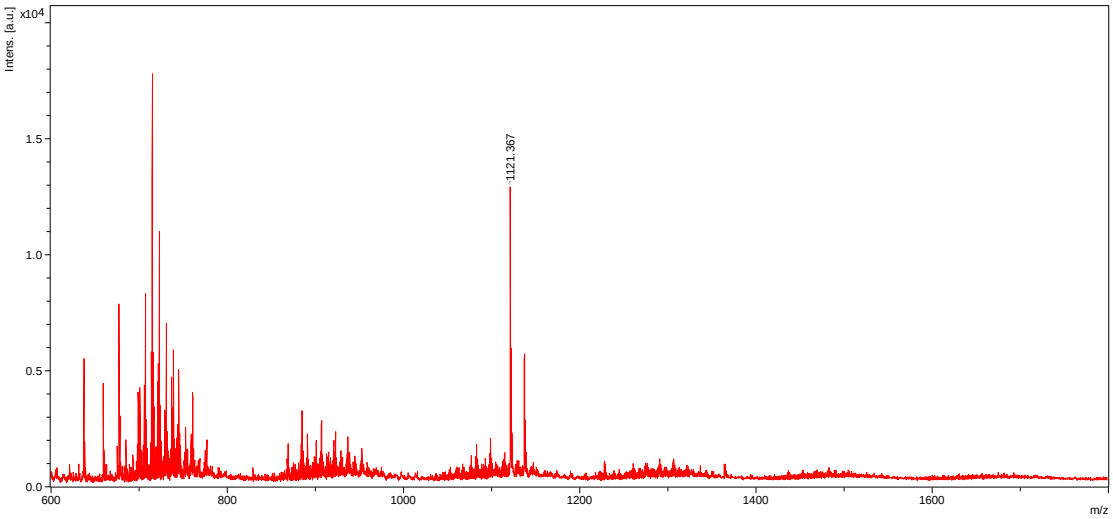


Fig E-135. The MALDI-TOF-MS result of ZWC1

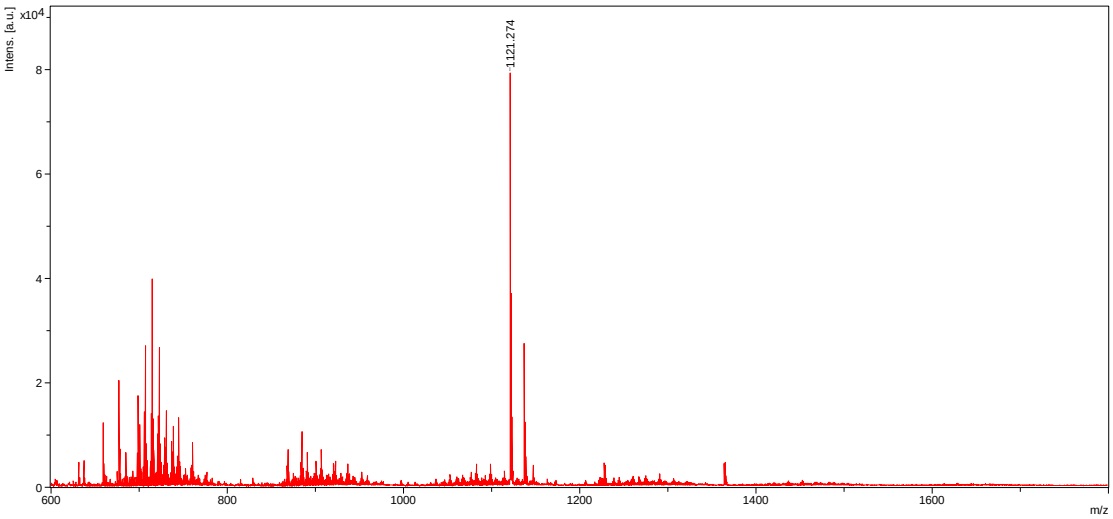


Fig E-136. The MALDI-TOF-MS result of ZWC2

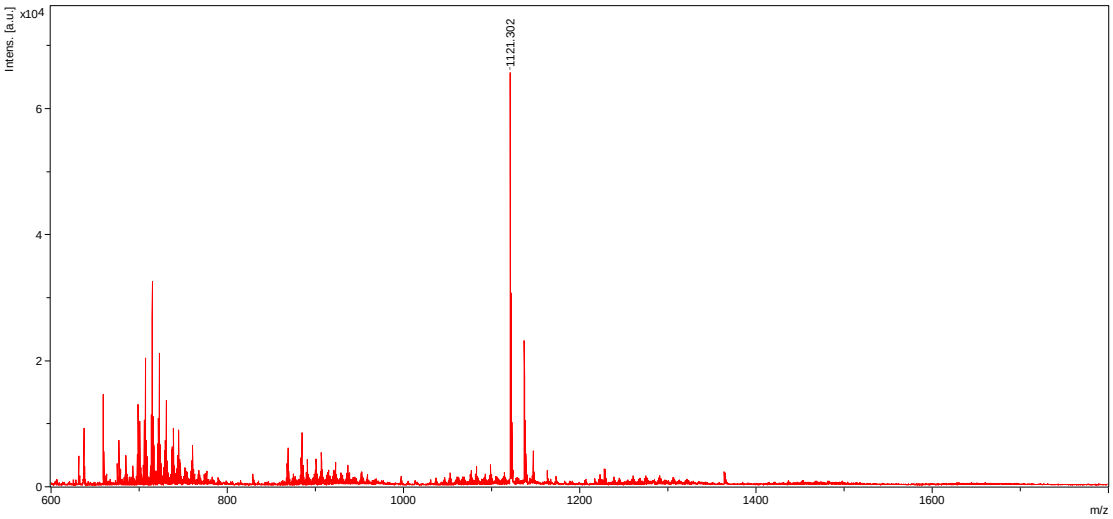


Fig E-137. The MALDI-TOF-MS result of ZWC3

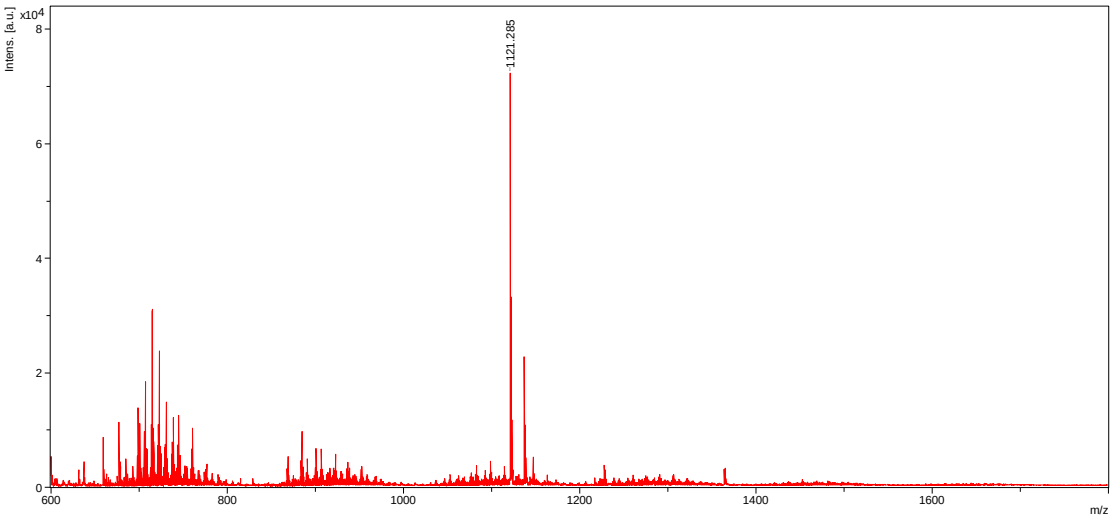


Fig E-138. The MALDI-TOF-MS result of ZWC4

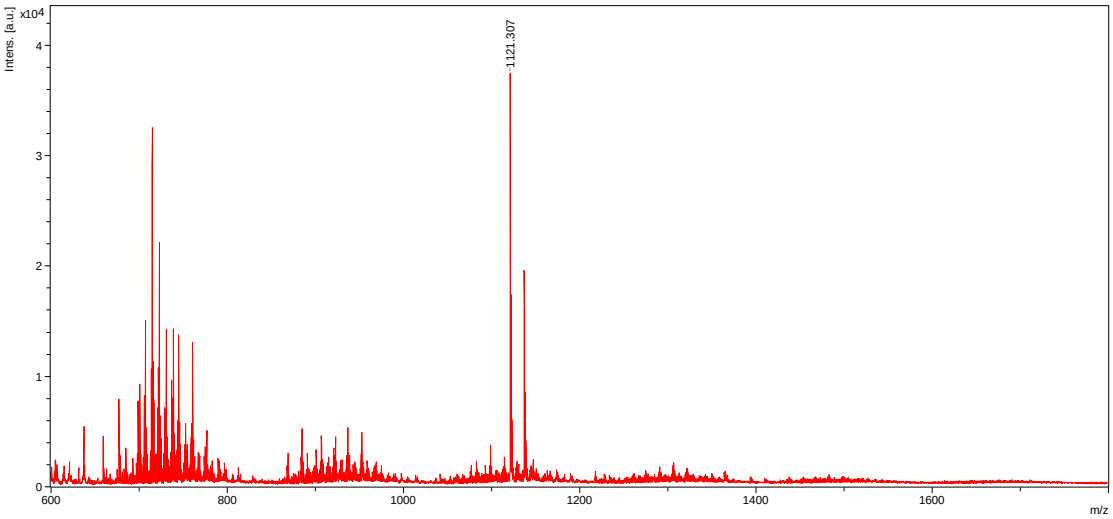


Fig E-139. The MALDI-TOF-MS result of ZWC5

Appendix 6. LC-MS/MS results

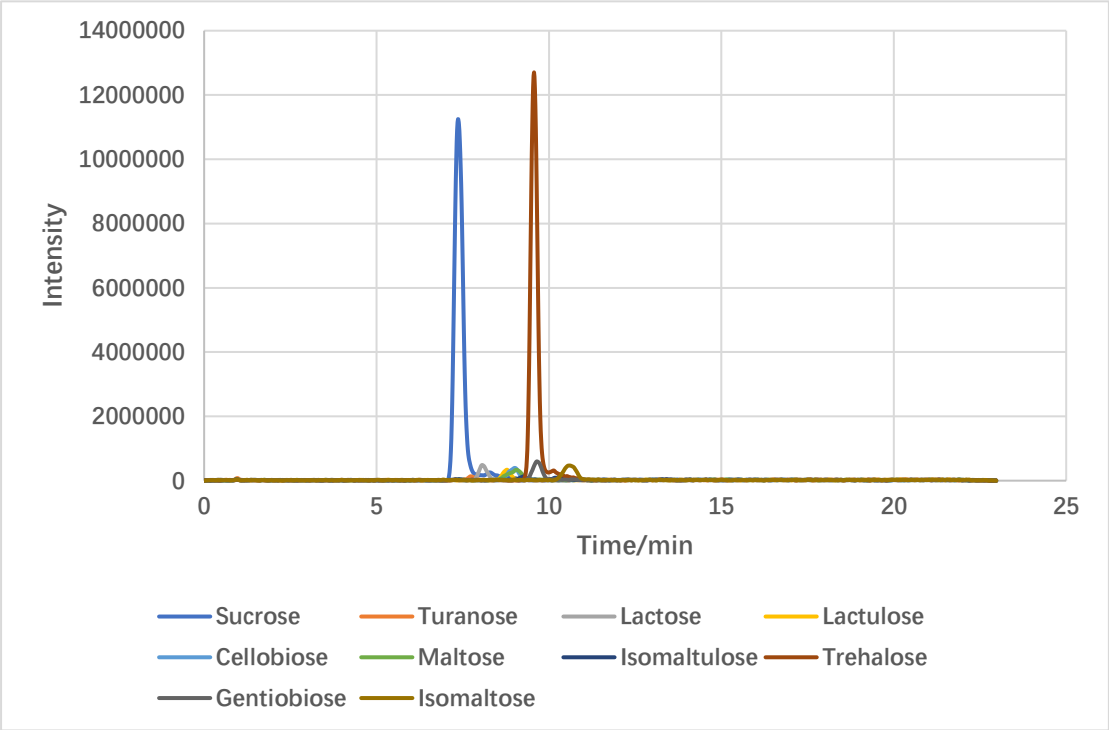


Fig F-1. The LC result of disaccharide standards

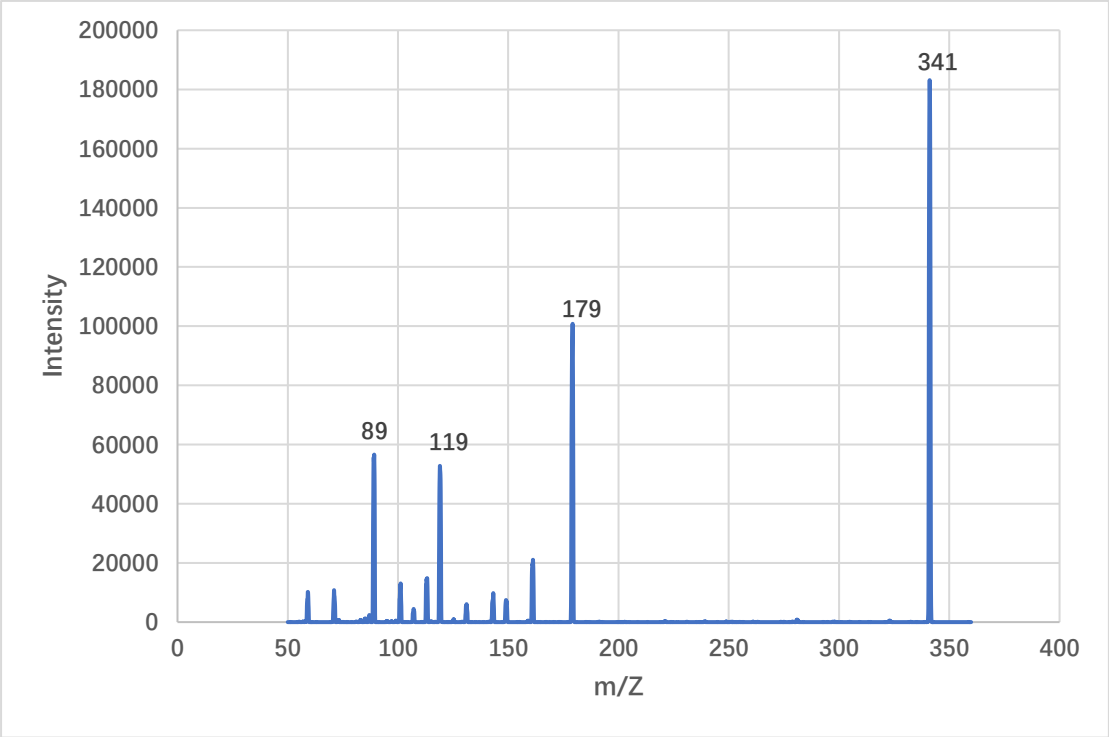


Fig F-2. The MS/MS result of Trehalose

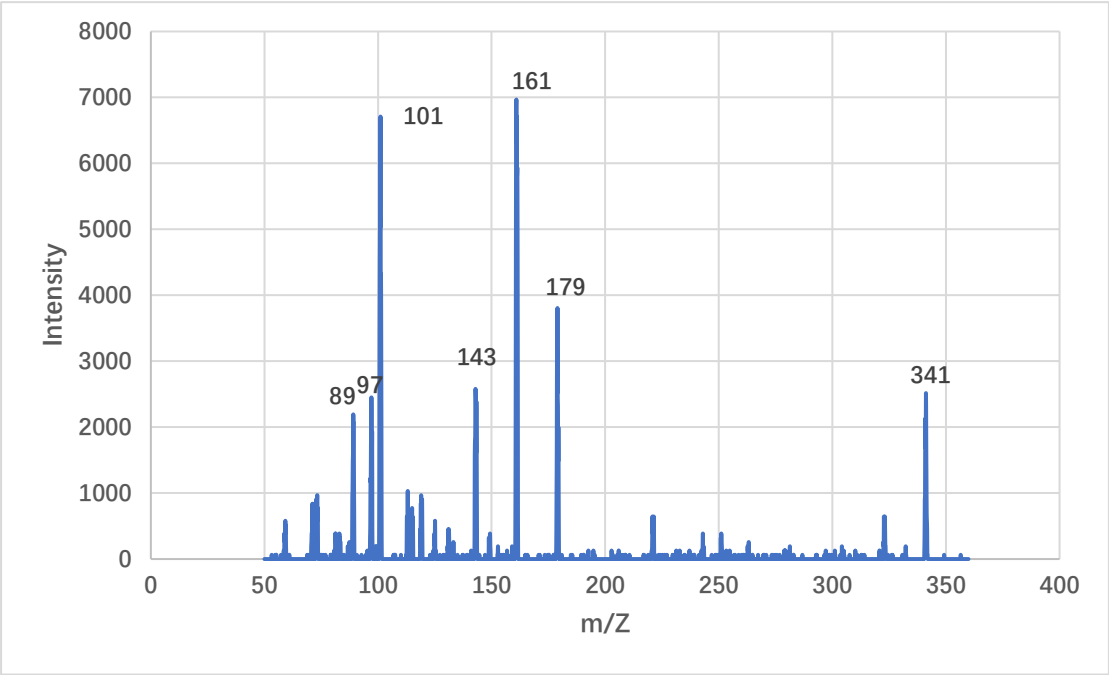


Fig F-3. The MS/MS result of Gentiobiose

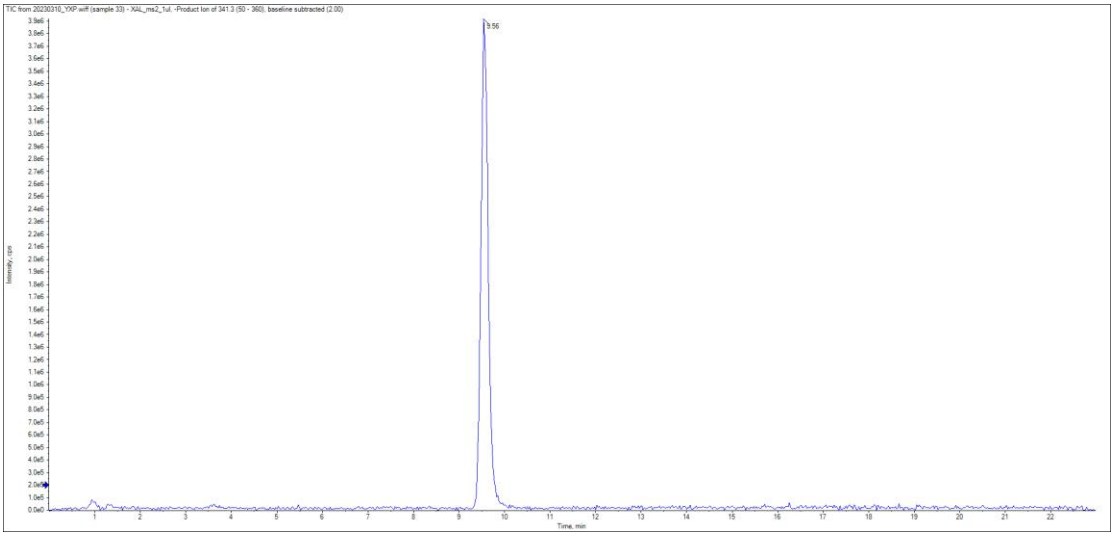


Fig F-4. The LC result of XAL

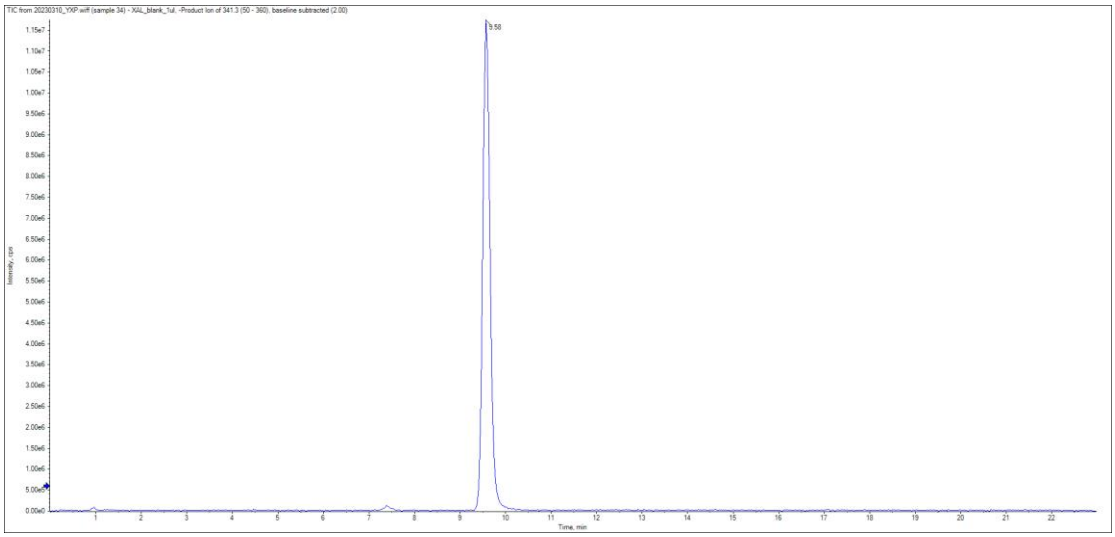


Fig F-5. The LC result of XAL-B1

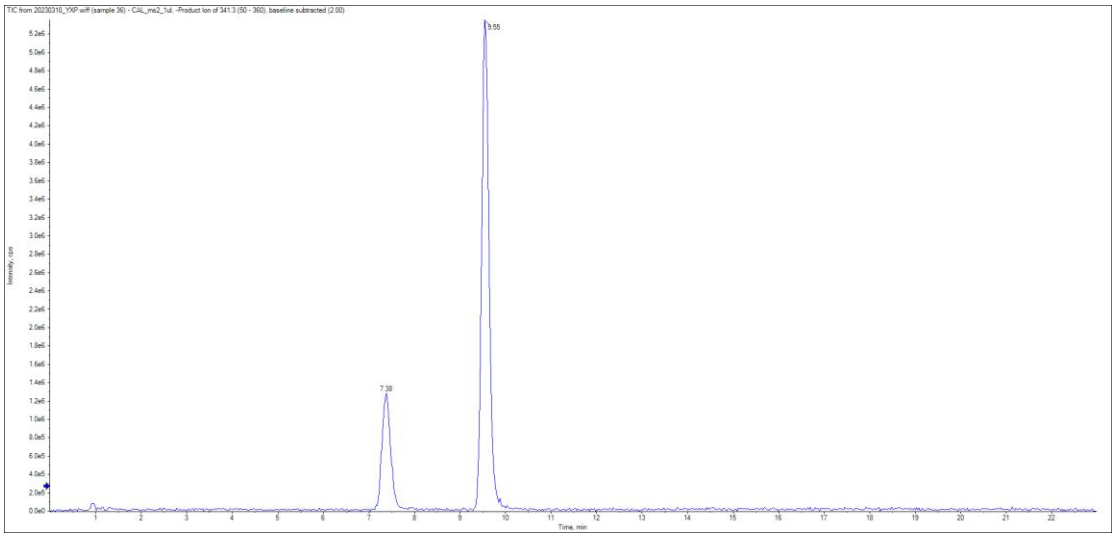


Fig F-6. The LC result of CAL

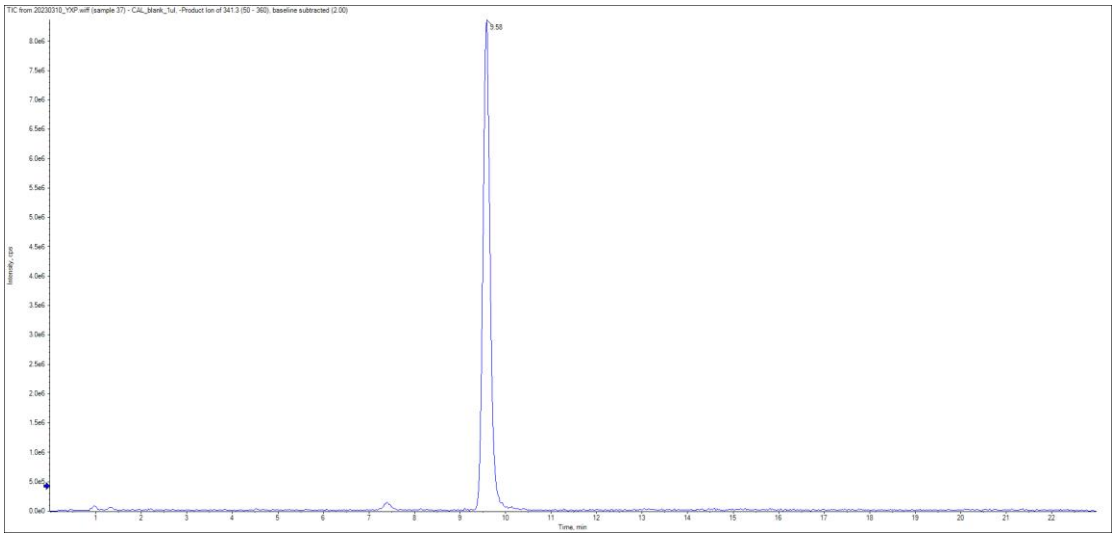


Fig F-7. The LC result of CAL-B1

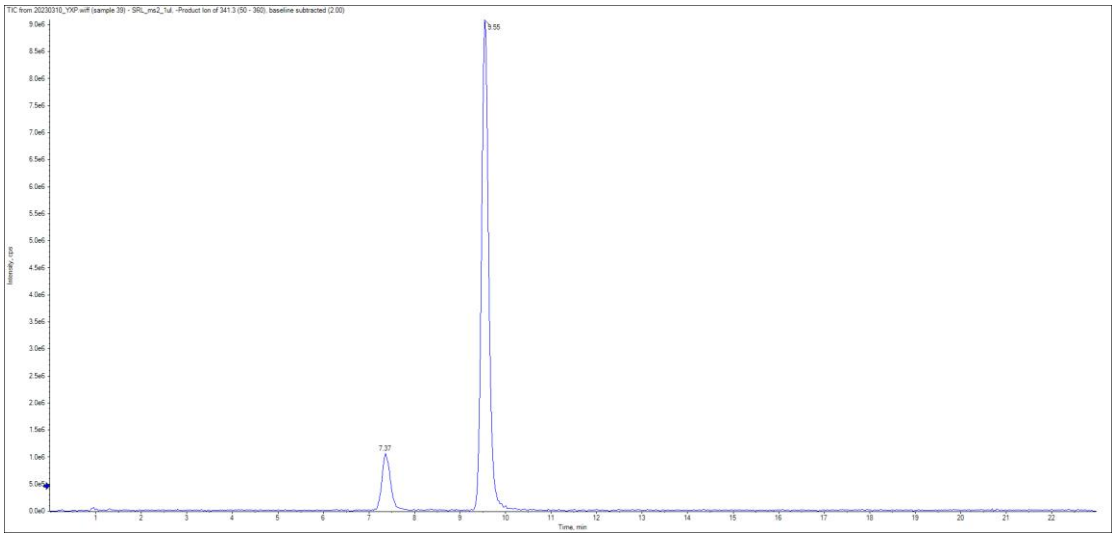


Fig F-8. The LC result of SRL

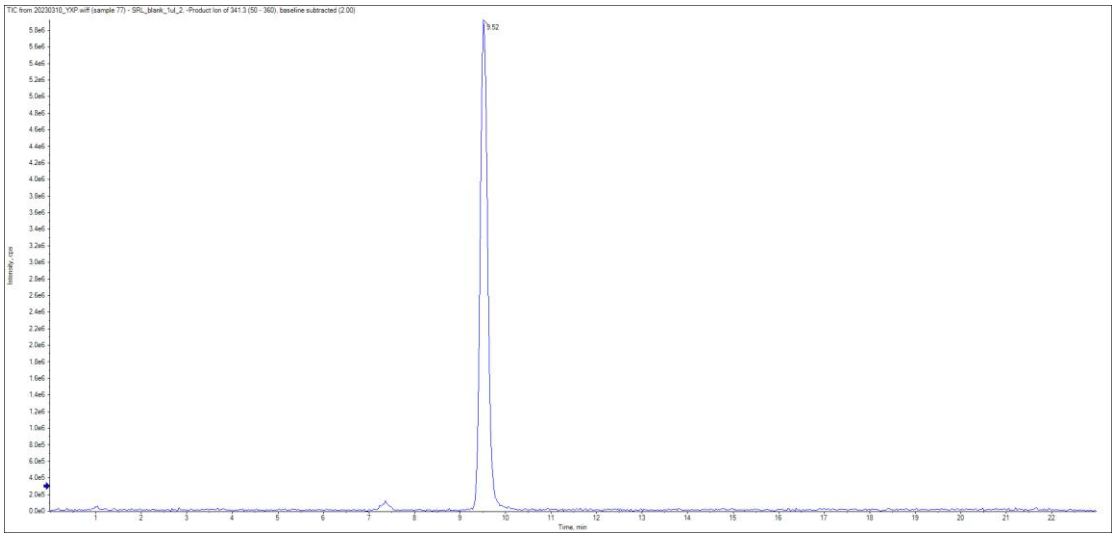


Fig F-9. The LC result of SRL-B1

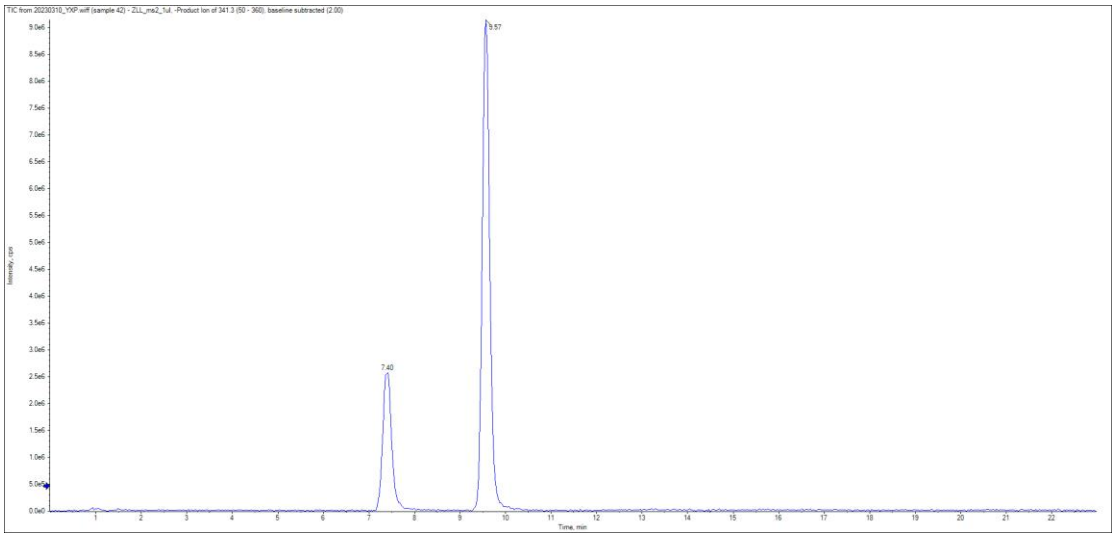


Fig F-10. The LC result of ZLL

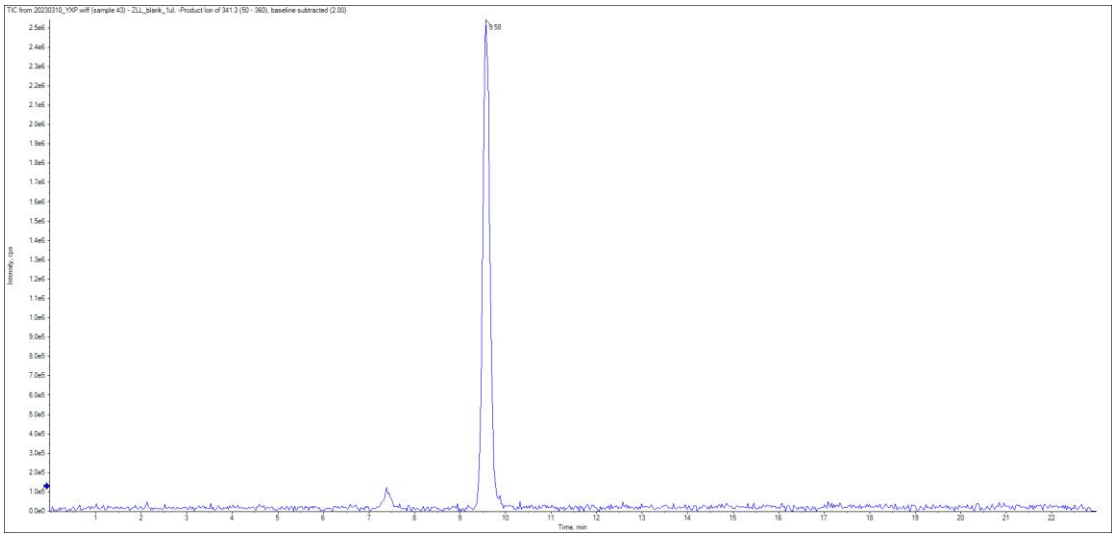


Fig F-11. The LC result of ZLL-B1

Appendix 7. Introduction of archeological sites

Sites in Henan Province

Xinzhengmen

Xinzhengmen is located in Kaifeng, Henan Province. It was built around 954-960 CE, when it was the Later Zhou Dynasty (951-960 CE) in Chinese history. Kaifeng was the capital of the Later Zhou Dynasty, the Northern Song dynasty (960-1127 CE) and the Jin kingdom (1115-1234 CE). Xinzhengmen was used as the gate of Kaifeng city wall, playing an important role in the defense system of the city. It was constructed with rammed earth and bricks. Xinzhengmen was rebuilt several times in these dynasties. The site is about 160 metres from south to north, 100 metres from east to west.

Samples from four city walls have been collected in Xinzhengmen, together with four sediment samples from the Northern Song dynasty (960-1127 CE), the Jin kingdom (1115-1234 CE), the Yuan dynasty (1271-1368 CE) and the Ming dynasty (1368-1644 CE). The surface of the city wall (around 2 cm thickness) was cleared and removed by scalpel first. Then the rammed earth and sediment samples were collected into sealed plastic bags.



Fig G-1. Vertical view of the Xinzhengmen site, the approximate location of collected samples are shown on the map: red dots for city wall samples and the green dots for sediment samples (4 are taken from different layers in the same location)

Zhengzhou Shangcheng

Zhengzhou Shangcheng is located in Zhengzhou, Henan Province. It was built in around 1500 BCE, when it was the capital of the Shang dynasty (1600-1046 BCE). Shangcheng was an ancient rammed earth city. A large number of artifacts and traces of human being activities have been found in it. The Zhengzhou Shangcheng site is a square in size. The length of each side is around 1700 metres.

Three samples have been collected on the top of the city wall in Zhengzhou

Shangcheng. The surface of the city wall (around 2 cm thickness) was cleared and removed by scalpel first. Then the rammed earth samples were collected into sealed plastic bags.

Xingyangguchengcheng

Xingyangguchengcheng is located in the northwest of Zhengzhou, Henan Province. It was built in the Warring States Period (475-221 BCE). Xingyang was an important city of the Han kingdom (403-230 BCE) during this period. After the Han kingdom was conquered, the city was reconstructed several times in the Qin (221-207 BCE) and the Han (202 BCE-220 CE) dynasties. The site is about 2000 metres from south to north, 1500 metres from east to west. The surviving city wall was made of rammed earth. There is also a metallurgical workshop site of the Han dynasty (202 BCE-220 CE) nearby.

Six samples have been collected from the side of the city wall in the Xingyangguchengcheng site, together with one sediment sample from the bottom of the city wall. The surface of the city wall (around 2 cm thickness) was cleared and removed by scalpel first. Then samples were collected into sealed plastic bags.

Bawangcheng

Bawangcheng is located on Mount Guangwu, which is in the northeast of Xingyang, Zhengzhou, Henan Province. It was built between the Qin dynasty (221-207BCE) and

the Han dynasty (202 BCE-220 CE). During this period the war between Xiang Yu, the king of the Chu kingdom, and Liu Bang, the first emperor of the Han dynasty, was fought for the dominion of the whole country. Xiang was also called ‘Bawang’, which means a powerful hero. He constructed the defense system along the front line to fight against Liu, so the city wall was also named after him. The site is about 340 metres from south to north, 400 metres from east to west. The remaining sections of defence constructions built by Liu are at the other end of Mount Guangwu.

Nine city wall samples have been collected from Bawangcheng. Three samples were taken from the top, three were from the bottom and three were between. The surface of the city wall (around 2 cm thickness) was cleared and removed by scalpel first. Then the rammed earth samples were collected into sealed plastic bags.

Pingtaocheng

Pingtaocheng is located in Guangwu, Zhengzhou, Henan Province. It may have been built in the Shang dynasty (1600-1046 BCE). Artifacts from the Shang dynasty (1600-1046 BCE), the Chunqiu (770-476 BCE) and the Warring States Periods (475-221 BCE), and also the Han dynasty (202 BCE-220 CE) have been found on this site. The surviving city walls of Pingtaocheng are the main part of the north wall and the northern part of the east wall.

Eight samples have been collected from the city wall of the Pingtaocheng site. Two

were collected from the east wall and others were from the north wall. The plants on the east wall were removed first, then the surface (around 2 cm thickness) of both the east and north walls was cleared and removed by scalpel. The rammed earth samples were collected into sealed plastic bags.

Sites in Zhejiang Province

Shangjiaoyang Tulou

Shangjiaoyang Tulou is located in Taishun, Wenzhou, Zhejiang Province. It was constructed in around 1858, in the late Qing dynasty (1636-1912 CE). The Zeng family built Shangjiaoyang Tulou to protect their family and property from the threat of the Taiping Heavenly Kingdom. Tulou is a traditional building type in Fujian Province. It is a big square or round house made of tabia. The Zeng family moved from Fujian Province and also brought their building techniques. Shangjiaoyang Tulou is about 625 square metres, surrounded by a small pond. The pond is used to protect Tulou from robbery and fire. All the drinking and domestic water for the whole family is also from the pond. The wall of Tulou is made of about one metre thick rammed tabia, which is supported by big stones on the bottom.

Three tabia samples have been collected on the surface of the internal wall in Shangjiaoyang Tulou, together with two from the external wall. Samples were collected by scalpel and put into sealed plastic bags.

Nanwan Emplacement

Nanwan Emplacement is located in Zhapu, Pinghu, Zhejiang Province. It was set on the flat ground between Mount Dengguang and Mount Xichang. The emplacement was built in 1895, in the late Qing dynasty (1636-1912 CE). The Qing government failed in the First Sino-Japanese War (1 August 1894 – 17 April 1895), which is commonly named as the War of Jiawu in Chinese history. Liao Shoufeng, who was the chief military and political official of Zhejiang Province, ordered in 1894 that a emplacement should be built in Nanwan to protect the coastline of Zhejiang. The construction of Nanwan Emplacement was completed in the following year. The emplacement faces south and covers 5178 square metres. There is an Armstrong Gun in the middle of the site. There are also two artillery bunkers remaining on the east and west side of the gun. The bunkers were built using lime, grit, sticky rice and alum, covering around 207 square metres. Entrances are set on both bunkers for the artillerymen.

One sample was provided by local archaeologists. It is a rammed earth sample collected from Nanwan Emplacement.

Tianfeigong Emplacement

Tianfeigong Emplacement is located in the south of Tangshan Park in Zhapu, Pinghu, Zhejiang Province. It was built in 1717, during the Qing dynasty (1636-1912 CE).

Tianfeigong Emplacement faces south. The surviving part of the site is a group of artillery bunkers, which are made from lime, grit, sticky rice and alum. These bunkers can be divided into four rooms, arranged in a circular plan. Earth on the surface of bunkers has heavily deteriorated. Exfoliation has also taken place in some parts of bunkers. Ten guns were set there at first, but only three of them remain now. Chemical conservation measures have been applied to the guns in Tianfeigong Emplacement between 2002 and 2004.

One sample was provided by local archaeologists. It is a rammed earth sample collected from Tianfeigong Emplacement.

Hongyuan Emplacement

Hongyuan Emplacement is located on the northeast slope of Mount Li in Beilun, Ningbo, Zhejiang Province. It was built in 1887, in the late Qing dynasty (1636-1912 CE). A commander's office, barracks and gunpowder magazine were also built there. Hongyuan Emplacement was constructed by tabia. Tabia is a mixture of yellow mud, lime and steamed sticky rice. The constructors flattened out the ground and used wooden planks to make the framework. Then the tabia was rammed into the framework in layers. The gun was set on a circular iron track and could be rotated around 360 degrees. The main part of Hongyuan Emplacement was demolished in 1936. Two large reinforced concrete forts were then constructed in the same place. After that, one of the reinforced concrete forts, as well as some tabia emplacement

walls, was blown up for the construction of a meteorological observatory. The remaining tabia walls built in 1887 are located on the north and west side of the meteorological observatory.

One sample was provided by local archaeologists. It is a tabia sample collected from Hongyuan Emplacement.

Jingyuan Emplacement

Jingyuan Emplacement is located on the east slope of Mount Jinji in Beilun, Ningbo, Zhejiang Province. It was built in 1880, in the late Qing dynasty (1636-1912 CE). There were five embrasures (holes for firing) on the wall of emplacement. Five barracks were also constructed there. In 1884, four Armstrong muzzle-loading cannons and a Whitworth breechloader cannon were set there. The construction technique of Jingyuan Emplacement was similar to that of Hongyuan Emplacement. The outside appearance of Jingyuan Emplacement now is relatively complete. When seen from the front, Jingyuan Emplacement is a trapezium. The length is 45 metres, the width is 9 metres, and the height is 4.4 metres. The top of the emplacement wall is 1.06 metres in thickness, and the bottom is 1.75 metres. The embrasures are 2.4 metres wide and 2 metres high. The barracks and walls inside the emplacement have been destroyed.

Two samples were provided by local archaeologists. They are tabia samples collected

from Jingyuan Emplacement.

Tomb of Zhao Boyun

The tomb of Zhao Boyun is located in Huangyan, Taizhou, Zhejiang Province. It is the only tomb of the Southern Song dynasty (1127-1279 CE) that has not been robbed in Zhejiang Province. The owner of the tomb is Zhao Boyun and his wife Li. Zhao is the seventh generation from Zhao Kuangyin, who is also known as Emperor Taizu of the Song in Chinese history. Zhao Kuangyin is the first emperor of the Song dynasty (960-1279 CE). His descendant Zhao Ziying, who is the father of Zhao Boyun, moved to Huangyan. Zhao Boyun was born in 1155 and died in 1216, and was buried with his wife, Li, who died in 1195 and was buried in 1196. The tomb can be divided into two parts. The right room belongs to Mrs. Zhao. It has been robbed, and the coffin in it has been mostly destroyed. Zhao's coffin was put in the left room, which is still well preserved. The coffin is made of wood and its surface is covered by red lacquer. The board is approximately 10 centimetres thick. There is just a little space between the coffin and the earth tomb wall. Rosin, sticky rice juice and tabia were added into the space to protect the coffin from deterioration. A large stone slab was put on the top of the room. Many clothes, jade decorations, bronze mirrors and other artifacts were also found in the tomb.

One rosin and two tabia samples were provided by archaeologists. They were

collected from the tomb of Zhao Boyun.

Longwan Emplacement

Longwan Emplacement is located on the slope of Mount Longwan in Yaoxi, Wenzhou, Zhejiang Province. The full name of Longan Emplacement is Wenzhou right barracks Longwan Emplacement. It was built in 1883, in the late Qing dynasty (1636-1912 CE). The emplacement was set in the estuary of Ou River. Another emplacement named Zhenou Emplacement was set in the other side of the Ou River in Leqing. The whole defensive system based on Fort Longwan and Zhenou played a very important role in protecting Wenzhou from the foreign enemies in recent history. Longwan Emplacement is oval in shape, 40 metres from south to north, and 60 metres from east to west. It faces south and can be entered from south door. The emplacement, which can be divided into three linked little castles, is 2.76 metres high. There is a small gunpowder magazine in every castle. There are seven cannons remaining in the site now. Two are in the middle castle, including the heaviest one, which is around 5.65 tonnes. Four are in the east castle and the other one is in the north castle. Longwan Emplacement was constructed from yellow mud, lime and grit. Those materials were rammed in layers. The emplacement was partly destroyed in the War of Resistance against Japan (also named Second Sino-Japanese War, 1937-1945 CE) and renovated after that.

One sample was provided by archaeologists. It is a rammed earth sample collected from Longwan Emplacement.

The house of the Zhang family

The house of the Zhang family is located in Yanguan ancient town in Haining, Jiaxing, Zhejiang Province. It is also named Baowei Tang. It was occupied by the Japanese army in the War of Resistance against Japan (1937-1945 CE). After 1949, this house was used as the office of local government. Currently, the house of the Zhang family is protected by Haining government as a cultural site. The house faces south and can be divided into two parts. The east part is in traditional Chinese style, while the west part is in western style. A 1.35 metres lane between the east and west houses, links the two parts together.

One tabia sample was provided by archaeologists. It is collected from the surface of the wall in the house of the Zhang family.

Ancheng city wall

Ancheng is located on the west bank of the Xitiao River in Anji, Huzhou, Zhejiang Province. As recorded on the local county annals, the army of the Ming dynasty (1368-1644 CE) captured Anji in 1356. The commander, Zhang Junde, ordered the building of an earthen city wall. Ancheng city wall was designed for both defence and

flood prevention functions. It consists of walls, platforms, gates, horse paths, bridges, moat etc. The perimeter of Ancheng city wall is about 3000 metres. The cross section of the city wall is a trapezium. The surviving city wall is 4-6 metres high, 6-8 metres thick on the bottom and 3-4 metres on the top. Ancheng city wall was constructed from rammed earth and faced with bricks and stones. It has been rebuilt several times. A variety of bricks have been used ranging from the Song dynasty to the Qing dynasty. Some of them have been moved from other sites.

Eight lime mortar samples have been collected from Ancheng city wall. They were taken out by scalpel from the gap between the bricks. The moss on the surface was removed, and then these mortar samples were put into sealed plastic bags. One sample was collected from the west gate and two others were collected besides the west gate. One sample was from the north gate and one was from the east gate. Three samples were collected from the north wall (one from western parts and two from east parts).

Bamudun tomb

Bamudun tomb, which belongs to the Mount Loong Aristocratic tombs of the Yue State, is located in Anji, Huzhou, Zhejiang Province. Mount Loong Aristocratic tombs of the Yue State cover around 2 million square metres of Mount Loong, Mount Wujia, Mount Shijiao and Mount Xianglu. More than 250 earthen tombs are included in Mount Loong Aristocratic tombs of the Yue State. The complex can be divided into six sections: Mount Jiulong, Bamudun and Jiumudun, Guchenglinchang, Huangjin,

the north of Mount Shijiao and Mount Xianglu, Yaogang and Mount Wujia. These tombs were built in the Zhou dynasty (1046-256 BCE). Some of them may belong to the Han dynasty (202 BCE-220 CE). Bamudun tomb is located 500 metres south of Gucheng, covering around 50000 square metres.

Three earth samples have been collected from Bamudun tomb. Two were collected in the burial cave and the other was from the top of the tomb. The surface layer (around 1 cm thickness) was cleared and removed by scalpel first. Then the earth samples were collected into sealed plastic bags.

Quzhou city wall

Quzhou city wall is located in Quzhou, Zhejiang province. It is mentioned in "The annals of the Quzhou" of the Ming dynasty (1368-1644 CE) that Quzhou city wall was first built by the Qu River in the fourth year of Tang Wude (621 CE) by the army and local people under the administration of Gong Yuchi (585-658 CE, famous general in the Tang dynasty). In the third year of Song Xuanhe (1121 CE), Quzhou city wall was re-constructed by the government. Then, the rammed earthen wall constructed in the Tang dynasty turned to brick structure. During 1121 to 1916 CE, Quzhou city wall was renovated several times by the governments of the Song, Yuan, Ming, Qing and the Republic of China. The remain of Quzhou city wall is around 2000 metres in length and 3 to 5 metres in height.

One lime mortar sample was provided by archaeologists.

Sites in Jiangxi Province

Wucheng

The Wucheng site is located in Zhangshu, Yichun, Jiangxi province. It was constructed around 1500 years ago, covering an area of around 4 square kilometres. The central part of the Wucheng site is a city of the Shang dynasty (1600-1046 BCE). Residential architectures, sacrificial relics and copper casting relics were found in the city.

Five earth samples have been collected from the northern part of the city wall in the Wucheng site. One was taken from the top, one from the middle and two from the bottom of the city wall. The other sample may be the raw material of the pottery. The surface was cleared and removed by scalpel. The rammed earth samples were collected into sealed plastic bags.

Zhuweicheng

The Zhuweicheng site is located in Zhangshu, Yichun, Jiangxi province. It was constructed around 5000 years ago. The remains of the late Neolithic Period, the Shang and Zhou dynasties could be found in the site. The Zhuweicheng site is about 360 metres from south to north, 410 metres from east to west. The city walls of the

Zhuweicheng site are from 10 to 21.8 metres in height. The walls were made of rammed earth, sand and stone.

Five earth samples have been collected from the northeast corner of the exterior city wall in the Zhuweicheng site. Three were taken from the top and two were from the bottom. The surface was cleared and removed by scalpel. The rammed earth samples were collected into sealed plastic bags.

Sites in Jiangsu Province

Mudu Wufengcheng

The Mudu Wufengcheng site is a part of the Mudu site, which is located in Mudu, Suzhou, Jiangsu province. The Mudu site was constructed in the late Chunqiu Period (770-476 BCE). The site could be divided into two parts: the north wall located in Wufeng Village, Mudu, Suzhou; the south wall located in Xinfeng Village, Xukou, Suzhou. The Mudu Wufengcheng site is the northern city wall. The remain of the city wall is around 1 kilometre in length, 10-20 metres in width and 3 metres in height.

Five earth samples have been collected from the city wall in the Mudu Wufengcheng site. The surface was cleared and removed by scalpel. The rammed earth samples were collected into sealed plastic bags.

Sites in Shaanxi Province

Mausoleum of Emperor Shihuang of the Qin

The mausoleum of Emperor Shihuang of the Qin is the mausoleum of Zheng Ying (259-210 BCE), who is also known as Shihuang of the Qin (the first emperor of the Qin dynasty (221-207 BCE)). The mausoleum, which is located at the north foot of Lishan Mountain, 5 kilometres east of Lintong District, Xi'an, Shaanxi Province, was constructed from 247 to 208 BCE. There are two rammed earth walls surrounding the mausoleum. The interior wall is around 4 kilometres in perimeter, while the exterior wall is around 6 kilometres. The remaining walls are around 8 to 10 metres in height.

One rammed earth sample was collected from the exterior wall by archaeologists.

Sites in Shanxi Province

Yangquan city wall

The Yangquan city wall site is located in Yangquan, Shanxi province. It is also known as the Pingtancheng site. The site was built around 2500 years ago by Yang Zhao (?-476 BCE), who is also known as Zhao Jianzi. The remaining part is a rammed earth city wall, which is around 3 to 16 metres in height.

One rammed earth sample was collected from the city wall by archaeologists.

Sites in Guangxi Zhuang autonomous region

Jiangjundi

The Jiangjundi site is located in Xialiantang Village, Wuxuan, Laibin, Guangxi Zhuang autonomous region. It was built in the sixth year of Qing Jiaqing (1801 CE).

One tabia sample was taken from the house wall of Jiangjundi by archaeologists.

Sites in Hebei Province

Laolongtou

Laolongtou, a part of the Great Wall, is adjacent to the Bohai Sea. Laolongtou was built in the early Ming dynasty (1368 CE) by Da Xu (1332-1385 CE, famous general in the Ming dynasty) and extended in 1579 CE by Jiguang Qi (1528-1588 CE, famous general in the Ming dynasty). The Laolongtou site consists of Ruhai stone fort, Sea God temple, Jinglutai, Nanhaikou, Chenghai watchtower, Ninghai fort and Binhai wall, covering an area of around 0.5 square kilometres.

Four rammed earth samples were collected from the Laolongtou site by archaeologists.

Zhengding city wall

The Zhengding city wall site is located in Zhengding, Shijiazhuang, Hebei province. It was constructed in the Northern Zhou dynasty (557-581CE), and renovated in 762 CE in the Tang dynasty (618-907 CE). Zhengding city wall was extended to around 12 kilometres in perimeter in the fourteenth year of Ming Zhengtong (1449 CE). In the fifth year of Ming Longqing (1571 CE), Zhengding city wall was re-constructed by Shoushi Gu (unknown), the county magistrate of Zhengding. Then, the rammed earthen wall turned to brick structure. The following renovations (until 2016) were all based this re-construction. The remains of Zhengding city wall are some gates and the earthen parts of the wall.

One lime mortar sample was taken from the North gate of Zhengding city wall by archaeologists.

Sites in Beijing

Yuanmingyuan, also known as the Old Summer Palace, is located in Haidian District, Beijing. It was built 1707 by Xuanye Aisin-Gioro (1654-1722 CE, also known as Emperor Kangxi of the Qing) and destroyed in 1860. Yuanmingyuan is one of the most famous royal garden in the Qing dynasty, covering an area of around 3.5 square kilometres. The remains of Yuanmingyuan is now Yuanmingyuan Ruins Park.

One rammed earth sample was collected from Haiyantang in Yuanmingyuan by the archaeologists.

Appendix 8. The intensity of *m/z* 1013 and 1121 peaks in the MALDI-TOF-MS spectra of the modern earth samples

Table H-1. The intensity of the peaks at around *m/z* 1013 and 1121 in the MALDI-TOF-MS spectra of the modern earth samples

	Shot 1		Shot 2		Shot 3		Shot 4		Shot 5		Shot 6		Shot 7		Shot 8		Shot 9	
	1013	1121	1013	1121	1013	1121	1013	1121	1013	1121	1013	1121	1013	1121	1013	1121	1013	1121
T1	9341	15331	9090	16227	8205	15662	8621	15507	9566	17257	9388	17825	7920	13211	8516	15698	9588	16015
T2	7254	7793	7281	7860	9244	10331	6163	7174	6420	7157	5423	5795	6788	7074	6006	7264	6470	7272
T3	47352	22221	54839	25983	44518	19898	44016	21246	38879	17822	43756	20663	52332	23820	57187	27611	53747	24224
T4	122936	16688	127088	16127	135726	18334	134814	17002	117249	14193	130090	14873	134013	17801	124307	15929	159793	21416
T5	150993	5863	112912	4118	104919	4076	162246	5867	160034	6176	153499	6344	189616	7881	168059	6945	166913	6929
T6	250342	6365	264794	6549	256815	6748	169690	4577	209418	5762	170044	4678	236949	6097	210439	5877	142336	3757
T7	62070	11067	80765	14588	64938	11735	66818	12438	57371	10259	63172	11844	64479	11716	81957	15762	83113	15058
T8	127766	6052	148781	7207	148145	6721	87252	4250	104001	5218	88490	3979	121794	6574	121856	5714	122916	6236
T9	184945	1638	178986	1445	176666	1455	245509	2051	210915	1911	211706	1853	204916	1837	204250	1859	139264	1118
T10	906	5564	1042	6087	760	5240	1444	9393	1003	5769	1726	11162	1468	9077	1131	7486	1411	9172
T11	1177	7958	971	6988	1086	8088	958	7384	1168	9385	1082	8118	1260	11011	1630	11460	1520	11375
T12	10850	14184	10578	13805	12351	16686	11234	14818	5957	8456	7978	9827	12297	15597	9944	13173	10952	13742
T13	1138	15219	1428	20420	897	12341	911	12157	921	12023	890	12223	1073	17033	1241	16119	858	12615
T14	1043	2803	1092	2913	1242	2962	4225	14448	4101	15099	5100	16238	4664	15036	4515	15586	4674	15570
T15	3167	21610	3659	23631	3267	22647	3148	19739	2633	18625	2791	18199	3152	23156	3277	20378	3503	22348

T16	**826**	**9523**	**923**	**11899**	**973**	**13346**	**1128**	**13720**	**804**	**13664**	**1017**	**11870**	**856**	**11076**	**934**	**11397**	**986**	**11596**
T17	**714**	**8209**	**730**	**9111**	**692**	**7855**	**640**	**7132**	**502**	**6595**	**679**	**8222**	**690**	**9763**	**828**	**10137**	**820**	**11576**
T18	**1153**	**2964**	**1741**	**3168**	**1900**	**4367**	**1937**	**4509**	**1924**	**3894**	**2309**	**4398**	**1706**	**4068**	**2029**	**4306**	**1904**	**4323**
T19	**913**	**13176**	**956**	**12601**	**909**	**12661**	**893**	**14024**	**1022**	**14522**	**839**	**12015**	**823**	**11775**	**717**	**9729**	**908**	**13588**
T20	**922**	**10016**	**681**	**6595**	**730**	**8413**	**901**	**8589**	**851**	**8987**	**660**	**8387**	**700**	**7145**	**792**	**7244**	**816**	**8579**
T21	**1043**	**17526**	**1097**	**14788**	**907**	**14250**	**896**	**14884**	**980**	**13932**	**919**	**14368**	**1115**	**17824**	**929**	**16119**	**1151**	**18730**
T22	**427**	**18509**	**415**	**20098**	**311**	**14808**	**394**	**12155**	**371**	**10712**	**362**	**10997**	**331**	**14610**	**389**	**15568**	**388**	**18126**
T23	**440**	**7389**	**358**	**7029**	**478**	**7514**	**373**	**5389**	**354**	**5760**	**297**	**4000**	**470**	**6898**	**387**	**6482**	**449**	**7927**
T24	**518**	**7723**	**584**	**9526**	**404**	**5794**	**356**	**6479**	**380**	**5471**	**402**	**6528**	**480**	**8665**	**482**	**7198**	**500**	**10530**
T25	-	-	-	-	-	-	-	-	-	-	-	-	-	-	-	-	-	-
T26	**382**	**10349**	**448**	**11139**	**448**	**11033**	**346**	**10046**	**421**	**10047**	**342**	**10660**	**421**	**10926**	**541**	**14906**	**506**	**9772**
T27	**390**	**8789**	**342**	**9513**	**359**	**8236**	**342**	**9912**	**290**	**7855**	**317**	**7753**	**367**	**6550**	**437**	**8626**	**364**	**6889**
T28	-	-	-	-	-	-	-	-	-	-	-	-	-	-	-	-	-	-
T29	**346**	**13798**	**428**	**13053**	**380**	**13225**	**351**	**10655**	**362**	**9973**	**403**	**12312**	**283**	**10511**	**332**	**11866**	**353**	**9327**
T30	**588**	**21372**	**558**	**28175**	**650**	**29067**	**579**	**26208**	**690**	**29568**	**742**	**28554**	**648**	**33889**	**625**	**33653**	**774**	**34084**

Reference

ABAKUMOV, E. V., CAJTHAML, T., BRUS, J. & FROUZ, J. 2013. Humus accumulation, humification, and humic acid composition in soils of two post-mining chronosequences after coal mining. *Journal of Soils and Sediments,* 13**,** 491-500.

AI, Q. 1999. Tomb of Lianying Li. *Beijing Archives***,** 41.

AN, J. 1992. On the Site of Chengziya Longshan Cultural City and its Related Problems. *Cultural Relics of Central China***,** 1-6.

ANYANG TEAM OF INSTITUTE OF ARCHAEOLOGY IN CHINESE ACADEMY OF SOCIAL SCIENCES 1985. The Excavation at Hougang In Anyang, 1979. *Acta Archaeological Sinica***,** 33-88.

ARTIOLI, G. & SECCO, M. Modern and ancient masonry: Nature and role of the binder. Brick and Block Masonry: Proceedings of the 16th International Brick and Block Masonry Conference, Padova, Italy, 26-30 June 2016, 2016. CRC Press, 3.

ARTIOLI, G., SECCO, M. & ADDIS, A. 2019. The Vitruvian legacy: Mortars and binders before and after the Roman world. *EMU Notes Mineral,* 20**,** 151-202.

Bai, W., Chi, X. & Zhou L. 2021. Research of Preservation and Activation of Kaiping Diaolou with Rammed Earth Wall. New Architecture, (4), 144-147.

Balasubramanian, A., Siddaramappa, R. and Rangaswami, G., 1972. Effect of organic manuring on the activities of the enzymes hydrolysing sucrose and urea and on soil

aggregation. Plant and Soil, 37, 319-328.

Bieleski, R.L., 1995. Onset of phloem export from senescent petals of daylily. Plant Physiology, 109(2), 557-565.

BONADUCE, I., BLAENSDORF, C., DIETEMANN, P. & COLOMBINI, M. P. 2008. The binding media of the polychromy of Qin Shihuang's Terracotta Army. *Journal of Cultural Heritage,* 9**,** 103-108.

BR COULAKI, H., ANDREOTTI, A., BONADUCE, I., COLOMBINI, M. & LLUVERAS, A. 2012. Characterization of organic media in the wall-paintings of the “Palace of Nestor” at Pylos, Greece: evidence for a secco painting techniques in the Bronze Age. *Journal of Archaeological Science,* 39**,** 2866-2876.

CAI, J. 1995. resource-based ecological round Tulou. *Architectural Journal***,** 42-44.

CAI, S. 2001. An Overview of Ancient Bridges in Jiangsu Province. *Traditional Chinese Architecture and Gardens***,** 48-54+65-68.

CAI, W. 2005. Discussion on the Proportion of Buddha Statues in the Three Early Grottoes of Mogao Grottoes. *Dunhuang Research***,** 33-40.

CAO, H. & CAO, R. 2016. The Discussion on the Origin of the Brick and Tile in Ancient China. *Brick & Tile World***,** 40-42.

CAPRIOLI, R.M., FARMER, T.B. and GILE, J., 1997. Molecular imaging of biological samples: localization of peptides and proteins using MALDI-TOF MS. *Analytical Chemistry,* 69(23), pp.4751-4760.

CHEN, J. 1961. The Investigation and Excavation of Sui and Tang Dongdu City. *Archaeology***,** 361-379.

Chen, N., Nedoluzhko, A. 2023. Ancient DNA: the past for the future. BMC Genomics 24, pp. 309-312.

Chen, W. 2018. The Structural Characteristics of Kaiping Barbican. Huazhong Architecture, 36(11), 147-151.

CHEN, Y. 2000. Ancient Bridges in Wuhan. *Literature and History of Wuhan***,** 45-48.

CHENG, M. & AN, S. 2015. Responses of soil nitrogen, phosphorous and organic matter to vegetation succession on the Loess Plateau of China. *Journal of Arid Land,* 7**,** 216-223.

CHENG, X. 2007. The History of Dragon Bridge. *Relics and Museolgy***,** 56-57.

CHENGDU CULTURAL RELICS AND ARCHAEOLOGY TEAM 2002. A Brief Report of the Preliminary Excavation of the Shuanghe Prehistory City Site, Chongzhou, Sichuan Province. *Archaeology***,** 3-19.

CHILD, A. M. & POLLARD, A. M. 1995. Immunochemistry applied to archaeology. *American Journal of Archaeology,* 99**,** 132-136.

COLOMBINI, M. P., MODUGNO, F., GIACOMELLI, M. & FRANCESCONI, S. 1999. Characterisation of proteinaceous binders and drying oils in wall painting samples by gas chromatography–mass spectrometry. *Journal of Chromatography A,* 846**,** 113-124.

CONTI, C., STRIOVA, J., ALIATIS, I., POSSENTI, E., MASSONNET, G., MUEHLETHALER, C., POLI, T. & POSITANO, M. 2014. The detection of copper resinate pigment in works of art: contribution from Raman spectroscopy. *Journal of Raman Spectroscopy,* 45**,** 1186-1196.

CUI, D. 1994. Tombs, Cities and Houses of Longshan Culture in Shandong Province. *Journal of Jinan University: Social Science Edition***,** 11-16.

CURRY, G. B., THENG, B. K. G. & ZHENG, H. 1994. Amino acid distribution in a Loess-Palaeosol sequence near Luochuan, Loess Plateau, China. *Organic Geochemistry,* 22**,** 287-298.

DAHER, C., PARIS, C., H , A. S. L., BELLOT-GURLET, L. & ÉCHARD, J. P. 2010. A joint use of Raman and infrared spectroscopies for the identification of natural organic media used in ancient varnishes. *Journal of Raman Spectroscopy,* 41**,** 1494-1499.

DARRIBÈRE, C. 2009. Evolved Gas Analysis (Translated by TANG, Y.), Shanghai, Donghua University Press.

David, J., Steinmetz, Z., Kučerík, J. and Schaumann, G.E., 2018. Quantitative analysis of poly (ethylene terephthalate) microplastics in soil via thermogravimetry–mass spectrometry. Analytical Chemistry, 90(15), pp.8793-8799.

DE'AN MUSEUM 1994. A Brief Report on Clearing-up of Xiong Family Tomb of the Ming Dynasty in De'an, Jiangxi Province. *Cultural Relics in Southern China***,** 5-9.

DEAN, W. E. 1974. Determination of carbonate and organic matter in calcareous sediments and sedimentary rocks by loss on ignition; comparison with other methods. *Journal of Sedimentary Research,* 44**,** 242-248.

DEGLOORKAR, N. K. & PANCHARATHI, R. K. 2020. Characterization of ancient

mortar for sustainability of an 800 year old heritage site in India. *Materials Today: Proceedings,* 32**,** 734-739.

DIAO, Q. & WEN, G. 1988. THE ORGANIC MATTER IN LOESS [J]. *Scientia Geographica Sinica,* 3.

DU, J. 2019. The Discovery and Research of the Sacrificial Remains in the Erlitou site, Yanshi. *Cultural Relics of Central China***,** 56-70.

DU, L. 2009. Research to the Use of Soil Materials in Chinese Traditional Architectural Technology-Take Shanxi for Example. master, Taiyuan University of Technology.

DUAN, P., DU, Y. & XIAO, H. 1984. The Preliminary Investigation and Excavation of the Yanshi Shangcheng site. *Archaeology***,** 488-504.

FANG, S. Q., ZHANG, H., ZHANG, B. J. & ZHENG, Y. 2014. The identification of organic additives in traditional lime mortar. *Journal of Cultural Heritage,* 15**,** 144-150.

Farrar, J., Hawes, M., Jones, D. and Lindow, S., 2003. How roots control the flux of carbon to the rhizosphere. Ecology, 84(4), 827-837.

Fuller, D.Q. and Castillo, C. (2015) 'Diversification and cultural construction of a crop: the case of glutinous rice and waxy cereals in the food cultures of eastern Asia', in J. Lee-Thorp and M. A. Katzenberg (eds.) *The Oxford Handbook of the Archaeology of Diet (online edn.)*. Oxford: Oxford Academic.

FU, X. 1981. A Preliminary Study on the Architectural Remainings of the Western Zhou Dynasty in Fengchu, Qishan, Shaanxi Province-One Study of Zhouyuan

Western Zhou Architectures. *Cultural Relics*, 65-74.

FU, X. 2009. Architectures of the Three Kingdoms, the Two Jin Dynasties, the Northern and Southern Dynasties, the Sui and Tang Dynasties and the Five Dynasties Beijing, China Architecture & Building Press.

FU, Z. 2010. A Comparative Study of Closed House-Hakka Traditional Dwelling Houses in Easter Guangxi and Northern Guangdong-Closed House at Hezhou Jiangsi's and Shixing Mantang's as examples. *Arts Exploration*, 32-35+46+148.

GAO, T. & LI, J. 1986. The Main Discoveries of the Excavation in the Residential Part of Area III from 1983 to 1984 in the Taosi Site *Archaeology*, 773-781.

GIORGI, G. 2009. Overview of Mass Spectrometric Based Techniques Applied in the Cultural Heritage Field. *Organic Mass Spectrometry in Art and Archaeology*.

Glaister, J. 1926. The Kastle-Meyer test for the detection of blood: considered from the medico-legal aspect. British Medical Journal, 1(3406), 650.

GUO, J. 2013. A Case Study on City Walls in Ming and Qing Dynasties: Analysis of the History and Characteristics of Taizhou Prefectural City Wall of Linhai. *Huazhong Architecture*, 174-177.

Hajdas, I., Guidobaldi, G., Haghipour, N., & Wyss, K. 2024. Sample Selection, Characterization, and Choice of Treatment for Accurate Radiocarbon Analysis: Insights from the ETH Laboratory. pp. 1–14.

HAN, F., HU, W., ZHENG, J., DU, F. & ZHANG, X. 2010. Estimating soil organic carbon storage and distribution in a catchment of Loess Plateau, China. *Geoderma*, 154, 261-266.

HAN, J. 1976. A Brief Excavation Report of the Fengxia Site in Beipiao County, Liaoning Province in the Spring of 1972. *Archaeology***,** 197-210, 186.

Hanson, J. R. 2019. *The organic chemistry of isotopic labelling*, Cambridge, Royal Society of Chemistry.

HARVEY, D. 2000. *Modern analytical chemistry*, McGraw-Hill New York.

HE, J. 1999. Excavation of the Yuan and Ming Underground Closets of the Fahua Pagoda at Jiading, Shanghai. *Cultural Relics***,** 4-15+97+2.

HE, N. 2018. The Collapsible Loess Foundation: the Key Problem of the City Wall Construction Technique of the Taosi Site. *Huaxia Archaeology***,** 65-76.

HENAN INSTITUTE OF CULTURAL RELICS AND ARCHAEOLOGY 2019. A Brief Excavation Report of the Guchengzhai Ancient City, Xinmi, Henan Province in 2016 and 2017. *Huaxia Archaeology***,** 3-13, 27.

HENAN MUSEUM & ZHENGZHOU MUSEUM 1977. A Brief Excavation Report of the Shang Dynasty City in Zhengzhou *Cultural Relics***,** 21-28, 61.

HODDER, I. 2006. The leopard's tale: revealing the mysteries of Çatalhöyük, London, Thames & Hudson.

HODDER, I. 2012. Entangled: An archaeology of the relationships between humans and things.

HU, W., ZHANG, K., ZHANG, H., ZHANG, B. & RONG, B. 2015. Analysis of polychromy binder on Qin Shihuang's Terracotta Warriors by immunofluorescence microscopy. *Journal of Cultural Heritage,* 16**,** 244-248.

HUANG, J. 1962. Investigation Report of the Yan Xiadu site. *Archaeology***,** 10-19.

HUANG, L. 2017. Elementary Introduction of the Shalu Battery in Guangzhou in the Late Qing Dynasty. *Identification and Appreciation to Cultural Relics***,** 72-75.

INSTITUTE OF NATURAL SCIENCE HISTORY OF CHINESE ACADEMY OF SCIENCES 2000. *The History of Chinese Ancient Architectural Technology*, Beijing: Science Press.

Jaeger III, C.H., Lindow, S.E., Miller, W., Clark, E. and Firestone, M., 1999. Mapping of sugar and amino acid availability in soil around roots with bacterial sensors of sucrose and tryptophan. Applied and Environmental Microbiology, 65(6), 2685-2690.

JEFFERY, G. H., Bassett, J., Mendham, J. & Denney, R. C. 1989. *Vogel's Textbook of Quantitative Chemical Analysis (5th edition)*, Harlow, Essex, Longman Scientific & Technical.

JI, D. 2001. The Rites of the Zhou Dynasty (pp. 429). Changsha: Yuelu Press.

JIANG, N. 1983. A Brief Excavation Report of the Kharchin Hedong site in Jianping County, Liaoning Province. *Archaeology***,** 973-981, 1003.

KERR, D. J. A. & MASON, V. H. 1926. The Haemochromogen Crystal Test for Blood. *British Medical Journal,* 1**,** 134-136.

KHAN, A. & LEMMEN, C. 2014. Bricks and urbanism in the Indus Civilization. History and Philosophy of Physics, from Cornell University Library, accessed from https://arxiv. org/pdf/1303.1426. pdf, on, 29**,** 2017.

LAI, Y. 1957. Discovery of a Ming Dynasty Tomb with Soft Body Remains in Xindu County, Sichuan. *Archaeology*, (2), 19-24.

LI, C. 2016a. A Study on the Early City and Civilization of the Central Plains. Doctor, Zhengzhou University.

LI, G.-L. & PANG, X.-M. 2014. Difference in organic carbon contents and distributions in particle-size fractions between soil and sediment on the southern Loess Plateau, China. *Journal of Mountain Science,* 11**,** 717-726.

LI, G., ZHANG, Y. & NI, Z. 2012. Comparative Experimental Research on Mortar Bonding Materials Used in Several Ancient City Walls. *Architecture Technology***,** 465-468.

LI, J. 2011. *The Principles of Constructions,* Beijing, People's Publishing House.

LI, J. 2019. Research and Cognition of Chinese Traditional Composite Mortars. Doctor, Zhejiang University.

LI, J. & ZHANG, B. 2019. Why Ancient Chinese People Like to Use Organic–Inorganic Composite Mortars?—Application History and Reasons of Organic–Inorganic Mortars in Ancient Chinese Buildings. *Journal of Archaeological Method and Theory,* 26**,** 502-536.

LI, K. 1996. Clearing-up of the Basement of the Yuquan Iron Pagoda at Dangyang, Hubei. *Cultural Relics***,** 43-57+98+100+1.

Li, M., Shangguan, Z. & Deng, L., 2021. Spatial distribution of carbon storages in the terrestrial ecosystems and its influencing factors on the Loess Plateau. Acta Ecologica Sinica, 41(17), pp.6786-6799.

LI, N., ZHANG, Z. & WANG, D. 2008. Primary Study on the "Sanhe Tu" from the Haizi and Weizi Emplacements in Tianjing Dagu site. *Science of Conservation and*

Archaeology, 20**,** 46-51.

LI, T. 2000. Large House Buildings in the Menbanwan Site in Yingcheng. *Jianghan Archaeology***,** 96-96.

Li, T., Song, F., Zhang, J., Liu, S., Xing, B. and Bai, Y., 2020a. Pyrolysis characteristics of soil humic substances using TG-FTIR-MS combined with kinetic models. Science of The Total Environment, 698, p.134237.

LI, X. 1999. The Structure of Suoyang City and "Plate Building of Rammed Earth" of City Walls. *Yangguan***,** 24.

LI, X. 2016b. A Summary of the Development of the Early Adobe Architectures in China. *Steppe Cultural Relics***,** 78-86.

LI, X. & DENG, Q. 2005. The Appreciation of Buddhist Stone Pillar-Take Buddhist Stone Pillars in Chaozhou Kaiyuan Temple as example. *Traditional Chinese Architecture and Gardens***,** 34-36.

LI, X. M., SUN, G. X., CHEN, S. C., FANG, Z., YUAN, H. Y. & SHI, Q. 2018. Molecular Chemodiversity of Dissolved Organic Matter in Paddy Soils. 52**,** 963-971.

Li, Y., Shi, W., Aydin, A., Beroya-Eitner, M.A. and Gao, G., 2020b. Loess genesis and worldwide distribution. Earth-Science Reviews, 201, p.102947.

LI, Z. 2015. Structure and Technology of Traditional Chinese Architecture, Shanghai, Tongji University Press.

LIANG, B. 2011. On the Construction Forms and Materials of Chinese Ancient Buildings. *Journal of Shanxi University(Philosophy and Social Science Edition)***,**

19-22.

LIANG, H. 2017. Practice and Exploration of Cleaning and Conservation of Artifacts Excavated at Archaeological Sites: A Case Study of the Indoor Archaeological Cleaning and Conservation of Tabia Coffins Unearthed in Shangsi County, Guangxi. *Cultural Relics in Southern China,* (4), 256-264+300.

LIANG, S. 1998. *Chinese Architecture History,* Tianjin, Baihua Literature and Art Publishing House.

LIANG, Z. & JIA, X. 2017. The Further Discussion on the Yaowangcheng Site and Its City Type. *Northern Cultural Relics***,** 24-39.

LIN, Z. & LIANG, W. 1980. Distribution and engineering properties of loess and loesslike soils in China. Schematic map of engineering geological zoning. *Bulletin of the International Association of Engineering Geology-Bulletin de l'Association Internationale de Géologie de l'Ingénieur,* 21**,** 112-117.

LIU, D. 1934. The Abstract of Stone-Based Pillar Bridge (Three Bridges of Xi'an: Ba, Chan, Feng). *Series Journal of China Construction Society,* 5**,** 50.

LIU, D. 1980. *History of Ancient Chinese Architecture,* Beijing, China Architecture & Building Press.

LIU, D. & TAN, L. 2016. A Review on the Development of Cementitious Materials in Ancient Buildings. *Science and Technology,* 26**,** 287.

LIU, J. 1993. Humble Opinions about the Bricks in the Zhou Dynasty. *Archaeology and Cultural Relics***,** 84.

LIU, J. 2006. The Preliminary Discussion on the Origin and Development of the

Brick. *Western Archaeology***,** 139-144.

LIU, Q., LI, Y., ZHANG, L. & YANG, L. 1993. A Brief Excavation Report of the No. 4 Relics of the Weiyang Palace in the Han Chang'an City. *Archaeology***,** 1002-1011.

LIU, T. 1965. A Brief Excavation Report of the Xiaoyushulinzi Site in Ningcheng County, Inner Mongolia. *Archaeology***,** 619-621.

LIU, W. & HUANG, Y. 2005. Compound specific D/H ratios and molecular distributions of higher plant leaf waxes as novel paleoenvironmental indicators in the Chinese Loess Plateau. *Organic geochemistry,* 36**,** 851-860.

LIU, X. 2003. Architectures of the Primitive Society, Xia, Shang, Zhou, Qin and Han Dynasties, Beijing, China Architecture & Building Press.

LIU, X., CUI, B. & ZHANG, B. 2016a. The Analysis of Traditional Lime Mortars from Zhejiang Province, China. *Spectroscopy and Spectral Analysis***,** 237-242.

Liu, X., Ma, X. & Zhang, B. 2016b. Analytical investigations of traditional masonry mortars from ancient city walls built during Ming and Qing Dynasties in China. International Journal of Architectural Heritage, 10(5), 663-673.

Liu, X., Yu, L., Xie, F., Li, M., Chen, L. & Li, X. 2010. Kinetics and Mechanism of Thermal Decomposition of Cornstarches with Different Amylose/Amylopectin Ratios. *Starch-Stärke,* 62(3-4), pp.139-146.

Liu, Y., Yang, L., Ma, C., & Zhang, Y. 2019. Thermal Behavior of Sweet Potato Starch by Non-isothermal Thermogravimetric Analysis. Materials, 12(5), pp. 699-710.

Liu, Y. & Zhang, X. 2002. Ancient and Modern Clinical Application of Cinnabar. *Journal of Practical Medical Techniques,* 9**,** 197-198.

Liu, Z., Wang, J., Wang, W. & Yang, R. 2016c. Spectral Analyses of the Lime Mortar in Ancient Chinese Architectures. The Journal of Light Scattering, 28(1), 45-50.

LUO, Z. 1960. Wall Painting Tomb of the Song Dynasty in Huai'an, Jiangsu Province. *Cultural Relics***,** 43-51+97.

LUO, Z. 1963. The Excavation of the Southern Dynasties Tomb in Youfang Village, Xishanqiao, Nanjing. *Archaeology***,** 290-300.

MA, D. 1961. A Brief Excavation Report of the Daming Palace in the Tang Dynasty during 1959-1960. *Archaeology***,** 341-344.

MA, D. 1987. The New Harvest of the Chang'an City in the Tang Dynasty. *Archaeology***,** 329-336, 310.

MA, S. 1939. *Fenghuangtai Jishi*, Shanghai, The Commercial Press.

Martin, F., Ramstedt, M., Söderhäll, K. and Canet, D., 1988. Carbohydrate and amino acid metabolism in the ectomycorrhizal ascomycete Sphaerosporella brunnea during glucose utilization: a 13C NMR study. Plant physiology, 86(3), 935-940.

Medeiros, P.M., Fernandes, M.F., Dick, R.P. and Simoneit, B.R., 2006. Seasonal variations in sugar contents and microbial community in a ryegrass soil. Chemosphere, 65(5), 832-839.

MENG, Q. 2011. Medicinal Value of Cinnabar. *Seek Medical And Ask The Medicine*, 9**,** 445.

MIAO, J., LI, X., CHENG, R. & LU, B. 1981. A Preliminary Investigation of

Cementing Materials Used in Ancient China. *Journal of the Chinese Ceramic Society***,** 234-240.

Muhs, D.R., 2013. Loess and its geomorphic, stratigraphic, and paleoclimatic significance in the Quaternary.

Muhs, D.R., Cattle, S.R., Crouvi, O., Rousseau, D.D., Sun, J. and Zárate, M.A., 2014. Loess records. Mineral dust: A key player in the earth system, pp.411-441.

MUNICCHIA, A. C., CANEVA, G., RICCI, M. A. & SODO, A. 2014. Identification of endolithic traces on stone monuments and natural outcrops: preliminary evidences. *Journal of Raman Spectroscopy,* 45**,** 1180-1185.

Ni, J., 2013. Carbon storage in Chinese terrestrial ecosystems: approaching a more accurate estimate. Climatic Change, 119(3), pp.905-917.

Niederer, M., Pankow, W. and Wiemken, A., 1989. Trehalose synthesis in mycorrhiza of Norway spruce: an indicator of vitality. European Journal of Forest Pathology, 19(1), 14-20.

OCHES, E. A. & MCCOY, W. D. 2001. Historical developments and recent advances in amino acid geochronology applied to loess research: examples from North America, Europe, and China. *Earth-Science Reviews,* 54**,** 173-192.

PAN, G. 2009. *Architectures of the Yuan and Ming Dynasties,* Beijing, China Architecture & Building Press.

Patwardhan, P.R., Satrio, J.A., Brown, R.C. and Shanks, B.H., 2009. Product distribution from fast pyrolysis of glucose-based carbohydrates. Journal of Analytical and Applied Pyrolysis, 86(2), pp.323-330.

Paul, E. A. (2007) Soil microbiology, ecology, and biochemistry. 3rd ed. Burlington, Mass.; Academic Press.

PEI, Q., GUO, Q., WANG, X., ZHAO, J., ZHAO, G. & LUO, J. 2019. Evolution and Characteristics of Traditional Building Techniques for Earthen Architectural Sites. *Sciences of Conservation & Archaeology*, 1.

PENG, S. 1995. Re-discussion on the Change and Development of Ancient Nanchang City. *Cultural Relics in Southern China*, 86-98.

PENG, S., ZHU, Y., GUO, Z. & WANG, L. 2004. The Excavation of the Dashanqian site in Harqin Banner, Inner Monglia in 1998. *Archaeology*, 31-39.

PETKOVSKI, E., KEYSER-TRACQUI, C., CRUB ZY, E., HIENNE, R. & LUDES, B. 2006. MALDI-TOF MS analysis of Y-SNPs in ancient samples. *International Congress Series*, 1288, 25-27.

POZZI, F. & LEONA, M. 2016. Surface-enhanced Raman spectroscopy in art and archaeology. *Journal of Raman Spectroscopy*, 47, 67-77.

Pye, K., 1995. The nature, origin and accumulation of loess. Quaternary Science Reviews, 14(7-8), pp.653-667.

QIAN, Y. 1999. The Characteristics and Historical Status of Xishan City. *Cultural Relics*, 41-45.

QIN, Y. 2010. The Survey and Preliminary Study of Yungang Grottoes' Clayey Sculptures. Master, Shanxi University.

QIU, G. & SUN, X. 1992. The Preliminary Investigation and Excavation of the Exterior City of the Northern Song Dongjing City. *Cultural Relics*, 52-61.

ROCCO MAZZEO, DARINN CAM, GIUSEPPE CHIAVARI, DANIELE FABBRI, HE LING & SILVIA PRATI 2004. Analytical study of traditional decorative materials and techniques used in Ming Dynasty wooden architecture. The case of the Drum Tower in Xi'an, P.R. of China. *Sciences of Conservation & Archaeology*, 5**,** 273-283.

Sedmak, J.J. & Grossberg, S.E. 1977. A rapid, sensitive, and versatile assay for protein using Coomassie brilliant blue G250. Analytical Biochemistry, 79(1-2), 544-552.

Shan, S., Zhang, R., Wang, Q., Zhu, Y. & Qi, G. 2022. Structural Analysis and Comparison of the Ming Dynasty Great Wall Mortar in Beijing Yanqing and Huairou. Bulletin of the Chinese Ceramic Society, 41(9), 3047-3058.

SHANDONG ARCHAEOLOGY TEAM OF CHINESE ACADEMY OF SOCIAL SCIENCES, SHANDONG INSTITUTE OF CULTURAL RELICS AND ARCHAEOLOGY & LIAOCHENG CULTURAL RELICS BUREAU 2005. Discovery and Excavation of the Longshan Cultural City Wall at the Jiaochangpu Site, Chiping, Shandong Province. *Archaeology***,** 3-6.

SHANDONG ARCHAEOLOGY TEAM OF CHINESE ACADEMY OF SOCIAL SCIENCES, SHANDONG INSTITUTE OF CULTURAL RELICS AND ARCHAEOLOGY & RIZHAO CULTURAL RELICS BUREAU 2015. The Investigation and Excavation in 2012 of the Yaowangcheng Site, Rizhao, Shandong Province. *Archaeology***,** 7-24.

SHANDONG INSTITUTE OF CULTURAL RELICS AND ARCHAEOLOGY &

CULTURAL RELICS RESEARCH OFFICE OF LIAOCHENG CULTURAL BUREAU 1997. The Investigation and Preliminary Excavation of the Longshan Culture Ancient City at the Jingyanggang Site, Yanggu County, Shandong Province. *Archaeology***,** 11-24.

SHANDONG INSTITUTE OF CULTURAL RELICS AND ARCHAEOLOGY & SCHOOL OF ARCHAEOLOGY CULTURE AND MUSEUM OF PEKING UNIVERSITY 2019. A Brief Excavation Report of the Chengziya site, Zhangqiu District, Jinan during 2013-2015. *Archaeology***,** 3-24.

SHAO, M. 2007. Study of Environment and Reinforcement of Main Part of the Ancient Ruins of Jiaohe. master, Lanzhou University.

SHEN, J., XIAO, G., WANG, Z., SUN, Q., WU, H., ZHANG, C. & GUO, Z. 2017. Distribution of n-alkanes in Miocene loess in Qinan, western Chinese Loess Plateau, and its palaeoenvironmental implications. *Science China Earth Sciences,* 60**,** 921-928.

SHEN, X., LIU, P. & LIU, A. 2006. Type, Value and Heritage Management Model of Diao Tower in Kai Ping. *Journal of Hunan University of Arts and Science(Social Science Edition)***,** 95-99.

Silverstein, R.M., Webster, F.X. & Kiemle, D.J. 2005. *Spectrometric Identification of Organic Compounds (7th edition)*. Hoboken, NJ: John Wiley & Sons., p. 74.

Smalley, I.J. 1966. The properties of glacial loess and the formation of loess deposits. Journal of Sedimentary Research, 36(3), pp.669-676.

Smalley, I.J. 1995. Making the material: The formation of silt sized primary mineral

particles for loess deposits. Quaternary Science Reviews, 14(7-8), pp.645-651.

Smalley, I.J. & Derbyshire, E. (1990) The definition of ‘ice-sheet’ and ‘mountain’ loess. Area (London 1969). 22 (3), 300–301.

Smalley, I.J. & Krinsley, D.H., 1978. Loess deposits associated with deserts. Catena, 5(1), pp.53-66.

Smalley, I.J., O'Hara-Dhand, K. and Kwong, J., 2014. China: materials for a loess landscape. Catena, 117, pp.100-107.

Smalley, I.J. & Vita-Finzi, C., 1968. The formation of fine particles in sandy deserts and the nature of" desert'loess. Journal of Sedimentary Research, 38(3), pp.766-774.

SONG, Y. 2008. *Translation and Annotation of "Tiangong Kaiwu"*, Shanghai, Shanghai Classics Publishing House.

Streeter, J.G., 1981. Seasonal distribution of carbohydrates in nodules and stem exudate from field-grown soya bean plants. Annals of Botany, 48(4), 441-450.

Su, X., Zhou, Z., Liu, Jun’e, Wang, P., Liu, Junyang, Li, Q., Zhao, F., 2022. The role of roots traits of climax community species to shear strength in the Loess Hilly Region, China. Soil and Tillage Research 221, 105417. https://doi.org/10.1016/j.still.2022.105417

SUN, M. 2006. A Study of the Protection and Reinforcement about the Ruins of Jiaohe, Turpan, China. Doctor, Lanzhou University.

THE ARCHAEOLOGICAL TEAM OF CHENGDU CITY & THE PIXIAN MUSEUM 2001. Excavation of a City Site at Pixian in Sichuan in 1997. *Cultural*

*Relics***,** 52-68.

Thevelein, J., 1984. Regulation of trehalose mobilization in fungi. Microbiological reviews, 48(1), 42-59.

TIAN, L. 2004. Finding a way to the Question of Conservation of Great Ruins & Traces. Doctor, Tianjin University.

Wang, B. 1936. The Official Construction Techniques of Stone Bridges in the Qing Dynasty. Beijing: The Society for Research in Chinese Architecture, 101-102.

WANG, C., LI, F., SHI, H., JIN, Z., SUN, X., ZHANG, F., WU, F. & KAN, S. 2013. The significant role of inorganic matters in preservation and stability of soil organic carbon in the Baoji and Luochuan loess/paleosol profiles, Central China. *CATENA,* 109**,** 186-194.

WANG, L., GUO, R., ZHOU, W., FAN, X., ZHAO, L. & MA, T. 2012. Determination of Contents of Protein and Starch in Plaster Materials Used in Colored Drawing on Chinese Ancient Buildings. *Journal of Lanzhou University(Natural Sciences)***,** 136-140.

WANG, Q., LI, Y. & WANG, Y. 2011. Optimizing the weight loss-on-ignition methodology to quantify organic and carbonate carbon of sediments from diverse sources. *Environmental Monitoring and Assessment,* 174**,** 241-257.

WANG, Q. & WANG, L. 2010. The Excavation of the Longshan Cultural City in the Xijincheng site, Boai County, Henan Province. *Archaeology***,** 22-35.

WANG, S. 2009. Study on the Causes for Deterioration and Environmental Regionalization of Earthen Heritage Sites in Northern China. Master, Lanzhou

University.

WANG, S. 2011a. The Study on the Charcoal Unearthed from the Taosi Site. *Archaeology***,** 91-96.

WANG, W. 2001. Design of Detection, Evaluation and Conservation of Huguo Bridge in Kunming. *Yunnan Communication Science and Technology***,** 44-48.

WANG, X. 2011b. Archaeology inTaosi: the Empirical Analysis of Technique. doctor, Shanxi University.

WANG, Y., HAN, X., JIN, Z., ZHANG, C. & FANG, L. 2016. Soil Organic Carbon Stocks in Deep Soils at a Watershed Scale on the Chinese Loess Plateau. *Soil Science Society of America Journal,* 80**,** 157-167.

Wei, G., Sun S., Wang, C., Zhang, B. & Chen, X. 2013. Study on the Traditional Lime Mortar from the Memorial Archway in the Southern Anhui Province. Spectroscopy and Spectral Analysis, (7), 1973-1976.

WEI, W. 2009. Investigation and Research on the Early Maijishan Cave Temples. doctor, Lanzhou University.

WHITNEY, A. V., VAN DUYNE, R. P. & CASADIO, F. 2006. An innovative surface-enhanced Raman spectroscopy (SERS) method for the identification of six historical red lakes and dyestuffs. *Journal of Raman Spectroscopy,* 37**,** 993-1002.

Winchester, R., & Wansbrough, H. (2013). Blood detection by chemical methods. XII-Biotech-A-Blood Detection, 1-6.

WOUTERS, J. 1985. High performance liquid chromatography of anthraquinones: analysis of plant and insect extracts and dyed textiles. *Studies in Conservation,* 30**,**

119-128.

WU, Q. 2005. Study on City Wall and Moat Military Defence System of Nanjing City in Ming Dynasty. *The Architect***,** 86-91.

WUNDERLICH, B. 1990. Thermal Analysis, San Diego, Academic Press, Inc.

XIE, H. 2004. Construction Technique of Rammed-earth Construction of Fujian Earth Building. *Housing Science***,** 39-42.

XIE, L. 2009. Lime, Grass and Paper as the Materials, the Sculpture of A'gong Stands on the Top Window-the Art of Lime Sculpture in Shixing Hakka Close House in the Ming and Qing dynasties. *Art***,** 105-107.

XIE, X. 2007. *Study on the Taosi Site, Xiangfen,* Beijing, Science Press.

XING, J. 1995. *Science and Technology of Ancient Times in Shaanxi,* Beijing, Science and Technology of China Press, 162.

XU, G. 2014. Present Situation and Conservation of Tonggusibaxi Ancient City Sites. Master, Lanzhou university.

XU, X. & SUN, D. 1963. Investigation of the Qin Capital Yongcheng site. *Archaeology***,** 27-30.

XU, X., ZHANG, K. L., XU, X. & PENG, W. Y. 2003. Spatial Distribution and Estimating of Soil Organic Carbon on Loess Plateau. *Journal of Soil and Water Conservation,* 17**,** 13-15.

YAN, S. 2016. Research on the Earth Wall of Vernacular Dwelling in Hubei Province. master, Wuhan University of Technology.

YANG, F., ZHANG, B., PAN, C. & ZENG, Y. 2009. Traditional Mortar Represented

by Sticky Rice Lime Mortar-One of the Great Inventions in Ancient China. *Science in China Series E Technological-Technological Sciences,* 52**,** 1641-1647.

YANG, F., ZHANG, B., ZENG, Y., PAN, C. & HE, X. 2008. Exploratory Research on the Scientific Nature and Application of Traditional Sticky Rice Mortar. *Palace Museum Journal***,** 105-114+159.

YANG, J. 2010. The Study on the Construction of Seagrass Cottage in Jiaodong Peninsula. Master, Southeast University.

YANG, J. 2016. Applied Research of Plant Materials in Ancient Chinese Architecture-Grass, Bamboo, Wood. Doctor, Southeast University.

YANG, J. 2019. From Materials: Enlightenment of Wood Selection and Application in Ancient Chinese Timber Buildings. *The Architect,* 200**,** 101-106.

YANG, K. 1981. The Origin and Evolution of the Ancient Chinese Mausoleum System. *Fudan Journal(Social Sciences Edition)***,** 59-68.

Yang, Y., Zhang, P.P., Song, Y., Li, Z.M., Zhou, Y.Y., Sun, H., Qiao, J., Wang, Y.Q. and An, S.S., 2024. The structure and development of Loess Critical Zone and its soil carbon cycle. Carbon Neutrality, 3(1), p.1.

Yao, Y., Wei, X., Kong, W., Li, M., Wang, Z., Zhao, Z. and Shao, M., 2023. Variations in the concentration, composition, and sources of WEOM in erosion and deposition landscapes over an erosion intensity gradient on the Loess Plateau of China. Catena, 222, p.106846.

YU, H. & CHEN, D. 2004. Protection and Development of Tourism Resources in Qiantang River Ancient Seawall. *Zhejiang Hydrotechnics***,** 9-10.

Zech, M. and Zech, R., 2018. 'Biomarkers and Stable Isotopes in Loess as Paleoenvironmental Indicators'. In: R. Schaetzl, E. Bettis, O. Crouvi, K. Fitzsimmons, D. Grimley, U. Hambach, F. Lehmkuhl, S.B. Marković, J.A. Mason, P. Owczarek, H.M. Roberts, D.-D. Rousseau, T. Stevens, J. Vandenberghe, M. Zárate, D. Veres, S. Yang, M. Zech, and J.L. Conroy, eds. Approaches and Challenges to the Study of Loess—Introduction to the LoessFest Special Issue. Quaternary Research, 89(3), pp.563-618.

ZENG, Q. G., ZHANG, G. X., LEUNG, C. W. & ZUO, J. 2010. Studies of wall painting fragments from Kaiping Diaolou by SEM/EDX, micro Raman and FT-IR spectroscopy. *Microchemical Journal,* 96**,** 330-336.

ZENG, Y., ZHANG, B., LIANG, X. & TIE, J. Study on the Mechanism of Natural Biological Macromolecules in Mortars of Ancient China. The fifth annual academic conference of China Association for Preservation Technology of Cultural Relics, 2007 Nanjing, Jiangsu Province, China. 11.

ZHAN, X., FU, S. & LIANG, J. 2006. *The History of Tiles in China,* Beijing, China Building Materials Press.

ZHANG, B., HU, W., ZHANG, K. & FANG, S. 2015. Research on the Egg White in Ancient Tabia Mortar by Enzyme-Linked Immunosorbent Assay(ELISA). *Journal of Building Materials***,** 716-720.

Zhang, B., Wei, G., Hu, S., Geng, Q., Yang, W. & Zheng, X. 2020a. Analysis of Mortar Composition of Shanhe Weir and Yangtou Weir in Hanzhong City. Spectroscopy and Spectral Analysis, 40(2), 637.

Zhang, C., Zhang, B., Cui, B. & Lin, G. 2020b. What factors contribute to high mechanical strength of tabia? Case study of the tabia from coastal forts sites at Zhejiang, China. Heritage Science, 8, 1-15.

ZHANG, G. & YIN, C. 1997. A Comprehensive Study of Neolithic City Sites in China. *Journal of Zhengzhou University***,** 58-62.

ZHANG, H., ZHAO, T. & WANG, X. 2008. The Construction Techniques of Earthen Sites in Ancient China. *Dunhuang Research,* 2008**,** 81-90.

ZHANG, J., LIU, Z. & XU, L. 2009. A Brief Excavation Report of the Zhichengmen Site of Chang'an City, Xi'an in 2008. *Archaeology***,** 49-60.

ZHANG, K. 2014. Enzymatic Detection Methods for Organic Matters in Mortars Containing Earth. master, Zhejiang University.

ZHANG, M., XU, T., DONG, H., SUN, Q., LEI, X. & SONG, J. 2006. The Investigation Report of the Zhougongmiao Site, Qishan, Shaanxi Province in 2003. *The Journal of Ancient Civilizations***,** 151-186.

ZHANG, Q., HUANG, L., LIAO, M., MIAO, H. & FAN, D. 2012. The Excavation Report of the Xiaoguwei Island Battery Site of the Qing Dynasty. *Guangzhou Cultural Relic***,** 84-100.

ZHANG, Z. 1998. The Preliminary Research of the Prehistoric Ancient Cities Along the Yangzi River. *Southeast Culture***,** 6-14.

ZHAO, H. & XU, H. 2020. A Brief Excavation Report of the No. 5 Foundation site in the Palace Area of the Erlitou site, Yanshi City, Henan Province. *Archaeology***,** 20-36.

ZHAO, J., LUO, X., MA, Y., SHAO, T. & YUE, Y. 2017. Soil characteristics and new formation model of loess on the Chinese Loess Plateau. *Geosciences Journal,* 21**,** 607-616.

ZHAO, T. 2007. Features the Gate of Guidefu Ancient City in Shangqiu. *Shanxi Architecture***,** 63-65.

ZHAO, Y. 2012. The Preliminary Discussion on the Wooden Remains of Liangzhu Culture. *Cultural Relics in Southern China***,** 74-83.

ZHEJIANG CULTURAL RELICS MANAGEMENT COMMITTEE 1960. The First and Second Excavation Reports of the Qianshanyang site, Wuxing. *Acta Archaeological Sinica***,** 73-90.

Zheng, L., Wu, X., Jin, P., & Wang Y. 2014. Analysis of the Component of the Lime Mortar from the Lanjiazhai Site in Dachang, Chongqing Wushan. Journal of Chongqing Normal University: Natural Science, (1), 42-47.

ZHENG, Q. 2000. Architectural Features and Humanistic Values of Ancient Pagodas in Taizhou. *Journal of Taizhou Teachers College***,** 91-96.

Zheng, Q. & Wang C. 2013. Starch Evidence of Glutinous Plant Content as the Additive to Ming Great Wall Mortar at Gubeikou, Beijing. Quaternary Sciences, 33(5), 575-581.

Zheng, Y., Zhang, H., Zhang, B.J. & Yue, L.H. 2016. A new method in detecting the sticky rice component in traditional Chinese tabia. Archaeometry, 58, 218-229.

Zhou, H. 2016. Study of Sticky Rice-Lime Mortar for the conservation of Stone Culture Relics. Doctor, Anhui University.

ZHOU, W. 2009. Analytical Studies on MakingTechniques and Plaster Materials Used in Painting and Colored Drawing of Aneient Wooden Architectural Buildings. master, Northwest University.

ZHOU, W., WANG, L., FAN, X., QI, Y. & MA, T. 2010. Study on the Making Techniques and Materials of the Oil-painting Samples from a Column in Bogda Khan Palace Museum. *Journal of Inner Mongolia University(Natural Science Edition)***,** 522-526.